Dissertation

submitted to the
Combined Faculties for the Natural Sciences and for Mathematics
of the Ruperto-Carola University of Heidelberg, Germany
for the degree of
Doctor of Natural Sciences

presented by
Sara Fahs, M.Sc.
born in Beirut, Lebanon

Oral examination:
17.05.2018

Interpreting the Activity of Metastasis-Promoting PRL-3 Through the Total Synthesis of Phosphatidylinositol Analogues

Referees:

Dr. Carsten Schultz, EMBL Heidelberg

Prof. Dr. Walter Nickel, University of Heidelberg

To my Grandfather, Saïd Mansour, who showed me the art in science, the science in art, and how boring life would be without poetry. May he rest in peace.

The research and results presented in this thesis were carried out at the European Molecular Biology Laboratories (EMBL), based in Heidelberg (Germany) under the supervision of Dr. Maja Köhn.

Publications:

Part of this work has been published, or prepared for submission

Fahs S, Lujan P, Köhn M. (2016), Approaches to Study Phosphatases**.** *ACS Chem. Biol.* **11**(11):2944-2961. doi: 10.1021/acschembio.6b00570

Stadlbauer S, Fahs S, Kar N, and Köhn M. (20xx), Solid Phase Synthesis and Bioactivity of Lipid chain PI(4,5)P_2 analogues [manuscript in preparation]

Acknowledgements

I would like to thank my thesis supervisor, Dr. Maja Köhn, for believing I could take on this project. Under her generous guidance and patience, I learned the practice to carry out the research and to present works as clearly as possible. I would also like to thank all my kind group members, particularly Sven Stadlbauer for putting me on track in inositol chemistry; Pablo Ríos, for teaching me to think critically, to meticulously analyze biological data, and to pipette like a pro; Alina Muschko for inspiring me with her courage to get things done; and Leslie Makotta for reminding me that science was never meant to kill joy.

Thanks to my collaborators (Ulrike Uhrig, Pedro Ballester, Mascha Jäckel) for believing in my fledgling ideas, and for backing me up with all the expertise they generously offered. My thanks also go to my TAC committee members (Carsten Schultz, Nassos Typas, Walter Nickel), for their encouragement, insightful comments, and hard questions.

Completing this work would have been more difficult were it not for the care and friendship provided by the chemical biology core facility and all its members, for they made me part of their family, that scientific hub at EMBL, which harbors the discipline I was specializing in. My special gratitude goes to David Will, for having forged a place for me, both in his state-of-the-art MedChem lab and in his heart, to learn and mature as a chemist and an independent researcher, inevitably contaminated with a weird Scottish sense of humor.

I would like to thank the superb kitchen ladies, for my PhD would have taken twice the amount of time, or more, had I cleaned the glassware after every mess I made.

I take pride in acknowledging the energy of my climbers' brigade, those beasts who provided a much needed form of escape from the (sometimes pointless) PhD torments, who helped me recall who I was and how to keep things in perspective. After all, challenging gravity has proven to be much harder than challenging a chemistry reaction that fails. I thank Bernhard Hampölz, my favorite mountain guide, for always offering the wild life I belong to. With him, I mastered the art of falling.

My acknowledgement would be incomplete without thanking the biggest foundation of my strength, my family. I will never cease finding genuine answers in the spirit of my Father Bilal. His pride is priceless, his life lessons countless, and his ambitions endless. All that I am or hope to be I owe to my mother Rima, that single, bright, free and powerful woman who kept raising the bar higher for me without knowing. My parents were never scientists, but they showed me what it is worth to be a good one. I wish they lived closer to me.

Thank you, Jakob Trendel, for endowing my critical writing period with deep laughs and intense, far-reaching discussions.

Table of Contents

Abstract

The discovery of phosphatidylinositol-phosphates (PIP*n*) within cell membranes, in the early 1950's, ignited the interest in their biological roles, and soon after scientific evidence proposed their tight association with processes involving cell signaling, cell adhesion, polarization and migration, as well as membrane trafficking and oncogenesis. PRL-3, an oncogenic phosphatase, has been recently shown to adopt phosphatidylinositol (4,5) bisphosphate ($PI(4,5)P_2$) as a natural substrate, through which it orchestrates several hallmarks of cancer, culminating in metastasis. Therefore, the PIP*n*-metabolizing enzyme PRL-3 became of great interest in biomedical research. To understand the binding mechanisms of $PI(4,5)P_2$ with PRL-3, the development of synthetic approaches to synthesize analogues of this natural product is paramount.

The goal of this work was to develop an approach to synthesize $PI(4,5)P_2$ mimetics with alkylation(s) on the inositol ring. The newly established synthetic route was first tested with the chiral 6-*O*-methoxy $PI(4,5)P_2$, after many arising synthetic challenges were overcome. The chemical literature is abundant with $PI(4,5)P_2$ analogues bearing thiophosphate groups, different lipid tail composition, and novel functional groups, but none with direct changes to the hydroxyl groups on the inositol ring have been reported so far. Within the resulting collection of novel, inositol-modified analogues, some showed significant biological activity with PRL-3, compared to the lipid tail-modified analogues and the one containing the natural $PI(4,5)P_2$ head group, which were also synthesized as part of this work. These active analogues were specific to PRL-3 as they did not show major activity with other $PI(4,5)P_2$ –metabolizing enzymes.

In parallel, *in silico* shape similarity screening methods were applied using $PI(4,5)P_2$ as a template, to look for specific PRL-3-active small molecule inhibitors. This led to an active compound, which stresses the potential of prediction tools in finding inhibitors for challenging targets.

Future applications of the synthesized $PI(4,5)P_2$ analogues can be numerous: investigating the binding requirements of specific PIP*n*- metabolizing phosphatases, understanding the biology of specific PIP*n*, designing ligands through *in silico* and synthetic methods to modulate their interaction, and probing their usefulness in the treatment of diseases.

Zusammenfassung

Die Entdeckung der Phosphatidylinositol-Phosphate (PIP*n*) in Zellmembranen in den frühen 50er Jahren entfachte das Interesse an ihren biologischen Rollen. Kurz darauf wurden ihre engen Verbindungen mit Prozessen, wie beispielsweise Signaltransduktion, Zelladhäsion, Polarisation und Migration, sowie Membrantransport und Onkogenese, belegt. PRL-3, eine onkogene Phosphatase, dephosphoryliert Phosphatidylinositol (4,5)bisphosphat (PI(4,5)P_2), wodurch es mehrere Prozesse von Krebs orchestriert, die in Metastasen münden. Daher ist das PIP*n*-metabolisierende Enzym PRL-3 von großem Interesse in der biomedizinischen Forschung. Um die Bindungsmechanismen von PI(4,5)P_2 mit PRL-3 zu verstehen, ist die Entwicklung von synthetischen Ansätzen zur Synthese von Analoga dieses Naturstoffes von größter Bedeutung.

Das Ziel dieser Arbeit war, einen Ansatz zur Synthese von PI(4,5)P_2-Mimetika mit Alkylierung(en) am Inositolring zu entwickeln. Der neu etablierte Syntheseweg wurde zuerst mit dem chiralen 6-*O*-Methoxy-PI(4,5)P_2 getestet, nachdem viele der auftretenden synthetischen Herausforderungen überwunden waren. Die chemische Literatur ist reich an PI(4,5)P_2-Analoga, die Thiophosphatgruppen, verschiedene Lipidschwanzzusammensetzungen und neue funktionelle Gruppen tragen, aber bisher wurden keine mit direkten Änderungen der Hydroxylgruppen am Inositolring hergestellt. Innerhalb der resultierenden Sammlung von neuen, am Inositolring modifizierten Analoga zeigten einige signifikant erhöhte biologische Aktivität mit PRL-3 verglichen mit den lipidschwanzmodifizierten Analoga und demjenigen, das die natürliche PI(4,5)P_2-Kopfgruppe enthielt. Diese wurden auch als Teil dieser Arbeit synthetisiert. Diese aktiven Analoga waren spezifisch für PRL-3, da sie keine oder wenig Aktivität mit anderen PI(4,5)P_2-metabolisierenden Enzymen zeigten.

Parallel dazu wurden *in-silico*-Struktur-Ähnlichkeits-Screening-Verfahren angewendet, wobei die Kopfgruppe von PI(4,5)P_2 als Templat verwendet wurde, um nach spezifischen PRL-3-aktiven kleinen Molekülen als Inhibitoren zu suchen. Dies führte zu einer aktiven Verbindung. Dies untermauert das Potenzial von Vorhersagewerkzeugen bei der Suche nach Inhibitoren für anspruchsvolle Zielproteine.

Zukünftig mögliche Anwendungen der synthetisierten PI(4,5)P_2-Analoga sind vielfältig, wie beispielsweise zur Untersuchung von Bindungsanforderungen spezifischer PIP*n*-metabolisierender Phosphatasen, zum Verständnis der Biologie spezifischer PIP*n*, zum Design von Liganden durch *in silico* und synthetische Methoden zur Modulation ihrer Wechselwirkungen, und zur Untersuchung ihrer Nützlichkeit bei der Behandlung von Krankheiten.

Chapter 1. Introduction

1.1. Phosphorylation and dephosphorylation

In Eukaryotes, one of the most common mechanisms by which gene product formation is tightly regulated is reversible phosphorylation. In fact, the reversible phosphorylation of proteins and other cellular molecules, such as the phosphatidylinositol phosphates (PIP*n*)[1] allows cells to adapt to environmental changes.

The abovementioned process is carried out by the coordinated action of protein kinases and protein phosphatases: kinases catalyze phosphate transfer from ATP molecules to functional groups of proteins (serine, threonine and tyrosine side chains) and non-protein substrates to be modified, thus leading to conformational changes eventually activating a cellular response; while phosphatases revert these covalent modifications by hydrolyzing the respective phosphate moieties on protein and non-protein substrates [2–4]. Constituting 2-4% of the genes in a typical eukaryotic genome[5,6], kinases and phosphatases equally stand as the architects of universal and crucial processes which are tightly regulated in cells in order to guarantee physiological balance, but are also implicated in numerous disease mechanisms upon their deregulation [7].

1.1.1. Phosphatase families

While strong advancement has been achieved, our understanding of phosphatases still lags behind that of kinases for many reasons[8], including their high evolutionary diversity and complexity based on different ancestors (i.e., evolutionary unrelated) compared to the evolution of kinases based on a common ancestor [5,9,10]. In fact, protein phosphatases evolved into mechanistically and structurally distinct superfamilies. There exists an extensive detailed perspective on these proteins in the literature[9,11,12].

Traditionally, these proteins have been grouped according to their substrate specificity and distinct catalytic mechanisms into the protein serine/threonine phosphatases (PSTPs) and the protein tyrosine phosphatases (PTPs). These broad and common classes were further classified into "superfamilies"[7,13]. However, newer structure-sequenced based classification methods differ from the traditional view. Phosphatases are now grouped into their evolutionary related families, and while many of the old relationships still exist, new ones have been identified[12,14]. Phosphatases within these families largely

have similar substrate specificity, however, this is not true for all members of all families[12,14].

The CC1[14]/Family 1[9,12] superfamily, traditionally called the class 1 protein tyrosine phosphatase (PTP) family, is of special interest to this work. This superfamily is defined by its catalytic signature Cx_5R, and well known for its diversity in domain structure and substrate preference. This family consists of non-transmembrane PTPs and receptor-like PTPs, which are both largely pTyr-specific, as well as the dual-specificity phosphatases (DSPs or DUSPs), which show diverse substrate specificity dephosphorylating not only pTyr containing proteins but also pSer/Thr, carbohydrates, mRNA, and, most importantly for this work, PIP*n*. Newer classifications also added some other PIP*n*-phosphatases to this family[1,15].

Despite their low abundance, PIP*n* control a multitude of central cellular processes, like signal transduction, intracellular membrane trafficking, cytoskeleton remodeling, nuclear events, control of cell growth and survival, and others (see chapter 1.3)[16]. Among the PTP superfamily, the phosphatases which dephosphorylate PIP*n* fall into four primary families: the Sac1 domain containing phosphatase, PTENs, myotubularins, and 4-phosphatase[15]. In addition, one receptor-type tyrosine-protein phosphatase (PTPRQ)[17] and phosphatase of regenerating liver-3 (PRL-3)[18,19], which is the major subject of this work, were shown to dephosphorylate PIP*n*.

1.1.2. The phosphatases of the regenerating liver (PRLs)

The phosphatases of the regenerating liver (PRL*s*) belong to the DUSP family of phosphatases (described above), and comprise three members: PRL-1, -2 and -3. This family is unique in many ways: first, the members do not share much sequence similarity with other phosphatases, but they share 76-87% similarity amongst each other. In fact, the closest related PTPs to the PRLs are the DUSPs Cdc14 and PTEN[20,21]. Second, the PRL*s* contain unique structural characteristics: they are the only ones amongst the PTPs to possess a CAAX box (where C is cysteine, A an aliphatic amino acid, and X any amino acid) at the C-terminus, which presents a prenylation motif that serves for localization to cellular membranes[22]. In addition, the PRLs contain a C-terminal polybasic stretch, which aids in membrane attachment through ionic interaction with negatively charged lipids[23]. Also, the PRL*s* show unusually shallow and hydrophobic active site characteristics, which makes them stand out from other phosphatases[20].

Nevertheless, the PRLs are known to follow the general PTP mechanism, taking into account that it is equipped with the conserved CX_5R motif of the active site p-loop, with the catalytic cysteine and arginine residue, and the invariant aspartic acid of the WPD-loop as general acid/base[24]. These structural elements, conserved around the active site, are common to PTPs: presented as a thiolate anion, the very acidic catalytic cysteine acts as a strong nucleophile, which attacks the phosphate moiety of a substrate[25]. This represents the first step of the dephosphorylation reaction, and is assisted by the conserved aspartic acid in the neighboring loop, which donates a proton to the dephosphorylated substrate. Then, and as the second step of the catalysis, the aspartate residue, now acting as a base, helps with the hydrolysis of the covalent intermediate by a water molecule, releasing inorganic phosphate and the original state enzyme (Figure 1)[7,24]. The conserved arginine in the P-loop is important for the stabilization of the phosphoryl-cysteine transition state[26]. The conserved WPD-loop aspartate in the PRLs however, as opposed to other PTPs, is not important as the general acid/base (mentioned above) in the dephosphorylation of phosphoinositides, demonstrating an alternative reaction mechanism[27].

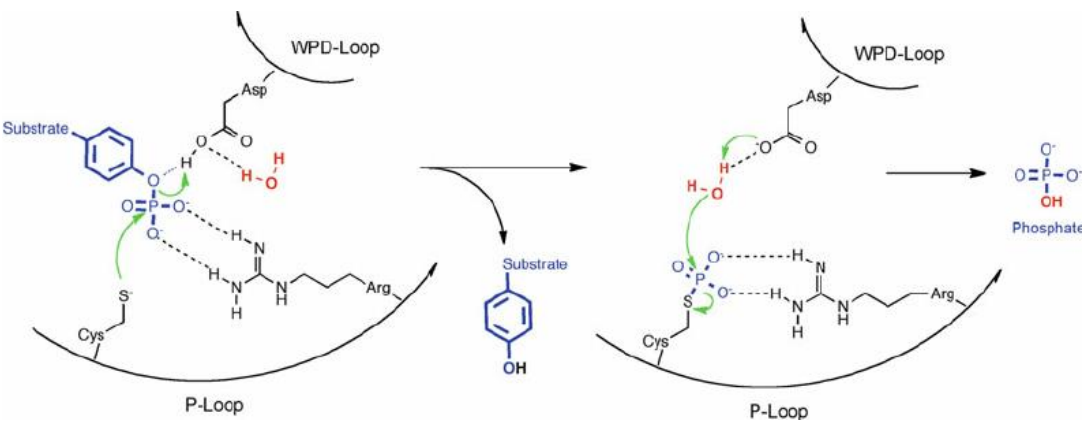

Figure **1** Common catalytic mechanism of the PTPs. The figure is adapted from Tautz et al[28].

1.1.3. PRL-3: a phosphatase critical for cell deregulation

In addition to being involved in cell growth, proliferation, and invasion[29,30], the functional role of PRL-3 in disease implications, and particularly in cancer metastasis is by now well established. For instance, PRL-3 is consistently highly expressed in metastatic colorectal tumors compared with non-metastatic tumors and the normal colorectal epithelia[31]. In

addition, consolidated work has denoted that PRL-3 could actually operate as a biomarker for poor prognosis in gastric cancer, ovarian cancer, breast cancer, and colon cancer[32–34]. It is not surprising that the DUSP PRL-3 would pose as a promising therapeutic target. Throughout various cancer cell lines in culture and in mouse models, PRL-3 was functionally characterized, either by overexpression or knockdown approaches which indicated that it promotes cell migration in vitro, and metastatic invasion in vivo[20,35]. PRL-3 has been further associated with even more hallmarks of cancer such as tumor angiogenesis[36], epithelial-to-mesenchymal transition (EMT)[37], and metastatic events in various tumor environments[34–36].

It is important to note the cellular localization of PRL-3 as a context for the abovementioned functions and disease implications: due to its C-terminal prenylation motif and the preceding polybasic stretch, PRL-3 localizes to the plasma membrane and early endosomes[38]. Because of its farnesylation potential, PRL-3 was shown to further shuttle between the nucleus and the cytosol, sometimes localizing in the endoplasmic reticulum[35]. Farnesylation was therefore suggested to conceal the nuclear localization signal (NLS) of the polybasic stretch, retaining the proteins bound to membranes[39]. These findings proposed that PRL-3 play a role in the plasma membrane, early endosomes and at the Golgi[40].

Such observations ignite the interest of what substrates PRL-3 binds to, and what kind of effectors it is linked with. Interestingly, potential, direct substrates/modulators of PRL-3 remain elusive today, despite the slowly growing literature of target identification: in fact, some potential targets for membrane-bound (active) PRL-3 have been suggested, after high-throughput phospho-proteomic or proteomic analyses, revealing chiefly proteins which either shape or control the cytoskeleton, such as ezrin[41], stathmin[42], keratin 8[43], cadherin CDH22, NHERF1[44], and most recently, integrin β1[22]. Intriguingly, most of these binding partners seem mainly of nuclear localization and nuclear-related functions, with so far unidentified connection to PRL-3 mechanisms of action[20]. In addition to the abovementioned strategies for identification or PRL-3 targets, if one regards its structural information as another platform for investigation, PRL-3 has been shown to have very dynamic protein rearrangement, highlighted by an open/free conformation with active site components pointing at different directions, according to NMR studies[45,46]. This is also one of the representative reasons for which structures of PRL-3 with physiological ligands do not exist to date: because of the highly flexible nature of the phosphatase, a

physiological state has not been apprehended just yet, which poses many obstacles for studying this enzyme's structure-activity relationship.
Nevertheless, PRL-3 was assigned one specific enzymatic substrate: phosphatidylinositol 4,5 bisphosphate ($PI(4,5)P_2$)[18,19].

1.1.4. $PI(4,5)P_2$, a special substrate for PRL-3

The identification of signaling pathways involving PRL-3 is key to uncovering its roles in cancer progression. PRL-3, as opposed to PRL-1 and -2, dephosphorylates $PI(4,5)P_2$ in vitro, making this substrate an individual one for PRL-3 among the PRL phosphatase family[18,19]. Our group showed recently that PRL-3 dephosphorylates $PI(4,5)P_2$ in cells (unpublished), which is also an unpublished observation by another group[19].This substrate could relate to the many phenotypes known for PRL-3. For instance, certain PIPs such as $PI(3,4,5)P_3$ and $PI(3,4)P_2$, and especially the depletion of $PI(4,5)P_2$ have been designated as being involved in promoting cell motility, such a role being important in cancer[47]. Since it is a small molecule substrate, $PI(4,5)P_2$ can act as a rational starting point for structure-activity relationship studies and inhibitor design.

1.2. Modulating PRL-3 activity: a challenging search

Small molecule modulators (activators or inhibitors) offer a way to detect cellular processes in which phosphatases are involved. This is a powerful complementary method to the genetic methods, because the usage of tool compounds focuses on acutely modulating enzymatic activity, which offers advantages such as handling simplicity, speed, and tunability. Particularly, small molecule inhibitors can eventually be used as lead compounds for drug discovery and are required for target validation[48–50]. Unfortunately, the small molecule PRL-inhibitors reported so far are either unselective relative to other phosphatases or among the PRL family, or they simply have been tested for only one of the PRLs and mostly exclusively *in vitro*[51,52]. One analog has been recently developed using *in silico* and biochemical screening assays[53], but is still not selective among the PRLs, in addition to its only moderate potency. There is, therefore, an unmet need for a specific inhibitor for PRL-3, and taking its natural substrate ($PI(4,5)P_2$) as a starting point is the most promising approach to fill this need due to it being a selective substrate within the PRL family.

1.2.1. Computational aid in the search of an inhibitor

To further build the search for an adequate small molecule, which could help study the mechanisms in which PRL-3 are involved, computational screening methods, which increase the chances of finding good tool compounds, were also examined. This had inspired the work of Hoeger et. al[53], who have relied on a novel computational method for molecular shape comparison, to screen for molecules which were similar in shape to a known, but unselective, PRL-3 inhibitor thienopyridone[52]. This technique, termed Ultrafast Shape Recognition (USR)[54], consists of probing online molecular databases for compounds that most closely resemble the shape of a given query (template) molecule. In this respect, it is an elegant alternative to other computational methods like docking, whereby the screened molecule, aligned to a macromolecular biological target (e.g., a protein), is simulated to provide an estimate of binding energy, thus the likelihood of being bioactive[55]. Docking has worked with a series of proteins with known crystal structure, but this was not the case for PRL-3, which crystal structure still needs to be better understood, despite the recent work on crystallizing it with binding partners[56]. In the Hoeger et. al[53] study, the query molecule was thienopyridone, the most potent cell-active inhibitor identified to date, with a reported IC_{50} of 173 nM for PRL-1, 277nM for PRL-2 and 128 nM for PRL-3. Thus, biochemical screening of hits generated by the *in silico* screen afforded a micromolar inhibitor that could be further optimized by a basic SAR study[53].

1.2.2. Virtual screening tools using natural substrates

In such computational methods, nevertheless, the abovementioned chemical template/query does not only have to be an inhibitor of a target protein, but could also be a known ligand, such as a natural substrate, or a patented compound[57]. This means that one could theoretically use the information provided by biochemical studies for the validation of a natural substrate in studying a target protein. Here, for instance, the valuable information of selective dephosphorylation of $PI(4,5)P_2$ by PRL-3 (amongst the PRL family), sets this phosphoinositide as an interesting starting point for computational prediction means, in order to learn more on binding mechanisms.

1.3. PIP*n*: substantial molecules in cell signaling

Phosphatidylinositol-phosphates (PIP*n*) belong to the large group of phosphorylated inositol compounds, amongst the two other members comprising the inositol polyphosphates (InsPs) and the diphosphoinositol polyphosphates (PP-InsPs). These compounds represent critical biomolecules, which order a hefty directory of important biological processes. Being an extremely diverse family of biosynthetically distinct signaling molecules, these compounds exist, at all times, with numerous combinations of phosphorylation patterns, resulting in an intricate network of correlative signaling blocks that regulate different cellular events[58]. The inositol family comprises nine possible 1,2,3,4,5,6-cyclohexanehexol isomers, these being the *myo*-, *cis*-, e*pi*-, *allo*-, *muco*-, *neo*-, L-*chiro*, D-*chiro*, and *scyllo*-inositols. While these regioisomers are proven to exist in some natural systems[59], the most prominent family member is *myo*-inositol, as it represents the main unit for the abovementioned abundant biologically active molecules. *myo*-inositol is a *meso*-cylohexane hexol (achiral) with five hydroxyl groups in the equatorial position and one in the axial. The carbon with the lone axial hydroxyl group is labelled with C2 (all the other hydroxyl groups being in equatorial positions, Figure 2). The recognized convention is to label the anti-clockwise counting with the prefix "D", which is currently being used for all biologically relevant compounds.

The PIP*n* are molecules with a lipophilic tail and a polar head group in form of an inositol ring that can be phosphorylated in the 3, 4 or 5 position (Figure 2).
The lipid tail consists of a glycerol backbone with two acyl carbon chains that are linked *via* a phosphodiester to C-1 of the inositol ring. Most common in animals is the arachidonic acid in sn-2- and stearic acid in sn-1-position on the glycerol backbone. The *myo*-inositol motif acts as the core scaffold for the head group of these glycerophospholipids. The PIP*n* family comprises seven isomers that are phosphorylated at different positions.

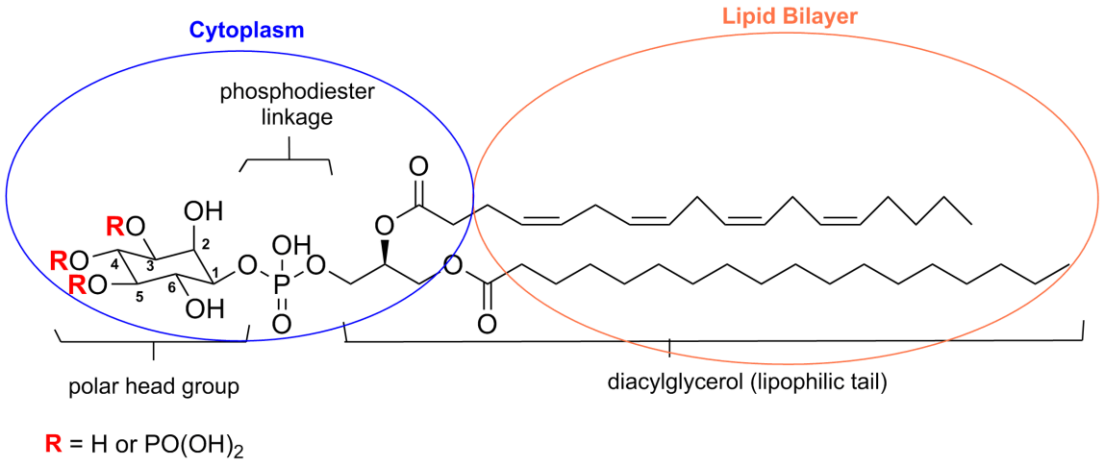

Figure **2** Phosphatidylinositol (PI) with 1-stearyl-2-arachidonoyl-glycerol-backbone. Example of a cellular-membrane PIP*n*: the structure of the phosphatidylinositol composition contains a polar head group and a lipophilic tail.

As can be seen in Figure 3, these family members contain every combination of phosphate groups at the 3-, 4- and 5- positions on the head group: therefore, each member can contain three (PI(3,4,5)P_3), two (PI(4,5)P_2, PI(3,4)P_2 and PI(3,5)P_2), or one (PI(3)P, PI(4)P, or PI(5)P) phosphate group(s) on the head group, in addition to the common phosphodiester.

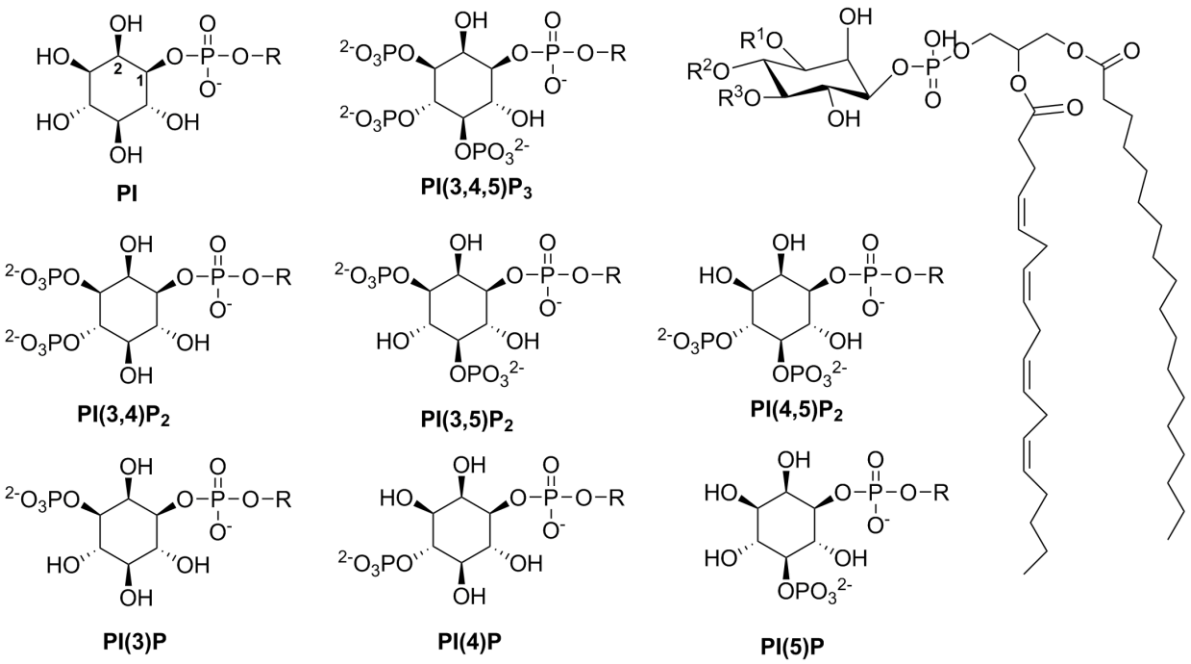

Figure **3** Structures of phosphatidylinositol (PI) and the seven phosphatidylinositol polyphosphates (PIP*n*) as found in nature.

What differentiates PIP*n* from the rest of the group of phosphorylated inositol molecules is that these phospholipids are anchored in cellular membranes, displaying the inositol head group on the (inner) membrane surface. This is key to understanding the localization requirements and implications of PIP*n*–proteins interactions, which convey various processes in cell signalling. In fact, specific PIP*n*, at specific locations, recruit different cytosolic proteins, which are, in turn, tangled in various structural functions and/or signal transduction.

Moreover, in addition to the specific recognition of these lipids by various protein domains, the sophistication of their signalling system also relies on the well-established participation of approximately a hundred isoforms of kinases and phosphatases in their concerted production and inactivation. These protein-lipid binding events, which are often reversible associations, result in regulating crucial processes in cell signalling, by affecting both protein function and subcellular localization[60]. They can in fact control protein function either by promoting direct modification of the protein itself upon binding, or by ushering the interaction of this now membrane-bound protein with other binding partners, also localized at the cellular membrane surface[60]. Adding to that the abovementioned structure-function diversity of PIP*n*, these molecules can direct proteins to distinct locations within the cell, depending on where the target lipid is present[61]. A key example for this thesis is the localization of PRL-3 to the plasma membrane, where its target lipid/substrate is $PI(4,5)P_2$ (see section **1.1.3.**).

1.3.1. Biological significance of PIP*n*

It is not surprising, therefore, that PIP*n* would be involved in intracellular signalling mechanisms which are known to play a vital role in essential cellular functions such as vesicle trafficking, apoptosis, cell proliferation and metabolism[62–64]. Thus, defects in binding and lipid compositions result in onset of serious regulatory diseases like chronic inflammation, autoimmunity, allergy, cancer, atherosclerosis, hypertension, heart hypertrophy, metabolic and degenerative diseases, among others[65–68]. The amount of PI in membranes is 4 % and the other phosphorylated PIP*n* amount all together to approximately 1%[69].

To appreciate the crucial role of PIP*n* in cellular homeostasis, one needs to recognise that signalling activities often arise through the activation of protein function upon binding to the cellular membrane: once the attached effector protein is activated, it can then detach (reversible associations, see above) and transduce that harnessed material throughout

the entire cell by traversing to diverse sites in solubilized form. This underlines the serious nature of lipid conversion balance, which needs to be tightly regulated to avoid abnormal interactions, quantities of lipid substrates, and spatial-temporal availability. This equilibrium takes place via the rigorous actions of kinases and phosphatases, a considerable amount of which genes could be mutated in various cancers[58]. An abridged scheme is shown in Figure 4. These enzymes, by continuously producing a vast directory of soluble inositol polyphosphates and membrane polyphosphoinositide lipids, represent key players in signalling cascades. For example, phosphoinositide 3-kinase (PI3K), regulated by cell-surface receptors, leads to the formation of $PI(3,4,5)P_3$, in turn a signalling lipid which modulates cell growth, proliferation and motility[70]. Most notably, PIP*n* are involved in inflammation, cancer and metabolic syndromes, as part of the lipid signalling dysregulation context[71].

The metabolism in which the PIP*n* are implicated is therefore quite complex and broad, whereby the continuous synthesis and interconversion of phosphorylated *myo*-inositol species takes place in the context of a myriad kinase and phosphatase enzyme linkage. The metabolic pathways in which the PIP*n* are associated have been the subject of extensive reviews, and the reader is referred to some of those for detailed mechanisms[72–75].

The capacity of the PIP*n*-protein interactome can therefore unravel as very complex and broad, the molecular detail of which relies on binding modules with conserved sequences, which target specific PIP*n* isomers. This association network has been the focus of many reviews in the last two decades[60,69,76–81]. Many of these binding domains have been recognized, and examples include the pleckstrin homology (PH), phox homology (PX), Fab1, YOTB, Vac1 and EEA1 (FYVE), epsin N-terminal homology (ENTH), AP180 N-terminal homology (ANTH), band 4.1 ezrin radixin moiesin homology (FERM), Tubby, and b-propellers that bind phosphoinositides (PROP- PIN) domains[58].

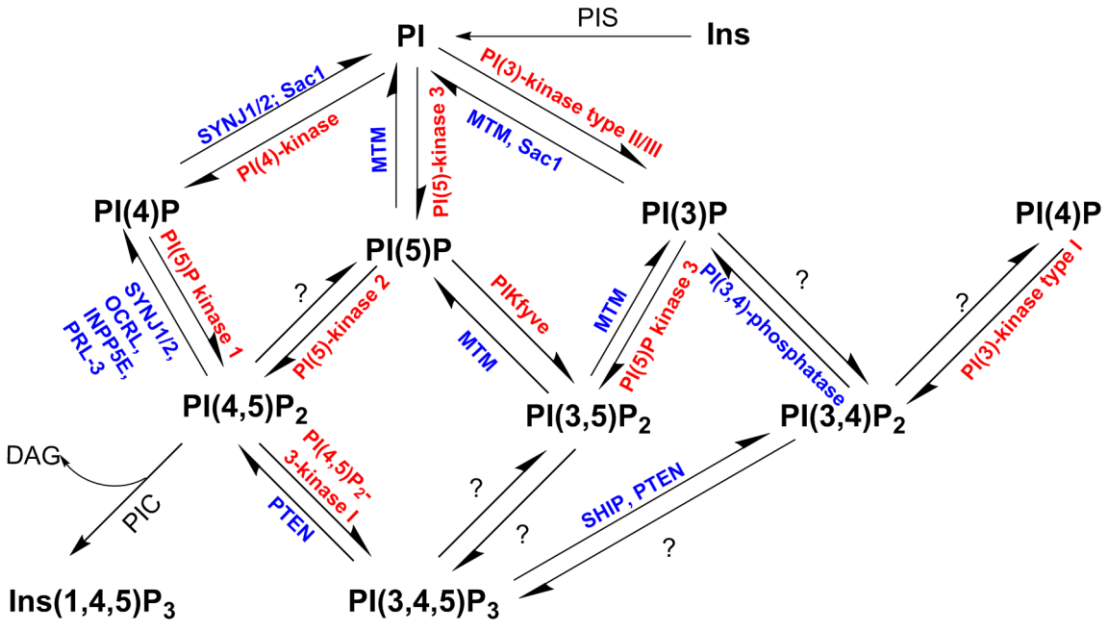

Figure **4** Metabolism and biosynthesis of PIPn. Phosphatases are in blue, kinases in red. The question mark stands for unknown enzymes. DAG, diacylglycerin and Ins(1,4,5)P3, Inositol(1,4,5)-triphosphate are second messengers; INPP5E, inositol polyphosphate 5-phosphatase; MTM, myotubularin; OCRL, Inositol polyphosphate 5-phosphatase; PIKfyve, phosphoinositide kinase containing fyve Zn-finger motive; PTEN, phosphatase and tensin homolog deleted on chromosome 10; PIS, phosphatidylinositol synthase; PIC, phospholipase C; Sac ,suppressor of actin domain containing phosphatase, SYNJ, Synaptojanin; SHIP, SH2 domain containing inositol phosphatase.

Such domains could be present in several different proteins, and PH domains are a typical example for that: in fact, sequence homology searches have connected more than 250 PH domain-containing proteins in humans[69]. But not all PH domains interact productively with PIP*n*. This is one proof that binding modules actually vary amongst proteins, even those carrying the same module(s). These variations take ground in three important nuances: specificity, structural requirements, and binding localization[60]. This also explains why some proteins bind with high affinity towards a particular phospholipid (FYVE domains generally target PI(3)P for instance), while others appear to be more promiscuous (PH domains were shown to target different PIPn isomers[69]).

In addition, binding modules amongst this network are not universal: binding can be principally driven by electrostatic attraction to the myo-inositol head group, with no requirement of the membrane milieu (such as PH domain of PLCδ to $PI(4,5)P_2$[82]), but for other domains/proteins (such as FYVE85[83] and PX86[84] domains), the membrane context is essential for binding to occur. This subtle difference is important, as it can be the consequence of a contact between the hydrophobic sequence of a certain protein and the

hydrophobic membrane core, thereby delivering a major input to the driving force for association. PRL-3 is a prominent and relevant example for this, as it requires the lipids to actually bind $PI(4,5)P_2$ itself[19] (which can bind PLCδ without the presence of a lipid bilayer), further illuminating the intricacy that should be interpreted to better apprehend binding at the molecular level.

$PI(4,5)P_2$ is actually a known substrate for the different phosphoinositide-specific phospholipase C (PLC) enzymes, thereby being the precursor of $Ins(1,4,5)P_3$ and DAG (diacylglycerol)[59]. It is also the substrate of the type I PI 3-kinases which produces $PI(3,4,5)P_3$. The significance of this lies in the fact that protein kinase C (PKC) docks, through its C1 PI effector proteins Ras-GRPs domain, onto DAG, while $Ins(1,4,5)P_3$ stimulates the release of Ca^{2+} ions from the endoplasmic reticulum (ER). The plasma-membrane-localized $PI(4,5)P_2$ represents a principal player in Ca^{2+} phosphoinositide-dependent signalling, by serving as the substrate for two potent receptor-regulated signal-generating enzymes[66]. Although its overall level does not considerably rise in stimulated cells, confined increases in $PI(4,5)P_2$ concentrations are likely to occur and recently, more and more supporting information suggests that this PIP even acts as a signaling molecule on its own: it can, for instance, influence actin cytoskeleton organization through interactions with actin-binding proteins[85].

The above-mentioned tightly controlled and dynamic network of phosphoinositide signalling is a reason for the metabolic instability and relatively low concentrations of PIPs, which pose as factors contributing to the incapacity to isolate useful amounts of these compounds in pure form for biological studies. For this reason, amongst many others, the chemical synthesis of PIPs and derivatives started as early as almost five decades ago, and remains, today, an attractive endeavour.

1.3.2. Chemical approaches to synthesize PIP*n* and analogues

After the continuous discovery of the essential biological roles of InsPs, PP-InsPs and PIP*n* in cell signaling, developing synthetic approaches to study them rose. In fact, the inability to isolate practically useful amounts of PIPn compounds from cells has led to a need of efficient syntheses, and the literature is wide-ranging and large since 1970[86]. First syntheses of myo-inositol 1,4,5-trisphosphate were reported in 1986 by Ozaki et. al[87] and these have been trailed by noteworthy synthetic progress to the extent that all of the problems inherent to inositol phosphate synthesis have now been principally overcome[88].

These problems are preeminent for the area of phospholipid synthesis, and can be summarized in three main synthetic facets: first, the synthesis of a suitable selectively protected inositol derivative, which would expose free hydroxyl groups at desired positions; second, a phosphorylation in an proficient manner, with a reagent carrying a suitable phosphate-protecting groups (this has been, for instance a major challenge for compounds with vicinal diols, where cyclic phosphate formation was a chief undesired side reaction[89]); and third, deprotection while avoiding migration of phosphate substituents to adjacent free hydroxyl functions. An additional necessity arose amongst this stage: the resolution of appropriate synthetic intermediates, allowing the preparation of optically pure inositol phosphates. This was unraveled by the use of chiral starting materials[90]. Consequently, establishing routes with selective protecting groups[91], different phosphorylation strategies[92–96] (Figure 5) and optical resolution of the enantiomers[87,97,98] with reagents such as (S)-(+)-O-acetyl-mandelic acid, (R)-(+)-1-phenyl-ethyl isocyanate, (R)-(+)-camphor dimethyl acetal, or L-menthyl chloroformate was completed.

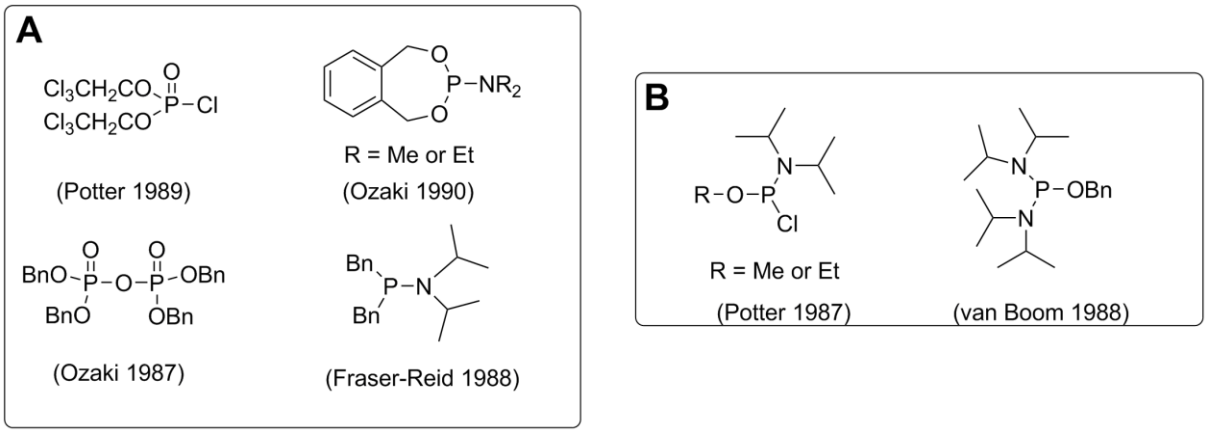

Figure **5** Phosphorylating and phosphitylating agents. A) Mono-functional PV and PIII reagents that were used for phosphorylation of vicinal diols. B) Bi-functional PIII reagents used for the phosphodiester link to attach the diacylglycerol backbones in PIPn.

Nevertheless, the complex nature of inositol phosphate metabolism is providing ever-growing new targets for synthesis: this interest further gave rise to the synthesis of modified inositol phosphates with novel biological properties. The synthesis of unnatural InsPs and PIP*n* analogues for structure-activity studies of proteins[58,99,100] as affinity probes for pulldown of effectors and metabolic studies has then become a major

discipline: a prodigious amount of reviews up to 2010 have covered the preparation of biologically important *myo*-inositol derivatives[58,101–109]. These include *myo*-inositol 1,4,5,6-tetrakisphosphate, *myo*-inositol pentakisphosphate and hexakisphosphate derivatives, diphosphoinositol phosphate derivatives, D-1,5- and D-3,5-diphosphoinositol 1,2,4,6-tetrakisphosphate $InsP_8$, diphosphoinositol analogues, replacement of the 5-Phosphate of $Ins(1,4,5)P_3$ with bioisosteres, inositol phosphate ligands that uncovered the capture site of PPIP5K2, photoactivated myo-inositol lipid derivatives, solid phase synthesis of myo-inositol DiC8-phospholipids, plasmanylinositols, and biphenyl phosphate derivatives (examples of each mentioned derivative are shown in Figure 6).

All of this demands the mastering of all three synthesis aspects mentioned above, particularly the synthesis of protected inositol derivatives, which require careful selection of a starting material (the inositol head group). The synthesis of PIPs starts by the synthesis of protected inositol derivatives. These can use the following as starting materials: *myo*-inositol, chiral starting materials such as naturally occurring inositol-like molecules (Galactinol, L-Quebrachitol, D-Pinitol or (-)-Quinninc acid), or other starting materials such as benzene-derivatives like *meso*-diol[89].

Due to the ready commercial availability of pure *myo*-inositol however, most syntheses have used the parent cyclitol as a starting material. In fact, the symmetry which comes with this material makes it easy to design numerous synthetic route from one starting material[89]. One of the most common and classic methods of manipulation of this starting material is shown in Scheme 1 (A): the reaction of this starting material with cyclohexanone or more efficiently with a cyclohexanone precursor such as l-ethoxycyclohexene, in the presence of an acid catalyst gives a mixture of three bisacetals which may be separated by crystallization and chromatography. Each of these bisacetals gives the monoacetal on mild hydrolysis of the less stable transacetal. Due to the conformational constraints imposed on the inositol ring by the bisacetal groups, each of the free hydroxyl groups and may be selectively manipulated under suitable conditions, providing access to a series of inositol derivatives having five hydroxyl groups differentially protected. Another classic manipulation uses orthoformate as a strategy (Scheme 1, B). In this strategy, the orthoformate offers a derivative in which positions 1, 3, and 5 can be simultaneously protected. The normal axial/equatorial relationship of the remaining free hydroxyl groups is reversed. The spatial juxtaposition of the axial hydroxyl groups allows highly selective alkylations to be performed at these positions[110].

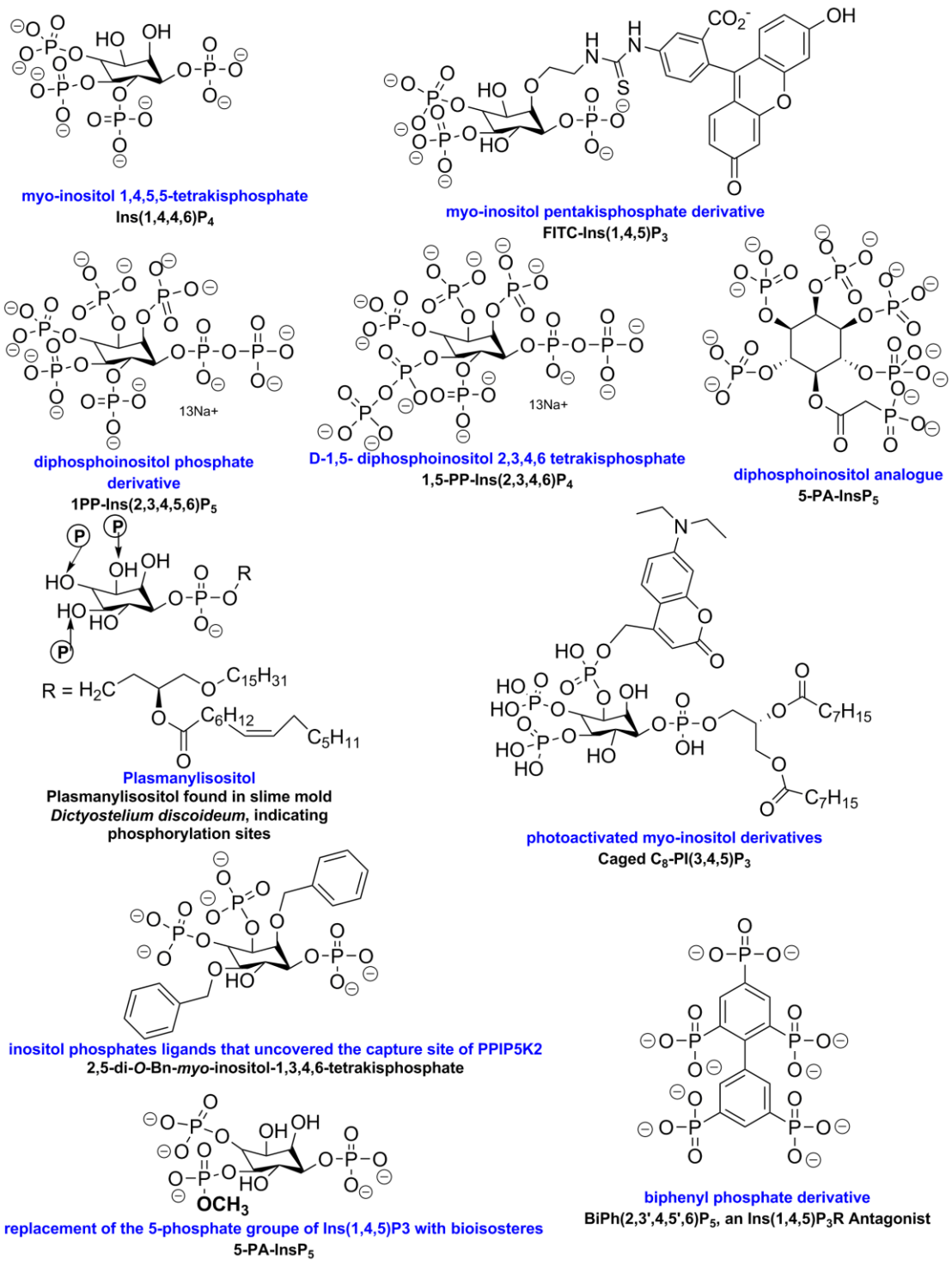

Figure **6** Examples of biologically important *myo*-inositol derivatives. Adapted from Potter *et. al* (2016)[111]. The categories of the derivatives are written in blue, the example molecule in black.

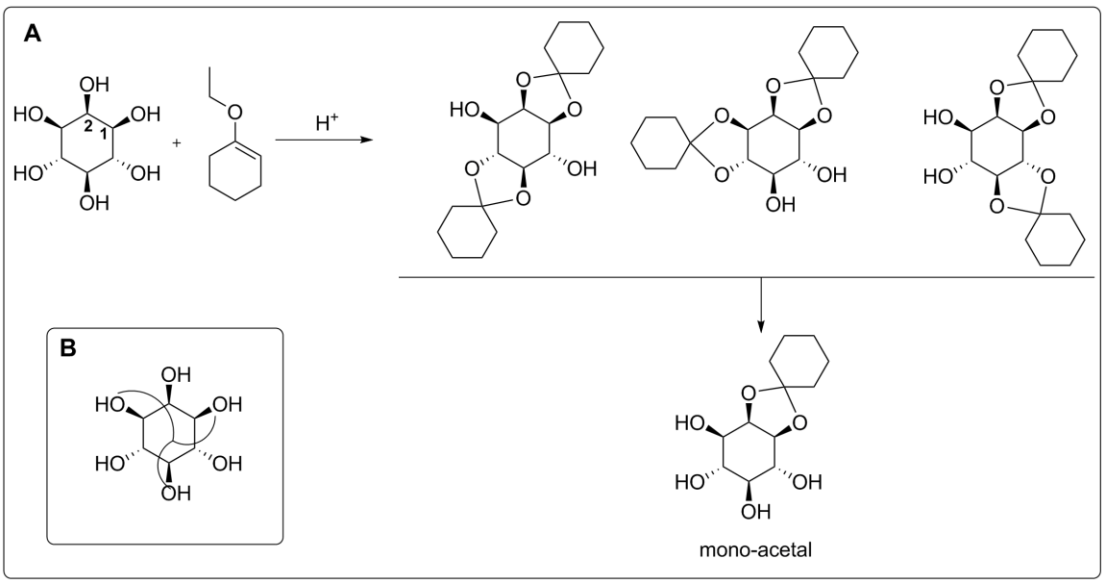

Scheme **1** A) Reaction of cyclohexanone precursors with *myo*-inositol to form three isomeric bisacetals, which can be selectively cleaved to yield a monoacetal. B) Orthoformate, on which the 1, 3, and 5 OH groups are protected simultaneously.

More details on the general synthetic considerations and synthetic strategies for the design of such compounds can be found in the extensive literature compiled by both the Billington and Potter groups[88,89,112]. In general, reviews of the chemical synthesis of phosphoinositides emphasize methods to be able to control regioselectivity and to obtain chiral intermediates, predominantly by the separation of diastereoisomeric derivatives with chiral auxiliaries, or by starting from the chiral group.

Of interest to this thesis work, the synthesis of PIP*n* analogues bears other challenging issues: not only the choice of selective protective groups, but also the corresponding conditions required for their global deprotection. In addition, final purification of such targets is achieved on the fully protected lipid precursor since it is very hard to fractionate the deprotected lipid from any related contaminants. Therefore, it is important that the global deprotection causes no degradation of the final lipid, and that protective group and reagent debris are easily separated from the product. These are the kind of challenges confronted and overcome when designing analogues of PI(4,5)P_2. Moreover, and during successive hydroxyl groups deprotection and/or any additional purification, excesses of acidity/basicity which could initiate acid- or base-catalyzed migration and/or hydrolysis should also be circumvented, and some decompositions during such handlings were actually reported; for instance, the de-acylation of the glyceride moiety[113].

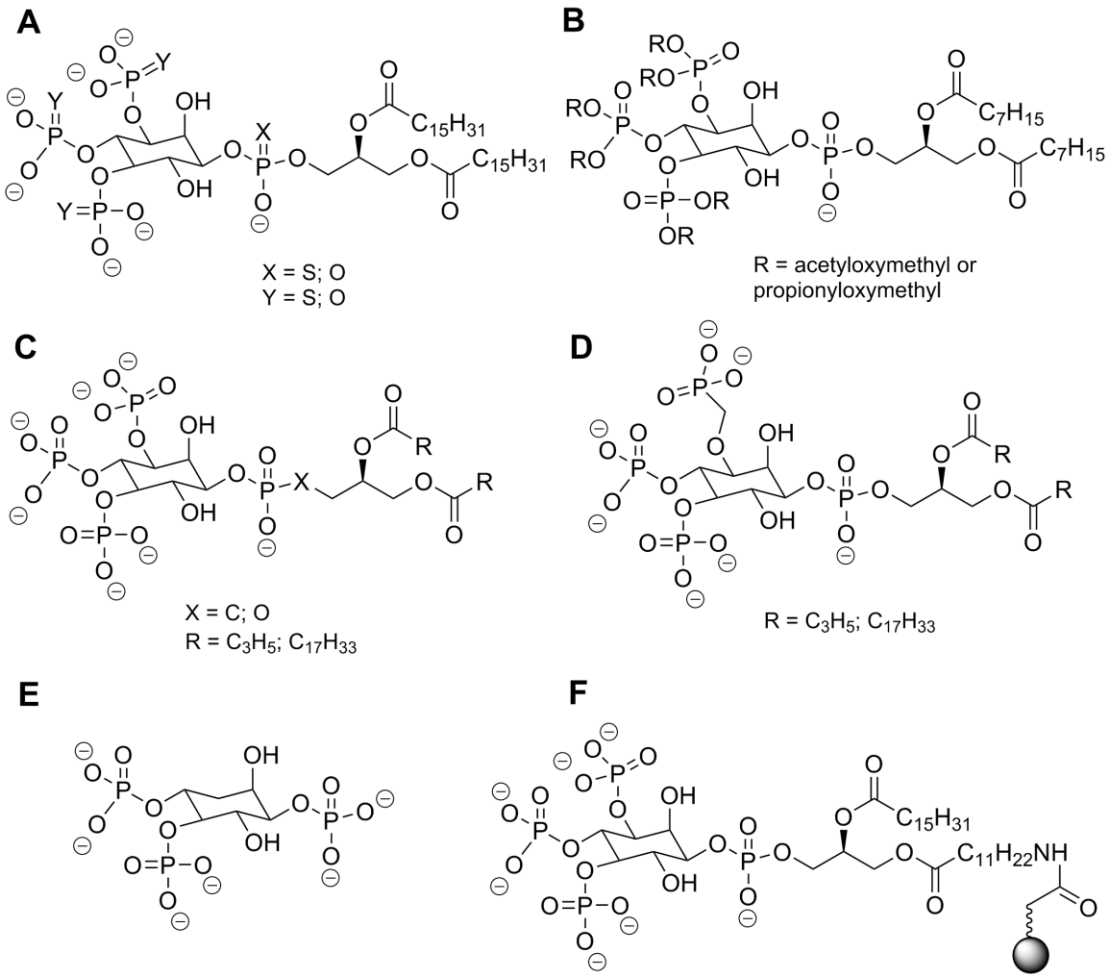

Figure **7** IP*n* and PIP*n* analogues. A) Thiophosphonate analogues; B) Membrane permeable PIP*n*. C) and D) PIP*n* with phosphonate groups; E) Deoxygenated I(1,4,5)P_3 in 3-position; F) PI(3,4,5)P_3 functionalized onto an affinity matrix.

Alterations of both the inositol-phosphate head group and the lipid tail were undertaken by groups like Potter *et al.*[102] van Boom and coworkers[96], Bruzik *et al*[91,114] and Prestwich and his group[115]. Their work contributed to the successful design of metabolically stable thiophosphates, phosphonates, deoxygenated inositols[116] and their PIP*n* with varied length of the individual acyl chains in the lipid tail (Figure 7). Such analogues find their use in many applications. For example, for intracellular applications, the need for membrane-permeable molecules arose. Due to the high polarity of the inositol head group, concealing agents like propionyloxymethyl and acetyloxymethyl were proposed with success by Schultz *et al.*[117] and Tsien and coworkers[118] to make the molecules membrane-permeable (Figure 7B). Another application example is affinity matrices,

whereby PIP*n* would be attached to a solid support in order to identify selective and competitive binding proteins.

Though many diverse analogues were advanced so far, there is still a missing number of analogues in the rather modest existing phosphatidylinositol-phosphate library[119]. There are a number of PIP*n*, with some alterations to the composition and the length (and the nature/structure) of the lipid tails as well as to the phosphate groups, but none so far that have direct alterations at the inositol ring, at least not PI(4,5)P_2. Evolving these tools for biological elucidation of protein structures and mechanisms is a constant effort in progress. In fact, and so far, only a few structure activity relationship (SAR) studies were done with PIP*n* analogues, to meet the needs for the development of PIP*n* analogue-based inhibitors. This is because chemical modifications of the inositol head group can be very challenging and arduous, due to multiple synthetic steps that often require tough purifications. Here, to conduct investigations if molecules based on by PI(4,5)P_2 could be used for the development of a selective PRL-3-inhibitor, it was sought to devise a practical synthetic route to derivatives of this phosphoinositide.

In the light of what has been said, it is evident that both current and future works of bioorganic, medicinal, and eventually computational chemists would support efforts directed towards the molecular understanding of, and the pharmacological intervention in, the phosphoinositide signalling system.

Chapter 2. Aim of this work

The general aim of this thesis work was to conduct structure-activity relationship studies with PIP-metabolizing proteins, by synthesizing a PIP*n* analogues library. This would help to understand PIP-binding requirements for specific proteins. Specifically, this was completed by synthesizing a library of phosphatidylinositol-4, 5-bisphosphates PI(4,5)P_2 analogues (Figure 8), and characterizing their biological activity with PRL-3. Considering the structure of PI(4,5)P_2, there are three possible areas of the molecule which could be modified for this purpose: I) the lipid tail, II) the inositol ring and III) the phosphates. In this thesis, the focus was put on the modification of the inositol ring by blocking the free hydroxyl-groups 2, 3 and 6 with alkyl groups, as this has not been done before, and on the modification of the lipid tails to understand the requirements regarding the nature of the alkyl chains for binding. Inventing and developing the synthetic route for one of the analogues, the 6-O-methoxy PI(4,5)P_2, and then expanding that route toward synthesis of a whole library of molecules was envisioned as the synthetic strategy.

After the successful synthesis of analogues their biological activity was aimed to be tested not only against PRL-3, but also against three other known PI(4,5)P_2-metabolizing phosphatases, to answer if selectivity targeting these enzymes can be achieved using the common substrate as a basis for ligand development.

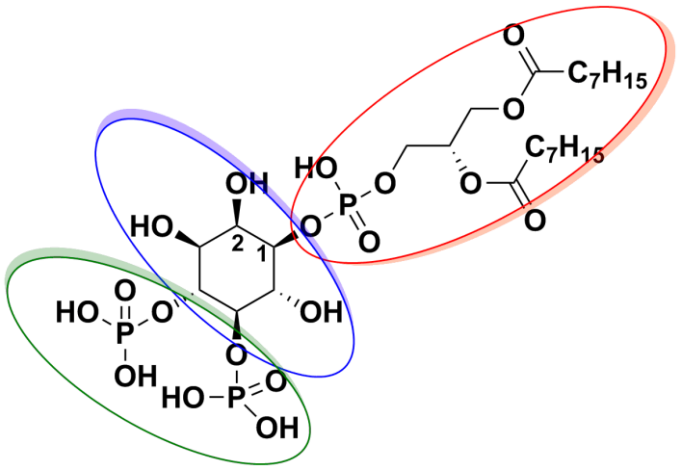

Figure **8** PI(4,5)P_2 from a medicinal chemistry viewpoint: the different sites of chemical modification are the lipid chains (red), the inositol ring (blue), and the phosphate groups (green).

Chapter 3. Results and Discussion

3.1. Total Organic Synthesis of PI(4,5)P_2 analogues

3.1.1. First Considerations for the Synthetic Approach

Considering the structure of the target molecule, a convergent synthetic strategy was deemed the most functional approach. In fact, it was first thought to follow the solid phase synthesis procedure of PIP*n* synthesis, established by the Koehn group in 2012[120]. In this strategy, PIP*n* analogues and derivatives would be synthesized in a combinatorial fashion, building on only four inositol building blocks to synthesize the seven phosphorylation patterns, which was made possible by a novel selective benzylidene acetal ring opening on a solid support[120] (Figure 9).

For that, a suggested solid phase synthesis for the preparation of methylated PI(4,5)P_2 molecules, shown in Figure 10, was considered. Although this strategy sets a basis for the modification of the inositol head group in a conjunctional mode, it was unsuccessful (not described here in detail), mainly for two reasons: 1) the lability of the compounds, which makes it hard to use stringent alkylating conditions on the ring after the phosphatidylinositol has been fully synthesized, and 2) the steric hindrance of the inositol ring in the fully synthesized PIP, making it even harder to alkylate effectively at desired positions. After unsuccessful previous trials (including different methylation strategies such as the usage of methyl iodide, dimethyl sulfate, sodium hydride, silver oxide, and trimethylsilyldiazomethane), it was deemed better to apply the modifications of the inositol ring on a precursor molecule before putting it up on solid phase and to then resume the phosphoinositide synthesis. This would be a better route, but only for one alkylated PIP, which is the one alkylated on the 6-OH group, as the remaining 2 OH groups (positions 2 and 3) would be sequestered by the benzylidene acetal protecting group and solid phase support linker, throughout the whole synthesis of the PIP (Figure 9). This would make alkylation at positions 2 and 3 of the inositol ring impossible until the end of the synthesis (i.e., cleavage of the benzylidene linker), which means it would have to be alkylated after the full labile and sterically hindered PIP had been synthesized. Therefore, it was thought that synthesizing the whole PI(4,5)P_2 modified analogues in solution would be the most equitable approach for this work.

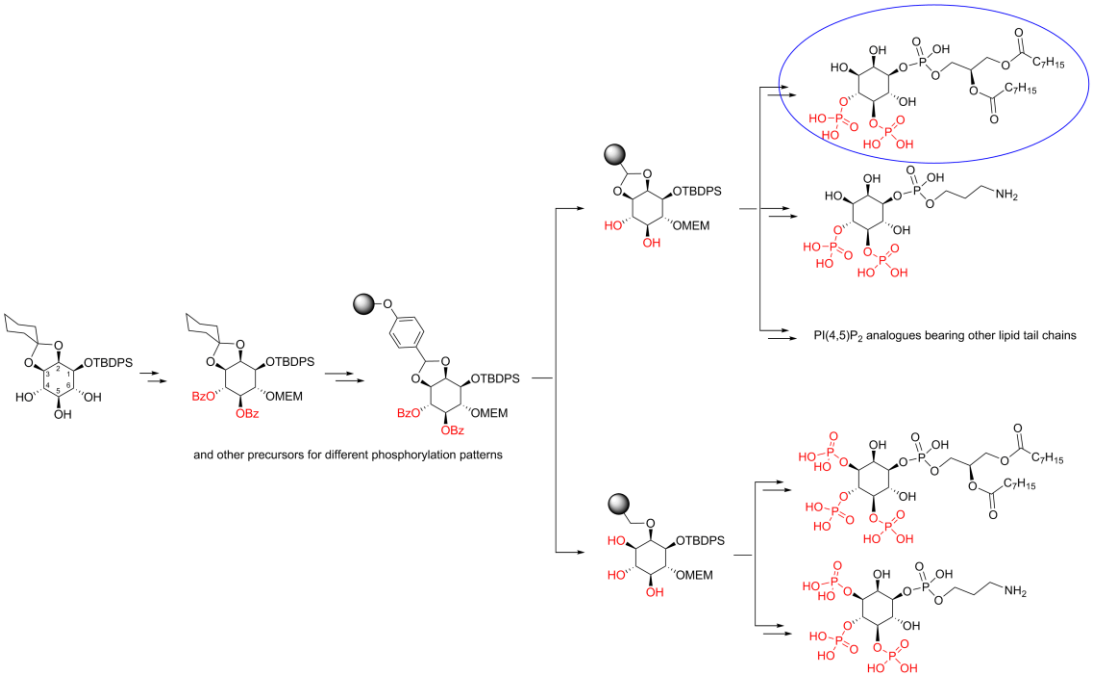

Figure **9** Outline of the solid phase strategy for soluble PIPn analogues and derivatives. NB: Adapted from Koehn et al. (2012)[120]. The encircled analogue is the analogue of interest for this work.

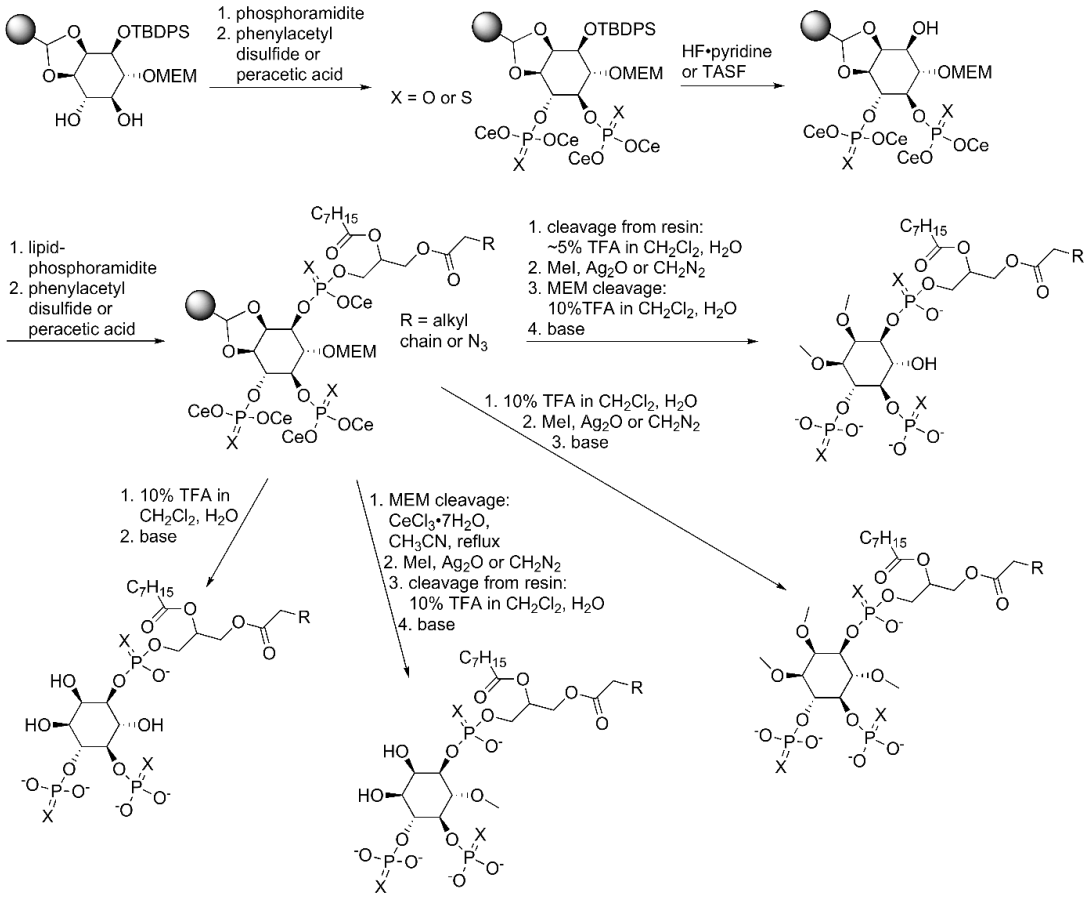

Figure **10** Outline of the solid phase strategy for the preparation of PI(4,5)P_2 analogues. Adapted from the Koehn research group [unpublished data].

3.1.2. Solution synthesis of the alkylated inositol ring precursors

Fortunately, the protective group strategy used the abovementioned solid phase synthesis strategy was a compatible and sound method to apply in solution phase synthesis of those PIPs. Nevertheless, each step in the total solution synthesis of these molecules required optimization and careful monitoring to aim for the best results and yields.

Three synthetic routes were designed for the monoalkylated, dialkylated and trialkylated analogues, respectively, for each of the methylated and the ethylated PI(4,5)P_2 (Schemes 2-5). In total, 6 target molecules (as alkylated precursors) were originally planned to be synthesized. The overall schemes of the differently alkylated final PI(4,5)P_2 analogues are shown below, followed by a comprehensive discussion on the total synthesis steps.

a. Synthesis plan for monoalkylated inositol precursors

Two monomethylated analogues, the 6-*O*-methylated and the 6-*O*-ethylated, were planned to be synthesized using the racemic starting material first, in order to establish a suitable synthetic route, and were tested for activity against PRL- 3. After successful establishment of this route with the racemic starting material, this synthetic route (Scheme 2) was then applied for the synthesis of the more expensive chiral analogues.

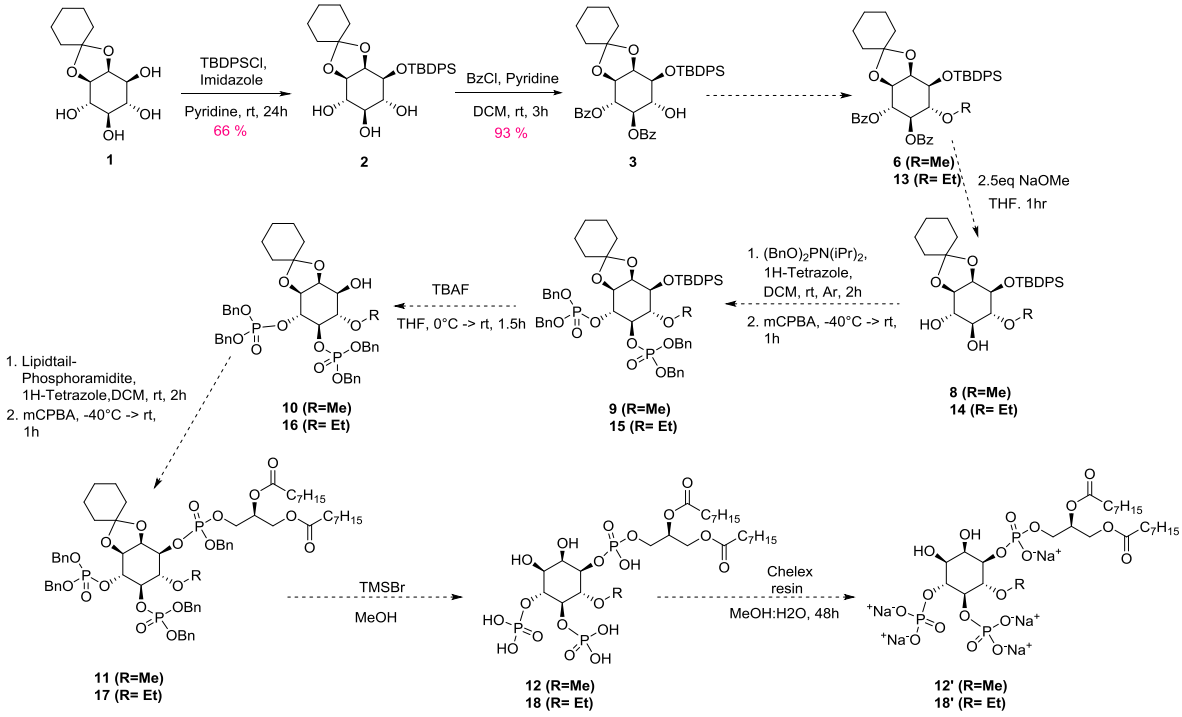

Scheme **2** Monoalkylation reaction pathway of 6-*O*-methylated/ethylated PI(4,5)P_2. Compounds 2 and 3 have been made according to prior synthesis establishment[120].

b. Synthesis plan for trialkylated inositol precursors

The 2,3,6-*O*-trimethylated PI(4,5)P_2 (protected, compound **27**) was also planned to be synthesized. Following deprotection of compound **27** it was planned to obtain the sodium salt form (**28'**) and free-acid form (**28**) of the final trialkylated compounds. The synthetic route is shown in Scheme 3.

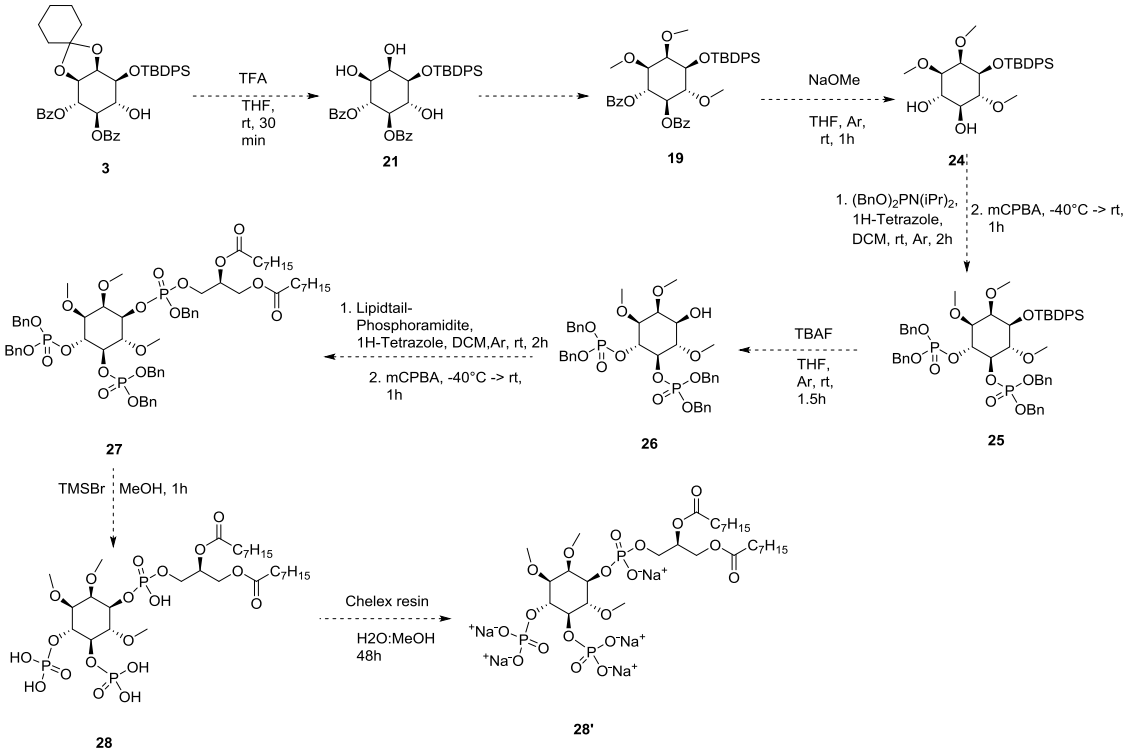

Scheme **3** Trialkylation reaction pathway of 2,3,6-O-methylated PI(4,5)P_2

c. Synthesis plan for dialkylated inositol precursors

Dialkylation of inositols can be used to generate several different combinations of regioisomers, each of which requires developing an additional protecting group strategy. For example, Scheme **4** shows a strategy for the synthesis of 3,6-*O*-methyl analogues utilizing the allyl protecting group, which can be removed in the final step. The dialkylated compounds **20** and **23** were thus planned to be synthesized.

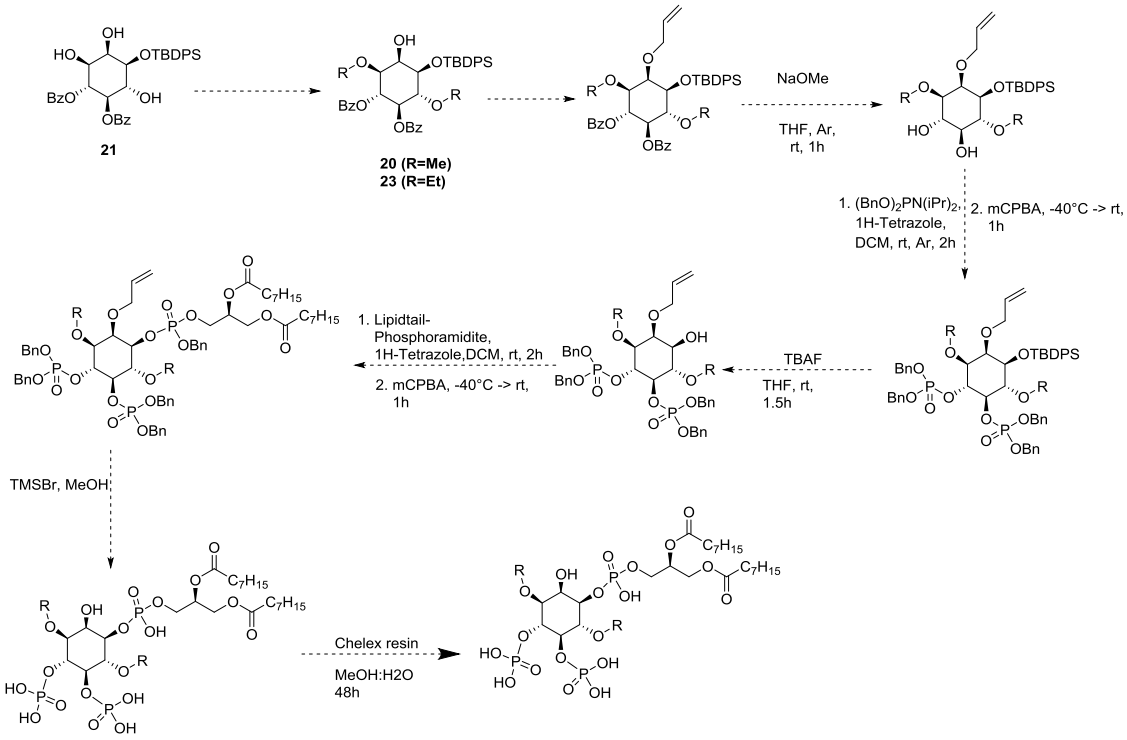

Scheme **4** Dialkylation reaction pathway of 3,6-*O*-methylated PI(4,5)P_2.

Another dialkylated analogue was considered to be synthesized, this time dialkylated at the 2- and 3-*O* positions, instead of the 3- and 6-*O* positions. The synthetic route is shown in Scheme 5.

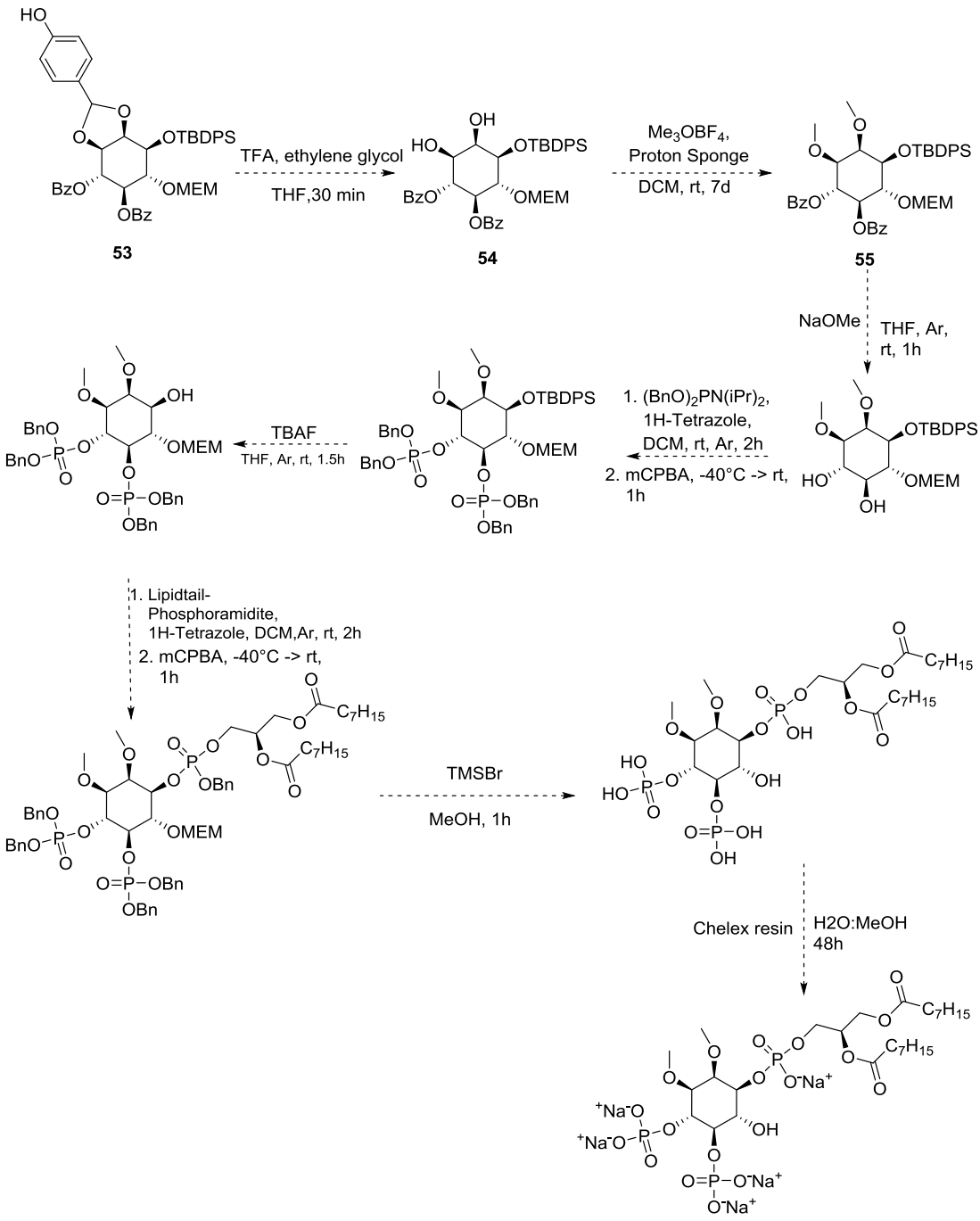

Scheme **5** Dialkylation reaction pathway of 2,3-*O*-methylated PI(4,5)P_2.

3.1.2.1. Synthesis of the starting material

The solution synthesis of the analogues always started with the building block **1**, available in the research group and purchased from Sichem®. A D-*myo*-inositol ring protected at positions 2 and 3 with a cyclohexylidene ketal group, this starting material allows reactions at the four remaining hydroxyl groups. The synthesis of the starting material

for mono-alkylation and trialkylation of the inositol ring was achieved in two or three steps, respectively. The protective group strategy has been established by Bruzik and coworkers[91,114], and used by the research group for the abovementioned solid phase strategy. First, 2,3-cyclohexyl ketal-protected inositol was selectively protected at the 1-OH position by introduction of the TBDPS group. After several repeats of this reaction considering the amount of precursors and analogues which had to be produced, it was finally optimized to yield the highest yield so far (66%) within the research group. The reaction was achieved by dissolving **1** and imidazole (2.25 eq) in dry pyridine, cooling the reaction solution down to -10°C before adding TBDPSCl (1.5 eq), then letting the reaction warm up to rt, stirring overnight. The product **2** was purified by automated column chromatography (Biotage®, see chapter 5), which afforded better yields than those achieved using classical glass column chromatography. Automated flash chromatography was used for the rest of this thesis work, unless when dealing with labile compounds like P(III)-compounds (see further sections). Analysis of the compound was carried out by ^{1}H- and ^{13}C-NMR and MS. Compound **2** was then selectively protected by *O*-benzoylation of positions 4 and 5 (Scheme 2), by dissolving in chloroform and pyridine (1:1) and cooling down the reaction solution to -40°C. A solution of benzoyl chloride (BzCl) was added dropwise and after the reaction mixture was slowly warmed to rt, an aqueous work-up was conducted and the crude product was purified by column chromatography. After reaction optimization regarding equivalents, time and purification techniques, **3** was isolated with a slightly higher yield of 93 % compared to the data found in literature (90 %)[91].The identity of this compound and confirmation of the correct regioisomer was confirmed by 2D-NMR studies (COSY, HSQC and HMBC, Figure 11).

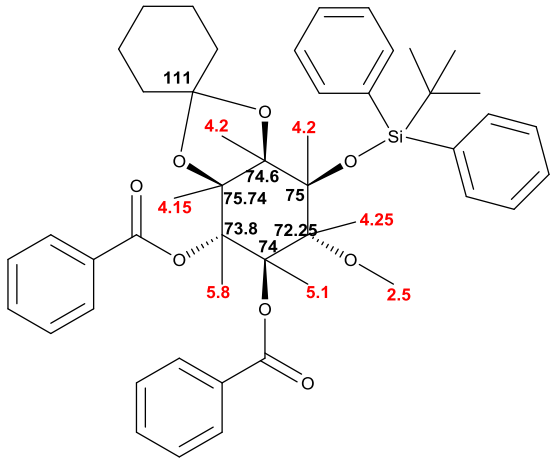

Figure **11** Constructed diagram of **3** after extensive structure elucidation using COSY, HSQC and HMBC.

Inositol **3** was the starting material for the monoalkylation reaction. For a possible dialkylation and trialkylation reaction, the cyclohexylidene protecting group had to be removed first. This was first attempted using the conditions used for the solid phase organic synthesis work, whereby the cyclohexylidene ketal would be cleaved to free the 2,3-OH groups for further protection with the benzylidene linker[120]. The conditions entailed using 75% formic acid in MeOH, but this led to only 30 % yield, in addition to the formation of side products, which might be due to the long reaction time (48 hours). Also, the solubility of the reactant in MeOH was unsatisfactory, and it would have been possible that the prolonged exposure to the basicity of this solvent has prompted the Benzoyl groups to react (fall off or migrate). Cleaving the cyclohexylidene group with TFA[114] was a very quick reaction with a better yield. But it also had to be optimized. The fastest and most efficient reaction was achieved by dissolving compound **3** in DCM and 200-300 µL water, then adding the TFA-solution (final ratio of TFA to DCM 1:1), and stirring the reaction mixture at rt. The reaction progress was monitored with TLC and after completion (in less than 15 minutes), the reaction solution was diluted with Toluene (3 times the existing volume) before the evaporating under reduced pressure. After purification by column chromatography the product was isolated with a yield of 86%. The synthesized product was analyzed by ^{1}H- and ^{13}C-NMR and MS. An additional problem had to be overcome in this type of reaction: comparing the reaction control TLC which showed total conversion to **21** with the TLC of the crude material shows a reformation of the product during the work up. This suggested a possible mechanism: the warm water bath in the rotary evaporator was facilitating a reattachment of the cyclohexylidene to the starting material. To overcome this, a 200 to 300 µL of ethylene glycol were added to the reaction mixture prior to evaporation, in order to scavenge the cleavage product cyclohexanone, thereby preventing it from interacting with the diol again (Scheme 6).

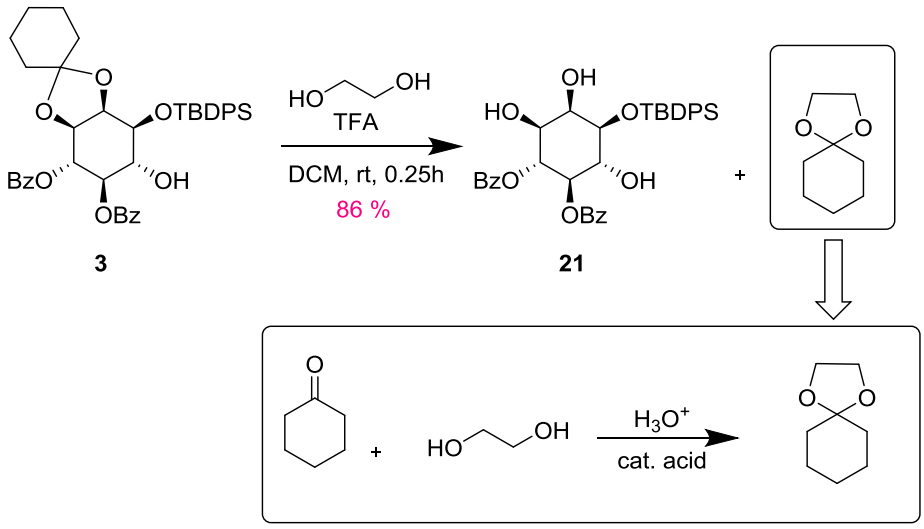

Scheme **6** Cyclohexylidene cleavage and scavenging with TFA and Ethylene Glycol, respectively.

The ketone group of cyclohexanone is a good electrophile, and could be made it an even better electrophile if protonated. Ethylene glycol has 2 hydroxyl groups, which are both good nucleophiles. Since these two hydroxyl groups are in the same molecule, if they both react with 1 other molecule (an electrophile) this would form a 5-membered ring (cyclic molecule). This is a big driving force for cyclic acetalization reactions, and ethylene glycol is very often used to form stable cyclic acetals. In fact, the free diol in the deprotected inositol ring also has the capacity for acetalization, but in a less flexible manner. Taking that with the fact that it is less abundant in the reaction, ethylene glycol would react first, and faster. In the ^{1}H- NMR, peaks corresponding to the protons of the free hydroxyl groups are clearly visible between 2.50 and 3.00 ppm (Figure 12) before the purification of **21**.

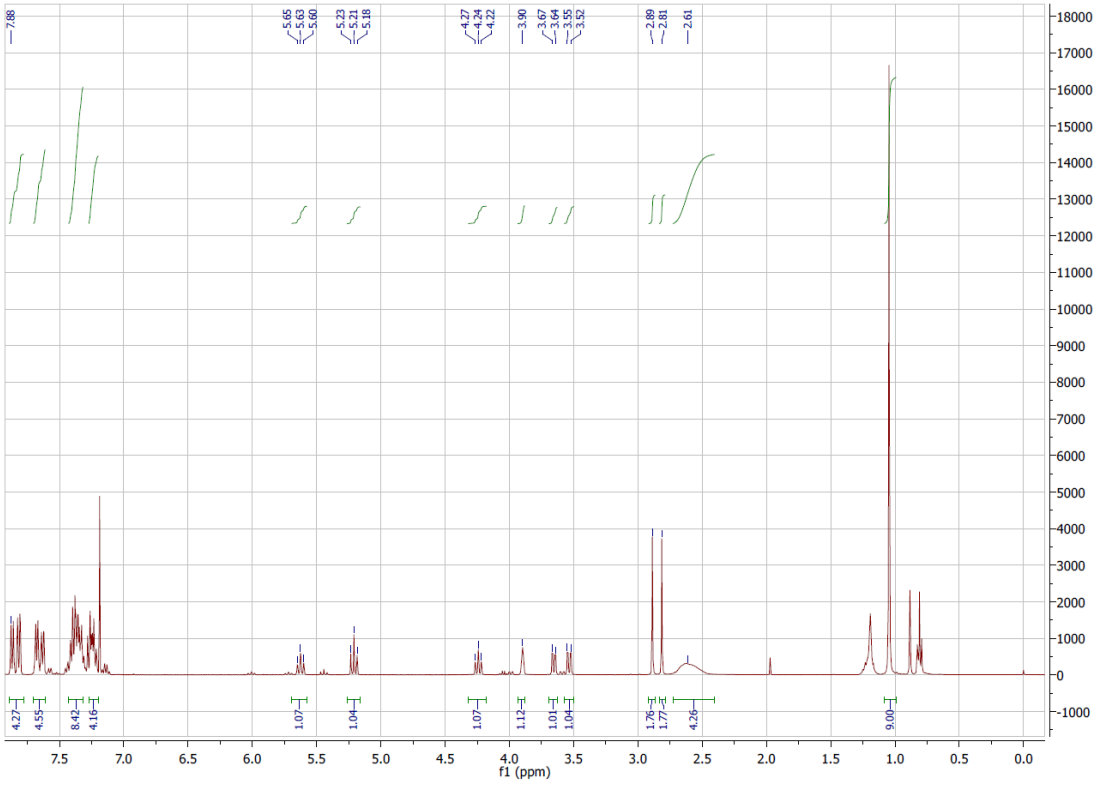

Figure **12** ^{1}H NMR of compound **21.**

For synthesis of lipid tail modified analogues in solution, the same starting material and protective group strategy was used, in addition to a MEM protecting group at position 6 of the ring, to ensure no OH-free group except the 1-OH, which would serve for attachment of the lipid tail phosphoramidite analogues (coupling reaction, see section **3.1.4.**). The reaction is shown in Scheme 7. To achieve this, compound **3** was dissolved in chloroform under Argon atmosphere, before DIPEA (14 eq) was added at rt, followed by MEM chloride (MEMCl, 9.8 eq). The reaction was heated under reflux to 58°C and left stirring overnight. Monitoring the reaction by UPLCMS showed the presence of the product, with full conversion, and with no signs of multiple regioisomers (only one peak, Figure 13). After working up the reaction with $NaCO_3$ and EtOAc extraction, the product could be isolated with a 66% yield, which could be due to the steric hindrance around the 6-OH by the benzoyl groups on one side and the TBDPS bulky group on the other side, thereby curtailing the reaction from going towards completion.

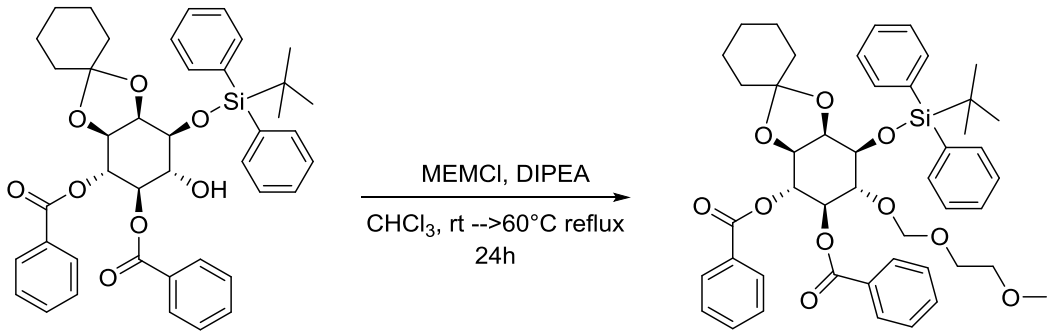

Scheme **7** MEM protection of the 6-OH on the protected inositol ring.

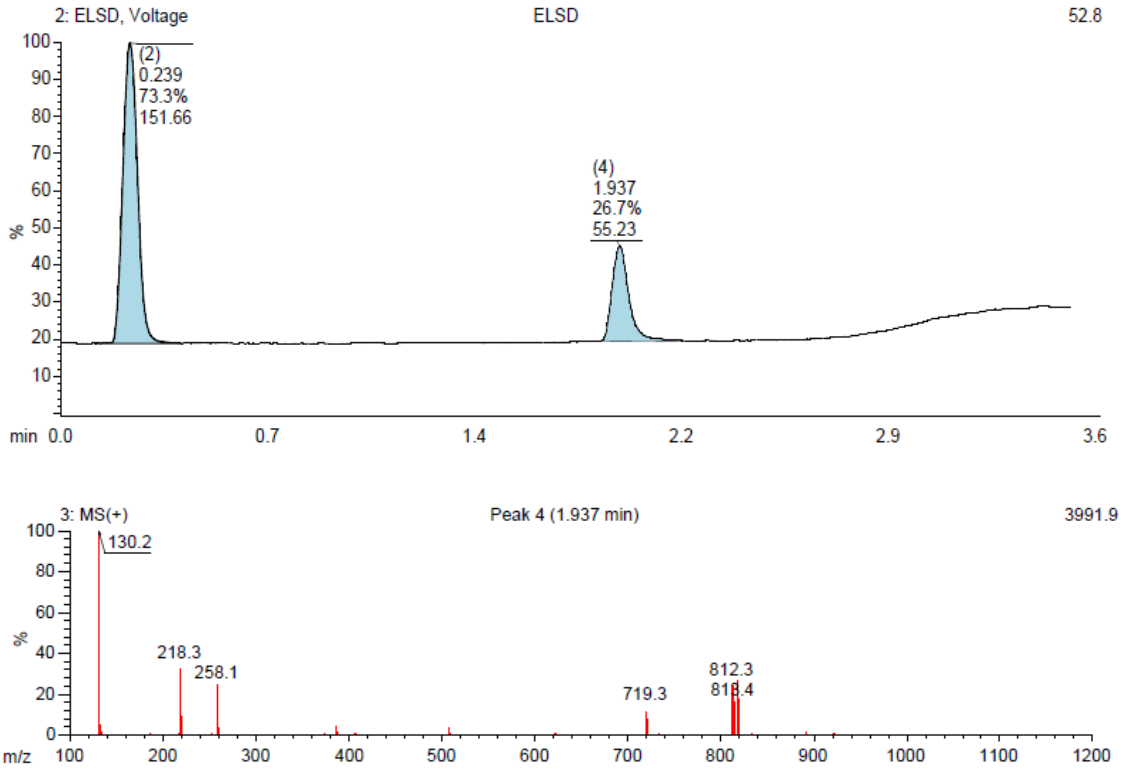

Figure **13** UPLCMS of the reaction control of compound **29** (10 hours after reaction start).

3.1.2.2. Alkylation of the inositol ring

This procedure was at the heart of the challenges that were met during this work. It was initially thought that the alkylation step, which succeeds the two previous selective protection steps (previous section), would be simply and efficiently achieved, but it was not.

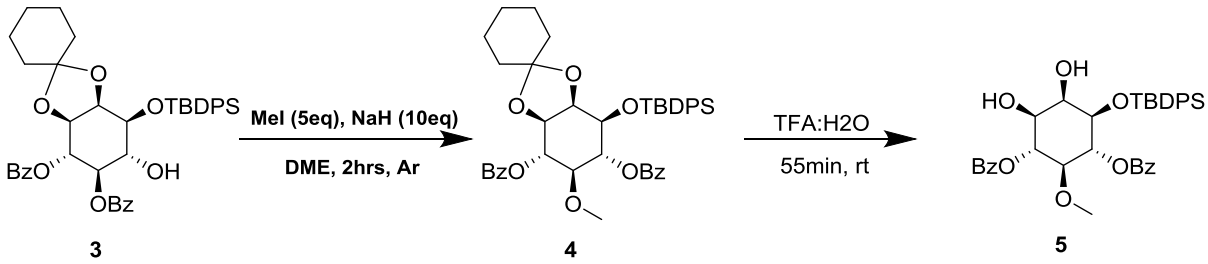

Scheme **8** Methylation of the 5-OH on the inositol ring upon usage of NaH and MeI. The cyclohexylidene ketal was cleaved for clearer structure elucidation upon 2D NMR.

The alkylation of the hydroxyl group in the 6 O-position on the inositol ring was very difficult to achieve, due to the steric hindrance of a bulky TBDPS group and a benzoyl group on the neighboring ring positions. This necessitated the usage of rich methylation agents, and strong bases for activation. Therefore, a variety of alkylating reagents with different bases were tried under a myriad of conditions (Table 1). These preliminary experiments indicated that the benzoyl protecting groups on the inositol ring were prone to migration. Following optimization of the solvent (Table 1) and reaction duration, conditions were found which gave a reasonable yield of a mono-methylated inositol. To confirm the identity of this fully-protected compound, thorough structure elucidation by NMR was carried out, after cleavage of the cyclohexylidene ketal PG to prevent noisy signals. Unfortunately, the compound was found to be the wrong regioisomer (compounds **4** and **5**, Scheme 8). Migration of the 5-O-benzoyl group to the 6-O position was found to have occurred, and methylation of the more stable 5-oxyanion had occurred. This is indicated in Figure 15, a reconstructed diagram based on the COSY spectrum in Figure 14.

Table **1** Bases and Solvents screened for methylation reaction, using MeI, in similar temperature conditions, equivalents of base, and time. MeI: Methyl Iodide; PG: Protective Group; DMF: Dimethyl Formamide, DME: Dimethoxyethane; ACN: Acetonitrile ; THF: Tetrahydrofuran ; DMSO: dimethyl sulfoxide.

Base	Solvent	Reaction Status
NaH	DMF	PG migration, low rate
	Dioxane	PG migration, low rate
	DME	High product rate, wrong regioisomer
Ag_2O	ACN	PG migration, very low rate
Cs_2CO_3	DMF	No reaction
	THF	PG migration, no reaction
	DMSO	PG migration, very low rate
Li_2CO_3	DMF	PG migration, no reaction
Na_2CO_3	DMF	PG migration, no reaction
K_2CO_3	DMF	PG migration, no reaction
DIPEA	DMF	PG migration, very low rate
DBU	DMF	PG migration, no reaction

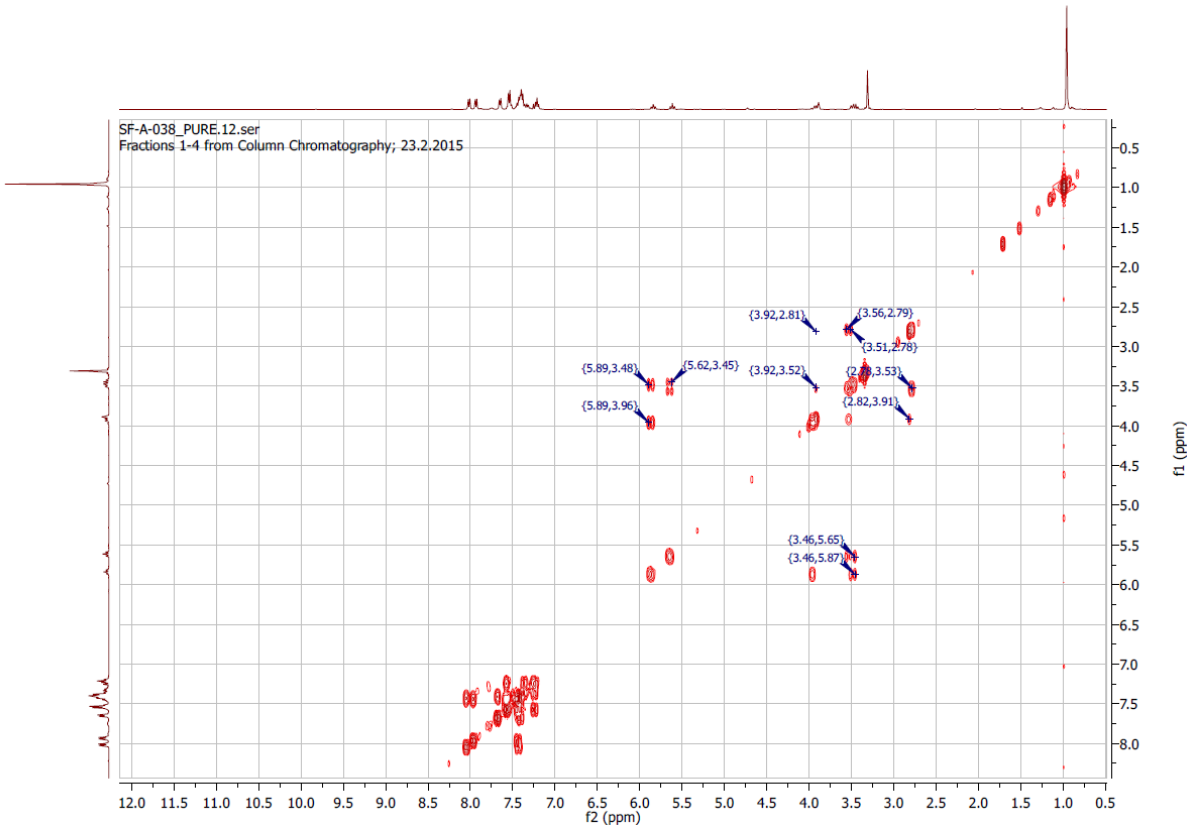

Figure **14** ^{1}H, ^{1}H COSY spectrum of compound **5.**

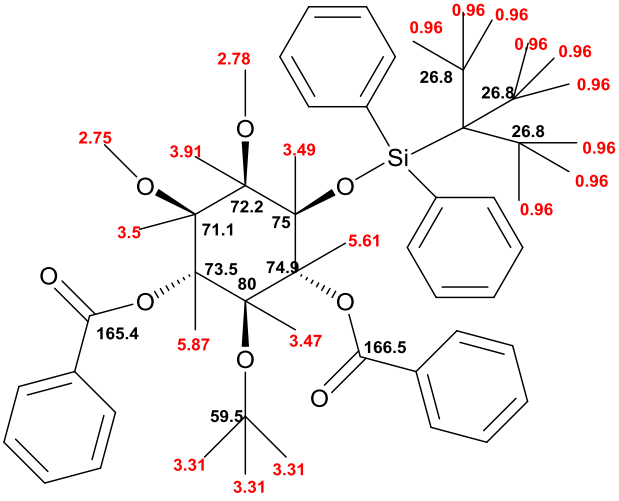

Figure **15** Constructed diagram of compound **5** after extensive structure elucidation using COSY, HSQC and HMBC. Protons are shown in red font, carbons in black.

A new protecting group strategy was designed involving replacement of the labile benzoyl groups by more stable benzyl groups. For this, the Dudley benzylation reaction was carried out[121]. Unfortunately, it was found that the TBDPS group was also prone to migration upon exposure to the strong bases used in Williamson ether synthesis (Scheme8, Figure 16).

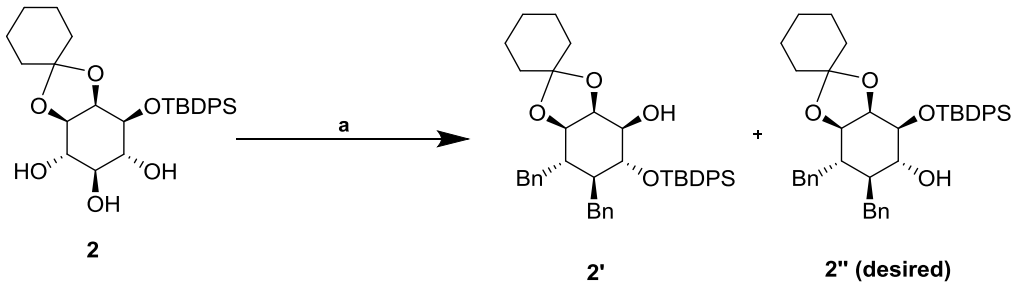

2 2' 2'' (desired)

Scheme **8** Attempt to use benzyl groups as PG instead of benzoyl groups. a) conditions: 2-benzyloxy-1-methylpyridinium triflate (4eq), MgO (4 eq), $PhCF_3$, 83°C, 1day.

Protection of compound **1** at the 1-OH position with monomethoxytrityl (MMT) instead of the bulky TBDPS group was also carried out, but the reaction was not selective (at least 2 regioisomers and one di-substituted inositol ring were formed), and never went to completion, so this attempt was soon aborted.

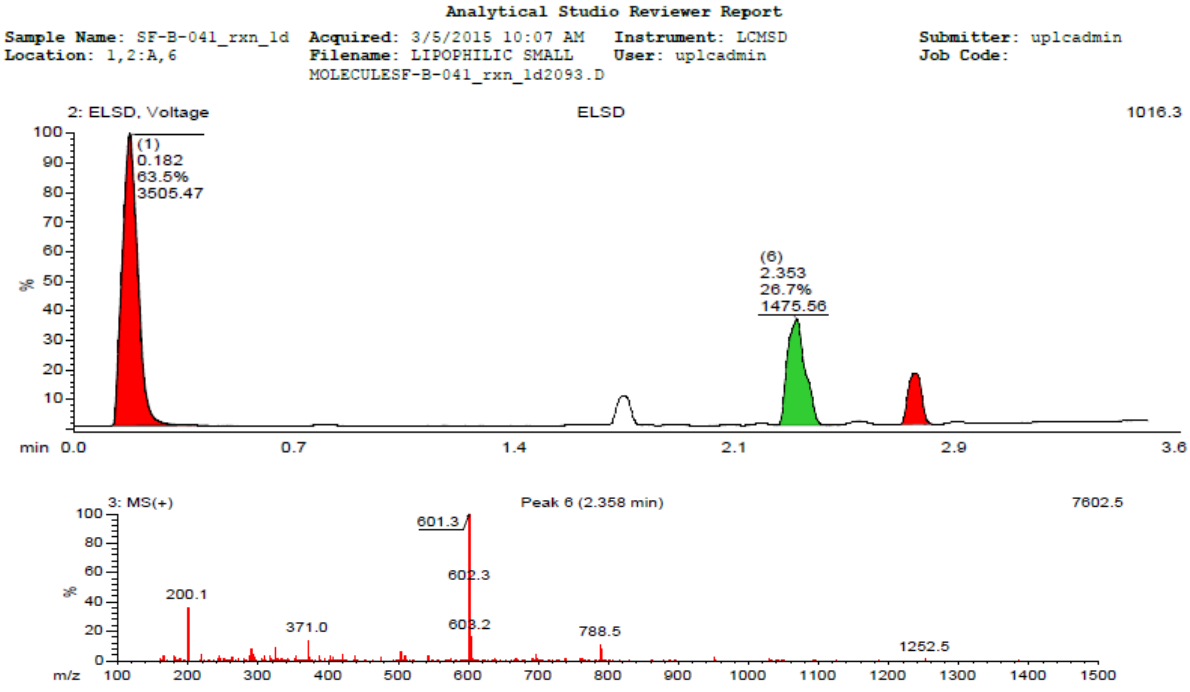

Figure **16** UPLCMS result of the benzylation reaction after one day: peak 6 depicted on the ELSD is actually a multitude of peaks at similar retention times, containing the same TBDPS-protected, dibenzylated compound mass, which indicates the presence of different regioisomers.

As a breakthrough in this synthesis, the methylation reaction on the 6-*O* position was finally achieved using a mild methylation reaction which employs a Meerwein's salt derivative, called trimethyl oxonium tetrafluoroborate, and proton sponge, known to

be a mild base but a strong nucleophile, which could overcome the hurdle of protecting group migration (Scheme 9). This procedure was inspired from the work of Paterson and Coster, who achieved the total synthesis of the potent cytotoxic macrolide, altohyrtin A (spongistatin 1)[122]. Since this reaction was successful, it was thought to make use of it further to protect the free hydroxyl groups of PI(4,5)P_2 with a group other than methyl, hence expand the library: the most direct and available one was the ethyl (Meerwein's salt as a reagent). This led to the design of a series of methylated and ethylated precursors were envisioned to be synthesized according to the planned synthetic routes shown in the previous section's schemes (above).

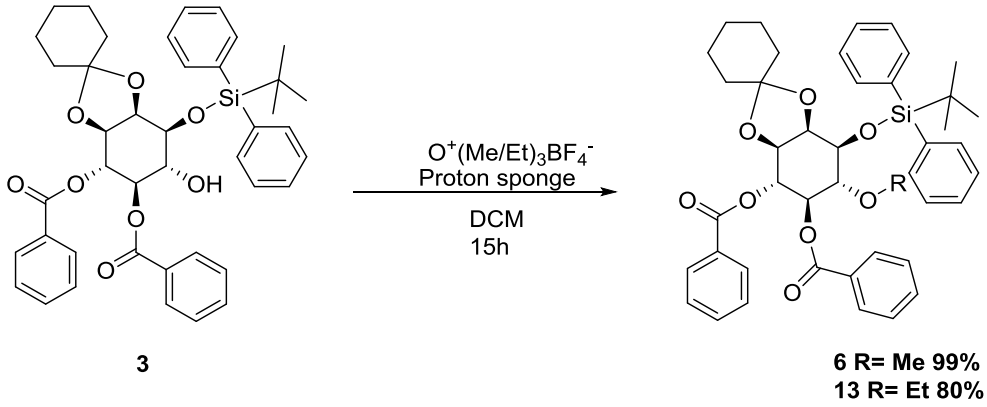

Scheme **9** Successful methylation of the 6-OH of compound **3.**

The reactant, dissolved in DCM, was cooled to 0°C before adding the proton sponge and the corresponding Meerwein salt derivative. The suspension was slowly warmed to room temperature and stirred for 48 hours. After filtration of the reaction mixture, the solvent of the supernatant was evaporated and the crude product was purified by column chromatography. **6** could be isolated in a yield of 99 % and **13** with 80 %. Both compounds were analyzed by ^{1}H- NMR, ^{13}C- NMR (Figures 18 and 19), COSY (Figure 17), HMBC, HSQC and HR-MS.

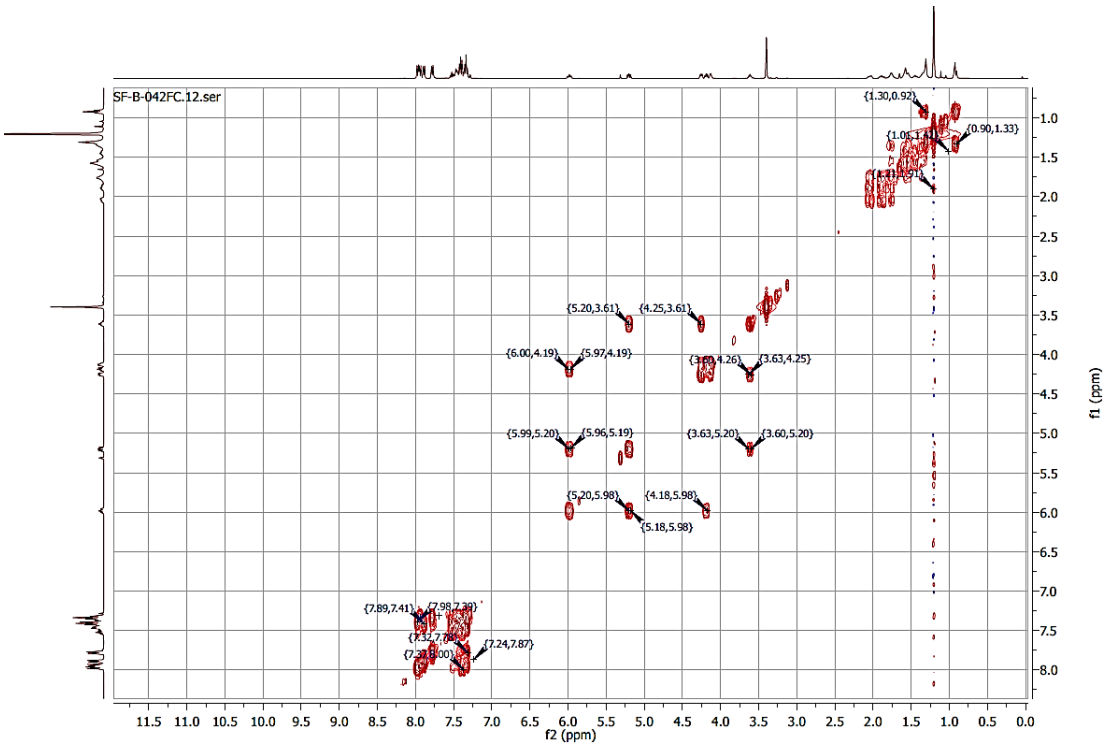

Figure **17** COSY spectrum of compound **6.**

The reaction of the ethyl group seems to be more hindered than with the smaller methyl moiety. In the ^{1}H - NMR of **6**, the methyl group is clearly distinguishable with a singlet at ca. 3.5 ppm (Figure 18). Comparing the ^{1}H - NMR of **6** and **13** (Figure 19) one can see that the proton in the 6-*O* position on the ring is shifted to the deep fields even further in the spectrum of **13** than in **6**.

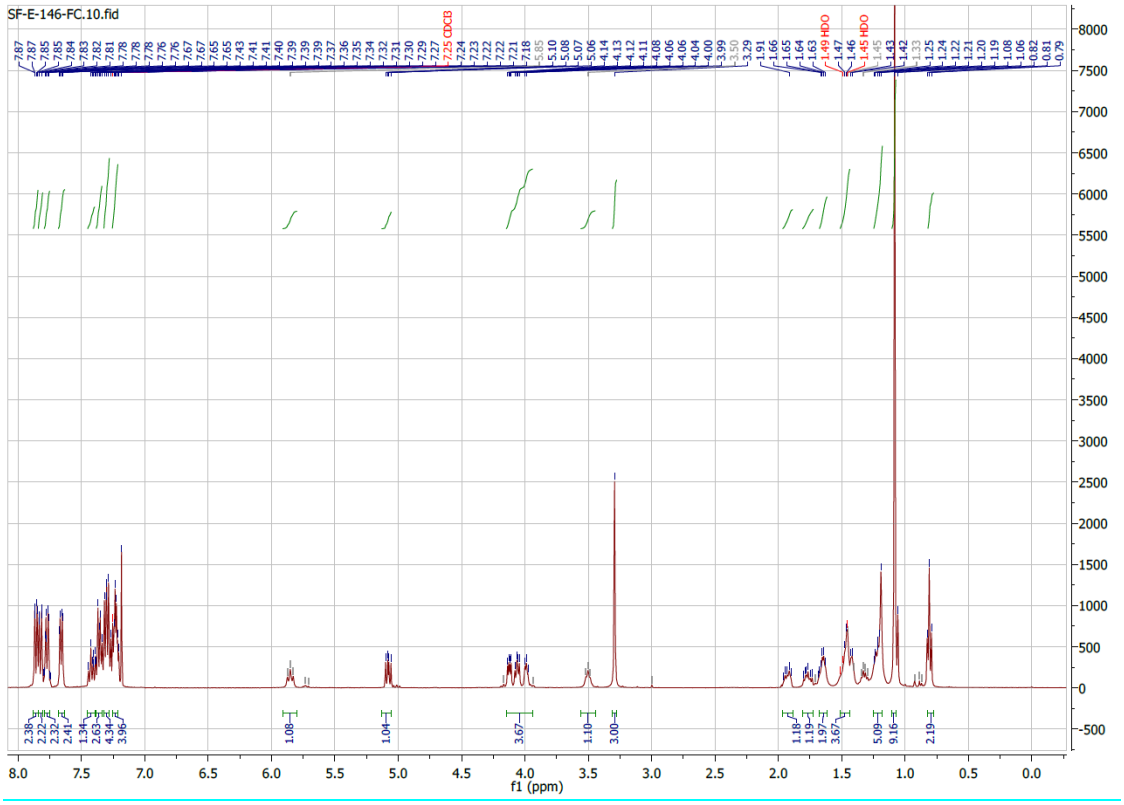

Figure **18** ^{1}H- NMR of **6** measured in $CDCl_3$.

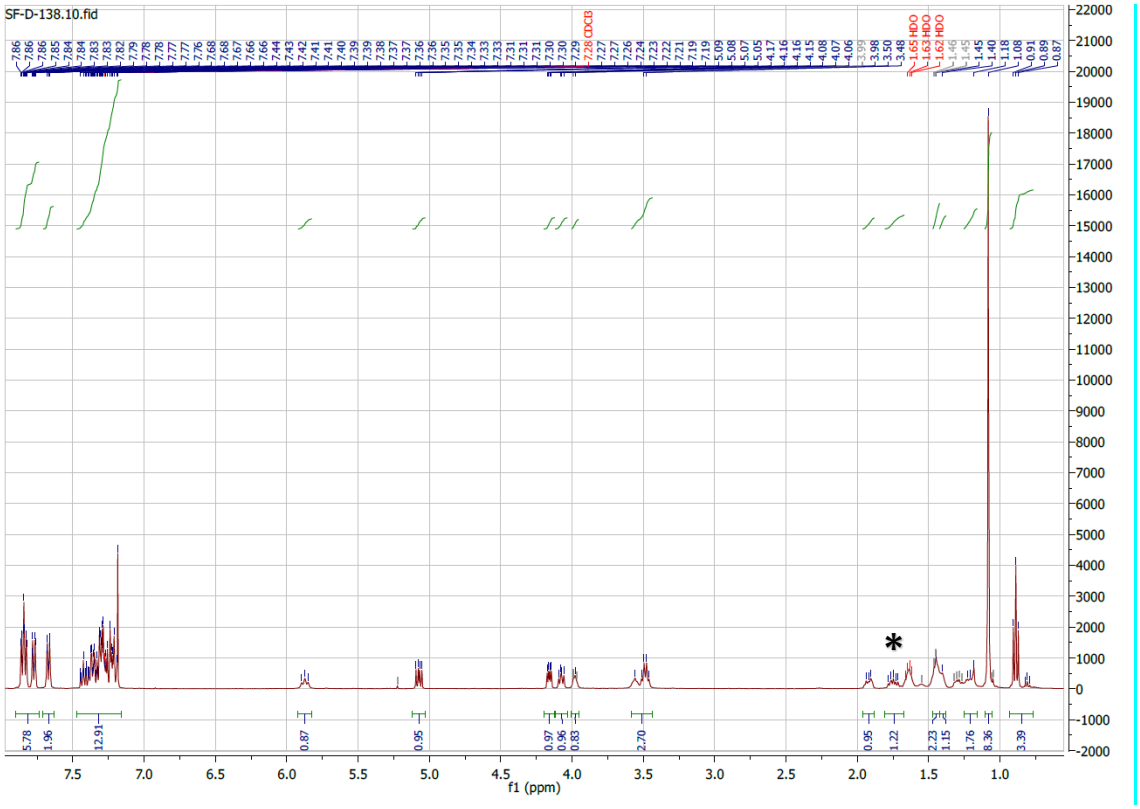

Figure **19** ^{1}H- NMR of **13** measured in $CDCl_3$.

For the di- and trialkylation of **21** the application of the Meerwein salts as reagent was successful as well. Both products were formed in a one-pot reaction (Scheme 10). However, there was a considerable difference between the di- and tri-alkylation yields, and also a difference between methylation and ethylation multi-alkylation yields.

After solving **21** in DCM and cooling the solution to 0°C, the respective Meerwein salt was added together with the proton sponge, and the solution was slowly brought to room temperature. After the reaction was finished, which was determined by TLC monitoring, and which took up to 6 days depending on the reaction, the reaction mixture was filtered, and the crude product purified by column chromatography. The methylation yielded 44% of **20** and 19% of **19**. The ethylating reaction produced 45% of **23** and only 15 % of **22**.

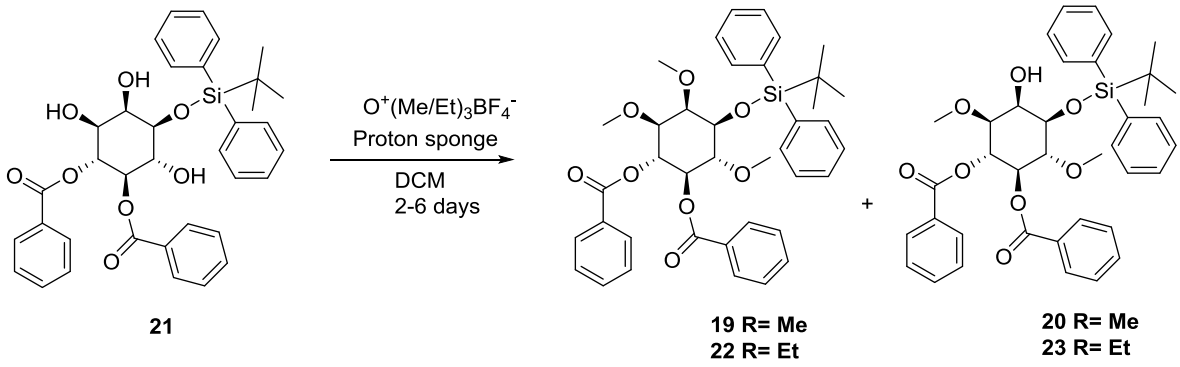

Scheme **10** Synthesis of di-and trialkylated myo-inositols.

The structural elucidation of every compound was conducted with ^{1}H- NMR, ^{13}C-NMR and HR-MS and COSY analysis confirmed the unsubstituted hydroxyl group in position 2 in case of compounds **20** and **23**. Both reactions were done using a very large excess of reagents (alkylating agent and base). These conditions were chosen because of the sterically hindered 6- position, but also because the hydroxyl group on the axial 2-position is the least reactive in the ring.

The ethylating reaction was probably slower than the methylation reaction due to the bigger bulk of the ethyl group, as was already observed in the mono-ethylation. The dialkylated compounds **20** and **23** were isolated in a much higher yield than the triakylated ones. This could be linked to the steric hindrance due to the neighboring TBDPS group for the axial hydroxyl group, as well as the relative inactivity of that group.

The respective yields were possible to increase by letting the reaction run as long as the monoalkylation. But the total yields of both reactions were significantly lower compared to the formation of **6** and **13**.

In other words, the major difficulty encountered in this synthesis was that trimethylation or triethylation using the oxonium salt never proceeded to completion, even when large excesses of alkylating reagent were used. There were always two products to separate (the dialkylated intermediate product and the trialkylated desired product). This separation was difficult due to the similarity in properties of the compounds. In order to obtain sufficient amounts of the successfully synthesized trimethylated PI(4,5)P_2, this was overcome by the multiple methylation reactions of both starting material and dimethylated minor product of previous trimethylation reactions. This was repeated many times, to try to utilize as much of the undesired dialkylated products as possible as starting materials for further methylation. The reactions took up to 7 days to achieve at least 50% conversion, and many solubility experiments were tried on the oxonium salts beforehand to achieve optimization. In the case of the triethylated derivative the alkylation reaction was so slow and with such poor conversion that it was decided to deprioritize this compound. For the total separation of the di- and trialkylated compounds, as well as from other impurities, two column chromatographic separations were sometimes necessary which naturally led to some loss of product. In the 2D-COSY NMR spectra of **19** and **20**, the peaks for the respective methoxy groups (marked with *) are clearly visible (Figures 20 and 21).

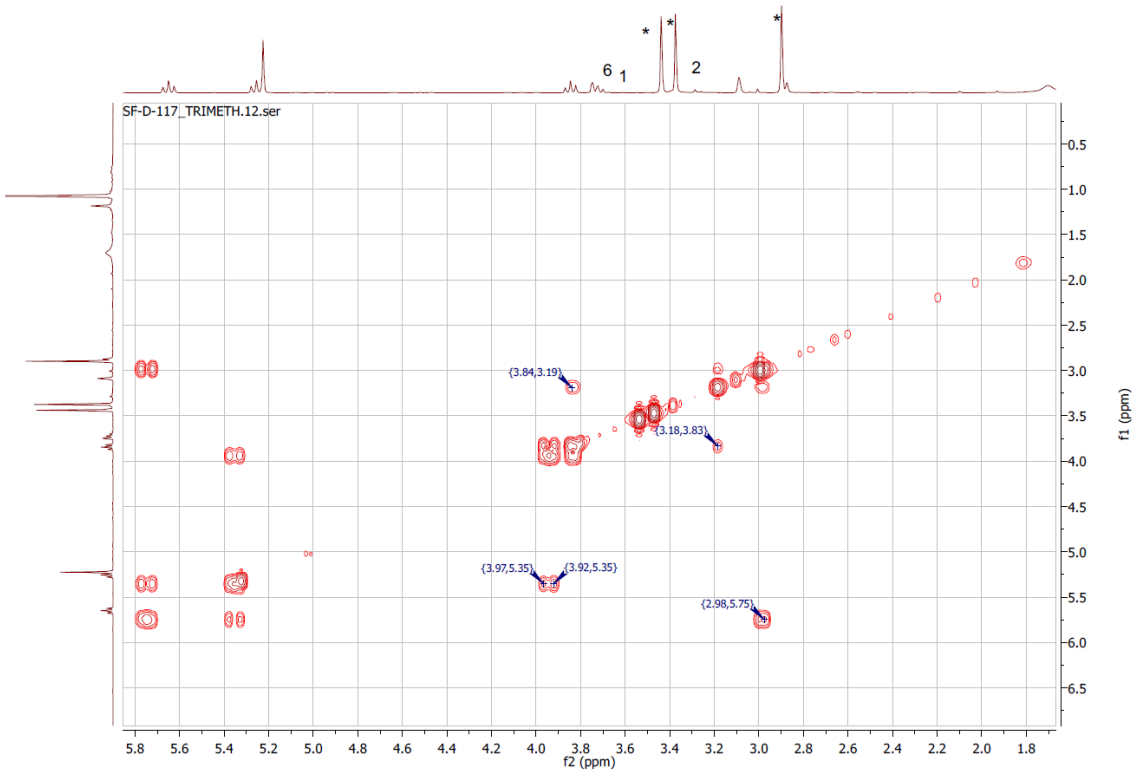

Figure **20** Section of 2D-COSY spectrum of compound **19** measured in $CDCl_3$ with annotated myo-inositol ring protons.

There is also a clear shift to the higher field of the proton signal of the hydrogen at the 2 position of the inositol ring discernable when comparing their respective spectra. This further supports the assumption that the hydroxyl group in the axial position is the last one to react in the multialkylation reactions. This can also be confirmed in the ^{1}H- NMR spectra from **22** and **23** (Figures 22 and 23). The methyl part of the ethoxy group can be seen in their distinctive triplet form while the methylene group signals are less distinguishable. The dialkylated compounds **20** and **23** were thus planned to be taken further down the PI(4,5)P_2 analogue synthesis. However, the steric hindrance of the TBDPS protecting group made further alkylation at the 2-*O* position difficult under non-forcing conditions. Unfortunately, attempts to introduce the allyl protecting group in the 2-*O* position were not successful, presumably also due to steric reasons. This route was put on hold for future revisit, and the 3,6-*O*-dialkylated PI(4,5)P_2 was not fully synthesized as part of this thesis work.

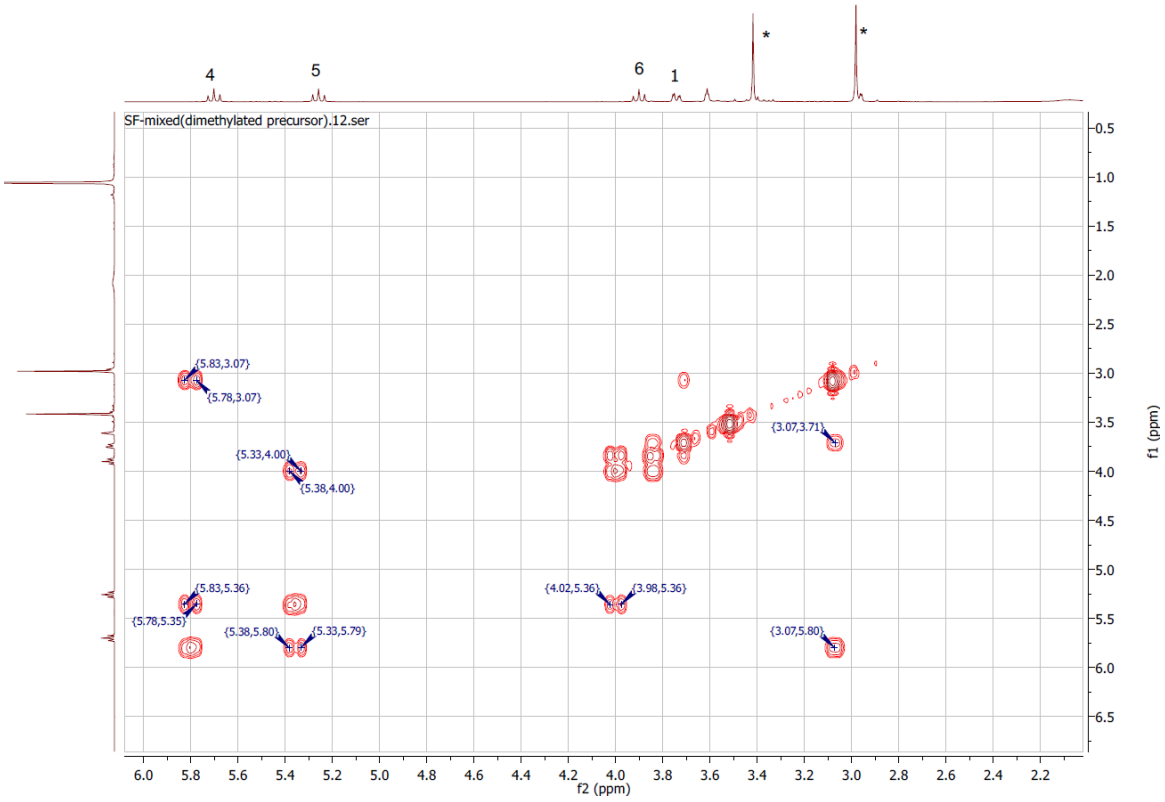

Figure **21** Section of 2D-COSY spectrum of compound **20** measured in $CDCl_3$ with annotated myo-inositol ring protons.

Yet another dialkylated analogue was considered to be synthesized, this time dialkylated at the 2- and 3-*O* positions, instead of the 3- and 6-*O* positions. The synthetic route is shown in Scheme 5. This was made possible with availability of the starting material (**9**), previously used for solid phase synthesis in the Köhn lab[120] (Figure 9). This compound is protected at the 6-*O* position by a MEM group, allowing for alkylation at the 2- and 3- *O* positions selectively, after cleaving the benzylidene linker. Methylation was chosen over ethylation in this case, for obvious feasibility reasons (see above). The cleavage of the benzylidene linker was successfully achieved, after using ethylene glycol as a scavenger to prevent it from reforming upon removal of acid. The methylation at the 2- and 3-*O* positions of the ring was successful too, following an established procedure as part of this thesis. Unfortunately, the MEM group was lost (partially) during the methylation reaction (scheme 5, second step). This could be overcome by re-protecting with a MEM group and carrying on the synthetic route as in Scheme 5. The 2,3-*O*-dimethylated inositol should provide an additional building block for the PI(4,5)P_2 analogues library. Due to time constraints, the 2,3-*O*-dimethylated PI(4,5)P_2 analogue was, however, not synthesized as part of this work.

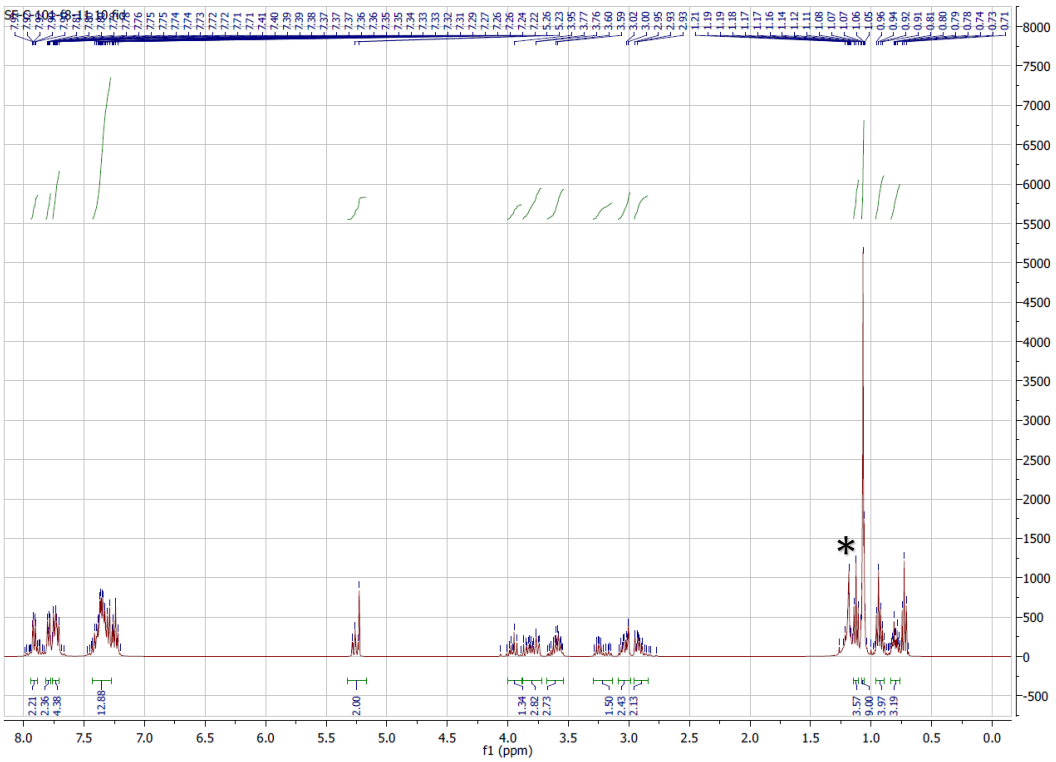

Figure **22** ^{1}H- NMR of compound **22** measured in $CDCl_3$.

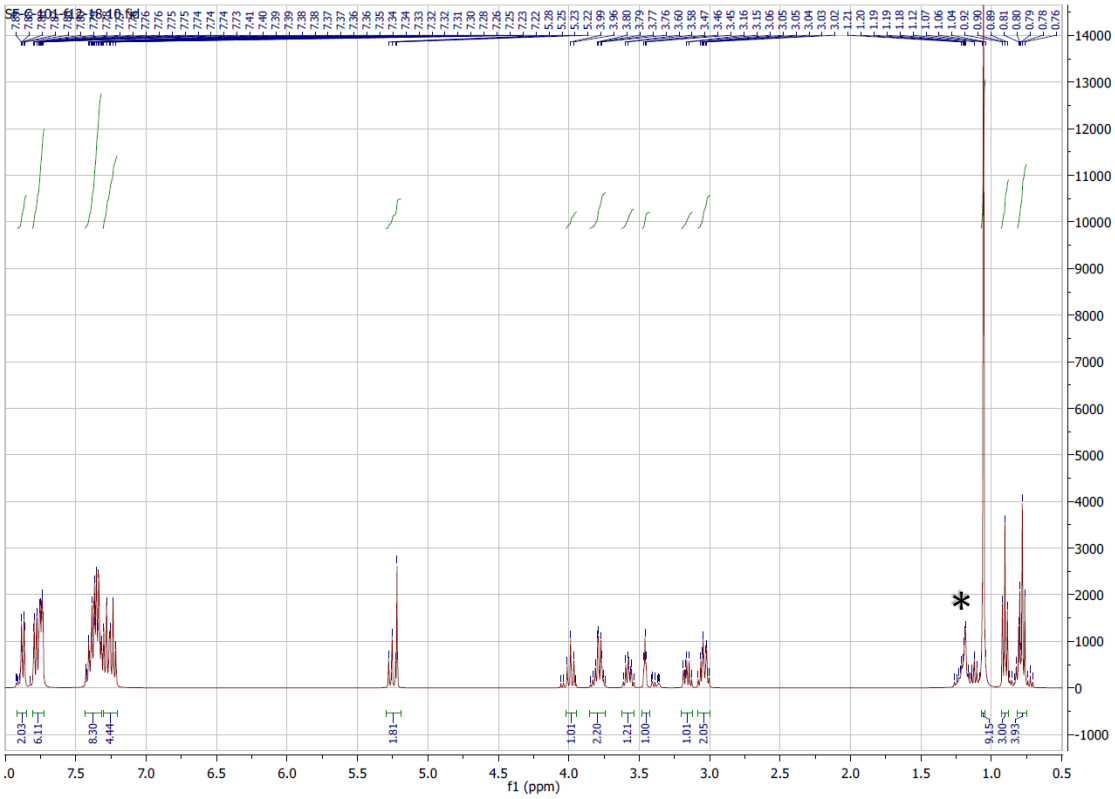

Figure **23** ^{1}H- NMR of compound **23** measured in $CDCl_3$.

3.1.2.3. Debenzoylation

The deprotection of the hydroxyl groups of the 4 and 5 position of the inositol ring was carried out following the procedures of Bruzik *et al.*[91] and Vanek and coworkers[123] (Scheme 11).

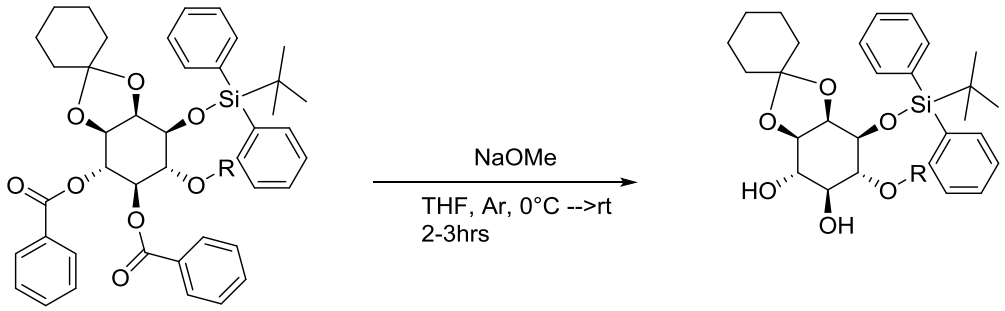

Scheme **11** General debenzoylation reaction.

The starting material was dissolved in the solvent and the solution cooled to 0°C before NaOMe dissolved in MeOH was added. The reaction was slowly warmed to room temperature and monitored by TLC. After complete conversion, the reaction solution was neutralized and worked up. The crude product was purified by column chromatography. Product **8** could be isolated in 74% yield and the conversion of **13** to **14** gave a yield of 99%. The discrepancy in the yields might be due to two independent reasons: 1) the bulkiness of the ethyl group which might push the reaction to go faster, and hence, more efficiently, and 2) the extent of the dry conditions. The structural confirmation of compounds **8** and **14** were both conducted with ^{1}H- NMR, ^{13}C- NMR and HR- MS. Since the first debenzoylation reaction was performed on compound **6**, it was used as a reference for optimization. Hence, the first time this reaction was conducted, NaOMe was used in a catalytic amount, and MeOH was used both as solvent and to regenerate the reactive species. But compared to the reaction by Bruzik and coworkers[91], which was also later applied for the formation of **8,** and in which the reagent was used in an equimolar amount (instead of catalytic), the reaction time is considerably longer and the yield is slightly lower. This is why it was opted to use the latter technique for the debenzoylation of all the analogues precursors (both the inositol-ring modified and the lipid tail modified), since it seemed that the best and quickest route to debenzoylate these hydroxyl positions in solution is by using NaOMe as a reagent, not as a catalyst.

In the ^{1}H- NMR, the shift of the proton signal assigned to the hydrogen on 4 and 5 position to the higher field has clearly shifted for both compounds compared to their respective starting materials (Figures 24 and 25). The peaks for the free hydroxyl groups were no longer visible in either spectrum in approximately the same area, after addition of D_2O to the NMR samples. This was a method to prove that the Hydroxyl groups were now free. The ^{13}C NMR spectra of the compounds also confirm the loss of the carbonyl compounds in the 170 ppm area (Appendix), in addition to less signal in the proton NMR at 7-8 ppm.

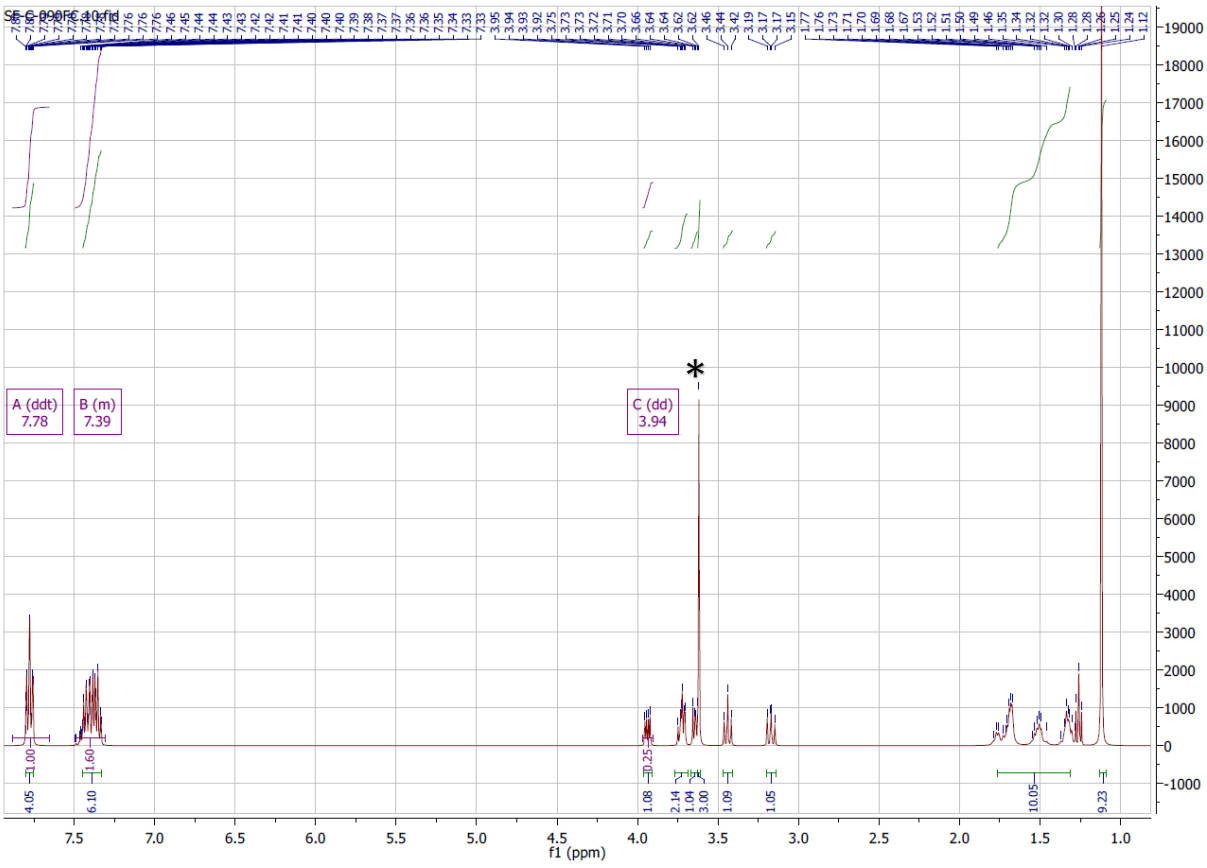

Figure **24** ^{1}H- NMR of **8** measured in $CDCl_3$.

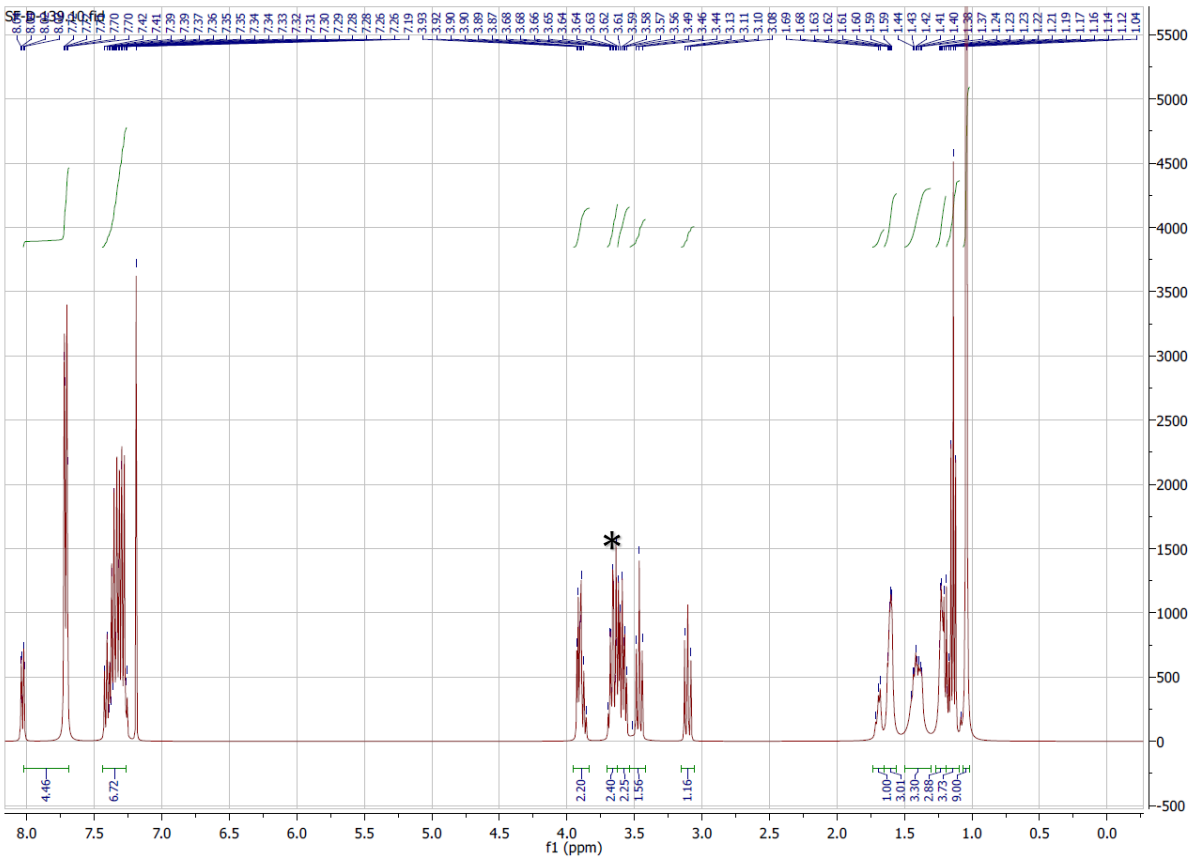

Figure **25** 1H- NMR of **14** measured in $CDCl_3$.

3.1.2.4. Phosphorylation

For the addition of the phosphate groups to the inositol ring, a procedure developed by Fraser- Reid *et al.*[124] utilizing the monofunctional phosphine was used (Scheme 12).

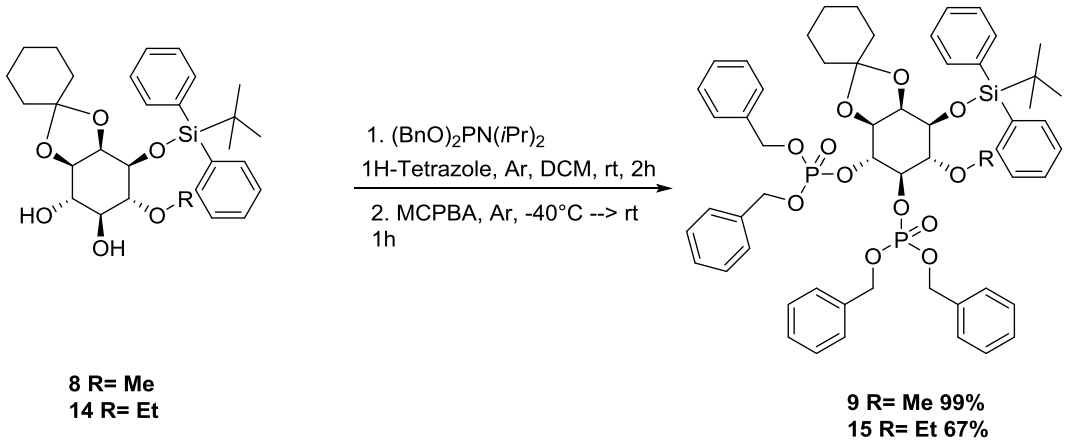

Scheme **12** General phosphorylation synthesis of alkylated myo-inositols.

After dissolving the respective starting material in solvent, 1H-tetrazole, then the phosphoramidite were added dropwise and the solution stirred until no starting material remained. Then the reaction mixture was cooled to -40°C and the phosphite groups were oxidized with mCPBA to give the protected phosphate groups. After warming the solution to room temperature, the reaction mixture was quenched and subjected to an aqueous work up. After purification of the products with column chromatography, **9** was isolated in a yield of 99% and **15** with 67%. The apparent difference in yield is thought to be mostly due to the steric hindrance of the ethoxy group, which is bulkier than the methoxy group, and with which the reaction was never pushed to completion. Therefore, changes in reaction conditions (equivalents of reagents and time) had to be closely investigated before obtaining the documented yield. Below is an explanation of the reaction conditions, which were optimized prior to the best (abovementioned) conditions.

The same phosphorylation method was applied for the trialkylated inositol ring after sufficient amount of the starting debenzoylated material was successfully obtained. The phosphorylation reactions were optimized according to three variables: the type of activator, the type of solvent, and the type of oxidation method. As can be seen in Table 2, the best activator was 1H-tetrazole, though extreme caution had to be considered as the use of an accidentally non-dry reagent solution had led to the total loss of product before oxidation. 2,5 Dicyanoimidazole, which has been used as an activator for phosphorylation in solid phase synthesis of PIPs[120], was not as good as 1H-tetrazole, at least in solution synthesis. The best solvent was DCM, not acetonitrile, nor chloroform, nor a mixture of either, and the best and cleanest oxidation method was the one using mCPBA (meta-Chloroperoxybenzoic acid) instead of peracetic acid (used in the solid phase synthesis[120]). In fact, the little amount of product that was formed in the reaction was not possible to isolate because a lot of side products formed during this kind of oxidation. Oxidation with peracetic acid lead to the formation of many side products that hinder the isolation of the product and oxidation on air is a very slow and indefinite technique.

Table **2** Phosphorylation reaction optimization.

Reaction	Activator	Solvent (dry)	Time stirred before oxidation (h)	Oxidation method	Yield
1	2,5 Dicyanoimidazole	DCM:AcCN	2	Peracetic acid	50%
2	1H-tetrazole	DCM:AcCN	2.5	mcpba	74%
3	1H-tetrazole	CHCl3	2	mcpba	82%
4	**1H-tetrazole**	**DCM**	**2**	**mcpba**	**99%**

For TLC monitoring of products and impurities during these first part of these reactions (i.e., before oxidation), a solution was devised to be able to run the P(III) compounds on silica without possible hydrolysis or oxidation, as these compounds are highly labile. For that, the TLC plate was treated with trimethylamine (TEA) fumes in a small TLC chamber prior to its use. The base TEA helped neutralize the acidic environment on the TLC plate, which contributed to the migration of the reaction components on the plate without decomposition. With that, one could tell if the presence of any additional spot(s) other than the desired product on the TLC were actual impurities. Overall, impurities in the optimized phosphorylating reactions were increasingly insignificant after final purification on silica columns, as can be seen in the ^{31}P NMR of products **9** and **15** in Figures 26 and 27, respectively. The structural elucidation of all the phosphorylated compounds was done by ^{1}H- NMR, ^{13}C- NMR, ^{31}P- NMR and HR- MS.

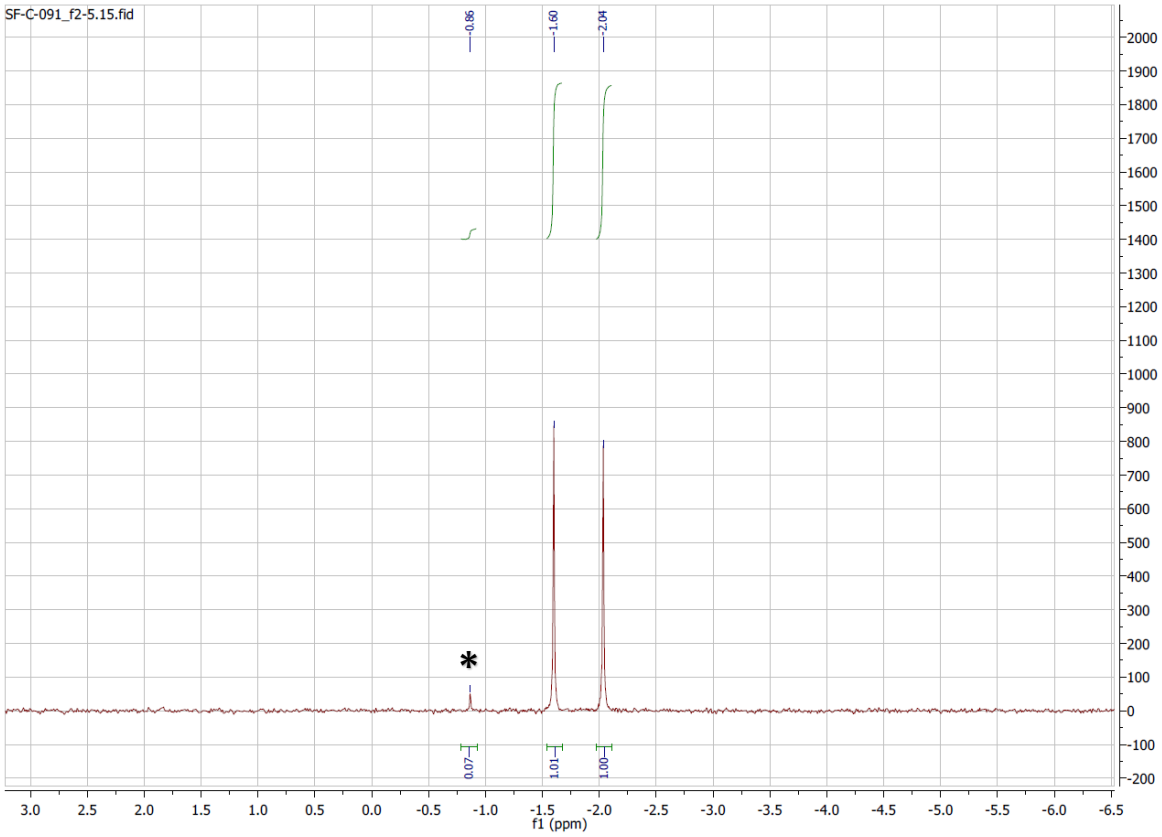

Figure **26** ^{31}P- NMR of **9** measured in $CDCl_3$ with only a minor impurity (*).

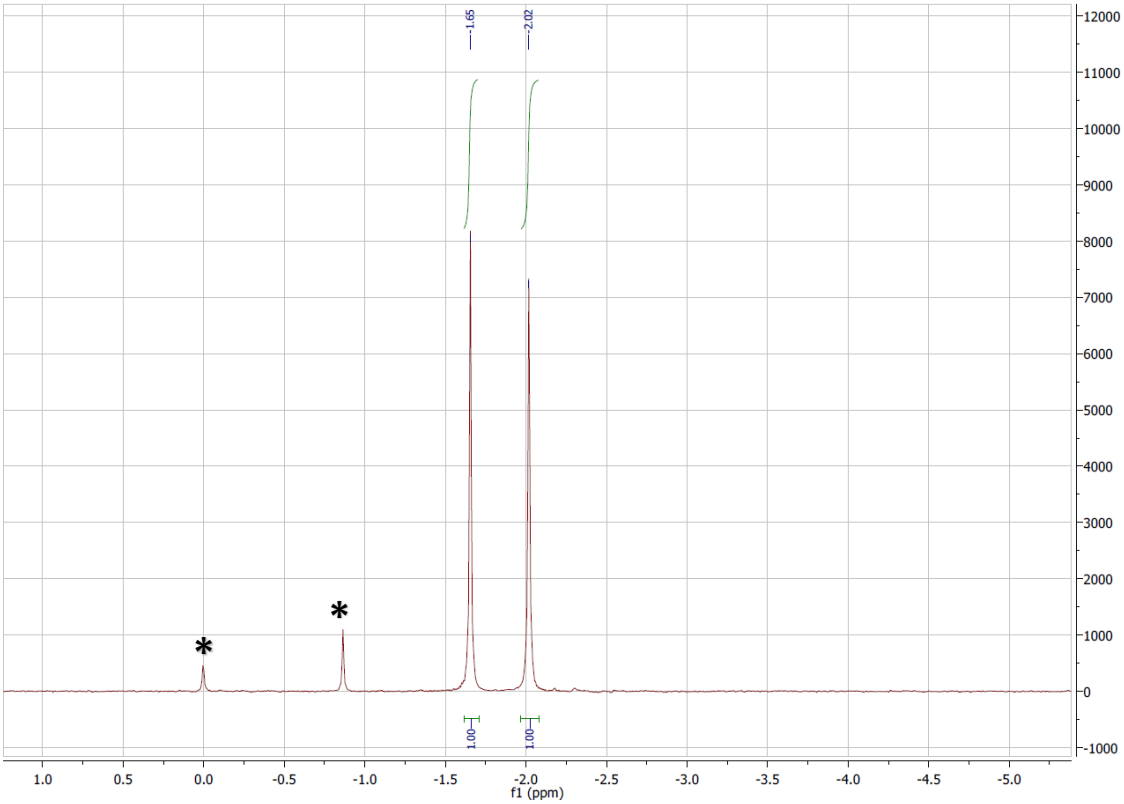

Figure **27** ^{31}P- NMR of **15** measured in $CDCl_3$ with only a minor impurity (*).

3.1.2.5. TBDPS deprotection

For the deprotection of the 1-hydroxyl group on the inositol ring by cleaving the TBDPS group, an adapted method by Bruzik *et al*[91], developed for the synthesis of PIPn, was applied (Scheme 13).

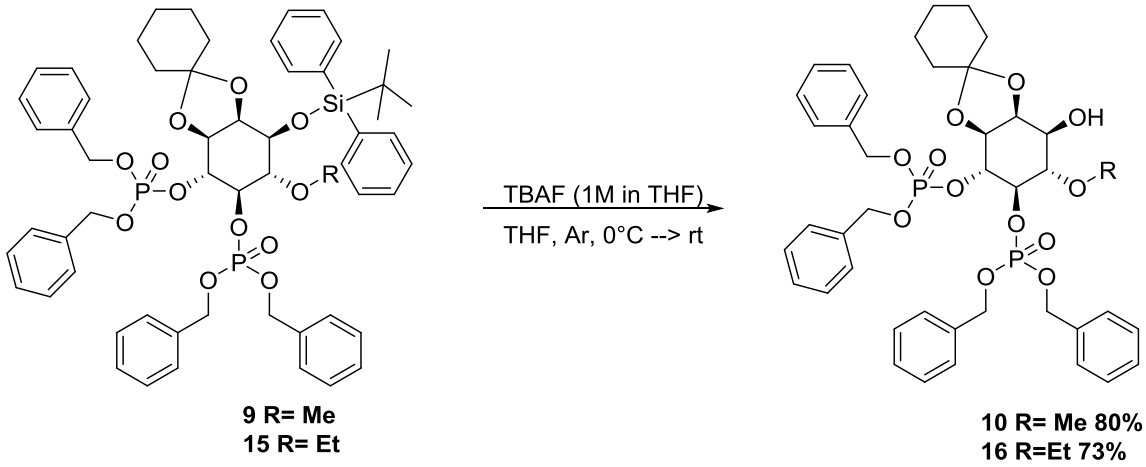

Scheme **13** General TBDPS deprotection reaction.

The respective starting materials were dissolved in THF and the solutions cooled to 0°C before TBAF was added. After warming the solution to room temperature and monitoring the reaction by TLC, the reaction was quenched, aqueously worked up and purified with column chromatography (see *Chapter 5* for more details).

Table **3** TBDPS deprotection optimization. *As part of the same solution synthesis outline, the native PI(4,5)P_2 substrate was also synthesized, but that included protecting at the 6-OH with a MEM group.

R-group	Reagent	Amount (eq)	Time (hr)	Temperature	Solvent	Yield (%)
Me	TASF	2.5	2.5	rt	DMF	34
Me	TBAF (solid)	2.5	2	rt	THF	47
Me	TBAF (1M in THF)	2.5	2.5	rt	THF	57
Me	TBAF (1M in THF)	2	3	0°C → rt	THF	80
Me	TBAF (1M in THF)	1.9	2.5	0°C → rt	THF	69
Et	TBAF (1M in THF)	1.9	2	0°C → rt	THF	73
Et	TBAF (1M in THF)	1.8	2.5	0°C → rt	THF	47
MEM*	TBAF (1M in THF)	1.8	2.5	0°C → rt	THF	82

In the optimized reaction, the amount of **10** yielded to 80% and of **16,** a yield of 73% could be isolated. Analyzed were both compounds by ^{1}H- NMR, ^{13}C- NMR, ^{31}P- NMR and HR- MS. After testing different solvents, it was determined that THF is the best solvent for the reaction and for monitoring thereof. The first two trials were directed with solid TASF and solid TBAF as reagents. Using TASF as reagent and DMF as solvent was inspired by the solid phase synthesis of such phosphoinositides[120], but it was soon shown to work much less efficiently in solution synthesis. Due to the hygroscopic nature of such reagents, the weighing and transport between scale and flask lends itself for the reagent to draw water from air which decreases the reactivity of the compound and leads to the necessity of using a higher amount. To avoid this problem a change to 1M-TBAF solution in THF was made. A variety of equivalents were tested from 1.7 to 2. The main results can be found in Table 3.

During the monitoring of the reaction with TLC it was apparent that more side product

was formed while increasing the amount of the reagent gradually. Using less reactant to avoid side product formation and letting the reaction run longer while monitoring the reaction with TLC led also to a decrease in yield. Reasons for this observation could be linked to the increase of side product, the longer the reaction mixture was stirred, as well as the lack of total conversion of the reaction. To avoid the increase of side product while using a higher amount of TBAF-solution, the reaction mixture was cooled to 0°C before the reagent was added. Surprisingly, the bigger the R group, the better the yield. This could be due to the bulkiness of the group, which pushes the leaving group to leave faster, but it is just an assumption. In the ^{31}P- NMR, it is apparent that the synthesized products can be isolated in 100% purity (Figures 28 and 29).

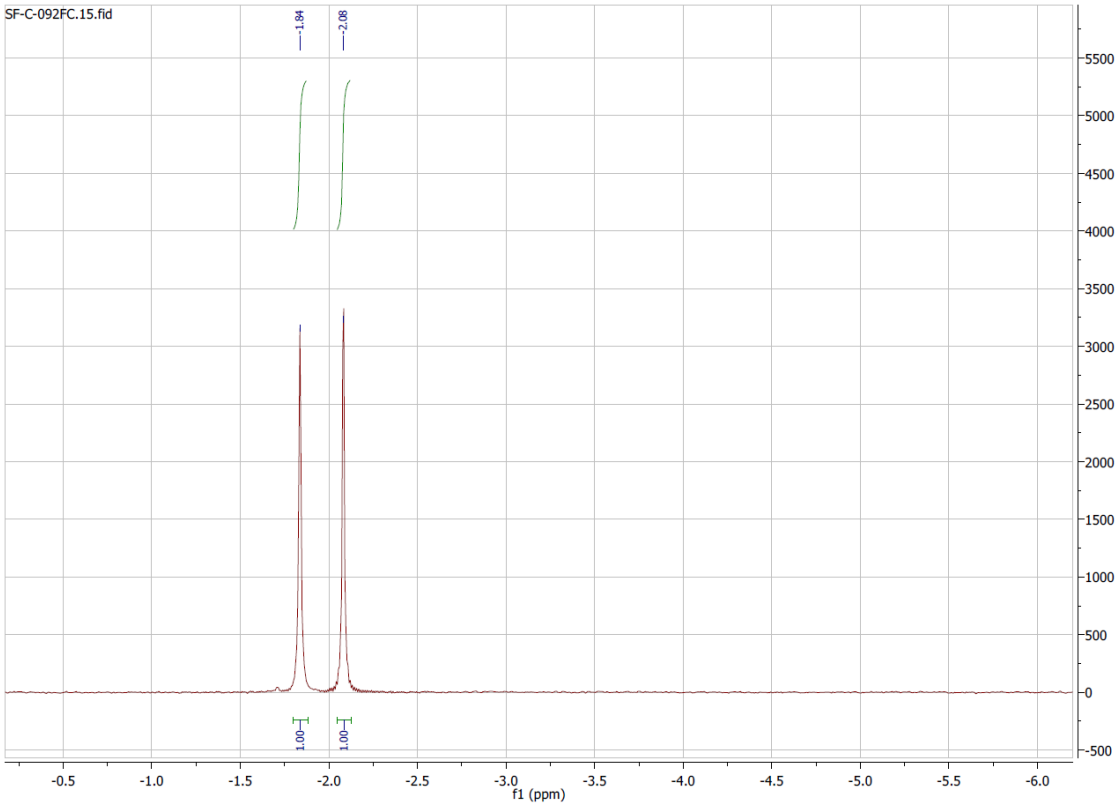

Figure **28** ^{31}P- NMR of compound **10** measured in $CDCl_3$.

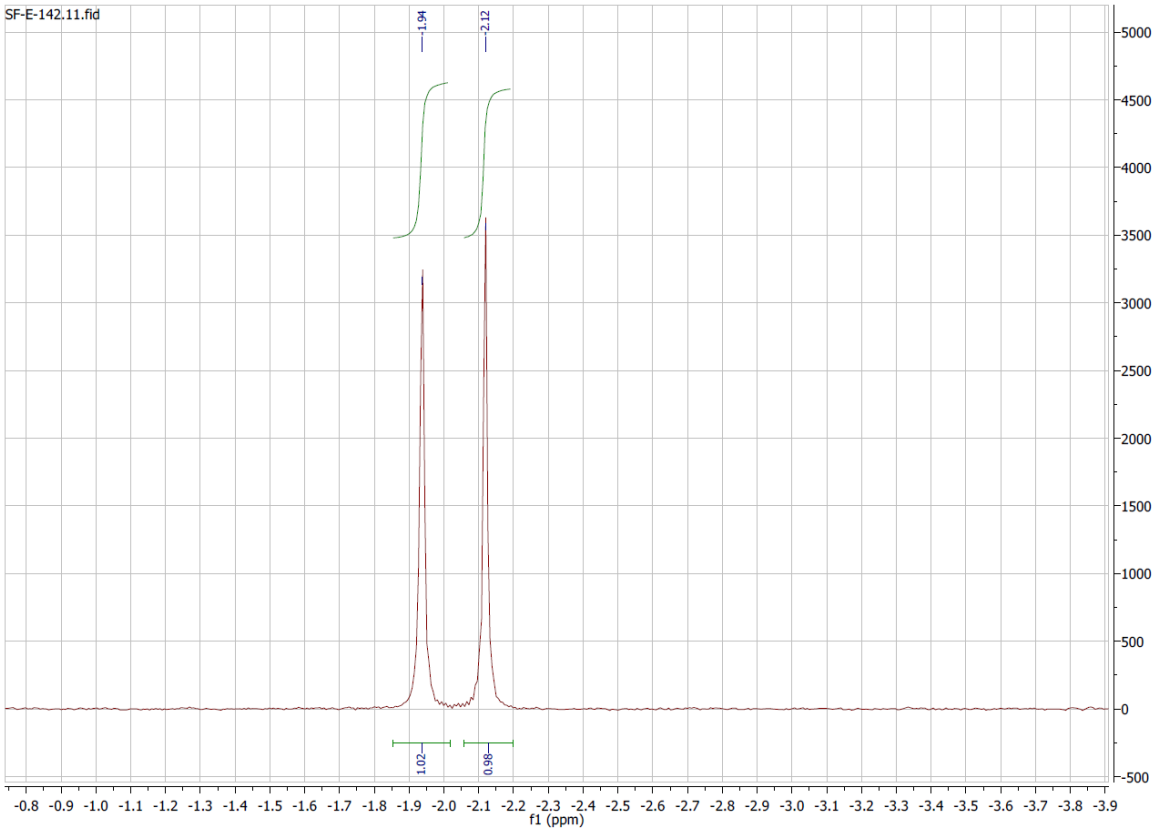

Figure **29** ^{31}P- NMR of compound **16** measured in $CDCl_3$.

3.1.3. Solution synthesis of the diverse lipid tails

Part of the overall total organic synthesis of PI(4,5)P_2 analogues involved synthesizing the lipid tail phosphoramidite prior to its attachment to the 1-*O* position of all the analogues.

The DiC8 lipid tail was successfully synthesized according to the synthetic route shown in Scheme 14. This is a previously established synthesis, used as part of the PIP solid phase synthesis[120].

The diisopropyl-*O*-benzyl phosphoramidite (**51**) was also synthesized using a different technique, involving bulb-to-bulb distillation. This afforded a large amount of reagent, which was used for further lipid tail synthesis, as well as three other lipid tail analogues: the di-carbamate, the di-adamantane, and the phenylpropanol chains (Schemes 15 and 16). These phosphoramidites were again synthesized and optimized following the technique used in Scheme 14 (see chapter 5 for more details about the procedures).

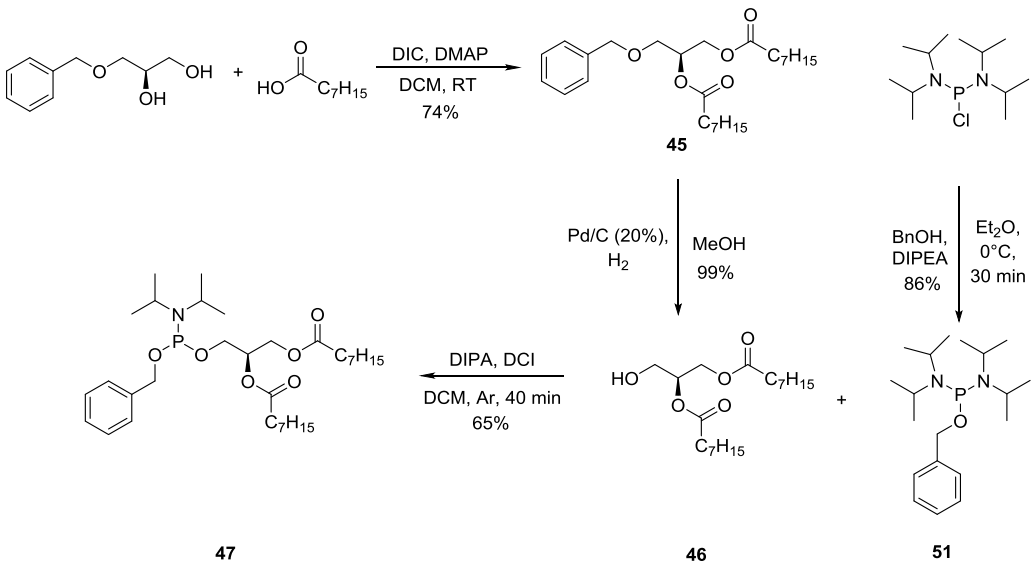

Scheme **14** Synthesis of phosphine **51** and the phosphoramidite **47.**

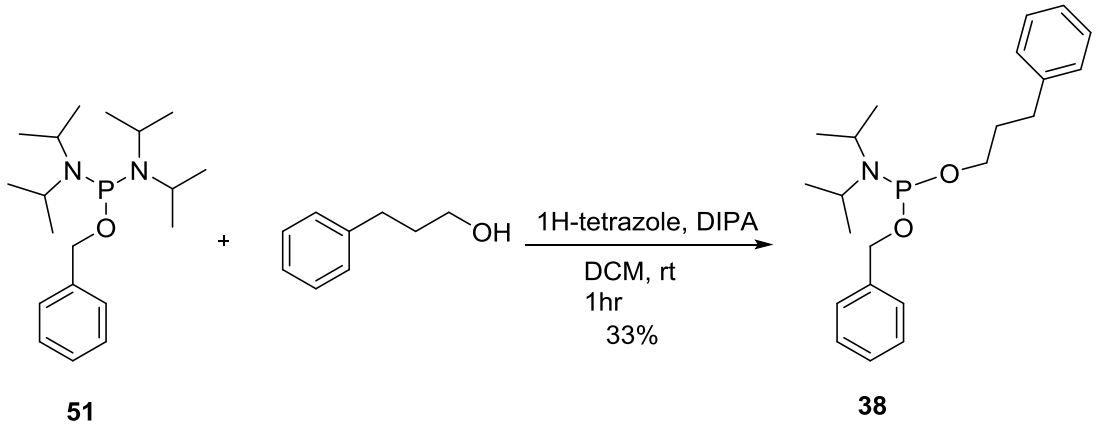

Scheme **15** Synthesis of phosphoramidite **38.**

The di-carbamate lipid chains were chosen to study the difference in analogue activity when the ester bonds of the lipid chains are replaced by the more stable carbamate bonds. The di-adamantane lipid chains were chosen based on a study by Gregory and coworkers [125], who synthesized phosphatidylinositol phosphate analogues containing adamantyl carboxylic ester groups, in place of the natural lipid side chains. These were shown to be significantly more soluble in water than other lipid chain analogues, and to not form large aggregates such as liposomes or micelles. These adamantyl analogues were also shown to bind to known phosphoinositide-binding proteins with similar affinities to native ligands[125], such as FYVE domains and others. The phenylpropanol lipid tail was selected

to be a simplified version of the hydrophobic lipid tail, to check for how significant large lipid tails are for binding. This reasoning was from a medicinal chemistry point of view aiming to design a potential inhibitor. The pathways of the lipid tails synthesis are shown in Schemes 14-16.

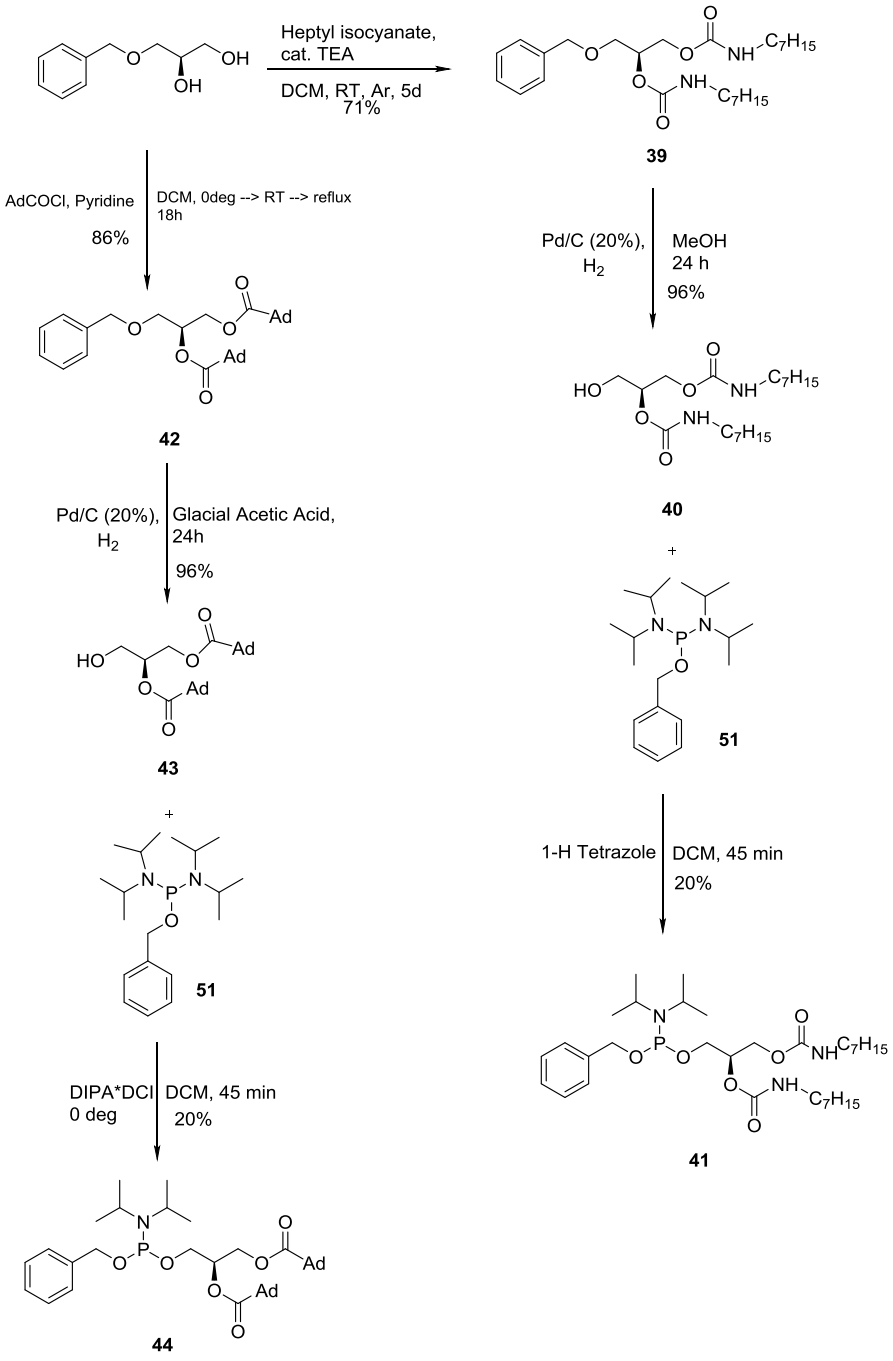

Scheme **16** Reaction pathways of the synthesis of the Di-adamantane and Di-carbamate glycerol lipid chains phosphoramidites **44** and **41,** respectively.

3.1.4. Synthesis of PI(4,5)P_2 analogues

The final steps in the solution phase synthesis of the analogues were: a) coupling of the separately synthesized phosphoramidite(s) with the free hydroxyl group on position 1 of the inositol precursors (in this case, compounds **10**, **16**, **26** and **32**), b) deprotection the full molecule to yield the free acid and c) salt formation using a salt exchange resin.

The DiC8 chains (compound **47**) were coupled to compounds **10**, **16** and **26** to strictly account for inositol modifications in the SAR studies. For the lipid tail attachment, the phosphorylation reaction method by Fraser-Reid and coworkers[124] was adapted for this purpose (Scheme 17), and applied for all the coupling reactions.

3.1.4.1. Lipid tail attachment

In DCM dissolved, the respective starting material was cooled to 0°C before the diC8 lipid tail phosphoramidite **47** and 1H-Tetrazole were added. After warming to rt and stirring until full conversion is achieved the reaction mixture was cooled to -40°C and oxidation with mCPBA was carried out. After the work up, the crude product was purified using column chromatography. **11** was isolated with a yield of 70%, the conversion of **16** to **17** led to a yield of 54%, and the conversion of **26** to **27** led to a yield of 76%. Structural elucidation was carried out by ^{1}H- NMR, ^{13}C- NMR, ^{31}P-NMR and HR -MS. Using the same reaction method for the attachment of the diC8 phosphoramidite that was used for the phosphorylation led to the formation of the desired products.

Comparing the synthesis of the three products, it was obvious that the reaction is a lot slower for the ethylated precursor as seen before in the bisphosphorylation and TBDPS cleaving reactions. The ethoxy group seems to hinder the reaction sterically through its size. Furthermore, it was not possible to achieve full conversion of the starting material by stirring longer and increasing the amount of the reagents. A solution to this might be to increase the amount of 1H-Tetrazole to ensure the full activation of the phosphoramidite. Coupling with the trimethylated inositol precursor achieved the best yields, since both the cyclohexylidene ketal and the ethoxy groups around the 1-OH were substituted by smaller, methoxy groups.

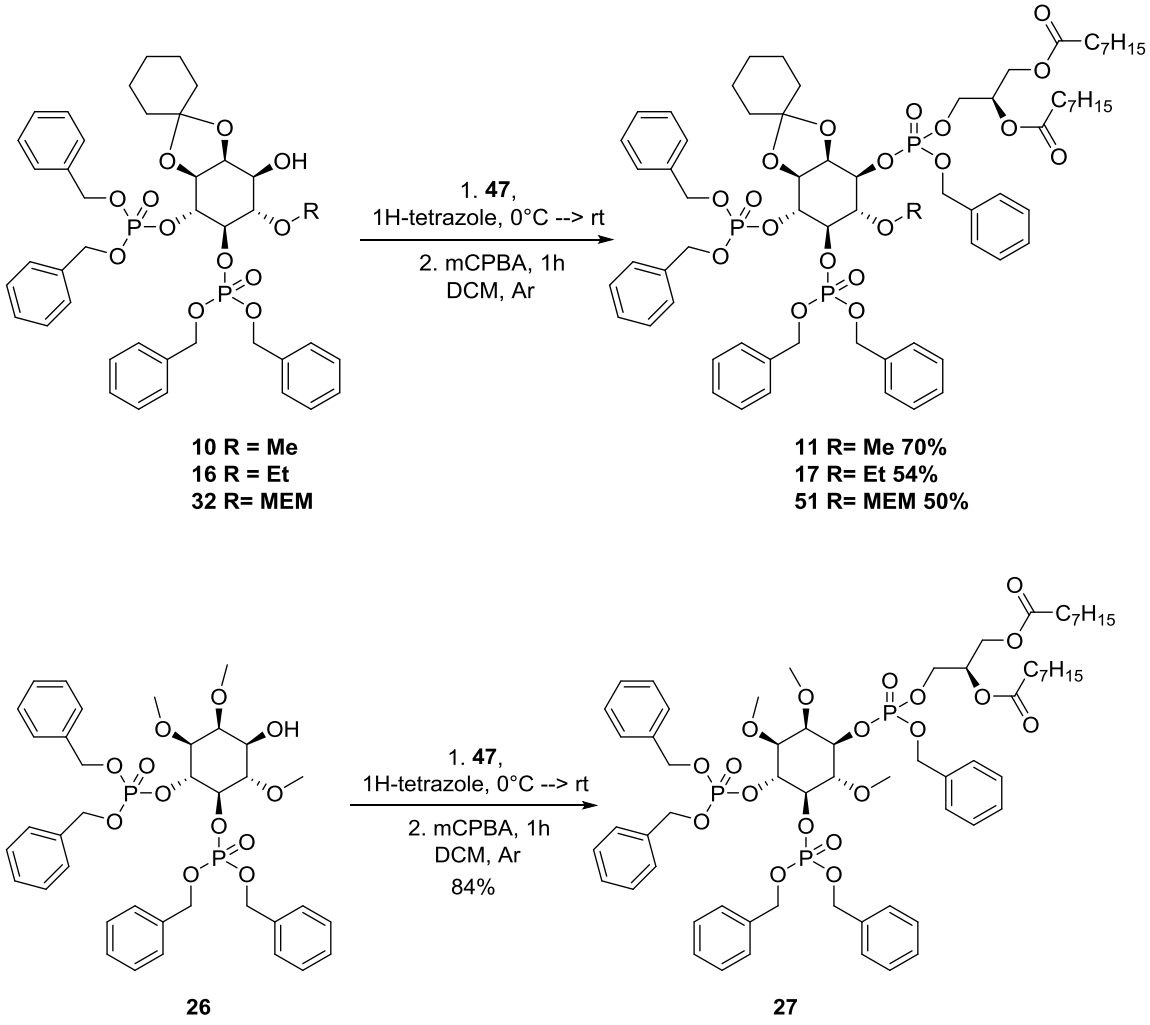

Scheme **17** Lipid tail attachment reaction to the three inositol precursors **10**, **16** and **26.**

In the ^{1}H-NMR of **11** the signal for the methoxyl group is split into a doublet for which both peaks integrate to 1.5 protons (Figure 30, marked with a "*"), which could be explained by the nuclear overhauser effect (NOE). In this case, the spin-spin coupling does not ensue through bonds, but through space. The protons of the methoxy group could hence be interacting with the protons of the benzyl protecting group in the phosphodiester, and the benzyl groups on the 5-phosphate, generating this effect. It might also be possible that through the bulky protecting groups the rotation around the single bond is inhibited and the environments on both sides of the methoxy group are dissimilar, thereby generating two separate signals.

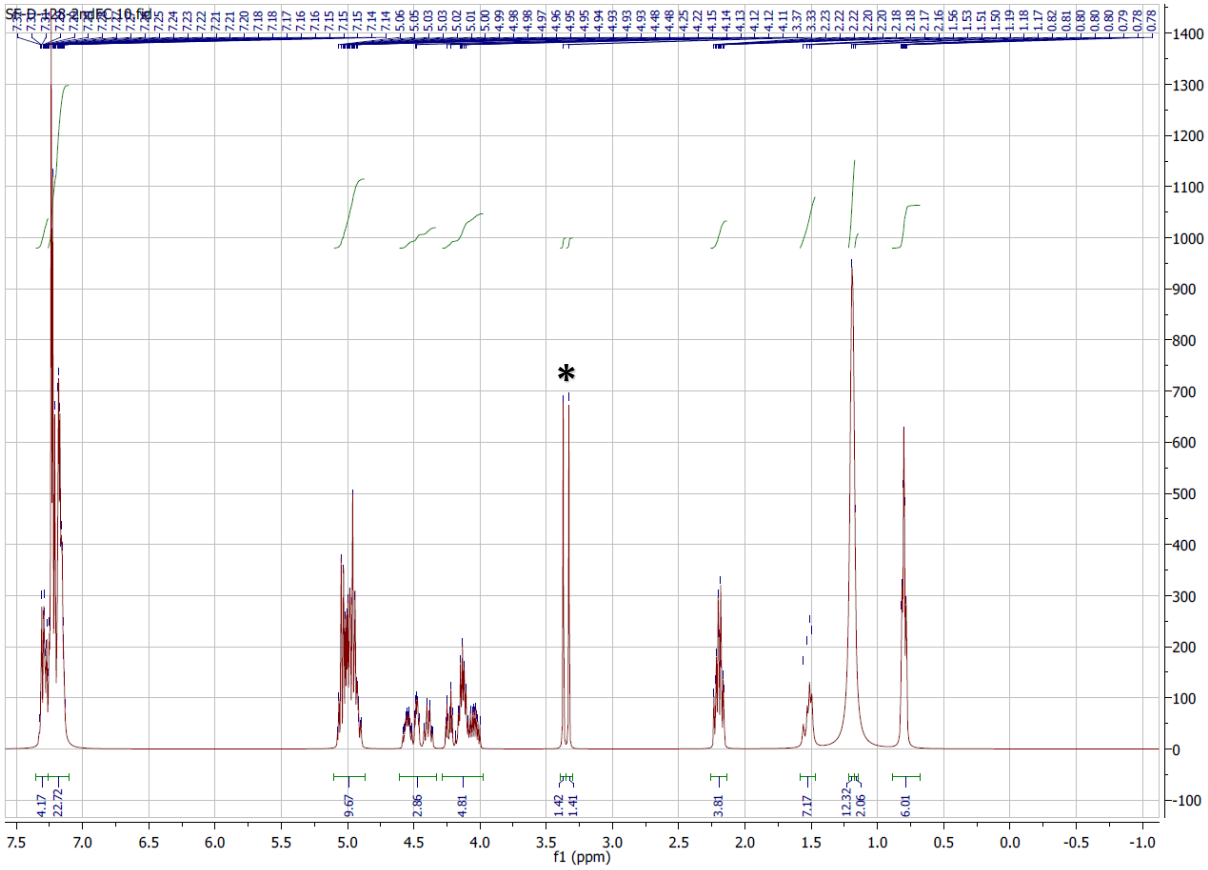

Figure **30** ^{1}H NMR of compound **11** measured in $CDCl_3$.

The other lipid tail analogues phosphoramidites (Section 3.1.3, compounds **38**, **41** and **44**) were coupled to the unmodified inositol ring precursor (protected with a MEM group at the 6-OH), to strictly account for lipid tail variances during SAR studies. Since no changes to the inositol ring had to be made for these steps, it was envisaged to synthesize the lipid tail modified PI(4,5)P_2 analogues using the solid phase strategy developed by the lab[126], provided that the total synthesis would be similar, except for the use of different lipid tails in the second last step of the synthesis.

With the help of Dr. Sven Stadlbauer, a former postdoctoral fellow in the Köhn group, the solid-phase synthesis of the phenylpropanol lipid tail PI(4,5)P_2 analogue was achieved, albeit with very low yields and amounts. The synthesis of the di-carbamate and di-adamantane lipid tail PI(4,5)P_2 analogues was, however, not successful using the solid-phase methodology, especially for the latter. Re-synthesis of the di-carbamate PI(4,5)P_2 analogue was repeated at larger scales using solid phase synthesis, which required the need of excess valuable reagents. It is believed that the di-adamantane PI(4,5)P_2 analogue was not successful because of the bulkiness of the adamantane molecules, which could hinder its passage through the resin mesh for coupling. It was therefore decided to

synthesize it using solution phase synthesis. Thus the di-adamantane glycerol phosphoramidite was resynthesized and purified as described already. The reaction steps are shown in Scheme 18, and show the selective MEM protection at the 6-*O* position after TBDPS and Benzoyl protection. Cleaving the TBDPS protecting group would leave the most reactive 1-OH free (**32**) for coupling to the phosphoramidite containing the lipid tails, a very fast organic reaction in solution.

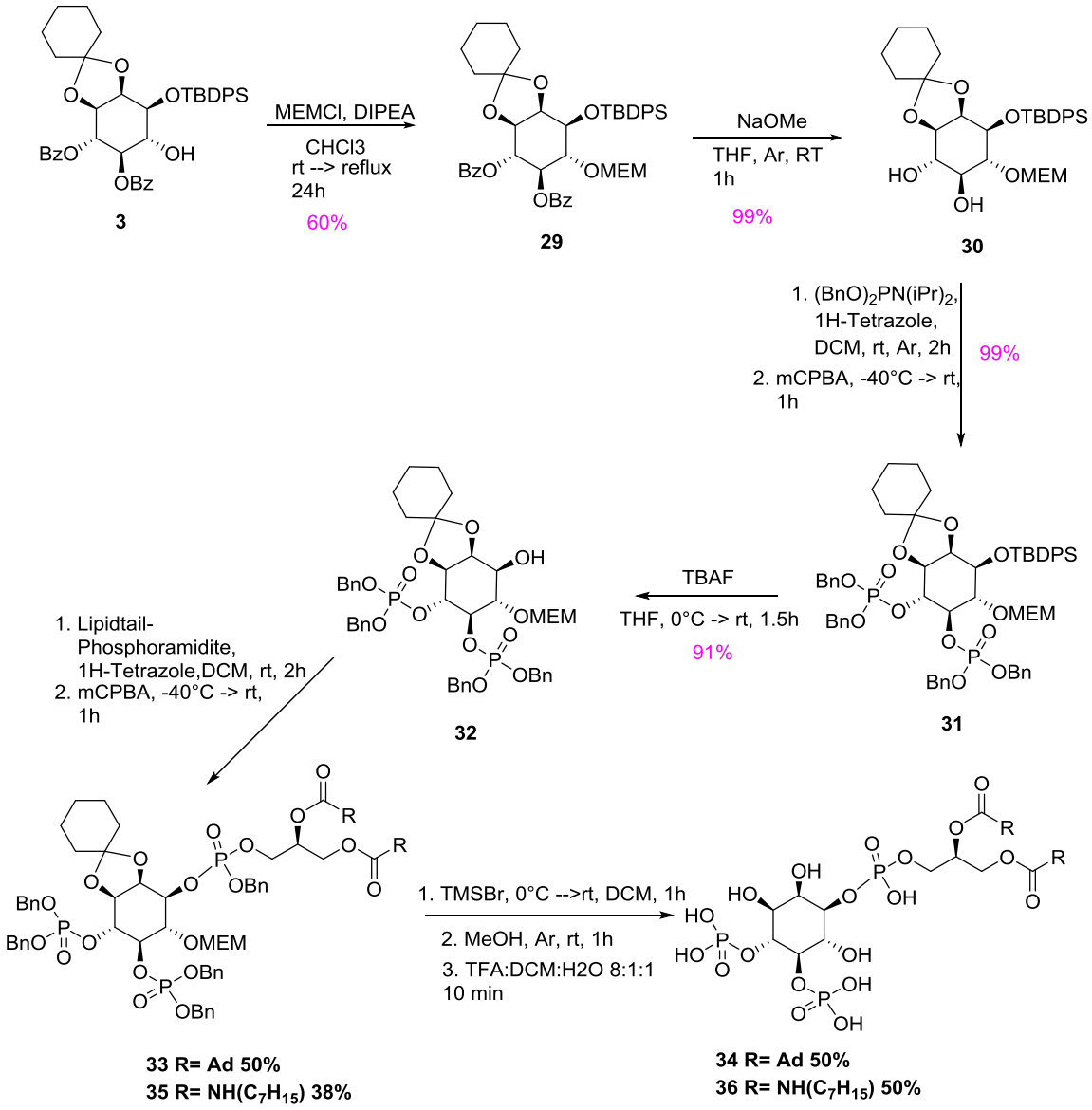

Scheme **18** Solution synthesis of the lipid modified PI(4,5)P_2 analogues. The last reaction step, which involves the overall deprotection of 33 and 35, is described in section 3.1.4.2.

Using this solution-phase route, three lipid tail modified analogues would be synthesized and the route compared to the reported solid phase syntheses, according to practicality.

This shows the importance of versatility in methods for achieving the most desired results.

3.1.4.2. Global deprotection

The deprotection of all attached protecting groups with TMSBr was conducted after the method of Köhn *et al*[126] (Scheme 19). The starting material dissolved in THF was cooled to 0°C, before TMSBr was added. After stirring for 1h, the solvent and the unreacted TMSBr were evaporated under reduced pressure and the precipitate dissolved in MeOH. This had first been attempted by evaporating on the rotary evaporator under inert conditions, but that resulted in total loss of the product. After evaporating under reduced pressure, the reaction mixture was stirred for another hour in MeOH and then evaporated (again, under reduced pressure), to yield the final product. The reactions with all compounds gave a quantitative yield. The compounds were analyzed by ^{1}H- NMR, ^{13}C-NMR, ^{31}P- NMR and HR- MS. After optimization of the deprotection strategy, in the ^{1}H-NMR spectra of the final compounds, it was obvious that the reaction was clean and proceeded without formation of side products, which makes a purification unnecessary. Usually, salt-exchange reactions would add a purification step to the final compounds, but salt exchange reactions were avoided for the analogues synthesized as part of this work (see section **3.1.4.3.**) An example of a free-acid final product is shown in Figure 31, for the analysis of compound **12**.

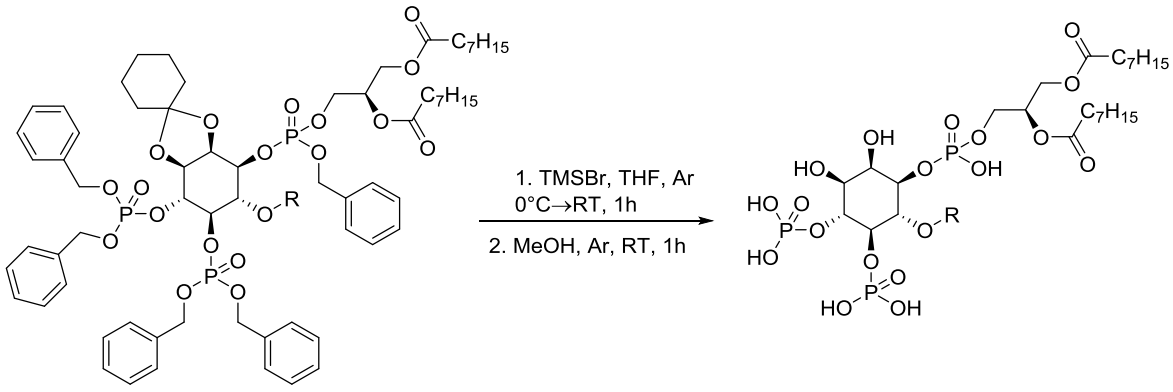

11 R= Me
17 R= Et
51 R= MEM

12 R= Me 80%
18 R=Et 70%
52 R= H 85%

Scheme **19** Global deprotection reaction for compounds **12**, **18** and **52.**

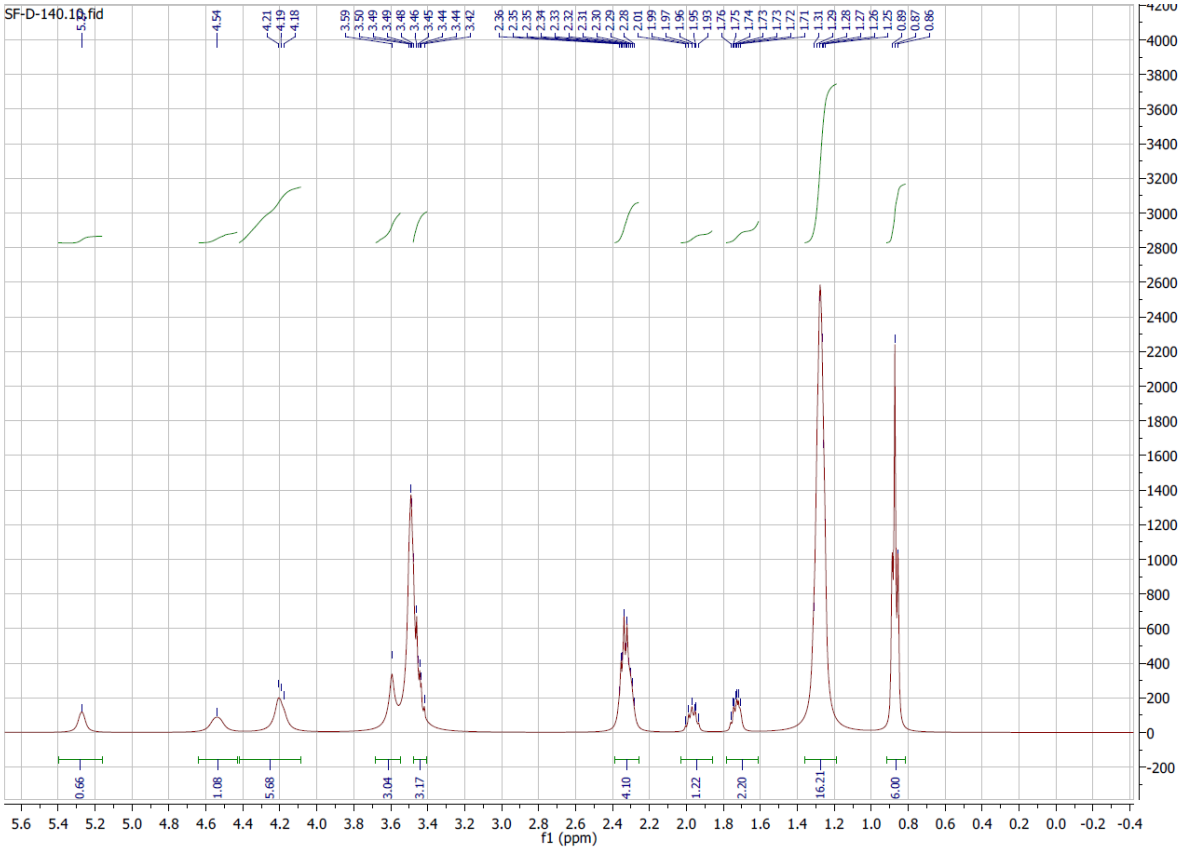

Figure **31** ^{1}H NMR of compound **12** measured in MeOH

For the deprotection of the trimethylated analogue, TMSBr was avoided, not only to avoid possible degradation of the very valuable compound **27** during the synthesis with a harsh reagent, but also because the only PGs to deprotect were benzyl groups, and for this, a lot of other cleaner methods were possible. The chosen method for deprotection of **27** was hydrogenation in glacial acetic acid, as this method would afford the clean product after freeze drying the solvent once the reaction is done (Scheme 20). The compounds were analyzed by ^{1}H- NMR, ^{13}C- NMR, ^{31}P- NMR and HR- MS.

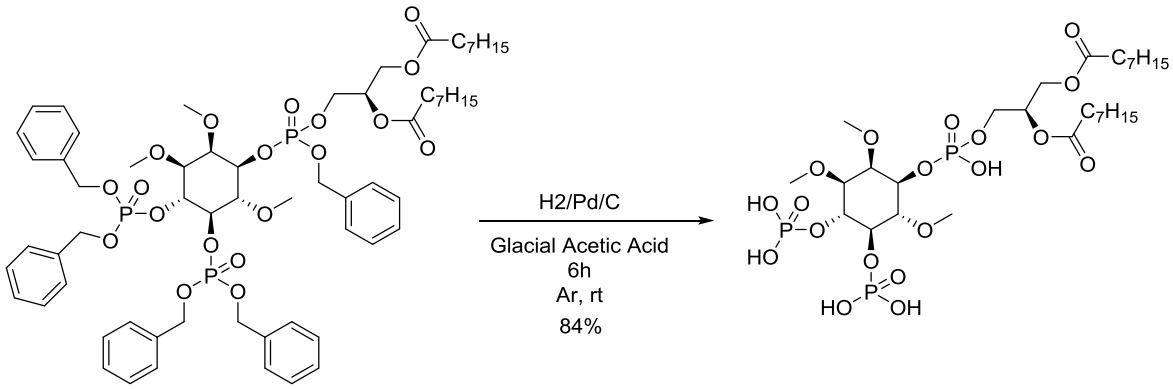

27 28

Scheme **20** Deprotection of compound 27, yielding the final compound 28 as a free acid.

For the deprotection of the other lipid tail modified compounds (**33** and **35**), TMSBr was not sufficient for full deprotection, and an additional step involving the use of TFA had to be done to get rid of the cyclohexylidene ketal (See *Chapter 5*, Section **5.2.3**).

3.1.4.3. Salt exchange of the final compounds

The conversion of the final compounds (free acids) to the sodium salts by ion exchange (Na form) was planned as the final step of the synthetic strategy, as was done in other works, including that of Koehn *et. al*[99,100,120]. This step, which would be considered as a purification step, counters every lost proton during deprotection steps: purification by ion exchange is used to remove contaminating acids, alkali metals, salts or mixtures from non-ionized or slightly ionized organic or in-organic substances. Salt exchange using the Dowex® cation-exchange media resin had already been used for such compounds[126]. The ion exchange technology is a good means to remove or exchange contaminants present in low concentrations.

In the case of the synthesized free acid final compounds however, this step was not proven proficient, for a couple of reasons, the first being the running time until the resin is exhausted, which can be long (up to 48 hours). This could subsequently create a basic environment, which could lead to loss of esters or migration. Another reason is that any contaminant that is not ionised cannot be removed by ion exchange, which could explain the amount of remaining impurities after salt exchange. Figures 32 and 33 show the proton and phosphorus NMR spectra of compound **12** before and after salt exchange, respectively.

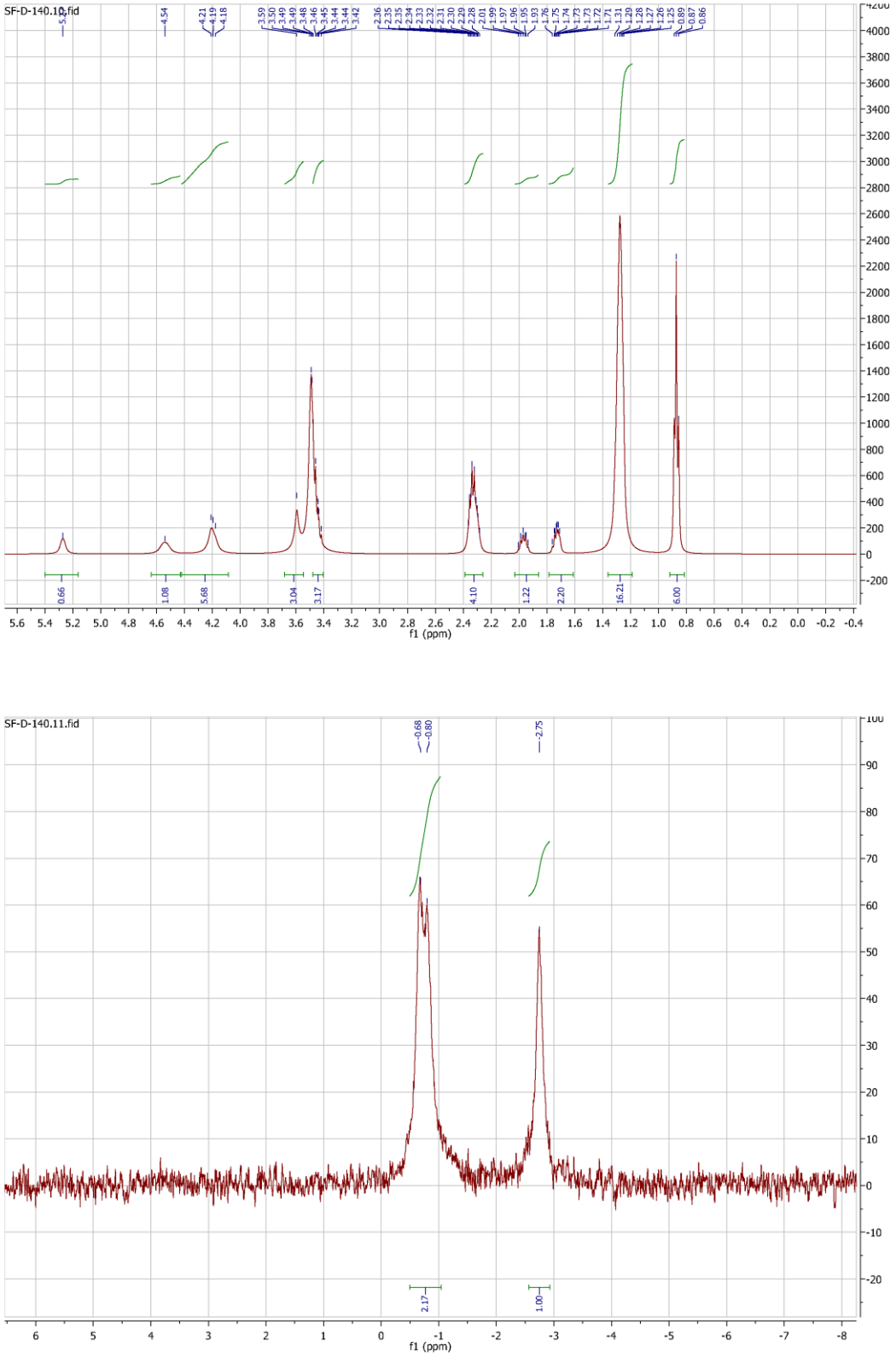

Figure **32** ^{31}P (below) and ^{1}H (above) NMR spectra of compound **12** before ion exchange.

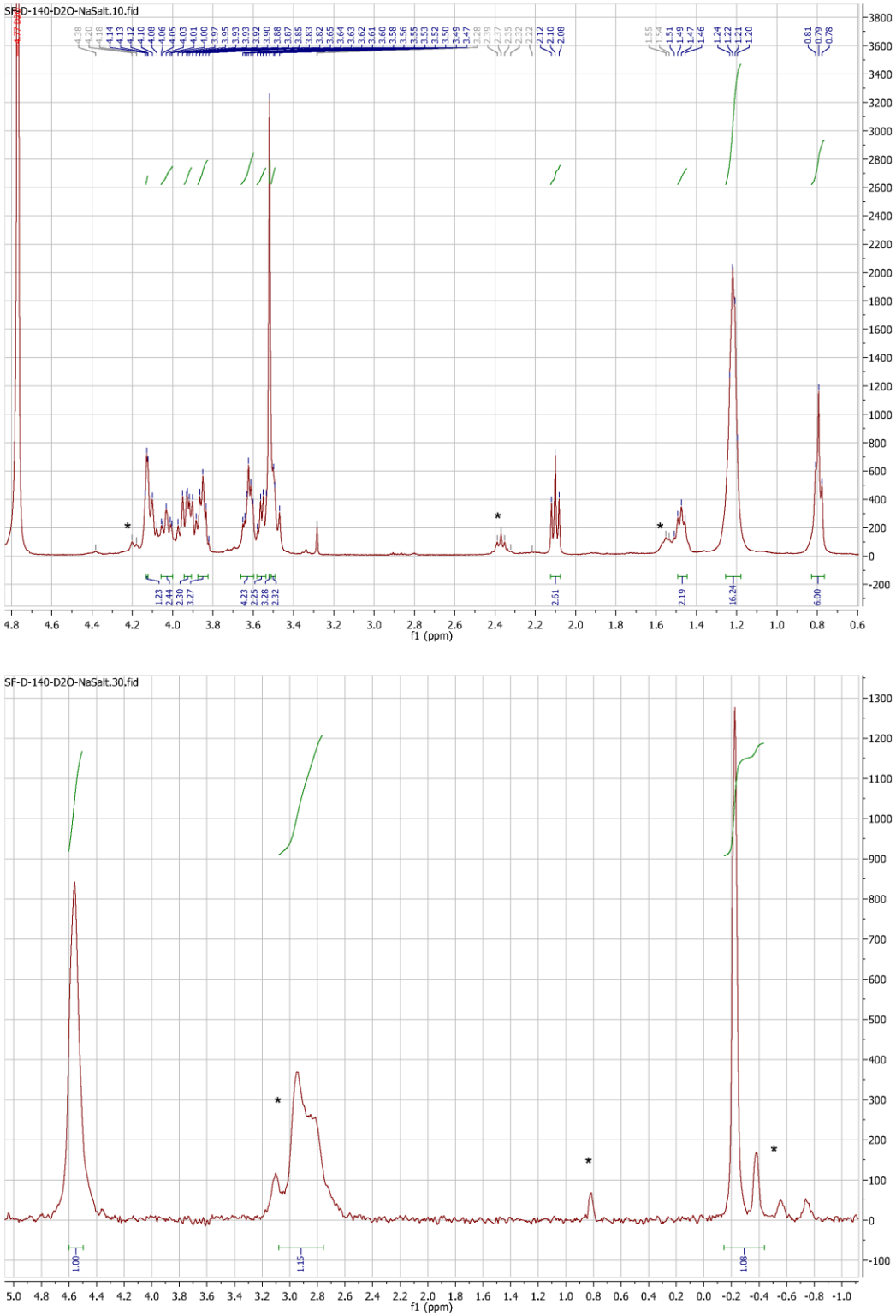

Figure **33** ^{31}P (below) and ^{1}H (above) NMR spectra of compound **12** after ion exchange. The impurities are marked with a "*".

The salt exchange step was thus an aborted step for the analogues. To make sure that this would not pose a problem for biochemical assays, as the non-ion exchanged analogues are more acidic, optimization of the assays using free acids instead of salts was done (see Section **3.2.**).

3.2. Biochemical evaluation of the PI(4,5)P$_2$ analogues

In order to assess if the modified PI(4,5)P$_2$-based compounds would be substrates of PRL-3, they were tested in a biochemical phosphatase assay. To investigate the hypothesis that introducing modifications could lead to selective recognition of the compounds, other PI(4,5)P$_2$-phosphatases were included in this study.

3.2.1. Activity assays with PRL-3 against PI(4,5)P$_2$ analogues

The six successfully synthesized and characterized PI(4,5)P$_2$ analogues (Figure 34) were available for testing, and were assayed for biological activity with PRL-3 using the commercially available Enzcheck assay[19], in addition to the original chiral PI(4,5)P$_2$-diC8 substrate as control (compound **52**, also synthesized in solution as part of this thesis work, see section 5.2.). The phosphatase activity of WT PRL-3 PI(4,5)P$_2$-based substrates was then analyzed. The phosphatase concentration was chosen to be in the low micro molar range, and thus quite high, because of the reported low activity of PRL-3 in vitro[25], and for the same reason, a high substrate concentration range was selected (25-250 µM). These conditions match previously reported ones[18,19,120].

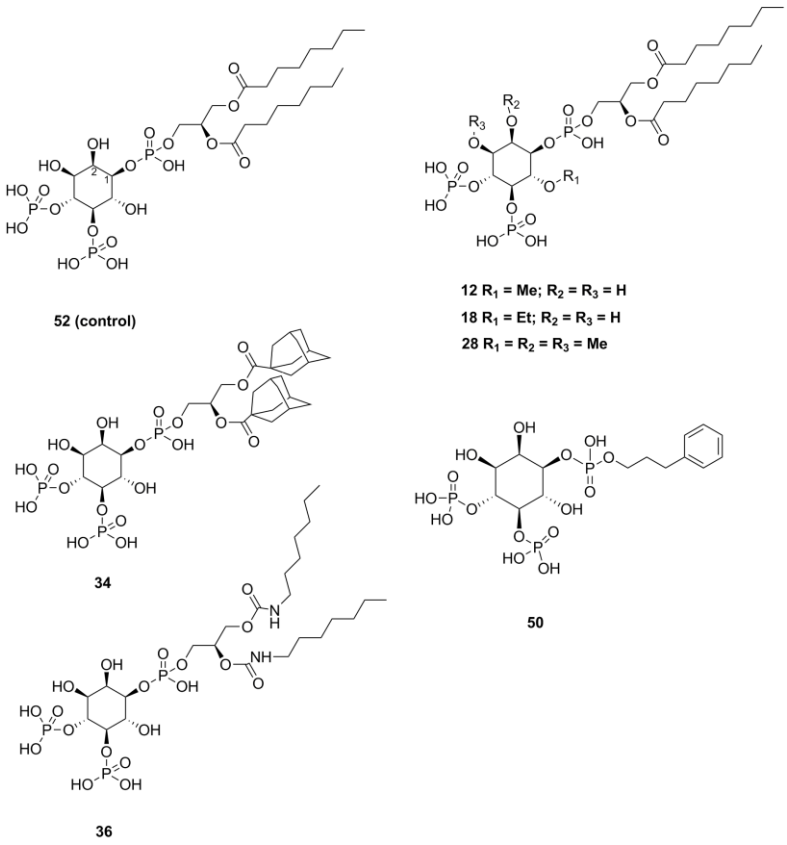

Figure **34** Structures of the PI(4,5)P$_2$ original substrate (**52**) and its 6 analogues (**12**, **18**, **28**, **34**, **36** and **50**).

The release of phosphate was monitored continuously over time. Each analogue was assayed at 5 different concentrations, twice in triplicates. The enzyme concentration was constant in all experiments, and so was the assay protocol (see Chapter 5). To account for possible changes in acidity of the well contents upon addition of the free-acid analogues, two control experiments were conducted prior to the assays to make sure that the free acid analogue (or substrate), would not perturb the pH of the reaction. First, a direct comparison between the salt form and the free acid form of the synthesized substrate was conducted using the assay, which showed similar results in phosphate release. Second, pH measurements before and after adding the free acid in the reaction wells showed that the acidity of the analogues did not change the pH; thus they were deemed compatible for the consequent experiments.

The release of phosphate from soluble PIP substrates carrying modifications either on the inositol ring (compounds **12**, **18** and **28**) or on the lipid chains (compounds **34**, **36** and **50**) by WT PRL-3 was continuously measured over 2 hours using the EnzChek assay. The dephosphorylation signal intensity was used to compare the substrate preferences of PRL-3 against the whole range of PI(4,5)P_2 analogues. The resulting substrate preference profiles are shown in Figures 35 and 36. The respective absorbance curve of each analogue, at different concentrations, is shown in Figure 35 (A-F). The initial velocities were then calculated from the slope of the linear part of the ensuing reaction, to generate the bar diagrams in Figure 36. These bar graphs allow quantitative analysis on the activity of the active analogues, and their significance with reference to the control (in % values). For compounds **36** and **50**, it was not possible to calculate the respective velocities as there was no slope that allowed this: the compounds were simply not active, and are not part of Figure 36.

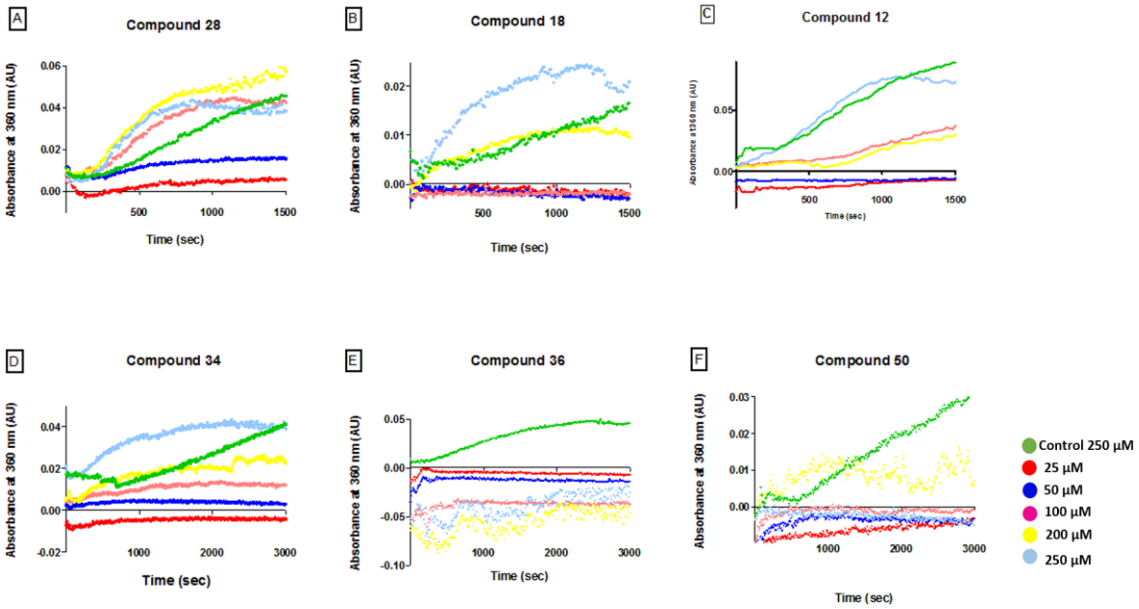

Figure **35** The dephosphorylation activity of PRL-3 toward the PI(4,5)P_2 analogues, at 5 different concentrations (25, 50, 100, 200 and 250 µM). The slopes are shown until 1500-3000 seconds of measurements because of the signal variation observed after that time point in all assays, which could either be due to the precipitation of the protein or the interaction of the analogues with the photoactive component in the assay. A) Absorbance measurements of compound **28**: the signal intensity at 100, 200, and 250 µM of this compound is higher than that of the natural substrate at 250 µM. B) Absorbance measurements of compound **18**: the signal intensity at 200 and 250 µM of this compound is higher than that of the natural substrate at 250 µM. C) Absorbance measurements of compound **34**: the signal intensity at 200 µM is comparable to that of the control, and that of 250 µM is higher than that of the control (at 250 µM). D) Absorbance measurements of compound **12**: although somewhat active, the signal intensity at 100 and 250 µM of this compound, is lower than that of the natural substrate. E) and F), Absorbance measurements of compounds **36** and **50**, respectively: those compounds were not active against PRL-3. Graphs are shown without error bars for clarity: the lower the signal intensity, the higher the relative error in the assay[18,19,120], leading to error bars that would mask other curves. An error was accounted for in Figure 36, where the slopes were quantified.

Before ongoing with the discussion on the analogues' biological activity, it is imperative to note that the assay appeared to give a strong variability with PRL-3 as a phosphatase. This is because PRL-3 does not follow a Michaelis-Menten trend, and because it shows only low enzymatic activity[18]. This is why PI(4,5)P_2 and its analogues' titration profiles reveal non-Michaelis–Menten kinetics, with sigmoidal curve shapes (Figure 35 - curves). Otherwise, such kinetics are not a general feature of the assay format, and the same kind of assay was actually used for the assessment of three other phosphatases which follow classical Michaelis–Menten profiles (see section **3.2.2.**). Other studies have also used this assay for classical Michaelis-Menten protein profiles[127]. A plausible reason for this could be the fact that PRL-3 is prone to oligomerize[128], and non-Michaelis–Menten behavior is

characteristic for oligomerizing enzymes[129], not to mention that phosphoinositides also have a propensity to oligomerize, making the issue less simple to tackle. Particularly with the analogues, the readout was noisy and poor, and the figure (curve) got unstable after a certain time point of measurement (1500 to 3000 seconds).

From what can be appreciated in Figures 35 and 36, the trialkylated analogue (**28**) shows the highest activity, which leads to reason that the more hydrophobic the inositol ring, the better the interaction, taking into consideration that the active site of PRL-3 is unusually shallow and hydrophobic, as opposed to other PTPs[20]. In fact, the 6-*O*-ethylated analogue (**18**) follows as second best, rather than the 6-*O*-methylated analogue (**12**) which suggests that the bulkier the group blocking the inositol's 6-OH, the better the interaction. However, more data should be generated on this, as the assay did not perform consistently with this analogue (**18**). In fact, two concentrations (25 and 50 μM) had to be excluded from the bar graphs for that compound, because the generated values were neither reproducible nor analyzable in the context of the rest of the data. Compound **12**, which has the least structural changes compared to the parent compound, showed the fewest changes compared to the control.

These results can be taken as a first stage towards understanding the specificity of PRL-3 in terms of catalytic reaction with its substrates. This can be supported by the fact that the three other analogues, which are only modified at the lipid tail part of the molecule (**34**, **36** and **50**) did not show significant activity compared with the inositol-modified ones (**12**, **18** and **28**) (Figure 35). Actually, only compound **34** was active amongst the three lipid tail modified analogues. This analogue, bearing a double chain of adamantanes instead of the unsaturated diC8 chains, appears to be slightly more active than the control. The analogues bearing carbamate and phenylpropanol chains were not active at all. This shows, first of all, that the diC8 chains are important for binding to PRL-3, as reported previously[120], and, second, that complete aberration of a double chain (as in **50**) or replacement of the esters (as in **36**) by a different atom did not show any improvement for interaction. However, it is not entirely clear why PRL-3 lacks phosphatase activity against compound **36** in this assay, given the similarity to the control compound. This might reflect that the nature of the lipid connection to the glycerol is of importance regarding the binding affinity of the compounds toward PRL-3.

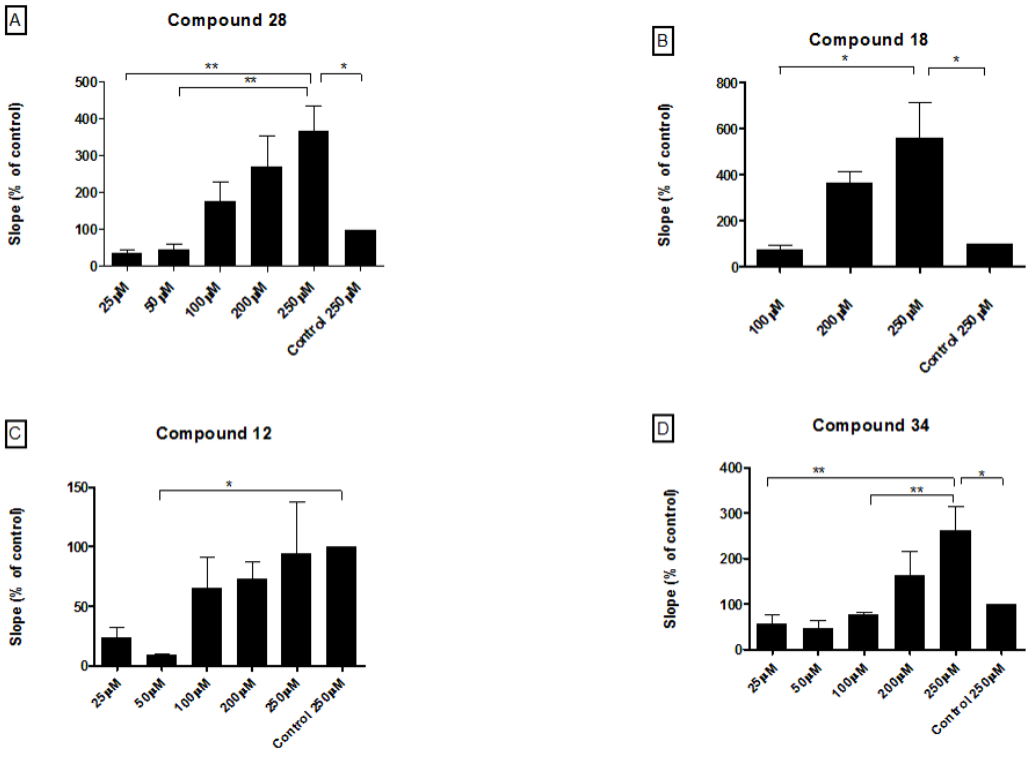

Figure **36** Results of the compounds activity towards PRL-3. PRL-3 (6 µM) was incubated with analogues at different concentrations and the assay conducted at 25 °C. Data are shown as mean ± SD. Statistics: *** p<0.0002; **** p<0.0001; ns – not significant. A) Compound 28 results. Tukey's multiple comparison test: ns: Control 250 µM vs 250 µM. B) compound 18 results: Tukey's multiple comparison test: ns: 100uM vs 250uM; 200uM vs 250uM; 250uM vs Control 250uM. Concentrations of 25 and 50µM were omitted because the data was not analyzable because it was too noisy. C) Compound 34 results: Tukey's multiple comparison test: ns: 25uM vs 50uM; 25uM vs 100uM; 25uM vs 200uM; 25uM vs Control 250uM; 50uM vs 100uM; 50uM vs 200uM; 50uM vs Control 250uM; 100uM vs 200uM; 100uM vs Control 250uM; 200uM vs 250uM; 200uM vs Control 250uM. D) Compound 12 results: Tukey's multiple comparison test: only the displayed relationship is significant, all others are not.

Thus, the inositol modified analogues show increased activity compared to both the control substrate and the lipid-modified substrates with PRL-3. Therefore, these compounds can be the basis for prolific structure activity relationship studies with PRL-3.

3.2.2. Activity assays with other phosphatases against PI(4,5)P_2 analogues

As stated earlier, phosphoinositide metabolism is tightly regulated by a set of specific kinases responsible for synthesis of phosphoinositides, and phosphatases that temporally and spatially catalyze phosphoinositide dephosphorylation[16]. Of these phosphatases, those, apart from PRL-3, that are known to dephosphorylate PI(4,5)P_2 were of specific interest for this study, as they would potentially hold an activity against the synthesized PI(4,5)P_2 analogues.

Using the DEPOD database[12], a literature review on PI(4,5)P_2 dephosphorylating phosphatases was conducted, with careful consideration of the type of activity assays used in the studies, and the availability of a recombinant protein to test in *in vitro* activity assays. Three phosphatases, that represent different families and are commercially available as recombinant proteins, were chosen and purchased for assaying the analogues in activity assays. These phosphatases are INPP5E, which belongs to the large family of the 5-phosphatases that cleave the 5 position phosphate of several inositol phosphates and lipids including PI(4,5)P_2[130]; OCRL, another inositol 5-phosphatase whose preferred substrate is PI(4,5)P_2, and that has been shown to promote biogenesis of membrane-trafficking intermediates through binding to this substrate[131]; and lastly, the SYNJ1 (Synaptojanin 1) phosphatase, which has recently been shown to modulate membrane curvature through degradation of its substrate PI(4,5)P_2[132]. The phosphatases were assayed like PRL-3 with the Enzchek assay[19], against the control phosphoinositide PI(4,5)P_2 and the synthesized analogues of it. An optimization of the activity assay was to be executed beforehand, as these proteins' activities had not been measured with this specific assay type to our knowledge.

The results of these assays, shown in Figure 37, provided substantial information on the specificity of the four phosphatases not only against PI(4,5)P_2 itself, but also against the different PI(4,5)P_2 analogues. As can be seen from Figure 37, the compounds that show significant activity towards the three PI(4,5)P_2–metabolizing phosphatases are the lipid-modified PI(4,5)P_2 analogues **34** and **36**. Compound **50** did not show significant activity with any of the phosphatases, further corroborating that the double lipid chain is important for binding of the substrate. Similar to PRL-3, OCRL is also weakly active *in vitro*. Interestingly, the inositol ring-modified analogues did not show any activity with SYNJ1 and INPP5E. This underlines the specificity of the inositol ring alkylated PI(4,5)P_2 analogues towards PRL-3, based on the hydrophobicity of its active site.

SYNJ1 and INPP5E are known to possess a basic region near their active site. Besides the 5-phosphatase domain, SYNJ1 bears an N-terminal Sac1 domain, which was later found to be a member of a new family of PI phosphatases[133]. The large *C*-terminal portion in SYNJ1 is a divergent proline-rich region (PRD), which contains a string of peptide motifs that mediate binding with a variety of endocytic proteins such as amphiphysin[134]. Furthermore, biochemical characterization showed that the 5 phosphatase domain dephosphorylates PI(4,5)P_2 at the 5-position of the inositol ring[15]. INPP5E was also shown to have a PRD region preceding the inositol polyphosphate phosphatase catalytic domain, making the catalytic active site's milieu largely basic[135], which could explain why

it could not accommodate the hydrophobic analogues in its catalytic pocket. On the other hand, OCRL does present a hydrophobic patch and a sequence motif defining the binding of the aliphatic moiety of the substrates to it.

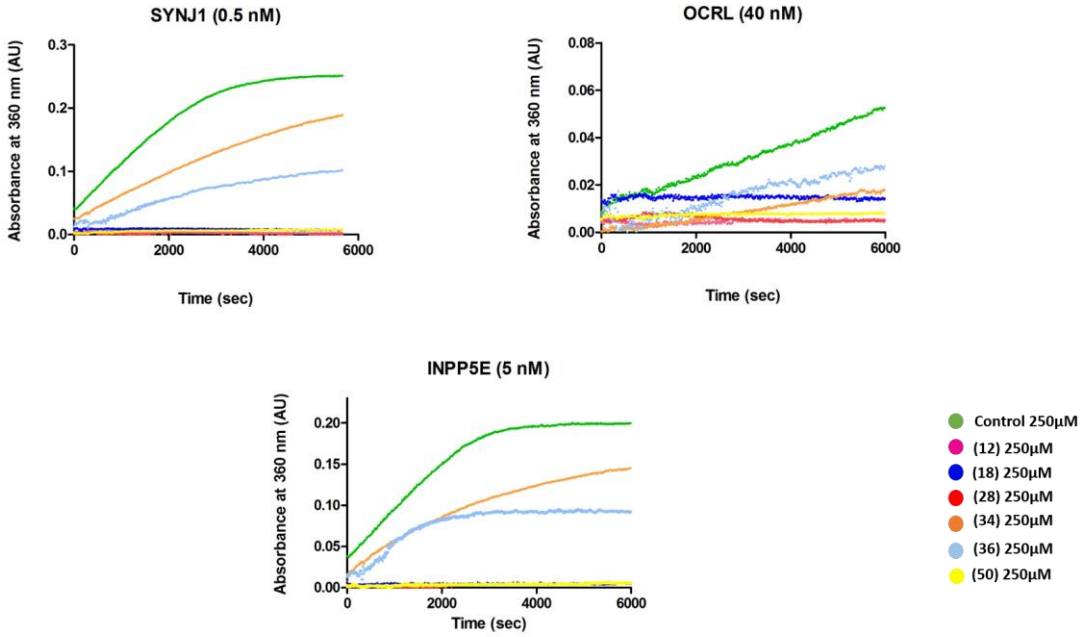

Figure **37** Activity of the 6 analogues with three different PI(4,5)P_2-metabolizing phosphatases, with respect to the parent substrate (control) PI(4,5)P_2.

The PH domain of OCRL actually lacks the basic PI(4,5)P_2 binding pocket present in the PH domain of PLCδ for instance[136]. One could then argue that this is why it might accommodate a hydrophobic analog like the inositol-modified PIP analogues. Still, these analogues show no significant activity with OCRL as opposed to the activity they show with PRL-3, and can thus still pose as specific substrates to the latter.

In addition, the analogues which actually show activity with SYNJ1, INPP5E and OCRL show no significant activity with PRL-3, further underlining that the main element of specificity would be the alkylated, increasingly hydrophobic inositol ring. Thus, these analogues could act as interesting tool compounds which could be further modified, leading to further understanding of the specific mechanisms for substrate recognition of PRL-3 to eventually create a selective inhibitor from the gained knowledge.

3.3. Virtual screening tools to aid inhibitor search using PI(4,5)P_2

During this thesis work, an alternative approach for designing PRL-3 probes and eventually inhibitors was explored, using the PI(4,5)P_2 molecule as a starting point for virtual screening of similar molecules. The Ultrafast Shape Recognition (USR) method[54], which can identify similarly shaped compounds within the largest molecular databases was applied to the PI(4,5)P_2 head-group in collaboration with Pedro Ballester, a former colleague from the EBI (Hinxton, UK), and the Chemical Biology Core Facility (EMBL, Heidelberg). Only the head-group of the template molecule was chosen and used because, firstly, the full molecule was too big for the computational system, and secondly, the phosphoinositide head is the part involved in enzymatic activity with the phosphatase (contains the cleavable phosphate group).

3.3.1. USR screening based on PI(4,5)P_2, data filtering, clustering and drug design

A set of screened compounds whose USR score30 was high (>0.8), was obtained. A second screen was made, and further filtering, clustering and analysis were done to make a rational choice on which molecules can be sourced or synthesized for testing PRL- 3's activity by biochemical screening. After obtaining a list of hits from a USR run, and with the help of Dr. Ulrike Uhrig from the Chemical Biology Core facility (EMBL, Heidelberg), 483 compounds were exported as structures from the ZINC database, and duplicates (same compound, different vendor) were removed, which left us with 216 compounds. The assignment into families based on 2D similarities resulted in 42 clusters and 35 singletons. Using computational chemistry methods (see chapter 5.1) to make a selection of the "best" representative of a cluster, a series of compounds were selected for synthesis and biochemical activity screening.

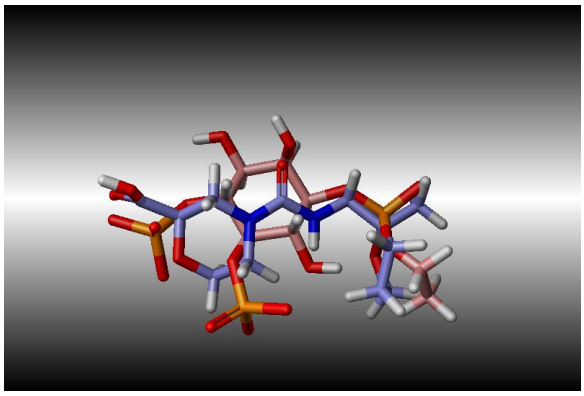

Figure **38** Overlay Sstructure of one of the identified hits from the USR run (compound in blue) with the original PI(4,5)P_2 head group (compound in yellow).

Figure 38 shows an example of a hit, which closely resembles the given lead molecule (PI(4,5)P_2 head-group in this case). In addition, since it is known that the lipid tails are crucial for binding to PRL-3 in the original molecule[120] (see chapter 3.2), the synthesis of these hits was planned to include attachment of the diC8 lipid chains before testing them on PRL-3. This necessitated devising a synthetic route for each of the finally selected target molecules. The potential target molecules are depicted in Figure 39.

Although the screening was carried out using a database of commercially available compounds, it turned out that all the potent compounds found were only theoretically commercially available and thus required custom synthesis from the vendor. This was found to be prohibitively expensive. Unfortunately, many of the compounds imposed a tough or impossible synthetic challenge. Nevertheless, two target molecules were identified (Figure 39) to be synthesized.

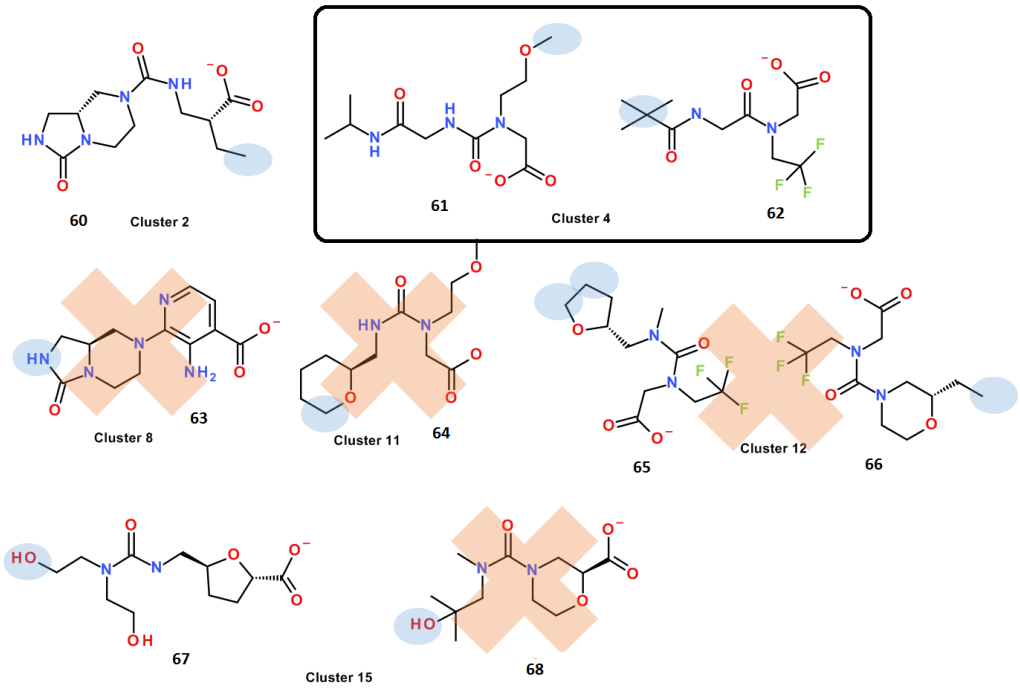

Figure **39** Target compounds from the results of the PI(4,5)P_2 similarity screening study. The areas shown in blue depict the location of the lipid tail attachment based on structural overlay. The crossed out molecules correspond to ruled out targets due to the synthetic challenges.

3.3.2. Synthesis of a potential target molecule from the similarity screen

With the collaboration of the Chemical Biology Core Facility at EMBL, Heidelberg, two target molecules were planned to be synthesized (Chapter 5.2.5). These were deemed to be the best hits according to computational overlay experiments done by Dr. Ulrike Uhrig (Figure 39, compound **61** and **62**). Dr. Mascha Jaekel successfully synthesized and characterized the molecules in Figure 40. Compound **61** was synthetically more difficult, and gave the hydantoin (**70**, Figure 40-C, Chapter 5.2.5) as major side product. The successfully synthesized molecule **62** (Figure 40-A), in addition to its protected precursor molecule **69** and the major side product **70** of the other target (Figure 40-C) were tested in inhibition assays (DiFMUP)[137] against PRL-3.

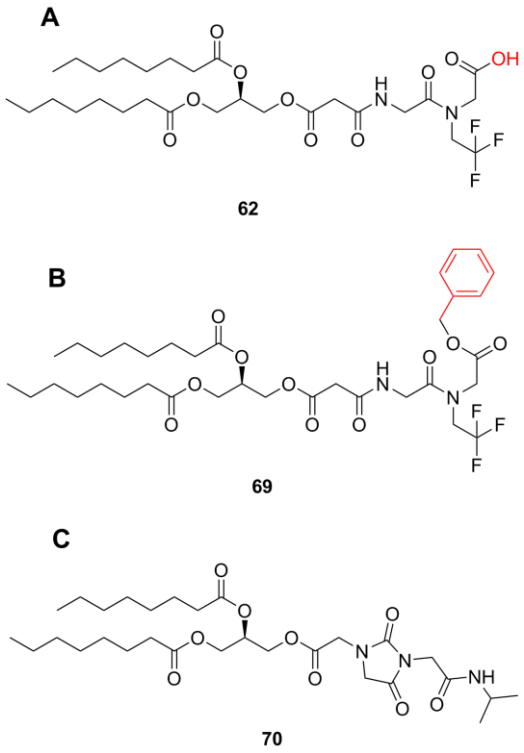

Figure **40** Synthesized molecules based on the USR screen, which were tested using inhibition assays against PRL-3 (chapter 3.3.3). A) Successfully synthesized target molecule. B) Precursor of A; with the carboxylic acid protected with a Bn group marked in red. C) Side product of the second target molecule (Chapter 5.2.5).

3.3.3. Inhibition assays with the synthesized targets

The abovementioned molecules were investigated for inhibition using 6,8-difluoro-4-methylumbelliferyl phosphate (DiFMUP) as a PRL-3 substrate[53] Judith Weyershaeuser, a PhD student in the Koehn group, performed the inhibition assays. The results of the inhibition assays are shown in Figure 41.

Excitingly, the first compound, **62**, which was the one successfully synthesized as an analogue of the hit in cluster 4 (Figures 39 and 40) showed inhibitory activity of PRL-3,

albeit with high concentrations (compound concentrations of 600 µM and 300 µM showed full inhibition of PRL-3), with an IC_{50} of 185 uM. The two other compounds **69** and **70** were not biologically active, and did not show any inhibition of PRL-3. The interesting observation here was the activity difference between compound **62** and its benzyl ester **69,** showing that the negative charges of the carboxylic acid are required for activity. As an outlook, it would be interesting to conduct structural overlay studies, to

account whether this carboxylic acid overlaps with the 5-or 4-phosphate group, helping to understand if this entity binds similarly to PRL-3 as the phosphate in the $PI(4,5)P_2$ substrate.

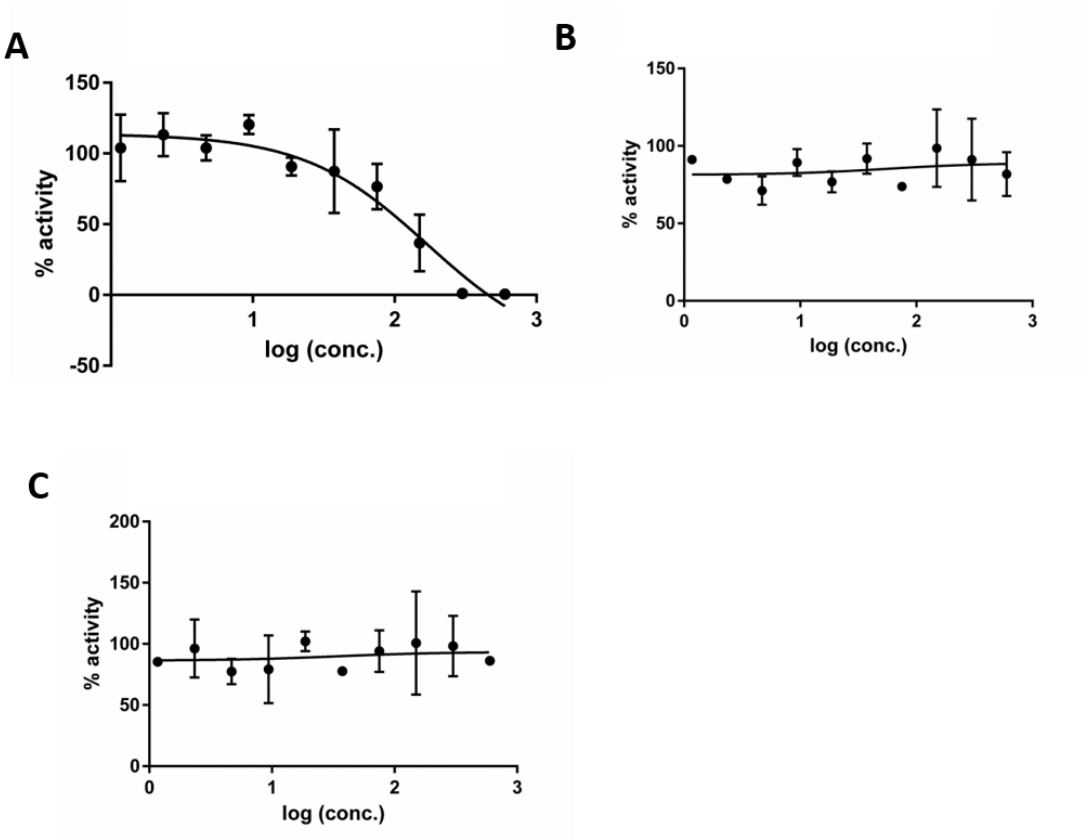

Figure **41** Results of the DiFMUP assay with the three synthesized compounds. The compound is **A)**, **B)** and **C)** belong to compounds **62**, **69** and **70**, respectively. **A)** compound **62**, depicted in Figure **40-A**, shows inhibition of PRL-3 activity with a mean IC_{50} value of 185 µM ± 22. B) and C) each show the inhibition measurement for compounds **69** (Figure **40-B**) and compound **70** (Figure **40-C**), with no inhibition of PRL-3.

Obviously, more SAR studies should be undertaken on such a compound, if it is even reasonable to consider it as an "optimizable" lead given the high IC_{50}. Nevertheless, in spite of the challenges regarding the synthesis of the compounds, the synthesis of only one hit molecule gave a molecule that inhibits PRL-3, which is a remarkable result and demonstrates the feasibility of this approach. The inhibitor has no structural similarity with any previously published inhibitors[27]. In addition, this inhibitor can pose as interesting analog for more lead design ideas for generating further $PI(4,5)P_2$ analogues/inhibitors; and it can potentially offer new valuable information for new templates in shape similarity *in silico* assays. Additionally, **62** could be overlayed, in future experiments, with the natural substrate to draw information on binding, by, for instance, identify which phosphate is implicated in the enzymatic reaction.

Chapter 4. Conclusion and Outlook

4.1. Total synthesis of novel PI(4,5)P_2 analogues

In this work, I have successfully established the synthetic route for the analogues **12**, **18**, **28**, **34**, **36** and **50,** which are modified PI(4,5)P_2 analogues, bearing chemical modifications either on the inositol ring or on the lipid tail moiety. Inferring the reasons for issues and solving the bottlenecks in the solution synthesis, particularly the selective alkylations on the free, less reactive OH groups of the inositol ring, was resolved satisfactorily. Furthermore, the route which was tested with the synthesis of **12** validated the synthetic approach that was established with the rest of the compounds.

The overall consideration of the established synthetic routes shows that the developed approach for the different reaction steps can be used to synthesize more and varied modified compounds in the pursuit of enlarging the existing library of PI(4,5)P_2 analogues. Moreover, these synthetic pathways can set the basis for differently modified analogues, such as analogues bearing modifications at the phosphate group moiety. Such modifications can be sulfurization instead of oxidation of the phosphate groups, inserting methylene phosphonates as phosphate analogues, or replacing the phosphate groups by cyclic compounds which could mimic the electronegative environment (examples include tetronic acids and carboxylic acids). The larger the library of such analogues, the easier it would be to combine various modifications in order to design the best potent probe (inhibitor/modulator).

Furthermore, I applied the solid phase strategy developed by my group in order to synthesize analogues bearing lipid tail modifications, which illuminates the possibility of using different synthetic strategies depending on the alteration nature of the compound. This offers back-up solutions to synthetic challenges whenever a compound proves to be challenging to synthesize.

As an outlook, these compounds could be employed to broaden the understanding of conditions for binding behavior of PI(4,5)P_2-binding and metabolizing proteins in the cell, thereby providing information about their efficacy in the treatment of diseases.

4.2. Biochemical application of unnatural PIP analogues as phosphatase substrates

Effectively, the six analogues synthesized as part of this work were used for SAR studies with PRL-3, helping to understand the structure activity relationships between PRL-3, a metastasis promoting phosphatase, and its recently discovered natural substrate PI(4,5)P_2. The inositol-modified analogues have shown significant biological activity with PRL-3, compared to the lipid tail-modified analogues and the control PI(4,5)P_2-diC8 compound. The most active compound was the trialkylated PI(4,5)P_2 **28**, where all the free hydroxyl groups were blocked, underlying the importance of the hydrophobicity required for better binding at PRL-3's remarkably hydrophobic active site. The phosphatase activity assays would still need to be optimized with such analogues nevertheless, as the combination of low-activity phosphatase, labile compounds and kinetics other than Michaelis-Menten makes it hard to extract very clear results.

In addition, the same analogues were used for SAR studies with three other PI(4,5)P_2–metabolizing phosphatases: SYNJ1, OCRL and INPP5E, aiming at deciphering the differences in activity of the analogues towards different phosphatases, which share the same natural substrate. Interestingly, the analogues that showed increased activity with PRL-3 did not show any significant activity with the other phosphatases, and those that proved to be poor substrates for PRL-3 turned out to have more significant activity with the other phosphatases. This sets the grounds for specificity of the inositol-ring modified PI(4,5)P_2 analogues toward PRL-3, as the other phosphatases can accommodate more hydrophilic substrates due to their generally basic catalytic active site (particularly SYNJ1 and INPP5E). The results show that these analogues, beyond being valuable tools for studying the activity of a specific target, can also act as specific modulators to clarify activity variance amongst diverse targets.

4.3. Computational power: a potential for inhibitor quest

The interest in developing inhibitors for oncogenic phosphatases such as PRL-3 was a stimulating complement in the context of this project's chemistry, and since computational methods were already accessible for screening small molecules which could mimic a known substrate or inhibitor, I thought of using the natural substrate as a template to search for similar small molecules which could help add more information to PRL-3's SAR studies. Using PI(4,5)P_2 as a query molecule in such computational software

was not an easy task though because of its relatively big structure. Still, the method was used on the head group by our collaborators (Pedro Ballester and the CBCF), which was known to be the direct interactor with PRL-3's active site, and generated a list of hits, from which a target molecule was successfully synthesized, bearing the diC8 lipid chains as a required moiety for binding. This final molecule was shown to inhibit PRL-3, albeit with high concentrations. This was surprisingly positive, as it could support the scientific reasoning behind employing a computational-experimental system as such.

In summary, this sets the ground for imminent exciting approaches that can combine predictive computational tools, total organic synthesis of natural products analogues, and medicinal chemistry-oriented SAR techniques to decipher, in the most effective way, the intricate mechanisms of oncogenic phosphatases, potentially making them "druggable" despite the challenges.

Chapter 5. Experimental

5.1. General: chemicals and methods

All the chemicals and anhydrous solvents used were obtained from commercial suppliers (Sigma-Aldrich, VWR, Acros Organics). The chiral starting material D-2,3-cyclohexylidene myo-inositol was purchased from SiChem GmbH, Bremen, Germany. The Wang resin (200-400 mesh, 0.88 mmol/g) was obtained from Bachem. The resin intermediates were dried properly on high vaccum before subjecting to the subsequent reactions.

^{1}H, ^{13}C and ^{31}P nuclear magnetic Resonance (NMR) spectra were recorded on a 400 MHz Bruker Avance DPX. Chemical shifts (δ) are measured in ppm and coupling constants (J) are given in Hz. (^{1}H and ^{13}C chemical shifts were referenced to the solvent peaks (7.26 and 77.0 ppm for $CDCl_3$, 4.84 and 49.05 for CD_3OD). Splitting patterns are designated as follows: s = singlet, d = doublet, t = triplet, q = quartet, m = multiplet, brs = broad singlet, dd = doublet of doublet and dt = doublet of triplet. ^{13}C and ^{31}P spectra were broadband hydrogen decoupled. For ^{1}H-assignment COSY and HMQC spectra were recorded. Assignment abbreviations for chemical groups: Ph = phenyl, cy = cyclohexylidene, myo = myo-inositol, MEM = methoxyethoxymethyl.

HPLC analysis and purifications were carried out on a Shimadzu High Performance Liquid Chromatograph/Mass Spectrometer LCMS-2010EV with a UV/Vis Photodiode array detector SPD-M20A Prominence. For the analytical and semipreparative injections the solvent delivery module LC-20AD was used. And for the preparative injections the LC pump unit LC-8A was used. The analytical column was a Macherey Nagel C_{18} EC 250/4.0 NUCLEODUR 100-5 C18 ec. For semipreparative separations the column was a Macherey Nagel C18 VP 250/10 NUCLEODUR 110-5 C18 ec and for preparative separations a Macherey Nagel C18 VP 250/21 NUCLEODUR 100-5 C18 ec column was used. Mass spectra (ESI) were recorded using a Waters Micromass ZQ mass spectrometer.

High resolution mass spectra were recorded using a MaXis II Q-Tof mass spectrometer (Bruker Daltonics) and at the University of Heidelberg with a Bruker ApexQe hybrid 9.4 T FT-ICR. Masses are given as m/z (% intensity).

ESI+-MS spectra were measured with an Agilent Infinity 1290 UPLC-MS System. An Acquity UPLC BEH C18 column (1.7µm; 2.1x50mm) was used at 40°C with an injected volume of 3 µL, a flow rate of 1mL/min and a runtime of 3 min. The solvents used were A.) water plus 0.1% TFA and B.) MeCN with 0.1% TFA.

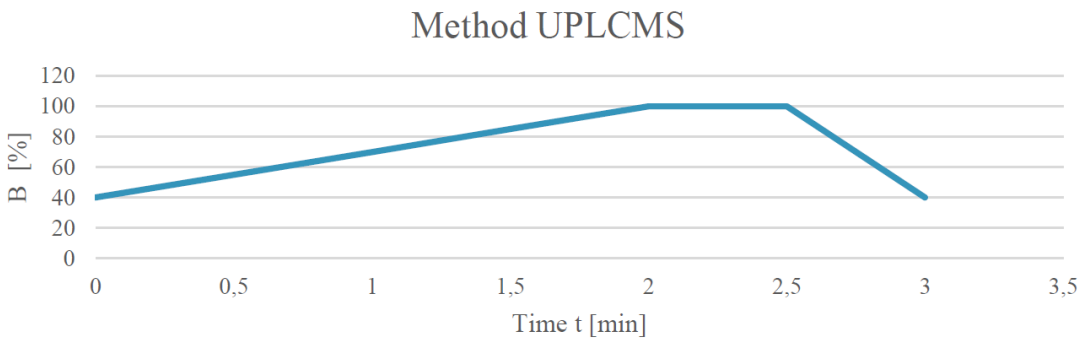

The MS method used was single quadrupole electrospray ionization.
HR-MS spectra were measured on a Bruker ICR Apex-Qe with the following method: ESI pos HPmix 200-1800.

Optical rotations values were measured at the sodium D-line in a 10 cm cell with a Schmidt + Haensch Polartronic H532 polarimeter at room temperature.

TLC analyses were conducted on Merck precoated silica gel (Merck, 60 F254) using UV light (254 nm) and the following staining solutions:

a) *p*-Anisaldehyde (prepared by addition of 15 mL AcOH and 3.5 mL of *p*-Anisaldehyde to a 350 mL ice cold EtOH, then cautiously adding 50 mL of conc. H_2SO_4 dropwise over 60 minutes. The unused portion was stored at 0°C).

b) Phosphomolybdic acid (prepared by dissolving 10 g of phosphomolybdic acid or PMA in 100 mL of absolute EtOH).

c) Potassium permanganate (prepared by dissolving 1.5 g of $KMnO_4$, 10 g of K_2CO_3, and 1.25 mL of a 10% NaOH solution in 200 mL of water).

Preparative column chromatography was performed using silica gel from Merck, (silica 60, grain size 0.063-0.200 mm, 70-230 mesh ASTM) or silica gel from Sigma-Aldrich (silica 60, 230-400 mesh). Phosphoramidites were purified on deactivated silica. Prior to use the silica was treated with the eluent containing 10% of dimethylethylamine. For the

purification 1% of dimethylethylamine was added to the eluent. Melting points were determined on a Büchi B-540 and are uncorrected.

Automated column chromatography was performed using an Isolera™ Prime, an advanced automated flash purification system by Biotage. Silica cartridges (Biotage® SNAP KP-Sil 10 g, 25 g, 50 g and 100 g), and silica samplets (Biotage® SNAP Samplet KP-SIL 1 g, 3 g, and 10 g) were appropriately used depending on the amount of compound to purify.

Expression and purification of recombinant proteins: Wild type PRL-3 was prepared as previously described[19] yielding pure protein in all cases. BL21 DE3 cells expressing the recombinant WT PRL-3 were lysed by sonication in buffer A [50 mM Tris-HCl (pH 7.4) containing 500 mM NaCl, 20 mM imidazole, 1 mM dithiothreitol (DTT), and 0.5 mM protease inhibitor cocktail]. The protein was purified using a FPLC Histrap HP 1 mL column using an elution gradient from 20 to 500 mM imidazole in buffer A. The purified PRL-3 was dialyzed against 50 mM Tris-HCl (pH 7.4), 150 mM NaCl, 5 mM DTT, and 10% glycerol. The integrity of all proteins was confirmed by molecular weight determination by electrospray ionization mass spectroscopy (ESI-MS)[19]. The other 3 proteins (SYNJ1, OCRL and INPP5E) were all purchased as purified, recombinant proteins from Origene®. The over-expressed recombinant proteins were purified using OriGene's 4C5-AntiDDK antibody (TA50011) affinity column. The proteins were shipped on dry ice, stored at - 80° C and divided in several aliquots to avoid repeated freeze/thaw cycles. The purity of each protein was examined by SDS-PAGE electrophoresis and coomassie staining. The proteins were received each in a vial (20 µg in a buffer solution containing 10% Glycerol, 100 mM Glycine, and 25 mM Tris-HCl, pH 7.3), at concentrations of 0.319; 0.174; and 0.409 µg/µL for SYNJ1, OCRL and INPP5E, respectively. The material safety data sheet (MSDS) of the purchased products is available online: http://www.origene.com/support/product/msds.mspx

EnzChek assay: The release of phosphate from lipid substrates was monitored using a commercially available phosphatase assay kit, EnzChek, according to the manufacturer's instructions. The EnzChek phosphatase assay kit was purchased from Molecular Probes. The assay was conducted in 96-well plate format and phosphate release was monitored by absorbance at 360 nm over time. PRL-3 (6 µM) in buffer (50 mM Tris-HCl (pH 7.5), 150 mM NaCl, 1 mM $MgCl_2$, and 4 mM DTT) was incubated with 250 or 500 µM of

phosphoinositide substrates in 96-well plates. The assay was conducted at 37 °C with shaking in a Tecan Safire TM plate reader. Assays in the absence of enzyme were included in the 96-well plate setup in triplicate for all the substrates analyzed. The measurements in the absence of enzyme were averaged and subtracted from the data to account for nonspecific hydrolysis of the substrates and for background absorption. In all assays, measurements were in triplicate and the standard deviation of the measurements is represented as error bars. Data were plotted using GraphPad Prism (GraphPad Software, Version 5). The protein was expressed and purified as described before[19].

Ligand-based virtual screening and computational analysis: To use 3D similarity, a reasonable 3D conformer of the template molecule (PI(4,5)P_2) is necessary. Here, the conformation of the headgroup of a PIP structure was selected from a co-crystallised protein-ligand complex which is deposited in the Protein database [www.ebi.ac.uk/pdbe/]: Crystal structure of PI3Kalpha in complex with PIP2-pdbcode 4ovv. This headgroup shows a chair conformation. In order to mimic the attached lipophilic tail, an ethyl moeity was added on the 1-*O*-Phosphorus group (instead of the DiC8 glycerol-based lipid chains). The structures to be screened were downloaded from the ZINC database (http://zinc.docking.org/substance/). USRCAT, a pharmacophoric extension of USR, was used to screen a single-conformer database with over 23 million purchasable molecules.

UFSRAT is available as a web-server (http://opus.bch.ed.ac.uk/ufsrat/)and thus it screened a different multi-conformer database of commercially available molecules. UFSRAT returns the top 200 molecules in a couple of seconds. The similarity threshold (USR score) which was used was 0.7. in the end. 388 compounds were exported as structures from the ZINC database, and duplicates (same compound, different vendor) were removed, which left 129 compounds. The assignment into families based on 2D similarities resulted in 14 clusters and 4 singletons. In order to prioritize the most interesting hit compounds they were aligned with another 3D-similarity program which is called Surflex-Sim[138]. In this method, the compounds are aligned on the template and a visual analysis is possible. Based on such a visual analysis of the alignments and taking into consideration that the final compounds to be synthesized must also contain a big lipophilic group, a series of hit structures were selected.

Using a manual chemical synthesis-driven method, a selection of the "best" representative of a cluster was made, and a series of compounds were selected for synthesis and biochemical activity screening.

DiFMUP assay: Phosphatase inhibition was generally carried out using DiFMUP (6,8-difluoro-4-methylumbelliferyl phosphate) as substrate. PRL -3 enzyme was used at 50 nM concentration in assay buffer (20 mM Tris-HCl 7.5; 150 mM NaCl; 10 mM DTT; 0,01% Triton-X) and incubated for at least 10 minutes prior to addition of substrate in order to ensure full activity due to the presence of high amounts of DTT in the buffer. Reactions were performed in 96-well plates from Perkin Elmer (OptiPlate, black). Inhibition kinetics were obtained with substrate concentrations at the respective *K*m value of the respective enzyme (for PRL-3 21 μM). For *K*m determination of phosphatases, reaction kinetics were monitored at 358/452 nm for 20 minutes on a multiwell plate reader after addition of substrate concentration series. Initial velocities of the obtained data curves were plotted against substrate concentration and data were fit for Michaelis-Menten parameters using GraphPad Prism software. The kinetics of inhibitor concentration series from 600 μM down to 1.17 μM were measured at 358/452 nm for 20 minutes on a multiwell plate reader after addition of substrate and corrected for the respective inhibitor baseline. IC_{50} data were obtained by plotting initial velocities versus inhibitor concentration (logarithmic scale) using GraphPad Prism software. The positive control for this assay was the purchased **Analog 3** with an IC_{50} of 31uM[53].

5.2. Synthetic procedures and analytical data

5.2.1. Solution synthesis of the lipid tail phosphoramidites

Benzyl (3-phenylpropyl) diisopropylphosphoramidite (38)

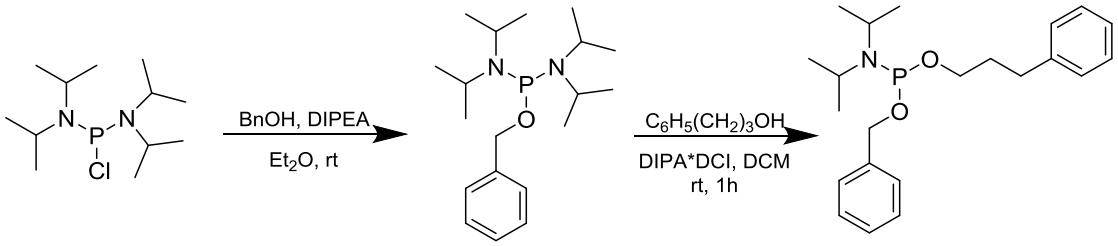

38

To a mixture of bis(diisopropylamino)chlorophosphine (1 g, 3.75 mmol) in 25 ml of diethyl ether was added diisopropylethylamine (1.96 ml, 11.2 mmol) at 0 °C, followed by dropwise addition of benzyl alcohol (311 µl, 3.00 mmol). After stirring for 30 min the solvent was evaporated and the residue treated with cyclohexane. The cyclohexane fraction was filtered through a filter canula into another schlenk flask and then evaporated. The residue was dried overnight in high vacuum. Then DIPA*DCI (411 mg, 1.88 mmol) in 8 mL of dichloromethane was added and the resulting solution cooled to 0 °C. Then, a solution of 3-phenyl-propanol (408 µl, 3.00 mmol) in 2 ml dichloromethane was added and the reaction mixture stirred for 40 min at 0 °C. After ^{31}P NMR shows full conversion, the solvent was evaporated, the residue suspended in cyclohexane/$NEtMe_2$ (99:1) and subjected to inert column chromatography (cyclohexane/$NEtMe_2$ (99:1)). Product fractions were combined and dried in high vacuum to yield the product as a pale yellow oil (145 mg, 33%).

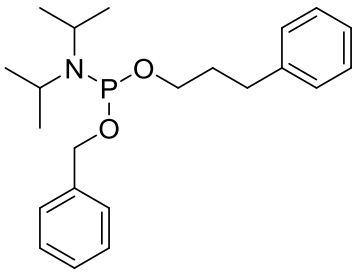

38

^{1}H NMR (400 MHz, $CDCl_3$) δ (ppm) = 7.30 – 7.09 (m, 10 H), 4.74 – 4.57 (m, 2 H), 3.68 – 3.53 (m, 4H), 2.64 (pseudo t, 2H), 1.86 (m, 2 H), 1.49 (d, 1H), 1.35 (s, 1H), 1.13 (m, 12 H).

^{13}C NMR (400 MHz, $CDCl_3$) δ (ppm) = 142.1, 139.6 (d, *J* = 7 Hz), 128.5, 128.3, 128.2, 127.2, 127.0, 125.7, 66.2 (d, *J* = 18 Hz), 62.9 (d, *J* = 18 Hz), 43.0 (d, *J* = 12 Hz), 33.0 (d, *J* = 8 Hz), 32.3, 24.7 (d, *J* = 7 Hz).

^{31}P NMR (162 MHz, $CDCl_3$): δ (ppm) = 146.6 (1P)

1,2-di-*O*-heptylcarbamoyl-*sn*-3-benzyloxyglycerol (39)

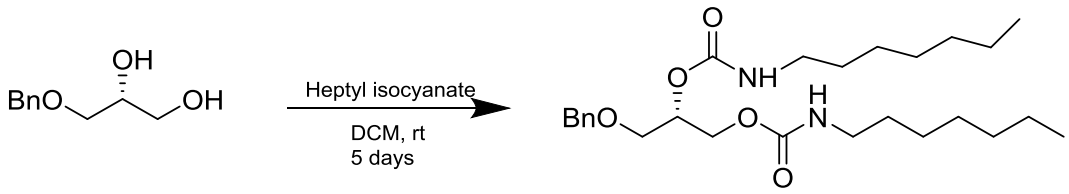

39

To (+)-benzyloxyglycerol (1.43 g, 4.42 mmol) in a round bottom flask was added heptylisocyanate (5.7 ml, 35.4 mmol) and trimethylamine (800 µL, 4.59 mmol) the reaction was stirred for 5 days at room temperature. The reaction was then concentrated and subjected to a column chromatography (*n*-heptane/ethylacetate = 68/32) to afford the product as a white solid (1.45 g, 71%).

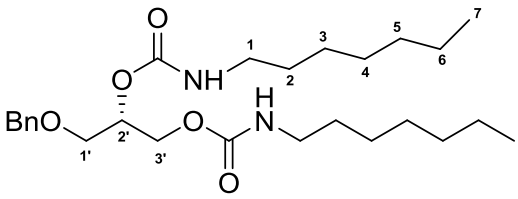

39

^{1}H NMR (400 MHz, $CDCl_3$) δ (ppm) = 7.34 – 7.14 (m, 5H, Ar-H), 5.14 – 4.91 (bs, 1H, NH), 4.61 (s, 1H, H-2'), 4.47 (q, *J* = 12.1 Hz, 2H, H-1'), 4.25 – 4.11 (m, 2H, H-3'), 3.53 (d, *J* = 4.9 Hz, 2H, H-1), 3.18 – 2.99 (m, 4H, H-2), 1.41 (q, *J* = 5.4 Hz, 2H, H-3), 1.21 (q, *J* = 4.3 Hz, 14H, H-3, H-4, H-5, H-6), 0.81 (t, *J* = 6.7 Hz, 6H, H-7).

^{13}C NMR (400 MHz, $CDCl_3$) δ (ppm) = 156.1, 155.7, 137.9, 138.4, 127.7, 127.7, 77.2, 73.3, 71.1, 68.7, 63.6, 41.1, 31.8, 29.9, 29.9, 29.0, 26.7, 22.6, 14.1

HRMS (MALDI+): m/z neg.: $[M+Na]^+$ calculated 487.3147, found 487.3142–0.9 ppm

$[\alpha]_D^{20}$ = +6.42 (*c* 1 mg/mL, MeOH)

1,2-di-*O*-heptylcarbamoyl-*sn*-glycerol (40)

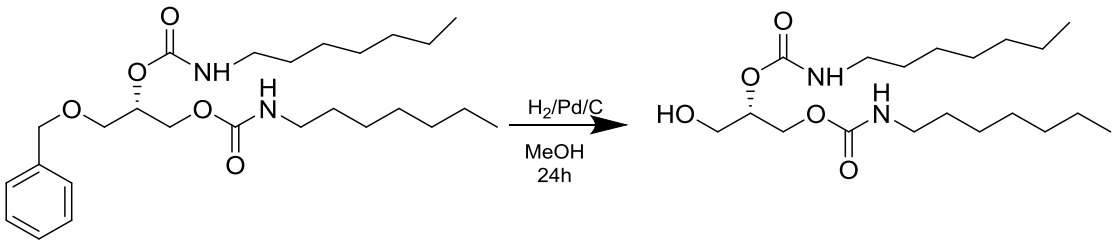

39 40

A mixture of **39** (1.45 g, 3.12 mmol) and 20 wt% $Pd(OH)_2/C$ (66 mg, 0.09 mmol) in 40 ml methanol was stirred under H_2 atmosphere for 12 h at room temperature. The reaction was filtered through a Celite pad and the filtrate was concentrated in vacuum to obtain **40** as a white foam (1.12 g, 96%).

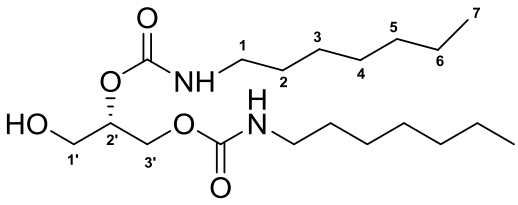

40

^{1}H NMR (400 MHz, $CDCl_3$) δ (ppm) = 4.82 (p, *J* = 5.3 Hz, 3H, H-1', H-2'), 4.21 (dt, *J* = 5.2 Hz, 2H, H-3'), 3.62 (d, *J* = 5.0 Hz, 2H, NH), 3.10 (q, *J* = 6.7 Hz, 4H, H-1), 1.42 (p, *J* = 7.0 Hz, 4H, H-2), 1.31 – 1.07 (m, 16H, H-3,4,5,6), 0.93 – 0.73 (m, 6H, H-7).

^{13}C NMR (400 MHz, $CDCl_3$) δ (ppm) = 156.6, 156.0, 77.2, 73.2, 62.6, 61.5, 41.2, 31.7, 29.9, 28.9, 28.9, 26.7, 26.7, 22.6, 14.1

HRMS(ESI+): m/z neg.: $[M+Na]^+$ calculated 397.2676, found 397.2673 – 0.9 ppm

$[\alpha]_D^{20}$ = (+) 4.55 (c = 1 mg/mL, MeOH)

(2R)-3-(((benzyloxy)(diisopropylamino)phosphanyl)oxy)propane-1,2-diyl bis(heptylcarbamate) (41)

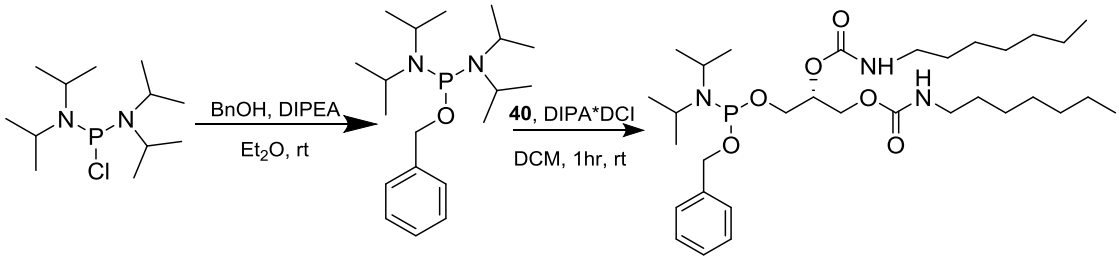

41

To a mixture of bis(diisopropylamino)chlorophosphine (1 g, 3.75 mmol) in 25 ml of diethyl ether was added diisopropylethylamine (1.96 ml, 11.2 mmol) at 0 °C, followed by dropwise addition of benzyl alcohol (311 µl, 3.00 mmol). After stirring for 30 min the solvent was evaporated and the residue treated with cyclohexane. The cyclohexane fraction was filtered through a filter canula into another schlenk flask and then evaporated. The residue was dried overnight in high vacuum. Then DIPA*DCI (411 mg, 1.88 mmol) in 8 mL of dichloromethane was added and the resulting solution cooled to 0 °C. Then, a solution of 1,2-di-*O*-heptylcarbamoyl-*sn*-glycerol (1.12 g, 3.0 mmol) in 2 ml dichloromethane was added and the reaction mixture stirred for 40 min at 0 °C. After ^{31}P NMR shows full conversion, the solvent was evaporated, the residue suspended in cyclohexane/$NEtMe_2$ (99:1) and subjected to inert column chromatography (cyclohexane/$NEtMe_2$ (99:1)). Product fractions were combined and dried in high vacuum to yield the product as pale yellow oil (462 mg, 20%).

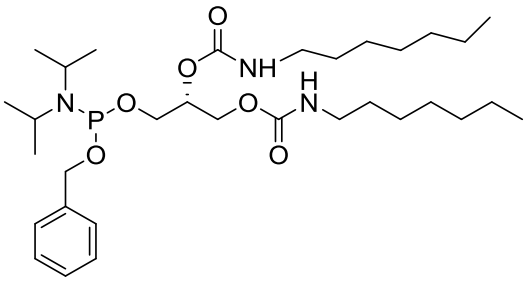

41

^1H NMR (400 MHz, $CDCl_3$) δ (ppm) = 0.81 (t, 3H), 1.11 (t, 3H), 1.20 (br s, 8H), 1.35 (t, 6H), 3.08 (m, 8H), 3.57 (m, 4H), 3.71 (m, 4H), 4.15 (m, 4H), 4.59 (m, 7 H), 4.98 (s, 2H), 7.17 – 7.29 (m, 5H)

^{13}C NMR (400 MHz, $CDCl_3$) δ (ppm) = 156.1, 155.6, 139.5 (d, *J* = 8 Hz), 139.4 (d, *J* = 7 Hz), 128.2, 127.3, 127.0, 71.8, 66.5, 66.3, 63.5, 62.1, 62.0, 43.1, 41.1, 31.8, 30.0, 29.0, 26.9, 26.7, 24.6, 22.6, 14.1

^{31}P NMR (400 MHz, $CDCl_3$) δ (ppm) = 148.42 and 148.48 (1P, diastereomers)

(S)-3-(benzyloxy)propane-1,2-diyl(3S,3'S,5S,5'S,7S,7'S)-bis(adamantane-1-carboxylate) (42)

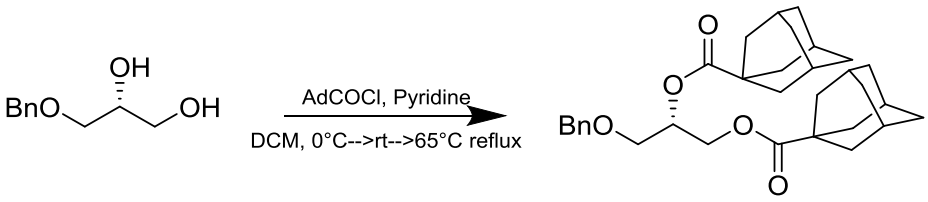

42

To a stirred solution of diol 1 (500 mg, 2.13mmol, 1 equiv.) in dry dichloromethane (10mL) under nitrogen was added 4-dimethylaminopyridine (33 mg, 0.27 mmol, catalytic). The resulting solution was cooled to 08C and dry pyridine (508 mg, 0.524mL, 6.40 mmol, 3 equiv.) was added dropwise. After stirring for 30 min, adamantancarbonyl chloride (1.12 g, 5.88 mmol, 3 equiv.) was added dropwise. The reaction mixture was then warmed up to room temperature and heated at 658C overnight. The reaction was quenched, once no starting material remained by TLC, by addition of water (30mL) and the aqueous phase was extracted with dichloromethane (4 x 30 mL). The combined organic layers were washed with 2M aqueous hydrochloric acid (30mL) and the acid phase was back-extracted with dichloromethane (30mL). The combined organic layers werewashed with brine (35mL), dried overMgSO4, filtered, and the solvent was removed under vacuum. Flash chromatography (10–20%ethyl acetate/petroleum spirit v/v) afforded the diester 3 (983mg, 1.83mmol, 86%) as a colourless solid.

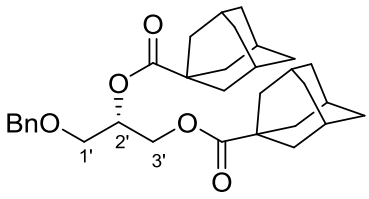

42

^{1}H NMR (400 MHz, $CDCl_3$) δ (ppm) = 7.42 – 7.16 (m, 5H, Ar-H), 5.24 – 5.19 (m, 1H, H-2'), 4.54 (s, 2H, H-1'), 4.34 (dd, *J* = 3.8 Hz, 1H, H-3'), 4.15 (dd, *J* = 6.3 Hz, 1H, H-3'), 3.58 (dd, *J* = 1.3 Hz, 2H, Ad-H), 2.02 (ddq, *J* = 3.2 Hz, 7H), 1.87 (dd, *J* = 2.9 Hz, 12H), 1.76 – 1.64 (m, 8H), 1.31 – 1.21 (m, 4H), 0.95 – 0.84 (m, 2H).

^{13}C NMR (400 MHz, $CDCl_3$) δ (ppm) = 177.3, 176.9, 159.5, 130.1, 129.5, 114.0, 73.1, 70.0, 68.1, 62.7, 55.4, 40.9, 39.0, 39.0, 36.7, 36.7, 28.1, 28.1.

$[\alpha]_D^{20}$ = (+) 7.38 (c = 0.5, $CHCl_3$)

HRMS (ESI+) m/z meas. 559.3030; calc. for C33H44O6 $[M+Na]^+$ 559.3030.

Characterization data of the compound was consistent with previously published work[125]

(S)-3-hydroxypropane-1,2-diyl(3S,3'S,5S,5'S,7S,7'S)-bis(adamantane-1-carboxylate) (43)

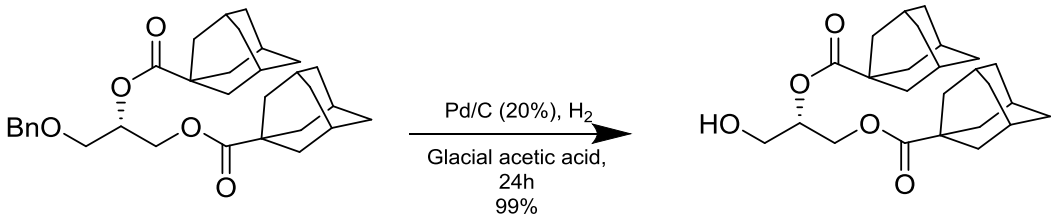

42 **43**

A mixture of **42** (1265 mg, 2.498 mmol) and 20 wt% $Pd(OH)_2/C$ (87.7 mg, 0.124 mmol, 0.05 eq) in 38 ml glacial acetic acid was stirred under H_2 atmosphere for 12 h at room temperature. The reaction was filtered through a Celite pad and the filtrate was concentrated in vacuum to obtain **43** as a white foam (1000 mg, 96%).

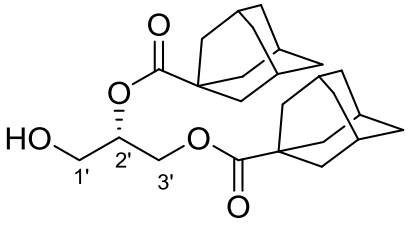

43

R_f 0.26 (20% EtOAc:heptane).

^{1}H NMR (400 MHz, $CDCl_3$) δ (ppm) = 5.07–5.03 (m, 5H, Ar-H), 4.30 (dd, J = 12 Hz, 5, 1H), 4.20 (dd, J = 6 Hz, 2H, H-3'), 3.71 (d, J = 5 Hz, 2H, H-1'), 2.04–1.98 (m, 6H), 1.89 (dd, J = 3 Hz, 12H), 1.76– 1.66 (m, 12H).

^{13}C NMR (400 MHz, $CDCl_3$) δ (ppm) = 71.9, 61.8, 61.7, 40.8, 40.8, 38.8, 38.8, 36.4, 27.8.

$[\alpha]_D^{20}$ = (-)1.82 (c 2.0, $CHCl_3$)

HRMS (ESI+) m/z meas. 439.2455; calc. for C25H36O5 $[M+Na]^+$ 439.2455.

Characterization data of the compound was consistent with previously published work[125]

(2R)-3-(((benzyloxy)(diisopropylamino)phosphanyl)oxy)propane-1,2-diyl (3R,3'R,5R,5'R,7R,7'R)-bis(adamantane-1-carboxylate) (44)

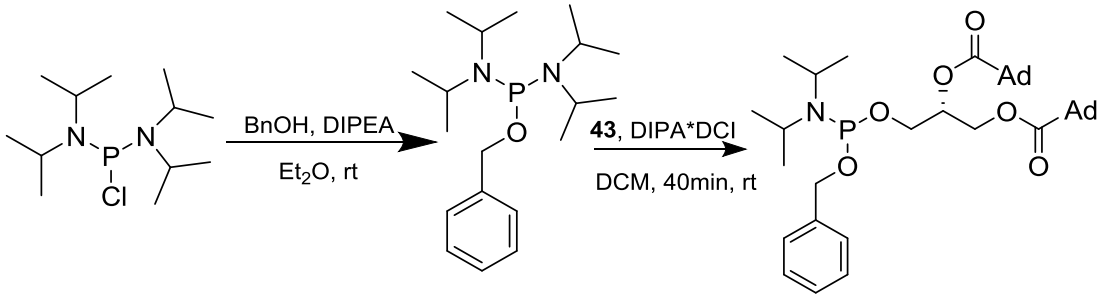

44

To a mixture of bis(diisopropylamino)chlorophosphine (800 mg, 3 mmol, 1 eq) in 25 ml of diethyl ether was added diisopropylethylamine (1.5 ml, 9 mmol, 3 eq) at 0 °C, followed by dropwise addition of benzyl alcohol (249.55 µl, 2.4 mmol, 0.8 eq). After stirring for 30 min the solvent was evaporated and the residue treated with cyclohexane. The cyclohexane fraction was filtered through a filter canula into another schlenk flask and then evaporated. The residue was dried overnight in high vacuum. Then DIPA*DCI (328.5

mg, 1.5 mmol, 0.5 eq) in 8 mL of dichloromethane was added and the resulting solution cooled to 0 °C. Then, a solution of **43** (1000 mg, 2.4 mmol, 0.8 eq) in 2 ml dichloromethane was added and the reaction mixture stirred for 40 min at 0 °C. After ^{31}P NMR shows full conversion, the solvent was evaporated, the residue suspended in cyclohexane/$NEtMe_2$ (99:1) and subjected to inert column chromatography (cyclohexane/$NEtMe_2$ (99:1)). Product fractions were combined and dried in high vacuum to yield the product as pale yellow oil (20%).

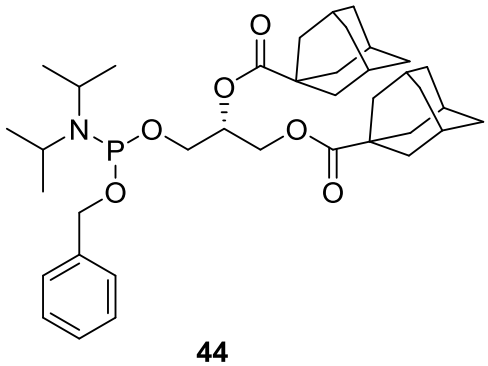

44

R_f 0.9 (30% EtOAc:heptane)

^{1}H NMR (400 MHz, $CDCl_3$) δ (ppm) = 7.42–7.30 (m, 5H), 5.18–5.12 (m, 1H), 4.76–4.59 (m, 2H), 4.35–4.30 (m, 1H), 4.16–4.10 (m, 1H), 3.82–3.60 (m, 4H), 2.00 (s, 6H), 1.88–1.86 (m, 12H), 1.73–1.66 (m, 12H), 1.22–1.15 (m, 12H).

^{13}C NMR (400 MHz, $CDCl_3$) δ (ppm) = 177.3, 176.9, 128.4, 127.4, 127.1, 70.8, 70.7, 65.6, 65.5, 65.4, 62.6, 62.5, 62.1, 61.9, 46.4, 43.3, 43.2, 40.9, 39.0, 36.7, 28.1, 24.9, 24.8, 24.7, 11.8.

^{31}P NMR (400 MHz, $CDCl_3$) δ (ppm) = 149.6, 149.5.

HRMS (ESI+) meas. m/z 676.3736; calc. for C38H56N1O6P $[M+Na]^+$ 676.3738.

Characterization data of the compound was consistent with previously published work[125]

(S)-3-(benzyloxy)propane-1,2-diyl dioctanoate (45)

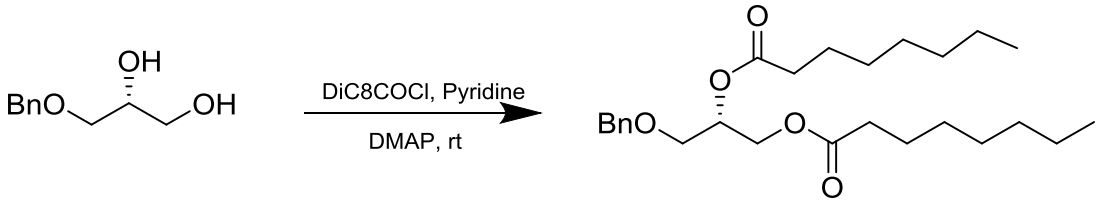

45

To a stirred solution of diol (1000 mg, 5.48 mmol, 1 eq) in dry pyridine (50 mL) under nitrogen was added 4-dimethylaminopyridine (33 mg, 0.27 mmol, catalytic). After stirring for 30 min, di-octanoyl chloride (1800 mg g, 11.5 mmol, 2.1 equiv.) was added dropwise. The reaction mixture was left stirring overnight. The reaction was stopped, once no starting material remained by TLC, by removal of pyridine under reduced pressure, dissolving in EtOAc and citric acid, and extracting EtOAc (4 x 30 mL). The combined organic layers were washed with water, then brine, dried overMgSO4, filtered, and the solvent was removed under vacuum. Flash chromatography (10–20% EtOAc/heptane) afforded the diester **45** (74%) as a colourless solid.

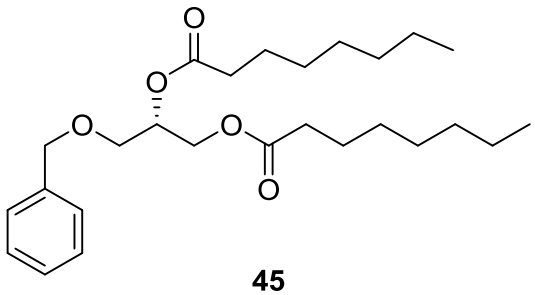

45

Characterization data of the compound was consistent with previously published work[120]

(S)-3-hydroxypropane-1,2-diyl dioctanoate (46)

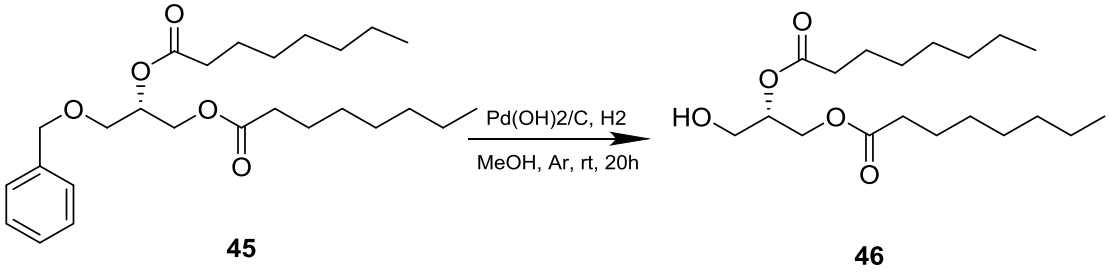

45 46

In a flask under Ar atmosphere **45** (1.278 g, 2.99 mmol, 1 eq) was dissolved in 35 mL of dry MeOH and the $Pd(OH)_2/C$ catalyst (100 mg, 0.147 mmol, 0.05 mol%) was added. Under stirring, the flask was flooded with H_2- Gas (1 atm) and left to stir for 20 h. After the reaction was finished, the reaction mixture was filtered through Celite and was washed three times with DCM. The solvent of the filtrate was evaporated under reduced pressure, which gave a crude with a quantitative yield of 1.022 g (2.96 mmol, 99 %). The crude product was used without further purification.

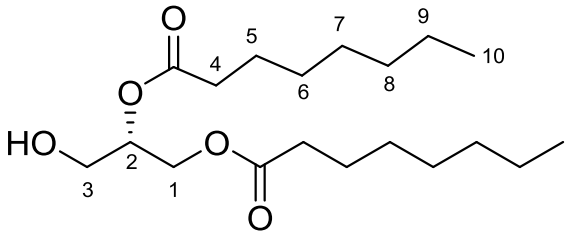

46

^{1}H-NMR (400.13 MHz, $CDCl_3$) δ (ppm) = 5.12 - 5.05 (m, 1H, H-2), 4.36 - 4.20 (m, 2H, H-1), 3.77 - 3.67 (m, 2H, H-3), 2.48 - 2.28 (m, 4H, H-4), 1.95 (s, 1H, OH), 1.61 (dt, *J* = 17.5 Hz, 7.2 Hz, 4H, H-5), 1.37 - 1.21 (m, 16H, H-6, H-7, H-8, H-9), 0.88 (t, *J* = 6.9 Hz, 6H, H-10).

^{13}C-NMR (100.92 MHz, $CDCl_3$) δ (ppm) = 174.1, 173.8 (C=0, 2C), 72.5 (CH, 1C, C-2), 62.4 (CH2, 1C, C-3), 61.9 (CH2, 1C, C-1), 34.6, 34.5 (CH2. 2C, C-4), 32.0, 29.4, 29.3 (CH2. 4C, C-6, C-7), 25.3, 25.2 (CH2.2C, C- 5), 23.0, 22.9, 21.4 (CH2, 4C, C-8, C-9), 14.4 (CH3, 2C, C-10).

HRMS (ESI+) m/z Meas. 345.3; Calc. for $C_{19}H_{37}O_5$ $[M+H]^+$ 345.3.

Characterization data of the compound was consistent with previously published work[120]

(2R)-3-(((benzyloxy)(diisopropylamino)phosphanyl)oxy)propane-1,2-diyl dioctanoate (47)

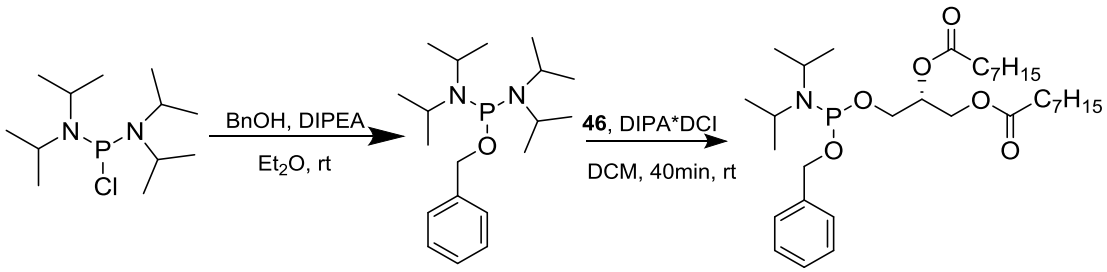

47

After suspending the starting material (528 mg, 1.97 mmol, 1 eq) in 15 mL of Et_2O in a flask under Ar atmosphere and cooling the solution to 0°C, a mixture of BnOH (192 mg, 1.77 mmol, 0.9 eq) and DIPEA (509 g, 3.94 mmol, 2.0 eq) in 10 mL Et_2O was added dropwise. The reaction was finished after 30 min stirring as determined by ^{31}P NMR. The solvent was evaporated and the precipitate dissolved in 8 mL cyclohexane. The solution was filtered under Ar and the solvent of the supernatant was evaporated before the product was dried under high vacuum. The yield of the crude product was 85% (593 mg, 1.75 mmol) with an 85% purity according to ^{31}P NMR. The crude product was used without further purification. In a flask under Ar atmosphere, the product (1.700 g, 5.027 mmol, 1.8 eq) was dissolved in 20 mL DCM and under stirring DCI*DIPA was added. The reaction solution was cooled to 0°C and **46**, dissolved in 10 mL DCM, was added dropwise. The reaction mixture was monitored by ^{31}P NMR. After 30 min the reaction was complete and the solvent was evaporated under reduced pressure. Purification of the crude was achieved with column chromatography (50 g SiO_2, cyclohexane/Me_2Net 95: 5). The product is a colorless liquid and could be isolated in a yield of 65%.

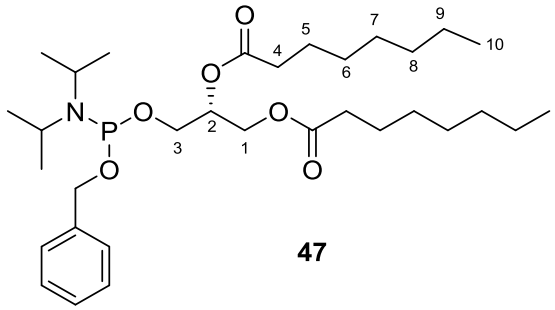

47

^{31}P-NMR (400.13 MHz, DCM locked on deuterated DMSO) δ (ppm) = 148.2 (s, 0.5P), 148.0 (s, 0.5P).

Characterization data of the compound was consistent with previously published work[120]

5.2.2. Solution synthesis of the alkylated inositol ring

1-*O*-*t*-Butyldiphenylsilyl-2,3-*O*-cyclohexylidene-*myo*-inositol (2)

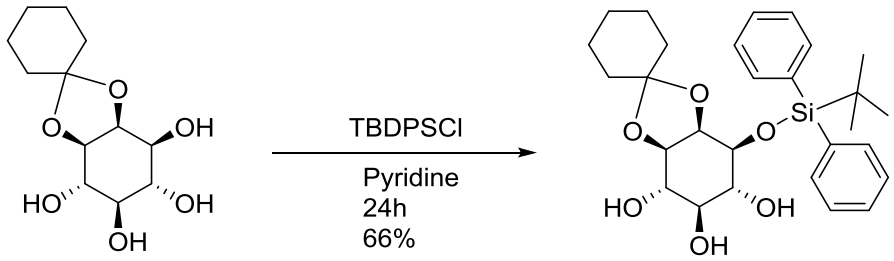

1 **2**

To the solution of tetrol **1** (1 g, 3.84 mmol, 1 eq) and imidazole (587.5 mg, 8.64 mmol, 2.25 equiv.) in pyridine (25 mL) at -10°C was added TBDPS-Cl (1.58g, 5.77mmol, 1.5 equiv.). The reaction mixture was stirred at RT for 24 hrs. After completion the reaction was subjected to aqueous work-up. Extraction with ethyl acetate gave the crude product, which was purified with column chromatography (4% MeOH in DCM) giving pure product (1.27g, 2.5 mmol, 66%) as white foam.

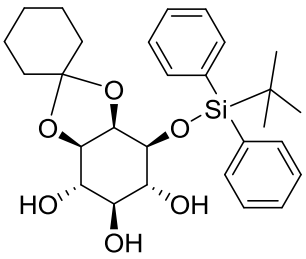

2

^{1}H-NMR (400 MHz, $CDCl_3$) δ 7.79-7.76 (m, 2H), 7.73-7.71 (m, 2H), 7.45-7.26 (m, 6H), 3.91-3.87 (m, 2H), 3.74-3.64 (m, 2H), 3.64-3.59 (m, 1H), 3.12 (t, *J* = 9.69 Hz, 1H), 3.03 (brs, 1H), 2.88 (brs, 1H), 2.57 (brs, 1H), 1.75-1.66 (m, 5H), 1.52-1.40 (m, 5H), 1.32 (m, 1H), 1.10 (s, 9H, 3xCH_3-TBDPS)

^{13}C-NMR (100 MHz, $CDCl_3$) δ 135.94, 133.7, 133.1, 130.11, 130.00, 127.66, 127.5, 78.28, 77.33, 77.01, 76.70, 75.70, 72.82, 38.2, 34.93, 26.97, 25.00, 24.01, 23.75, 19.5

$[\alpha]_D^{20}$ = -19.4° (c = 1.0 mg/mL in CH_3Cl)

Characterization data of the compound was consistent with previously published work[120]

1-*O*-*t*-Butyldiphenylsilyl-2,3-*O*-cyclohexylidene- 4,5-O-dibenzoyl-*myo*-inositol (3)

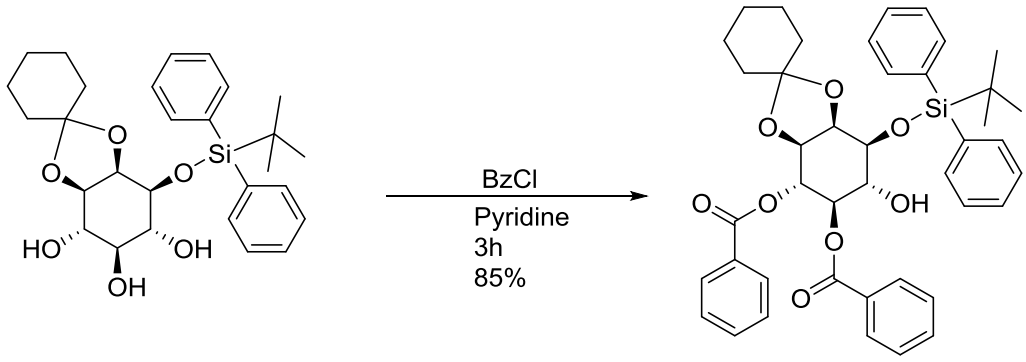

2 **3**

The solution of triol **2** (2.6 g, 5.22 mmol, 1 equiv.) in pyridine (27 mL) was cooled down to -40ºC. A solution of BzCl (605 µL, 5.22 mmol, 1 equiv.) in CH_3Cl (27 mL) was added dropwise to the mixture. The system was stirred at this temperature for 1h. The reaction was then quenched with citric acid and extracted with ethyl acetate. The product was purified on a *Biotage* column at a constant concentration of EtOAc (25%) in heptane.

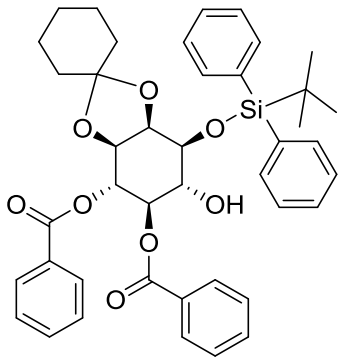

3

^{1}H-NMR (400 MHz, $CDCl_3$) δ 7.95-7.91 (d, 2H, Ar-H), 7.88-7.86 (d, 2H, Ar-H), 7.84- 7.82 (d, 2H, Ar-H), 7.73-7.71 (d, 2H, Ar-H), 7.48-7.28 (m, 12H, Ar-H), 5.83 (t, 1H, CH-4-*myo*), 5.1-5.05 (t, 1H, CH-5- *myo*), 4.24-4.20 (t, 1H, CH-6-*myo*), 4.15-4.10 (m, 2H, CH-2-*myo*, CH-3-*myo*), 4.06-4.00 (dd, *J* = 8.7 Hz, 1H, CH-1-*myo*), 2.5 (bs, 1H, 6-OH), 2.03-1.25 (m, 10H, cy), 1.15 (s, 9H, CH_3-TBDPS).

^{13}C NMR (101 MHz, $CDCl_3$) δ 166.42, 165.56, 136.06, 135.91, 134.81, 133.29, 133.15, 133.03, 132.94, 130.11, 129.84, 129.62, 129.34, 128.28, 128.20, 127.94, 111.23, 77.35,

77.04, 76.72, 75.75, 75.35, 74.43, 73.79, 72.18, 37.46, 34.63, 31.89, 29.03, 27.01, 25.07, 23.79, 19.46, 14.12.

Characterization data of the compound was consistent with previously published work[120]

1-*O*-*t*-Butyldiphenylsilyl-2,3-*O*-cyclohexylidene- 4,6-O-dibenzoyl-5-O-methyl-*myo*-inositol (4)

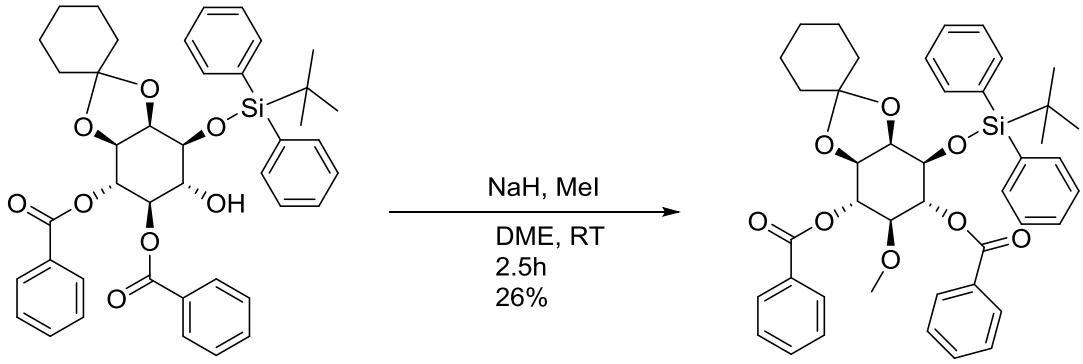

3 **4**

To a solution of compound **3** (300 mg, 0.424 mmol) in anhydrous DME (12 ml), NaH (10 eq, 4.24 mmol, 169.8 mg) was carefully added, then the reaction was treated with methyl iodide (131.97 µl, 5 eq, 2.12 mmol). The reaction was allowed to stir at room temperature for 2.5 hours, during which monitoring for the product using UPLCMS was undergone. The product was purified by flash chromatography in a 10 to 90% EtOAc gradient in Heptane.

To allow better and more simplified structure elucidation NMR studies of the abovementioned compound, a cleavage of the cyclohexylidene ketal was undergone first. 2D NMR studies were attempted on compound **4**, but the cyclohexylidene ketal protons have crowded the spectra in a way that it was very difficult to analyze the other protons (data not shown). The product was purified by flash chromatography in a 23% to 32% EtOAc gradient in Heptane (gradient optimized according to Rfs).

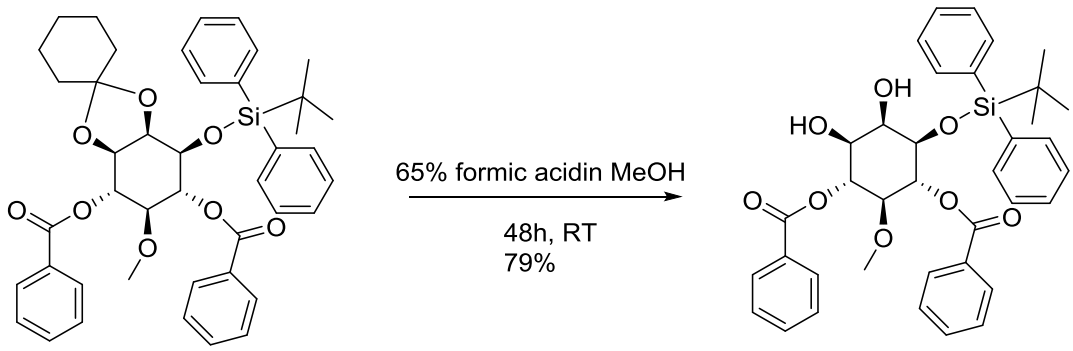

4 **5**

Compound **4** (74 mg) was dissolved in a solution of 65% formic acid in methanol, and the reaction was allowed to stir for 72 hours. It was quenched with $NaHCO_3$ and extracted with EtOAc. The product was purified by flash column chromatography using an EtOAc gradient of 23% to 32% in heptane. The product was monitored on UPLCMS with the corrected mass.

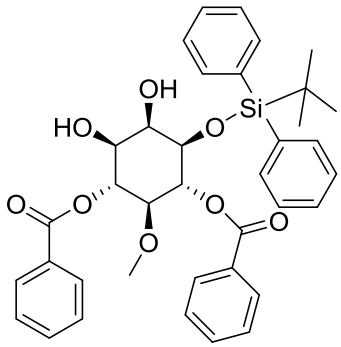

5

^{1}H-NMR (400 MHz, $CDCl_3$) δ 8.03-8.01(m, 2H, Ar-H), 7.94-7.93 (m, 2H, Ar-H), 7.66-7.64 (m, 2H, Ar-H), 7.55-7.53 (m, 4H, Ar-H), 7.43-7.31 (m, 8H, Ar-H), 7.25-7.19 (m, 2H, Ar-H), 5.84 (t, J = 9.52 Hz, 1H, CH-4-*myo*), 5.61 (t, J = 9.68 Hz, 1H, CH-6-*myo*), 3.94-3.89 (m, 2H, CH-2-*myo*, CH-3-*myo*), 3.53-3.43 (m, 2H, CH-1-*myo*, CH-5-*myo*), 3.31 (s, 3H, methyl), 2.78 (m, 1H, OH),2.75 (m, 1H, OH), 0.96 (s, 9H, CH_3-TBDPS).

^{13}C-NMR (100 MHz, $CDCl_3$) δ 166.9, 165.9, 135.8, 135.6, 133.4, 133.1, 133.0, 132.13, 130.3, 130.1, 129.83, 129.7, 129.2, 128.37, 128.25, 128.18, 127.9, 97.8, 78.2, 74.5, 74.1, 72.3, 71.8, 71.0, 70.6, 67.6, 58.7, 27.0, 26.9, 19.11

HRMS (ESI+): m/z meas. 663.2400; calc. for C39H39O8Si $[M+Na]^+$ = 663.2409; 1.3 ppm

$[\alpha]_D^{20}$ = only racemate is available

1-*O*-*t*-Butyldiphenylsilyl-2,3-*O*-cyclohexylidene- 4,5-O-dibenzoyl-6-O-methyl-*myo*-inositol (6)

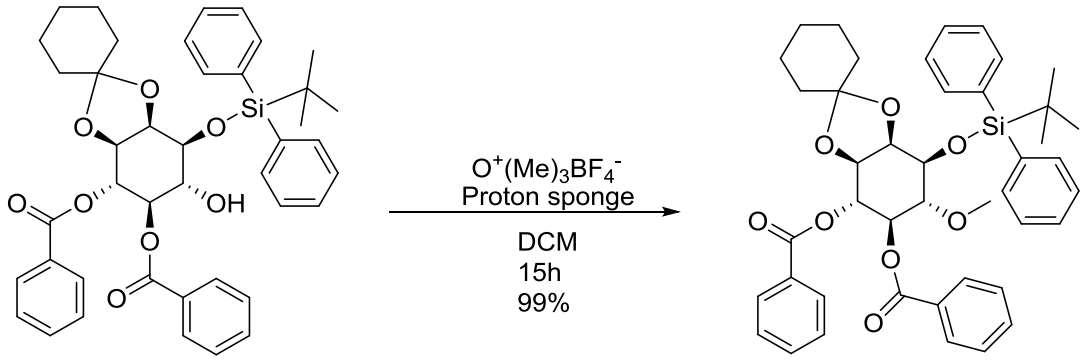

3 **6**

A solution of compound **3** (750 mg, 1.06 mmol) in anhydrous DCM (20 ml) was cooled down to 0° C. Proton Sponge (1249.4 mg, 5.83 mmol, 5.5 eq) was added, followed by trimethyl oxonium tetrafluoroborate (827.6 mg, 5.6 mmol). The reaction was left stirring at RT overnight. Monitoring for the product was done using TLC (3:7 EtOAc: Heptane) and UPLCMS. The product was purified by flash chromatography in an isocratic solvent system (54% EtOAc in Heptane).

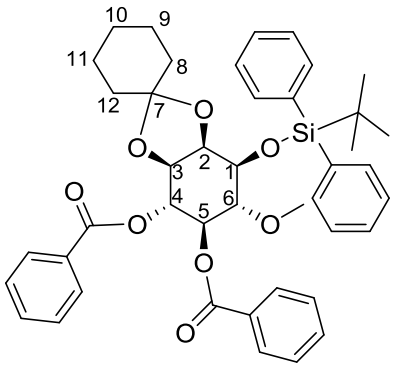

6

^{1}H-NMR (400 MHz, $CDCl_3$) δ 7.98-7.93 (m, 6H, Ar-H), 7.88-7.77 (m, 2H, Ar-H), 7.54- 7.28 (m, 12H, Ar-H), 5.98 (t, 1H, CH-4-*myo*), 5.22-5.18 (dd, J = 9.7 Hz, 1H, CH- 5- *myo*), 4.35-4.32 (dd, J = 7.8 Hz, 1H, CH-1-*myo*), 4.15-4.12 (m, 2H, CH-6-*myo*, CH-3- *myo*), 4.01 (brs, 1H, CH-2-*myo*), 3.27 (s, 3H, H-CH_3), 1.99 (m, 1H, cy), 1.84 (m, 1H, cy), 1.74 (m, 2H, cy), 1.52-1.31 (m, 6H, cy), 1.20 (s, 9H, CH_3-TBDPS)

^{13}C-NMR (100 MHz, $CDCl_3$) δ 165.8, 165.5, 136.1, 135.8, 133.5, 133.3, 133.0, 132.8, 129.9, 129.8, 129.7, 129.6, 128.2, 128.1, 127.8, 127.5, 96.7, 75.1, 74.8, 74.2, 71.2, 67.4, 58.8, 37.2, 34.3, 27.0, 26.9, 25.0, 23.9, 23.8, 19.3

Rf: 0.63 (in 1:1 heptane:EtOAc)

$[\alpha]_D^{20}$ = (-) 7.25 (c = 5mg/mL in $CHCl_3$)

HRMS (ESI)+ m/z meas. 743.3013; calc. for $C_{43}H_{48}O_8Si$ $[M+Na]^+$ 743.3011 -0.4 ppm.

(1R,2R,3R,4R,5R,6S)-4-((tert-butyldiphenylsilyl)oxy)-5,6-dihydroxy-3-methoxycyclohexane-1,2-diyl dibenzoate (7) - Cleavage of the cyclohexylidene acetal in compound 6

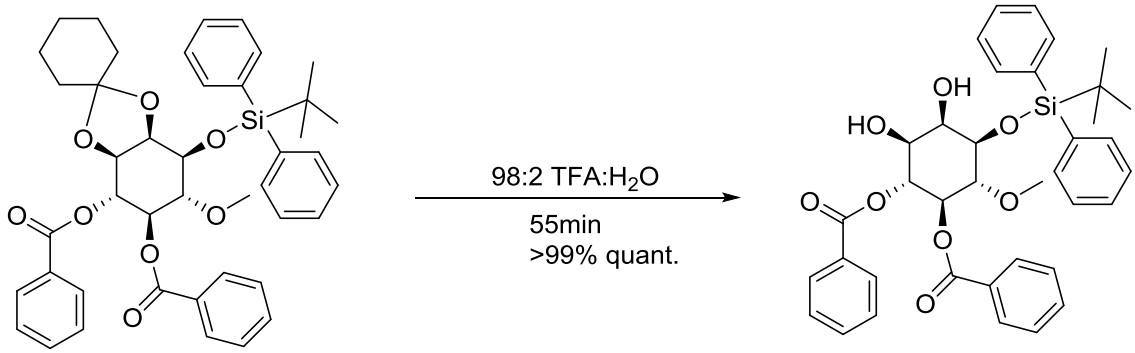

6 **7**

638 mg of crude compound (**6**) were dissolved in 10 ml of a TFA solution in water (98:2 TFA:H_2O) and the reaction was stirred (swirled) for 10 minutes. Minute amounts of ethylene glycol were added as a scavenger to prevent the starting material from reforming upon evaporation of TFA. The reaction was monitored using TLC (1:1 Heptane:EtOAc) and UPLCMS. When the reaction was deemed finished, TFA was then evaporated, then co-evaporated with ethanol (4 times) to get rid of the acid as much as possible. The crude was dissolved in NaCO3 to quench any residual acid, and extracted with DCM (4 times). The organic layers, after being inspected for the presence of the product as opposed to the aqueous layers, were combined, washed with water then brine, then dried over sodium sulfate and filtered. The product was purified through flash chromatography in a 1:1 EtOAc/heptane solvent system.

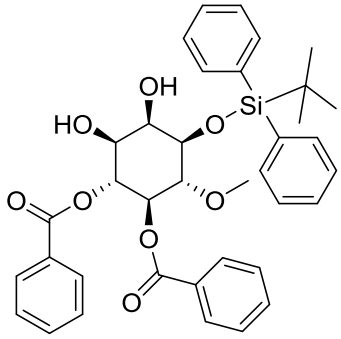

7

^{1}H-NMR (400 MHz, $CDCl_3$) δ 7.90- 7.79 (dd, 4H, Ar-H), 7.69- 7.62 (dd, 4H, Ar-H), 7.44-7.22 (m, 12H, Ar-H), 5.58-5.53 (t, *J* = 9.9 Hz, 1H, *myo*-H), 5.32- 5.27 (t, *J*= 9.7 Hz, 1H, *myo*-H), 4.41- 4.39 (m, 1H, *myo*-H), 3.89-3.83 (m, 1H, *myo*-H), 3.65 (t, *J* = 2.8 Hz, 1H, *myo*-H), 3.44 (dd, *J* = 9.9 Hz, 2.9 Hz, 1H, *myo*-H), 3.35 (s, 3H, methoxy), 1.05 (s, 9H, $(CH_3)_3$).

^{13}C-NMR (100 MHz, $CDCl_3$) δ 167.08, 165.72, 135.98, 135.69, 133.47, 133.18, 133.15, 132.51, 130.22, 130.03, 129.83, 129.80, 129.69, 129.50, 129.24, 128.39, 128.27, 128.12, 128.01, 127.78, 81.37, 77.36, 77.24, 77.04, 76.72, 73.87, 73.61, 72.99, 72.45, 70.75, 69.12, 64.14, 61.28, 60.16, 27.02, 19.41.

$[\alpha]_D^{20}$ = **-** 8.7745455

HRMS (ESI)+ m/z meas. 663.2391; calc. for C37H40O8Si $[M+Na]^+$ 663.2385 -0.9 ppm.

1-*O*-*t*-Butyldiphenylsilyl-2, 3-*O*-cyclohexylidene-6-O-methyl-*myo*-inositol (8)

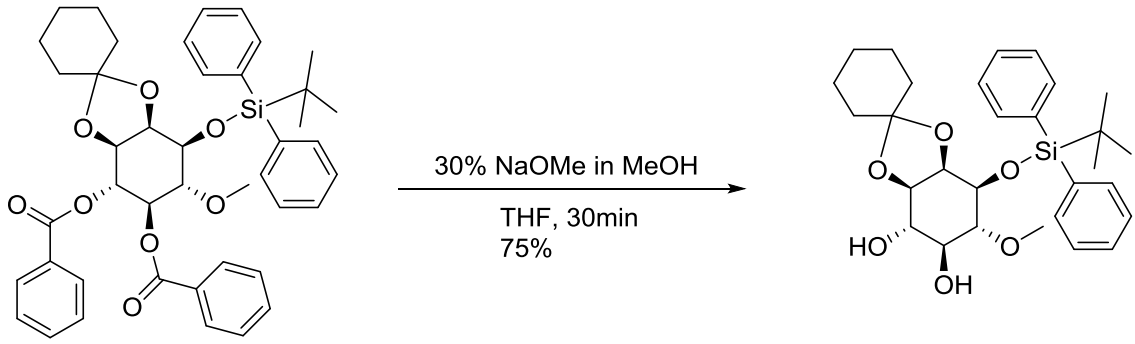

6 **8**

Compound **7** (156.5 mg, 0.217 mmol) was dissolved in anhydrous THF (10 mL), and the reaction mixture was allowed to stir at 0°C. NaOMe (2.5 eq) was added dropwise, and the reaction was taken up to room temperature 5 minutes later. 30 minutes later, the reaction was stopped, quenched with citric acid, and extracted with EtOAc 4 times. The aqueous layers were washed with water, brine, dried over sodium sulfate and filtered. The crude

was purified on flash chromatography in a 36% to 99% EtOAc gradient in DCM, with a yield of 75%.

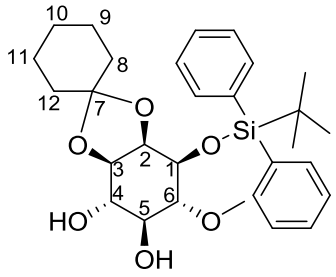

8

^{1}H-NMR (400 MHz, $CDCl_3$) δ (ppm) 7.78 (t, *J* = 7.6 Hz, 4H, Ar-H), 7.47 - 7.32 (m, 6H, Ar-H), 3.94 (md, *J* = 8.7 Hz, 1H, *myo*-H-1), 3.72 (t, *J* = 7.9 Hz, 2H, *myo*-H-2, *myo*-H-4), 3.65 (d, *J* = 6.3 Hz, 1H, *myo*-H-3), 3.62 (s, 3H, H-13), 3.44 (t, *J* = 8.7 Hz, 1H, *myo*-H-6), 3.17 (t, *J* = 9.4 Hz, 1H, *myo*-H-5), 2.36 (br.s, 2H, OH), 1.80 - 1.63 (m, 4H, H-8, H-12), 1.56 - 1.43 (m, 3H, H-9, H-11), 1.36 - 1.26 (m, 3H, H-10, H-11), 1.12 (s, 9H, $C(CH_3)_3$).

^{13}C-NMR (100 MHz, $CDCl_3$) δ (ppm) 136.4, 136.3 (CH, 4C, Ar-C), 134.5, 133.7 (Cq, 2C, Ar-C), 130.2, 128.1, 127.9 (CH, 6C, Ar-C), 111.3 (Cq, 1C, C-7), 83.3 (CH, 1C, *myo*-C-6), 78.3 (CH, 1C, *myo*-C-3), 76.0 (CH, 1C, *myo*-C-2), 75.8 (CH, 1C, *myo*-C-4), 73.8 (CH, 1C, *myo*-C-5), 72.5 (CH, 1C, *myo*-C-1), 61.6 (CH_3, 1C, C-13), 38. 5 (CH_2, 1C, C-12), 35.0 (CH_2, 1C, C-8), 27.4 (CH_3, 3C, $C(CH_3)_3$), 25.4 (CH_2, 1C, C-10), 24.4 (CH_2, 1C, C-11), 24.1 (CH_2, 1C, C-9), 19.7 (Cq, 1C, $C(CH_3)_3$).

$[\alpha]_D^{20}$ = - 11.7892

HRMS (ESI)+ m/z meas. 535.2489; calc. for C29H40O6Si $[M+Na]^+$ 535.2486 -0.5 ppm

1-O-t-Butyldiphenylsilyl-2,3-O-cycloexylidene-4,5-di-O-dibenzylphosphoryl-6-O-methyl-myo-inositol

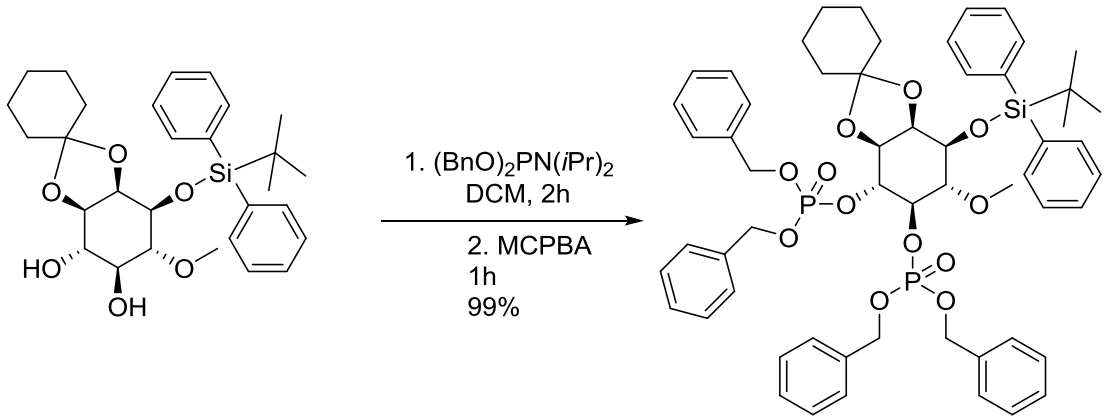

8 **9**

Compound **8** (230mg, 0.45 mmol) was dissolved in anhydrous DCM (20 ml and allowed to stir for a few minutes before adding 1H-tetrazole (0.45 M in ACN, 6mL, 2.7 mmol, 6 eq). The phosphoramidite (464.8 mg, 1.34 mmol, 3 eq) was immediately added in anhydrous acetonitrile (2.2 ml). The reaction was allowed to stir for 2 hours. The reaction was cooled down to -40 ° C, followed by the addition of mcpba (77% w/w, 7.6 mmol, 1255µL) and was allowed to stir for one more hour.

The reaction was quenched with $NaCO_3^-$ and extracted with DCM (200 ml). The organic layer was washed three more times with $NaCO_3^-$, then with water and brine, and condensed to give oil (pale color). The crude was purified using a 100 g silica biotage column, in a gradient from 56% to 60% EtOAc in heptane. Sample loading on the column was done twice, as the total mass of the crude (1267 mg) had to be divided in two for column loading limit (with respect to the Rfs differences on TLC).

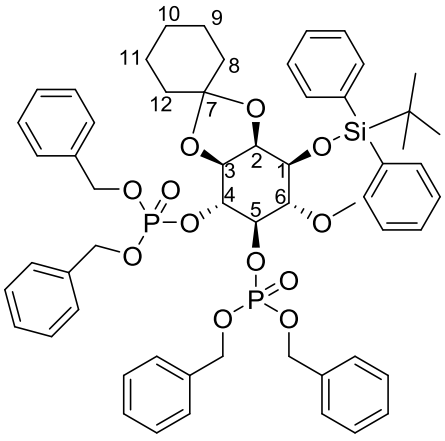

9

^{1}H-NMR (400 MHz, $CDCl_3$) δ 7.81 (d, *J* = 8.0 Hz, 2H, Ar-H), 7.75 (d, *J* = 8.0 Hz, 2H, Ar-H), 7.39 - 7.18 (m, 26H, Ar-H), 5.10 - 4.95 (m, 9H, CH_2-Ar, *myo*-H-4), 4.32 (td, *J* = 9.2 Hz, 1H, *myo*-H-5), 4.12 - 4.05 (m, 1H, *myo*-H-1), 4.02 - 3.93 (m, 2H, *myo*-H-2, *myo*-H-3), 3.56 - 3.49 (m, 1H, *myo*-H-6), 3.20 (s, 3H, H-13), 1.88 - 1.59 (m, 7H, H-8, H-9, H-11, H-12), 1.52 - 1.40 (m, 3H, H-9, H-10), 1.11 (s, 9H, $C(CH_3)_3$).

^{13}C-NMR (100 MHz, $CDCl_3$) δ 136.5 (CH, 4C, Ar-C) 133.6, 133.6 (Cq, 4C, Ar-C), 130.3, 130.1, 128.8, 128.8, 128.7, 128.7, 128.7, 128.6, 128.4, 128.4, 128.3, 128.2, 128.2, 128.1, 128.1, 127.9, 127.8 (CH, 26C, Ar-C), 111.4 (Cq, 1 C, C-7), 82.4 (CH, 1C, *myo*-C-6), 80.6 (CH, 1C, *myo*-C-4), 79.6 (CH, 1C, *myo*-C-5), 76.1 (CH, 1C, *myo*-C-3), 74.8 (CH, 1C, *myo*-C-2), 69.8 (CH, 1C, *myo*-C-1), 69.6, 69.51 (CH_2, 4C, CH2-Ar), 60.2 (CH_3, 1C, C-13) 37.2, 34.5, 28.0 (CH_2, 3C, C-12, C-8, C-10) 27.4 (CH_3, 3C, $C(CH_3)_3$), 25.4, 24.1 (CH_2, 2C, C-9, C-11), 19.7 (Cq, 1C, $C(CH_3)_3$).

^{31}P-NMR (400.13 MHz, $CDCl_3$) δ (ppm) = - 1.6 (s, 1P), -2.04 (s, 1P).

$[\alpha]_D^{20}$ = (-) 2.54 (c = 7 mg/mL in $CHCl_3$)

HRMS (ESI)+ m/z meas. 1055.3694; calc. for C57H66O12P2Si $[M+Na]^+$ 1055.3691 -0.3 ppm

2,3-O-cycloexylidene-4,5-di-O-dibenzylphosphoryl-6-O-methyl-myo-inositol (10)

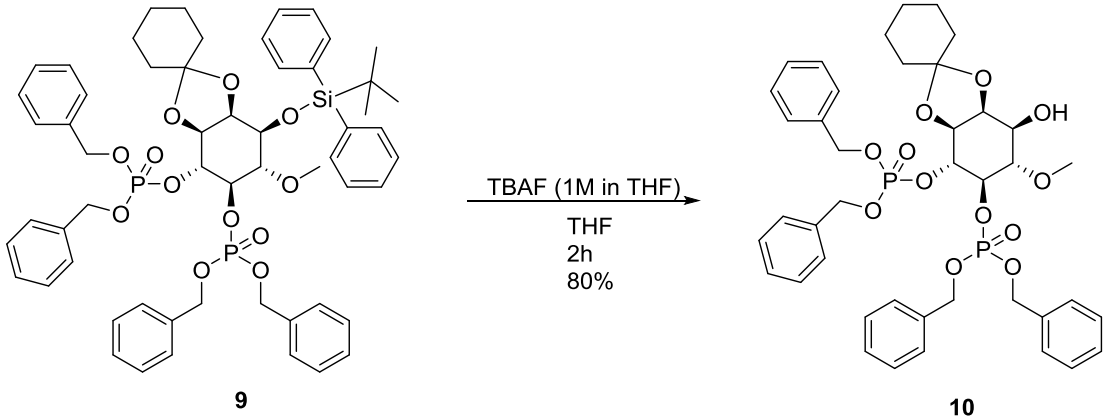

9 **10**

To a solution of **9** (421 mg, 0.4 mmol) in THF (anhydrous, 15 ml) was added a solution of TBAF (707uL, 1.9 eq) in 0.8 ml THF (anhydrous) at 0°C. The reaction was left stirring at room temperature. The reaction mixture turned slightly yellow upon addition of the TBAF reagent. The reaction was stopped after 2 hours, worked up with $NaCO_3^-$ and extracted

with Ethyl Acetate. The crude was purified using flash column chromatography at gradient of 80% to 100% EtOAc in Heptane.

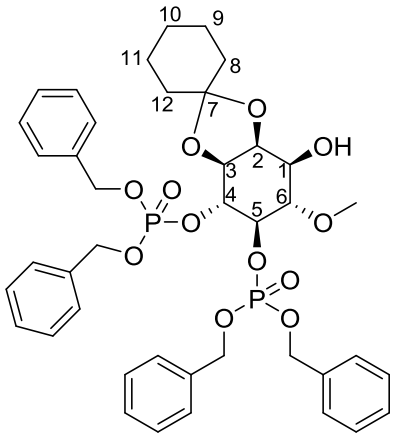

10

^{1}H NMR (400 MHz, $CDCl_3$) δ 7.33 - 7.29 (m, 8H, Ar-H), 7.27 - 7.22 (m, 12H, Ar-H), 5.13 - 4.99 (m, 8H, CH2-Ar), 4.94 (dd, *J* = 8.5 Hz, 1H, *myo*-H-4), 4.50 - 4.44 (m, 1H, *myo*-H-5), 4.42 (dd, *J* = 6.5 Hz, 1H, *myo*-H-2), 4.26 (t, *J* = 7.0 Hz, 1H, *myo*-H-3), 3.98 (dd, *J* = 6.9 Hz, 1H, *myo*-H-1), 3.75 - 3.70 (m, 1H, *myo*-H-6), 3.44 (s, 3H, H-7), 2.54 (br. s, 1H, OH), 1.77 - 1.71 (m, 2H, H-12), 1.66 - 1.53 (m, 6H, H-11, H-9, H-8), 1.37 - 1.31 (m, 2H, H-10).

^{13}C NMR (101 MHz, $CDCl_3$) δ (ppm) = 136.3, 136.2 (Cq, 4C, Ar-C), 128.8, 128.8, 128.7, 128.6, 128.6, 128.6, 128.3, 128.3, 128.2, 128.1 (CH, 20C, Ar-C), 111.7 (Cq, 1C, C-7), 82.0 (CH, 1C, *myo*-C-6), 80.1 (CH, 1C, *myo*-C-4), 79.3 (CH, 1C, *myo*-C-5), 76.2 (CH, 1C, *myo*-C-3), 74.4 (CH, 1C, *myo*-C-2), 69.9, 69.7, 69.7, 69.7, 69.6, 69.6 (CH2, 4C, CH2-Ar), 68.5 (CH, 1C, *myo*-C-1), 59.9 (CH3, 1C, C-13), 37.0 (CH2, 1C, C-12), 34.7, 25.3, 24.2 (CH2, 3C, C-11, C-9, C-8), 23.9 (CH_2, 1C, C-10).

^{31}P-NMR (400.13 MHz, $CDCl_3$): δ - 1.84 (s, 1P), - 2.08 (s, 1P).

$[\alpha]_D^{20}$ = (-) 3.2 (c = 8 mg/mL in $CHCl_3$)

HRMS (ESI)+ m/z meas. 817.2512; calc. for C41H48O12P2 $[M+Na]^+$ 817.2513.

(3aR,4S,5R,6R,7R,7aS)-4-((tert-butyldiphenylsilyl)oxy)-5-ethoxyhexahydrospiro[benzo[d][1,3]dioxole-2,1'-cyclohexane]-6,7-diyl dibenzoate (13)

A solution of compound **3** (325 mg, 0.46 mmol) in anhydrous DCM (15 ml) was cooled down to 0° C. Proton Sponge (985.826 mg, 4.6 mmol, 10 eq) was added, followed by triethyl oxonium tetrafluoroborate (873.9 mg, 4.6 mmol, 10 eq). The reaction was left stirring at RT overnight. Monitoring for the product was done using TLC (3:7 EtOAc: Heptane) and UPLCMS. The product was purified by flash chromatography in an isocratic solvent system (54% EtOAc in Heptane).

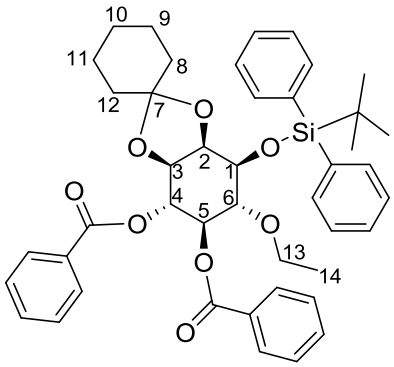

13

^{1}H-NMR (400.13 MHz, $CDCl_3$) δ (ppm) = 7.92 (t, *J* = 6.7 Hz, 4H, Ar-H), 7.85 (d, *J* = 6.7 Hz, 2H, Ar-H), 7.75 (d, *J* = 6.8 Hz, 2H, Ar-H), 7.54 - 7.27 (m, 12H, Ar-H), 5.95 (t, *J* = 9.1 Hz, 1H, *myo*-H-4), 5.15 (md, *J* = 10.1 Hz, 1H, *myo*-H-5), 4.24 (md, *J* = 7.3 Hz, 1H, *myo*-H-1), 4.18 - 4.13 (m, 1H, *myo*-H-3), 4.07 (t, *J* = 4.2 Hz, 1H, *myo*-H-2), 3.64 (t, *J* = 5.9 Hz, 1H, *myo*-H-6), 3.56 (q, *J* = 6.9 Hz, 2H, H-13), 2.04 - 1.96 (m, 1H, H-12), 1.88 - 1.78 (m, 1H, H-12), 1.72 (t, *J*

= 8.1 Hz, 2H, H-8), 1.51 (m, 4H, H-9/11), 1.43 - 1.30 (m, 2H, H-10), 1.16 (s, 9H, $C(CH_3)_3$), 0.97 (t, *J* = 7.0 Hz, 3H, H-14).

^{13}C-NMR (100.92 MHz, $CDCl_3$) δ (ppm) = 166.1, 166.0 (C=O, 2C), 136.6, 136.4 (CH, 4C, Ar-C), 134.0, 133.9 (Cq, 2C, Ar-C), 133.3, 133.2, 130.2, 130.1 (CH, 4C, Ar-C), 130.1, 130.1 (CH, 4C, Ar-C), 128.6, 128.5, 128.04, 127.9 (CH, 8C, Ar-C), 111.3 (Cq, 1C, C-7), 80.1 (CH, 1C, *myo*-C-6), 75.5 (CH, 1C, *myo*-C-3), 75.2 (CH, 1C, *myo*-C-2), 74.6 (CH, 2C, *myo*-C-5, *myo*-C-4), 71.2 (CH, 1C, *myo*-C-1), 68.2 (CH_2, 1C, C-13), 37.6 (CH_2, 1C, C-12), 34.8 (CH_2, 1C, C-8), 27.4 (CH_3, 3C, $C(CH_3)_3$)), 25.5 (CH_2, 1C, C-10), 24.4 (CH_2, 1C, C-11), 24.2 (CH_2, 1C, C-9), 19.7 (Cq, 1C, $C(CH_3)_3$), 15.7 (CH_3, 1C, C-14).

$[\alpha]_D^{20}$ = (-) 7.36 (c= 3 mg/mL in $CHCl_3$)

HRMS (ESI)+ m/z meas. 757.3171; calc. for $C_{44}H_{50}O_8Si$ $[M+Na]^+$ 757.3167 -0.5 ppm.

(3aR,4S,5R,6S,7S,7aR)-4-((tert-butyldiphenylsilyl)oxy)-5-ethoxyhexahydrospiro[benzo[d][1,3]dioxole-2,1'-cyclohexane]-6,7-diol (14)

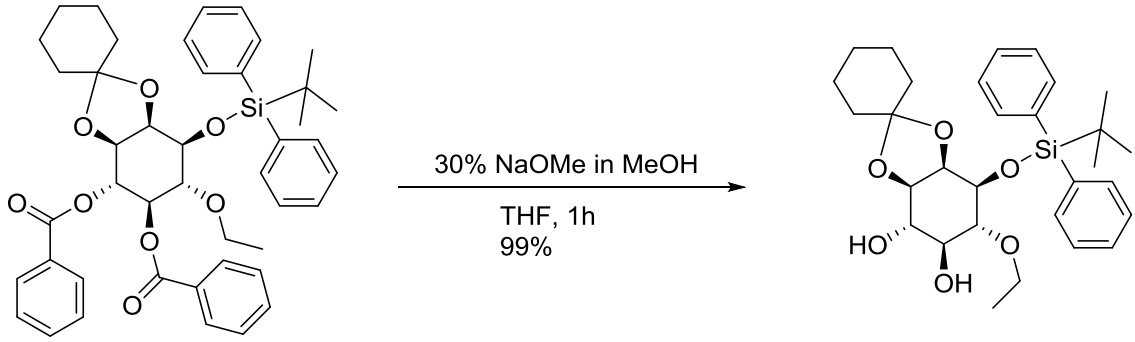

13 **14**

The solution of compound **13** (225 mg, 0.306 mmol, 1 eq) in dry THF (10 mL) was cooled down to 0°C and under stirring was treated, dropwise, with a 30% solution of NaOMe in MeOH (175 µL, 0.766 mmol, 2.5 eq). The reaction mixture was slowly warmed to RT while stirring for 1 h. The reaction solution was quenched with 5 mL of a conc. solution of citric acid in MeOH and 3 mL water. The aqueous phase was washed three times with EtOAc and the combined organic phases first dried with NaSO4, before the solvent was evaporated. The product was purified *Biotage* column in a gradient of 25% to 100% EtOAc in heptane. The product is a white solid and was isolated in 99% yield.

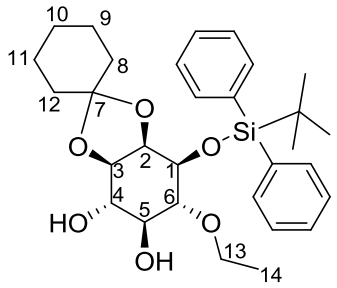

14

R_f (1:1 DCM:EtOAc) = 0.43

^{1}H-NMR (400.13 MHz, $CDCl_3$) δ (ppm) = 7.81 - 7.75 (m, 4H, Ar-H), 7.45 - 7.32 (m, 6H, Ar-H), 4.01 - 3.93 (m, 2H, *myo*-H-1, H-13), 3.76 - 3.67 (m, 3H, *myo*-H-2, *myo*-H-4, H-13), 3.64 (dd, *J* = 5.2 Hz, 1H, *myo*-H-3), 3.53 (t, *J* = 8.8 Hz, 1H, *myo*-H-6), 3.17 (dd, *J* = 9.0 Hz, 1H, *myo*-H-5), 1.79 - 1.63 (m, 4H, H-8, H-12), 1.55 - 1.40 (m, 3H, H-9, H-11), 1.34 - 1.26 (m, 3H, H-10, H-11), 1.21 (t, *J* = 7.0 Hz, 3H, H-14), 1.10 (s, 9H, $C(CH_3)_3$).

^{13}C-NMR (100.92 MHz, $CDCl_3$) δ (ppm) = 136.4, 136.3 (CH, 4C, Ar-C), 134.5, 133.7 (Cq, 2C, Ar-C), 130.2, 130.2, 128.0, 127.9 (CH, 6C, Ar-C), 110.7 (Cq, 1C, C-7), 81.4 (CH, 1C, *myo*-C-6), 78.3 (CH, 1C, *myo*-C-3), 75.9 (CH, 1C, *myo*-C-2), 75.8 (CH, 1C, *myo*-C-4), 73.6 (CH, 1C, *myo*-C-5), 72.7 (CH, 1C, *myo*-C-1), 69.2 (CH_3, 1C, C-13), 38.4 (CH_2, 1C, C-12), 34.9 (CH_2, 1C, C-8), 27.4 (CH_3, 3C, $C(CH_3)_3$), 25.4 (CH_2, 1C, C-10), 24.4 (CH_2, 1C, C-11), 24.1 (CH_2, 1C, C-9), 19.7 (Cq, 1C, $C(CH_3)_3$), 15.9 (CH_3, 1C, C-14).

$[\alpha]_D^{20}$ = (-) -5.1133333 (c = 3 mg/mL in $CHCl_3$)

HRMS (ESI)+ m/z meas. 549.2645; calc. for C30H42O6Si $[M+Na]^+$ 549.2643 -0.4 ppm

Tetrabenzyl((3aR,4S,5S,6R,7R,7aS)-4-((tert-butyldiphenylsilyl)oxy)-5-ethoxyhexahydrospiro[benzo[d][1,3]dioxole-2,1'-cyclohexane]-6,7-diyl) bis(phosphate) (15)

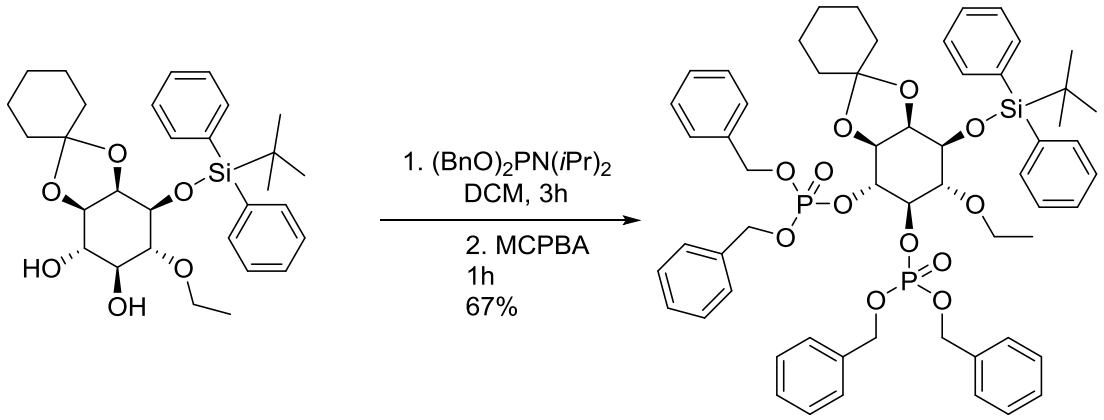

14 **15**

Compound **14** (150 mg, 0.285 mmol) was dissolved in anhydrous DCM (6 mL) and allowed to stir for a few minutes before adding 1H-tetrazole (0.45 M in ACN, 3.8 mL, 1.71 mmol, 6 eq). The reaction was brought down to 0 °C before the phosphoramidite (265.82 mg, 0.769 mmol, 2.7 eq) was immediately added in anhydrous DCM (2 ml). The reaction was allowed to stir for 3 hours at RT. After product formation, monitored by TLC measurements, the reaction was cooled down to -40 ° C, followed by the addition of mcpba (77% w/w, 1.14 mmol, 255.4µL, 4eq) and was allowed to stir for one more hour. After being deemed finished, the reaction was quenched with $NaCO_3^-$ and extracted with DCM (200 ml). The organic layer was washed three more times with $NaCO_3^-$, then with water and brine, and condensed to give oil (pale color). The crude was purified using a 50 g silica Biotage column, in an isocratic gradient of 23% EtOAc in heptane. The product was obtained as a colorless oil with a yield of 67%.

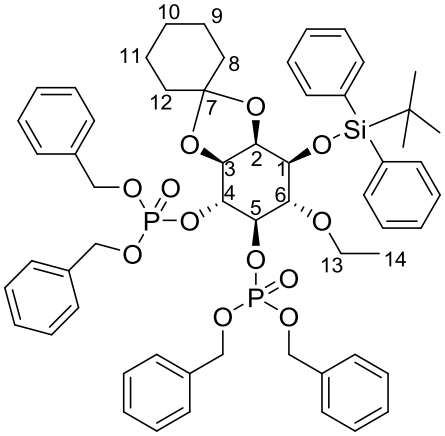

15

^{1}H-NMR (400.13 MHz, $CDCl_3$) δ (ppm) = 7.82 (d, *J* = 7.3 Hz, 2H, Ar-H), 7.76 (d, *J* = 7.3 Hz, 2H, Ar-H), 7.37 - 7.21 (m, 26H, Ar-H), 5.10 - 4.95 (m, 9H, CH_2-Ar, *myo*-H-4), 4.35 (td, *J* = 9.1, Hz, 1H, *myo*-H-5), 4.13 (s, 1H, *myo*-H-1), 4.07 (s, 2H, *myo*-H-2, *myo*-H-3), 3.58 (t, *J* = 4.7 Hz, 1H, *myo*-H-6), 3.35 (s, 1H, H-13), 3.26 (s, 1H, H-13), 1.90 - 1.79 (m, 2H, H-12), 1.75 - 1.57 (m, 3H, H-8, H-10), 1.53 - 1.35 (m, 5H, H-9, H-10, H-11), 1.11 (s, 9H, $C(CH_3)_3$), 0.90 (t, *J* = 6.8 Hz, 3H, H-14).

^{13}C-NMR (100.92 MHz, $CDCl_3$) δ (ppm) = 136.6, 136.6 (CH, 4C, Ar-C), 133.8, 133.8 (Cq, 4C, Ar-C), 130.2, 130.1, 128.9, 128.8, 128.7, 128.7, 128.7, 128.6, 128.4, 128.4, 128.3, 128.2, 128.1, 128.0, 127.8, 127.8 (CH, 26C, Ar-C), 111.2 (Cq, 1C, C-7), 80.8 (CH, 1C, *myo*-C-6), 80.7(CH, 1C, *myo*-C-4), 80.1 (CH, 1C, *myo*-C-5), 75.9 (CH, 1C, *myo*-C-3), 74.5 (CH, 1C, *myo*-C-2), 69.8 (CH, 1C, *myo*-C-1), 69.5, 69.4 (CH_2, 4C, CH2-Ar), 67.3 (CH_2, 1C, C-13) 36.9, 34.4 (CH_2, 2C, C-12, C-8) 27.3 (CH_3, 3C, $C(CH_3)_3$), 25.5, 24.3, 24.1 (CH_2, 3C, C-9, C-10, C-11), 19.6 (Cq, 1C, $C(CH_3)_3$), 15.4 (CH_3, 1C, C-14).

^{31}P-NMR (400.13 MHz, CDCl3) δ (ppm) = - 1.68 (s, 1P), -2.04 (s, 1P).

$[\alpha]_D^{20}$ = (-) 15.584444 (c = 9 mg/mL in $CHCl_3$)

HRMS (ESI)+ m/z meas. 1069.3856; calc. for $C_{58}H_{68}O_{12}P_2Si$ $[M+Na]^+$ 1069.3847 -0.8 ppm.

Tetrabenzyl((3aS,4S,5S,6R,7R,7aS)-5-ethoxy-4-hydroxyhexahydrospiro [benzo[d][1,3]dioxole-2,1'-cyclohexane]-6,7-diyl)bis (phosphate) (16)

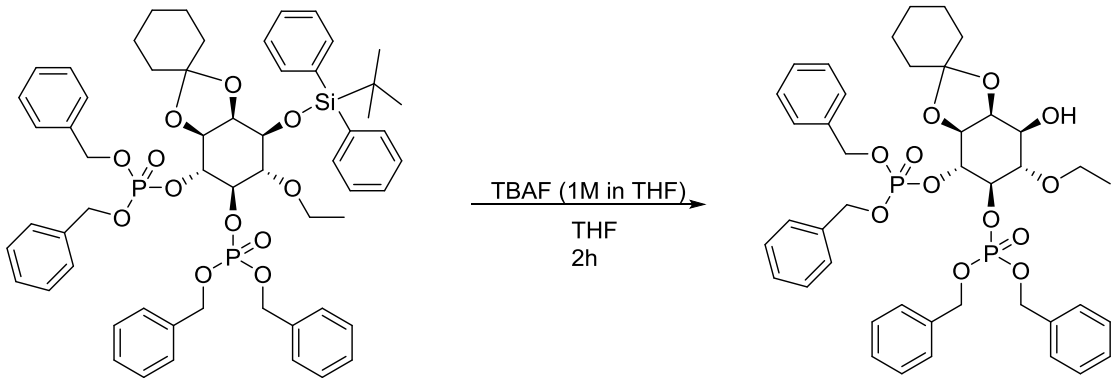

15 16

To a solution of **15** (170 mg, 0.162 mmol) in THF (anhydrous, 8.5 ml) was added a solution of TBAF (308uL, 1.9 eq) in 0.8 ml THF (anhydrous) at 0°C. The reaction was left stirring at room temperature. The reaction mixture turned slightly yellow upon addition of the TBAF reagent. The reaction was stopped after 2 hours, worked up with $NaCO_3^-$ and extracted with Ethyl Acetate. The crude was purified using flash column chromatography at gradient of 30% to 100% EtOAc in Heptane. The product was purified as a colorless oil and was isolated in a yield of 73%.

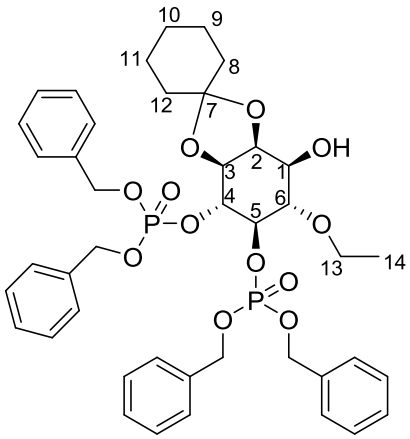

16

^{1}H-NMR (400.13 MHz, $CDCl_3$) δ (ppm) = 7.30 (d, *J* = 6.0 Hz, 9H, Ar-H), 7.25 (d, *J* = 4.3 Hz, 11H, Ar-H), 5.17 - 5.00 (m, 8H, CH_2-Ar), 4.98 (dd, *J* = 14.3 Hz, 1H, *myo*-H-4), 4.51 - 4.41 (m, 2H, *myo*-H-5, *myo*-H-2), 4.28 (t, *J* = 7.2 Hz, 1H, *myo*-H-3), 4.02 - 3.96 (m, 1H, *myo*-H-1), 3.89 - 3.82 (m, 1H, *myo*-H6), 3.79 - 3.69 (m, 1H, H-13), 3.59 - 3.50 (m, 1H, H-13), 2.12 (s, 1H,

OH), 1.80 - 1.69 (m, 2H, H-12), 1.67 - 1.45 (m, 6H, H-11, H-9, H-8), 1.40 - 1.30 (m, 2H, H-10), 1.08 (t, *J* = 6.9 Hz, 3H, H-14).

^{13}C-NMR (100.92 MHz, $CDCl_3$) δ (ppm) = 136.6, 136.5, 136.2, 136.3 (Cq, 4C, Ar-C), 128.8, 128.8, 128.7, 128.6, 128.6, 128.5, 128.4, 128.3, 128.2, 128.1 (CH, 20C, Ar-C), 111.6 (Cq, 1C, C-7), 80.3 (CH, 1C, *myo*-C-6), 80.2 (CH, 1C, *myo*-C-4), 79.8 (CH, 1C, *myo*-C-5), 76.0 (CH, 1C, *myo*-C-3), 74.3 (CH, 1C, *myo*-C-2), 69.9, 69.7, 69.7, 69.6, 69.6 (CH_2, 4C, CH_2-Ar), 68.3 (CH, 1C, *myo*-C-1), 67.5 (CH_2, 1C, C-13), 36.9 (CH_2, 1C, C-12), 34.7, 25.3, 24.2 (CH_2, 3C, C-11, C-9, C-8), 23.9 (CH_2, 1C, C-10), 15.7 (CH_3, 1C, C-14).

^{31}P-NMR (400.13 MHz, CDCl3) δ (ppm) = - 1.9 (s, 1P), -2.1 (s, 1P).

$[\alpha]_D^{20}$ = (-) 3.1086667 (c = 30 mg/mL in CH_3Cl)

HRMS (ESI)+ m/z meas. 831.2673; calc. for C42H50O12P2 $[M+Na]^+$ 831.2670 -0.4 ppm.

(1R,2R,3R,4R,5R,6*S*)-4-((tert-butyldiphenylsilyl)oxy)-3,5,6-trimethoxycyclohexane-1,2-diyldibenzoate(19),
<u>and</u>
(1R,2R,3R,4R,5R,6*S*)-4-((tert-butyldiphenylsilyl)oxy)-5-hydroxy-3,6-dimethoxycyclohexane-1,2-diyl dibenzoate (20)

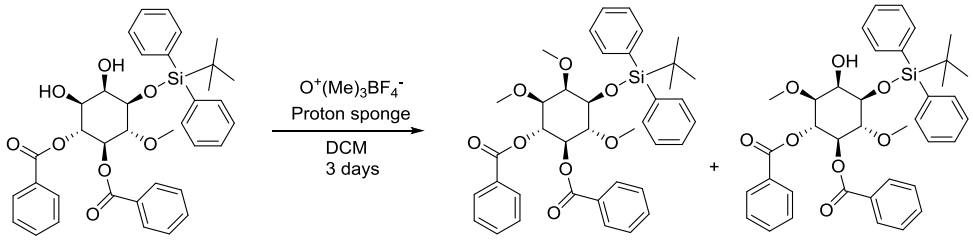

7 19 20

A solution of compound **7** (216.4 mg, 0.35 mmol) in anhydrous DCM (15 ml) was cooled down to 0° C. Proton Sponge (757.43 mg, 3.53 mmol, 10 eq) was added, followed by trimethyl oxonium tetrafluoroborate (522.12 mg, 3.53 mmol, 10 eq). The reaction was left stirring at RT for 3 days. Monitoring for the product was done using TLC (3:7 EtOAc: Heptane) and UPLCMS. The reaction mixture was filtered and the solvent of the supernatant removed under reduced pressure. Products **19** and **20** were purified by

flash chromatography in an isocratic solvent system (25% EtOAc in Heptane), in a 19% and 44% yield, respectively.

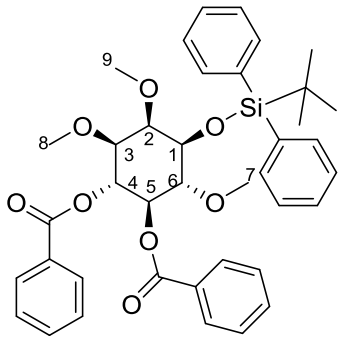

19

^{1}H-NMR (400.13 MHz, CD_3OD) δ (ppm) = 7.99 - 7.94 (m, 2H, Ar-H), 7.89 - 7.85 (m, 2H, Ar-H), 7.80 (td, *J* = 8.0 Hz, 4H, Ar-H), 7.50 - 7.28 (m, 12H, Ar-H), 5.72 (t, *J* = 10.0 Hz, 1H, *myo*-H-4), 5.36 - 5.30 (m, 1H, *myo*-H-5), 3.92 (t, *J* = 9.5 Hz, 1H, *myo*-H-6), 3.81 (dd, *J* = 9.6 Hz, 1H, *myo*-H-1), 3.51 (s, 3H, H-7), 3.44 (s, 3H, H-9), 3.15 (s, 1H, *myo*-H-2), 2.97 (s, 3H, H-8), 2.94 (d, *J* = 1.9 Hz, 1H, *myo*-H-3), 1.15 (s, 9H, $C(CH_3)_3$).

^{13}C-NMR (100.92 MHz, CDCl3) δ (ppm) = 165.3, 165.1 (C=O, 2C), 136.5, 136.3, 133.3, 133.1 (CH, 6C, Ar-C), 132.0, 131.9 (C_q, 2C, Ar-C), 130.4, 130.2, 130.1, 130.0 (CH, 6C, Ar-C), 129.9 (C_q, 2C, Ar-C), 128.6, 128.5, 128.4, 128.2, 128.1 (CH, 8C, Ar-C), 82.0 (CH, 1C, *myo*-C-6), 81.0 (CH, 1C, *myo*-C-3), 77.6 (CH, 1C, *myo*-C-2), 74.4 (CH, 1C, *myo*-C-1), 74.3 (CH, 1C, *myo*-C-5), 72.5 (CH, 1C, *myo*-C-4), 61.9 (CH_3, 1C, C-7), 61.4 (CH_3, 1C, C-9), 58.2 (CH_3, 1C, C-8), 27.4 (CH_3, 3C, $C(CH_3)_3$), 19.7 (C_q, 1C, $C(CH_3)_3$).

$[\alpha]_D^{20}$ = (-) 24.191111 (c = 17 mg/mL in CH_3Cl)

HRMS (ESI)+ m/z meas. 691.2699; calc. for C39H44O8Si $[M+Na]^+$ 691.2698.

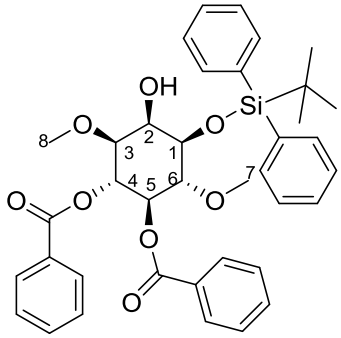

20

^{1}H-NMR (400.13 MHz, CD_3OD) δ (ppm) = 7.97 - 7.93 (m, 2H, Ar-H), 7.88 - 7.84 (m, 2H, Ar-H), 7.83 - 7.76 (m, 4H, Ar-H), 7.49 - 7.39 (m, 8H, Ar-H), 7.38 - 7.29 (m, 4H, Ar-H), 5.77 (t, *J* = 10.0 Hz, 1H, *myo*-H-4), 5.32 (t, *J* = 9.9 Hz, 1H, *myo*-H-5), 3.97 (t, *J* = 9.5 Hz, 1H, *myo*-H-6), 3.81 (d, *J* = 9.4 Hz, 1H, *myo*- H-1), 3.68 (s, *J* = 2.52 Hz, 1H, *myo*-H-2), 3.48 (s, 3H, H-7), 3.06 (s, 3H, H-8), 3.03 (d, *J* = 2.6 z, 1H, *myo*-H-3), 2.34 (s, 1H, OH), 1.13 (s, 9H, $C(CH_3)_3$).

^{13}C-NMR (100.92 MHz, $CDCl_3$) δ (ppm) = 166.2, 166.1 (C=O, 2C), 136.4, 136.2, 133.4, 133.2, (CH, 6C, Ar-C), 132.6, 130.6 (Cq, 2C, Ar-C), 130.4, 130.3, 130.1, 130.1, 130.0 (CH, 6C, Ar-C), 129.9 (Cq, 2C, Ar-C), 128.7, 128.6, 128.2, 128.1 (CH, 8C, Ar-C), 81.7 (CH, 1C, *myo*-C-6), 79.5 (CH, 1C, *myo*-C-3), 74.1 (CH, 1C, *myo*-C-1), 73.9 (CH, 1C, *myo*-C-5), 72.1 (CH, 1C, *myo*-C-4), 68.9 (CH, 1C, *myo*- C-2), 61.8 (CH_3, 1C, C-7), 58.3 (CH_3, 1C, C-8), 27.3 (CH_3, 3C, $C(CH_3)_3$), 19.8 (Cq, 1C, $C(CH_3)_3$).

$[\alpha]_D^{20}$ = (-) 21.92514 (c = 17 mg/mL in CH_3Cl)

HRMS (ESI)+ m/z meas. 677.2548; calc. for $C_{38}H_{42}O_8Si$ $[M+Na]^+$ 677.2541.

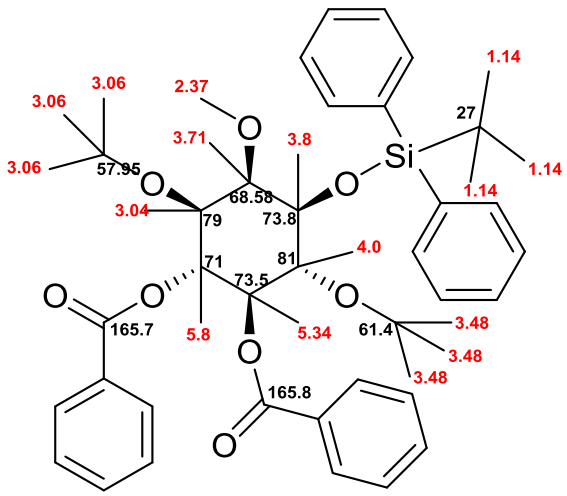

Figure 2 Constructed diagram of 19 after structure elucidation using COSY, HSQC and HMBC. Protons are marked in red, carbons in black

(1R,2R,3R,4R,5R,6*S*)-4-((tert-butyldiphenylsilyl)oxy)-3,5,6-trihydroxycyclohexane-1,2-diyl dibenzoate (21)

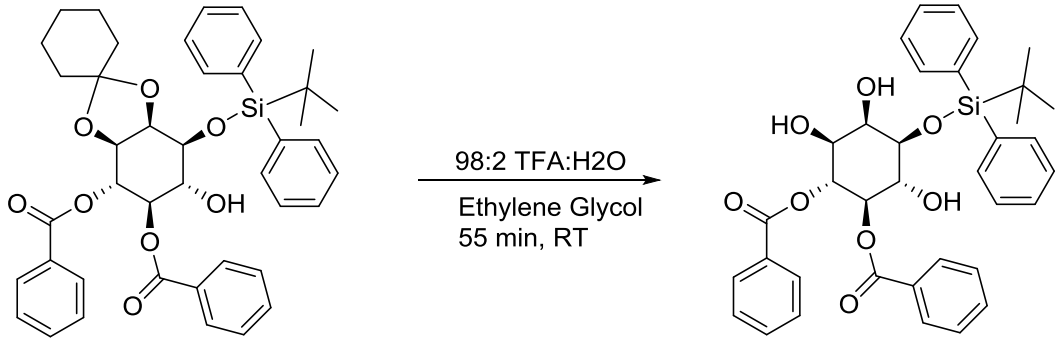

3 21

3 (358.80 mg, 0.51 mmol, 1 eq) was dissolved in 10 mL DCM and 1 mL water and stirred while adding 15 mL of TFA dropwise. 1 mL of ethylene glycol was added at the reaction start. The reaction mixture was stirred for 30 min before diluting it with 10 mL cyclohexane, then removing the solvent mixture and TFA in vacuo. Purification of the compound was reached through column chromatography (cyclohexane/EtOAc 4:1). The product is a white solid and could be obtained in 85% yield.

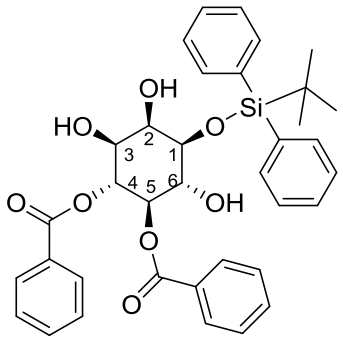

21

Rf (Cyclohexane/EtOAc 2:1) = 0.44.

^{1}H-NMR (400.13 MHz, $CDCl_3$) δ (ppm) = 7.96 - 7.86 (m, 4H, Ar-H), 7.78 - 7.69 (m, 4H, Ar-H), 7.50 - 7.37 (m, 8H, Ar-H), 7.37 - 7.28 (m, 4H, Ar-H), 5.70 (t, *J* = 9.9 Hz, 1H, *myo*-H-4), 5.28 (t, *J* = 9.9 Hz, 1H, *myo*-H-5), 4.31 (t, *J* = 9.5 Hz, 1H, *myo*-H-6), 3.97 (s, 1H, *myo*-H-2), 3.73 (dd, *J* = 9.3 Hz, 1H, *myo*-H-1), 3.61 (dd, *J* = 9.9 Hz, 1H, *myo*-H-3), 2.96 (s, 1H, OH), 2.89 (s, 1H, OH), 2.71 (br.s, 1H, OH), 1.12 (s, 9H, $C(CH_3)_3$).

^{13}C-NMR (100.92 MHz, $CDCl_3$) δ (ppm) = 167.4, 166.6 (C=O, 2C), 136.2, 136.0, 133.5, 133.5, 133.2 (CH, 6C, Ar-C), 132.9, 130.7 (Cq, 2C, Ar-C), 130.6, 130.5, 130.2, 130.1 (CH, 6C,

Ar-C), 129.7, 129.6 (Cq, 2C, Ar-C), 128.6, 128.6, 128.4, 128.4 (CH, 8C, Ar-C), 75.0 (CH, 1C, *myo*-C-1), 74.0 (CH, 1C, *myo*-C-4), 73.2 (CH, 1C, *myo*-C-5), 72.9 (CH, 1C, *myo*-C-2), 72.4 (CH, 1C, *myo*-C-6), 71.3 (CH, 1C, *myo*- C-3), 27.4 (CH_3, 3C, $C(CH_3)_3$), 19.7 (Cq, 1C, $C(CH_3)_3$).

$[\alpha]_D^{20}$ = (-) 3.74 (c = 4 mg/ml in $CHCl_3$)

HRMS (ESI+) m/z meas. 649.2231; calc. for C36H38O8Si $[M+Na]^+$ 649.2228 -0.4 ppm

(1R,2R,3R,4R,5R,6S)-4-((tert-butyldiphenylsilyl)oxy)-3,5,6-triethoxycyclohexane-1,2-diyl dibenzoate (22) and (1R,2R,3R,4R,5R,6S)-4-((tert-butyldiphenylsilyl)oxy)-3,6-diethoxy-5-hydroxycyclohexane-1,2-diyl dibenzoate (23)

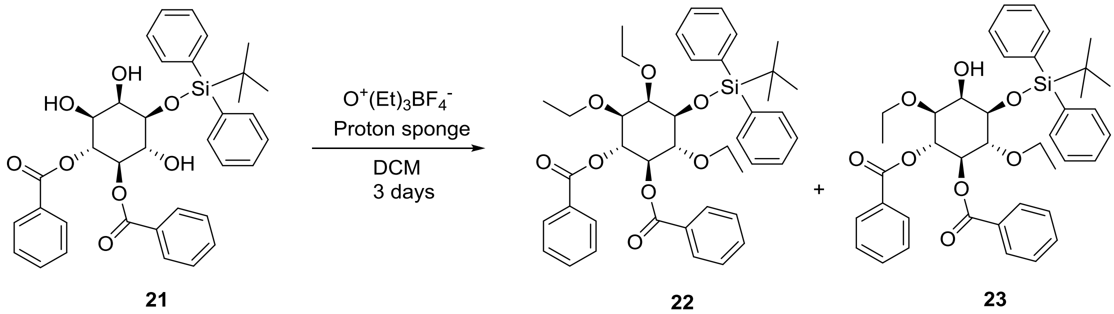

22 and **23** were obtained from **21** (116 mg, 0.185 mmol, 1 eq) analogously as the procedure described for **19** and **20** with proton sponge (792.9 g, 3.7 mmol, 20 eq), Et3OBF4 (626.96 g, 3.3 mmol, 18 eq) and stirring for 48 h. The products were colorless solids. **22** was isolated with 15% yield and **23** in a yield of 45%.

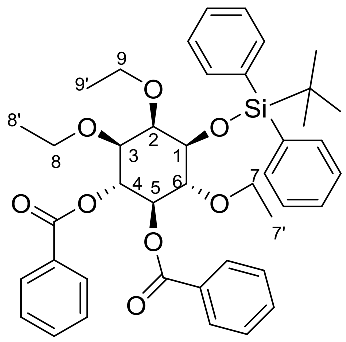

22

^{1}H-NMR (400.13 MHz, CD_3OD) δ (ppm) = 8.01 - 7.96 (m, 2H, Ar-H), 7.89 - 7.76 (m, 6H, Ar-H), 7.49 - 7.29 (m, 12H, Ar-H), 5.70 (t, *J* = 10.0 Hz, 1H, *myo*-H-4), 5.33 (t, *J* = 9.7 Hz, 1H, *myo*-H-5), 4.02 (t, *J* = 9.5 Hz, 1H, *myo*-H-6), 3.93 - 3.86 (m, 1H, H-7), 3.83 (dd, *J* = 9.6 Hz, *myo*-H-1) 3.72 - 3.60 (m, 2H, H-7, H-9), 3.32 (dq, *J* = 14.1 Hz, 1H, H-9), 3.16 -

3.06 (m, 2H, *myo*-H-2, H-9), 3.04 - 2.93 (m, 2H, *myo*-H-3, H-9), 1.20 (t, *J* = 7.0 Hz, 3H, H-9‘), 1.14 (s, 9H, C(CH_3)$_3$), 1.01 (t, *J* = 7.0 Hz, 3H, H-7‘), 0.80 (t, *J* = 7.0 Hz, 3H, H-8‘).

^{13}C-NMR (100.92 MHz, $CDCl_3$) δ (ppm) = 166.2, 166.1 (C=O, 2C), 136.5, 136.3 (CH, 4C, Ar-C), 135.1, 133.6 (C_q, 2C, Ar-C), 133.2, 133.0 (CH, 2C, Ar-C), 130.5, 130.3 (C_q, 2C, Ar-C), 130.3, 130.1, 130.0, 129.9, 128.6, 128.5, 128.1, 128.0 (CH, 14C, Ar-C), 79.9 (CH, 1C, *myo*-C-6), 79.0 (CH, 1C, *myo*-C-3), 77.3 (CH, 1C, *myo*-C-2), 74.3 (CH, 1C, *myo*-C-1), 74.3 (CH, 1C, *myo*-C-5), 72.6 (CH, 1C, *myo*-C-4), 69.5 (CH_2, 1C, C-7), 68.7 (CH_2, 1C, C-9), 65.9 (CH_2, 1C, C-8), 27.4 (CH_3, 3C, C(CH_3)$_3$), 19.6 (C_q, 1C, C(CH_3)$_3$), 16.2 (CH_3, 1C, C-9’), 16.0 (CH_3, 1C, C-7’), 15.4 (CH_3, 1C, C-8’).

$[\alpha]_D^{20}$ = (-) 3.204 (c = 5 mg/ml in $CHCl_3$)

HRMS (ESI)+ m/z meas. 733.3176; calc. for C42H50O8Si $[M+Na]^+$ 733.3167 -1.2 ppm

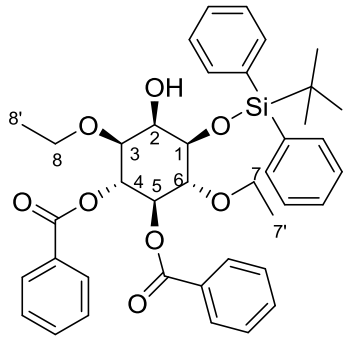

23

^{1}H-NMR (400.13 MHz, CD_3OD) δ (ppm) = 7.97 - 7.92 (m, 2H, Ar-H), 7.88 - 7.78 (m, 6H, Ar-H), 7.50 - 7.28 (m, 12H, Ar-H), 5.74 (t, *J* = 10.0 Hz, 1H, *myo*-H-4), 5.32 (t, *J* = 9.9 Hz, 1H, *myo*-H-5), 4.06 (t, *J* = 9.5 Hz, 1H, *myo*-H-6), 3.89 - 3.82 (m, 2H, *myo*-H-1, H-7), 3.69 - 3.61 (m, 1H, H-7), 3.53 (t, *J* = 2.5 Hz, 1H, *myo*-H-2), 3.27 - 3.20 (m, 1H, H-8), 3.11 (qd, *J* = 7.0 Hz, 2H, *myo*-H-4), 1.13 (s, 9H, C(CH_3)$_3$), 0.98 (t, *J* = 7.0 Hz, 3H, H-7‘), 0.86 (t, *J* = 7.0 Hz, 3H, H-8‘).

^{13}C-NMR (100.92 MHz, $CDCl_3$) δ (ppm) = 166.2, 166.0 (C=O, 2C), 136.4, 136.2 (CH, 4C, Ar-C), 134.6 (C_q, 1C, Ar-C), 133.3, 133.2 (CH, 2C, Ar-C), 133.1 (C_q, 1C, Ar-C), 130.4, 130.2 (CH, 2C, Ar-C), 130.1 (C_q, 2C, Ar-C), 130.0, 129.9, 128.7, 128.6, 128.2, 128.1 (CH, 12C, Ar-C), 79.6 (CH, 1C, *myo*-C-6), 77.9 (CH, 1C, *myo*-C-3), 74.3 (CH, 1C, *myo*-C-1), 73.8 (CH, 1C, *myo*-C-5), 72.1 (CH, 1C, *myo*-C- 4), 70.0 (CH, 1C, *myo*-C-2), 69.5 (CH_2, 1C, C-7), 66.3 (CH_2, 1C, C-8), 27.3 (CH_3, 3C, C(CH_3)$_3$), 19.7 (C_q, 1C, C(CH_3)$_3$), 15.9 (CH_3, 1C, C-7’), 15.5 (CH_3, 1C, C-8’).

$[\alpha]_D^{20}$ = (-)13.906 (c = 10 mg/mL in $CHCl_3$)

HRMS (ESI)+ m/z meas. 705.2858; calc. for C40H46O8Si $[M+Na]^+$ 705.2854 -0.6 ppm

(1S,2S,3R,4S,5R,6R)-4-((tert-butyldiphenylsilyl)oxy)-3,5,6-trimethoxycyclohexane-1,2-diol (24)

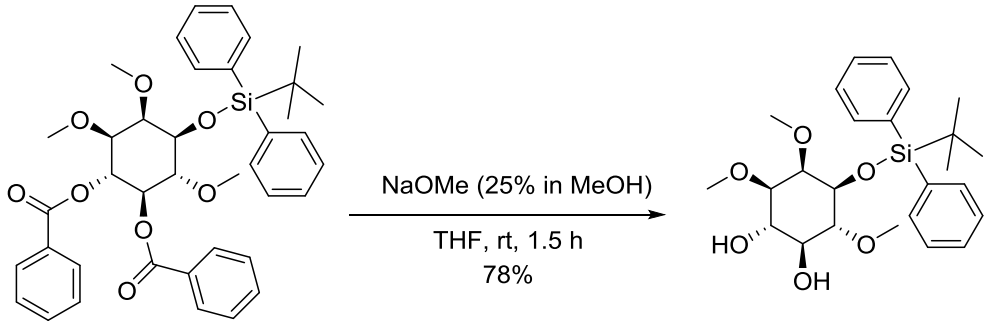

19 **24**

Compound 24 was obtained by dissolving 19 (253 mg, 0.378 mmol, 1 eq) in anhydrous THF (8mL), and adding NaOMe (216 uL, 0.946 mmol, 2.5 eq) dropwise at 0°C. The reaction solution turned turbid and pale yellow upon addition of the NaOMe solution. The reaction solution was left stirring at rtf o 1.5 hours. Monitoring for the product was done using TLC (3:7 EtOAc: Heptane) and UPLCMS. The reaction mixture was quenched with citric acid, extracted 4 times with EtOAc, washed with water, then with brine, dried over NaSO4 and condensed, yielding a crude weighing 260 mg. The product was purified over flash column chromatography at a gradient of 40% to 100% EtOAc in Heptane, yielding a colorless solid with a yield of 78%.

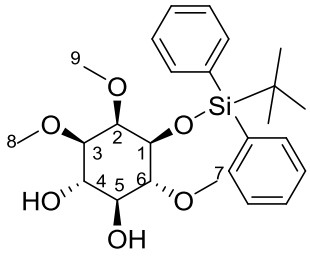

24

^{1}H-NMR (400.13 MHz, CD_3OD) δ (ppm) = 7.69-7.71 (m, 3H, Ar-H), 7.39-7.32 (m, 6H, Ar-H), 7.19-7.18 (m, 1H, Ar-H), 3.65 (s, 3H, H-7), 3.57 (t, *J* = 10.0 Hz, 1H, *myo*-H-4), 3.46 (m,

1H, *myo*-H-5), 3.28 (s, 3H, H-9), 3.19-3.17 (t, *J* = 9.5 Hz, 1H, *myo*-H-6), 2.94 (s, 3H, H-8), 2.49-2.45 (m, 3H, myo-H-1,2,3), 1.07 (s, 9H, C(CH3)3).

^{13}C-NMR (100.92 MHz, $CDCl_3$) δ (ppm) = 136.13, 136.00, 134.70, 133.10 (CH, 4C, Ar-C), 130.14, 130.03 (C_q, 2C, Ar-C), 129.82, 128.46, 127.88, 127.70 (CH, 4C, Ar-C), 82.87 (CH, 1C, *myo*-C-6), 81.88 (CH, 1C, *myo*-C-3), 77.36 (CH, 1C, *myo*-C-2), 77.04 (CH, 1C, *myo*-C-5), 74.53 (CH, 1C, *myo*-C-1), 71.87 (CH, 1C, *myo*-C-4), 61.82 (CH_3, 1C, C-7), 60.82 (CH_3, 1C, C-8), 57.06 (CH_3, 1C, C-9), 27.11 (CH_3, 3C, C(CH_3)$_3$), 19.21 (C_q, 1C, C(CH_3)$_3$).

$[\alpha]_D^{20}$ = (-) 2.0621359 (c = 10.3 mg/mL in CH_3Cl)

HRMS (ESI)+ m/z meas. 483.2179; calc. for $C_{25}H_{36}O_6Si$ $[M+Na]^+$ 483.2173 -1.1 ppm.

Tetrabenzyl((1R,2R,3S,4R,5R,6S)-4-((tert-butyldiphenylsilyl)oxy)-3,5,6-trimethoxycyclohexane-1,2-diyl) bis(phosphate) (25)

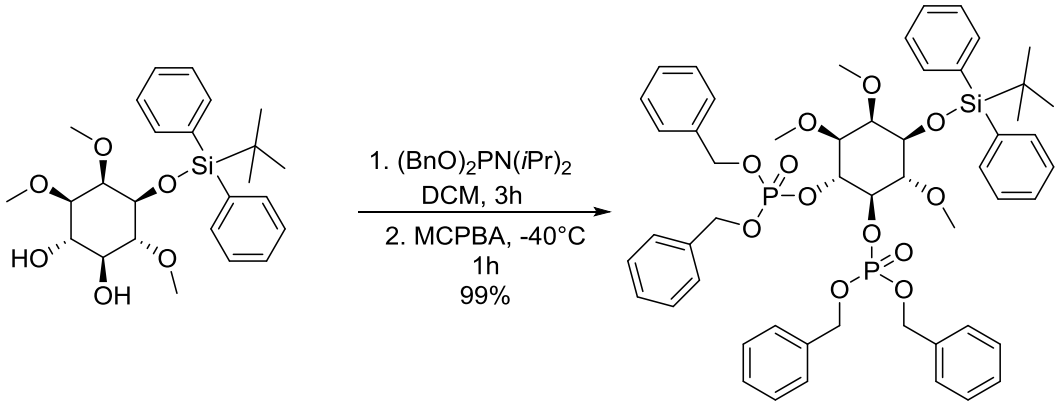

24 **25**

Compound **24** (126 mg, 0.273 mmol) was dissolved in anhydrous DCM (7 mL) and allowed to stir for a few minutes before adding 1H-tetrazole (0.45 M in ACN, 3.6 mL, 1.642 mmol, 6 eq). The reaction was brought down to 0 °C before the phosphoramidite (275.86 mg, 0.821 mmol, 3 eq) was immediately added in anhydrous DCM (2 ml). The reaction was allowed to stir for 3 hours at RT. After product formation, monitored by TLC measurements, the reaction was cooled down to -40 ° C, followed by the addition of mcpba (77% w/w, 1.642 mmol, 367.99mg, 6eq) and was allowed to stir for one more hour. After being deemed finished, the reaction was quenched with $NaCO_3^-$ and extracted with DCM (200 ml). The organic layer was washed three more times with $NaCO_3^-$, then with water and brine, and condensed to give oil (pale color). The crude (605 mg) was

purified using a 10 g silica Biotage column, in a gradient of 23% to 33% EtOAc in heptane. The product was obtained as a colorless oil with a yield of 99%.

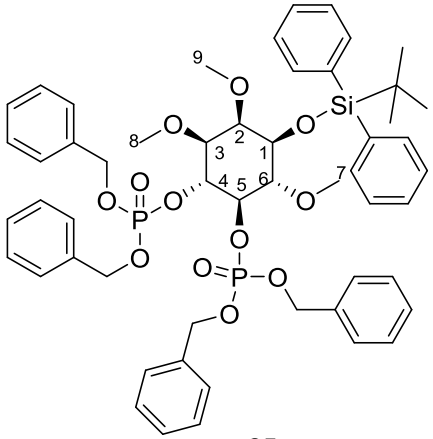

25

^{1}H-NMR (400.13 MHz, CD_3OD) δ (ppm) = 7.69 (d, *J* = 7.1 Hz, 2H, Ar-H), 7.41 – 7.30 (m, 4H, Ar-H), 7.30 – 7.21 (m, 6H, Ar-H), 7.18 – 7.12 (m, 16H, Ar-H), 4.99 (ddd, *J* = 9.7 Hz, 2H, CH_2-Ar), 4.94 (d, *J* = 5.9 Hz, 3H, CH_2-Ar, *myo*-H-6), 4.90 (d, *J* = 7.1 Hz, 4H, CH2-Ar), 4.63 (d, *J* = 9.2 Hz, 1H, *myo*-H-5), 4.27 (m, 1H, *myo*-H-4), 3.66-3.56 (m, 2H, *myo*-H-6, *myo*-H-3), 3.52 (s, 3H, H-9), 3.24 (s, 3H, H-8), 2.74 (s, 3H, H-7), 1.16 (m, 2H, *myo*-H-1, *myo*-H-2), 1.06 (s, 9H, $C(CH_3)_3$).

^{13}C-NMR (100.92 MHz, $CDCl_3$) δ (ppm) = 136.22 (CH, 4C, Ar-C), 136.06, 135.91, 134.56, 132.86 (Cq, 4C, Ar-C), 130.07, 129.95, 129.08, 128.75, 128.60, 128.57, 128.52, 128.42, 128.33, 128.27, 128.19, 128.08, 128.02, 128.00, 127.96, 127.93, 127.83, 127.80, 127.60, 127.45 (CH, 22C, Ar-C), 81.36 (CH, 1C, *myo*-C-6), 77.35 (CH, 1C, *myo*-C-5), 77.24 (CH, 1C, *myo*-C-3), 77.03 (CH, 1C, *myo*-C-4), 76.72 (CH, 1C, *myo*-C-2), 76.11 (CH, 1C, *myo*-C-1), 74.01, 73.55, 71.03, 70.96, 69.33l, 69.20, 61.80, 60.86 (CH_2, 8C, CH_2-Ar), 57.00 (CH_3, 3C, $C(CH_3)_3$), 27.08 (CH_3, 3C, $C(CH_3)_3$), 22.57 (CH_3, 3C, $C(CH_3)_3$), 19.25 (Cq, 1C, $C(CH_3)_3$).

^{31}P-NMR (400.13 MHz, $CDCl_3$) δ (ppm) = - 1.69 (s, 1P), -2.54 (s, 1P).

$[\alpha]_D^{20}$= (-) 6.5072727 (c = 11 mg/mL in CH_3Cl)

HRMS (ESI)+ m/z meas. 1003.3381; calc. for C53H62O12P2Si $[M+Na]^+$ 1003.3378 -0.3 ppm.

Tetrabenzyl((1R,2R,3S,4R,5S,6S)-4-hydroxy-3,5,6-trimethoxycyclohexane-1,2-diyl) bis(phosphate) (26)

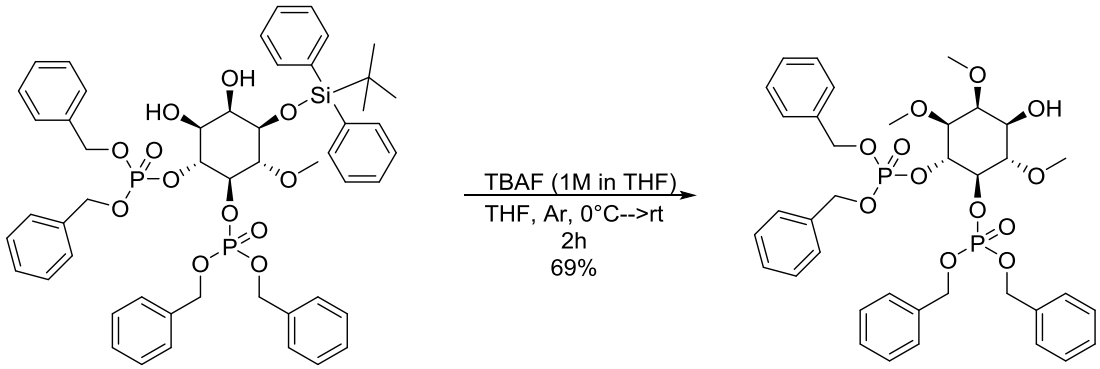

25 26

To a solution of **25** (275 mg, 0.28 mmol) in THF (anhydrous, 15 ml) was added a solution of TBAF (500uL, 1.8 eq) in 0.8 ml THF (anhydrous) at 0°C. The reaction was left stirring at room temperature. The reaction mixture turned slightly yellow upon addition of the TBAF reagent. The reaction was stopped after 2 hours, worked up with $NaCO_3^-$ and extracted with Ethyl Acetate. The crude (298mg) was purified using flash column chromatography at gradient of 80% to 100% EtOAc in Heptane, and was obtained as a pale yellow oil (solid) with a 69% yield.

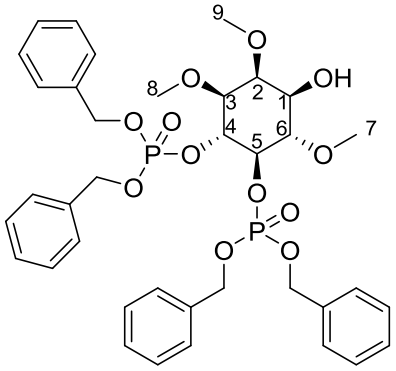

26

^{1}H NMR (400 MHz, $CDCl_3$) δ = 7.21 (s, 10H, Ar-H), 7.17 (t, *J* = 3.5 Hz, 10H, Ar-H), 4.97 (m, 8H, CH2-Ar), 4.75 (d, *J* = 9.1 Hz, 1H, *myo*-H-4), 4.33 (d, *J* = 8.9 Hz, 1H, *myo*-H-5), 3.77 (m, 1H, *myo*-H-6), 3.56 (s, 3H, H-7), 3.49 – 3.44 (m, 1H, *myo*-H-3), 3.42 (s, 3H, H-8), 3.40 (d, *J* = 9.2 Hz, 1H, *myo*-H-2), 3.27 (s, 1H, H-9), 3.15 (dd, *J* = 9.5, 1.8 Hz, 1H, *myo*-H-1).

^{13}C NMR (101 MHz, $CDCl_3$) δ (ppm) = 136.20, 136.12, 136.04 (Cq, 8C, Ar-C), 128.45, 128.41, 128.36, 128.34, 128.27, 128.18, 128.15, 128.12, 127.92, 127.87, 127.83, 127.69 (Cq, 12C, Ar-C), 81.76 (Cq, 1C, C-7), 81.12 (Cq, 1C, C-8), 78.80 (Cq, 1C, C-9), 77.96 (CH, 1C, *myo*-C-6), 77.35 (CH, 1C, *myo*-C-4), 77.24 (CH, 1C, *myo*-C-5), 77.04 (CH, 1C, *myo*-C-3), 76.72 (CH, 1C, *myo*-C-2), 71.86 (CH, 1C, *myo*-C-1), 69.43, 69.37, 69.29, 69.21 (CH2, 4C, CH2-Ar).

^{31}P-NMR (400.13 MHz, CDCl3): δ - 1.6 (s, 1P), - 2.05 (s, 1P).

$[\alpha]_D^{20}$ = (-) 14.218462 (c = 13 mg/mL in CH_3Cl)

HRMS (ESI)+ m/z meas. 765.2202; calc. for C37H44O12P2 $[M+Na]^+$ 765.2200 -0.2 ppm.

(3aR,4S,5R,6R,7R,7aS)-4-((tert-butyldiphenylsilyl)oxy)-5-((2-methoxyethoxy)methoxy)hexahydrospiro[benzo[d][1,3]dioxole-2,1'-cyclohexane]-6,7-diyl dibenzoate (29)

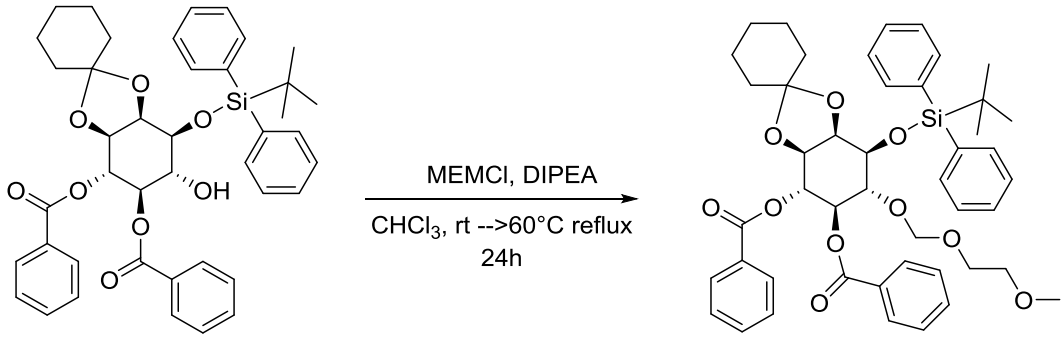

3 **29**

Compound **3** (2501 mg, 3.56mmol, 1 eq) was dissolved in anhydrous $CHCl_3$ (35 mL) under Argon atmosphere. DIPEA (dry, 8.7 mL, 49.9 mmol, 14 eq) was then added at room temperature, followed by MEMCl (3.98 mL, 34.93 mmol, 9.8 eq). The reaction was heated to 60°C under reflux, and was left stirring overnight. When deemed finished, the reaction was quenched with NaCO3-, extracted three times with EtOAc, washed with water, then brine, dried over NaSO4 and condensed to yield a crude weighing 3001 mg. Purification of the product was achieved by column chromatography (isocratic gradient 18% EtOAc in heptane). The product is a colourless oil and was isolated with a 60% yield.

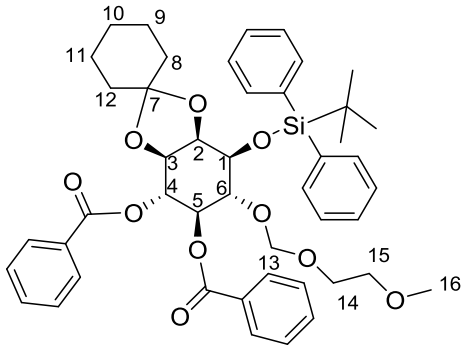

29

R_f: 0.34 (in 7:3 heptane:EtOAc)

^{1}H NMR (400 MHz, $CDCl_3$) δ (ppm) = 7.87 – 7.82 (m, 2H, Ar-H), 7.77 (ddd, *J* = 18.5 Hz, 4H, Ar-H), 7.68 – 7.61 (m, 2H, Ar-H), 7.44 – 7.18 (m, 12H, Ar-H), 5.13 (dd, *J* = 9.8 Hz, 1H, CH-4-*myo*), 4.91 (d, *J* = 6.5 Hz, 1H, CH- 5- *myo*), 4.65 (d, *J* = 6.9 Hz, 1H, CH-1-*myo*), 4.24 (dd, *J* = 7.9 Hz, 1H, CH-3- *myo*), 4.03 (d, *J* = 9.1 Hz, 1H, CH-6-*myo*), 3.90 (s, 1H, CH-2-*myo*), 3.52 – 3.23 (m, 2H, H-14), 3.11 (s, 1H, H-16), 3.07 – 2.86 (m, 2H, H-15), 1.92 (d, *J* = 14.2 Hz, 1H, cy), 1.72 (dd, *J* = 12.8 Hz, 2H, cy), 1.39 (d, *J* = 24.4 Hz, 4H, cy), 1.20 (d, *J* = 12.0 Hz, 3H, cy), 1.06 (s, 9H, CH_3-TBDPS).

^{13}C-NMR (100.92 MHz, $CDCl_3$) δ (ppm) = 165.87, 165.53 (C=O, 2C), 136.16, 135.86, 133.57, 133.27 (CH, 4C,Ar-C), 133.07, 132.88 (Cq, 2C, Ar-C), 129.97, 129.87, 129.81, 129.70 (CH, 4C, Ar-C), 129.65, 129.57, 128.27, 128.16 (CH, 4C, Ar-C), 127.85, 127.59 (CH, 2C, Ar-C), 111.11 (Cq, 1C, C-7), 96.79 (CH, C-13), 77.35 (CH, 1C, *myo*-C-6), 77.23 (CH, 1C, *myo*-C-3), 77.03 (CH, 1C, *myo*-C-2), 76.72 (CH, 2C, *myo*-C-5, *myo*-C-4), 75.11 (CH, C-14), 74.81 (CH, C-15), 71.75 (CH, 1C, *myo*-C-1), 67.44 (CH, C-16), 58.83, 37.31 (CH_2, 1C, C-12), 34.34 (CH_2, 1C, C-8), 27.08 (CH_3, 3C, $C(CH_3)_3$), 25.08 (CH_2, 1C, C-10), 23.99 (CH_2, 1C, C-11), 23.82 (CH_2, 1C, C-9), 19.35 (Cq, 1C, $C(CH_3)_3$).

$[\alpha]_D^{20}$ = (-)7.3428571 (c = 7 mg/ml in $CHCl_3$)

HRMS (ESI)+ m/z meas. 817.3387; calc. for C46H54O10Si $[M+Na]^+$ 817.3378 -1.1 ppm.

(3aR,4S,5R,6S,7S,7aR)-1-((tert-butyldiphenylsilyl)oxy)-6-((2-methoxyethoxy)methoxy)hexahydrospiro[benzo[d][2,3]dioxole-2,1'-cyclohexane]-4,5-diol (30)

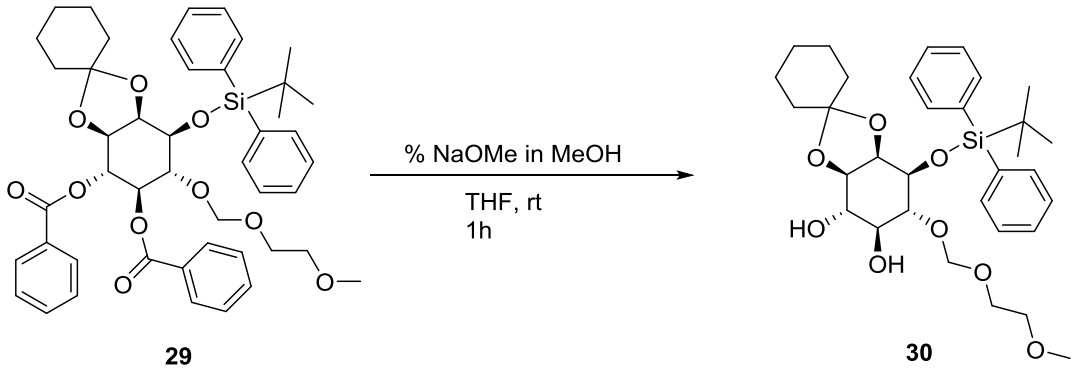

29 30

Compound 29 (1700 mg, 2.14 mmol, 1 eq) was dissolved in THF (dry, 40 mL) and the reaction mixture was cooled down to 0°C. NaOMe solution was added dropwise, and the reaction was brought up to RT by removing the ice bath 10 minutes after the reaction start. The reaction mixture turned yellow upon addition of NaOMe. 1 hour later, the reaction was deemed finished, stopped and worked up by quenching with citric acid, extracting 4 times with EtOAc. The organic layers were then combined, washed with water, brine, then dried over NaSO4-, filtered and condensed, yielding a yellow crude with a sharp aromatic smell, weighing 1880 mg. Purification of the product was achieved by column chromatography (gradient of 20%-100% EtOAc in heptane). The product was isolated with >99% quantitative yield.

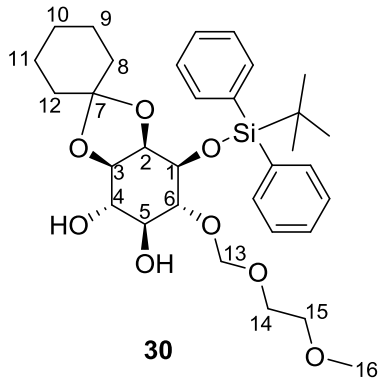

30

^{1}H NMR (400 MHz, $CDCl_3$) δ (ppm) = 7.68 (ddd, *J* = 17.5 Hz, 4H, Ar-H), 7.44 – 7.17 (m, 6H, Ar-H), 4.69 (q, *J* = 7.3 Hz, 2H, C-13), 3.81 (ddd, *J* = 27.0 Hz, 3H, CH-4-*myo*, CH-5-*myo*, CH-6-*myo*), 3.63 (ddd, *J* = 12.7 Hz, 4H, H-14, H-15), 3.48 (p, *J* = 2.3 Hz, 2H, CH-3-*myo*, CH-1-

myo), 3.31 (s, 3H, H-16), 3.04 (t, *J* = 9.0 Hz, 1H, CH-2-*myo*), 1.63 (d, *J* = 10.5 Hz, 4H, H-12, H-8), 1.31 (d, *J* = 4.9 Hz, 6H, H-9, H-10, H-11), 1.02 (s, 9H, CH_3 -TBDPS).

^{13}C-NMR (100.92 MHz, $CDCl_3$) δ (ppm) = 136.01, 135.95, 135.80, 135.78 (CH, 4C,Ar-C), 133.91, 133.45 (Cq, 2C, Ar-C), 133.28, 133.20, 130.11, 129.83 (CH, 4C, Ar-C), 127.84, 127.64 (CH, 2C, Ar-C), 110.47 (Cq, 1C, C-7), 97.76 (CH, C-13), 97.68 (CH, C-14), 85.45 (CH, C-15), 83.83 (CH, C-16), 77.57 (CH, 1C, *myo*-C-6), 77.36 (CH, 1C, *myo*-C-3), 77.04 (CH, 1C, *myo*-C-2), 76.72 (CH, 1C, *myo*-C-5), 75.60 (CH, 1C, *myo*-C-4), 75.56 (CH, 1C, *myo*-C-1), 38.18 (CH_2, 1C, C-12), 34.78 (CH2, 1C, C-8), 27.00 (CH_3, 3C, $C(CH_3)_3$), 25.02 (CH_2, 1C, C-10), 24.01 (CH_2, 1C, C-11), 23.79 (CH_2, 1C, C-9), 19.35 (Cq, 1C, $C(CH_3)_3$).

$[\alpha]_D^{20}$ = (+) 30.28875 (c = 16 mg/mL in CH_3Cl)

HRMS (ESI)+ m/z meas. 609.2877; calc. for C32H46O8Si $[M+Na]^+$ 609.2854 -3.8 ppm

Tetrabenzyl((3aR,4S,5S,6R,7R,7aS)-1-((tert-butyldiphenylsilyl)oxy)-6-((2-methoxyethoxy)methoxy)hexahydrospiro[benzo[d][2,3]dioxole-2,1'-cyclohexane]-4,5-diyl) bis(phosphate) (31)

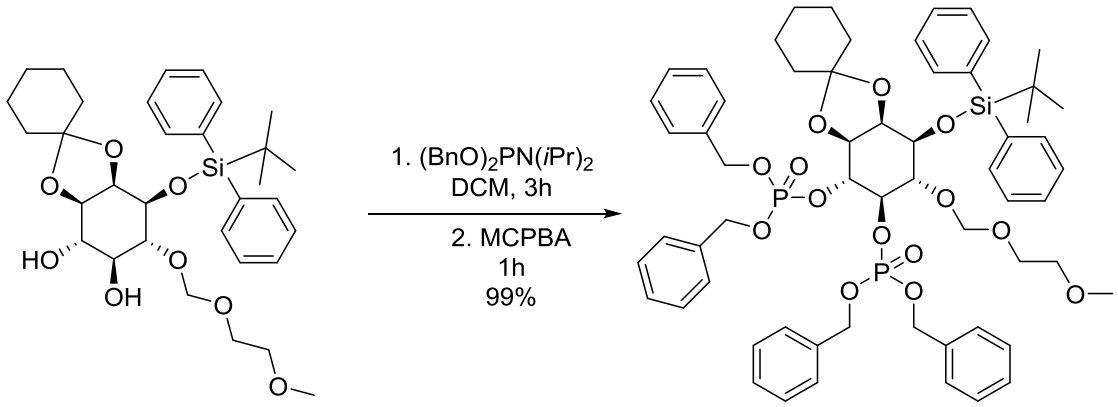

30 **31**

Compound **30** (1100 mg, 1.8 mmol) was dissolved in anhydrous DCM (20 ml and allowed to stir for a few minutes before adding 1H-tetrazole (0.45 M in ACN, 24 mL, 11 mmol, 6 eq). The phosphoramidite (1.8 mL, 5.6 mmol, 3 eq) was immediately added in anhydrous acetonitrile (2.2 ml). The reaction was allowed to stir for 3 hours. The reaction was cooled down to -40 ° C, followed by the addition of mcpba (77% w/w, 11 mmol, 2465.28 mg, 6 eq) and was allowed to stir for one more hour.

The reaction was quenched with $NaCO_3^-$ and extracted with DCM (200 ml). The organic layer was washed three more times with $NaCO_3^-$, then with water and brine, and condensed to give oil (pale color). The crude (2 g) was purified using a 100 g silica biotage column, in a gradient from 15% to 100% EtOAc in heptane. Sample loading on the column was done twice, as the total mass of the crude had to be divided in two for column loading limit (with respect to the Rfs differences on TLC). The product could be isolated with a yiled of 99%.

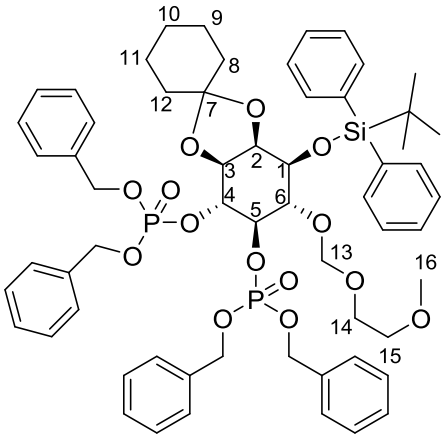

31

R_f: 0.39 (in 3:2 EtOAc:Heptane)

^{1}H NMR (400 MHz, $CDCl_3$) δ (ppm) = 7.77 – 7.61 (m, 4H, Ar-H), 7.41 – 7.06 (m, 26H, Ar-H), 5.26 – 5.08 (m, 2H, H-13), 5.07 – 4.80 (m, 8H, CH_2-Ar), 4.47 – 4.27 (m, 2H, *myo*-H-4, *myo*-H-5), 4.16 – 3.96 (m, 3H, *myo*-H-1, H-14), 3.48 (s, 1H, *myo*-H-2), 3.39 – 3.22 (m, 4H, *myo*-H-3, *myo*-H-6, H-15), 3.22 – 3.14 (s, 3H, H-16), 1.38 (d, *J* = 21.9 Hz, 10H, H8-9-10-11-12), 1.03 (s, 9H, $C(CH_3)_3$).

^{13}C-NMR (100.92 MHz, $CDCl_3$) δ (ppm) = 136.29, 136.14, 136.01 (CH, 4C, Ar-C), 133.33 (Cq, 4C, Ar-C), 129.93, 129.71, 129.08, 128.75, 128.65, 128.59, 128.56, 128.45, 128.40, 128.36, 128.33, 128.26, 128.09, 128.04, 128.01, 127.81, 127.70, 127.46 (CH, 26C, Ar-C), 110.98 (Cq, 1 C, C-7), 99.99 (CH, 1C, *myo*-C-6), 77.36 (CH, 1C, *myo*-C-4), 77.24 (CH, 1C, *myo*-C-5), 77.04 (CH, 1C, *myo*-C-3), 76.72 (CH, 1C, *myo*-C-2), 73.92 (CH, 1C, *myo*-C-1), 71.56 (CH_2, 4C, CH2-Ar), 71.03 (CH_3, 1C, C-13), 70.96 (CH_3, 1C, C-14), 69.48 (CH_3, 1C, C-15), 69.16 (CH_3, 1C, C-16), 67.58, 58.90, 33.86 (CH_2, 3C, C-12, C-8, C-10), 27.08, 25.18 (CH_3, 3C, $C(CH_3)_3$), 23.98, 23.73 (CH_2, 2C, C-9, C-11), 19.24 (Cq, 1C, $C(CH_3)_3$).

^{31}P-NMR (400.13 MHz, CDCl3) δ (ppm) = - 1.51 (s, 1P), -2.01 (s, 1P).

$[\alpha]_D^{20}$ = (+)6.252546 (c = 20 mg/mL in CH_3Cl)

HRMS (ESI+) m/z meas. 1129.4065; Calc. for C60H72O14P2Si $[M+Na]^+$ 1129.4059 - 0.6ppm

Tetrabenzyl((3aS,4S,5S,6R,7R,7aS)-4-hydroxy-5-((2-methoxyethoxy)methoxy) hexahydrospiro[benzo[d][1,3]dioxole-2,1'-cyclohexane]-6,7-diyl)bis(phosphate) (32)

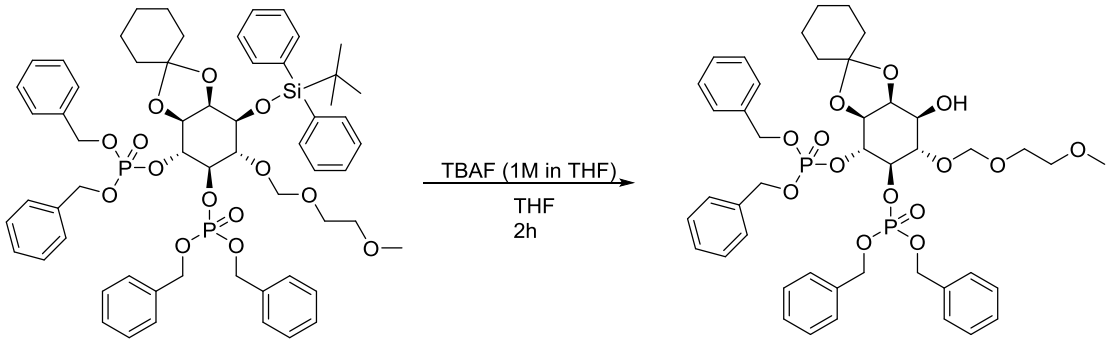

31 32

To a solution of **31** (1981 mg, 1.79 mmol) in THF (anhydrous, 35 ml) was added a solution of TBAF (3.2 mL, 1.8 eq) in 0.8 ml THF (anhydrous) at 0°C. The reaction was left stirring at room temperature. The reaction mixture turned slightly yellow upon addition of the TBAF reagent. The reaction was stopped after 2 hours, worked up with $NaCO_3^-$ and extracted with Ethyl Acetate. The product was purified using flash column chromatography at gradient of 20% to 100% EtOAc in Heptane. The product was purified as a colorless oil and was isolated in a yield of 85%.

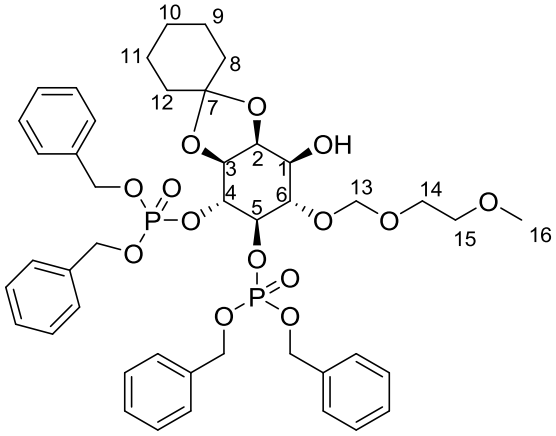

32

R_f: 0.28 (in 4:1 EtOAc:Hep)

^{1}H NMR (400 MHz, $CDCl_3$) δ (ppm) = 7.31 – 7.03 (m, 20H, Ar-H), 5.29 – 4.78 (m, 6H, CH2-Ar), 4.65 (dd, *J* = 15.0, 7.1 Hz, 2H, CH2-Ar), 4.45 – 4.27 (m, 2H, H-13), 4.13 (dd, *J* = 7.0, 5.3 Hz, 1H, *myo*-H-4), 4.05 (q, *J* = 7.1 Hz, 1H, *myo*-H-5), 3.87 (t, *J* = 8.7 Hz, 1H, *myo*-H-2), 3.79 – 3.64 (m, 2H, H-14), 3.52 – 3.45 (m, 1H, *myo*-H-3), 3.42 (dd, *J* = 5.2, 3.6 Hz, 2H, H-15), 3.29 (s, 3H, H-16), 1.96 (d, *J* = 15.8 Hz, 2H, *myo*-H-1, *myo*-H-6), 1.75 – 1.15 (m, 10H, H-8-9-10-11-12).

^{13}C NMR (101 MHz, $CDCl_3$) δ (ppm) = 136.13, 135.92, 135.85 (Cq, 4C, Ar-C), 128.54, 128.51, 128.47, 128.44, 128.43, 128.37, 128.34, 128.29, 128.22, 128.10, 128.02, 127.98, 127.93, 127.89, 127.81 (CH, 20C, Ar-C), 111.42 (Cq, 1C, C-7), 97.20 (CH, 1C, C-13), 80.63 (CH, 1C, *myo*-C-6), 80.13 (CH, 1C, *myo*-C-4), 77.35 (CH, 1C, *myo*-C-5), 77.24 (CH, 1C, *myo*-C-3), 77.04 (CH, 1C, *myo*-C-2), 76.72 (CH, 1C, C-14), 76.37 (CH, 1C, C-15), 71.53 (CH, 1C, C-16), 69.56, 69.50, 69.32, 68.53 (CH_2, 4C, CH2-Ar), 67.79 (CH, 1C, *myo*-C-1), 37.27 (CH_2, 1C, C-12), 35.01, 24.90, 23.82 (CH_2, 3C, C-11, C-9, C-8), 23.54 (CH_2, 1C, C-10).

^{31}P-NMR (400.13 MHz, $CDCl_3$) δ (ppm) = - 1.5 (s, 1P), -2.05 (s, 1P).

$[\alpha]_D^{20}$ = (-)21.628571 (c = 14 mg/mL in CH_3Cl)

HRMS (ESI)+ m/z meas. 891.2881; calc. for C76H95O21P3 $[M+Na]^+$ 891.2881 -1.1 ppm

5.2.3. Solution synthesis of PI(4,5)P_2 analogues

(2R)-3-(((benzyloxy)(((3aS,4R,5R,6S,7S,7aR)-4,5-bis((bis(benzyloxy)phosphoryl) oxy)-6-methoxyhexahydrospiro[benzo[d][1,3]dioxole-2,1'-cyclohexan]-7-yl)oxy) phosphoryl)oxy)propane-1,2-diyldioctanoate (11)

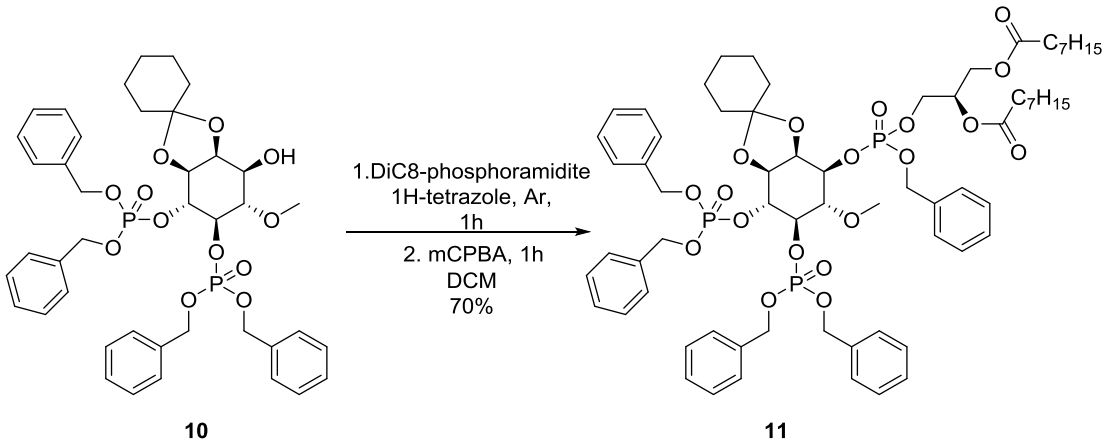

10 11

Compound 10 (100 mg, 0.12 mmol, 1 eq) and 0.45 M 1H-Tetrazole in ACN (0.8 mL, 0.375 mmol, 3 eq) were dissolved in 8 mL DCM in a flask under Ar atmosphere. The solution was cooled to 0°C before the DiC8-phosphoramidite **47** (109.8 mg, 0.18 mmol, 1.5 eq) dissolved in DCM (1mL) was added dropwise. After removing the ice bath and stirring for 1 h, the reaction mixture was cooled to -40°C and mCPBA (56 mg, 0.25 mmol, 2 eq) dissolved in 1.5 mL DCM was added. After warming the solution slowly to RT, the reaction mixture was quenched with 2 mL of a 10%- solution of $KHSO_4$ in water. The organic phase was washed with sat. $NaHCO_3^-$ solution, water and brine, before it was dried with NaSO4 and the solvent evaporated under reduced pressure. Purification of the product was achieved by column chromatography (heptane/ EtOAc linear gradient 12% to 86%). The product is a colourless oil and was isolated with a 70% yield.

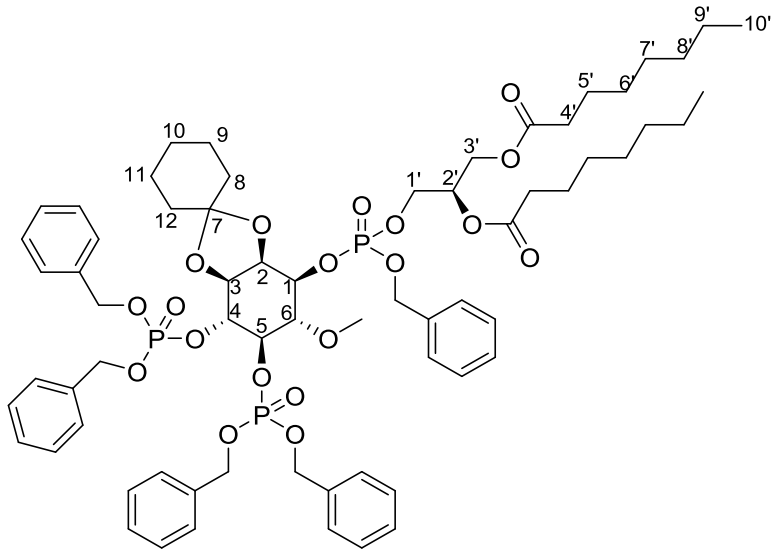

11

^{1}H NMR (400 MHz, $CDCl_3$) δ 7.41 - 7.27 (m, 14H, Ar-H), 7.26 - 7.19 (m, 11H, Ar-H), 5.26 - 5.17 (m, 1H, H-2‘), 5.16 - 4.96 (m, 10H, CH2-Ar), 4.78 (td, *J* = 14.9 Hz, 1H, *myo*-H-4), 4.62 (ddt, *J* = 14.0 Hz, 1H, *myo*-H-1), 4.58 - 4.51 (m, 1H, *myo*-H-2), 4.51 - 4.42 (m, 1H, *myo*-H-5), 4.37 - 4.25 (m, 1H, H-1‘), 4.25 - 4.16 (m, 3H, *myo*-H-3, H-3‘), 4.16 - 4.06 (m, 1H, H-1‘), 3.84 - 3.74 (m, 1H, *myo*-H-6), 3.44, 3.40 (s, 3H, H-13), 2.27 (dt, *J* = 14.5 Hz, 4H, H-4‘), 1.79 - 1.72 (m, 2H, H-12), 1.66 - 1.41 (m, 10H, H-5‘, H-8, H-9, H-11), 1.33 (s, 2H, H-10), 1.26 (s, 16H, H-6‘, H-7‘, H-8‘, H-9‘), 0.87 (t, *J* = 5.7 Hz, 6H, H-10‘).

^{13}C-NMR (100.92 MHz, $CDCl_3$): δ (ppm) = 173.5, 173.1 (C=O, 2C), 136.2, 136.2, 136.1, 136.1, 136.0 (Cq, 5C, Ar-C), 129.0, 129.0, 128.9, 128.8, 128.8, 128.7, 128.7, 128.6, 128.6, 128.3, 128.3, 128.3, 128.2, 128.2, 128.14 (CH, 20C, Ar-C), 112.1 (Cq, 1C, C-7), 80.2 (CH, 1C, *myo*-C-6), 79.4 (CH, 1C, *myo*-C-4), 78.5 (CH, 1C, *myo*-C-5), 76.3 (CH, 1C, *myo*-C-3), 75.5 (CH, 1C, *myo*-C-1), 73.8 (CH, 1C, *myo*-C-2), 70.0, 69.9, 69.8, 69.8, 69.7 (CH_2, 5C, CH_2-Ar), 69.6 (CH, 1C, C-2’), 66.0 (CH_2, 1C, C-3’), 62.0 (CH_2, 1C, C-1’), 60.7 (CH_3, 1C, C-13), 37.1, 37.0 (CH_2, 2C, C-12), 34.8 (CH_2, 1C, C-8), 34.5, 34.3 (CH_2, 2C, C-4’), 32.0, 29.4, 29.3 (CH_2, 6C, C-6’, C-7’, C-8’), 25.2, 25.2 (CH_2, 3C, C-5’, C-10), 24.2, 23.9 (CH_2, 1C, C-9, C-11), 22.9 (CH_2, 2C, C-9’), 14.4 (CH_3, 2C, C-10’).

^{31}P-NMR (400.13 MHz, $CDCl_3$): δ (ppm) = -1.68 (d, 1P), -1.79 (s, 0.5P), -1.92 (s, 0.5P), -2.09 (d, 1P).

$[\alpha]_D^{20}$ = (-)6.6171429 (c = 7 mg/ml in $CHCl_3$)

HRMS (ESI)+ m/z meas. 1313.5125; calc. for C67H89O19P3 $[M+Na]^+$ 1313.5103 -1.6ppm.

(2R)-3-(((((1R,2R,3S,4R,5R,6S)-2,3-dihydroxy-6-methoxy-4,5-bis(phosphonooxy)cyclohexyl) oxy)(hydroxy)phosphoryl) oxy)propane-1,2-diyl dioctanoate (12)

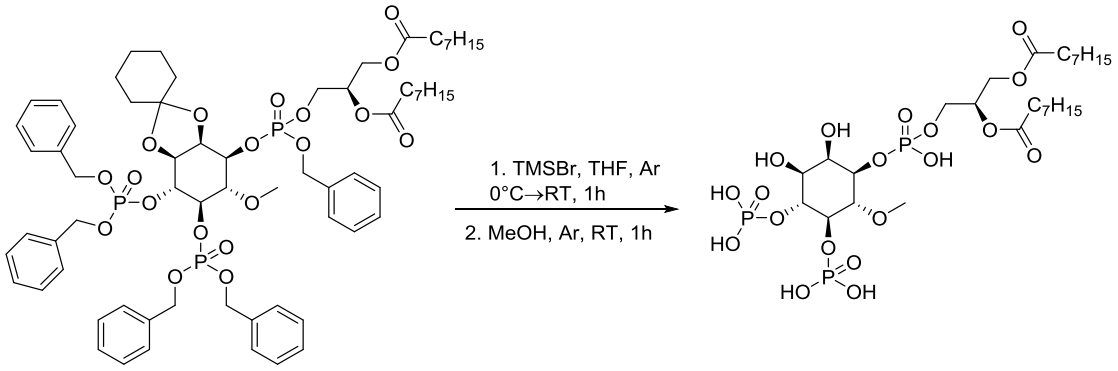

11 **12**

Compound **11** (100 mg, 0.077 mmol, 1 eq) was dissolved in 2 mL THF in a flask under Ar atmosphere and cooled to 0°C. TMSBr (2 mL, excess) was diluted in 1 mL THF, added and stirred for 5 min before ice bath was removed and the reaction warmed to RT. After stirring for 1 h, TMSBr and THF were evaporated and the precipitate dissolved in 5.6 mL dry MeOH. The reaction solution was stirred for 1 h before the solvent was removed under reduced pressure. The product could be isolated as a white solid in a quantitative yield. (70 mg, 0.092 mmol).

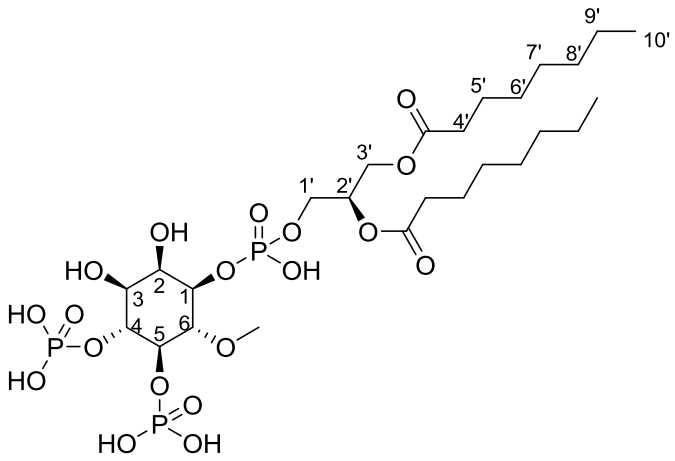

12

^{1}H-NMR (400.13 MHz, CD_3OD) δ (ppm) = 5.33 - 5.22 (m, 1H, H-2'), 4.50 (q, *J* = 9.2 Hz, 1H, *myo*-H-4), 4.45 - 4.37 (m, 1H, H-1'), 4.28 - 4.06 (m, 6H, *myo*-H-1, *myo*-H-2, *myo*-H-5, H-1', H-3'), 3.69 - 3.61 (m, 2H, *myo*-H-3, *myo*-H-6), 3.59 (s, 3H, H-7), 2.41 - 2.29 (m, 4H, H-4'),

1.67 - 1.55 (m, 4H, H-5'), 1.38 - 1.25 (m, 16H, H-6', H-7', H-8', H-9'), 0.91 (t, *J* = 6.8 Hz, 6H, H-10').

^{13}C-NMR (100.92 MHz, $CDCl_3$) δ (ppm) = 174.9, 174.5 (C=O, 2C), 81.6 (CH, 1C, *myo*-C-6), 80.5 (CH, 1C, *myo*-C-5), 80.0 (CH, 1C, *myo*-C-4), 78.7 (CH, 1C, *myo*-C-1), 72.3 (CH, 1C, *myo*-C-2), 71.3 (CH, 1C, *myo*-C-3), 71.3 (CH_2, 1C, C-2'), 66.2 (CH_2, 1C, C-3'), 63.2 (CH, 1C, C-1'), 61.8 (CH_3, 1C, C-7), 35.1, 34.9 (CH2, 2C, C-4') 33.7, 32.9, 30.2, 30.1, 30.1 (CH_2, 6C, C-6', C-7', C-8'), 26.0 (CH_2, 2C, C-5'), 23.9, 23.7 (CH_2, 2C, C-9'), 14.4 (CH_2, 2C, C-10').

^{31}P-NMR (400.13 MHz, $CDCl_3$) δ (ppm) = 0.68 (s, 1P), -0.8 (s, 1P), -2.75 (s, 1P)

$[\alpha]_D^{20}$ = (-) 0.9547826

HRMS (ESI)+ m/z meas. 759.2168; calc. for C26H50O19P3 $[M+H]^+$ 759.2165 -0.4 ppm.

(2R)-3-(((benzyloxy)(((3aS,4R,5R,6S,7S,7aR)-4,5-bis((bis(benzyloxy) phosphoryl)oxy)-6-ethoxyhexahydrospiro[benzo[d][1,3]dioxole-2,1'-cyclohexan]-7-yl)oxy)phosphoryl)oxy)propane-1,2-diyl dioctanoate (17)

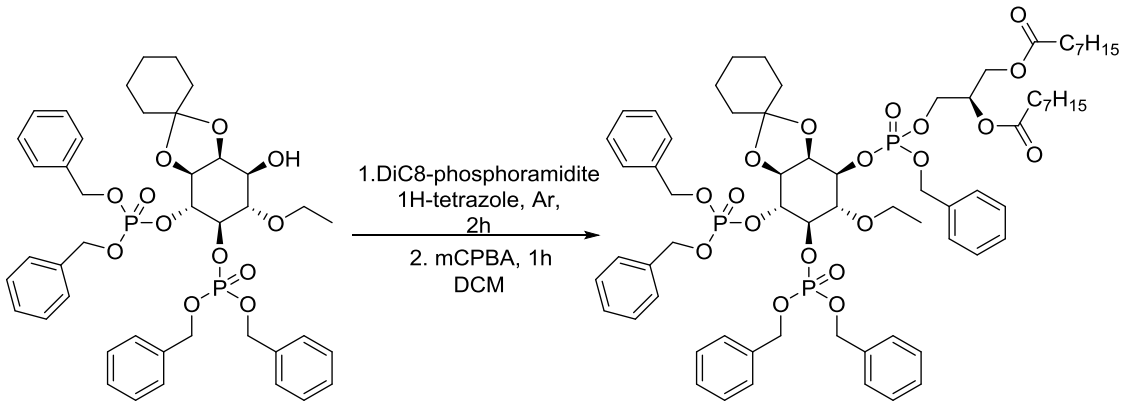

16 17

Compound 16 (63 mg, 0.078 mmol, 1 eq) and 0.45 M 1H-Tetrazole in ACN (0.52 mL, 0.234 mmol, 3 eq) were dissolved in 5 mL DCM in a flask under Ar atmosphere. The solution was cooled to 0°C before the DiC8-phosphoramidite **47** (67.9 mg, 0.11 mmol, 1.5 eq) dissolved in DCM (1.5 mL) was added dropwise. After removing the ice bath and stirring for 2 h, the reaction mixture was cooled to -40°C and mCPBA (26.92 mg, 0.156 mmol, 2 eq) dissolved in 0.8 mL DCM was added dropwise. After warming the solution slowly to RT, the reaction mixture was quenched with 2 mL of a 10%- solution of KHSO4 in water. The organic phase was washed with sat. $NaHCO_3^-$ solution, water and brine, before it was dried with NaSO4 and the solvent evaporated under reduced pressure. Purification of the product was achieved by biotage column chromatography (25g Silica

cartridge; linear gradient of 12% to 100% EtOAc in Heptane). The product is a colourless oil and was isolated with a 54% yield.

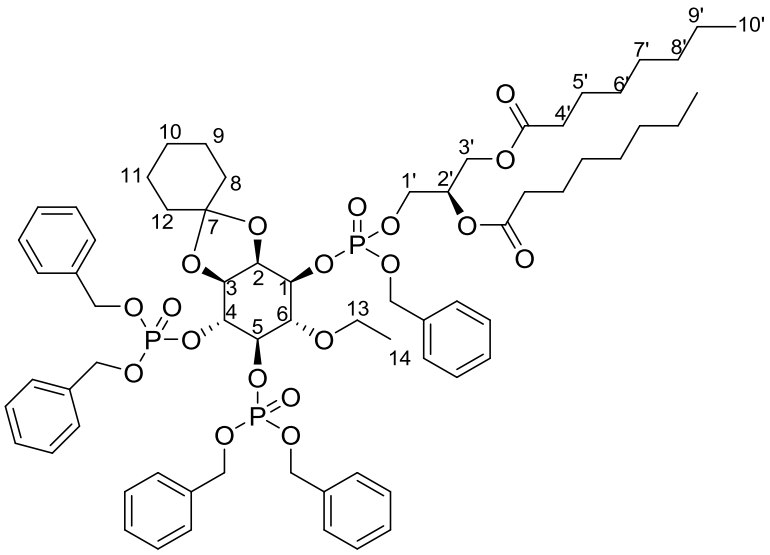

17

^{1}H-NMR (400.13 MHz, $CDCl_3$) δ (ppm) = 7.41 - 7.17 (m, 25H, Ar-H), 5.26 - 5.13 (m, 1H, H-2‘), 5.15 - 4.93 (m, 10H, CH2-Ar), 4.88 - 4.74 (m, 1H, *myo*-H-4), 4.69 - 4.52 (m, 2H, *myo*-H-1, *myo*-H-2), 4.48 (dt, *J* = 15.9 Hz, 1H, *myo*-H-5), 4.35 - 4.04 (m, 5H, *myo*-H-3, H-1‘, H-3‘), 3.92 (dt, *J* = 14.3, 6.8 Hz, 1H, *myo*-H-6), 3.68 (dt, *J* = 20.3 Hz, 1H, H-13), 3.62 - 3.51 (m, 1H, H-13), 2.32 - 2.16 (m, 4H, H-4‘), 1.74 (s, 4H, H-12, H-8), 1.64 - 1.34 (m, 10H, H-10, H-9, H-8, H-5‘), 1.26 (s, 16H, H-6‘, H-7‘, H-8‘,H-9‘), 1.04 (dt, *J* = 14.2 Hz, 3H, H-14), 0.87 (t, *J* = 6.0 Hz, 6H, H-10‘).

^{13}C-NMR (100.92 MHz, $CDCl_3$) δ (ppm) = 173.5, 173.3 (C=O, 2C),136.3, 136.2, 136.1, (Cq, 5C, Ar-C), 129.0, 128.9, 128.8, 128.8, 128.8, 128.7, 128.7, 128.6, 128.6, 128.4, 128.3, 128.3, 128.2, 128.1 (CH, 25C, Ar-C), 112.0 (Cq, 1C, C-7), 79.2 (CH, 1C, *myo*-C-4), 79.0 (CH, 1C, *myo*-C-5), 78.4 (CH, 1C, *myo*-C-6), 76.1 (CH, 1C, *myo*-C-3), 74.9 (CH, 1C, *myo*-C-1), 73.5 (CH, 1C, *myo*-C-2), 70.0, 69.9, 69.8, 69.7 (CH_2, 5C, CH_2-Ar), 69.6 (CH, 1C, C-2’), 68.0 (CH_2, 1C, C-13), 66.0 (CH_2, 1C, C-3’), 62.0 (CH_2, 1C, C-1’), 36.9, 36.8 (CH_2, 2C, C-12), 34.7 (CH_2, 1C, C-8), 34.5, 34.3 (CH_2, 2C, C-4’), 32.0, 29.4, 29.4, 29.3 (CH_2, 6C, C-6’, C-7’, C-8’), 25.3, 25.2, 25.1 (CH_2, 3C, C-5’, C-10), 24.2, 23.9 (CH_2, 1C, C-9, C-11), 22.9 (CH_2, 2C, C-9’), 15.5 (CH_3, 1C, C-14), 14.4 (CH_3, 2C, C-10’).

^{31}P-NMR (400.13 MHz, $CDCl_3$) δ (ppm) = -1.77 (dd, *J*= 4.43 Hz, 1P), -1.93 (s, 0.5P), -2.06 (s, 0.5P), 2.11 (dd, *J* = 4.84 Hz, 1P).

$[\alpha]_D^{20}$ = (-) 1.3037 (c = 9 mg/mL in CH_3Cl)

HRMS (ESI)+ m/z meas. 1327.5310; calc. for C68H91O19P3 $[M+Na]^+$ 1327.5260 -3.8 ppm.

(2R)-3-(((((1R,2S,3R,4R,5S,6R)-2-ethoxy-5,6-dihydroxy-3,4-bis(phosphonooxy)cyclohexyl)oxy)(hydroxy)phosphoryl)oxy)propane-1,2-diyl dioctanoate (18)

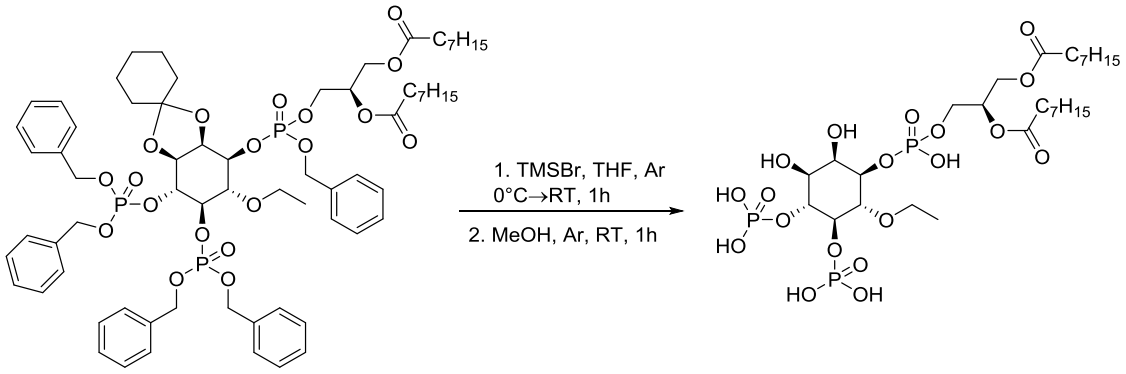

17 18

Compound **17** (55 mg, 0.04 mmol, 1 eq) was dissolved in 1.3 mL THF in a flask under Ar atmosphere and cooled to 0°C. TMSBr (0.9 mL, excess) was diluted in 0.5 mL THF, added and stirred for 5 min before ice bath was removed and the reaction warmed to RT. After stirring for 1 h, TMSBr and THF were evaporated and the precipitate dissolved in 3 mL dry MeOH. The reaction solution was stirred for 1 h before the solvent was removed under reduced pressure. The product could be isolated as a white solid in a quantitative yield. (20 mg, 0.023 mmol).

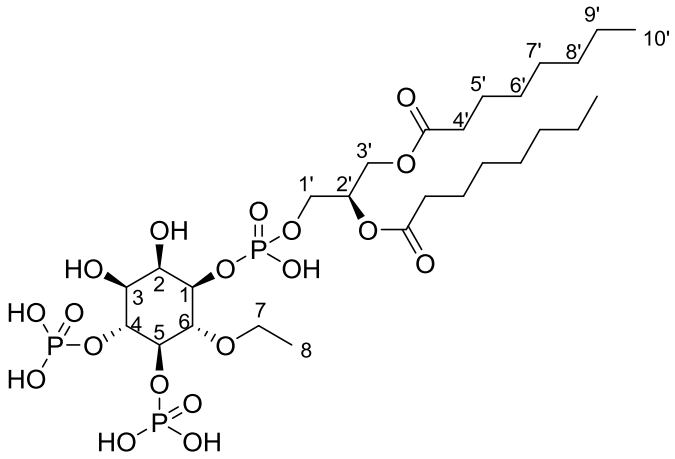

18

^{1}H-NMR (400.13 MHz, CD_3OD) δ (ppm) = 5.27 (d, *J* = 4.3 Hz, 1H, H-2‘), 4.49 (d, *J* = 8.1 Hz, 1H, *myo*-H-4), 4.41 (dd, *J* = 12.0, 2.8 Hz, 1H, H-1‘), 4.29 - 4.07 (m, 6H, *myo*-H-2, *myo*-H-5, H-1’, H-3’), 3.88 - 3.68 (m, 3H, H-6, H-7), 3.60 (d, *J* = 8.9 Hz, 1H, *myo*-H-3), 2.42 - 2.27 (m, 4H, H-4’), 1.61 (d, *J* = 6.6 Hz, 4H, H-5‘), 1.32 (s, 16H, H-6‘, H-7‘, H-8‘, H-9‘), 1.21 (t, *J* = 6.8 Hz, 3H, H-8), 0.90 (t, *J* = 6.3 Hz, 6H, H-10‘).

^{13}C-NMR (100.92 MHz, $CDCl_3$) δ (ppm) = 174.9, 174.5 (C=O, 2C), 80.6 (CH, 1C, *myo*-C-5), 80.0 (CH, 1C, *myo*-C-4), 79.5 (CH, 1C, *myo*-C-6), 78.8 (CH, 1C, *myo*-H-1), 72.3 (CH, 1C, *myo*-C-2), 71.4 (CH, 1C, *myo*-C-3), 71.3, 71.2 (CH_2, 1C, C-2’), 70.1 (CH_2, 1C, C-7), 66.2, 66.2 (CH_2, 1C, C-3’), 63.1, 63.1 (CH, 1C, C-1’), 35.0, 34.9 (CH_2, 2C, C-4’), 32.9, 30.2, 30.1, 30.1 (CH_2, 6C, C-6’, C-7’, C-8’), 26.0 (CH_2, 2C, C-5’),23.7 (CH_2, 2C, C-9’), 15.8 (CH_3, 1C, C-8), 14.4 (CH_2, 2C, C-10’).

^{31}P-NMR (400.13 MHz, $CDCl_3$) δ (ppm) = -0.79 (br. S, 2P), -2.77 (br. s, 1P).

$[\alpha]_D^{20}$ = (-) 1.464 (c = 9 mg/mL in CH_3Cl)

HRMS (ESI)+ m/z meas. 775.4163; calc. for $C27H53O9P3$ $[M+H]^+$ 775.4156 -1.0 ppm.

(2R)-3-(((benzyloxy)(((1R,2S,3R,4R,5S,6R)-4,5-bis((bis(benzyloxy)phosphoryl) oxy)-2,3,6-trimethoxycyclohexyl)oxy)phosphoryl)oxy)propane-1,2-diyl dioctanoate (27)

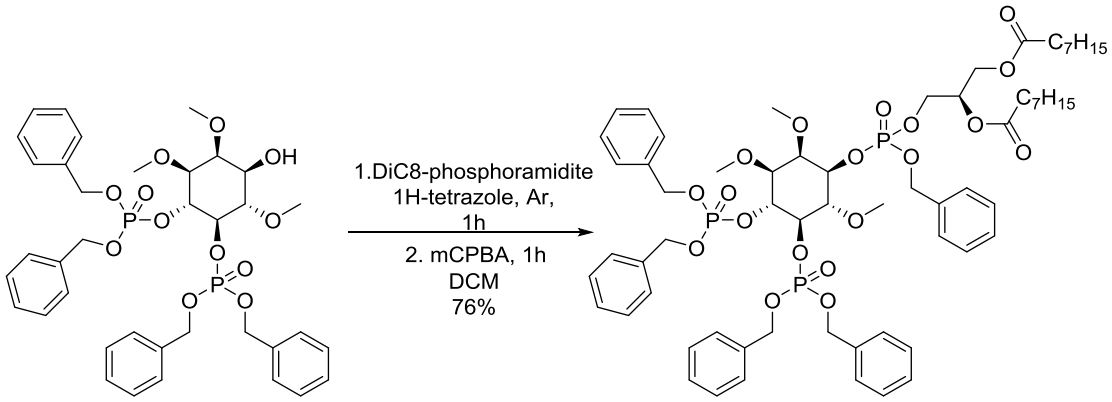

26 **27**

Compound **26** (150 mg, 0.2 mmol, 1 eq) and 0.45 M 1H-Tetrazole in ACN (1.3 mL, 0.6 mmol, 3 eq) were dissolved in 10 mL DCM in a flask under Ar atmosphere. The solution was cooled to 0°C before the DiC8-phosphoramidite **47** (174.53 mg, 0.3 mmol, 1.5 eq) dissolved in DCM (1.5 mL) was added dropwise. After removing the ice bath and stirring for 1 h, the reaction mixture was cooled to -40°C and mCPBA (89.64 mg, 0.4 mmol, 2 eq) dissolved in 1 mL DCM was added. After warming the solution slowly to RT, the reaction mixture was quenched with 2 mL of a 10%- solution of KHSO4 in water. The organic phase was washed with sat. NaHCO3- solution, water and brine, before it was dried with NaSO4 and the solvent evaporated under reduced pressure. Purification of the product was achieved by column chromatography (heptane/ EtOAc linear gradient 20% - 100%). The product is a colourless oil and was isolated with a 76% yield.

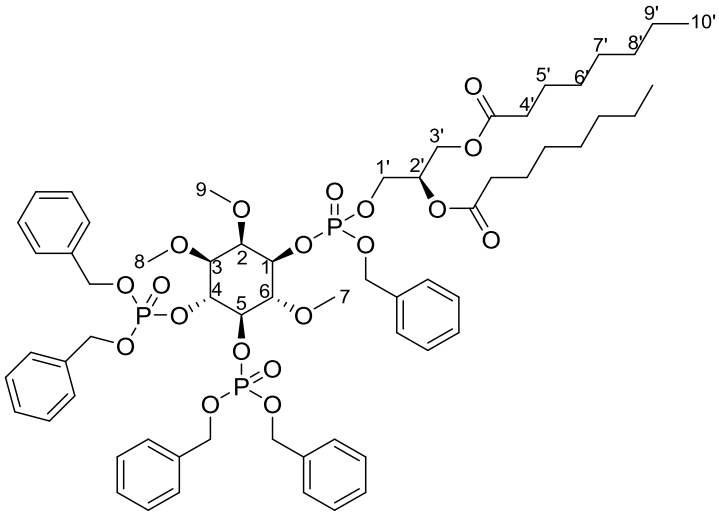

27

R_f = 0.4 m (4:1 EtOAC:Heptane)

^{1}H NMR (400 MHz, $CDCl_3$) δ (ppm) = 7.30 (qd, *J* = 7.5 Hz, 5H, Ar-H), 7.26 – 7.09 (m, 20H, Ar-H), 5.14 (d, *J* = 5.1 Hz, 1H, H-2') 5.10 – 4.86 (m, 10H, CH_2-Ar), 4.74 (d, *J* = 9.1 Hz, 1H, *myo*-H-4), 4.33 (m, 1H, *myo*-H-1), 4.26 – 4.18 (m, 1H, *myo*-H-2), 4.14 – 4.00 (m, 4H, H-1' H-3'), 3.96 (d, *J* = 8.2 Hz, 1H, *myo*-H-3), 3.63 (t, *J* = 8.4 Hz, 1H, *myo*-H-5), 3.52 (s, 3H, H-7), 3.33 (s, 3H, H-9), 3.24 (s, 3H, H-8), 3.10 (t, *J* = 10.8 Hz, 1H, *myo*-H-6), 2.26 – 2.14 (m, 4H, H-4'), 1.51 (q, *J* = 9.5 Hz, 4H, H-5'), 1.20 (dd, *J* = 9.5 Hz, 16H, H-6', H-7', H-8', H-9'), 0.85 – 0.72 (m, 6H, H-10').

^{13}C-NMR (100.92 MHz, $CDCl_3$) δ (ppm) = 173.21, 172.82 (C=O, 2C), 136.29, 136.16, 136.04, 135.97, 135.42 (Cq, 5C, Ar-C), 130.09, 129.71, 128.87, 128.79, 128.74, 128.72, 128.44, 128.41, 128.36, 128.33, 128.30, 128.18, 128.11, 128.06, 127.94, 127.88, 127.68 (CH, 20C, Ar-C), 80.08 (CH, 1C, *myo*-C-6), 79.71 (CH, 1C, *myo*-C-4), 78.78 (CH, 1C, *myo*-C-5), 78.16 (CH, 1C, *myo*-C-3), 77.83 (CH, 1C, *myo*-C-1), 77.35 (CH, 1C, *myo*-C-2), 77.24, 77.04, 76.72, 76.07, 69.83 (CH_2, 5C, CH_2-Ar), 69.78 (CH, 1C, C-2'), 69.53 (CH_2, 1C, C-3'), 69.47 (CH_2, 1C, C-1'), 69.39 (CH_3, 1C, C-7), 69.13 (CH3, 1C, C-9), 69.07 (CH_3, 1C, C-8), 58.12, 34.12 (CH_2, 2C, C-4'), 34.00, 33.98, 31.66, 29.72, 29.07, 29.03 (CH2, 6C, C-6', C-7', C-8'), 28.94, 24.83 (CH_2, 2C, C-5'), 22.61 (CH_2, 2C, C-9'), 14.09 (CH_3, 2C, C-10').

^{31}P-NMR (400.13 MHz, $CDCl_3$): δ (ppm) = -1.66 (d, 1P), -1.76 (s, 0.5P), -1.86 (s, 0.5P), -2.11 (d, 1P).

$[\alpha]_D^{20}$ = (-) 10.596667 (c = 12 mg/mL in CH_3Cl).

HRMS (ESI)+ m/z meas. 1261.4813; calc. for $C_{63}H_{85}O_{19}P_3$ $[M+Na]^+$ 1261.4790 ppm

(2R)-3-((hydroxy(((1R,2R,3S,4R,5R,6S)-2,3,6-trimethoxy-4,5-bis(phosphonooxy)cyclohexyl)oxy) phosphoryl)oxy)propane-1,2-diyl dioctanoate (28)

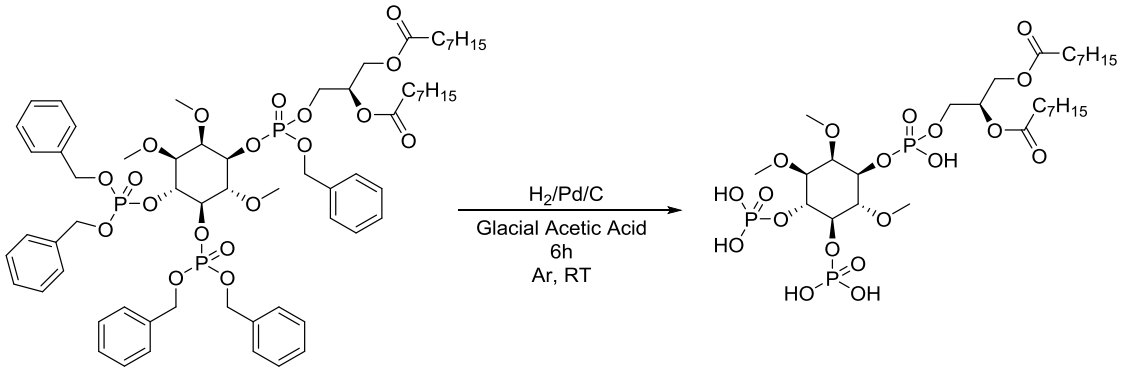

27 28

Palladium catalyst (10 wt. %, 35.8 mg, 0.028 mmol, 0.36 eq) was dissolved in glacial acetic acid (4 mL) containing the starting material 27 (118 mg, 0.095 mmol, 1 eq) at room temperature. The air in reaction flask was removed under reduced pressure, and filled with H_2 three times, before the double H_2 balloon was kept while the reaction stirred. When deemed finished, the reaction was stopped, filtered over celite, frozen in liquid N_2, then freeze dried using a cooled-down condenser trap. The product was obtained as a white powder, with a yield of 84%.

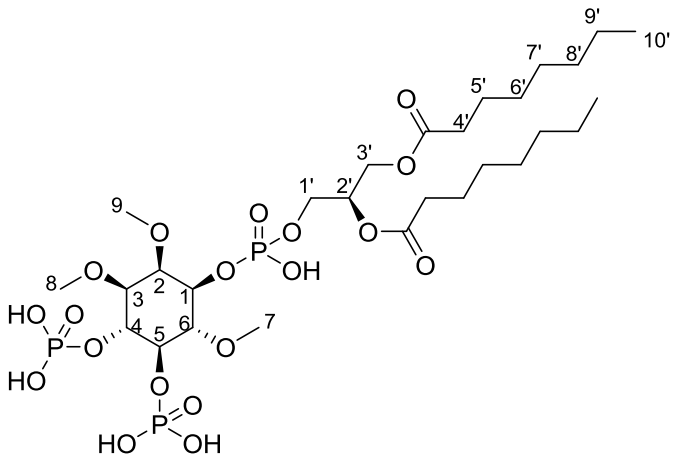

28

^{1}H NMR (400 MHz, $CDCl_3$) δ (ppm) = 5.18 (d, *J* = 5.7 Hz, 1H, H-2'), 4.44 – 4.34 (m, 1H, *myo*-H-4), 4.34 – 4.30 (m, 1H, H-1'), 4.09 (t, *J* = 6.4 Hz, 3H, *myo*-H-2, *myo*-H-5, H-3'), 3.97 (s, 1H, *myo*-H-3), 3.50 (d, *J* = 15.3 Hz, 6H, H-7, H-8), 3.40 (s, 3H, H-9), 2.25 (dt, *J* = 11.7 Hz, 4H,

myo-H-1, *myo*-H-6, H-1', H-3'), 1.52 (q, *J* = 7.1 Hz, 4H, H-4'), 1.21 (dt, *J* = 8.1 Hz, 20H, H-5', H-6', H-7', H-8', H-9'), 0.81 (t, *J* = 6.5 Hz, 6H, H-10').

^{13}C-NMR (100.92 MHz, $CDCl_3$) δ (ppm) = 175.27, 174.91 (C=O, 2C), 82.33 (CH, 1C, *myo*-C-6), 81.63 (CH, 1C, *myo*-C-5), 79.12 (CH, 1C, *myo*-C-4), 78.75 (CH, 1C, *myo*-C-1), 71.82 (CH, 1C, *myo*-C-2), 71.74 (CH, 1C, *myo*-C-3), 66.42 (CH_2, 1C, C-2'), 63.64 (CH_2, 1C, C-3'), 59.54 (CH, 1C, C-1'), 49.92 (CH_3, 1C, C-7), 49.85 (CH_3, 1C, C-8), 49.71 (CH_3, 1C, C-9), 49.00, 48.79 (CH_2, 2C, C-4'), 35.47, 35.28, 33.31, 31.19, 30.59 (CH_2, 6C, C-6', C-7', C-8'), 30.57, 30.55 (CH_2, 2C, C-5'), 26.43, 24.13 (CH_2, 2C, C-9'), 14.87 (CH_2, 2C, C-10').

^{31}P-NMR (400.13 MHz, $CDCl_3$) δ (ppm) = -0.32 (d, *J* = 25.6 Hz, 2P), -1.71 (s, 1P).

$[\alpha]_D^{20}$ = (-) 1.3266055 (c = 10.9 mg/mL in CH_3Cl).

HRMS (ESI)+ m/z meas. 789.2635; calc. for C76H95O21P3 $[M+H]^+$ 789.2623 -1.5 ppm

(2R)-3-(((benzyloxy)(((3aS,4R,5R,6S,7S,7aR)-4,5-bis((bis(benzyloxy) phosphoryl)oxy)-6-((2-methoxyethoxy)methoxy)hexahydrospiro[benzo[d] [1,3]dioxole-2,1'-cyclohexan]-7-yl)oxy)phosphoryl)oxy)propane-1,2-diyl(3R,3'R,5R,5'R,7R,7'R)-bis(adamantane-1-carboxylate) (33)

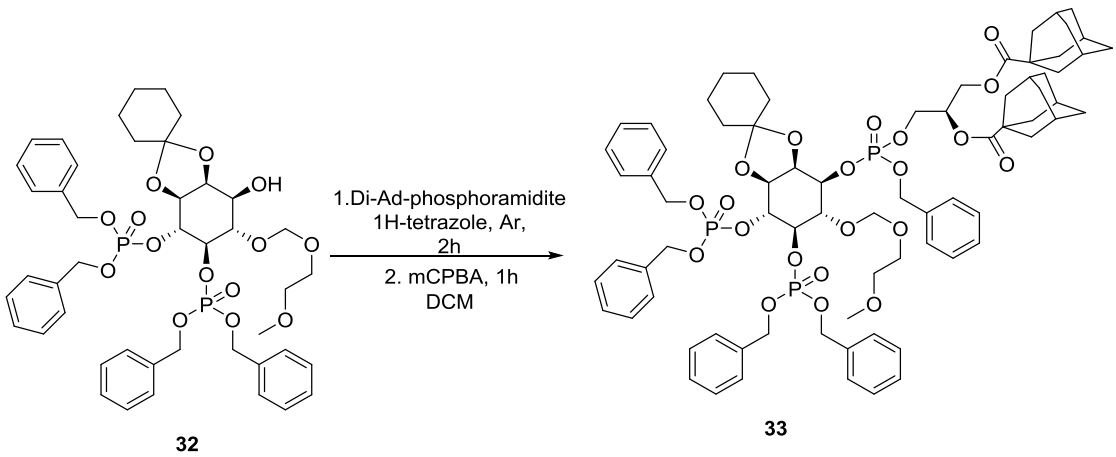

32 33

Compound **32** (90.36 mg, 0.104 mmol, 1 eq) and 0.45 M 1H-Tetrazole in ACN (1.04 mL, 0.468 mmol, 3 eq) were dissolved in 8 mL DCM in a flask under Ar atmosphere. The solution was cooled to 0°C before compound **44** (102 mg, 0.156 mmol, 1.5 eq) dissolved in DCM (1 mL) was added dropwise. After removing the ice bath and stirring for 2 h, the reaction mixture was cooled to -40°C and mCPBA (104.88 mg, 0.468 mmol, 3 eq)

dissolved in 1 mL DCM was added dropwise. After warming the solution slowly to RT, the reaction mixture was quenched with 2 mL of a 10%- solution of KHSO4 in water. The organic phase was washed with sat. NaHCO3- solution, water and brine, before it was dried with NaSO4 and the solvent evaporated under reduced pressure. Purification of the product was achieved by biotage column chromatography (50g Silica cartridge; linear gradient of 50% to 90% EtOAc in Heptane). The product is a colourless oil and was isolated with a 50% yield.

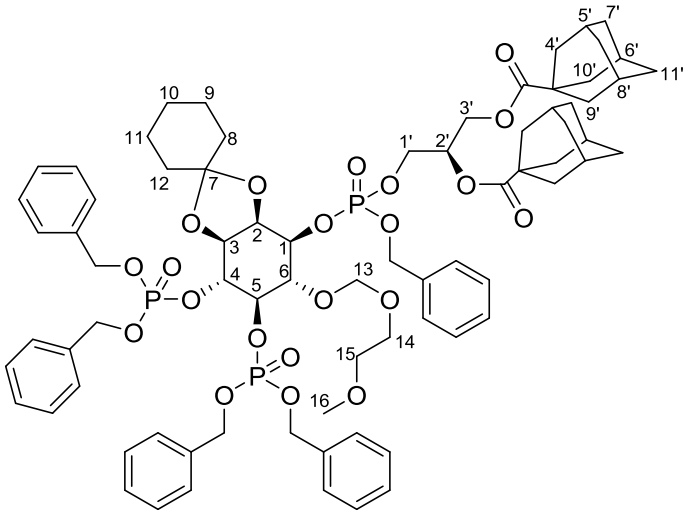

33

^{1}H NMR (400 MHz, $CDCl_3$) δ (ppm) = 7.44 – 7.30 (m, 8H, Ar-H), 7.30 – 7.19 (m, 17H, Ar-H), 5.30 (s, 2H, H-13), 5.14 – 4.94 (m, 10H, CH_2-Ar), 4.87 – 4.78 (m, 2H, *myo*-H-4, *myo*-H-1), 4.75 (dd, *J* = 9.8 Hz, 1H, H-2'), 4.67 – 4.59 (m, 2H, H-1', H-3'), 4.33 – 4.22 (m, 3H, *myo*-H-5, H-1', H-3'), 4.21 – 4.10 (m, 2H, *myo*-H-6, H-14), 4.05 (d, *J* = 5.9 Hz, 2H, H-15), 3.73 – 3.57 (m, 2H, *myo*-H-2, *myo*-H-3), 3.27 (s, 3H, H-16), 2.07 – 1.90 (m, 8H, H-9', H-4'), 1.84 (q, *J* = 3.2 Hz, 12H, H-10', H-5', H-7', H-6', H-11', H-8'), 1.69 (q, *J* = 12.0 Hz, 8H-cy), 1.47 (d, *J* = 14.5 Hz, 2H).

^{13}C NMR (101 MHz, $CDCl_3$) δ (ppm) = 174.2, 173.8, 135.8, 135.5, 133.1, 126.0, 125.9, 125.8, 125.7, 125.3, 125.25, 125.2, 125.1, 124.9, 124.7, 124.6, 77.3, 75.3, 74.6, 74.3, 74.0, 73.5, 73.1, 72.8, 66.9, 58.9, 38.1, 36.2, 36.1, 33.9, 25.3, 25.2, 20.4

^{31}P-NMR (400.13 MHz, $CDCl_3$) δ (ppm) = -1.64 (d, *J* = 2.4 Hz, 1P), -1.92 (d, *J* = 45.6 Hz, 1P), -2.18 (d, *J* = 3.0 Hz, 1P)

$[\alpha]_D^{20}$ = (-)5.8571429 (c = 7.7 mg/mL in CH_3Cl)

HRMS (ESI)+ m/z meas. 1459.5492; calc. for C76H95O21P3 [M+Na]$^+$ 1459.5471 -1.5 ppm

(2R)-3-((hydroxy(((1R,2R,3S,4R,5R,6S)-2,3,6-trihydroxy-4,5-bis(phosphonooxy) cyclohexyl)oxy)phosphoryl)oxy)propane-1,2-diyl(3R,3'R,5R,5'R,7R,7'R)-bis(adamantane-1-carboxylate) (34)

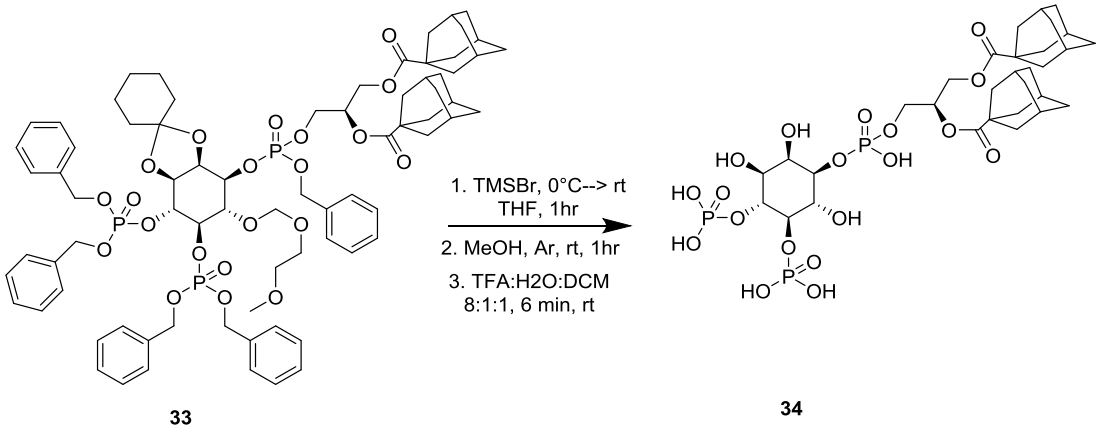

33 34

Compound **33** (70 mg, 0.0487 mmol, 1 eq) was thoroughly dried before dissolving it in anhydrous THF (3 mL) at rt, under argon atmosphere. The solvents used for this reaction was dried over molecular sieves. The reaction mixture was allowed to stir at 0°C. TMSBr (0.9 mL, excess), was added dropwise to the stirring reaction, and the reaction was slowly brought up to rt and stirred for an hour. TMSBr and THF were evaporated and the precipitate dissolved in 3 mL dry MeOH. The reaction solution was stirred for 1 h before the solvent was removed under reduced pressure. The crude was then dissolved in a 2 mL solution of TFA:DCM:H2O mixture (8:1:1) and allowed to stir for 6 minutes before diluting with cyclohexane and co-evaporating under reduced pressure. Upon condensation, the product was formed as a white solid and could be isolated with a 50% yield.

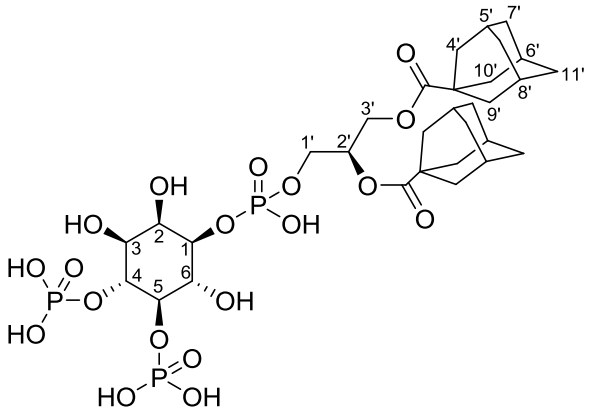

34

^{1}H NMR (400 MHz, $CDCl_3$) δ (ppm) = 5.35–5.27 (m, 1H, CH_2CHCH_2), 4.49 (dd, *J* = 12 Hz, 3, 1H), 4.30–4.22 (m, 3H), 4.15– 3.90 (m, 5H), 3.71 (dd, *J* = 10 Hz, 3, 1H), 2.05–2.00 (m, 6H), 1.93– 1.86 (m, 12H), 1.89–1.68 (m, 12H).

^{13}C NMR (101 MHz, $CDCl_3$) δ (ppm) = 180.2, 179.9, 77.8, 77.7, 75.9, 75.8, 71.3, 71.2, 70.9, 70.7, 70.6, 63.7, 62.6, 40.9, 40.8, 38.3, 35.8, 35.7, 27.5, 27.4.

^{31}P-NMR (400.13 MHz, $CDCl_3$) δ (ppm) = 0.49 (d, *J* = 67.1 Hz, 2P), -1.50 (s, 1P)

Characterization data of the compound was consistent with previously published work[125]

(2R)-3-(((benzyloxy)(((3aS,4R,5R,6S,7S,7aR)-4,5-bis((bis(benzyloxy) phosphoryl)oxy)-6-((2-methoxyethoxy)methoxy)hexahydrospiro[benzo[d] [1,3]dioxole-2,1'-cyclohexan]-7-yl)oxy)phosphoryl)oxy)propane-1,2-diyl bis(heptylcarbamate) (35)

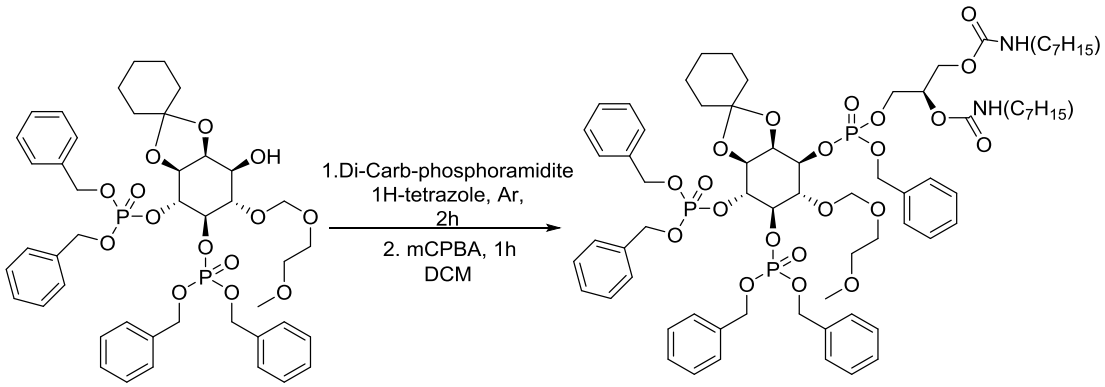

32 35

Compound **32** (207.3 mg, 0.238 mmol, 1 eq) and 0.45 M 1H-Tetrazole in ACN (1.58 mL, 0.714 mmol, 3 eq) were dissolved in 15 mL DCM in a flask under Ar atmosphere. The solution was cooled to 0°C before compound **41** (219 mg, 0.358 mmol, 1.5 eq) dissolved in DCM (2 mL) was added dropwise. After removing the ice bath and stirring for 2 h, the reaction mixture was cooled to -40°C and mCPBA (160 mg, 0.714 mmol, 3 eq) dissolved in 2 mL DCM was added dropwise. After warming the solution slowly to RT, the reaction mixture was quenched with 2 mL of a 10% solution of $KHSO_4^-$ in water. The organic phase was washed with sat. $NaHCO_3^-$ solution, water and brine, before it was dried with $NaSO_4$ and the solvent evaporated under reduced pressure. Purification of the product was achieved by biotage column chromatography (25g Silica cartridge; linear gradient of 30% to 100% EtOAc in Heptane). The product is a colourless oil and was isolated with a 38% yield.

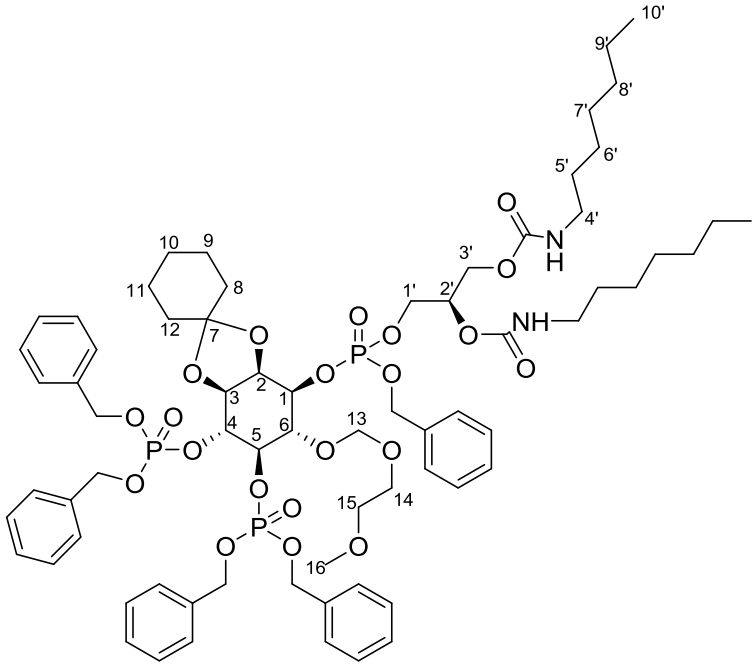

35

^{1}H NMR (400 MHz, $CDCl_3$) δ (ppm) = 7.32 (dd, *J* = 6.0 Hz, 2H, NH), 7.29 – 7.11 (m, 25H, Ar-H), 5.03 (ddd, *J* = 9.6 Hz, 5H, CH_2-Ar, H-13, H-2'), 4.99 – 4.88 (m, 8H, CH_2-Ar), 4.76 (dd, *J* = 6.9 Hz, 2H, H-1'), 4.67 (dd, *J* = 6.9 Hz, 2H, H-3'), 4.58 – 4.42 (m, 2H, *myo*-H-4, *myo*-H-1), 4.29 – 4.17 (m, 2H, H-14), 4.14 (dq, *J* = 9.9 Hz, 2H, H-15), 4.04 (t, *J* = 7.2 Hz, 1H, *myo*-H-5), 3.65 – 3.52 (m, 1H, *myo*-H-3), 3.34 (dt, *J* = 4.5 Hz, 2H, *myo*-H-2, *myo*-H-6), 3.21 (s, 3H, H-16), 3.09 – 2.92 (m, 4H, H-4'), 1.73 – 1.59 (m, 2H, H-5'), 1.27 – 1.04 (m, 28H, H-8,9,10,11,12, H-6',7',8',9'), 0.81 – 0.75 (m, 6H, H-10').

^{13}C NMR (101 MHz, $CDCl_3$) δ (ppm) = 155.83, 155.36, 136.00, 135.92, 135.74, 135.67, 135.63, 129.15, 128.76, 128.66, 128.61, 128.56, 128.53, 128.48, 128.45, 128.42, 128.39, 128.35, 128.30, 128.28, 128.04, 128.01, 127.99, 127.96, 127.91, 127.87, 127.79, 127.73, 111.72, 111.66, 96.24, 79.11, 77.36, 77.25, 77.05, 76.73, 75.51, 74.14, 72.94, 71.66, 71.62, 70.12, 69.67, 69.61, 69.54, 69.49, 69.42, 67.82, 67.77, 66.47, 62.47, 60.41, 58.89, 58.87, 41.16, 36.35, 34.25, 31.76, 29.91, 29.88, 29.82, 28.97, 28.93, 26.75, 26.69, 24.94, 23.88, 23.58, 22.61, 21.08, 14.22, 14.08, 1.04.

^{31}P-NMR (400.13 MHz, CDCl3) δ (ppm) = -1.69 (d, *J* = 11.8 Hz, 1P), -1.99 – -2.63 (m, 2P).

$[\alpha]_D^{20}$ = (-)8.1460123 (c = 16.3 mg/mL in CH_3Cl)

HRMS (ESI)+ m/z meas. 1417.5715; calc. for C70H97N2O21P3 $[M+Na]^+$ 1417.5689 -1.9 ppm

(2R)-3-((hydroxy(((1R,2R,3S,4R,5R,6S)-2,3,6-trihydroxy-4,5-bis(phosphonooxy)cyclohexyl)oxy)phosphoryl)oxy)propane-1,2-diyl bis(heptylcarbamate) (36)

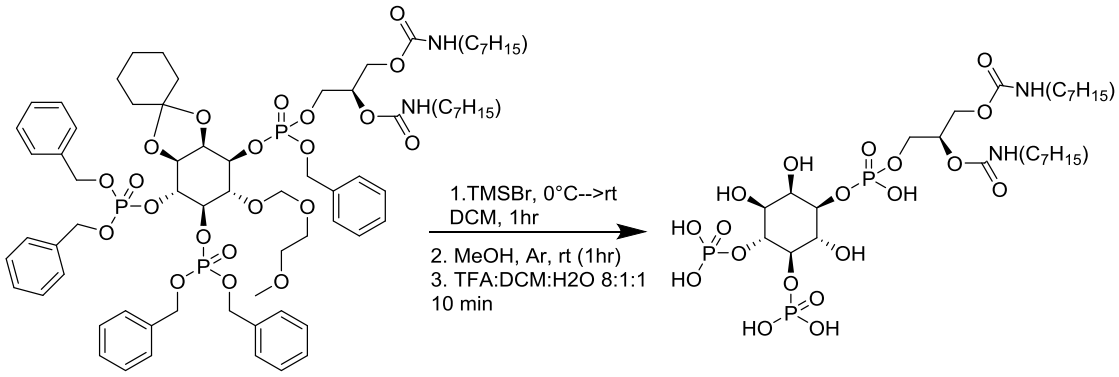

35 36

Compound **35** (120 mg, 0.086 mmol, 1 eq) was thoroughly dried before dissolving it in anhydrous DCM (2.5 mL) at rt, under argon atmosphere. The solvents used for this reaction was dried over molecular sieves. The reaction mixture was allowed to stir at 0°C. TMSBr (1 mL, excess), was added dropwise to the stirring reaction, and the reaction was slowly brought up to rt and stirred for an hour. TMSBr and DCM were evaporated and the precipitate dissolved in 2.5 mL dry MeOH. The reaction solution was stirred for 1 h before the solvent was removed under reduced pressure. The crude was then dissolved in a 2 mL solution of TFA:DCM:H2O mixture (8:1:1) and allowed to stir for 6 minutes before diluting with cyclohexane and co-evaporating under reduced pressure. Upon condensation, the product was formed as a white solid and could be isolated with a 50% yield.

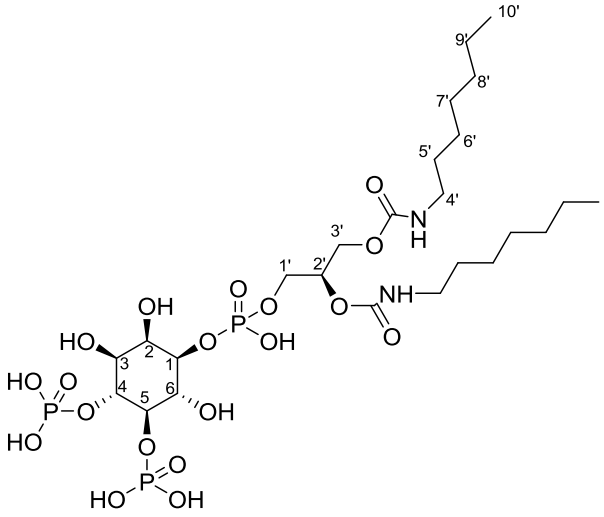

36

^{1}H NMR (400 MHz, DMSO) δ (ppm) = 7.19 (dt, *J* = 39.7 Hz, 2H, NH), 4.85 (t, *J* = 5.1 Hz, 1H, H-2'), 4.06 – 3.83 (m, 4H, H-1',3'), 3.64 – 3.40 (m, 2H, *myo*-H-1, *myo*-H-4), 2.87 (dq, *J* = 12.8 Hz, 4H, H-4'), 2.42 (p, *J* = 1.8 Hz, 4H, *myo*-H-5, *myo*-H-2, *myo*-H-3, *myo*-H-6), 1.41 – 0.97 (m, 24H, H-5'-9'), 0.77 (t, *J* = 6.8 Hz, 6H, H-10').

^{13}C NMR (101 MHz, DMSO) δ (ppm) = 155.63, 155.05, 70.72, 69.68, 68.41, 63.69, 60.21, 53.94, 53.87, 53.67, 53.60, 53.40, 53.33, 53.13, 52.86, 41.70, 41.10, 41.10, 40.44, 31.74, 31.14, 28.92, 26.65, 22.58, 13.80.

^{31}P-NMR (400.13 MHz, DMSO) δ (ppm) = 0.56 (s, 1 P), -0.14 (d, *J* = 40.2 Hz, 1P), -0.73 (s, 0.5P), -1.91 (s, 0.5P)

$[\alpha]_D^{20}$ = 6.5133333 (c = 3 mg/ml in $CHCl_3$)

HRMS (ESI)+ m/z meas. 835.4610; calc. for C37H75N4O9P3 $[M+Na]^+$ 835.4639, 3.5 ppm

(2R)-3-(((benzyloxy)(((3aS,4R,5R,6S,7S,7aR)-4,5-bis((bis(benzyloxy) phosphoryl)oxy)-6-((2-methoxyethoxy)methoxy)hexahydrospiro[benzo[d] [1,3]dioxole-2,1'-cyclohexan]-7-yl)oxy)phosphoryl)oxy)propane-1,2-diyl dioctanoate (51)

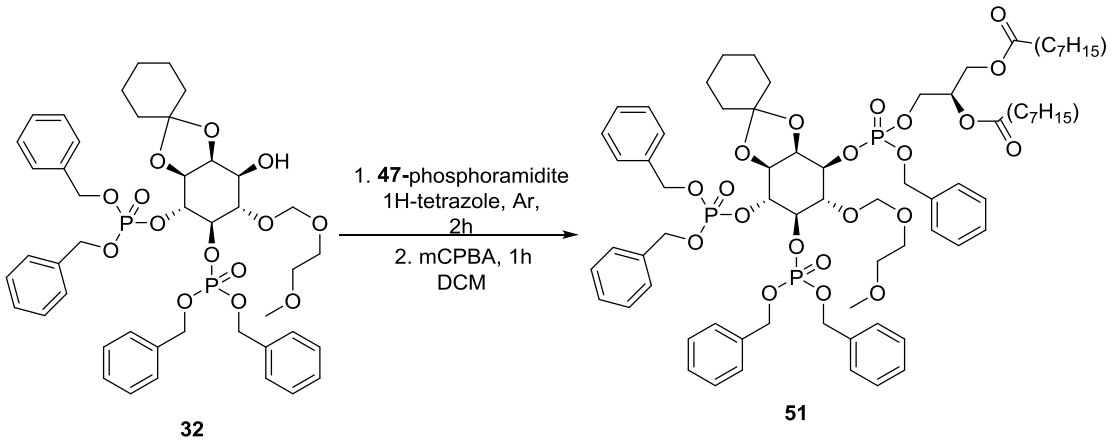

32 51

Compound **32** (97 mg, 0.11 mmol, 1 eq) and 0.45 M 1H-Tetrazole in ACN (1.46 mL, 0.66 mmol, 6 eq) were dissolved in 15 mL DCM in a flask under Ar atmosphere. The solution was cooled to 0°C before compound **47** (129.98 mg, 0.22 mmol, 2 eq) dissolved in DCM (2 mL) was added dropwise. After removing the ice bath and stirring for 2 h, the reaction mixture was cooled to -40°C and mCPBA (147.9 mg, 0.66 mmol, 6 eq) dissolved in 2 mL DCM was added dropwise. After warming the solution slowly to RT, the reaction mixture was quenched with 2 mL of a 10% solution of $KHSO4^-$ in water. The organic phase was washed with sat. $NaHCO3^-$ solution, water and brine, before it was dried with NaSO4 and the solvent evaporated under reduced pressure. Purification of the product was achieved by biotage column chromatography (10g Silica cartridge; linear gradient of 25% to 100% EtOAc in Heptane). The product is a colorless oil and was isolated with an 85% yield.

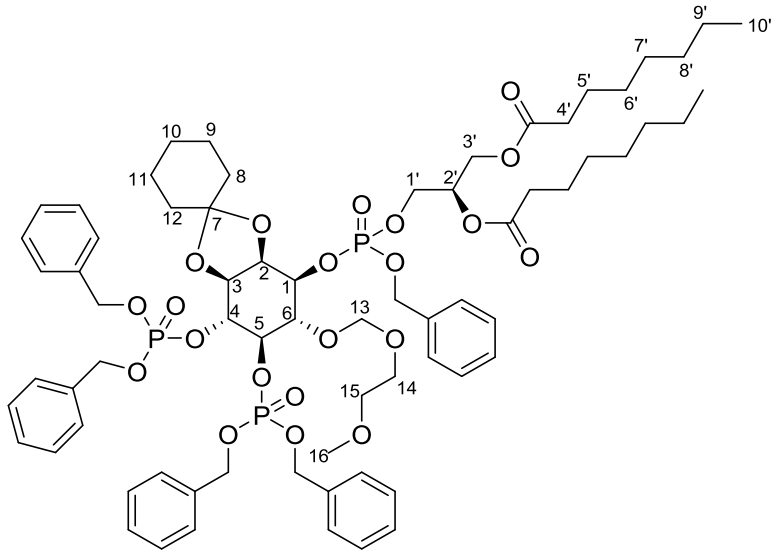

51

^{1}H NMR (400 MHz, $CDCl_3$) δ (ppm) = 7.32 – 7.25 (m, 4H, Ar-H), 7.25 – 7.20 (m, 8H, Ar-H), 7.19 – 7.14 (m, 13H, Ar-H), 5.06 – 4.98 (m, 5H, CH_2-Ar), 4.98 – 4.88 (m, 5H, CH2-Ar), 4.76 (dd, *J* = 16.3 Hz, 2H, H-13, H-2'), 4.68 (dd, *J* = 9.1 Hz, 1H, H-13), 4.57 (ddt, *J* = 10.1 Hz, 2H, H1'), 4.26 – 4.16 (m, 3H, *myo*-H-4, H-14), 4.15 – 4.10 (m, 1H, *myo*-H-1), 4.09 – 3.97 (m, 2H, H-3'), 3.59 (ddd, *J* = 11.9 Hz, 2H, H-14), 3.35 – 3.26 (m, 2H, *myo*-H-5, *myo*-H-3), 3.20 (d, *J* = 2.0 Hz, 3H, *myo*-H-2, H-15), 2.19 (dtd, *J* = 12.9, 7.1, 6.7, 4.5 Hz, 4H, H-4'), 1.66 (d, *J* = 6.2 Hz, 7H, H-16, H-5'), 1.27 – 1.11 (m, 22H, H-8,9,10,11,12, H-6',7',8',9'), 0.80 (dq, *J* = 6.7 Hz, 6H, H-10').

^{13}C NMR (101 MHz, $CDCl_3$) δ (ppm) = 173.18, 173.17, 172.80, 172.76, 136.00, 135.88, 135.80, 135.44, 128.64, 128.63, 128.52, 128.50, 128.48, 128.46, 128.44, 128.42, 128.37, 128.34, 128.28, 128.03, 128.01, 127.97, 127.94, 127.93, 127.86, 127.83, 111.62, 111.60, 96.28, 96.20, 78.66, 77.35, 77.23, 77.03, 76.71, 75.69, 73.18, 71.64, 69.65, 69.55, 69.49, 67.76, 61.64, 58.88, 36.48, 34.24, 34.08, 33.97, 31.67, 29.73, 29.08, 29.04, 28.95, 24.83, 24.82, 24.80, 23.88, 23.59, 22.62, 14.09.

^{31}P-NMR (400.13 MHz, $CDCl_3$) δ (ppm) = -1.62 (d, *J* = 4.4 Hz, 1P), -1.86 (d, *J* = 22.6 Hz, 1P), -2.14 (d, *J* = 4.5 Hz, 1P)

$[\alpha]_D^{20}$ = (-)5.9584615

HRMS (ESI+) m/z meas. 1387.5483; calc. for C70H95O21P3 $[M+Na]^+$ 1387.5471 -0.9 ppm

(2R)-3-((hydroxy(((1R,2R,3S,4R,5R,6S)-2,3,6-trihydroxy-4,5-bis(phosphonooxy)cyclohexyl)oxy)phosphoryl)oxy)propane-1,2-diyl dioctanoate (52)

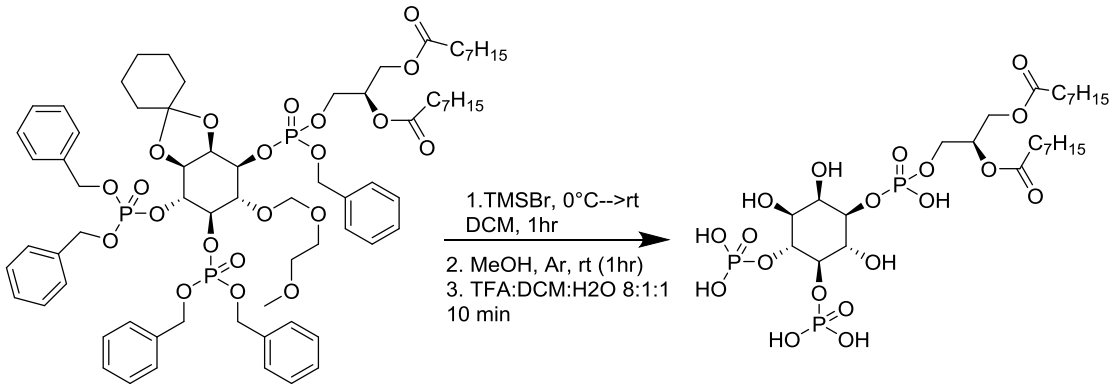

51 52

Compound **51** (120 mg, 0.0879 mmol, 1 eq) was thoroughly dried before dissolving it in anhydrous DCM (0.5 mL) at rt, under argon atmosphere. The solvents used for this reaction was dried over molecular sieves. The reaction mixture was allowed to stir at 0°C. TMSBr (1 mL, excess), was added dropwise to the stirring reaction, and the reaction was slowly brought up to rt and stirred for an hour. TMSBr and DCM were evaporated and the precipitate dissolved in 2.5 mL dry MeOH. The reaction solution was stirred for 1 h before the solvent was removed under reduced pressure. The crude was then dissolved in a 2 mL solution of TFA:DCM:H2O mixture (8:1:1) and allowed to stir for 10 minutes before diluting with cyclohexane and co-evaporating under reduced pressure. Resuspension in water and freeze drying yielded a white solid as the product (85%).

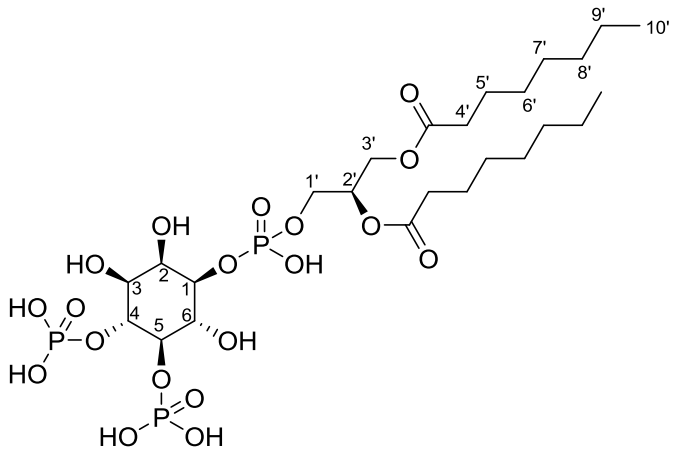

52

Characterization data of the compound was consistent with previously published work[120]

5.2.4. Solid phase synthesis of lipid tail-modified PI(4,5)P*2* analogues

1-*O*-[(3-phenylpropanoyl)benzyl]phosphoryl-2,3-O-(*p*-Wang-resin-oxy) benzylidene-4,5-di-*O*-(di-*O*-benzyl-phosphate)-6-*O*-methoxyethoxymethyl-*myo*-inositol (48)

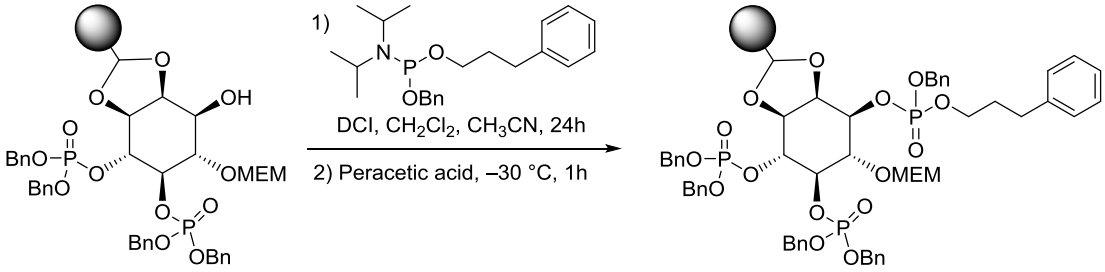

To the preswelled resin prepared according to previously established and published procedures[120] (148 mg, 0.077 mmol, loading 0.522 mmol/g) in anhydrous CH_2Cl_2 (2 mL) was added dicyanoimidazole (91 mg, 0.772 mmol) in acetonitrile (1 mL), followed by immediate addition of phosphoramidite **38** (284 mg, 0.772 mmol) in acetonitrile (1 mL). The resin was then allowed to shake for 40 h at room temperature, which was then cooled to –30°C, followed by addition of peracetic acid (167 µL, 0.92 mmol, 40% in acetic acid). After careful stirring of the resin for 1 h at the same temperature, it was filtered and

washed with DCM (3 X), DMF (3x), MeOH (3x), and finally DCM (3x). The resin was dried overnight in vacuo. The formation of the product was confirmed by test cleavage using 10% TFA in DCM.

MS (ESI): m/z (%): 1071.3 (100) $[M+H]^+$ (TFA test cleavage)

1-*O*-[(3-phenylpropanoyl)benzyl]phosphoryl-4,5-di-*O*-(di-*O*-benzyl-phosphate)-6-*O*-methoxyethoxymethyl-*myo*-inositol (49)

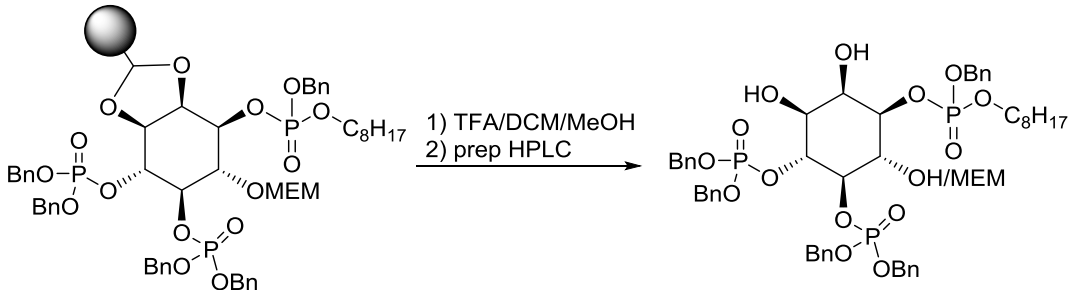

To the pre-swelled resin **48** (168 mg, 0.068 mmol, loading 0.469 mmol/g) in CH_2Cl_2 was added a mixture of 10% TFA in CH_2Cl_2 containing 1% methanol. The resin was shaken for 1 h, filtered and washed with CH_2Cl_2 for several times. All the washings were combined and evaporated to give the crude product, which was purified by HPLC yielding a mixture of free hydroxyl and MEM protected hydroxyl group at the 6-position. This mixture was used directly for the next step.

HPLC conditions:

t_R = 18.4 min; m/z (%): 989 $[M\text{-}MEM+H]^+$. The area under the peak represents 1.

t_R = 18.9 min; m/z (%): 1100 $[M+Na]^+$. The area under the peak represents 1.

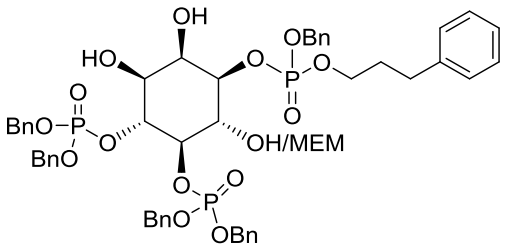

^{1}H NMR (400 MHz, $CDCl_3$) δ (ppm) = 7.66-7.88 (m, 25 H, Ar-H), 4.56–4.48 (q, *J* = 9.7 Hz, 1H, CH-4-*myo*), 4.22 (m, 1H, CH_2), 4.19–4.05 (m, 5H, CH-2-myo, CH-5-myo, CH_2), 4.01–3.96 (m, 1H, CH-1-*myo*), 3.64 (m, 1H, CH-6 *myo*), 3.62 (m, 1H, CH-3-*myo*), 2.

^{31}P-NMR (400.13 MHz, $CDCl_3$) δ (ppm) = 0.61 (d, 1P), –0.16 (d, 1P), –1.26 (d, 2P)

M-MEM: $[\alpha]_D^{20}$ = (–)3.122 (*c* = 0.9 mg/mL, $CHCl_3$)

HRMS (ESI^+): m/z pos.: $[M\text{-}MEM+H]^+$ calculated, 989.2827 found 989.2836 –0.9 ppm

$[M\text{-}MEM+Na]^+$ calculated, 1011.2646, found 1011.2653–0.7 ppm

$[M\text{-}MEM+K]^+$ calculated, 1027.2385, found 1027.2396–1.0 ppm

1-*O*-[(3-phenylpropanoyl)]phosphoryl-4,5-di-*O*-(phosphate)-*myo*-inositol (50):

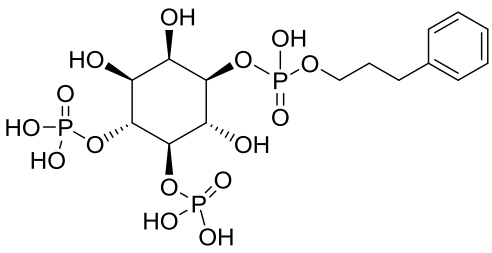

To compound **49** (19.6 mg, 0.019 mmol) in 0.5 mL of THF in a Schlenk flask was added bromotrimethylsilane (1.0 mL, excess) and the reaction was stirred for 2 h at room temperature. The reaction was then concentrated under vacuum to remove excess TMSBr and other byproducts. The residue was then stirred with methanol (2.5 mL) for 1 h followed by removal of the solvent under vacuum to give the product as white solid, which was dissolved in a methanol/ water mixture (1:1) and stirred with 20 mg of prewashed Chelex Na^+ ion exchanger resin for 24 h. The resin was filtered off and washed three times with water. The combined filtrates were concentrated in vacuo and then lyophilized to obtain **50** as an off-white solid (8.6 mg, 84%).

^{1}H NMR (400 MHz, $CDCl_3$) δ (ppm) = 7.66-7.88 (m, 25 H, Ar-H), 4.56–4.48 (q, *J* = 9.7 Hz, 1H, CH-4-*myo*), 4.22 (m, 1H, CH_2), 4.19–4.05 (m, 5H, CH-2-myo, CH-5-*myo*, CH_2, H-CH_2), 4.01–3.96 (m, 1H, CH-1-*myo*), 3.64 (m, 1H, CH-6 *myo*), 3.62 (m, 1H, CH-3-*myo*), 2.

^{31}P-NMR (400.13 MHz, $CDCl_3$) δ (ppm) = 0.61 (d, 1P), –0.16 (d, 1P), –1.26 (d, 2P)

M–MEM: $[\alpha]_D^{20} = -2.90$ (c = 0.004, $CHCl_3$)

HRMS (ESI+): m/z pos.: [M-MEM+H]+ calculated, 989.2827 found 989.2836 –0.9 ppm

[M-H]- calculated, 537.0334, found 537.0342–1.6 ppm

5.2.5. Synthesis of the PI(4,5)P_2 computational screen hit analogues (by the CBCF)

The synthesis of the final molecule which showed inhibition of PRL-3 is depicted in the scheme below:

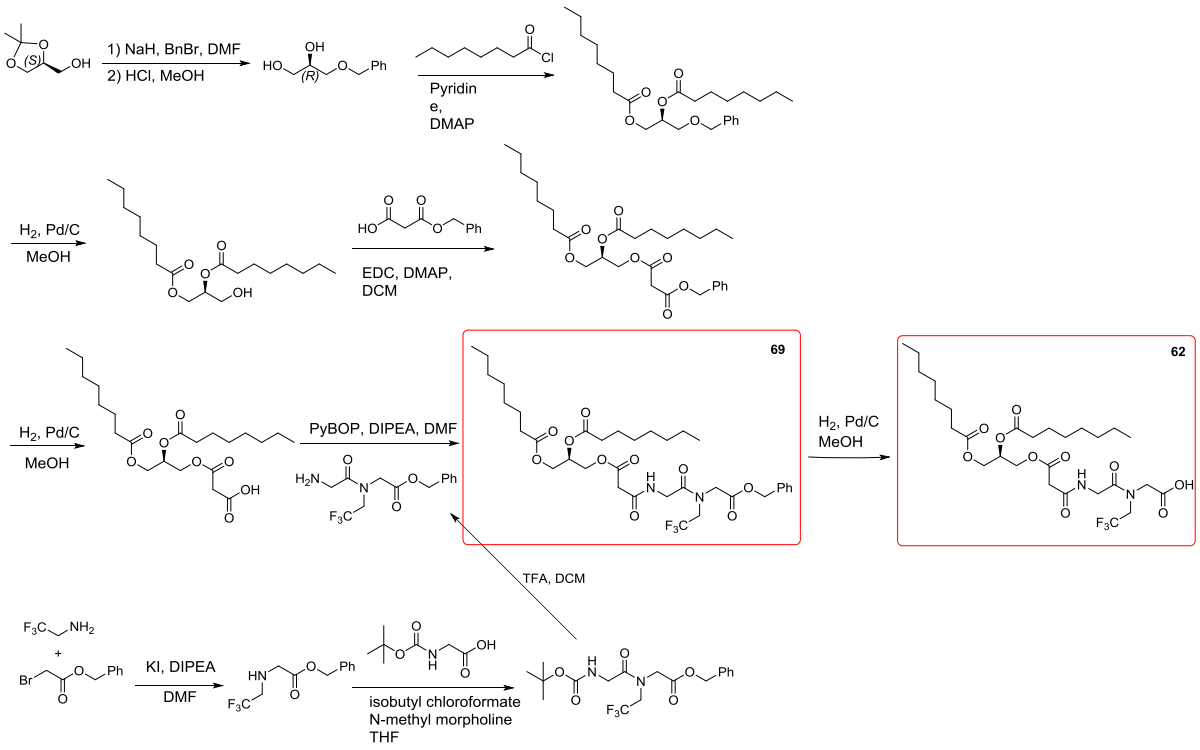

The designed final compound is termed **62** and its negative control benzyl ester **69**. The synthesis of product **61,** which was not completed and only yielded compound **70,** is depicted in the scheme below:

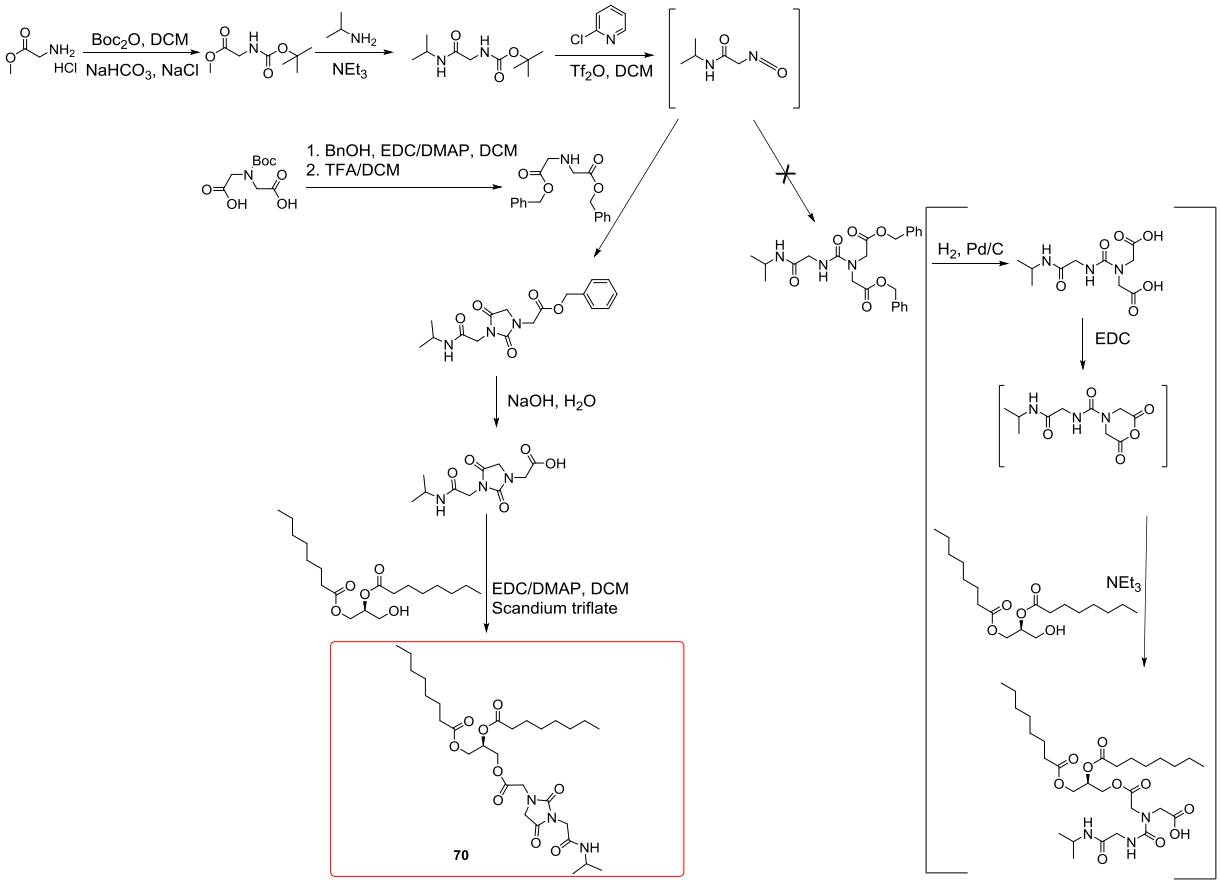

The analytics of the abovementioned three compounds (**62**, **69** and **70**) are shown below.

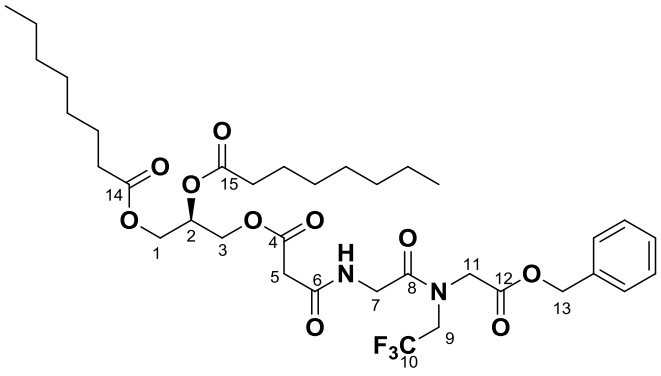

69

^{1}H NMR (400 MHz, $CDCl_3$) δ (ppm) = 7.70 (s, 1H, NH), 7.35 (s, 5H, Ar-H), 5.27 (s, 1H, H-2), 5.19 (s, 1H, H-13), 5.16 (s, 1H, H-13), 4.37 (s, 1H, H-1), 4.23 (d, *J* = 25.4 Hz, 4H, H-11, H-3), 4.14 (dd, *J* = 5.8 Hz, 2H, H-7), 4.08 (s, 1H, H-9), 3.95 (m, 1H, H-9), 3.37 (d, *J* = 3.0 Hz, 2H, H-5), 2.30 (m, 4H, CH_2), 1.60 (m, 2H, CH_2), 1.27 (s, 16H, CH-lipid chain), 0.87 (s, 6H, CH_3 x2).

^{13}C NMR (101 MHz, $CDCl_3$) δ (ppm) = 173.38 (C-14), 173.07 (C-15), 169.53, 169.33 (C-6), 168.33, 168.22 (C-8), 168.10, 167.91 (C8), 164.91 (C-4), 135.03, 134.54 (C-7), 129.03 C-Ph), 128.91, 128.79, 128.76, 128.73, 128.49, 128.38, 128.04 (C-10), 122.80, 122.46, 120.02, 119.67, 68.61, 68.22 (C-13), 67.56, 63.53 (C-13), 61.94 (C-13), 49.60, 49.26, 49.20, 48.92, 48.64, 47.92 (C-9), 47.58, 47.24 (C-11), 46.90, 41.47 (C-11), 41.24, 41.04 (C-9), 40.96 (C-5), 34.23, 34.12, 31.75, 29.15, 29.10, 29.00, 24.94, 22.70 (C-CH_2), 14.16 (C-CH_3).

^{19}F NMR ($CDCl_3$) δ (ppm) = -70.11, -70.47

HRMS (ESI$^+$): m/z = $[M+H]^+$ 713.3 (UPLCM/MS data)

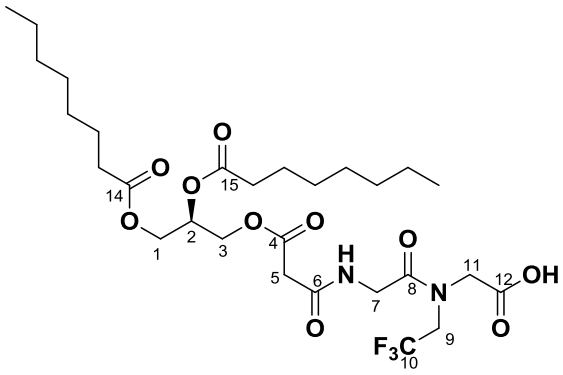

62

^{1}H NMR (400 MHz, MeOD) δ (ppm) = 5.35 – 5.21 (m, 1H, H-2), 4.37 (dd, *J* = 4.0 Hz, 2H, H-3), 4.30 – 4.09 (m, 8H, H-1, H-5, H-9, H-7), 3.42 (d, *J* = 6.3 Hz, 1H), 2.33 (td, *J* = 2.5 Hz, 4H, H-CH_2), 1.67 – 1.54 (m, 4H, H-CH_2), 1.39 – 1.22 (m, 16H, CH_2), 0.91 (t, *J* = 6.7 Hz, 6H, CH_3).

^{13}C NMR (101 MHz, $CDCl_3$) δ (ppm) = 173.63, 173.60, 173.31, 173.27, 171.07, 170.75, 170.04, 169.74, 168.53, 168.23, 166.10, 166.06, 125.75, 125.46, 122.97, 122.68, 120.18, 77.48, 77.16, 76.84, 65.16, 63.59, 62.12, 62.08, 49.36, 49.07, 47.66, 47.31, 41.89, 41.23, 41.05, 40.91, 34.28, 34.15, 31.78, 29.19, 29.13, 29.04, 24.96, 22.73.

^{19}F NMR ($CDCl_3$) δ (ppm) = -70.20, -70.65

HRMS (ESI$^+$): m/z = $[M+H]^+$ 627.2 (UPLCM/MS data)

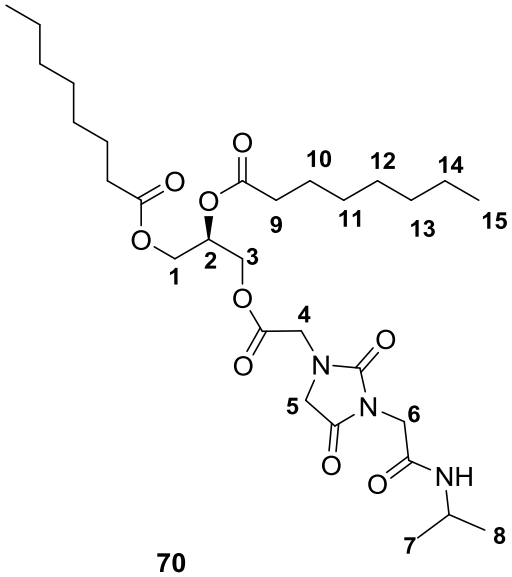

70

^{1}H NMR (400 MHz, $CDCl_3$) δ (ppm) = 5.63 (d, *J* = 7.8 Hz, 1H, NH), 5.28 (td, *J* = 5.1Hz, 1H, H-2), 4.39 (dd, *J* = 11.9 Hz, 4H, H-1, H-3), 4.29 (d, *J* = 4.5 Hz, 2H, H-4), 4.24 – 4.10 (m, 6H, H-5, H-6), 4.10 – 3.99 (m, 3H, H-7), 2.32 (td, *J* = 7.6 Hz, 4H, 2xH-9), 1.61 (dt, *J* = 7.6 Hz, 4H, 2xH-10), 1.33 – 1.22 (m, 16H, 2xH11-14), 1.15 (d, *J* = 6.6 Hz, 6H, 2xH-15).

^{13}C NMR (101 MHz, $CDCl_3$) δ (ppm) = 173.38, 173.11, 169.42, 168.23, 164.69, 156.90, 77.48, 77.16, 76.84, 63.80, 61.84, 50.55, 44.04, 41.94, 34.27, 34.14, 31.78, 29.83, 29.18, 29.14, 29.03, 24.98, 24.97.

HRMS (ESI$^+$): m/z = $[M+H]^+$ 585.3 (UPLCM/MS data).

Chapter 6. Summary

In this doctoral work, the objective was to develop and establish a strategy for the total organic synthesis of PI(4, 5)P_2 analogues, alkylated on the inositol ring, in order to study the mechanisms of interaction between PI(4, 5)P_2 and the metastasis-promoting phosphatase PRL-3.

After the development of the synthetic route, the effort for the synthesis of 6-*O*-methylated PI(4,5)P_2 was made. To establish the route, each reaction step was optimized by testing different reaction conditions. After developing the needed protecting group strategy for selective inositol ring alkylation, the reaction with the alkylating Meerwein salt as reagent was carried out, gave good yields, and was further used for different alkylated analogues.

Moreover, and using both solid phase and solution phase organic synthesis strategies, lipid chain-modified PI(4,5)P_2 analogues were also synthesized to gain more insight on the importance of the functional groups in the natural substrate binding to PRL-3. By using the established synthetic route, a bigger and more versatile library of differently substituted alkylated PI(4,5)P_2 and other PIP*n* analogues could be synthesized in the future. These analogues synthesized here were utilized for SAR studies to gain information for binding requirements of the following PI(4,5)P_2-metabolizing proteins: PRL-3, SYNJ1, OCRL and INPP5E. Curiously, the inositol-alkylated analogues were specific to PRL-3 with respect to the other phosphatases, and the lipid tail-modified analogues showed more significant activity with the other phosphatases than with PRL-3. This sets the initial basis for specificity of these analogues with a phosphatase that bears an unusually shallow and hydrophobic active site (PRL-3).

Complementary to the main work of this project, *in silico* shape similarity screening methods were used with PI(4,5)P_2 as a template, to search for specific PRL-3-active lead compound which could support designing an optimal inhibitor. This computational experiment led to an active compound (further optimized through synthesis before testing), underlying the potential of prediction tools in finding inhibitors for challenging targets.

The synthesized PI(4,5)P_2 analogues will be valuable in many applications, ranging from investigating the binding requirements of specific PIP*n*- metabolizing phosphatases, to

designing ligands through *in silico* and synthetic methods to modulate their interaction with interesting targets like phosphatases. Generally, such adaptable analogues could forge novel agents in chemical biology, both in probing biological activity and in the treatment of diseases.

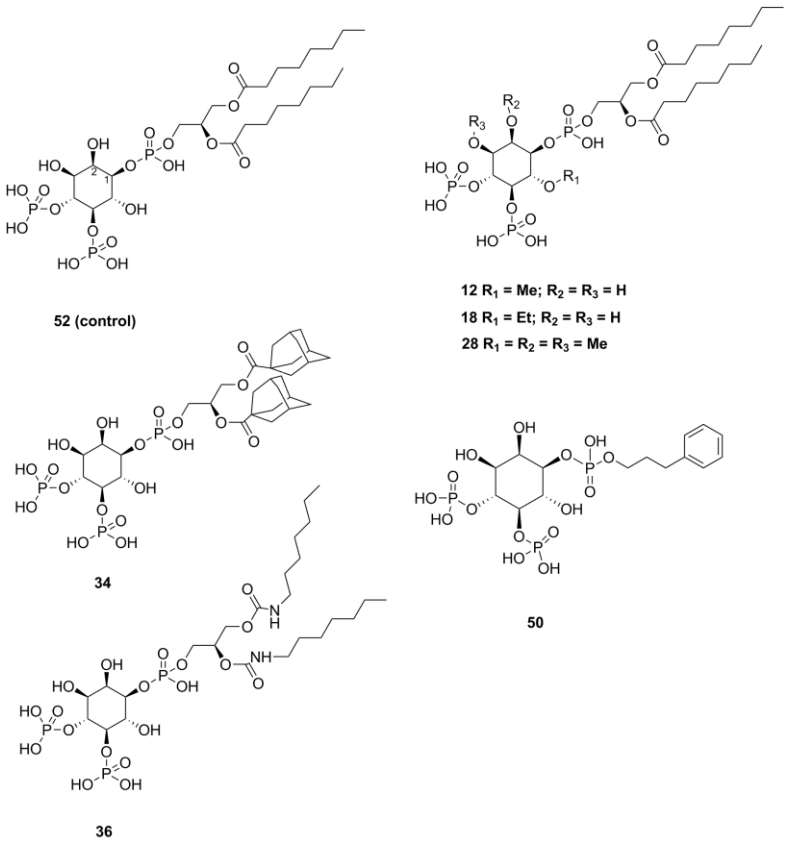

Figure **42** Overview of the structures of the PI(4,5)P_2 original substrate (**52**) and its six analogues (**12, 18, 28, 34, 36** and **50**), all of which were synthesized as part of this work.

Chapter 7. Appendices

7.1. Structural Directory

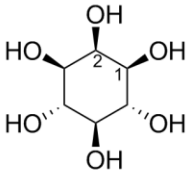

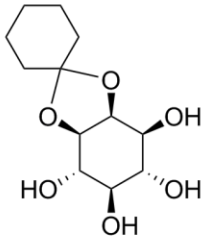

1

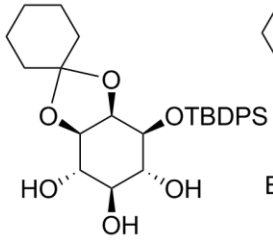

2

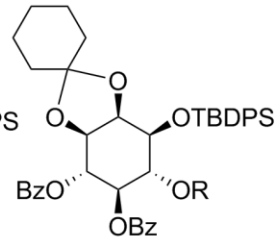

3 R = H
6 R = Me
13 R = Et
29 R = MEM

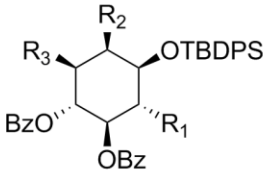

21 $R_1 = R_2 = R_3 = H$
19 $R_1 = R_2 = R_3 = Me$
20 $R_2 = H$; $R_1 = R_3 = Me$
22 $R_1 = R_2 = R_3 = Et$
23 $R_2 = H$; $R_1 = R_3 = Et$
7 $R_1 = Me$; $R_2 = R_3 = H$

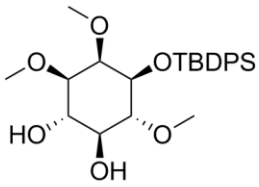

24

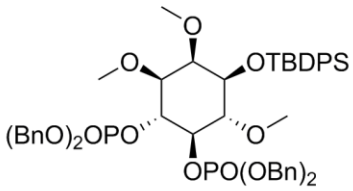

25

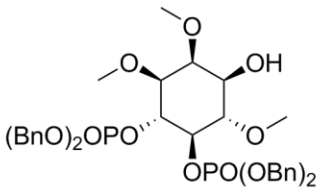

26

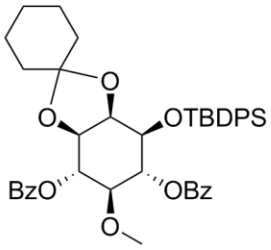

4

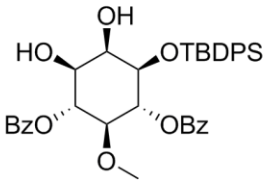

5

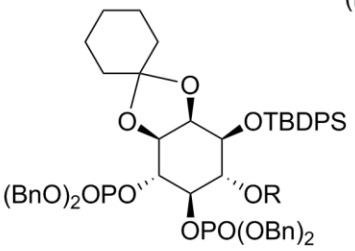

9 R = Me
15 R = Et
31 R = MEM

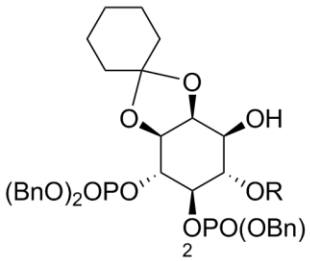

10 R = Me
16 R = Et
32 R = MEM

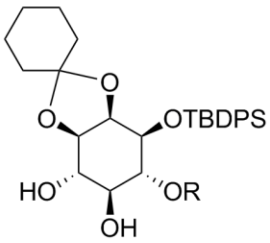

8 R = Me
14 R = Et
30 R = MEM

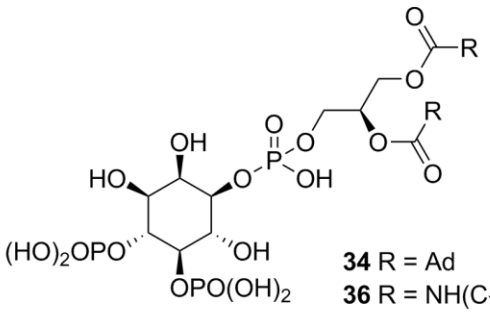

34 R = Ad
36 R = $NH(C_7H_{15})$

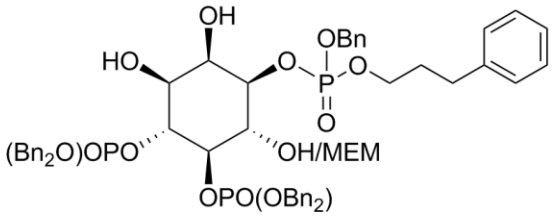

49

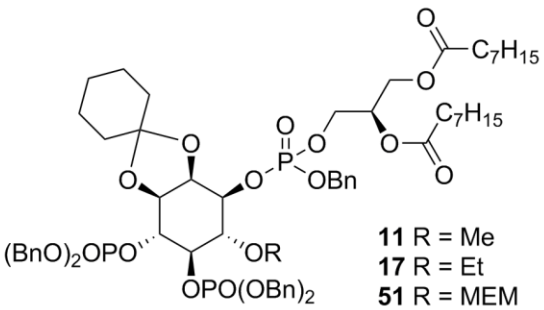

11 R = Me
17 R = Et
51 R = MEM

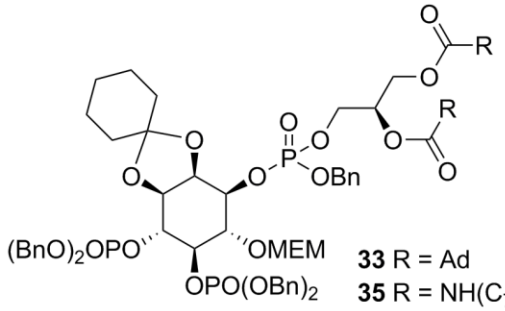

33 R = Ad
35 R = $NH(C_7H_{15})$

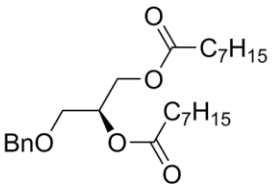

45

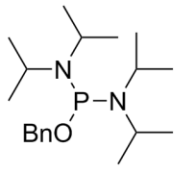

51

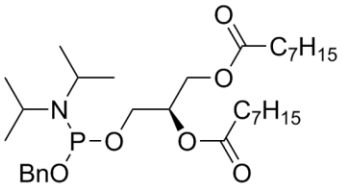

47

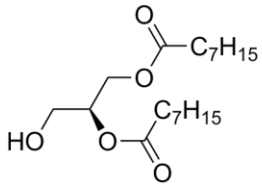

46

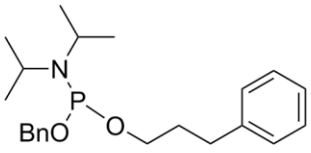

38

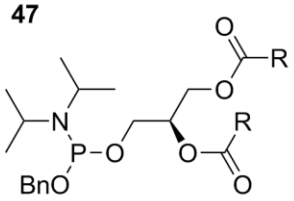

41 R = $NH(C_7H_{15})$
44 R = Ad

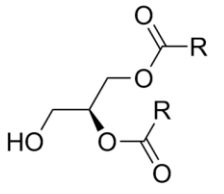

40 R = $NH(C_7H_{15})$
43 R = Ad

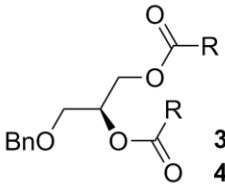

39 R = $NH(C_7H_{15})$
42 R = Ad

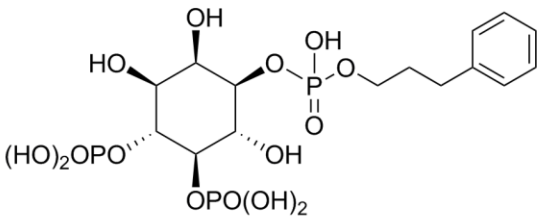

50

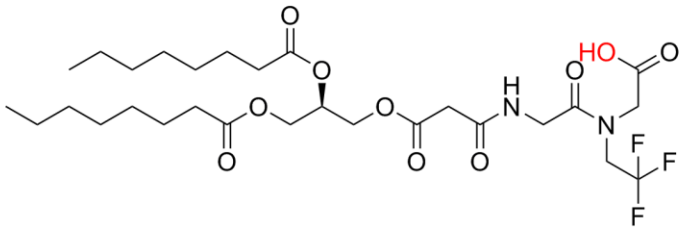

MJ06-49

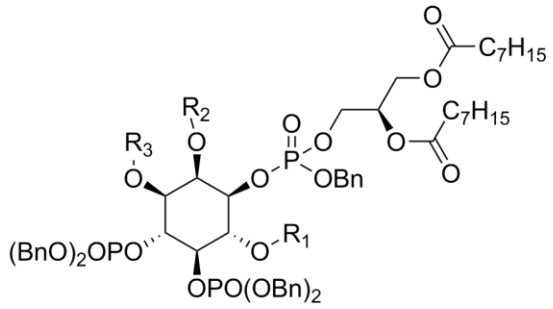

27

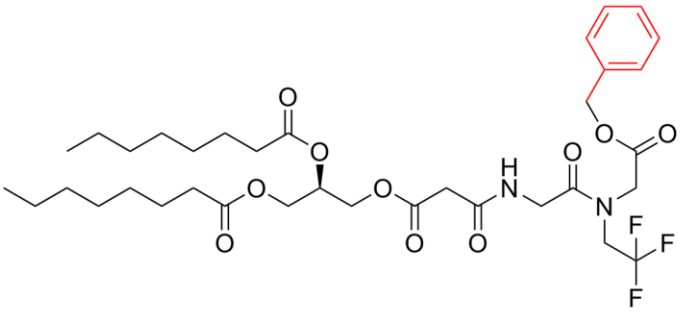

MJ06-47-2

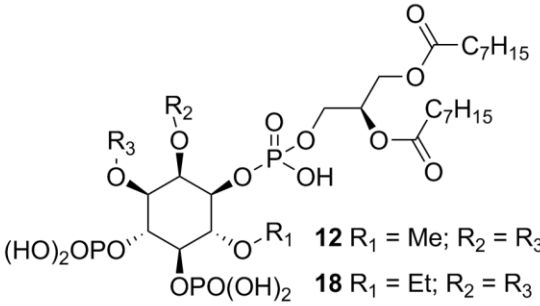

12 R_1 = Me; R_2 = R_3 = H
18 R_1 = Et; R_2 = R_3 = H
28 R_1 = R_2 = R_3 = Me
52 R_1 = R_2 = R_3 = H

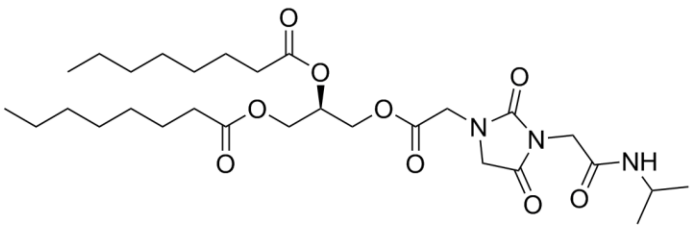

MJ05-47-2

7.2. Abbreviation directory

PIP*n*	phosphatidylinositol-phosphates
AcCN/ACN	acetonitrile
AM	acetyloxymethyl
Ar	Argon
BnOH	benzylalcohol
BzCl	benzoylchloride
CHD22	Cadherin 22
COSY	homonuclear correlation spectroscopy
DAG	diacylglycerol
DCM	dichloromethane
DIC	*N,N'*-diisopropylcarbodiimide
DIPA*DCI	diisopropylcarbodiimide
DIPEA	*(N,N'*-di-*iso*-propyl)-ethylamine
DMAP	4-Dimethylaminopyridine
DMF	dimethylformamide
DMSO	dimethylsufoxide
DUSPs/DSPs	Dual specificity phosphatases
EMT	Epithelial-mesenchymal transition
ESI	electrospray ionization
Et	ethyl
Et_2O	diethylether
EtOAc	ethylacetate
HMBC	Heteronuclear Multiple Bond Correlation.
HR-MS	high resolution mass spectrometry
HSQC	Heteronuclear Multiple Quantum Correlation
InsP	inositol-phosphates
mCPBA	*meta*-chloroperoxybenzoic acid
Me	methyl
MEM	2-Methoxyethoxymethyl ether
MEMCl	2-Methoxyethoxymethyl chloride
MeOH	methanol
MHz	megaherz
MMT	Monomethoxy trityl
MTM	myotubularin
NaOMe	sodium methoxide
NHERF1	Na^+/H^+ Exchanger Regulatory Factor
NMR	nuclear magnetic resonance
NOE	nuclear overhauser effect
PIC	phospholipase C
PIKfyve	phosphoinositide kinase with fyve Znn-motive
PIS	phosphatidylinositol synthase
PM	propionyloxymethyl

PRD	Proline-rich domain
PSTPs	Protein serine/threonine phosphatases
PTPs	Protein Tyrosine phosphatases
PTEN	Phosphatase and tensin homolog deleted on chromosome 10
RT	room temperature
SAR	Structure-activity relationships
TBAF	Tetra-*n*-butylammonium fluoride
TBDPS	Tert-butyl diphenylsilane
TBDPSCl	Tert-butyl diphenylsilylchloride
THF	tetrahydrofuran
TMSBr	bromotrimethylsilane
TLC	Thin layer chromatography
TFA	Trifluoroacetic acid
USR	Ultrafast shape recognition

7.3. NMR Spectra

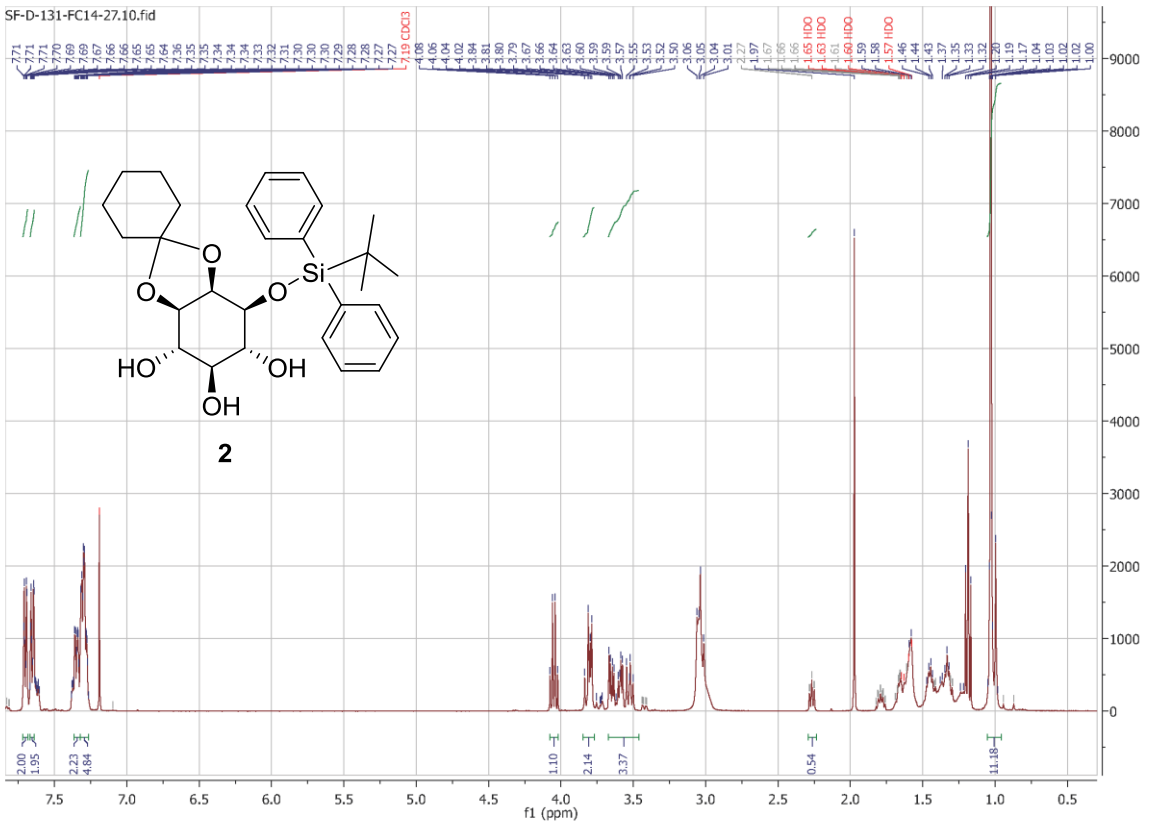

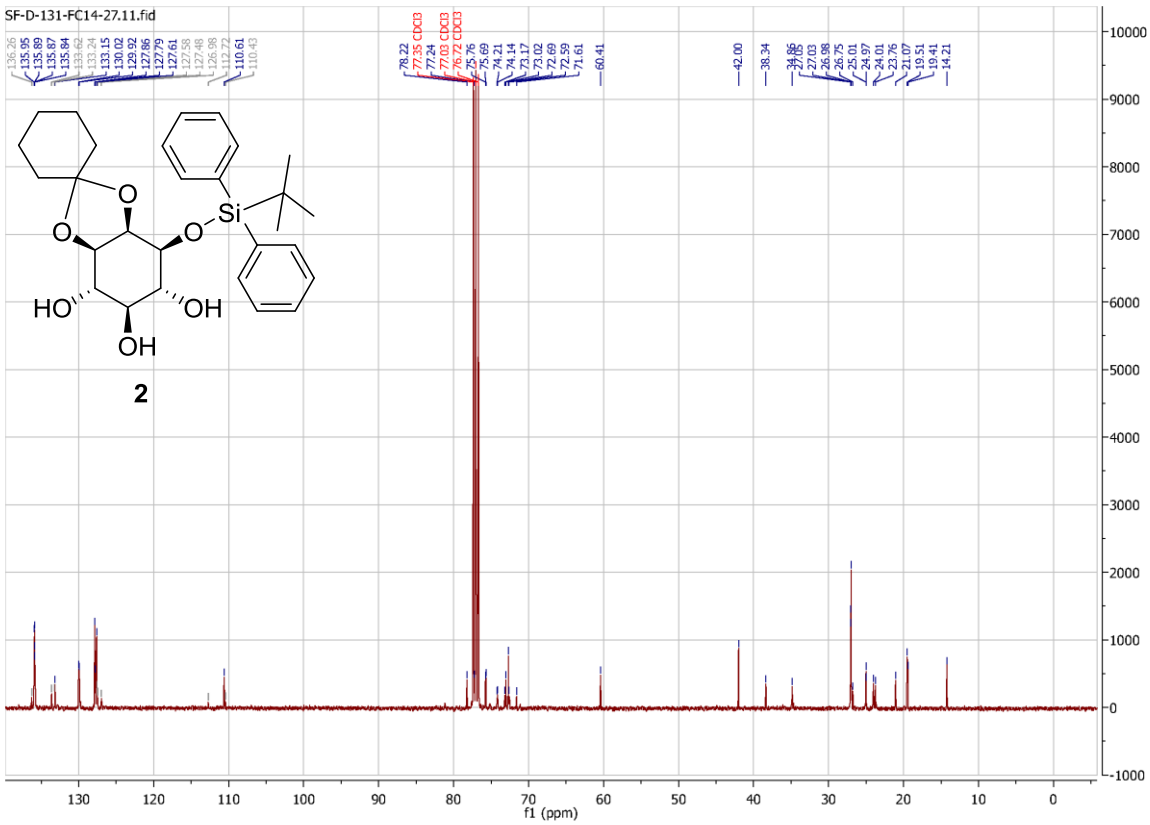

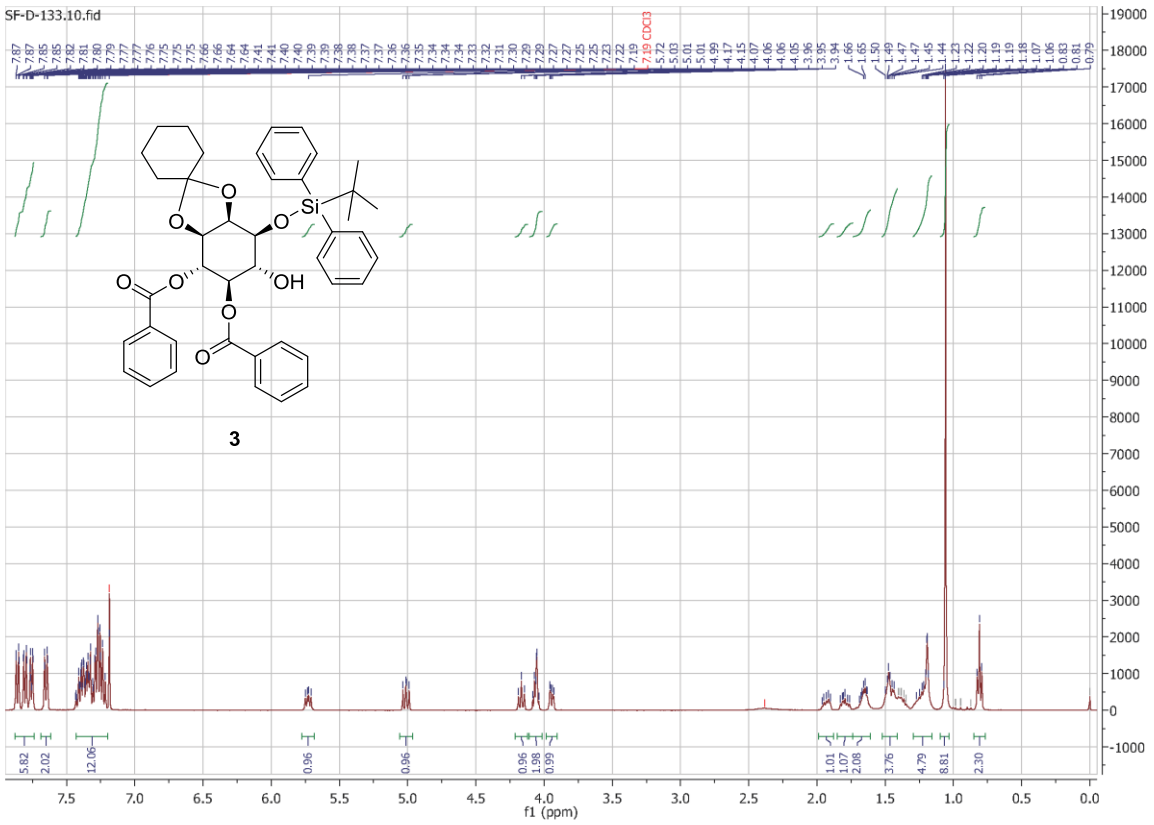
SF-D-133.10.fid
3
f1 (ppm)

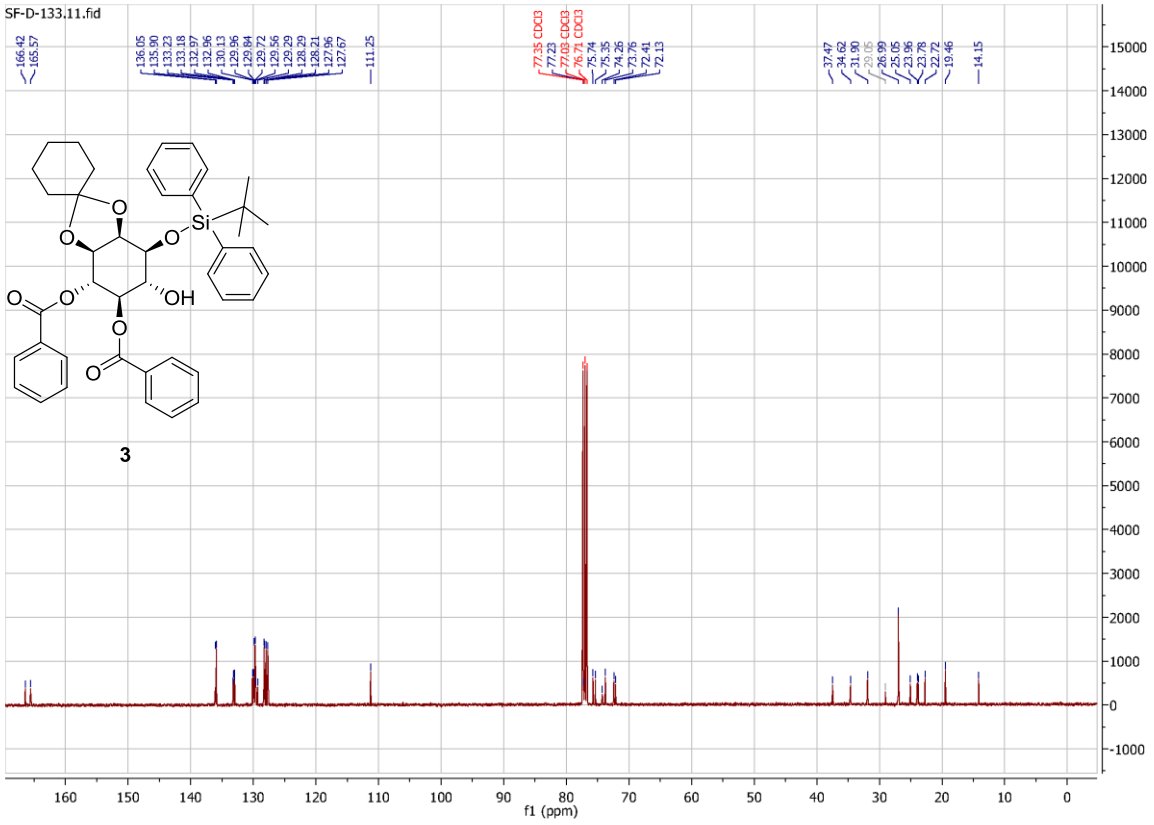
SF-D-133.11.fid
3
f1 (ppm)

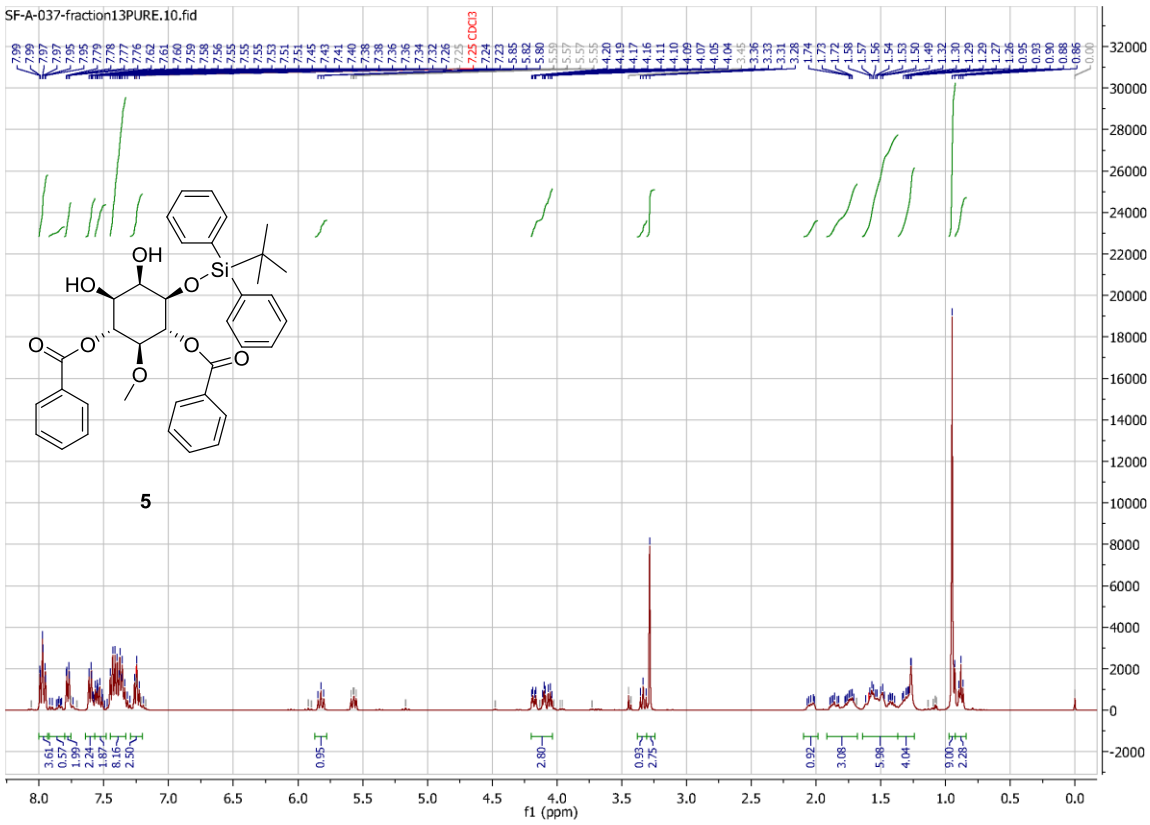
SF-A-037-fraction13PURE.10.fid
OH
HO
Si
O
O
O
O
O
O
5
f1 (ppm)

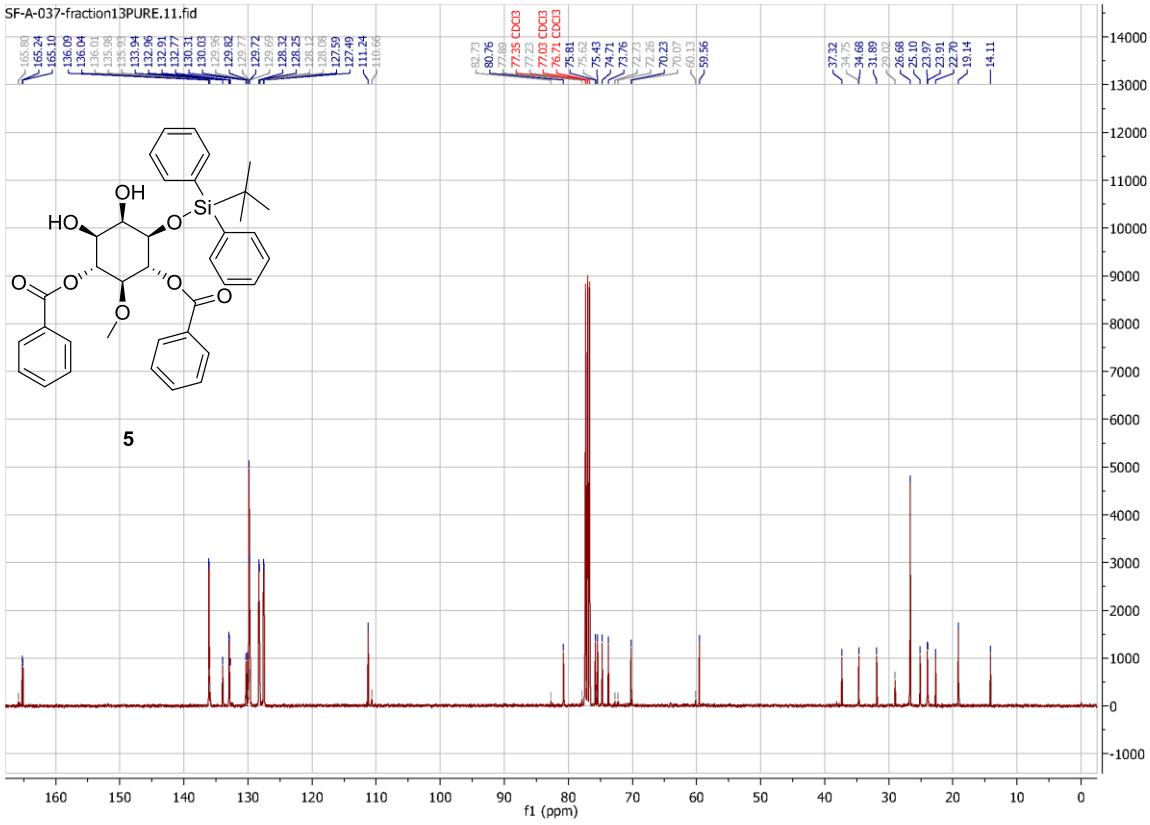
SF-A-037-fraction13PURE.11.fid
OH
HO
Si
O
O
O
O
O
O
5
f1 (ppm)

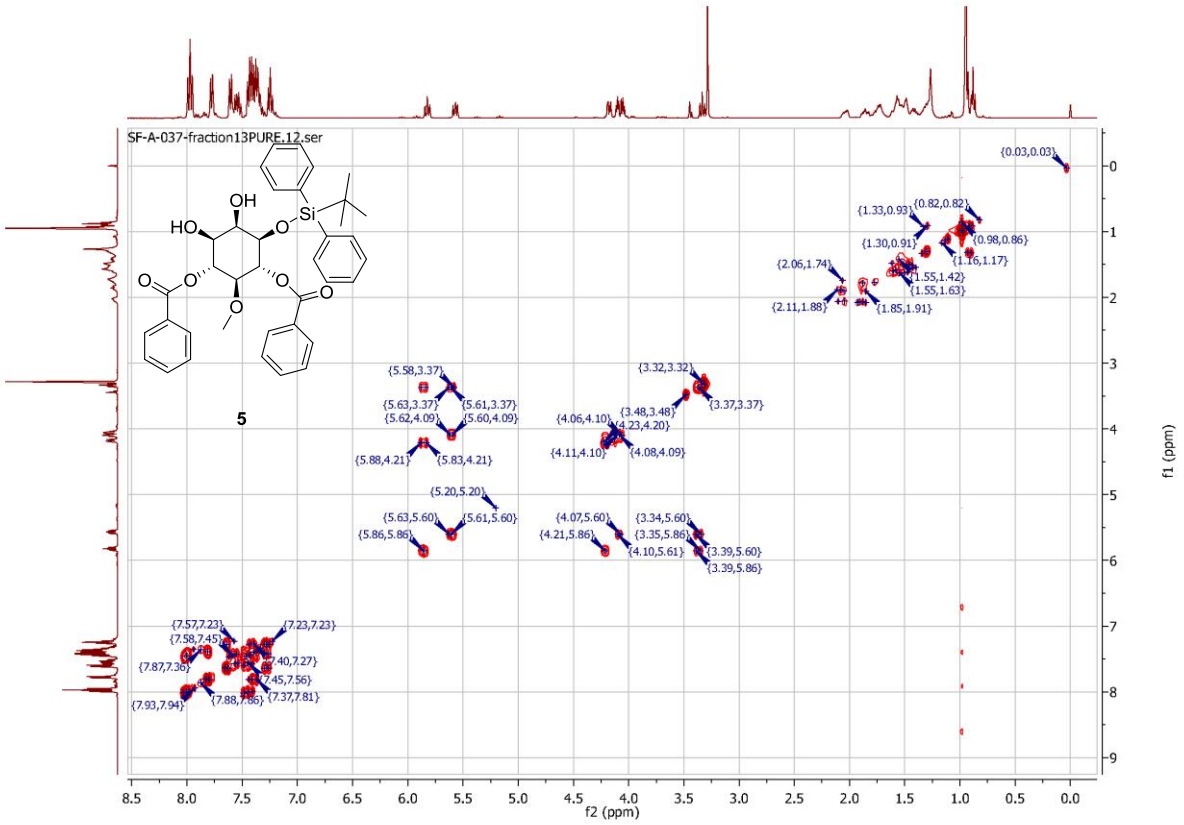
SF-A-037-fraction13PURE.12.ser
OH
HO
Si
O
O
O
O
O
O
5
{0.03,0.03}
{1.33,0.93}
{0.82,0.82}
{1.30,0.91}
{0.98,0.86}
{1.16,1.17}
{2.06,1.74}
{1.55,1.42}
{1.55,1.63}
{2.11,1.88}
{1.85,1.91}
{5.58,3.37}
{5.63,3.37}
{5.61,3.37}
{5.62,4.09}
{5.60,4.09}
{5.88,4.21}
{5.83,4.21}
{3.32,3.32}
{3.37,3.37}
{4.06,4.10}
{3.48,3.48}
{4.23,4.20}
{4.11,4.10}
{4.08,4.09}
{5.20,5.20}
{5.63,5.60}
{5.61,5.60}
{5.86,5.86}
{4.07,5.60}
{3.34,5.60}
{4.21,5.86}
{3.35,5.86}
{4.10,5.61}
{3.39,5.60}
{3.39,5.86}
{7.57,7.23}
{7.23,7.23}
{7.58,7.45}
{7.87,7.36}
{7.40,7.27}
{7.45,7.56}
{7.93,7.94}
{7.88,7.86}
{7.37,7.81}
f2 (ppm)
f1 (ppm)

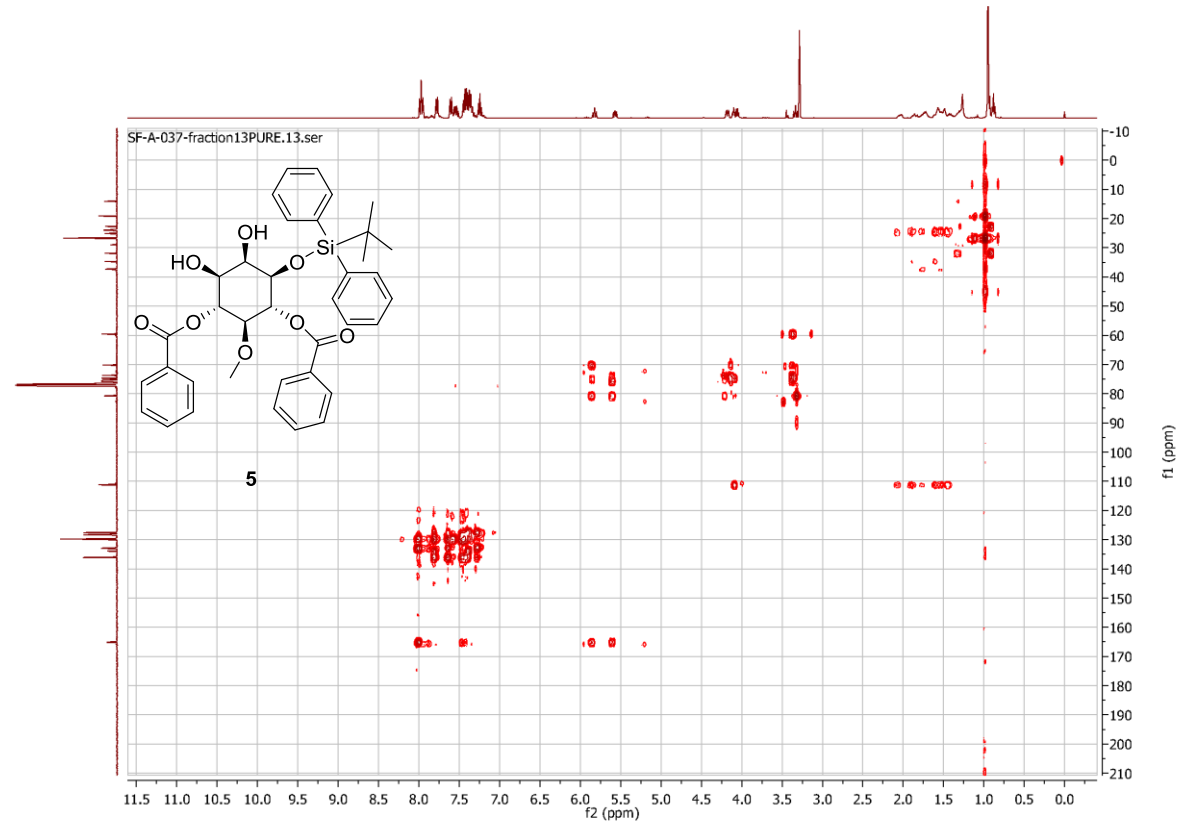
SF-A-037-fraction13PURE.13.ser
OH
HO
Si
O
O
O
O
O
O
5
f2 (ppm)
f1 (ppm)

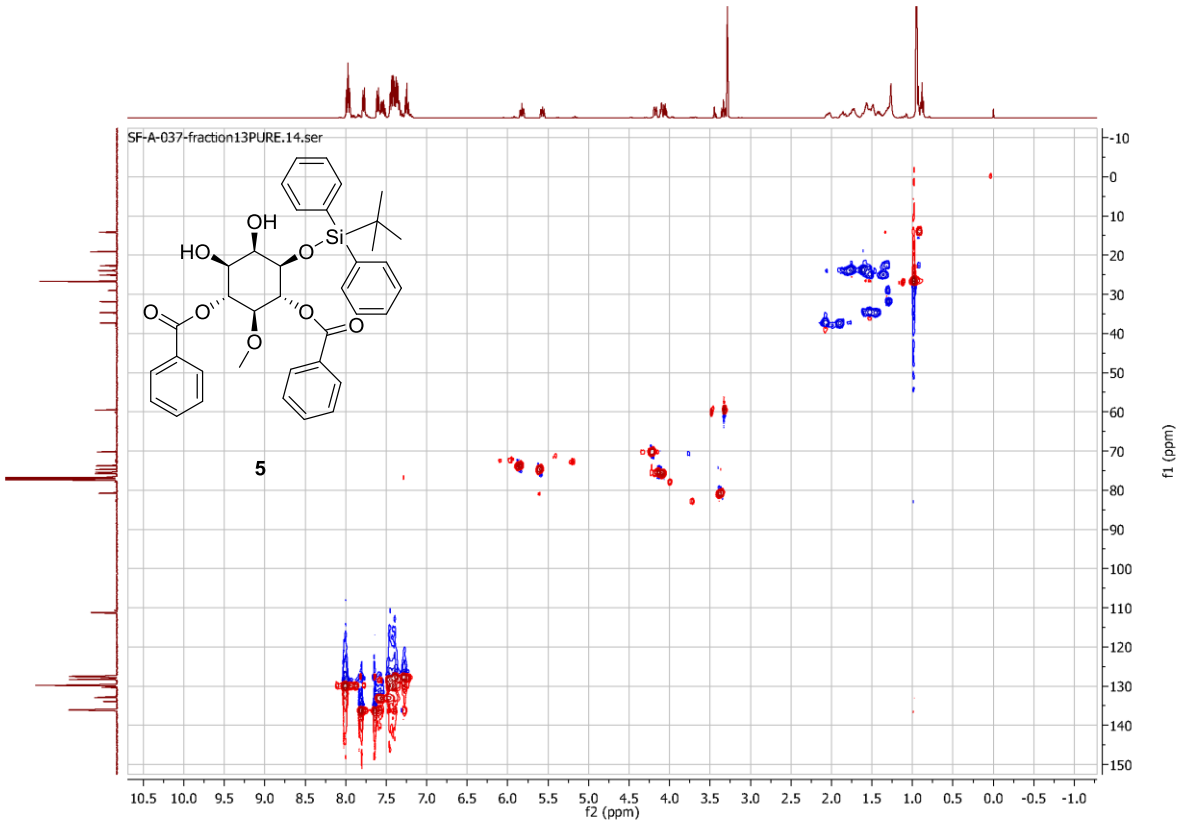
SF-A-037-fraction13PURE.14.ser
OH
HO
O
Si
O
O
O
O
O
O
5
f2 (ppm)
f1 (ppm)

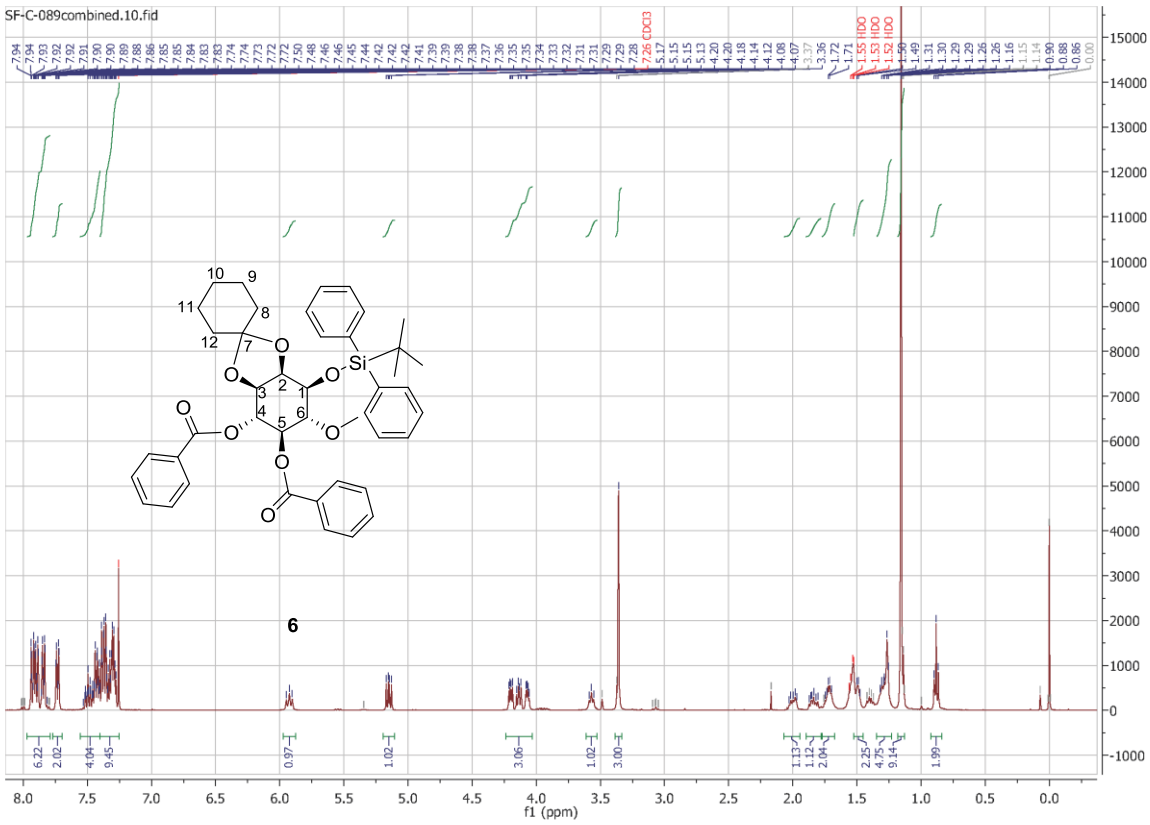
SF-C-089combined.10.fid
6
f1 (ppm)

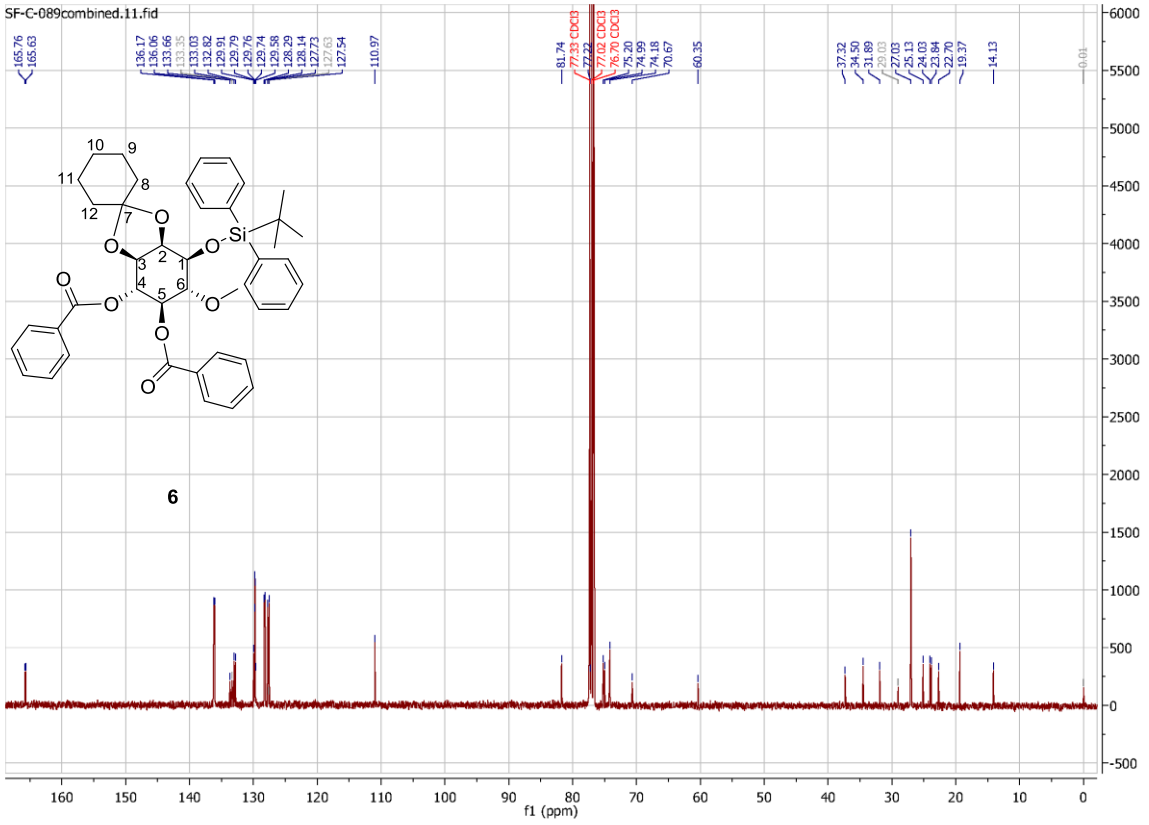
SF-C-089combined.11.fid
6
f1 (ppm)

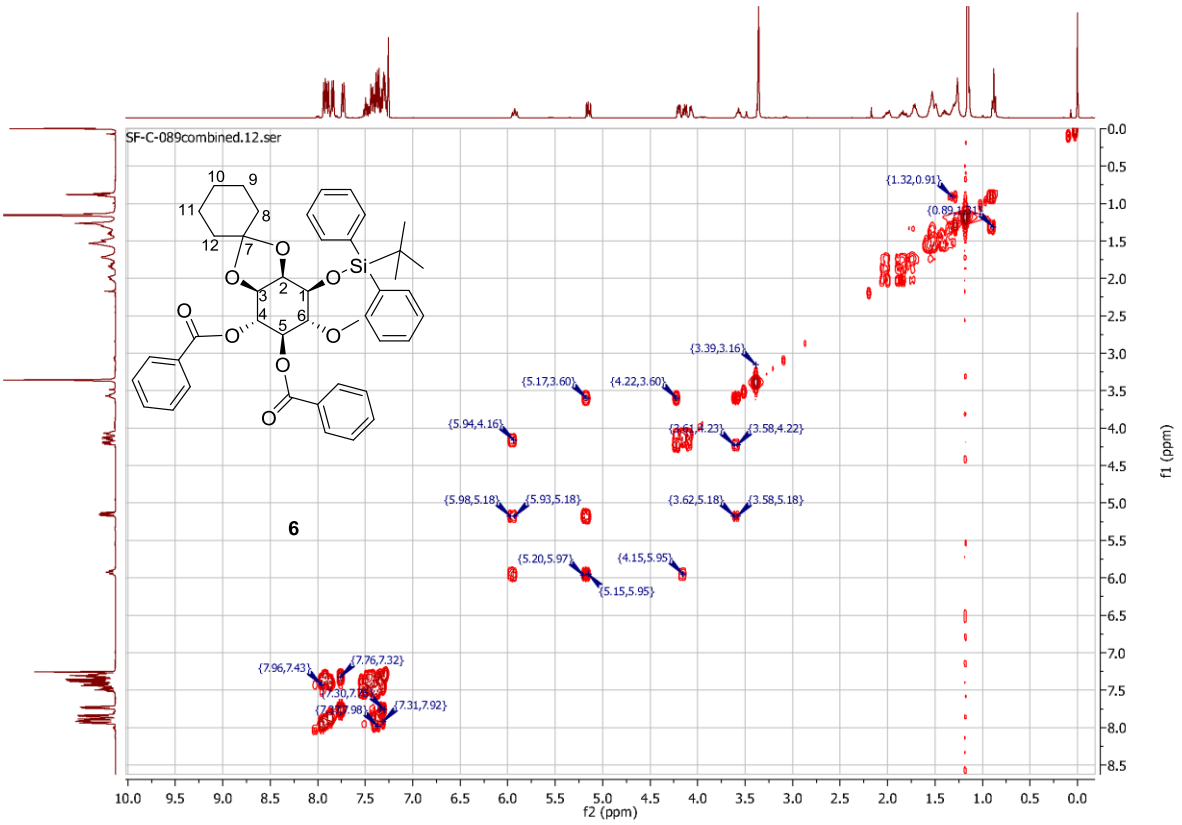
SF-C-089combined.12.ser
6
{1.32,0.91}
{3.39,3.16}
{5.17,3.60}
{4.22,3.60}
{5.94,4.16}
{3.61,4.23}
{3.58,4.22}
{5.98,5.18}
{5.93,5.18}
{3.62,5.18}
{3.58,5.18}
{5.20,5.97}
{4.15,5.95}
{5.15,5.95}
{7.96,7.43}
{7.76,7.32}
{7.31,7.92}
f2 (ppm)
f1 (ppm)

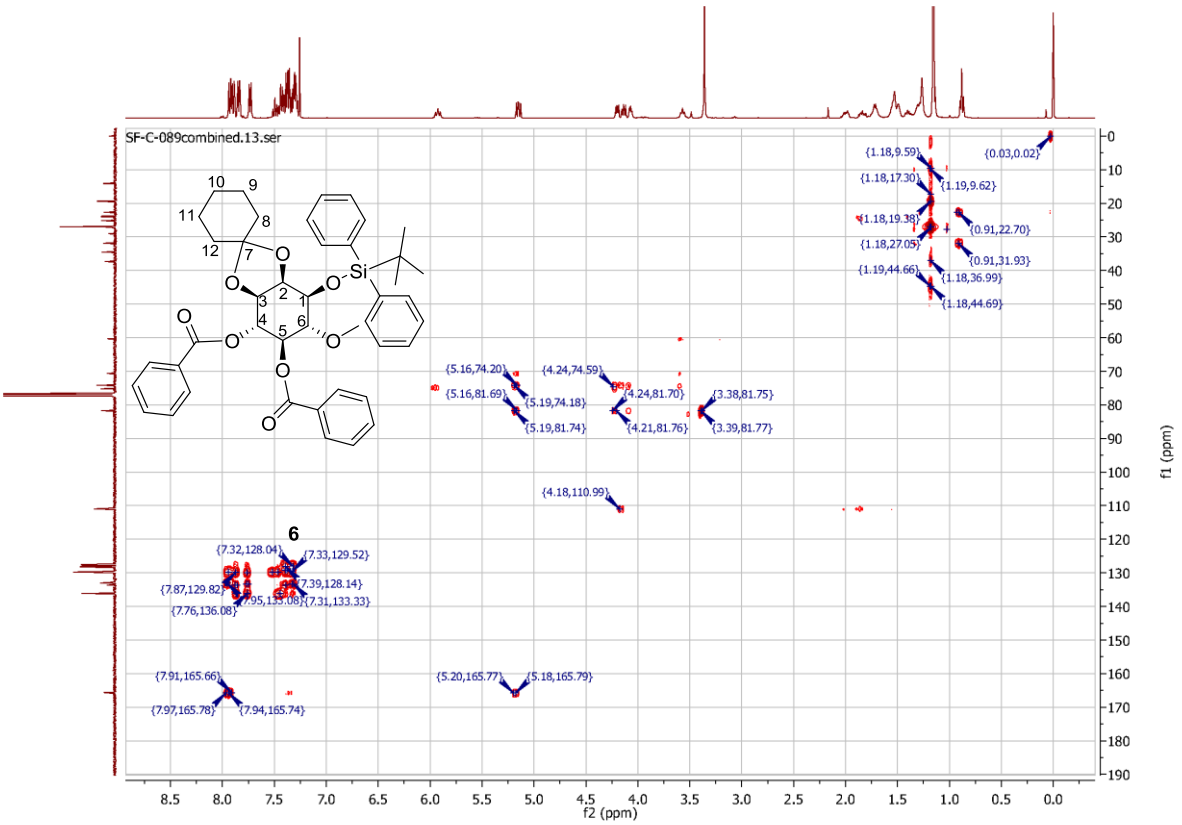
SF-C-089combined.13.ser
6
{1.18,9.59}
{0.03,0.02}
{1.18,17.30}
{1.19,9.62}
{1.18,19.38}
{0.91,22.70}
{1.18,27.05}
{0.91,31.93}
{1.19,44.66}
{1.18,36.99}
{1.18,44.69}
{5.16,74.20}
{4.24,74.59}
{5.16,81.69}
{5.19,74.18}
{4.24,81.70}
{3.38,81.75}
{5.19,81.74}
{4.21,81.76}
{3.39,81.77}
{4.18,110.99}
{7.32,128.04}
{7.33,129.52}
{7.87,129.82}
{7.39,128.14}
{7.76,136.08}
{7.31,133.33}
{7.91,165.66}
{5.20,165.77}
{5.18,165.79}
{7.97,165.78}
{7.94,165.74}
f2 (ppm)
f1 (ppm)

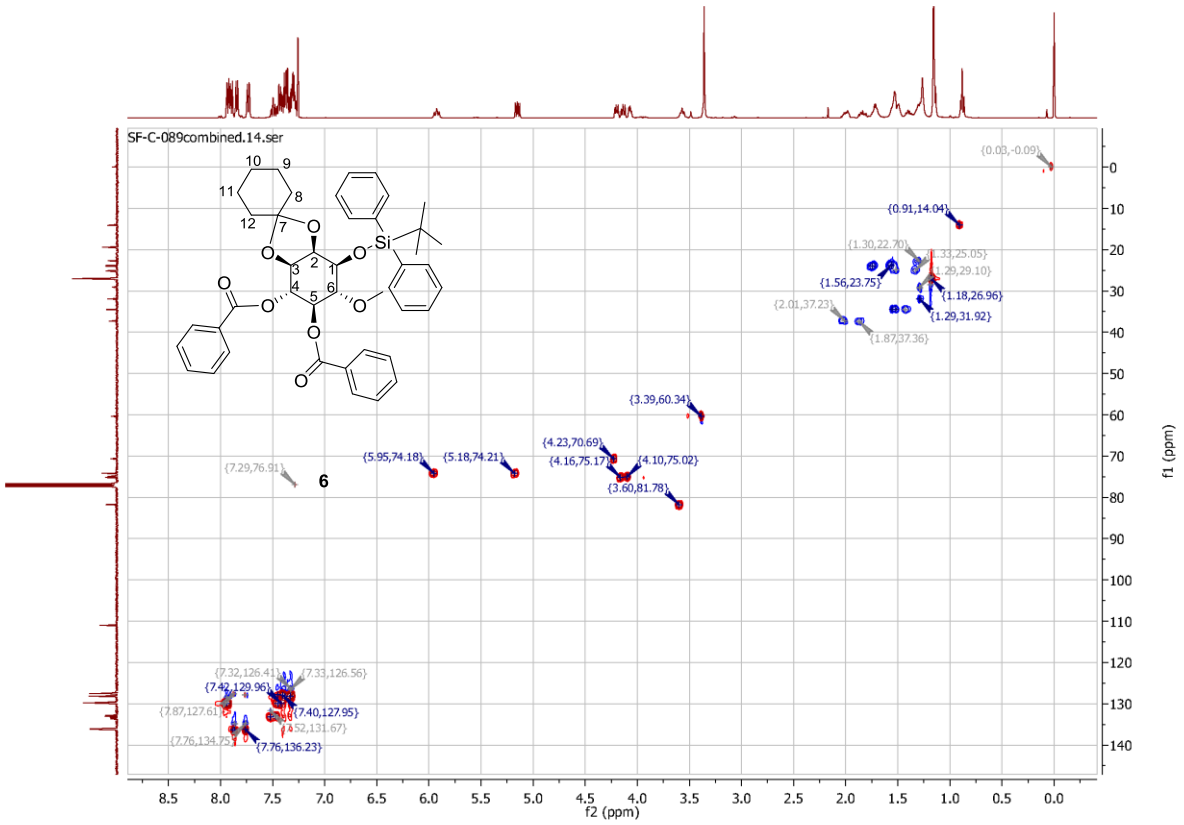
SF-C-089combined.14.ser
{0.03,-0.09}
{0.91,14.04}
{1.30,22.70}
{1.33,25.05}
{1.29,29.10}
{1.56,23.75}
{1.18,26.96}
{2.01,37.23}
{1.29,31.92}
{1.87,37.36}
{3.39,60.34}
{4.23,70.69}
{4.16,75.17}
{4.10,75.02}
{3.60,81.78}
{5.95,74.18}
{5.18,74.21}
{7.29,76.91}
6
{7.32,126.41}
{7.33,126.56}
{7.42,129.96}
{7.87,127.61}
{7.40,127.95}
{7.52,131.67}
{7.76,134.75}
{7.76,136.23}
f2 (ppm)
f1 (ppm)

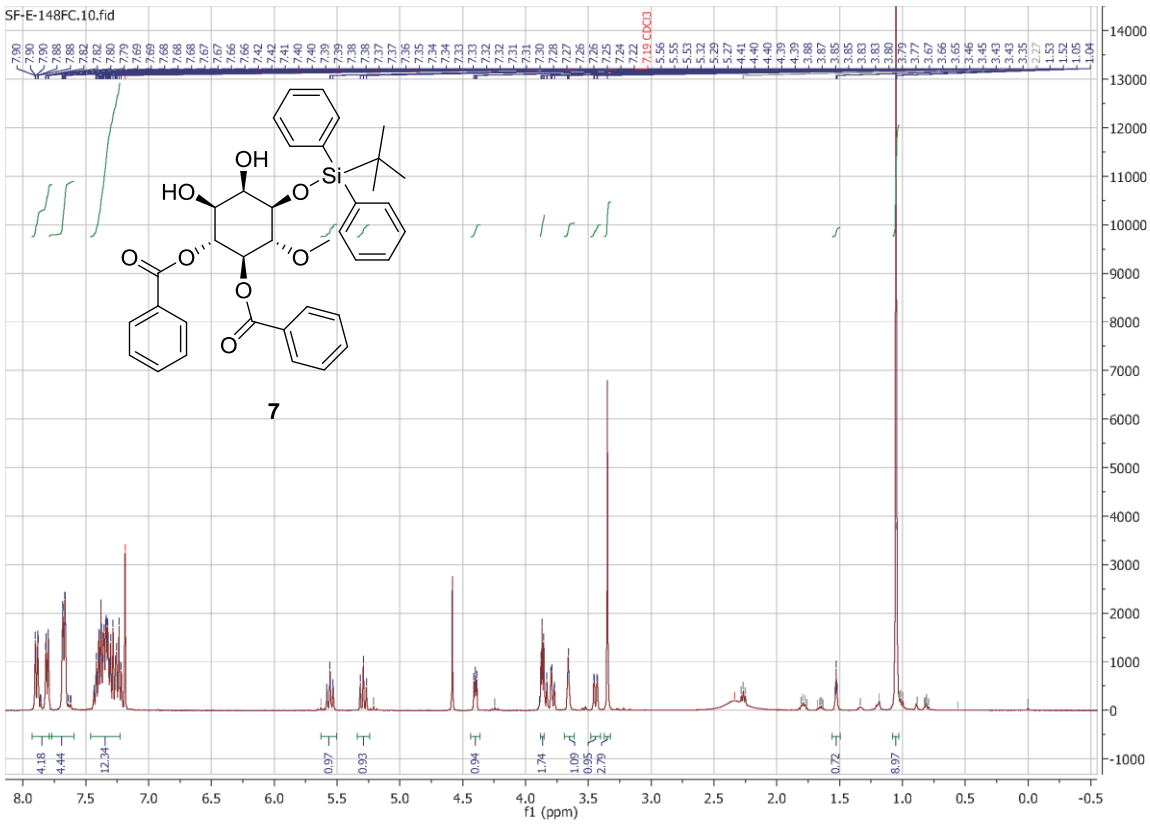
SF-E-148FC.10.fid
OH
HO
Si
O
O
O
O
O
7
f1 (ppm)

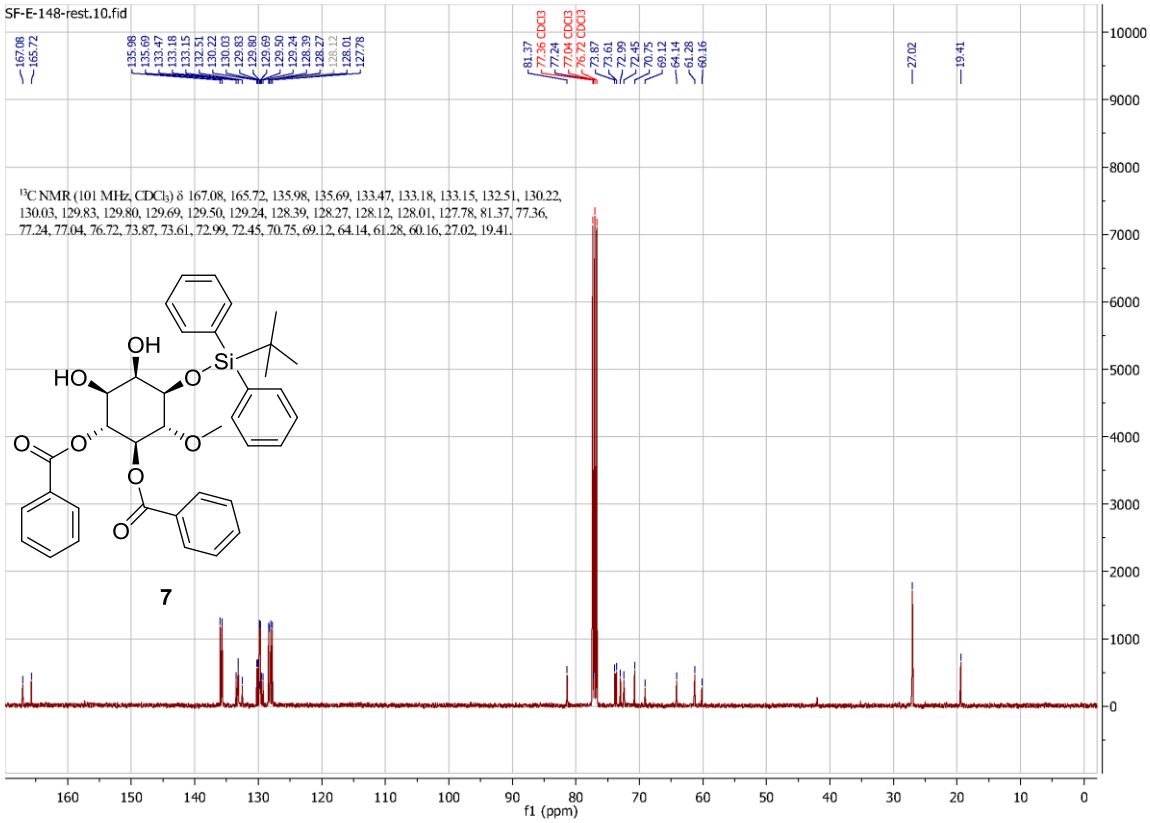
SF-E-148-rest.10.fid
^{13}C NMR (101 MHz, $CDCl_3$) δ 167.08, 165.72, 135.98, 135.69, 133.47, 133.18, 133.15, 132.51, 130.22, 130.03, 129.83, 129.80, 129.69, 129.50, 129.24, 128.39, 128.27, 128.12, 128.01, 127.78, 81.37, 77.36, 77.24, 77.04, 76.72, 73.87, 73.61, 72.99, 72.45, 70.75, 69.12, 64.14, 61.28, 60.16, 27.02, 19.41.
OH
HO
Si
O
O
O
O
O
7
f1 (ppm)

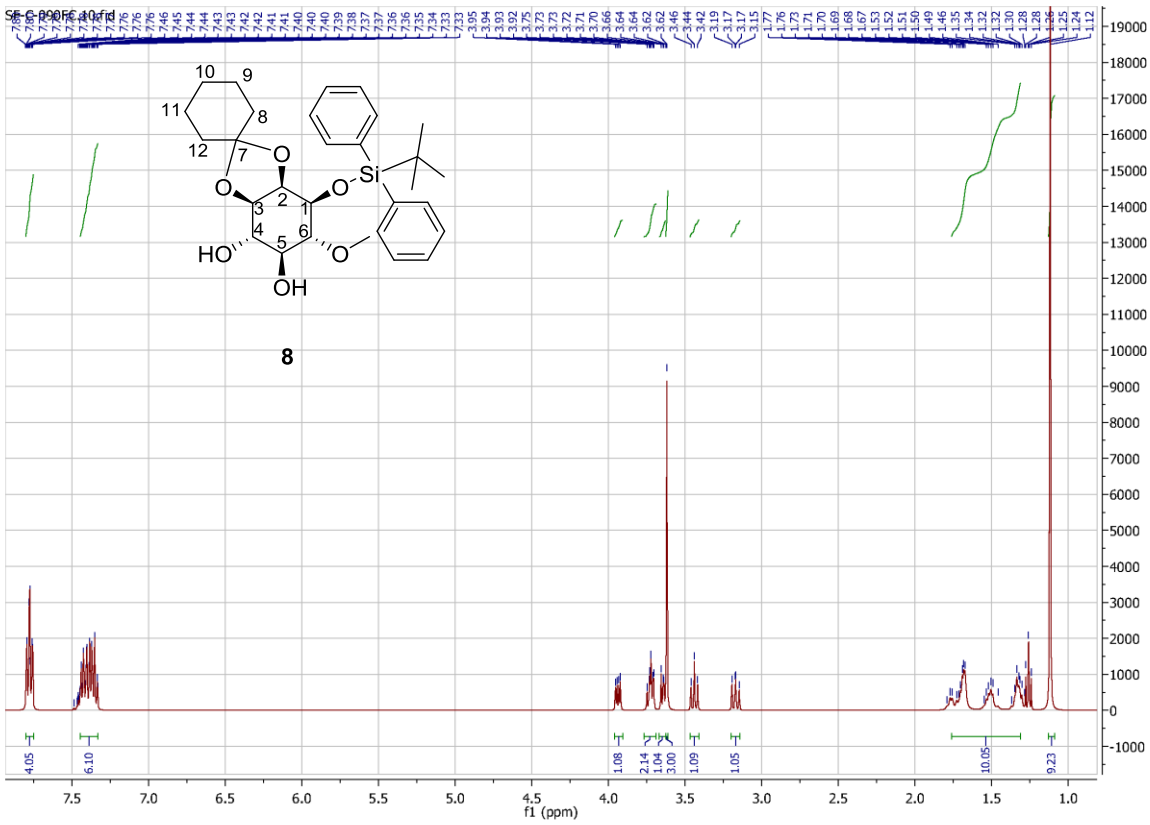
SF-C-090FC.10.fid
8
f1 (ppm)

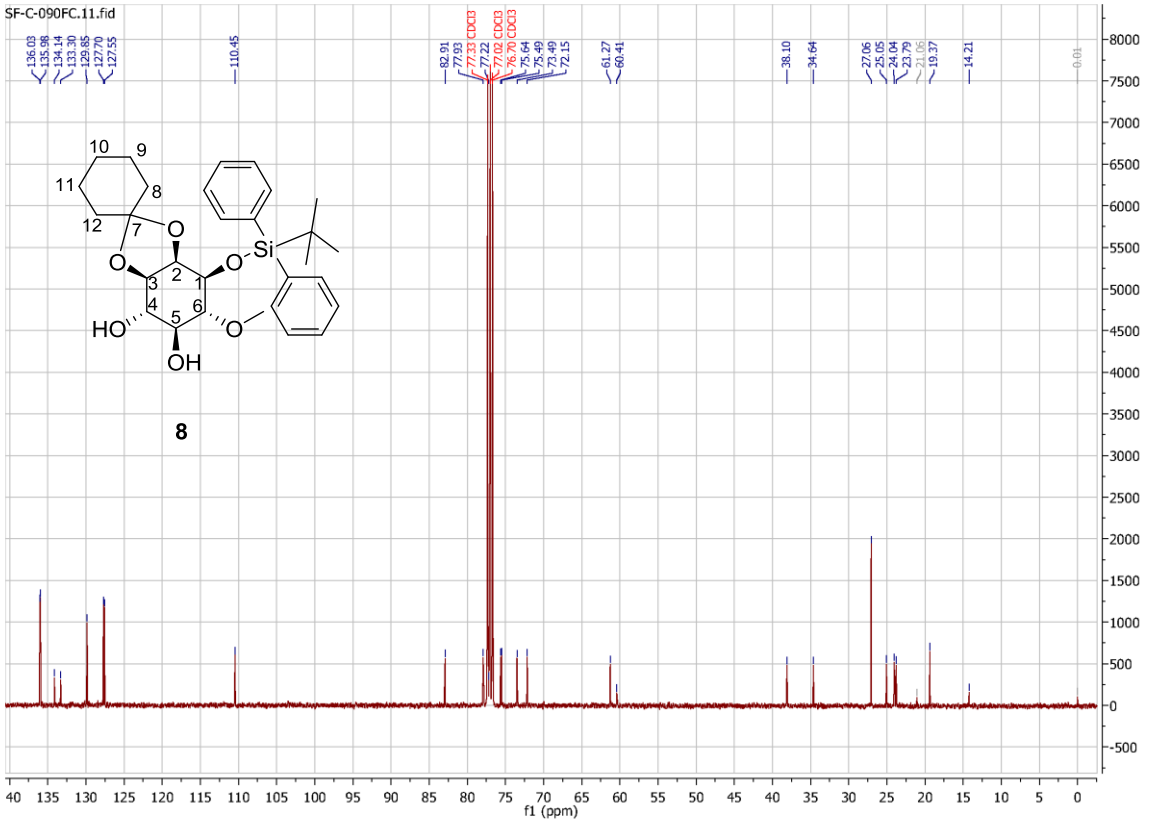
SF-C-090FC.11.fid
8
f1 (ppm)

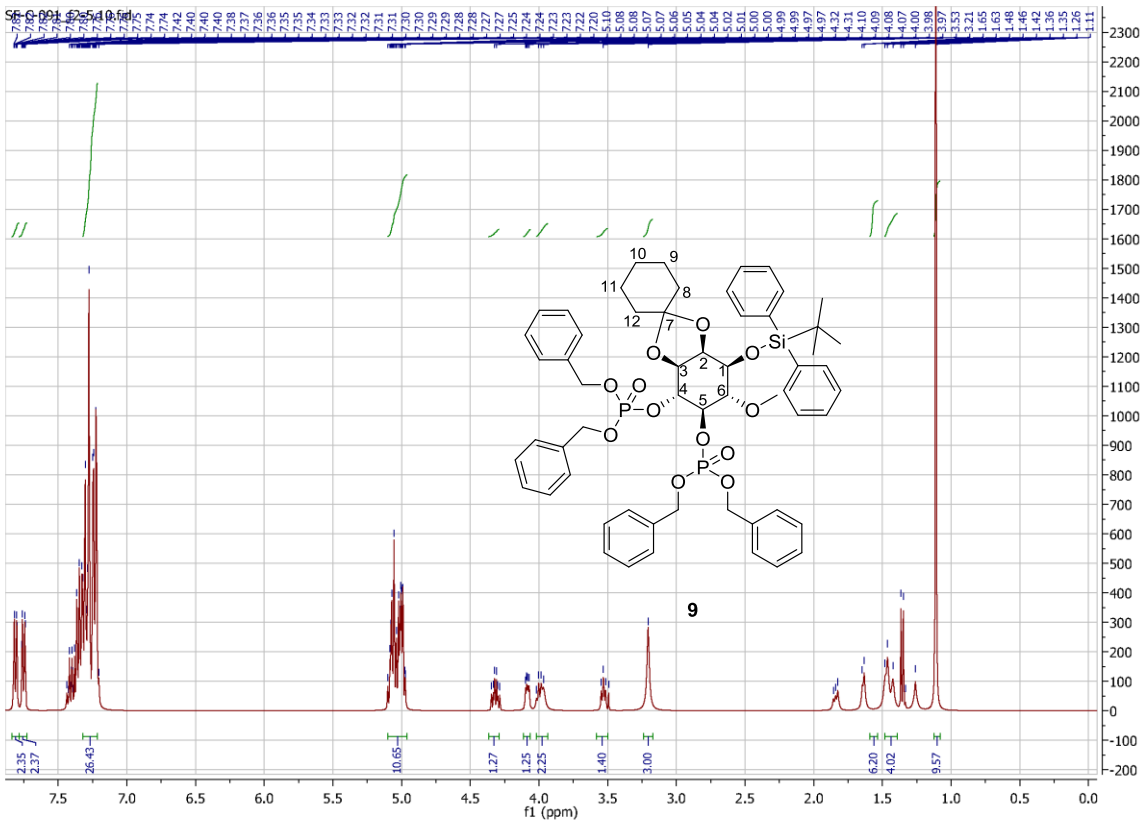
9

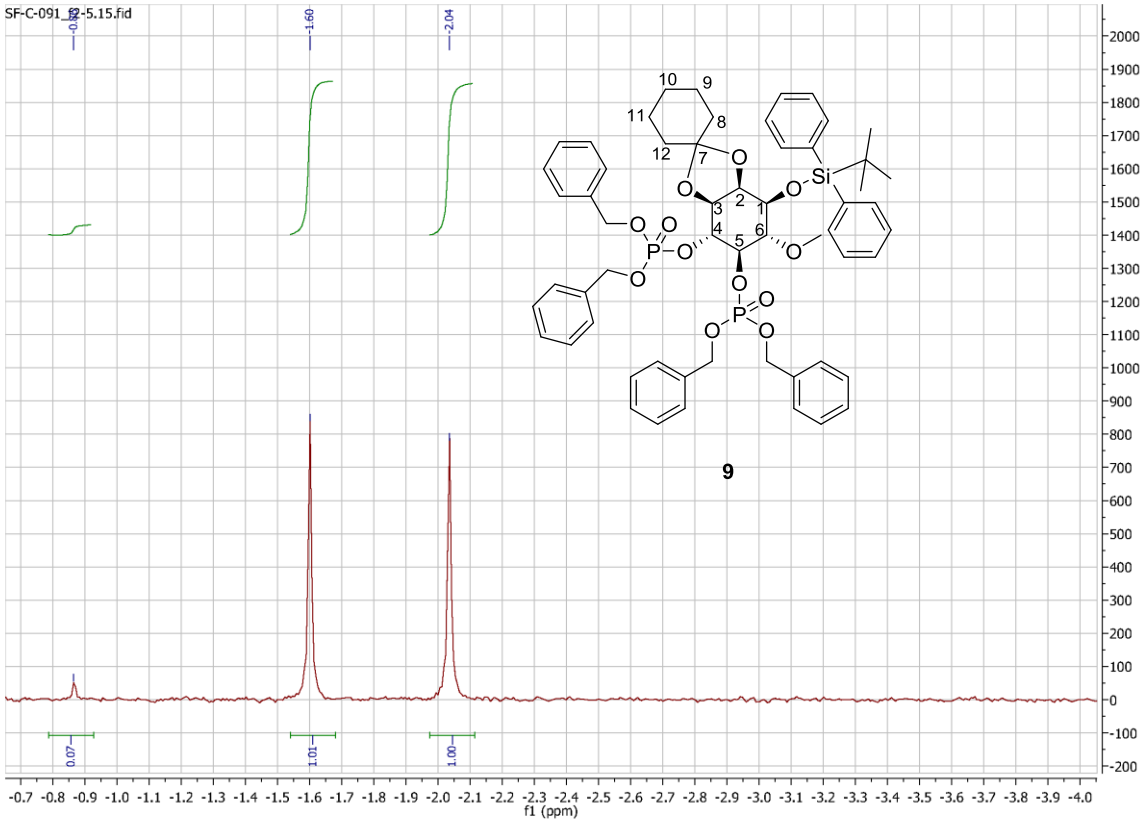
SF-C-091_S2-5.15.fid
9

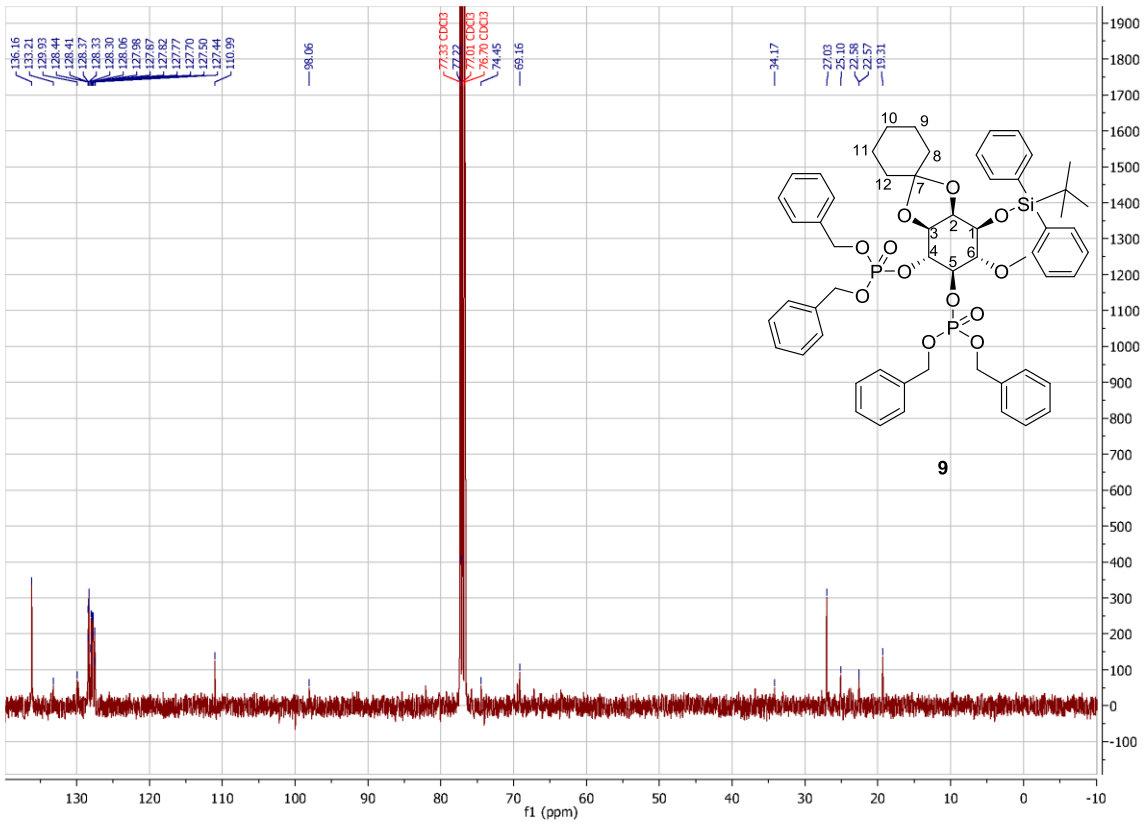
136.16
133.21
129.93
128.44
128.41
128.37
128.33
128.30
128.06
128.06
127.87
127.82
127.77
127.70
127.50
127.44
110.99
98.06
77.33 CDCl3
77.22
77.01 CDCl3
76.70 CDCl3
74.45
69.16
34.17
27.03
25.10
22.58
22.57
19.31
9
f1 (ppm)

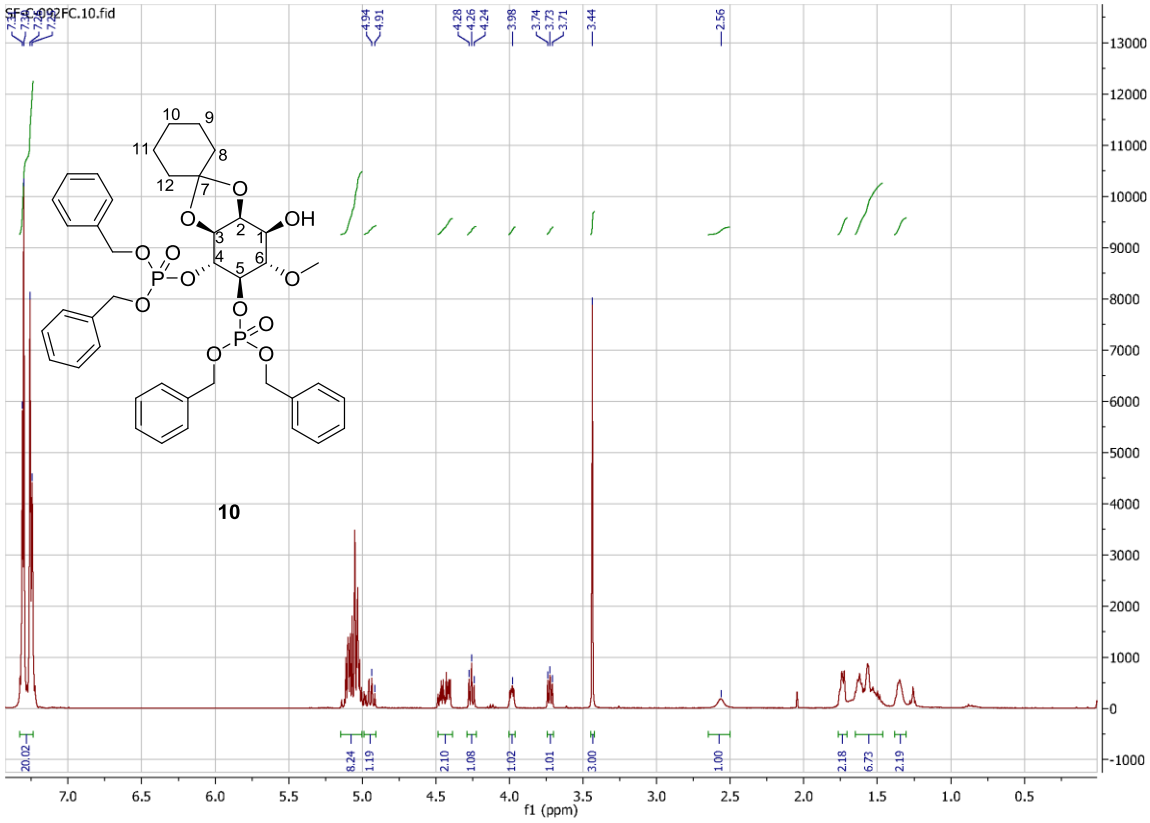
SFsC-092FC.10.fid
10

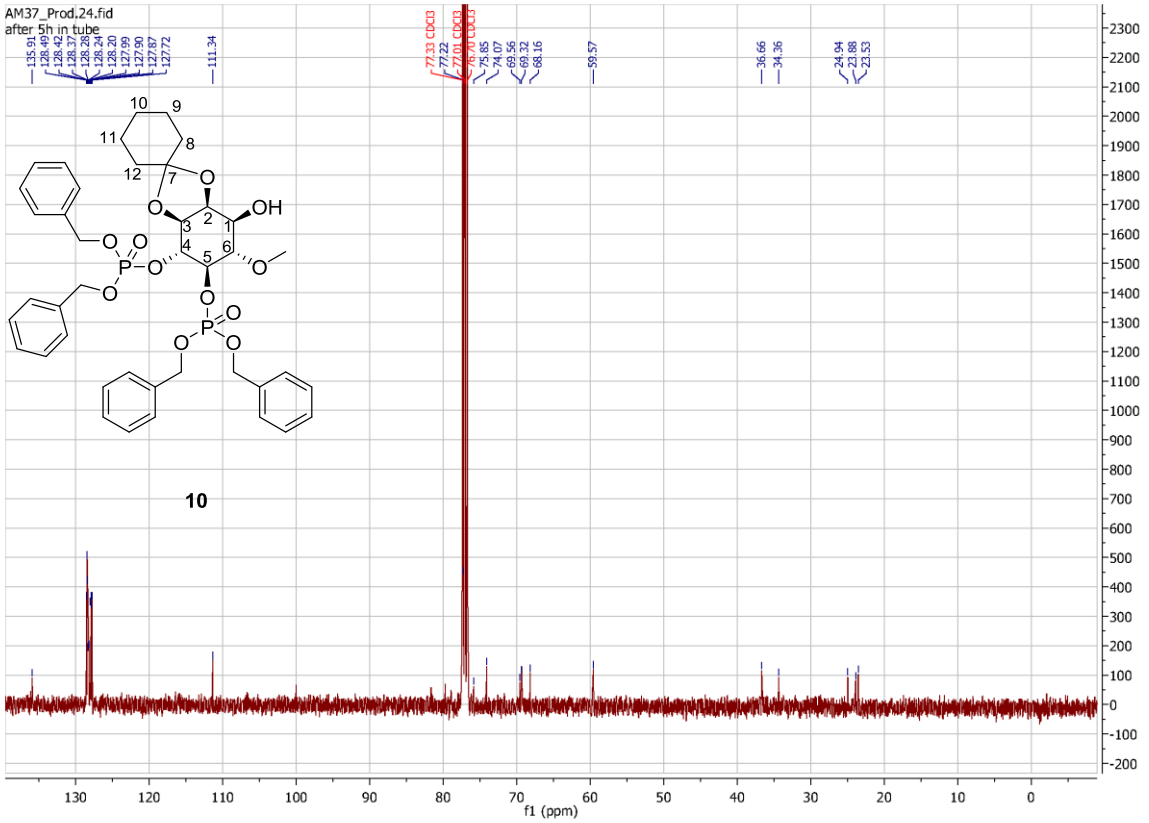
AM37_Prod.24.fid
after 5h in tube
10

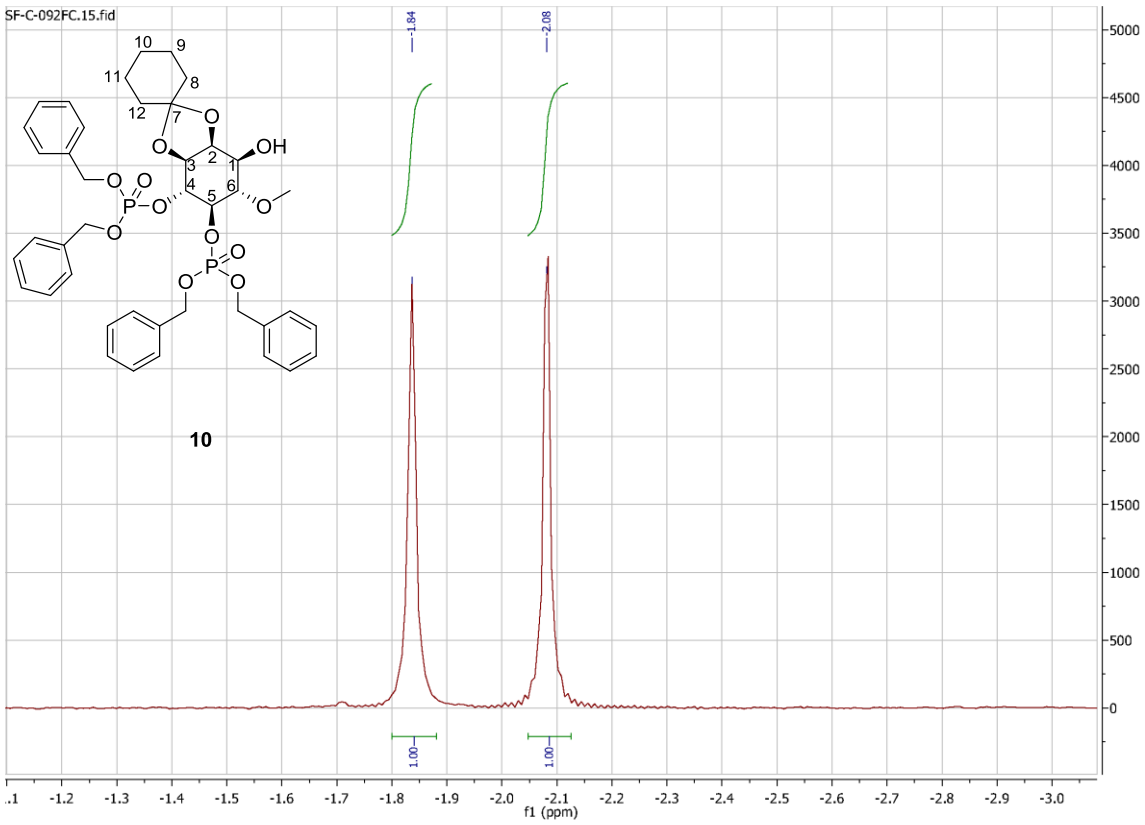
SF-C-092FC.15.fid
10
-1.84
-2.08
1.00
1.00
f1 (ppm)

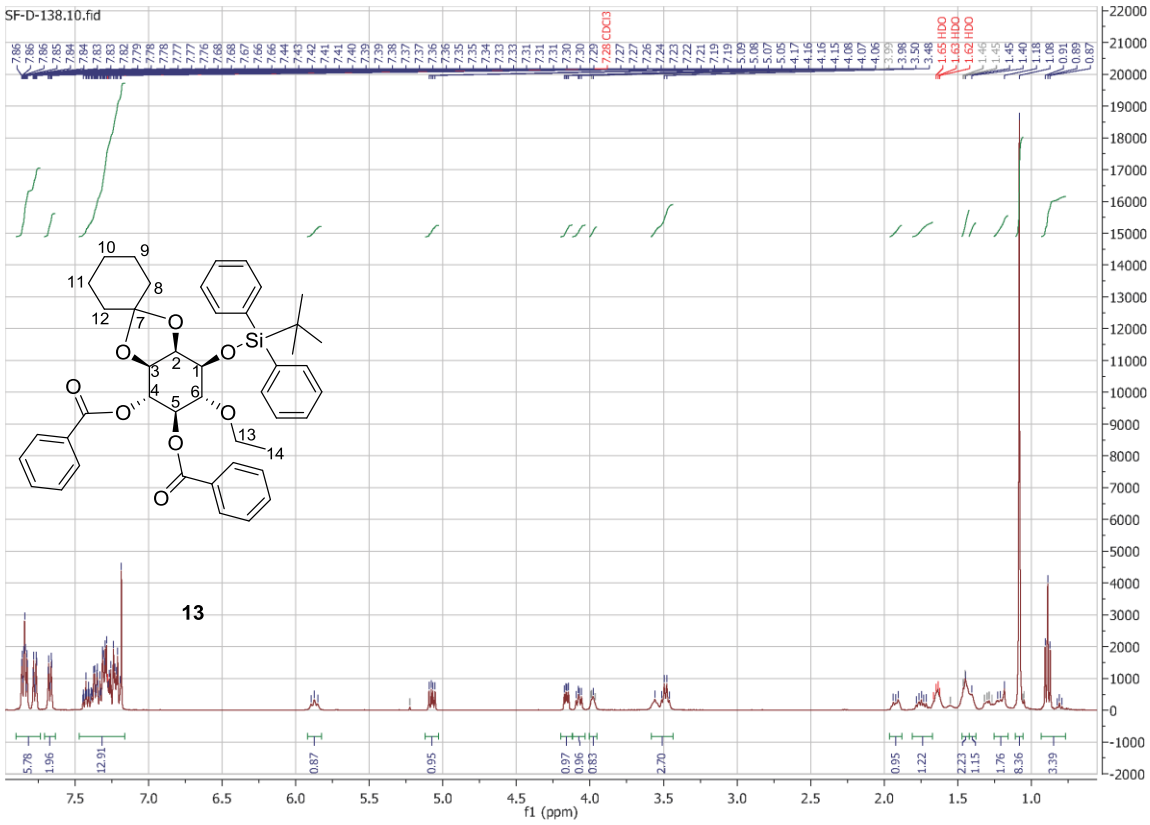
SF-D-138.10.fid
13
f1 (ppm)

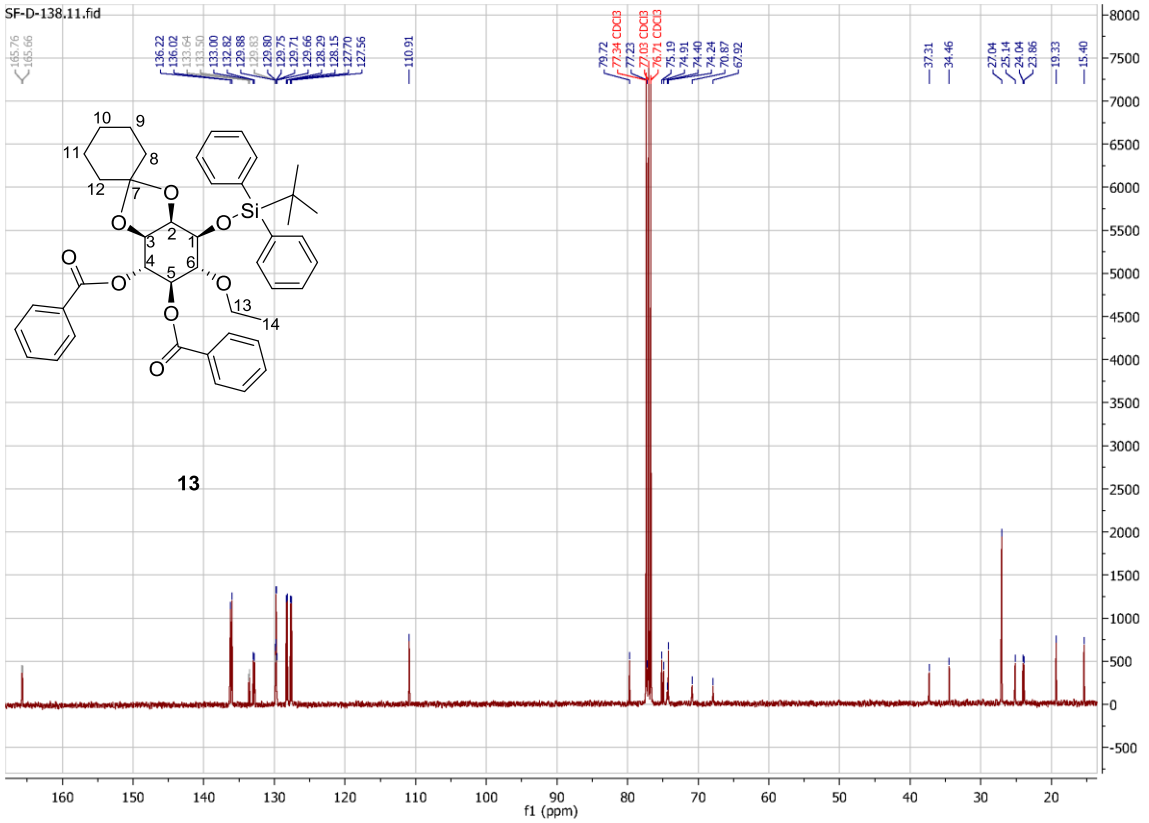
SF-D-138.11.fid
13
f1 (ppm)

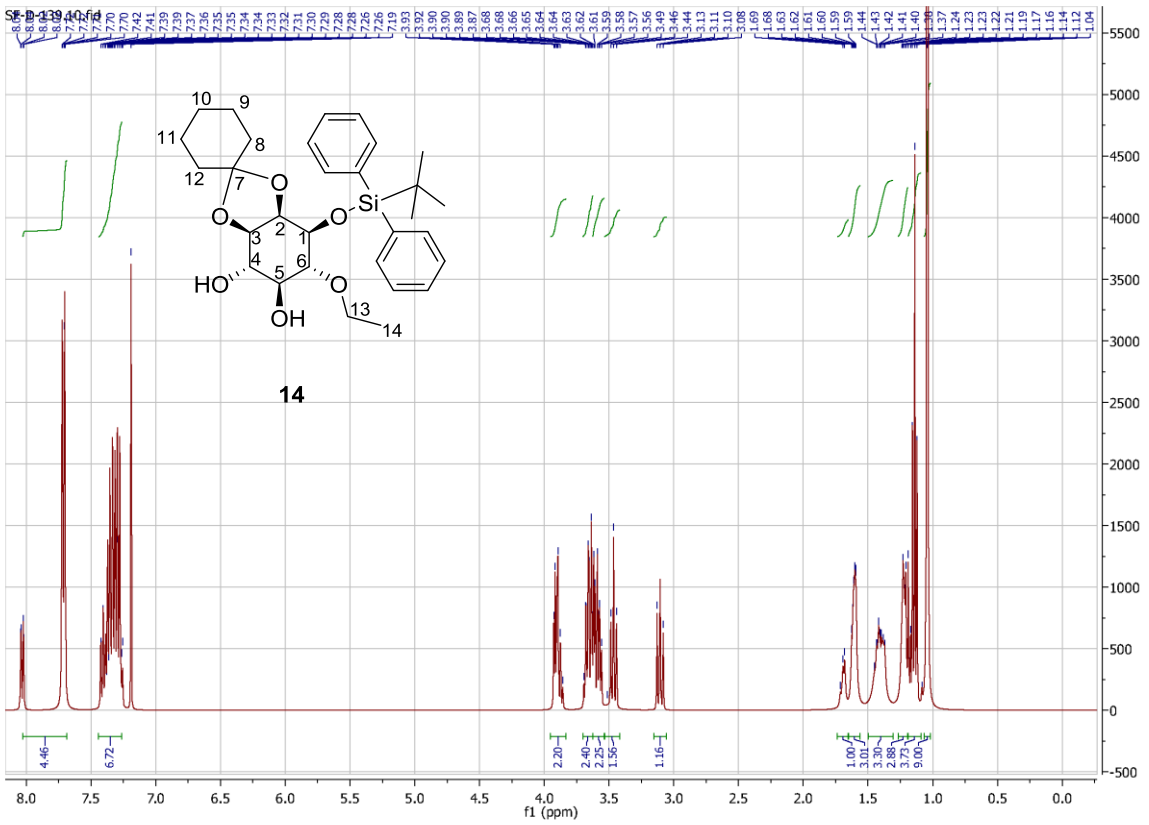

14

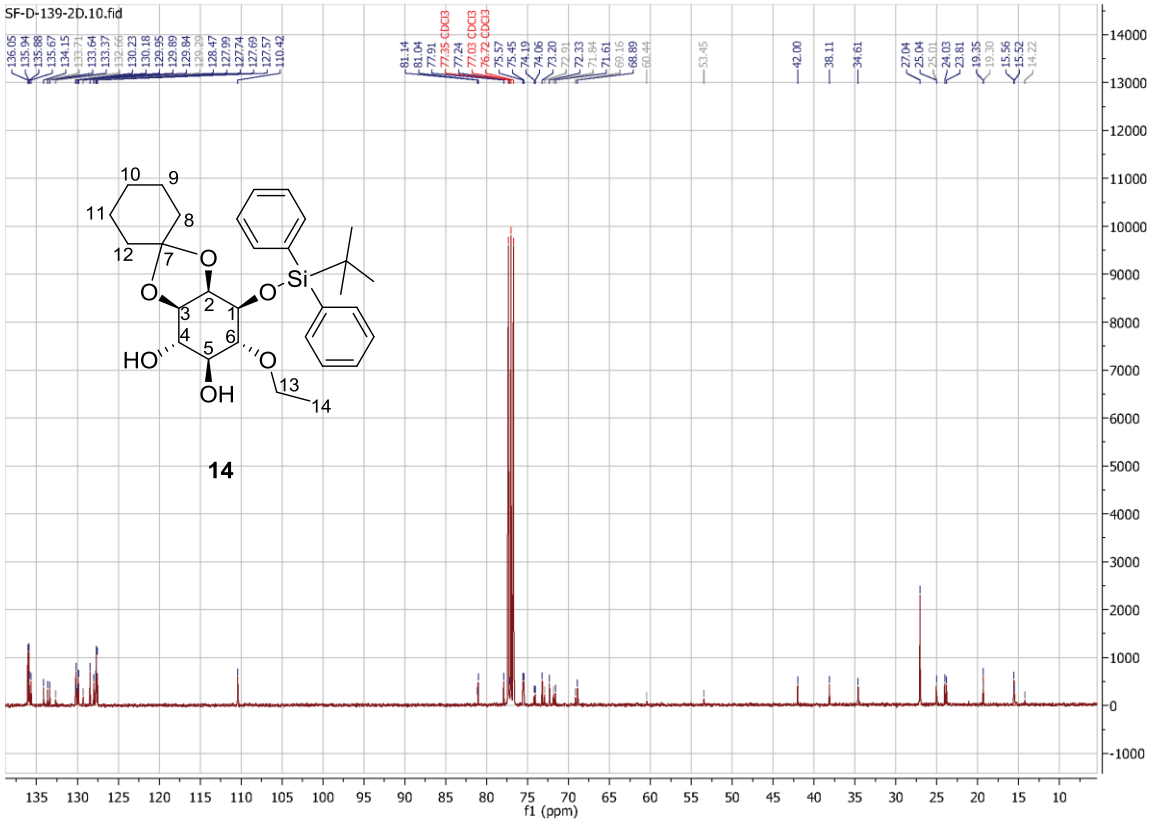

14

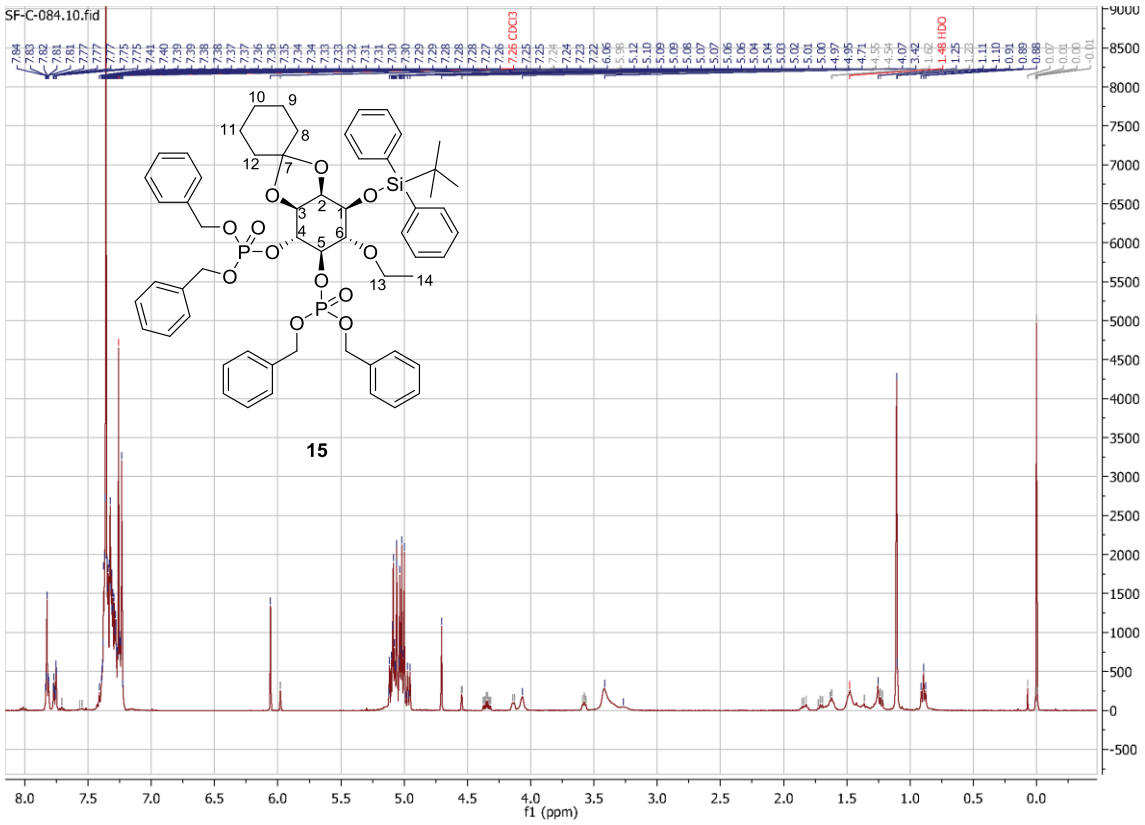
SF-C-084.10.fid
15
f1 (ppm)

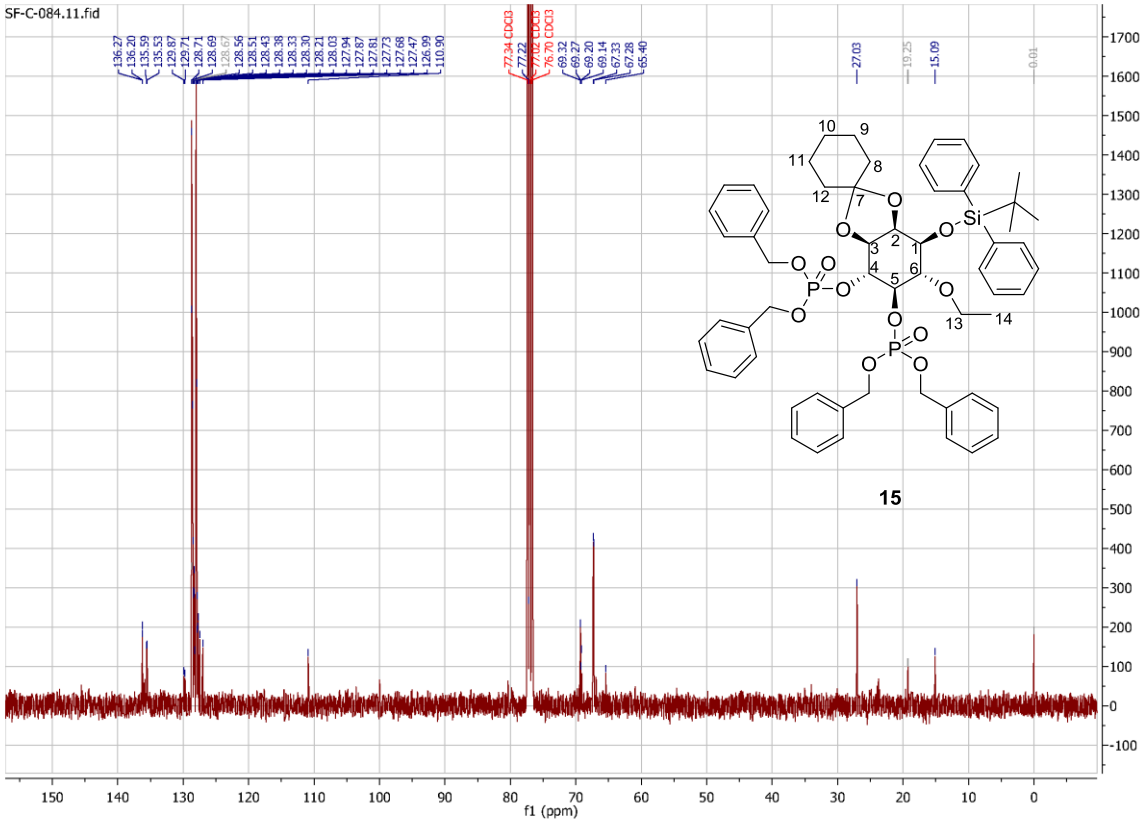
SF-C-084.11.fid
15
f1 (ppm)

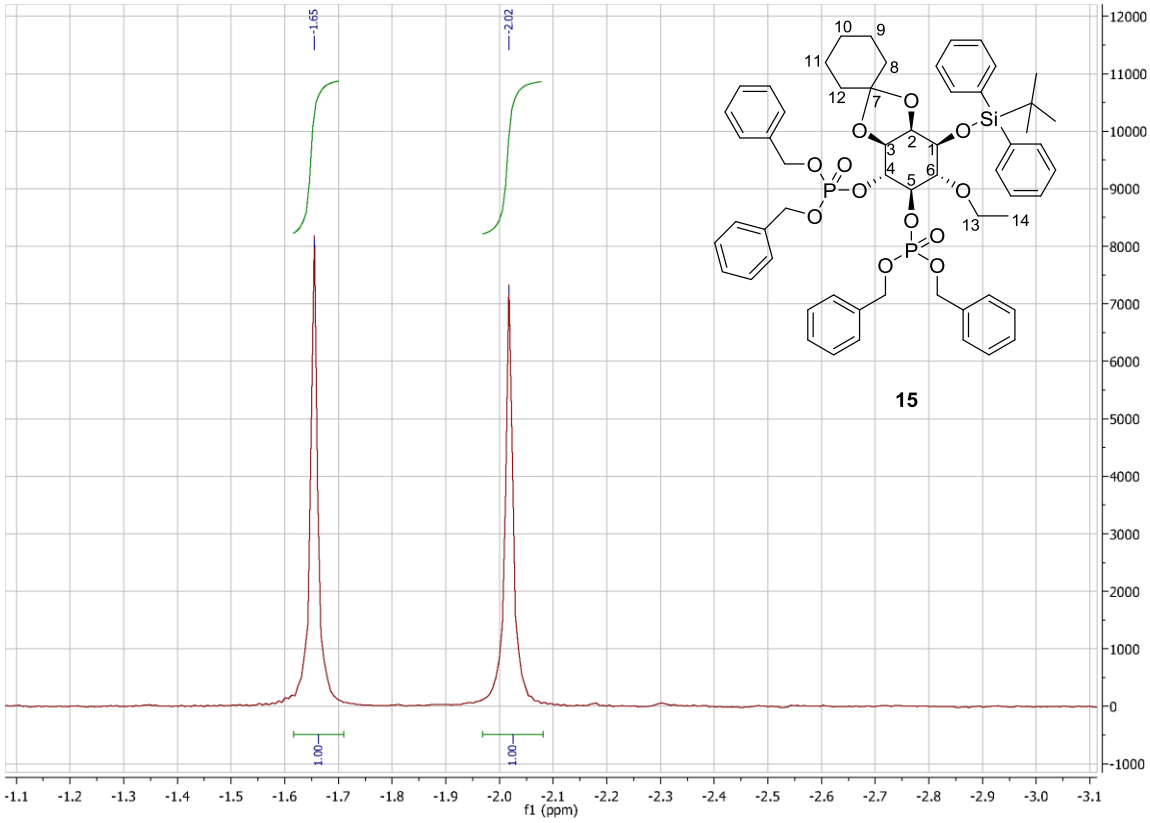
-1.65
-2.02
1.00
1.00
f1 (ppm)
15

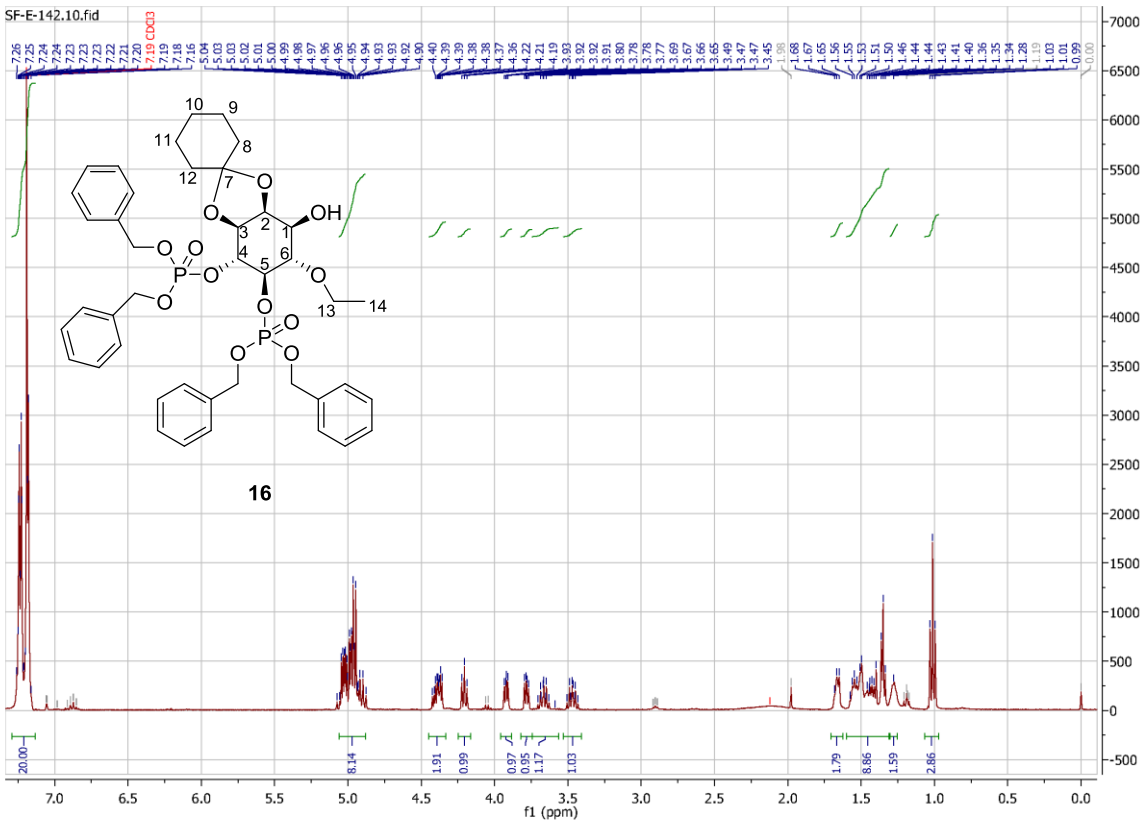
SF-E-142.10.fid
16
f1 (ppm)

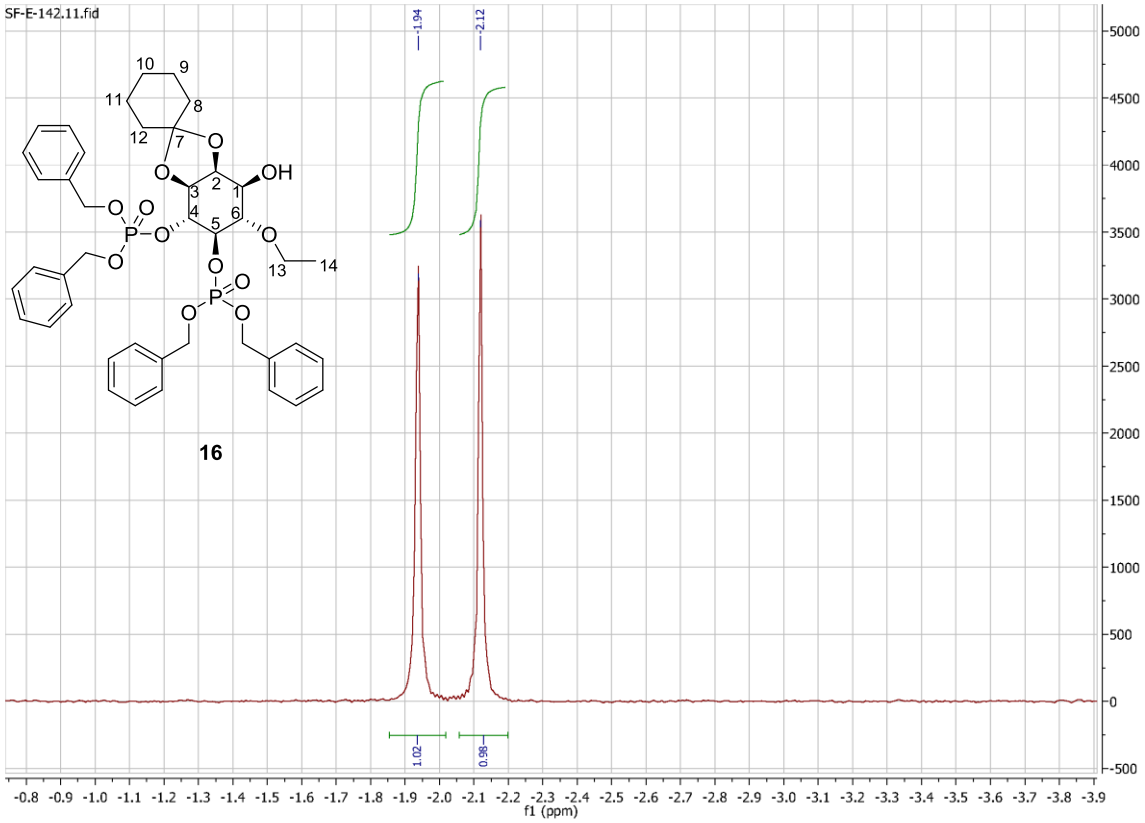
SF-E-142.11.fid
16
f1 (ppm)

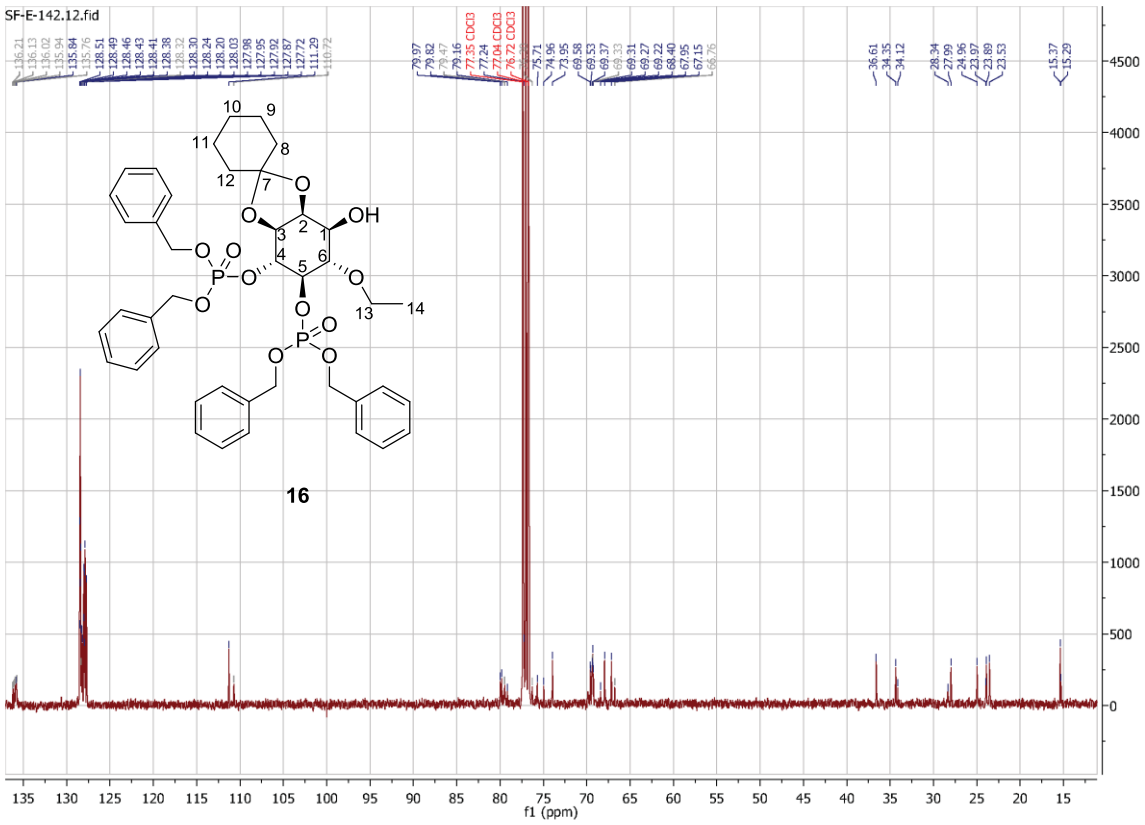
SF-E-142.12.fid
16
f1 (ppm)

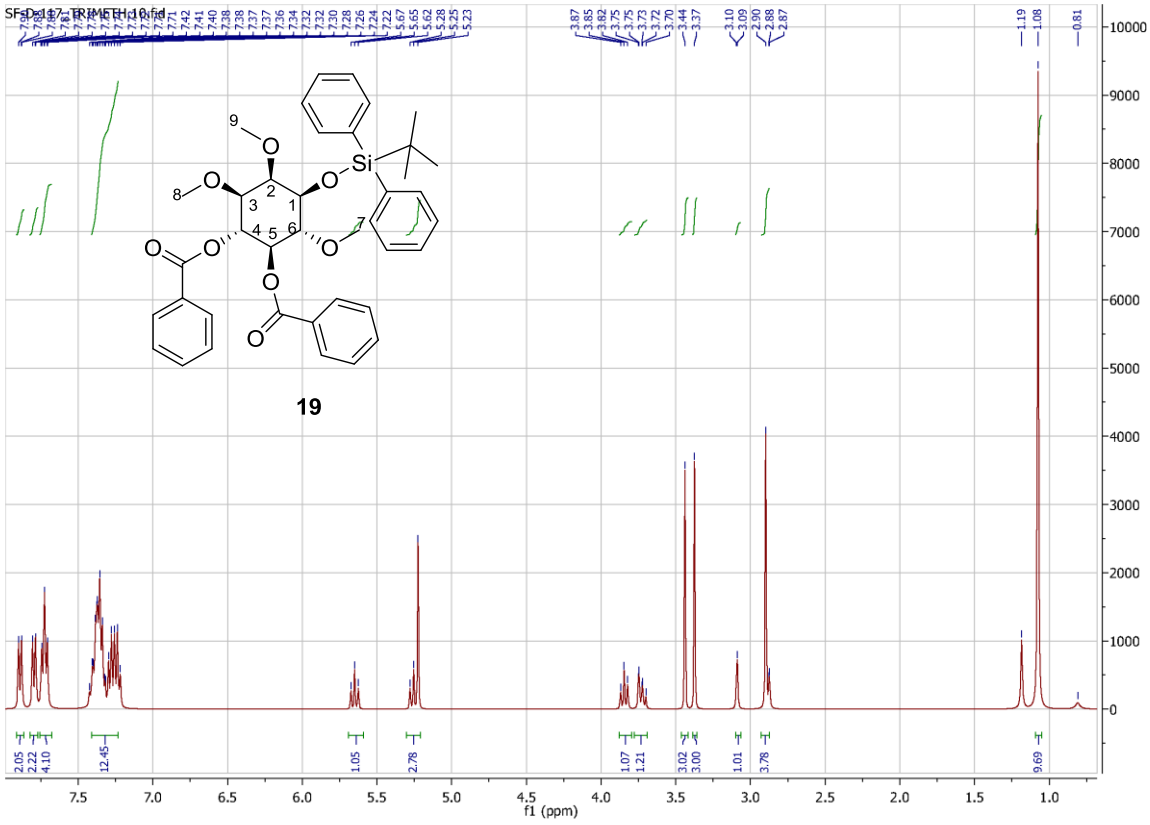
19
f1 (ppm)

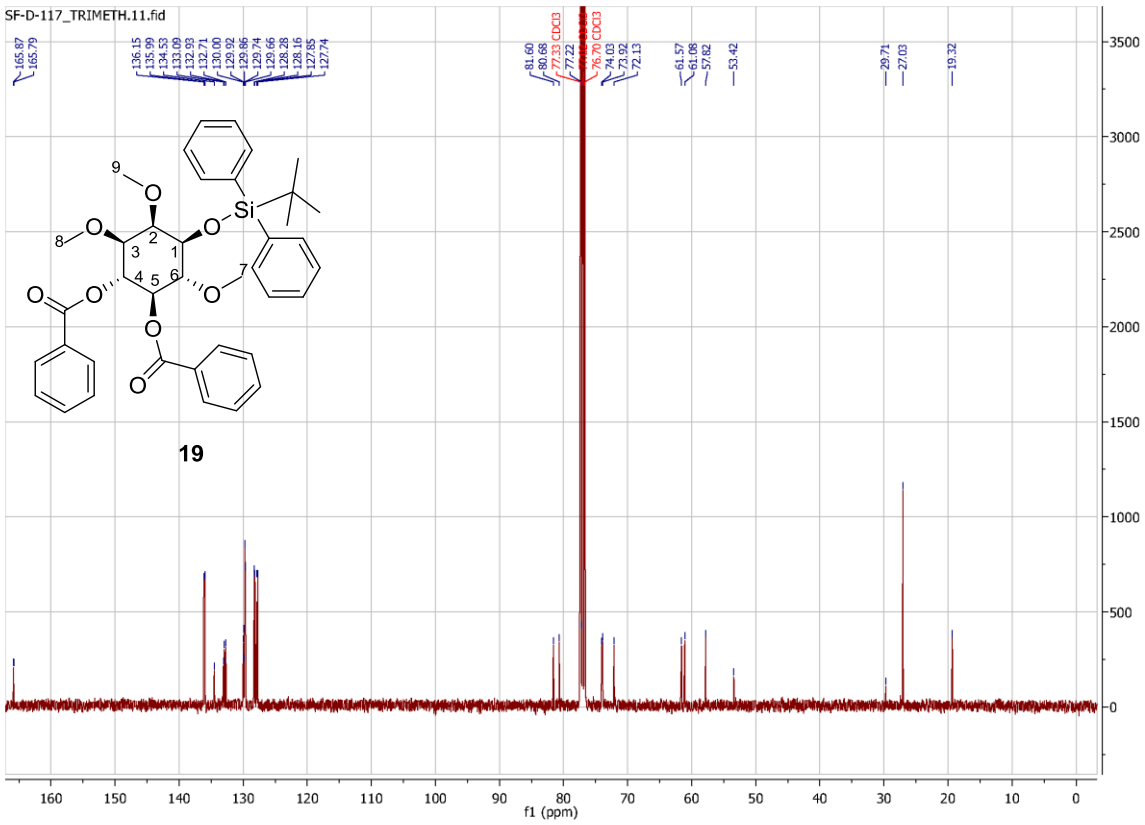
SF-D-117_TRIMETH.11.fid
165.87
165.79
136.15
135.99
134.53
133.09
132.93
132.71
130.00
129.92
129.86
129.74
129.66
128.28
128.16
127.85
127.74
81.60
80.68
77.33 CDCl3
77.22
76.70 CDCl3
74.03
73.92
72.13
61.57
61.08
57.82
53.42
29.71
27.03
19.32
9
O
8
O
2
3
1
O
Si
4
5
6
7
O
O
O
O
19
3500
3000
2500
2000
1500
1000
500
0
160
150
140
130
120
110
100
90
80
70
60
50
40
30
20
10
0
f1 (ppm)

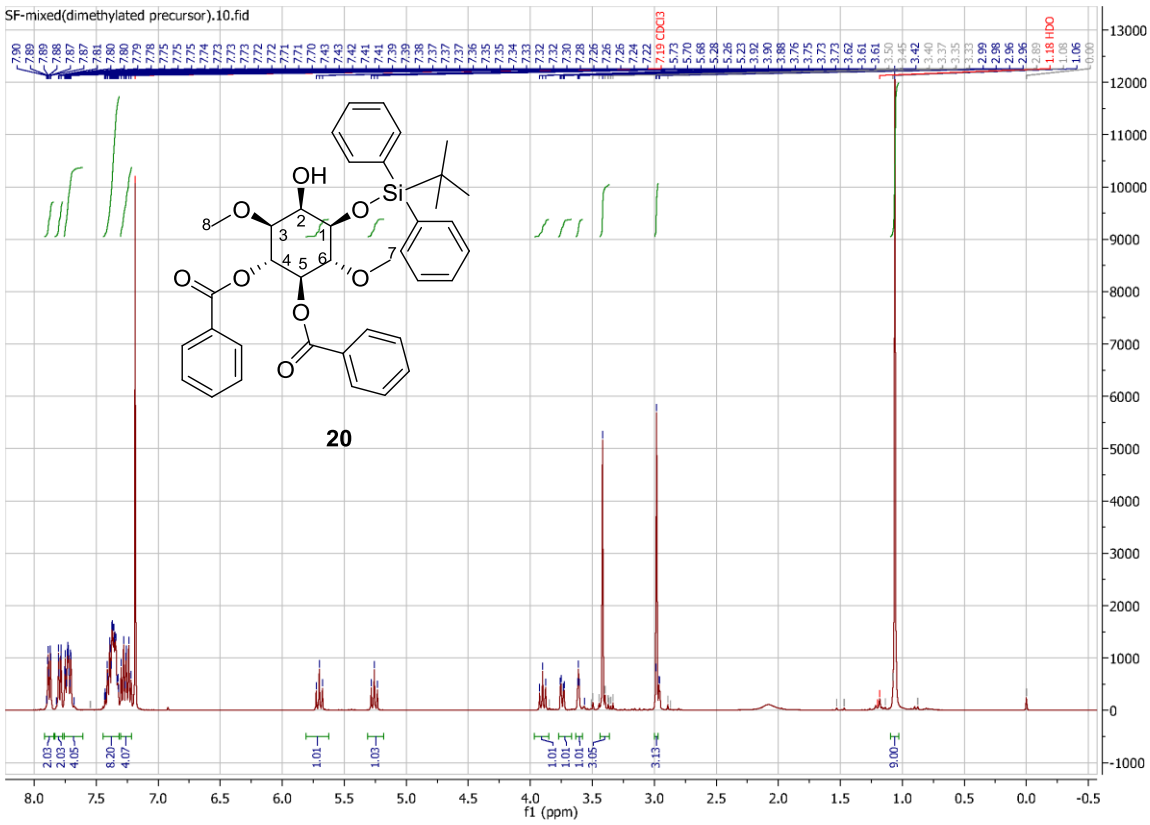
SF-mixed(dimethylated precursor).10.fid
OH
Si
O
8
1
2
3
4
5
6
7
20
f1 (ppm)

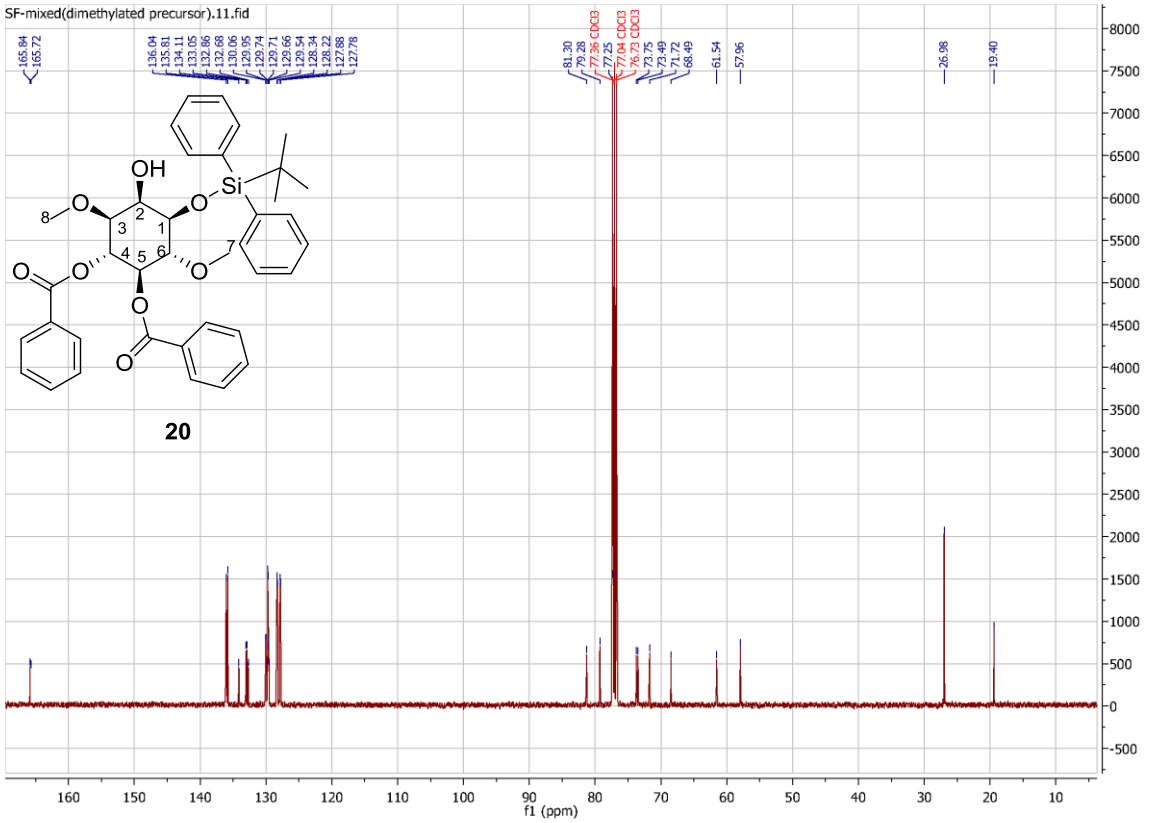
SF-mixed(dimethylated precursor).11.fid
OH
Si
O
8
1
2
3
4
5
6
7
20
f1 (ppm)

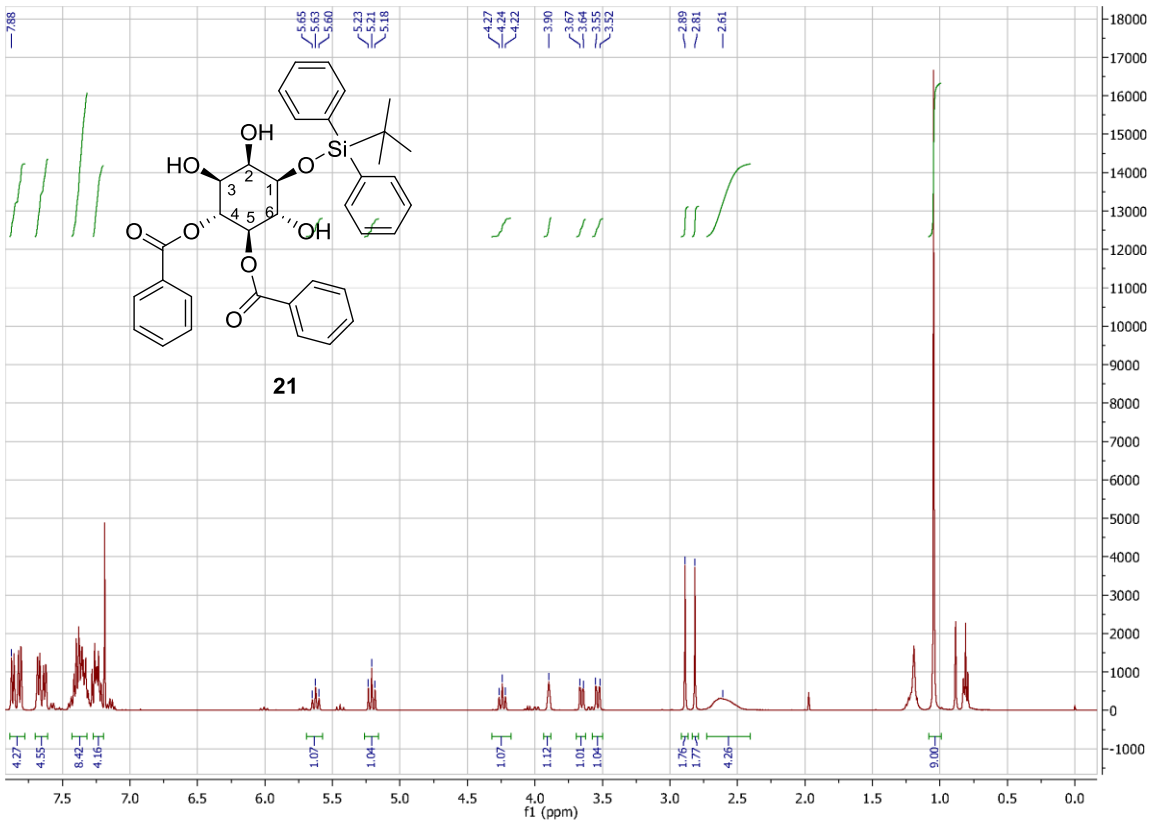
7.88
5.65
5.63
5.60
5.23
5.21
5.18
4.27
4.24
4.22
3.90
3.67
3.64
3.55
3.52
2.89
2.81
2.61
OH
HO
O
Si
2
3
1
4
5
6
O
O
OH
O
O
21
4.27
4.55
8.42
4.16
1.07
1.04
1.07
1.12
1.01
1.04
1.76
1.77
4.26
9.00
f1 (ppm)

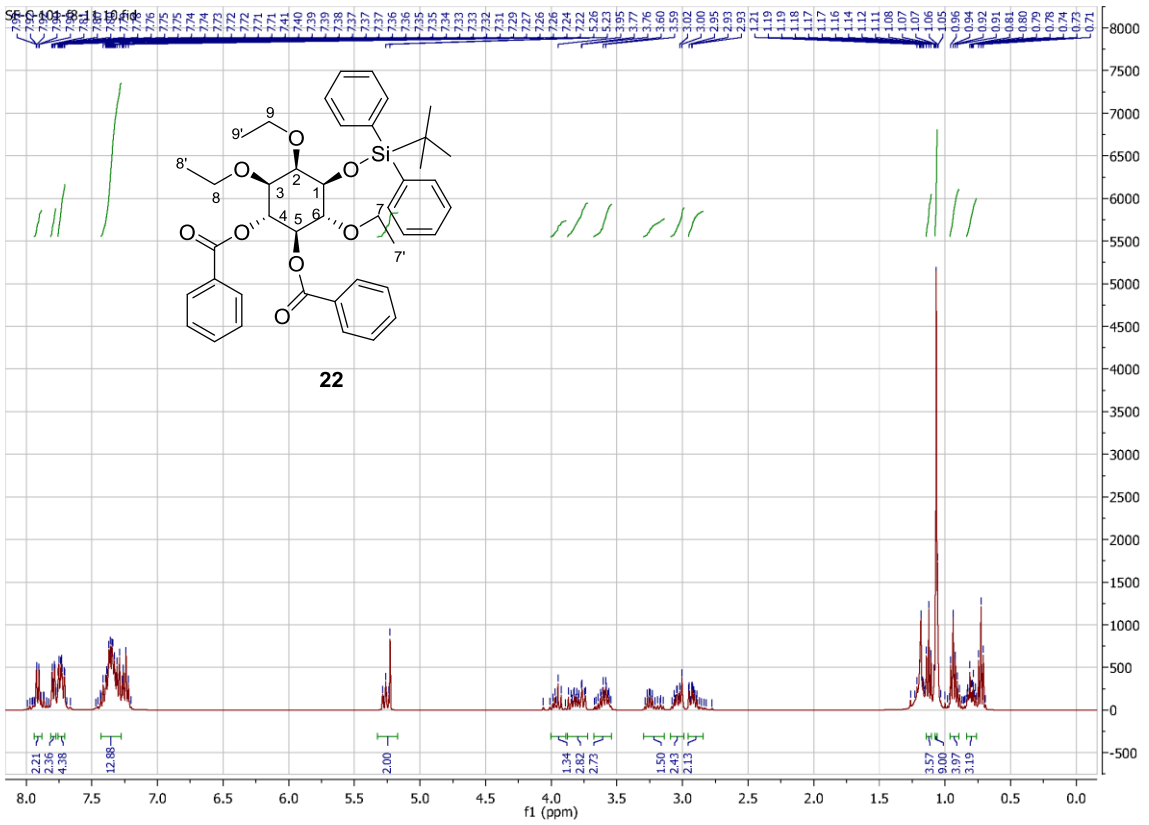
SF-C-101-8-11.10.fid
22
f1 (ppm)

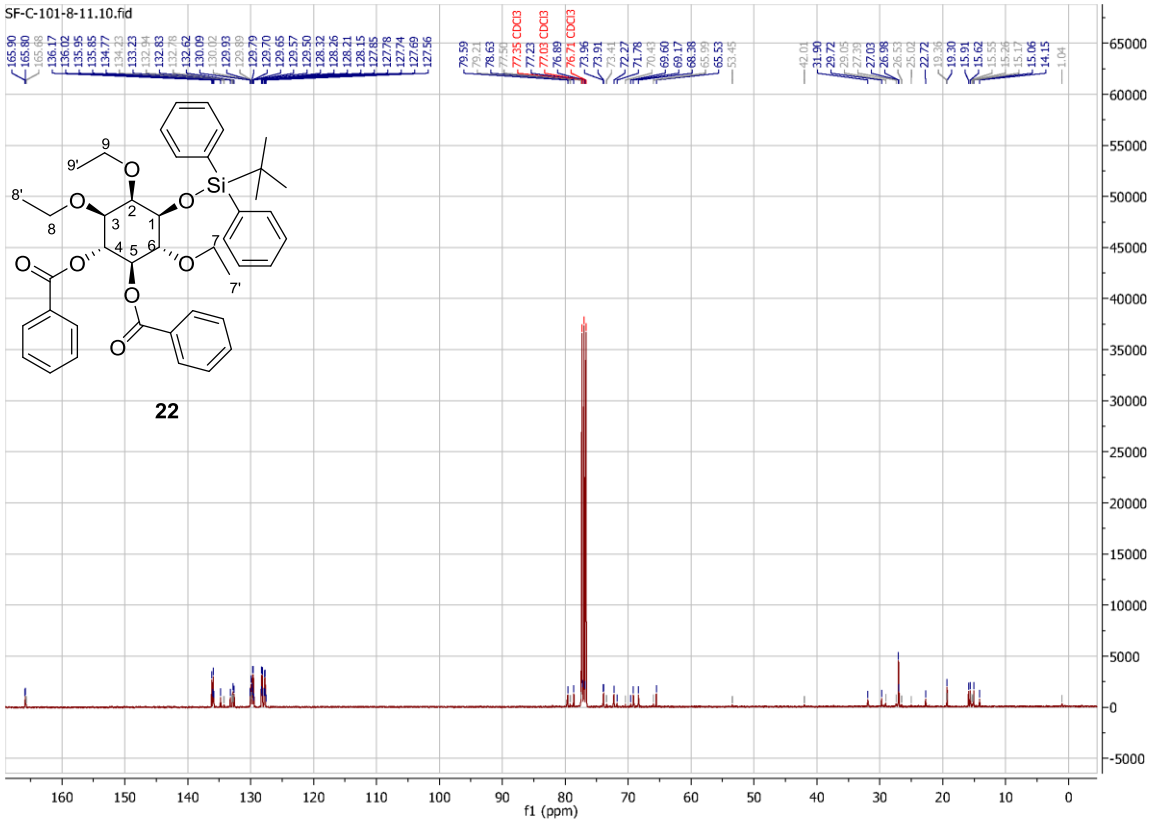
SF-C-101-8-11.10.fid
22
f1 (ppm)

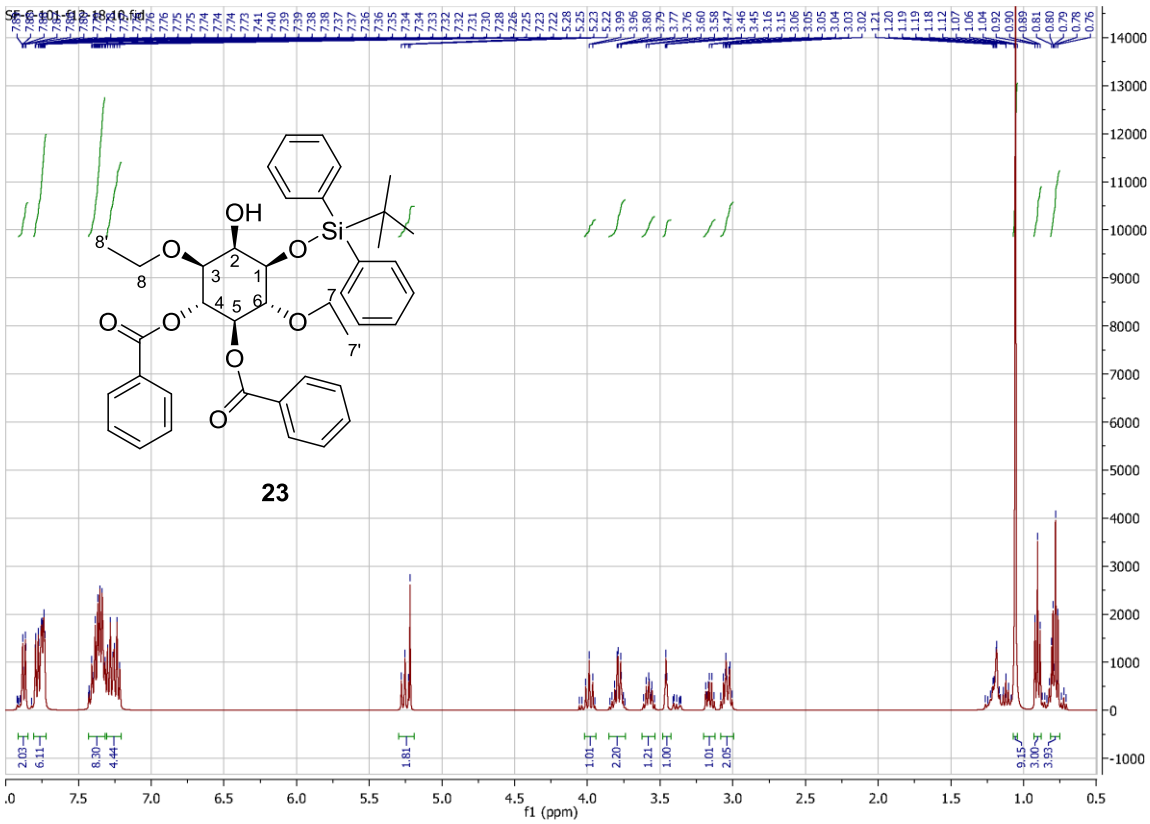
OH
Si
O
8'
8
1
2
3
4
5
6
7
7'
23
f1 (ppm)

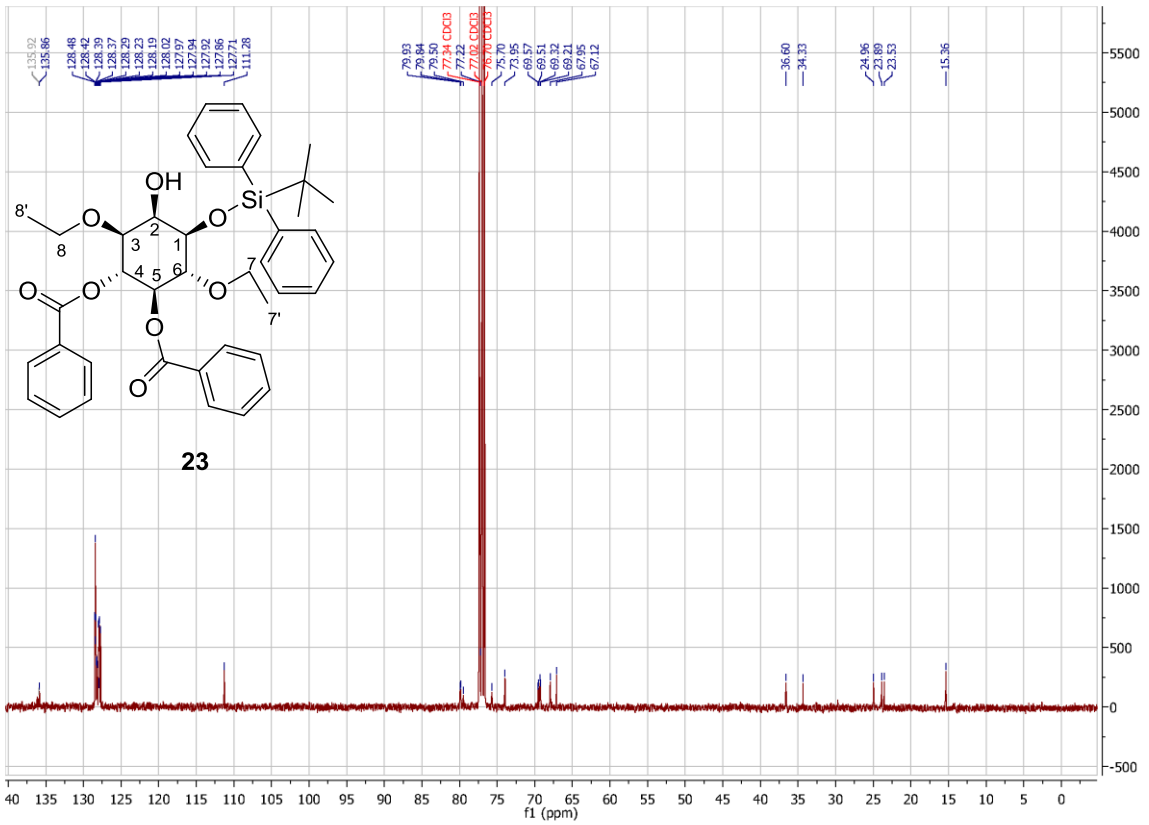
OH
Si
O
8'
8
1
2
3
4
5
6
7
7'
23
f1 (ppm)

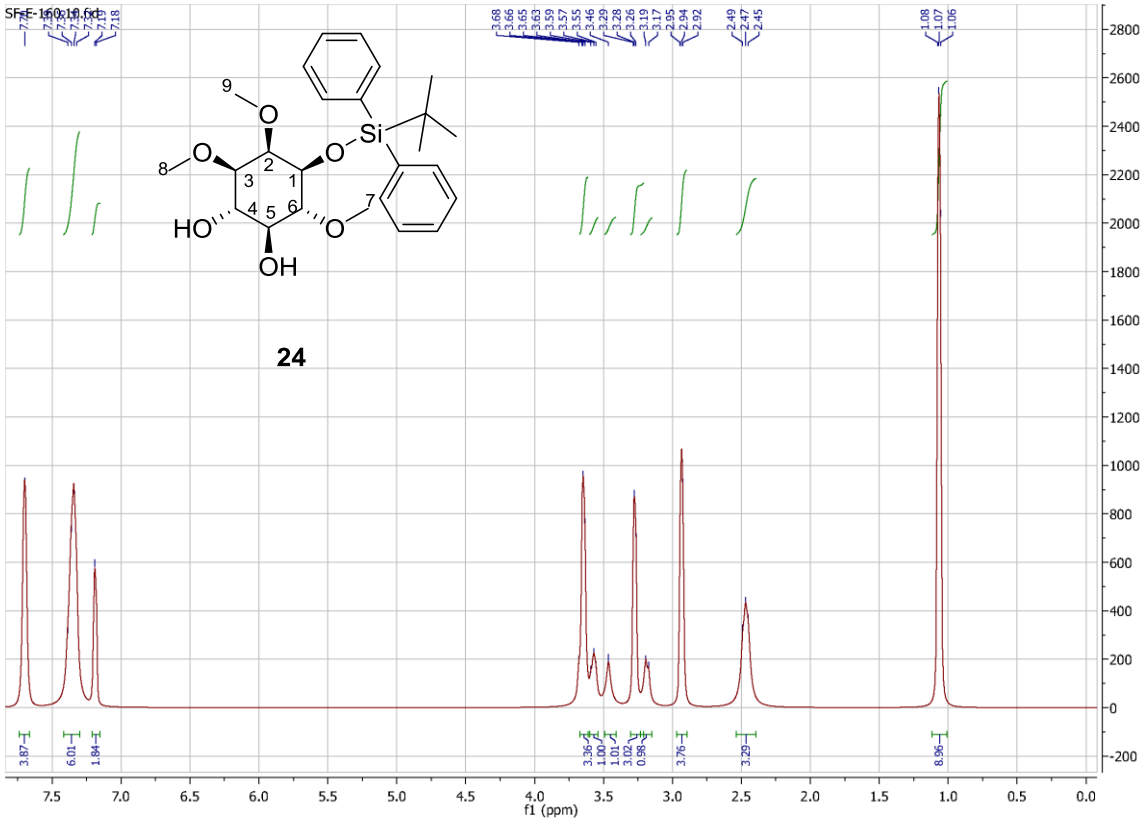
SF-E-160.10.fid
24
f1 (ppm)

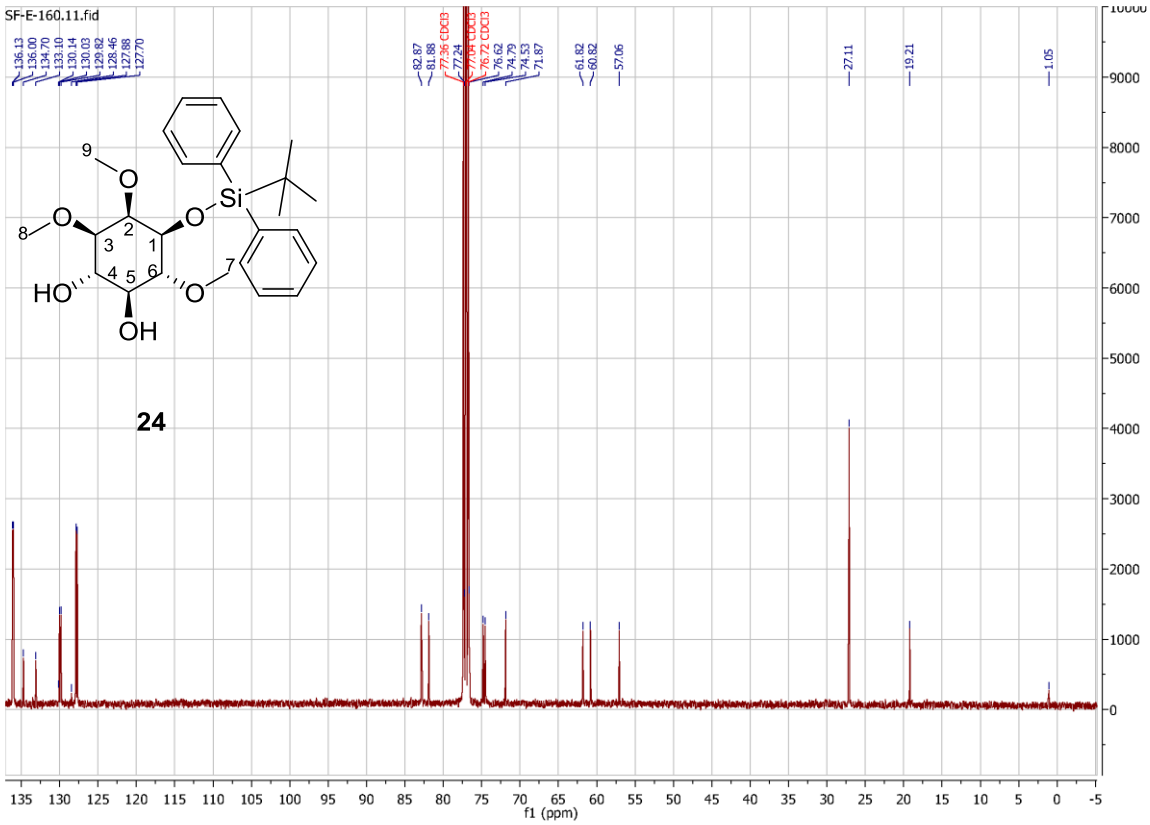
SF-E-160.11.fid
24
f1 (ppm)

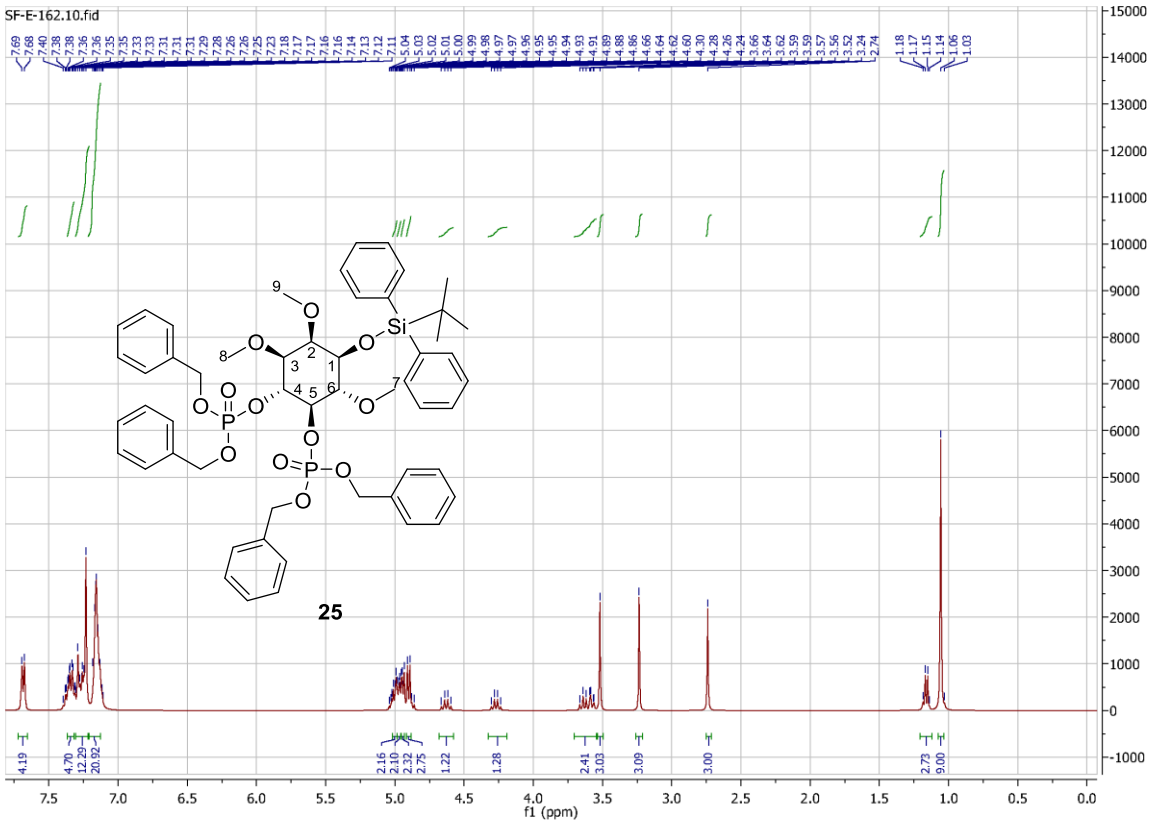
SF-E-162.10.fid
25
f1 (ppm)

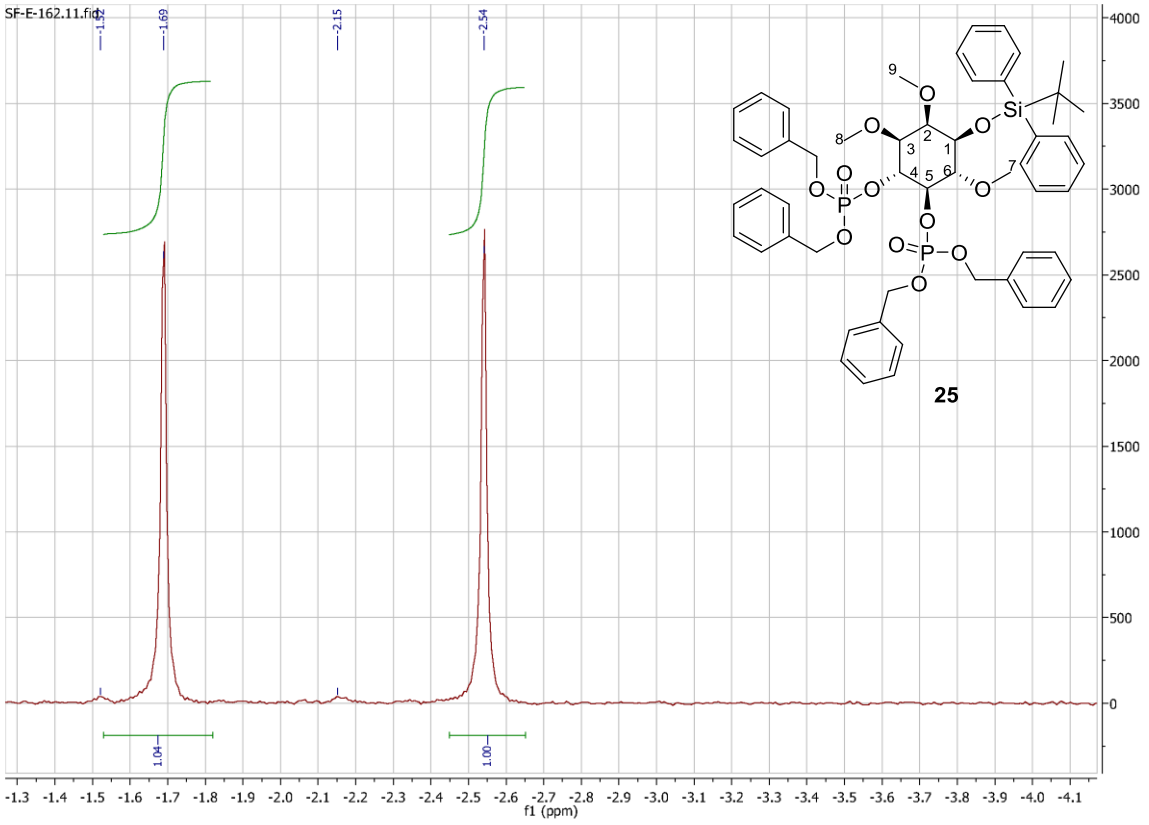
SF-E-162.11.fid
25
f1 (ppm)

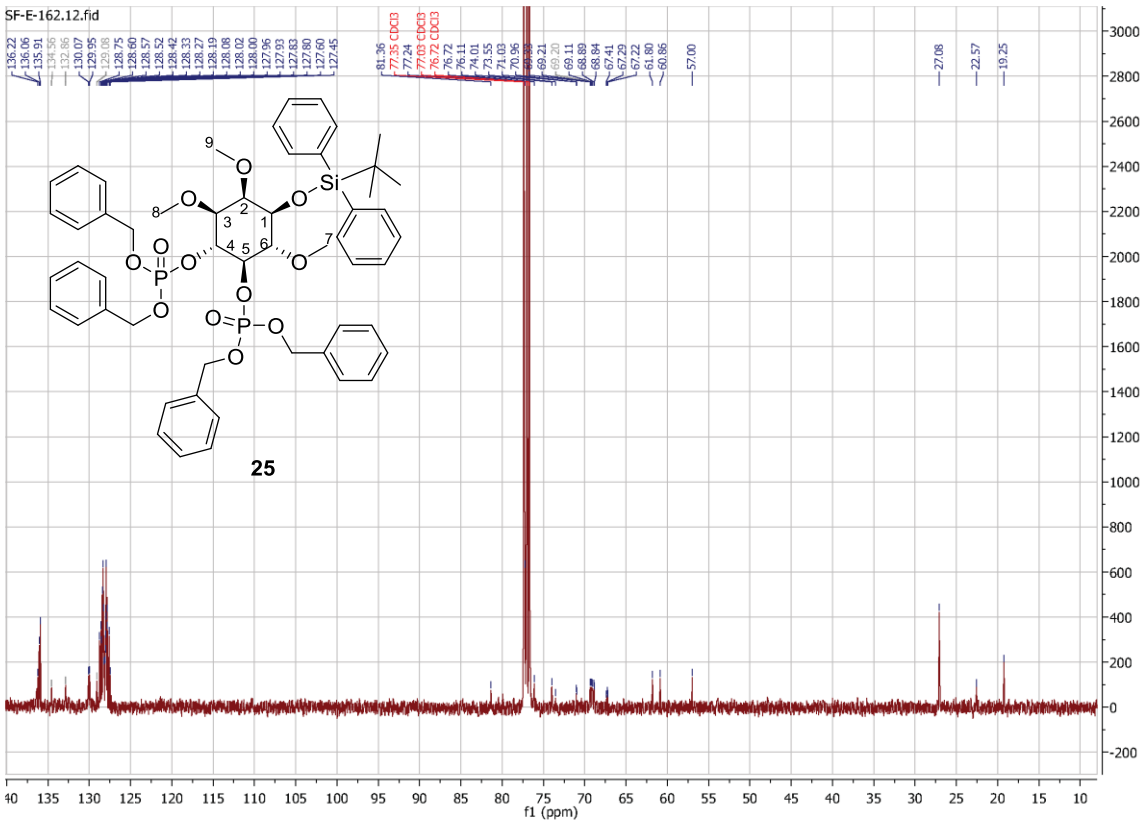

25

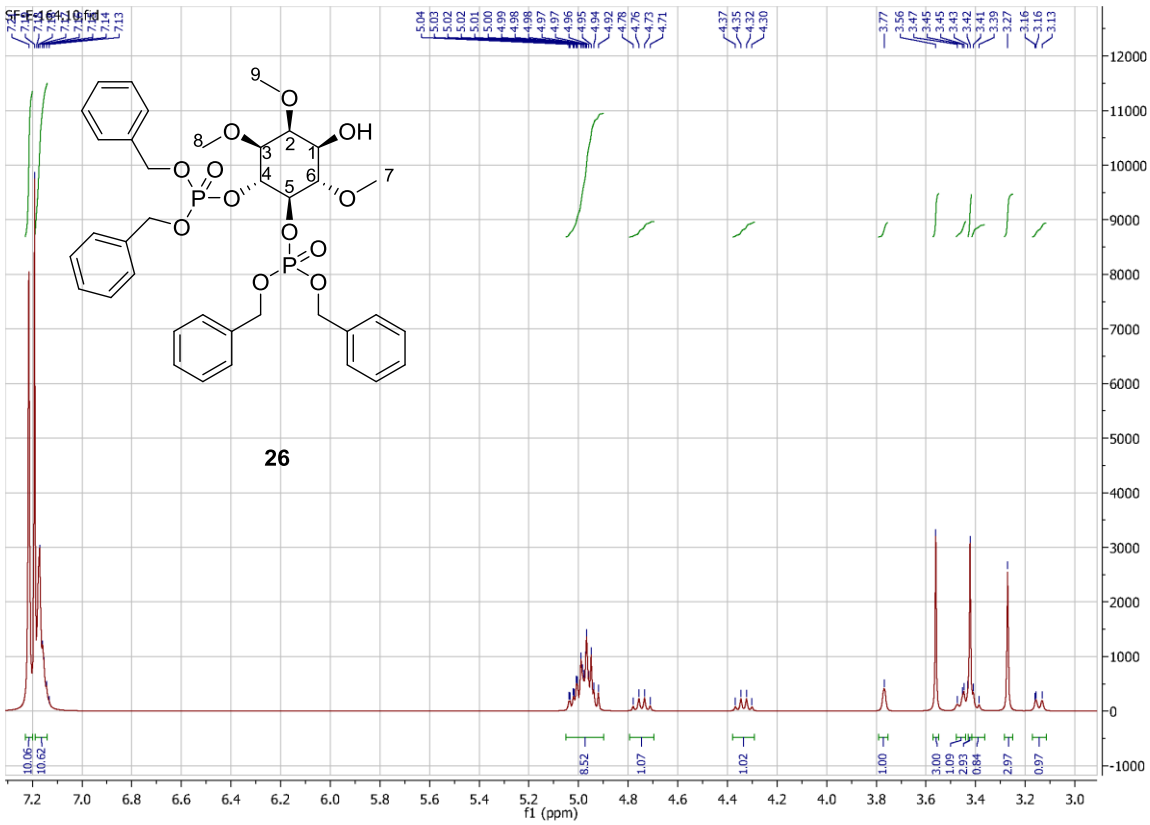

26

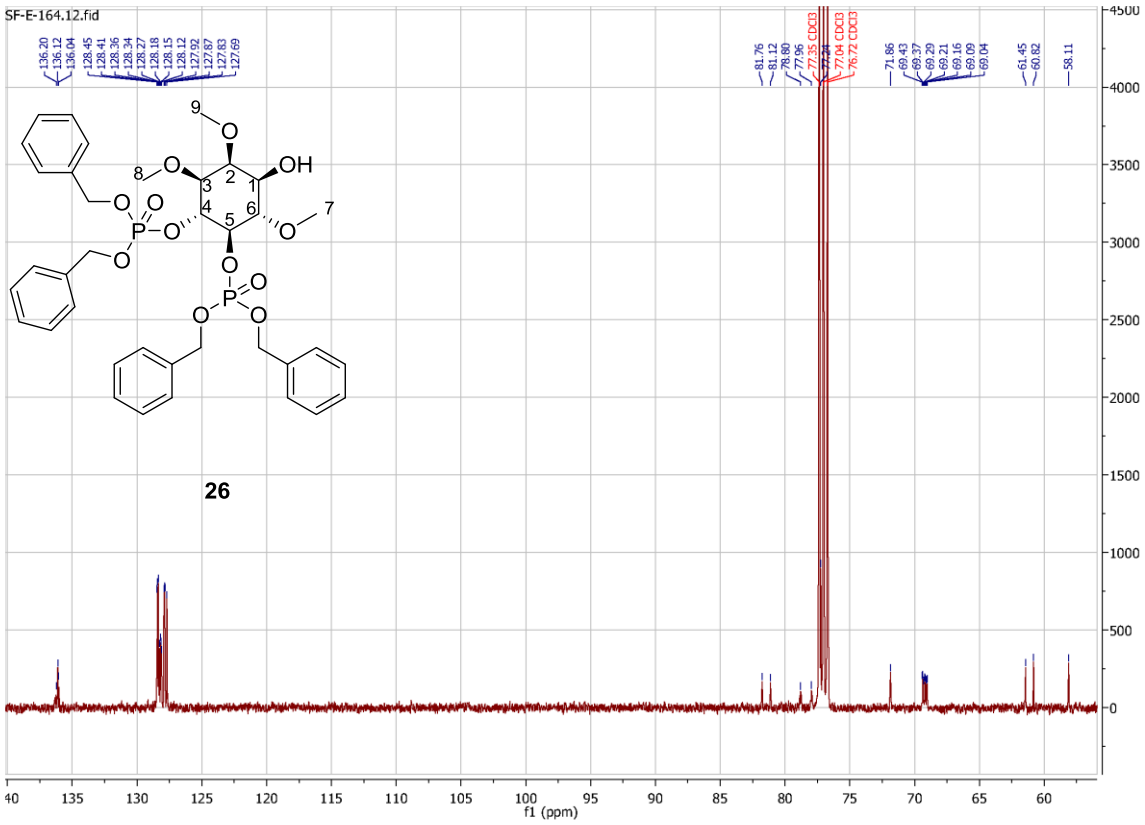
SF-E-164.12.fid
136.20
136.12
136.04
128.45
128.41
128.36
128.34
128.27
128.18
128.15
128.12
127.92
127.87
127.83
127.69
81.76
81.12
78.80
77.96
77.35 CDCl3
77.24
77.04 CDCl3
76.72 CDCl3
71.86
69.43
69.37
69.29
69.21
69.16
69.09
69.04
61.45
60.82
58.11
OH
26
f1 (ppm)

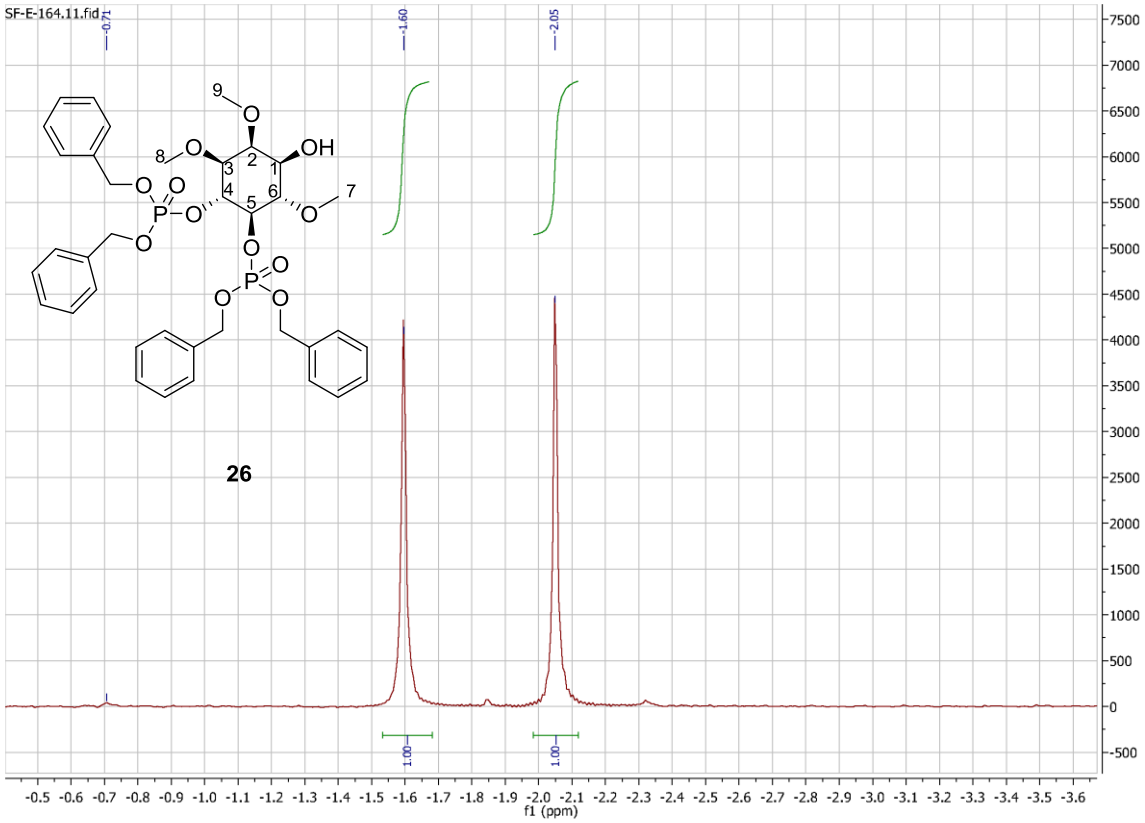
SF-E-164.11.fid
-0.71
-1.60
-2.05
OH
26
1.00
1.00
f1 (ppm)

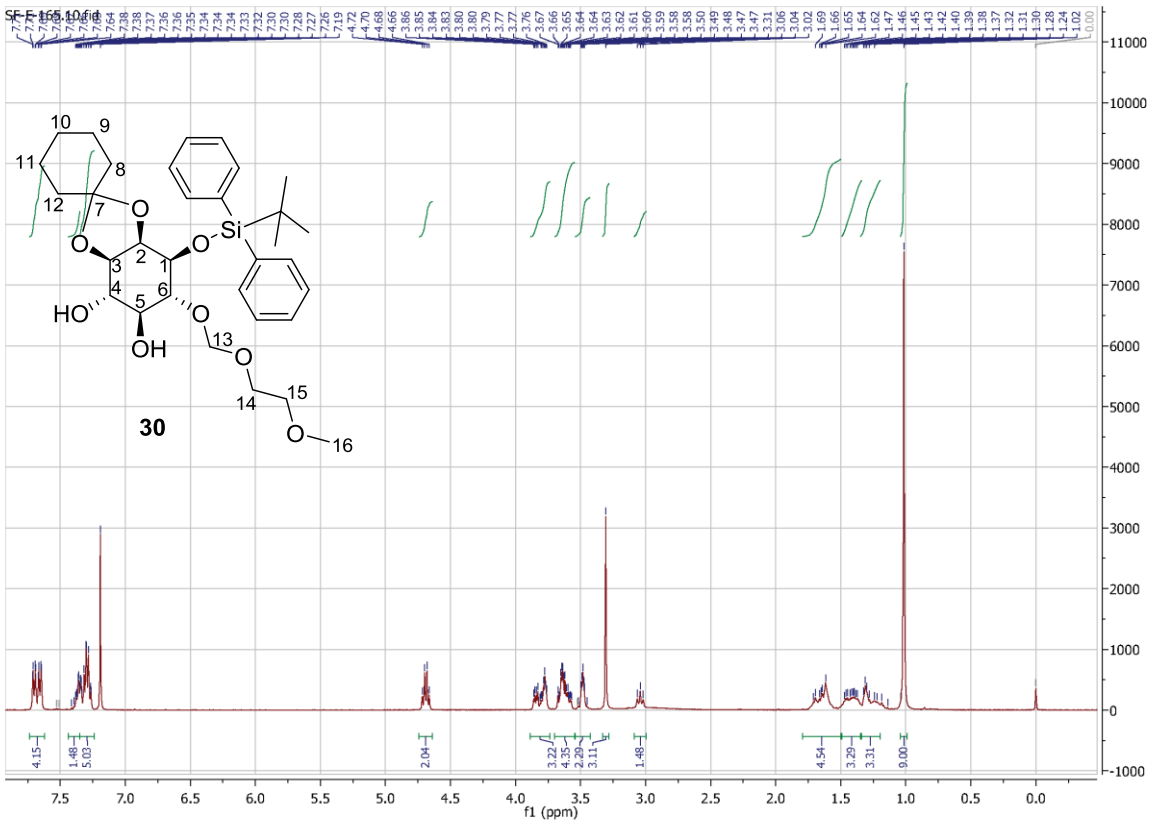
SF-E-165.10.fid
30
f1 (ppm)

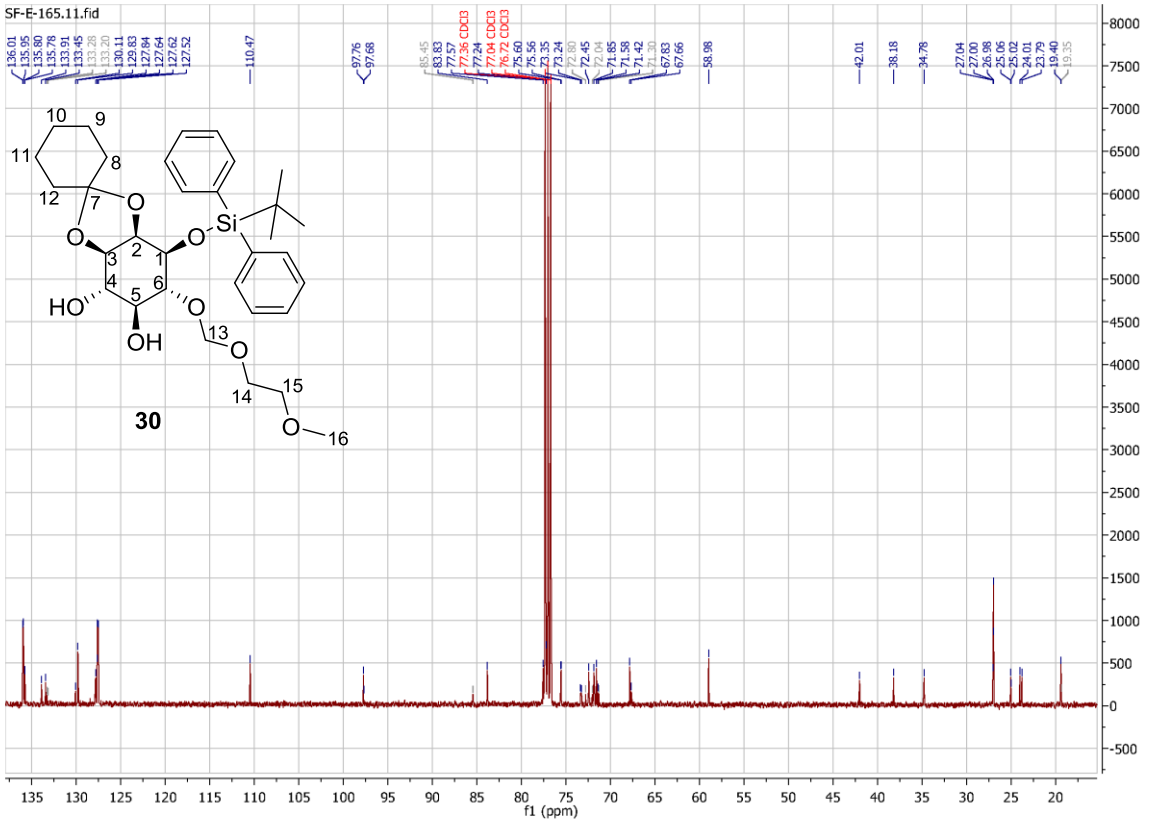
SF-E-165.11.fid
30
f1 (ppm)

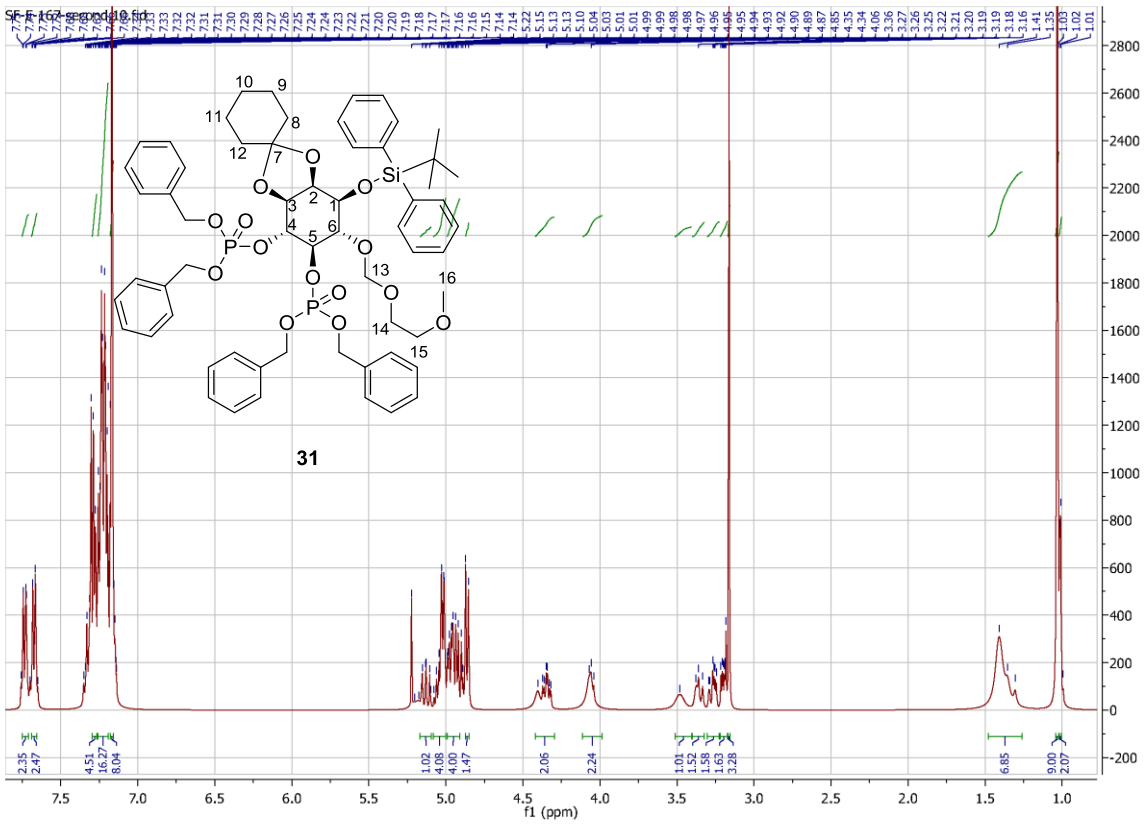
SF-E-167-second-10.fid
31
f1 (ppm)

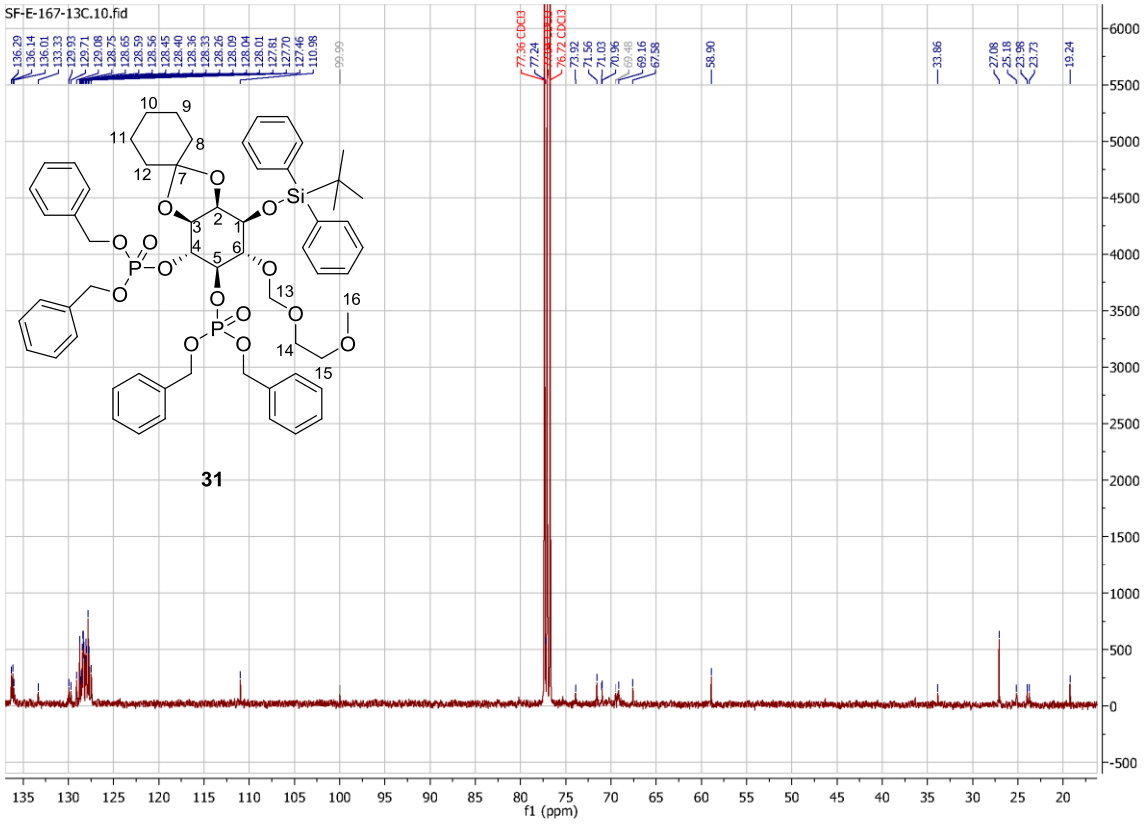
SF-E-167-13C.10.fid
31
f1 (ppm)

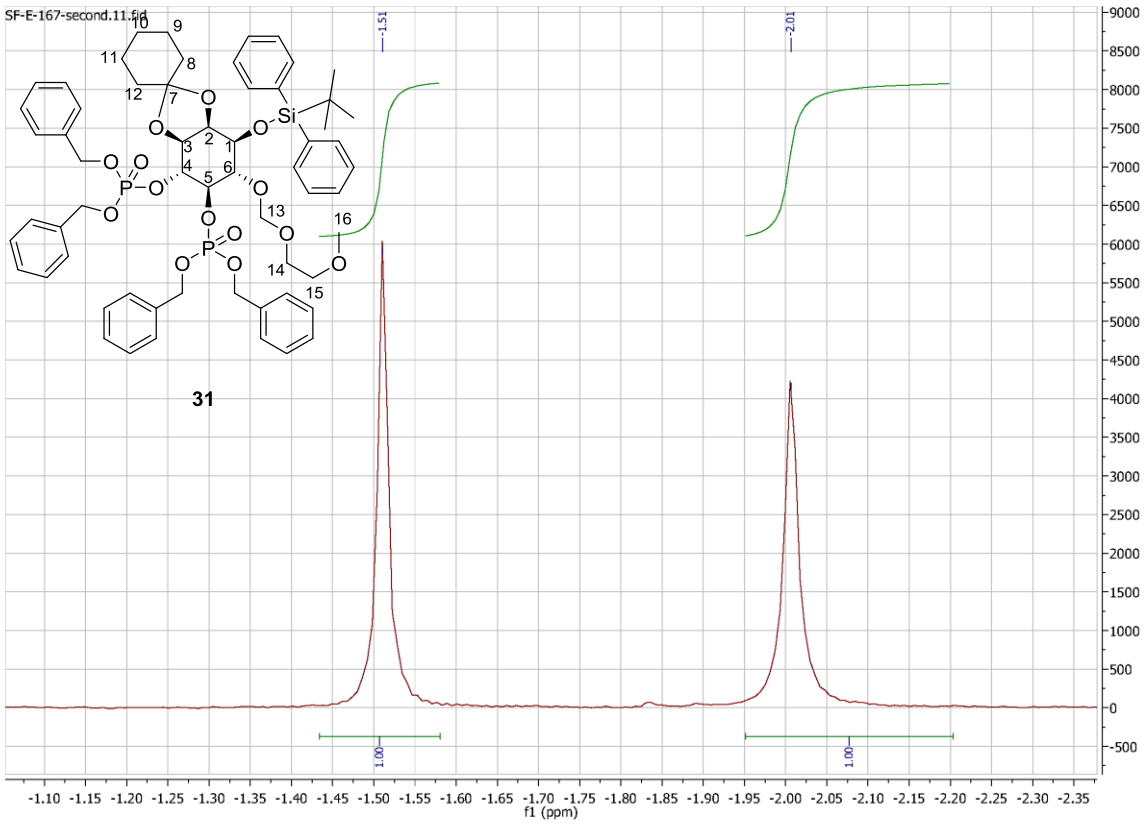
SF-E-167-second.11.fid
31
-1.51
-2.01
1.00
1.00
f1 (ppm)

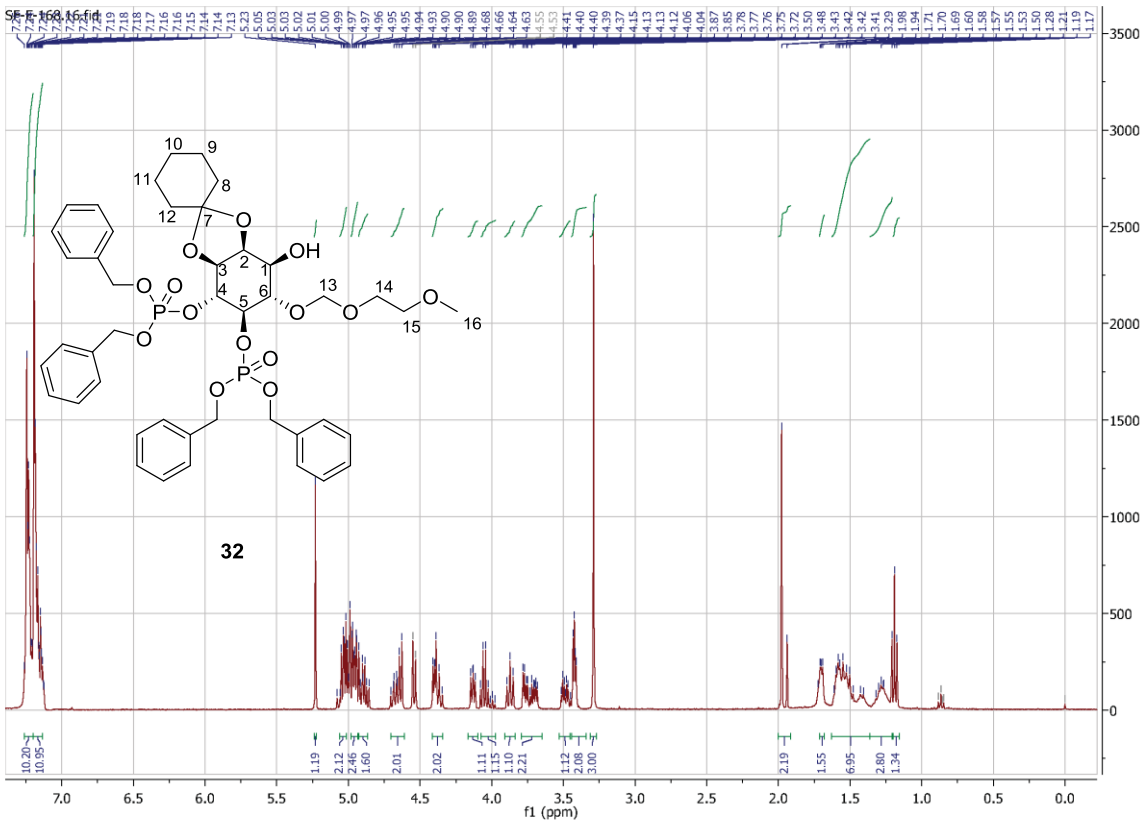
SF-E-168.16.fid
32
f1 (ppm)

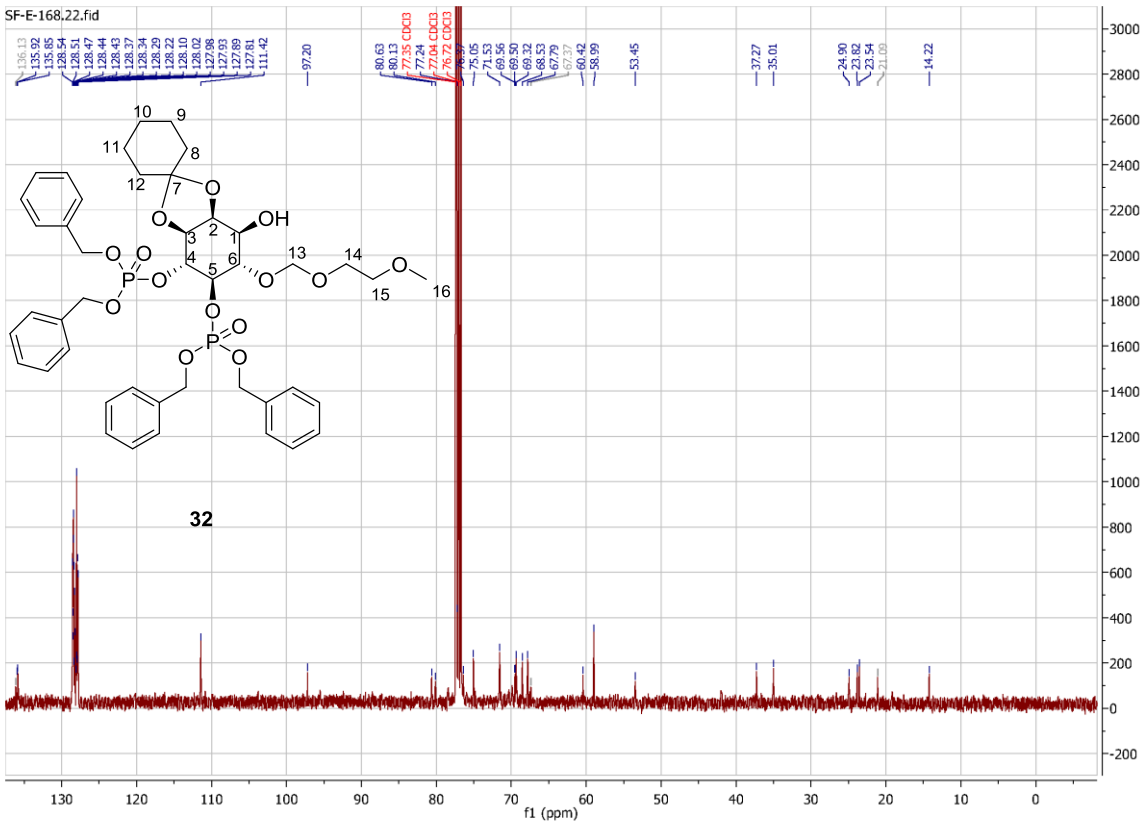
SF-E-168.22.fid
32
f1 (ppm)

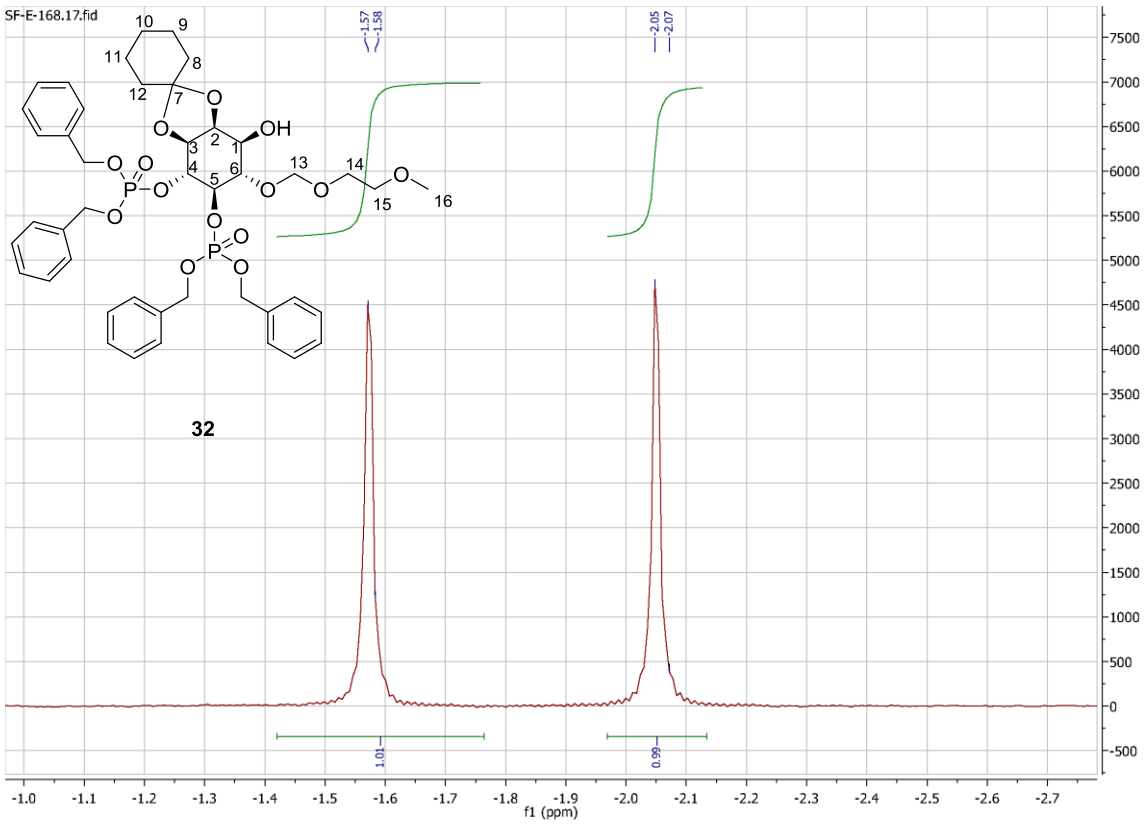
SF-E-168.17.fid
32
-1.57
-1.58
-2.05
-2.07
1.01
0.99
f1 (ppm)

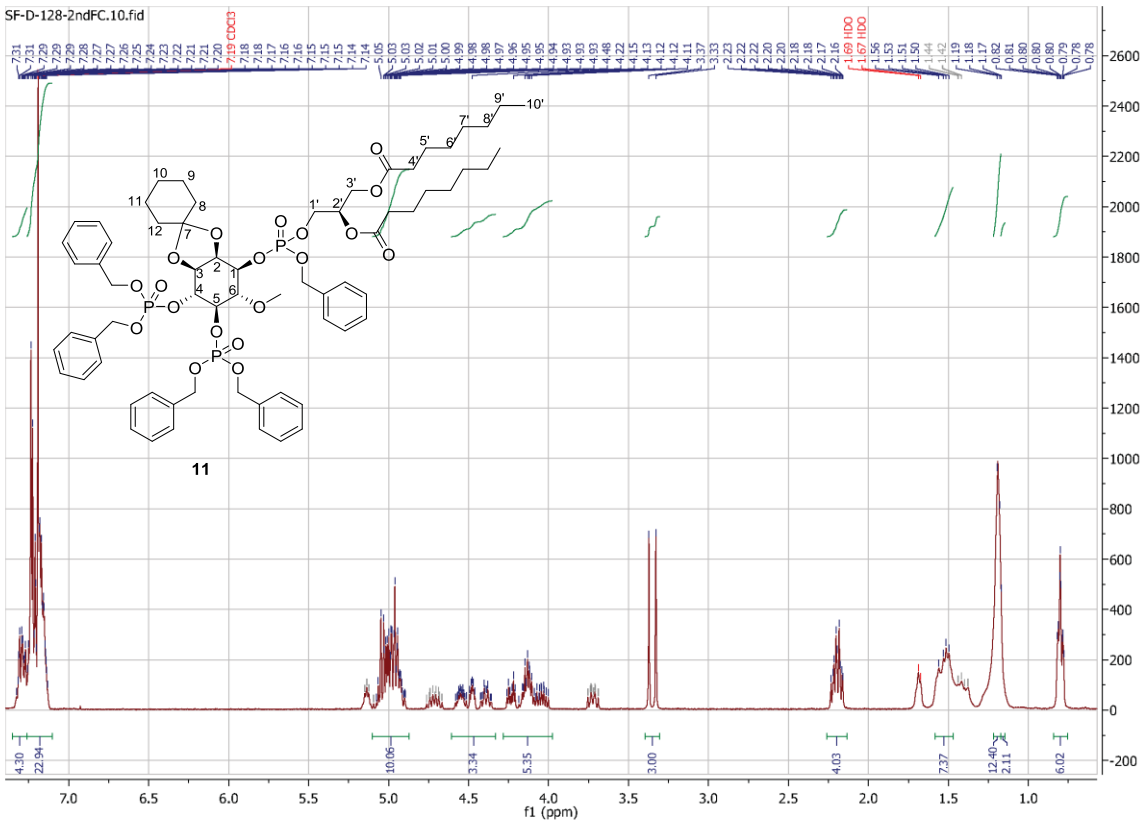
SF-D-128-2ndFC.10.fid
11
f1 (ppm)

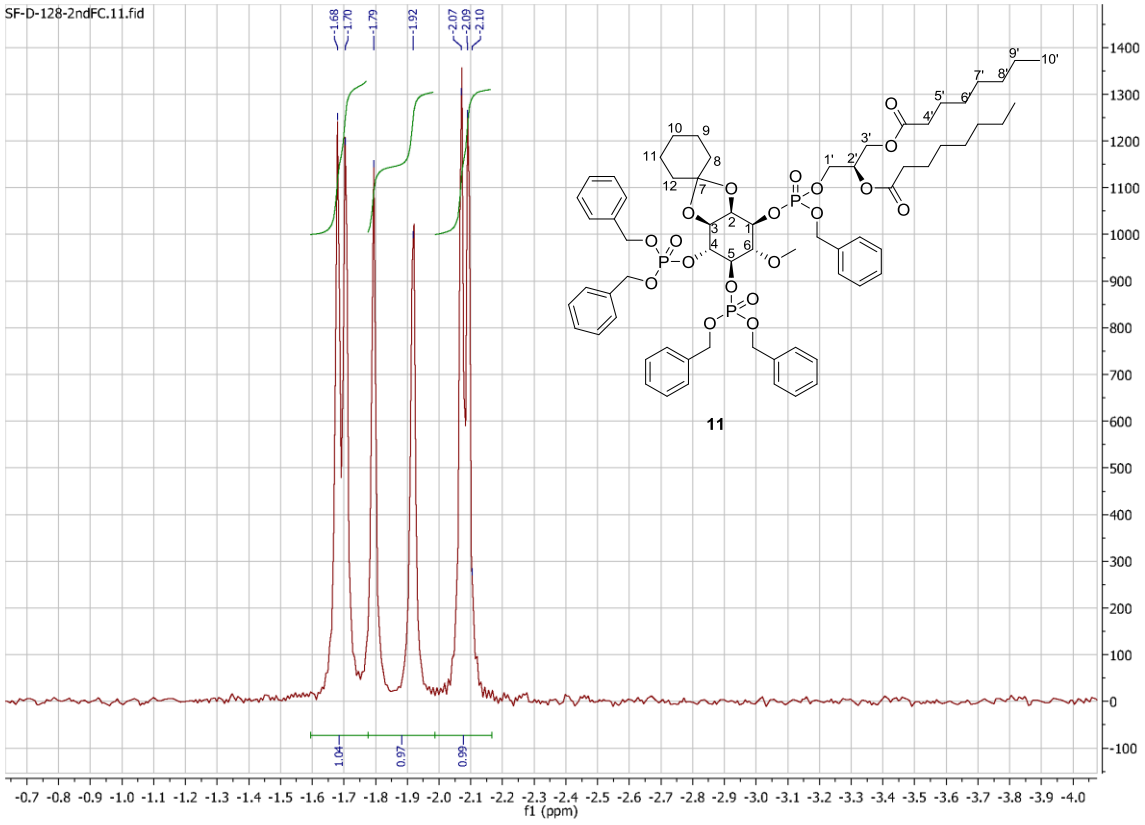
SF-D-128-2ndFC.11.fid
11
f1 (ppm)

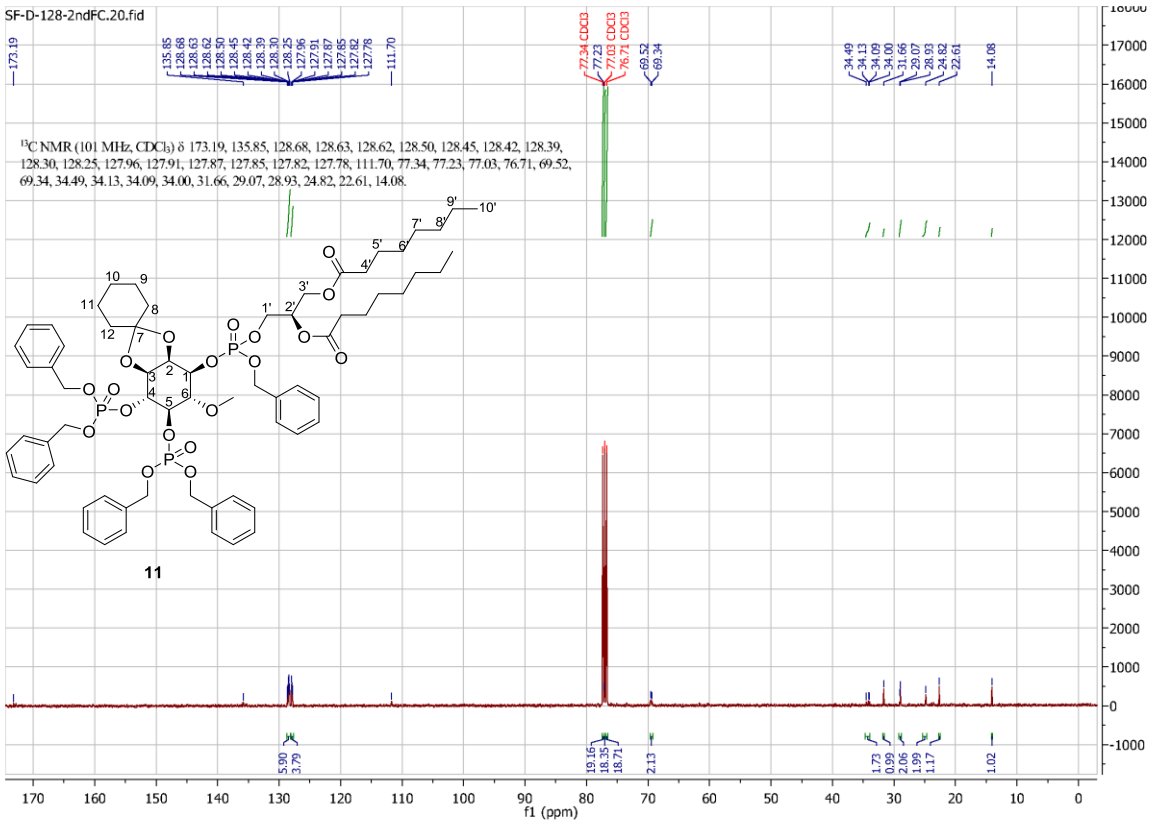
SF-D-128-2ndFC.20.fid
^{13}C NMR (101 MHz, $CDCl_3$) δ 173.19, 135.85, 128.68, 128.63, 128.62, 128.50, 128.45, 128.42, 128.39, 128.30, 128.25, 127.96, 127.91, 127.87, 127.85, 127.82, 127.78, 111.70, 77.34, 77.23, 77.03, 76.71, 69.52, 69.34, 34.49, 34.13, 34.09, 34.00, 31.66, 29.07, 28.93, 24.82, 22.61, 14.08.
11
f1 (ppm)

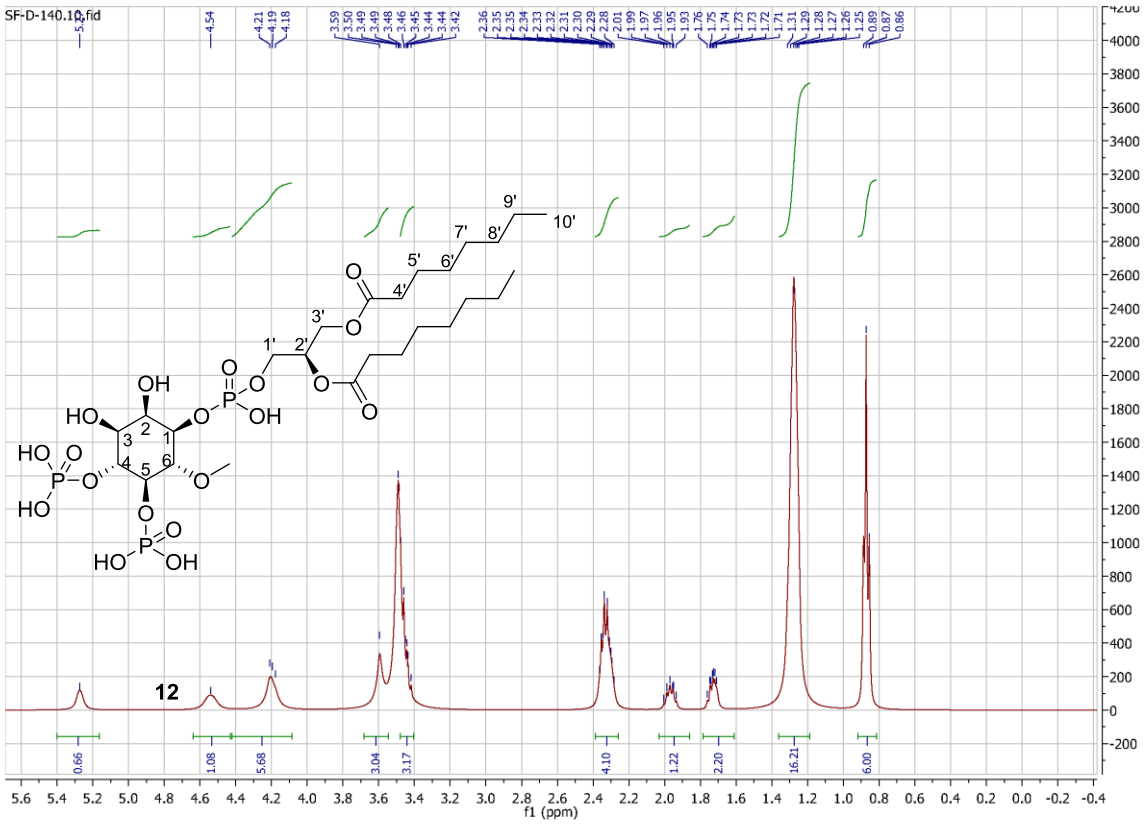
SF-D-140.10.fid
12
f1 (ppm)

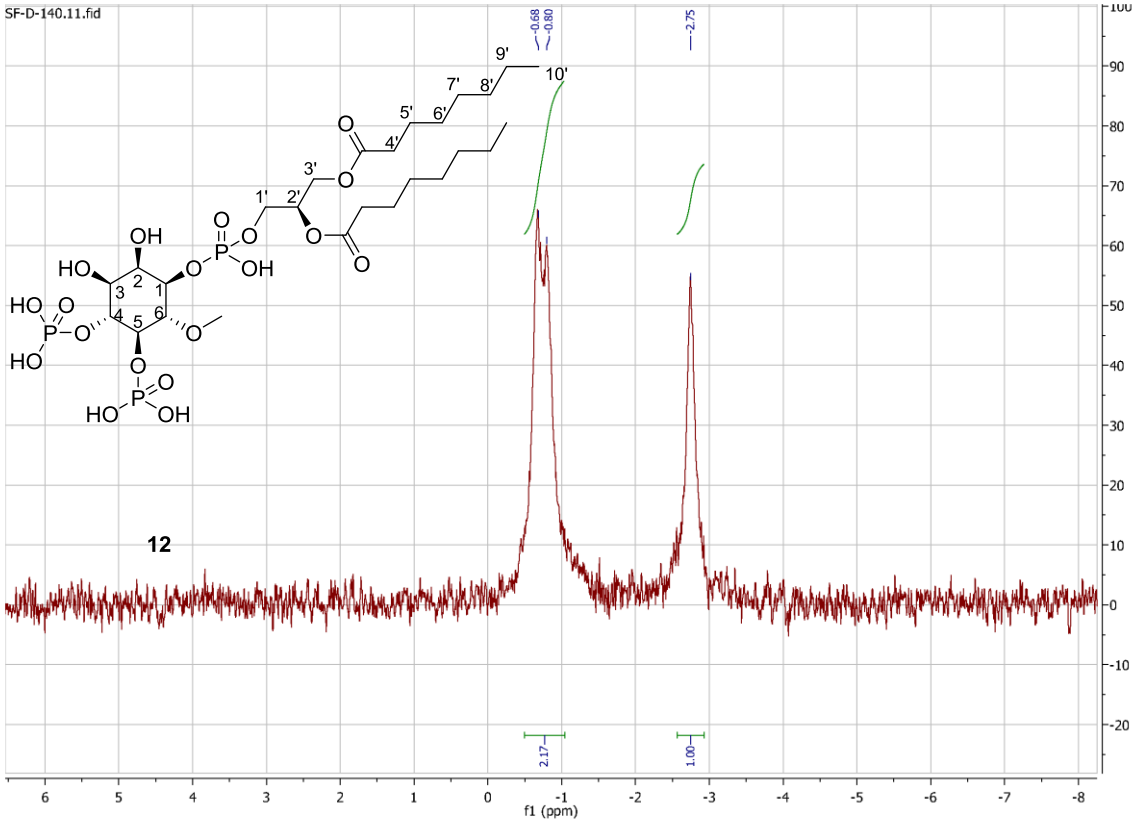
SF-D-140.11.fid
12
f1 (ppm)

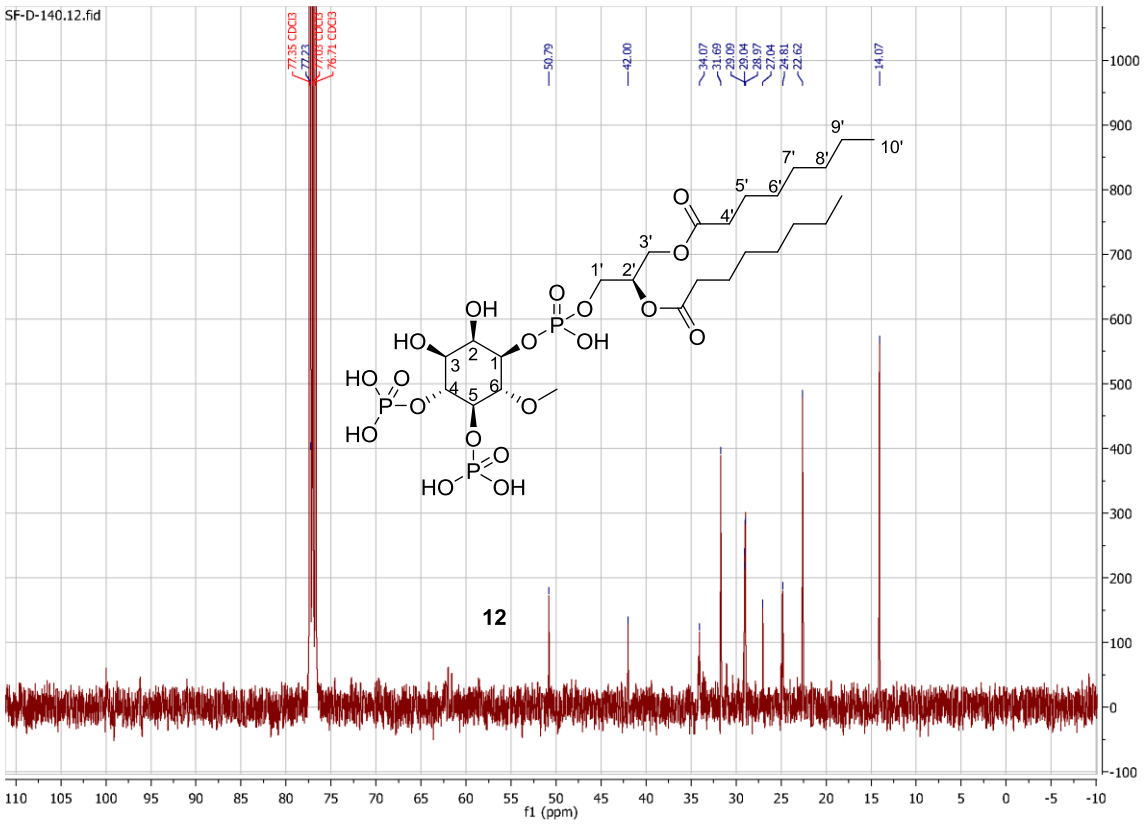
SF-D-140.12.fid
77.35 CDCl3
77.00 CDCl3
76.71 CDCl3
50.79
42.00
34.07
31.69
29.09
29.04
28.97
27.04
24.81
22.62
14.07
12
f1 (ppm)

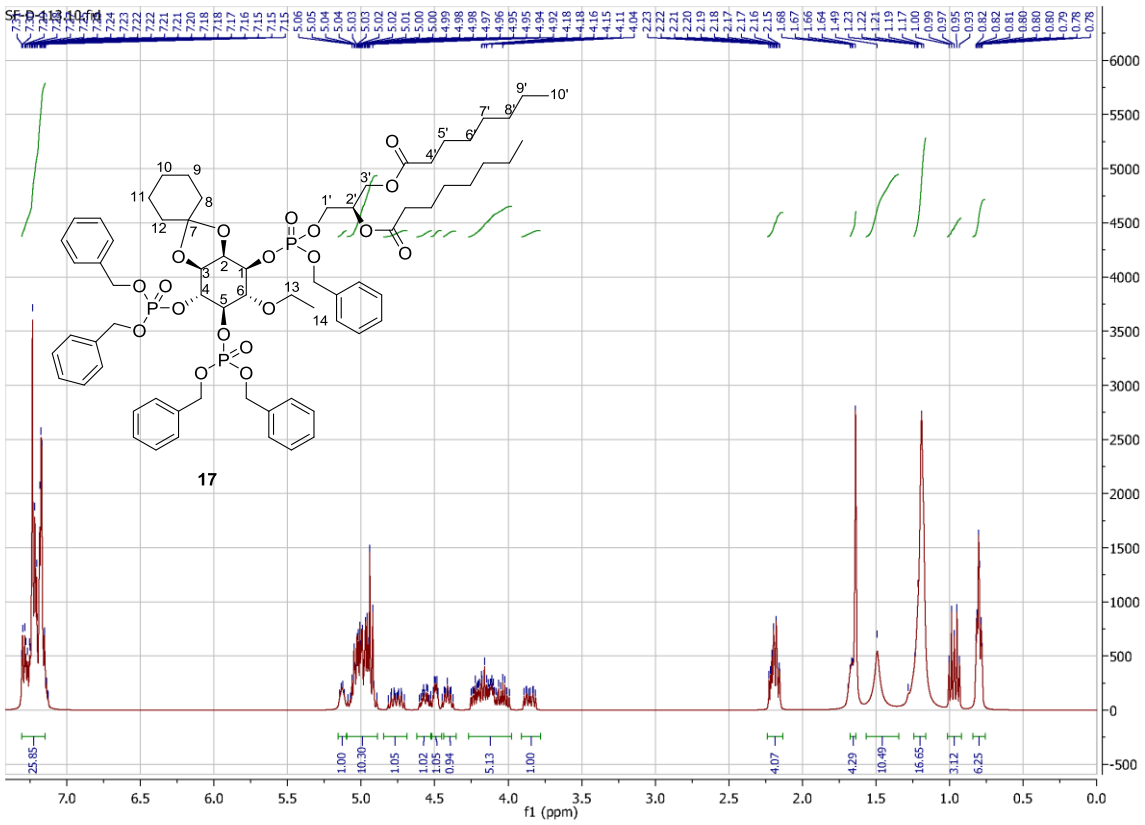
SF-D-113.10.fid
17
f1 (ppm)

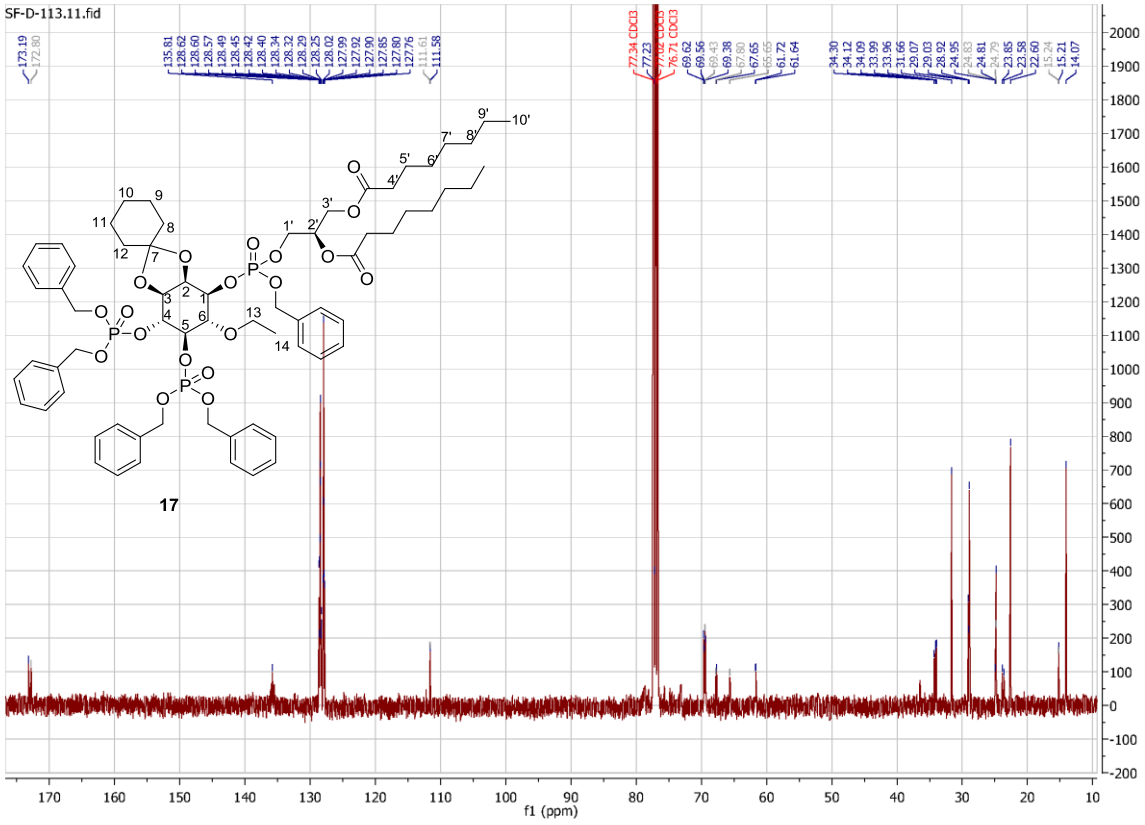
SF-D-113.11.fid
17
f1 (ppm)

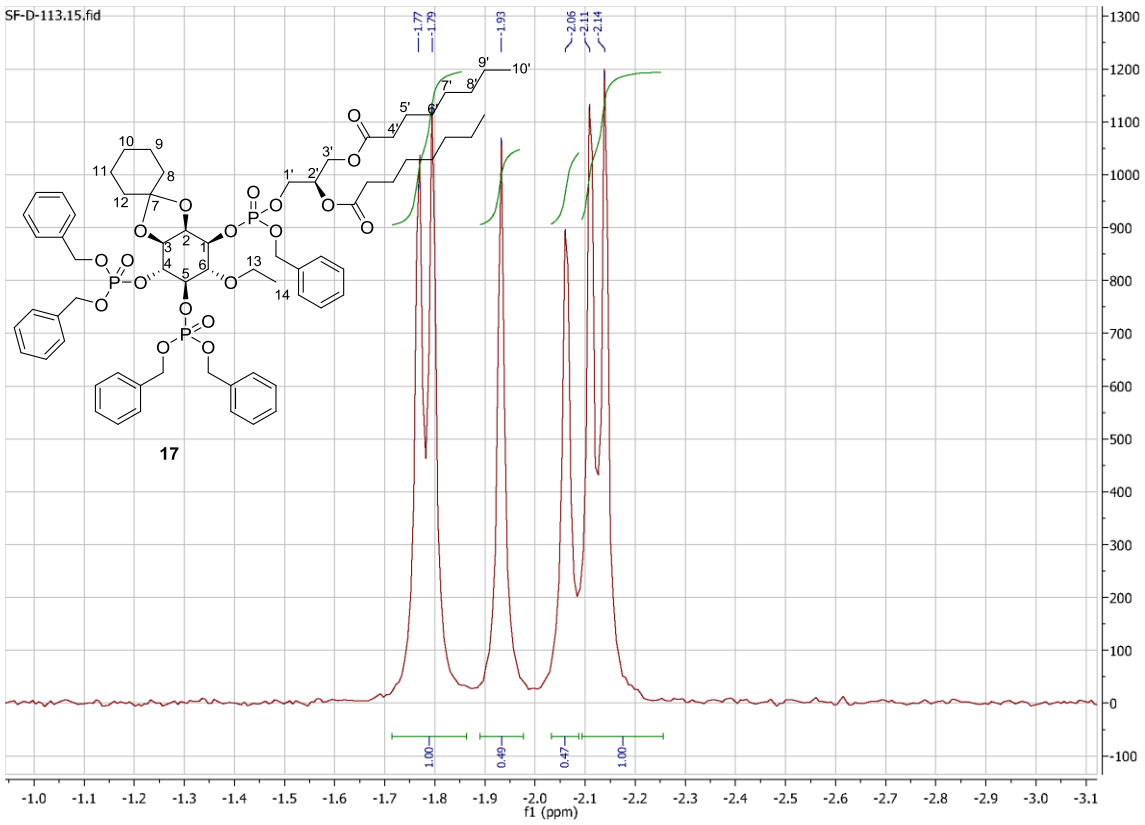

17

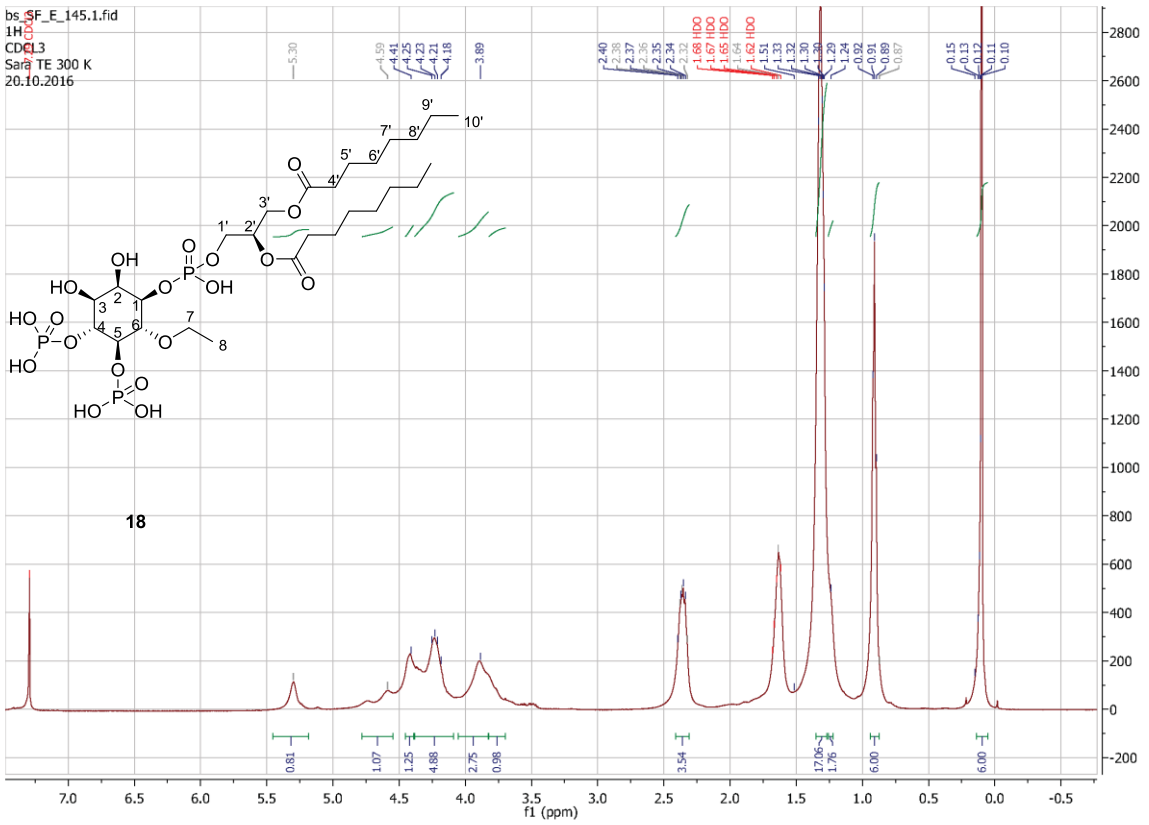
bs_SF_E_145.1.fid
1H
CDCL3
Sara TE 300 K
20.10.2016
18
f1 (ppm)

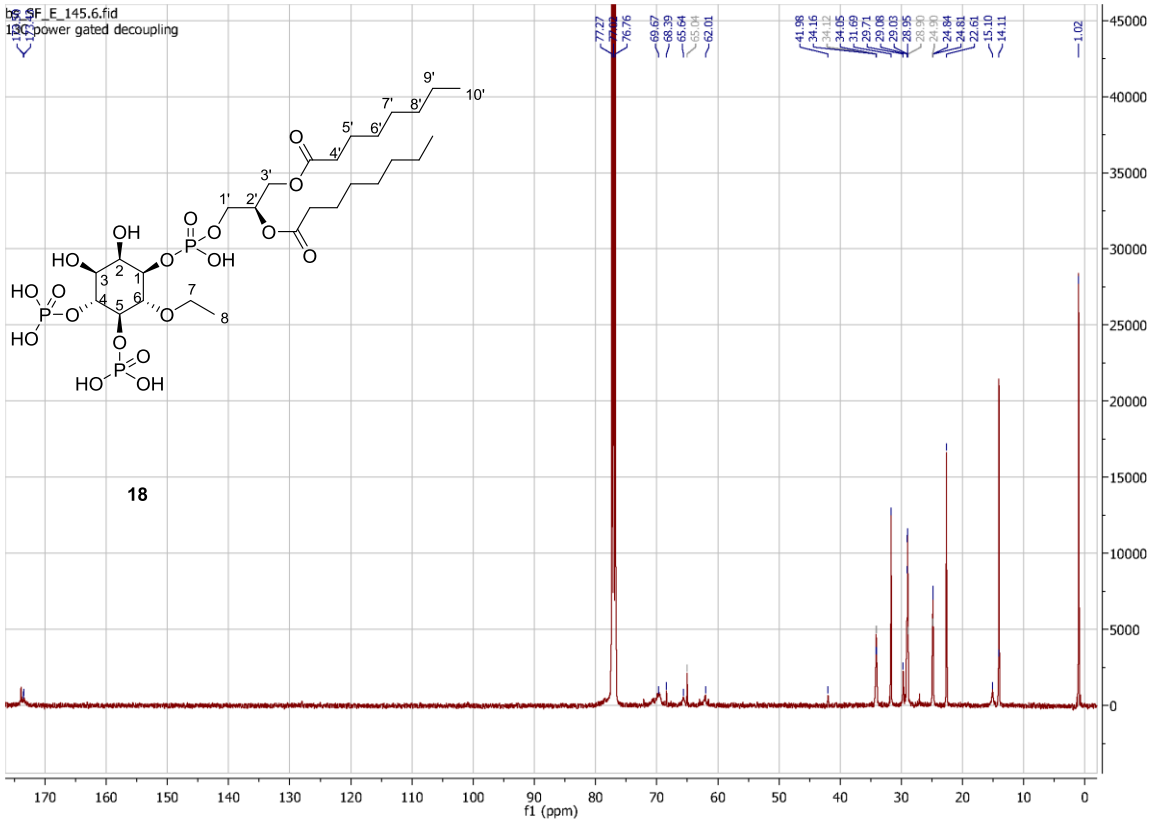
bs_SF_E_145.6.fid
13C, power gated decoupling
18
f1 (ppm)

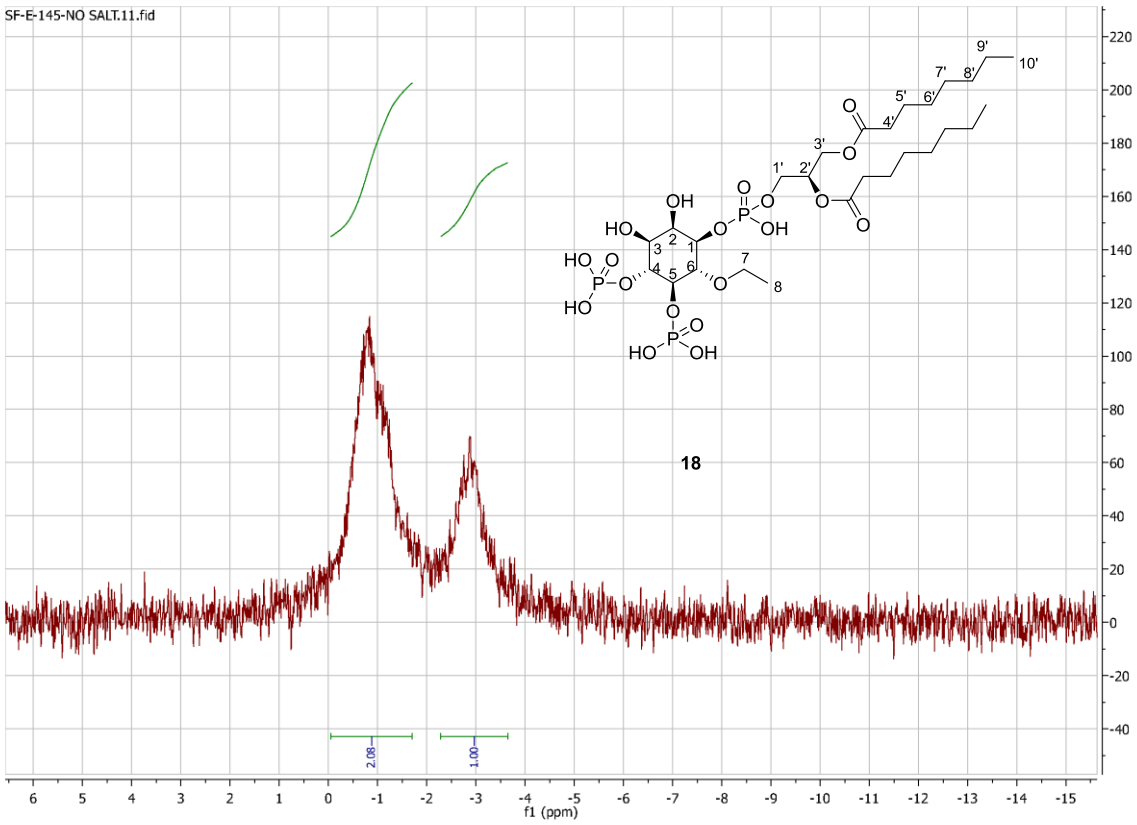
SF-E-145-NO SALT.11.fid
18
f1 (ppm)

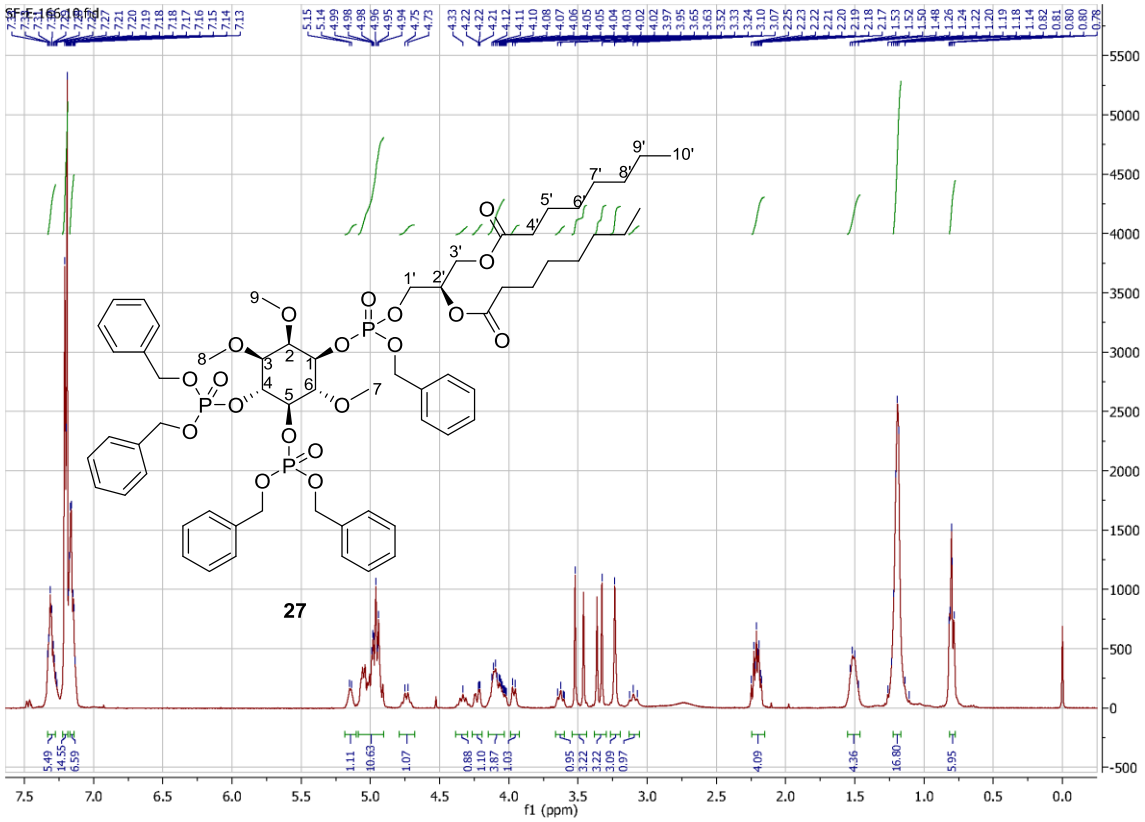
SF-E-166.10.fid
27
f1 (ppm)

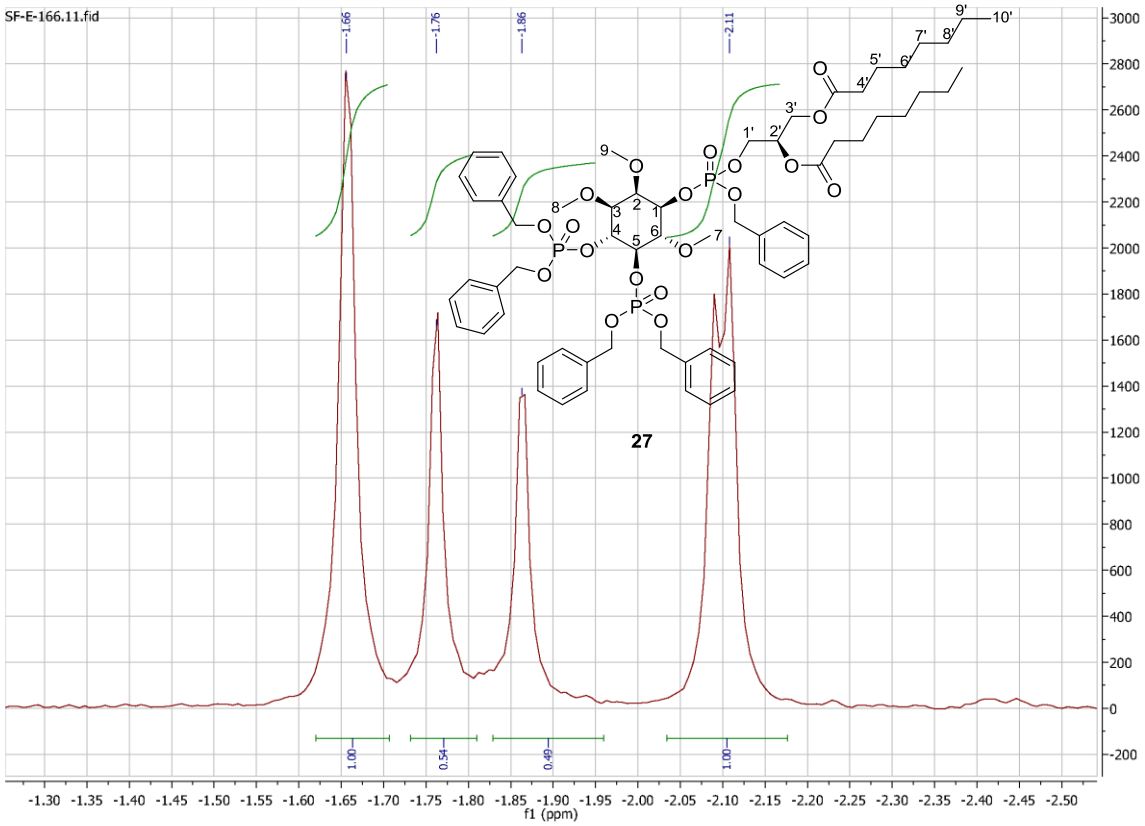
SF-E-166.11.fid
-1.66
-1.76
-1.86
-2.11
27
f1 (ppm)

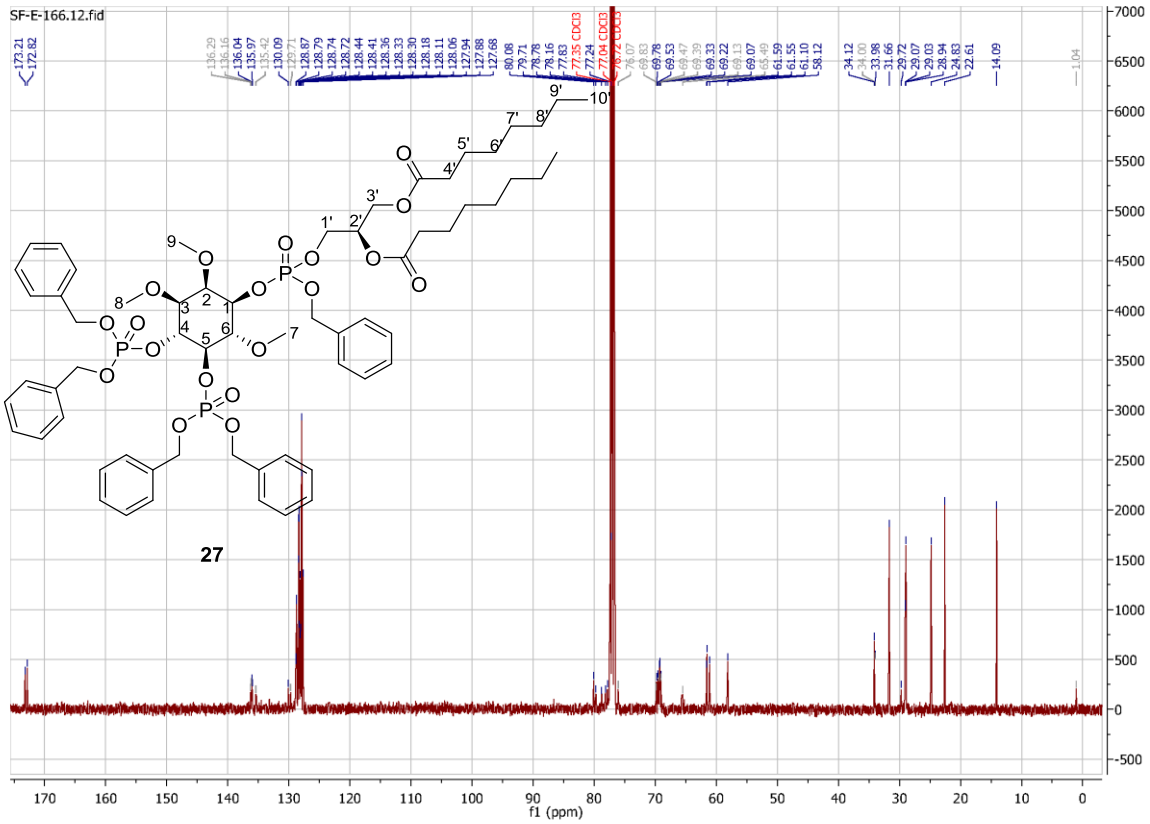
SF-E-166.12.fid
27
f1 (ppm)

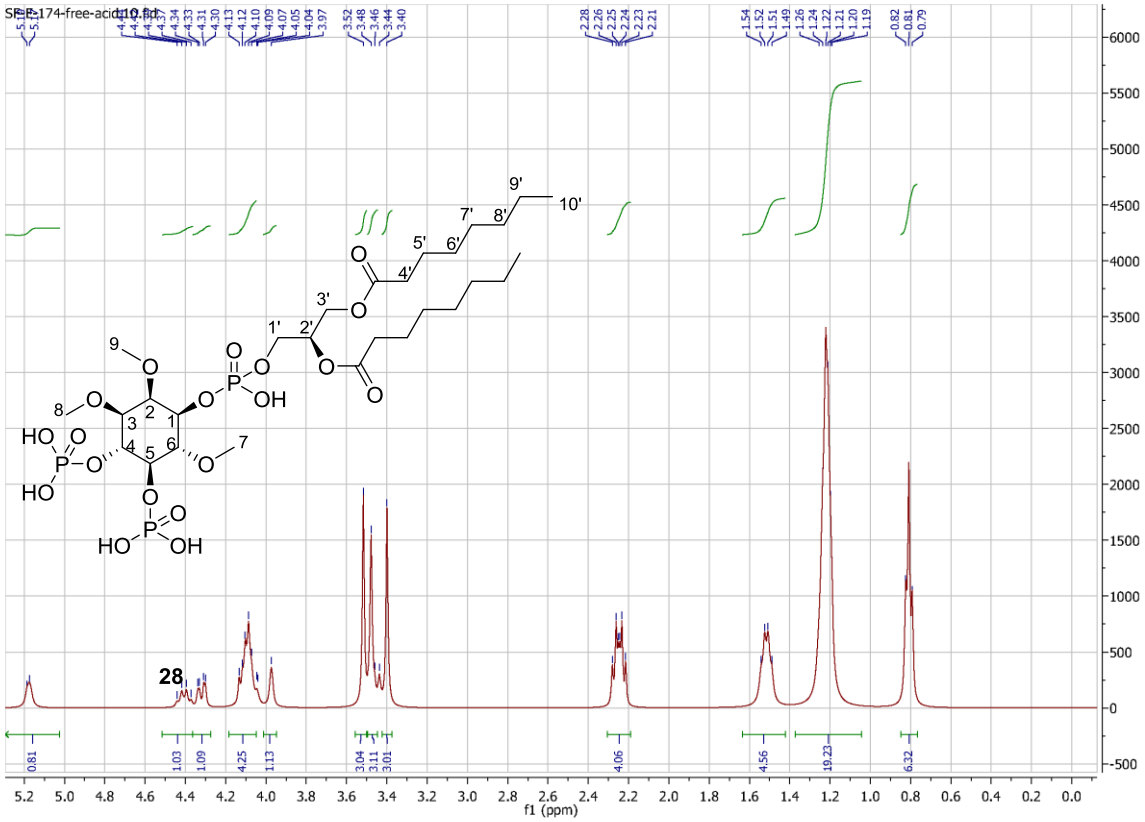
SF-E-174-free-acid.10.fid
28
f1 (ppm)

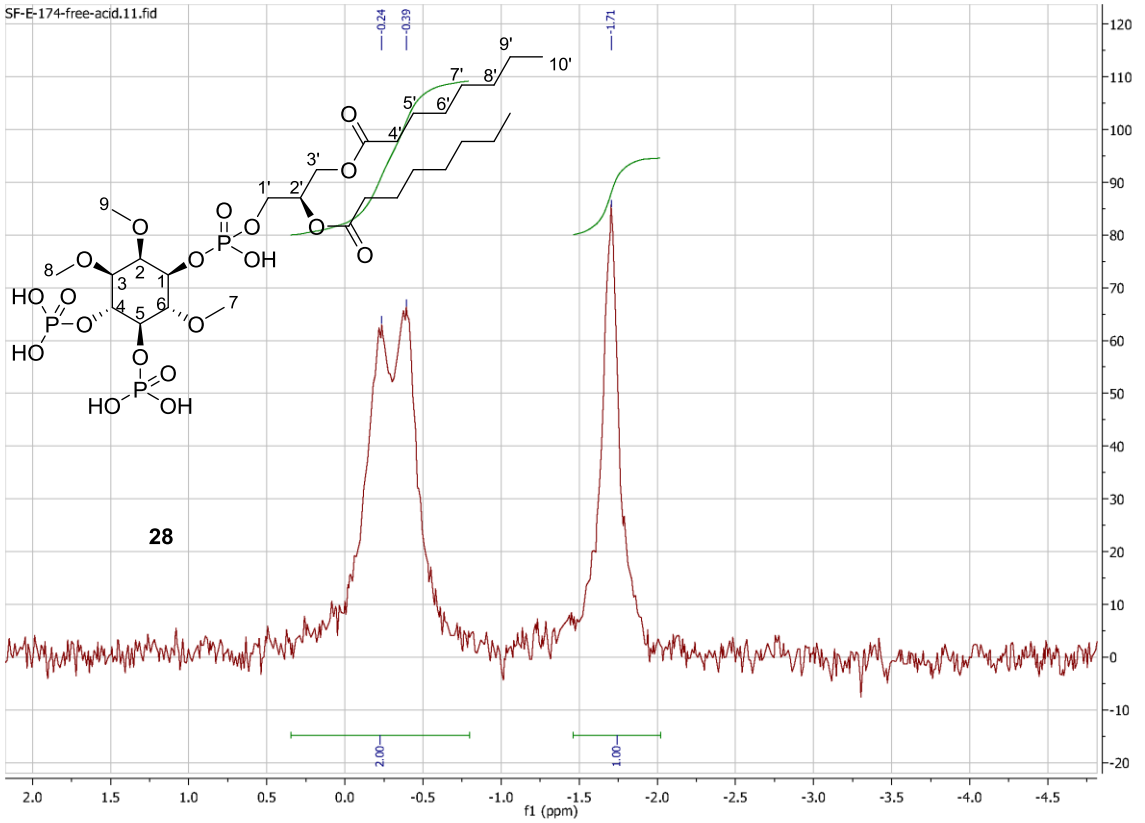
SF-E-174-free-acid.11.fid
28
f1 (ppm)

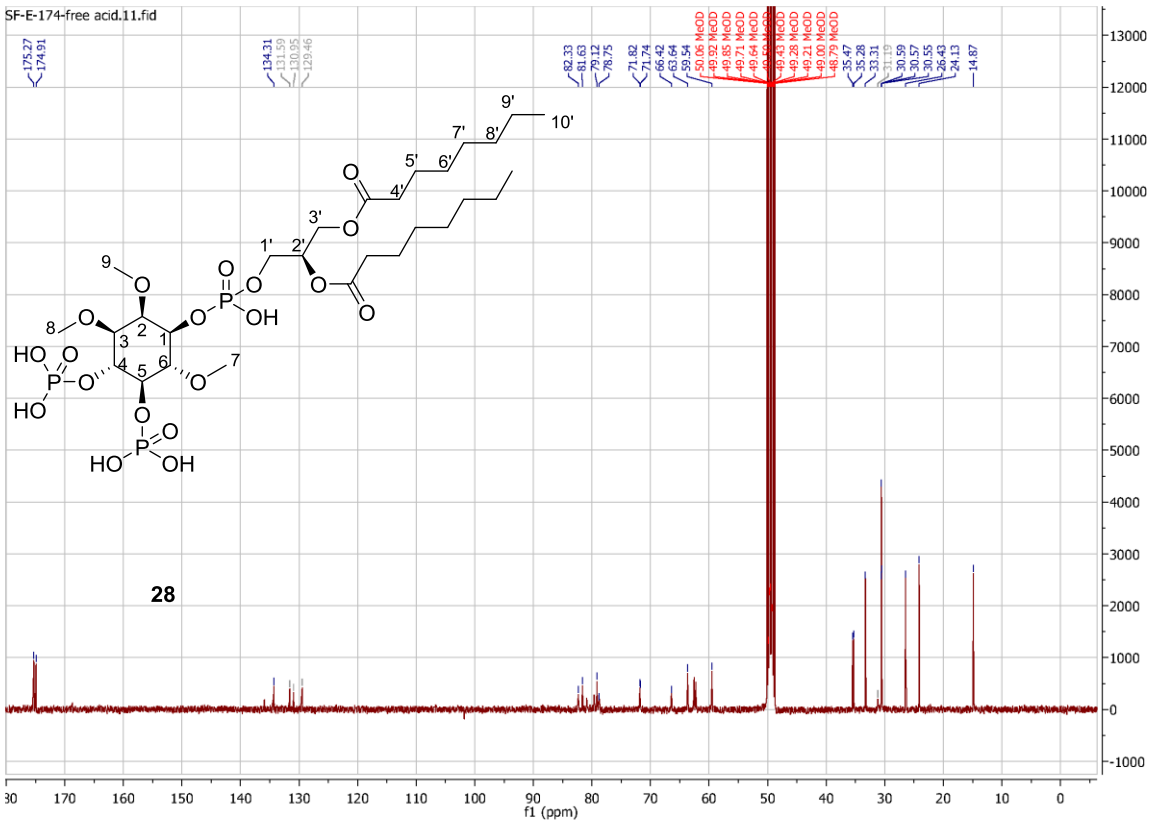
SF-E-174-free acid.11.fid
28
f1 (ppm)

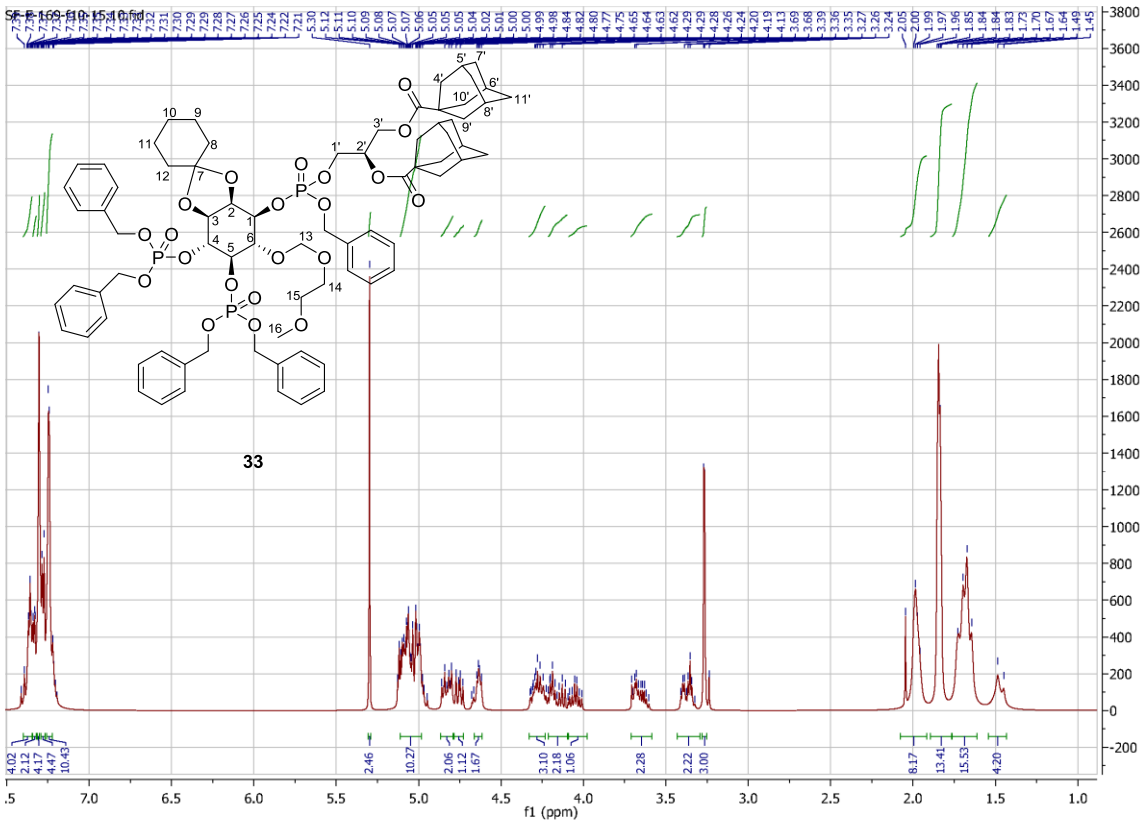
SF-E-169-10-15-10.fid
33
f1 (ppm)

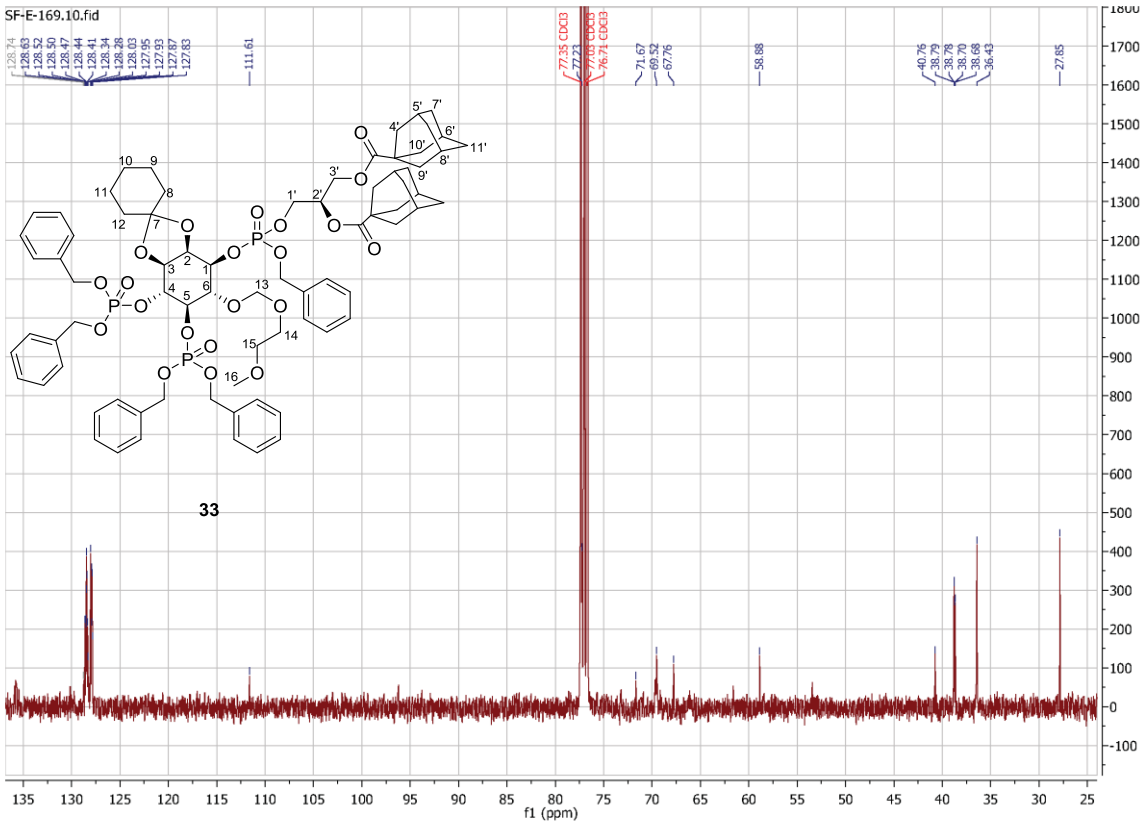
SF-E-169.10.fid
77.35 CDCl3
77.23
77.03 CDCl3
76.71 CDCl3
71.67
69.52
67.76
58.88
40.76
38.79
38.78
38.70
38.68
36.43
27.85
111.61
33
f1 (ppm)

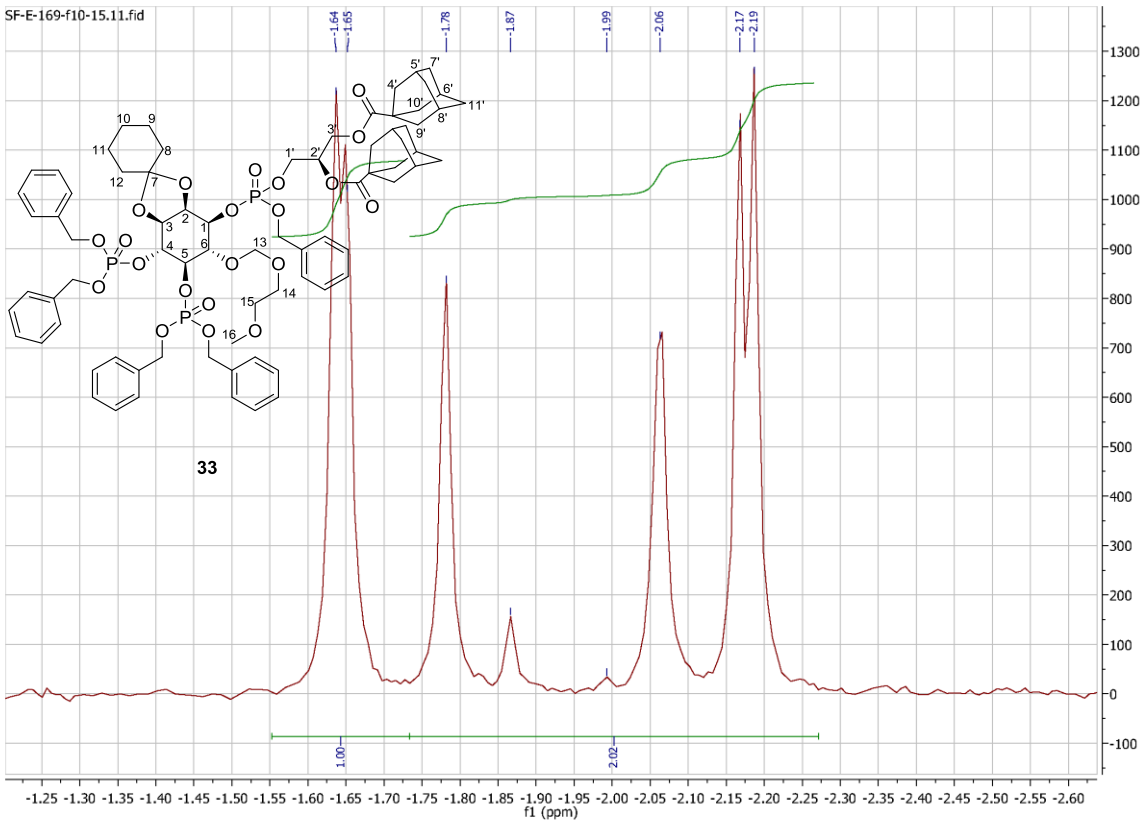
SF-E-169-f10-15.11.fid
-1.64
-1.65
-1.78
-1.87
-1.99
-2.06
-2.17
-2.19
1.00
2.02
f1 (ppm)

33

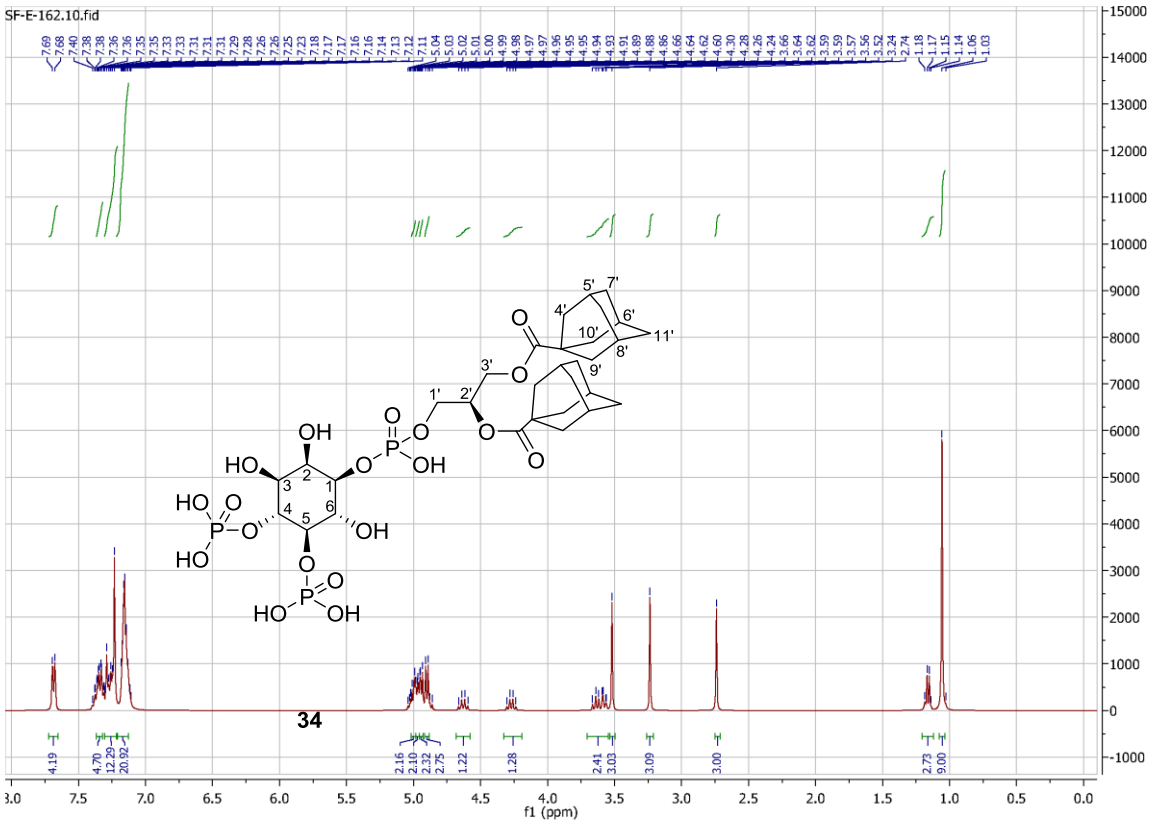
SF-E-162.10.fid
34
f1 (ppm)

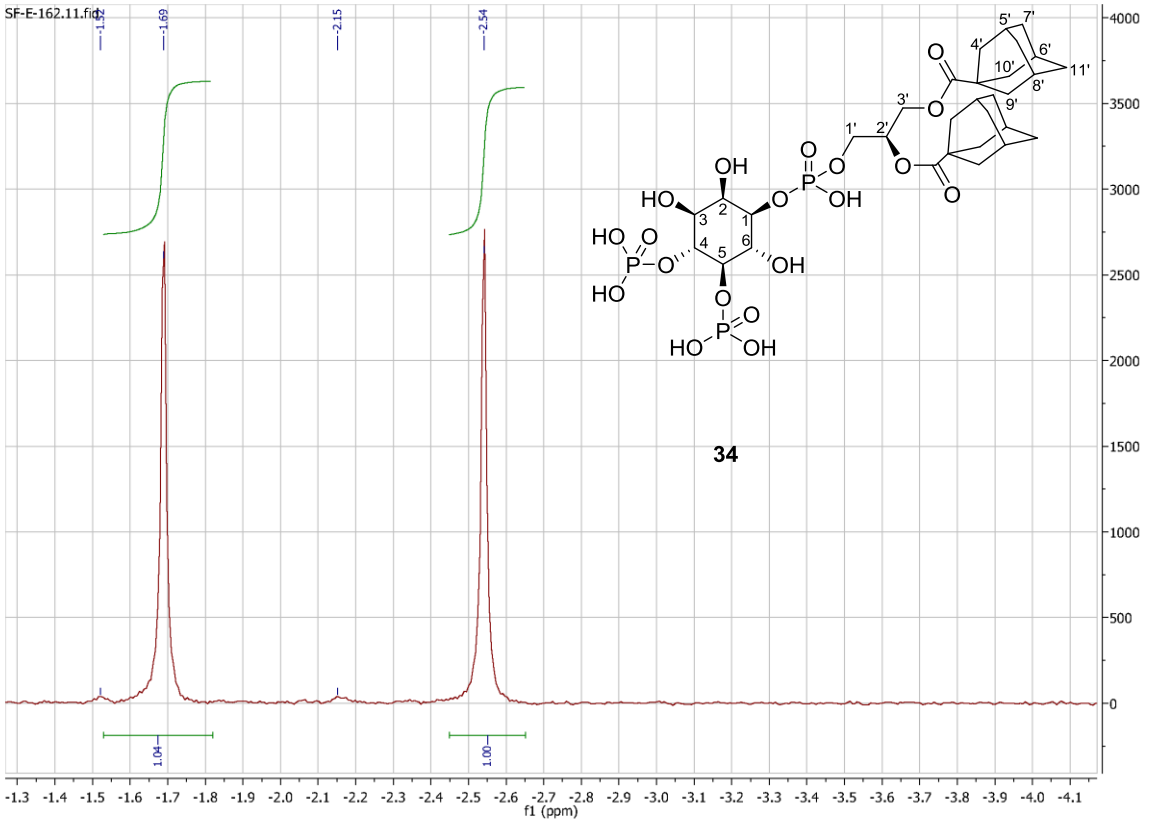
SF-E-162.11.fid
34
f1 (ppm)

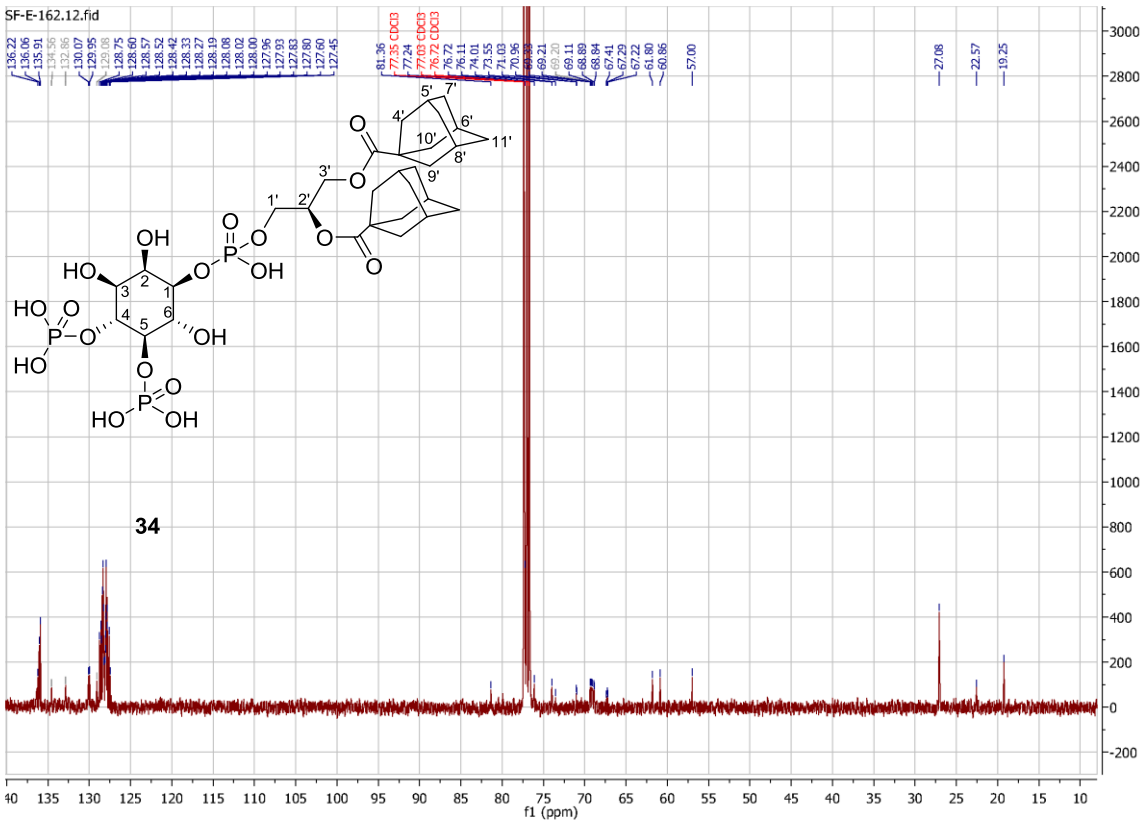
SF-E-162.12.fid
34
f1 (ppm)

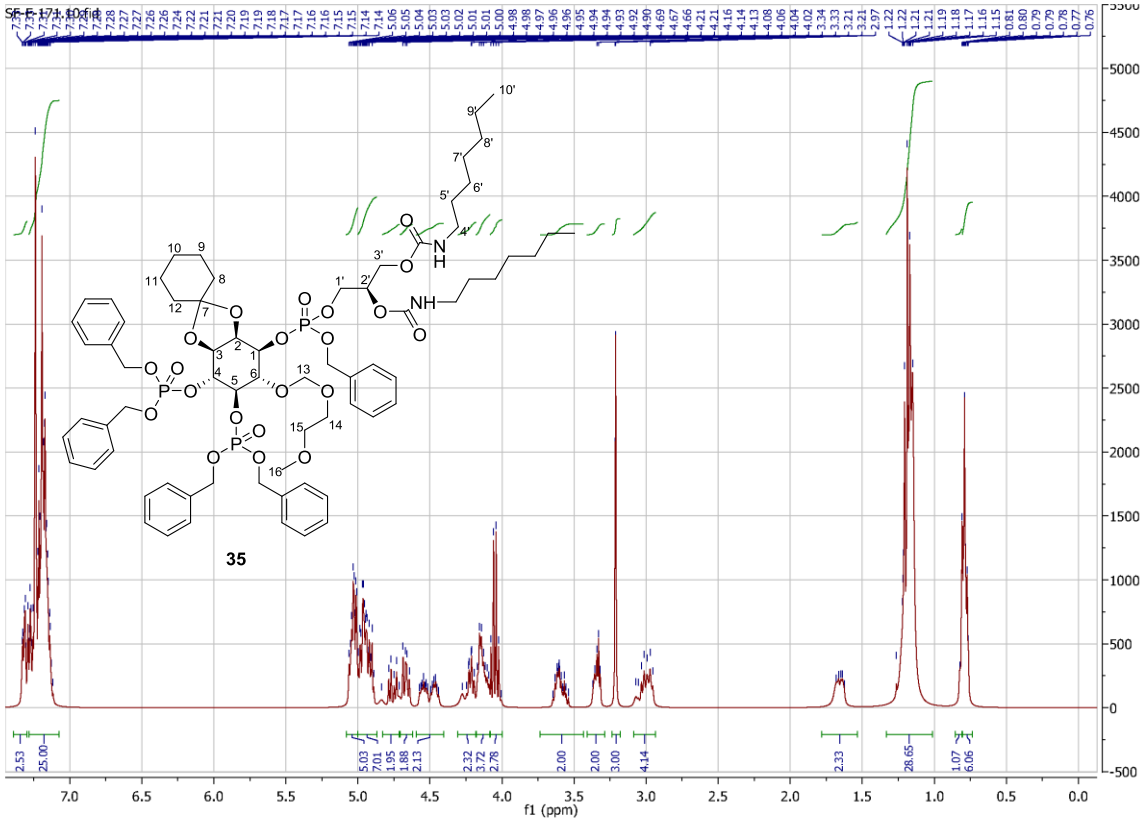
35
f1 (ppm)

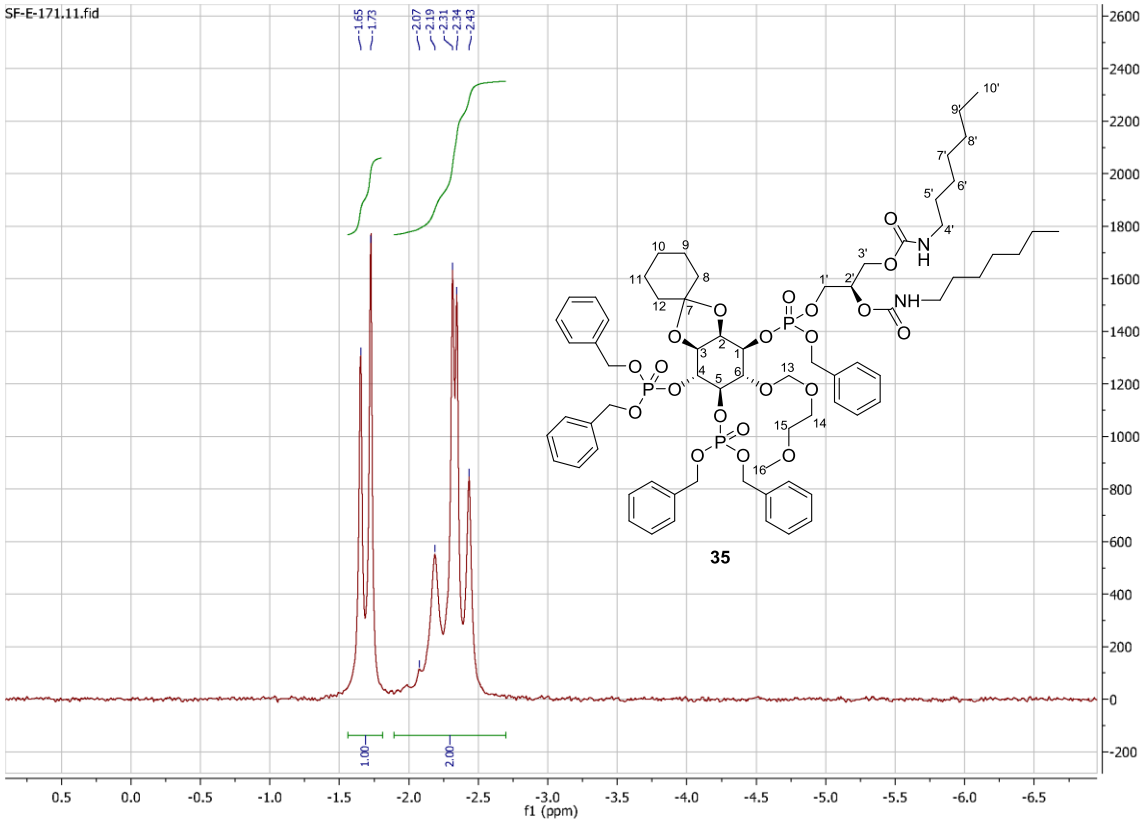
SF-E-171.11.fid
35
f1 (ppm)

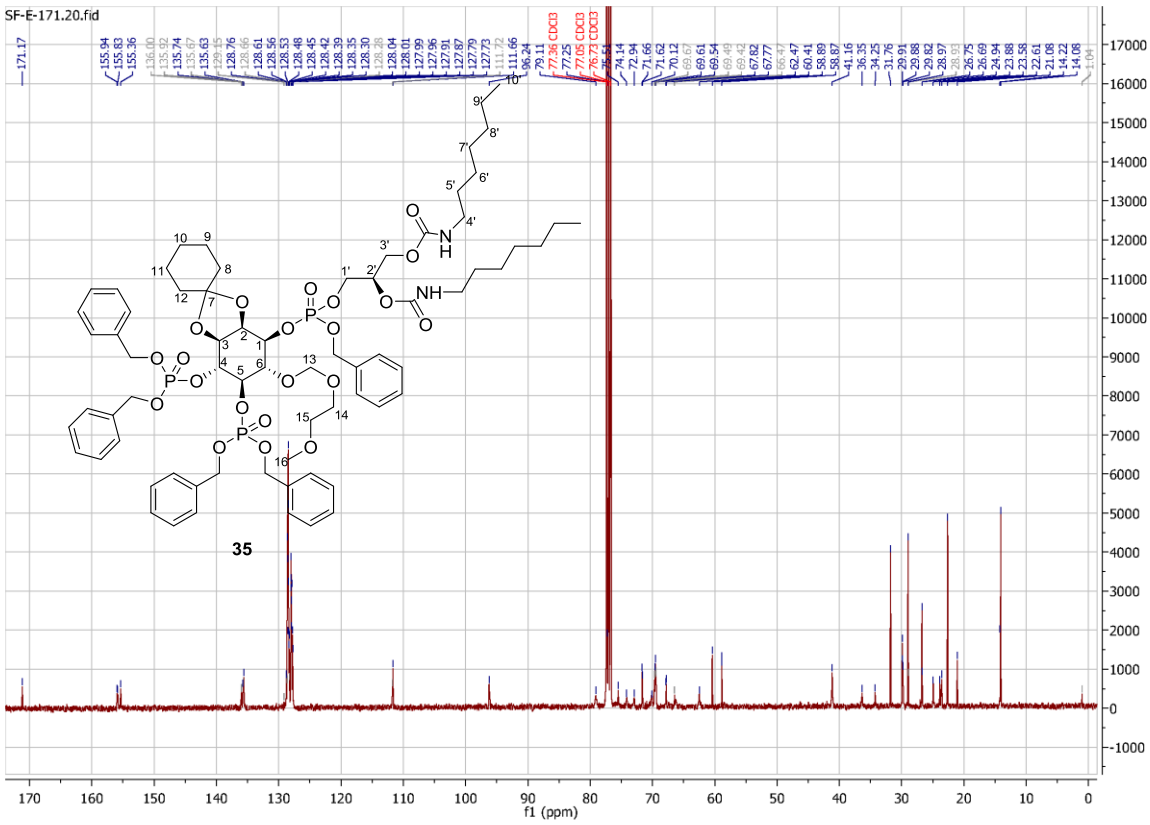
SF-E-171.20.fid
35
f1 (ppm)

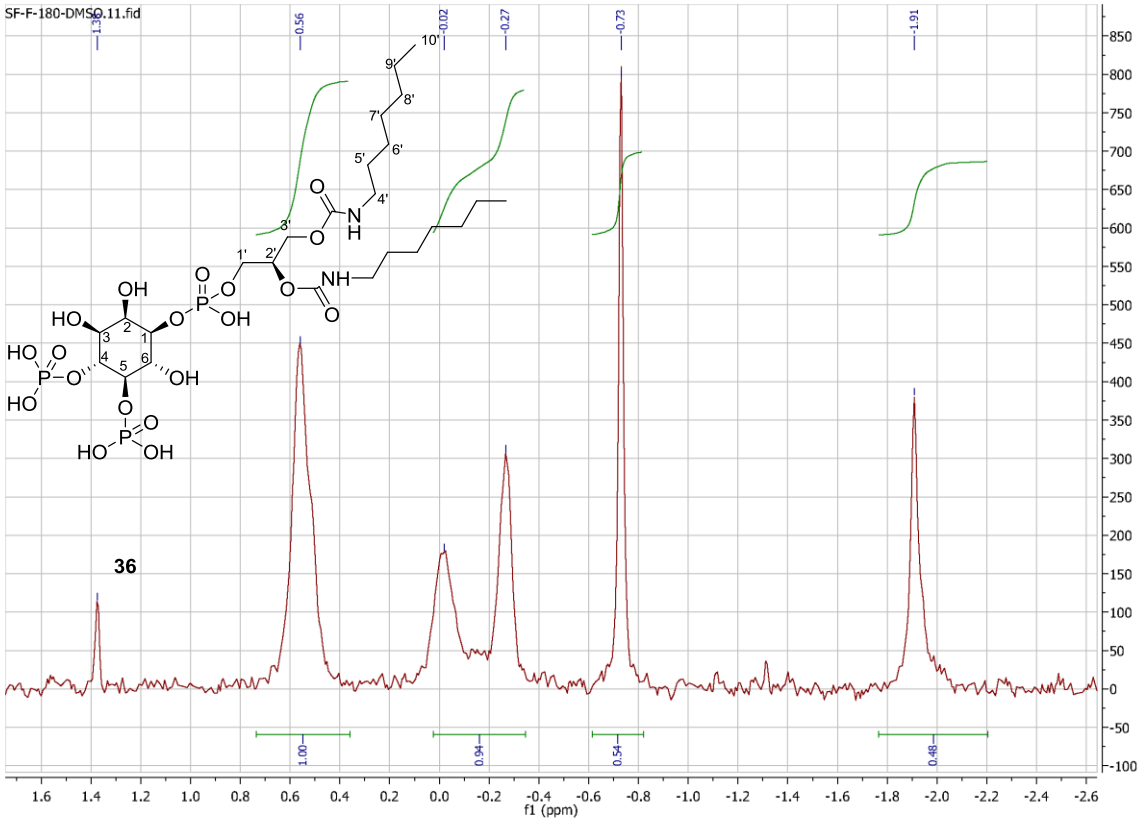
SF-F-180-DMSO.11.fid
36
f1 (ppm)

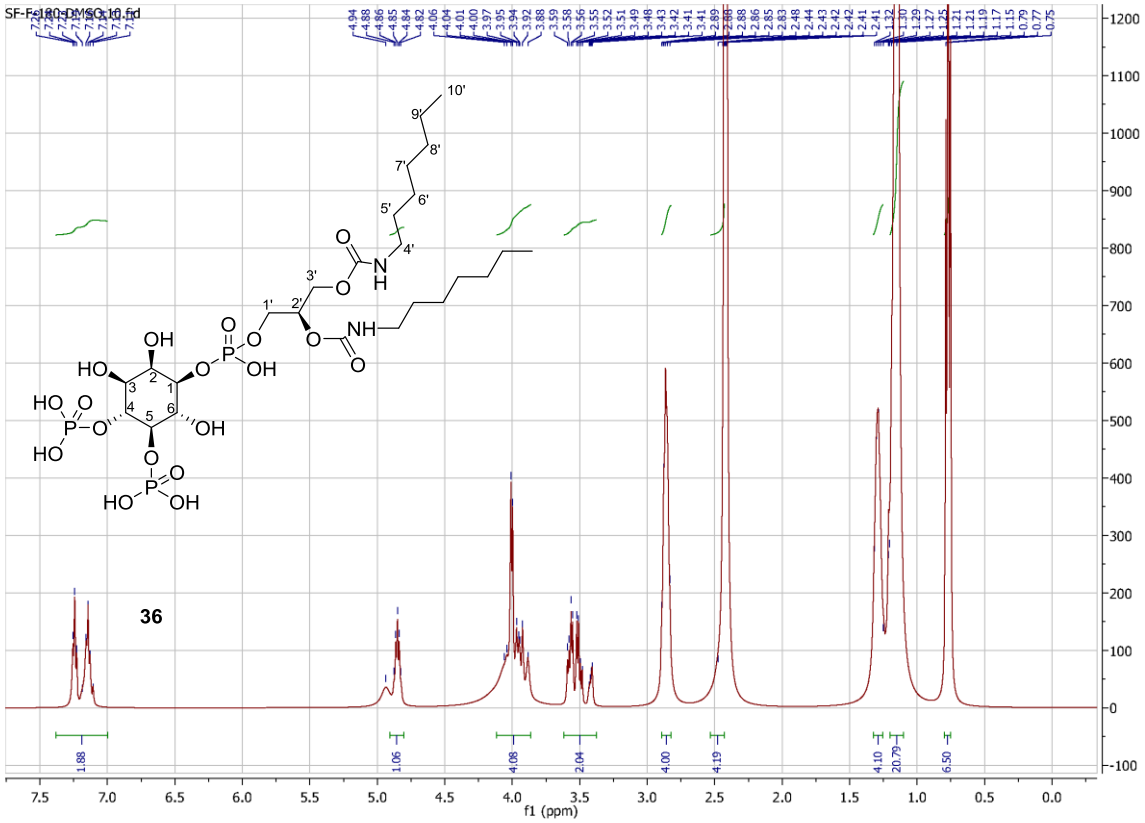
SF-F-180-DMSO.10.fid
36
f1 (ppm)

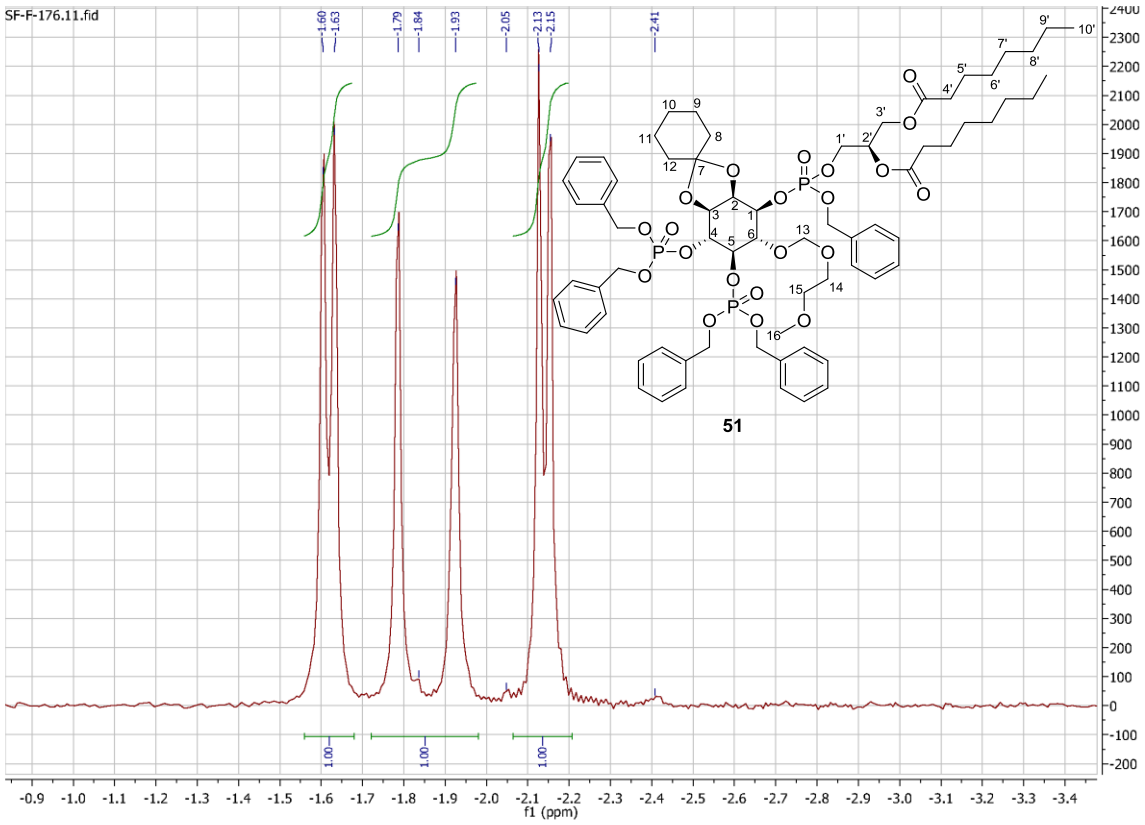
SF-F-176.11.fid
51
f1 (ppm)

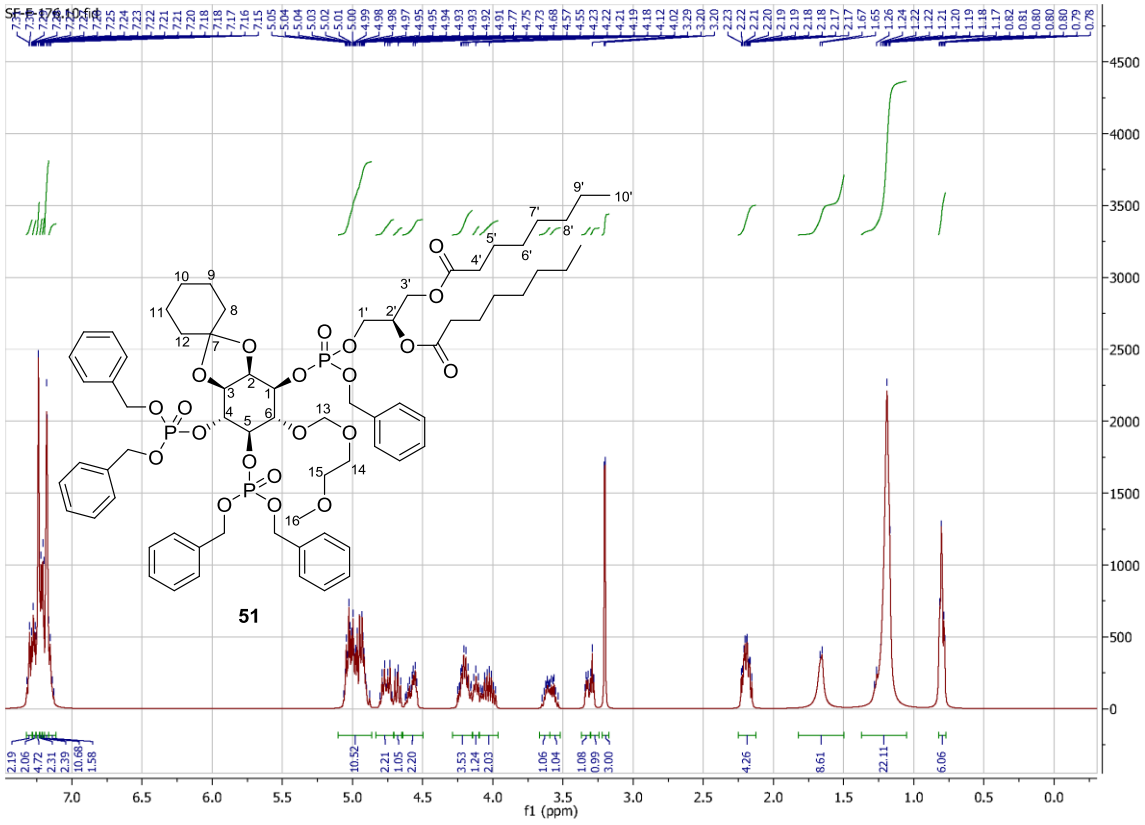
51
f1 (ppm)

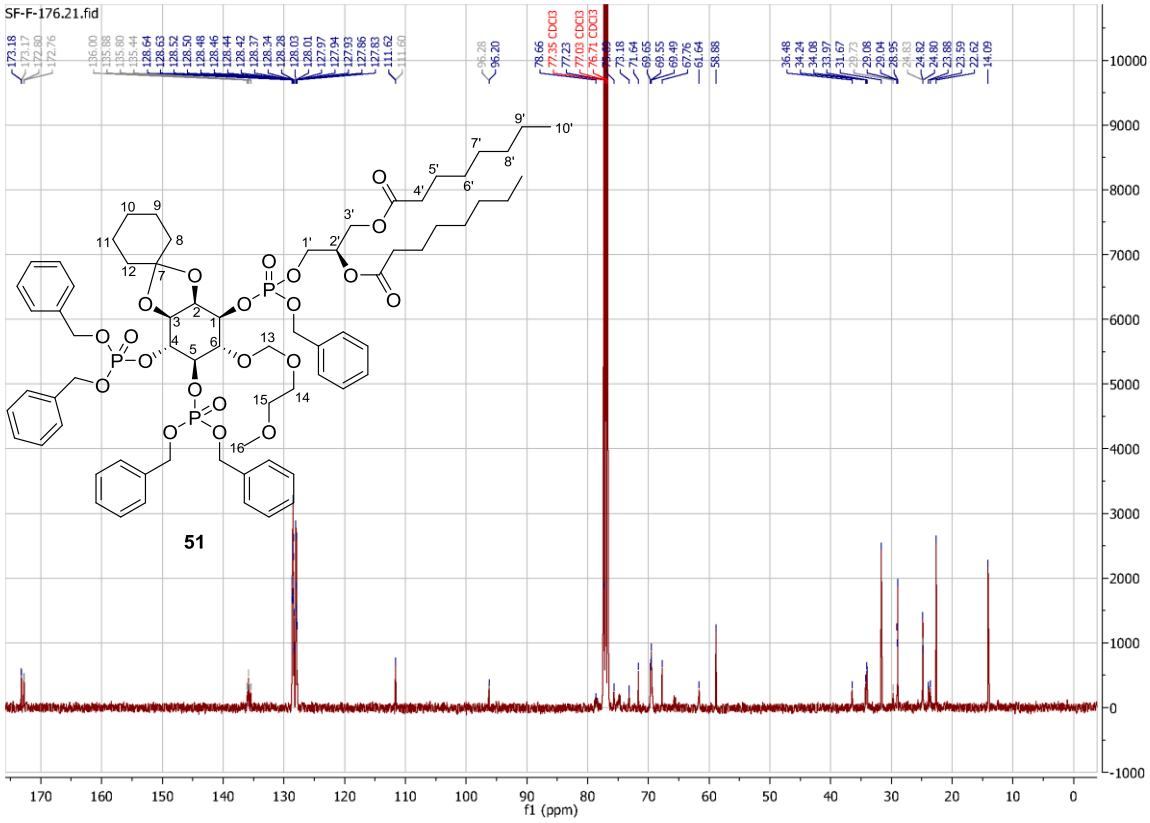
SF-F-176.21.fid
51
f1 (ppm)

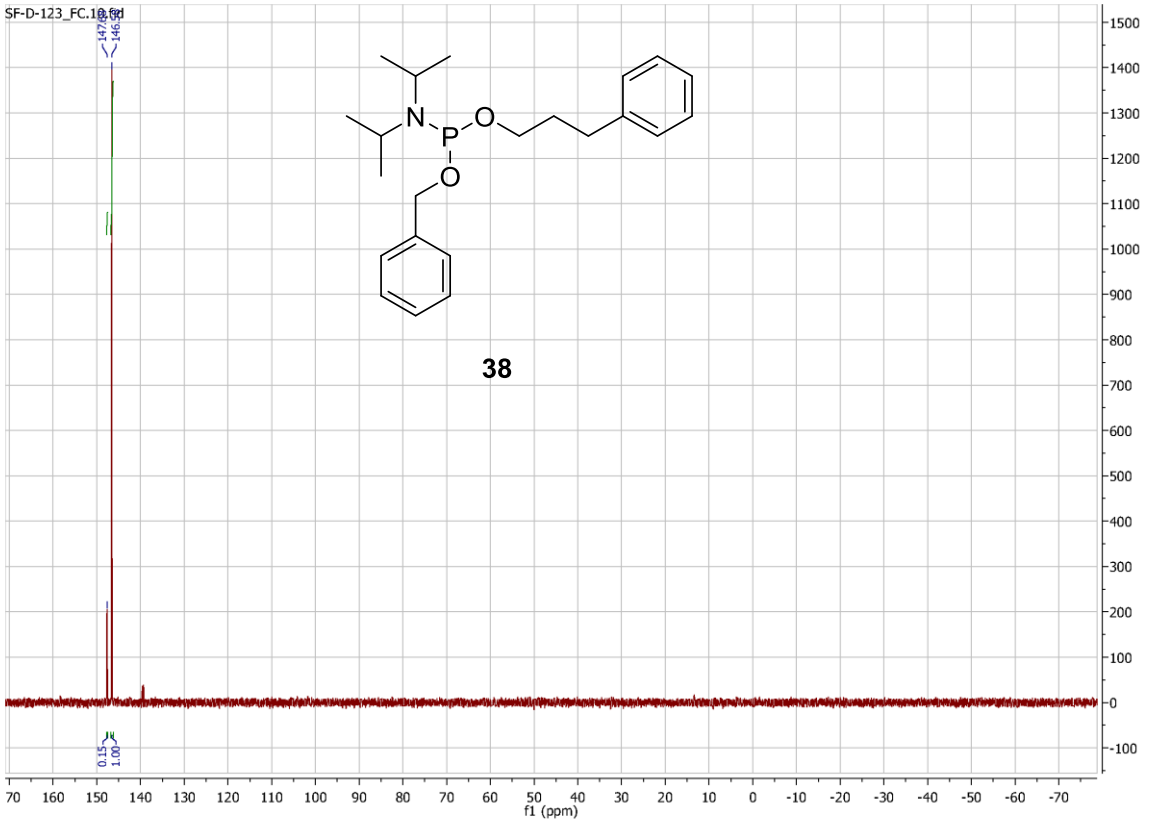
SF-D-123_FC.10.fid
38
f1 (ppm)

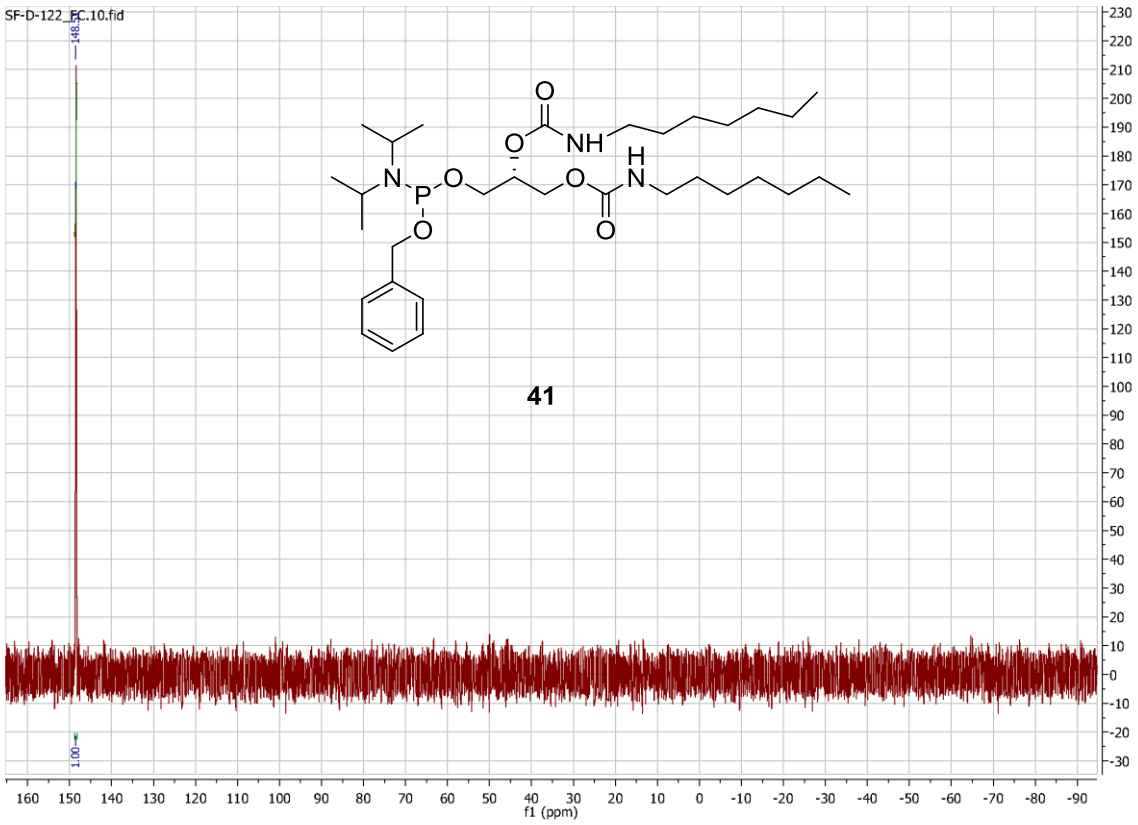
SF-D-122_EC.10.fid
148.5
1.00
f1 (ppm)

41

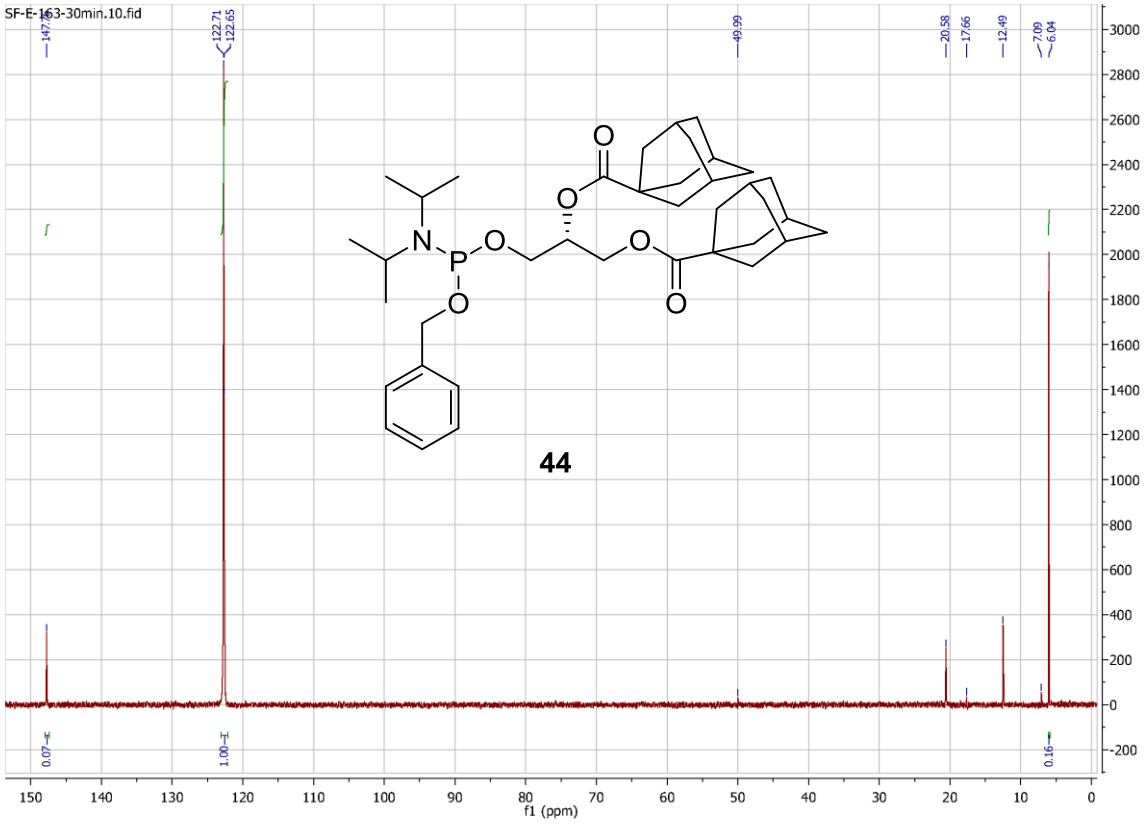
SF-E-163-30min.10.fid
147.76
122.71
122.65
49.99
20.58
17.66
12.49
7.09
6.04
0.07
1.00
0.16
f1 (ppm)

44

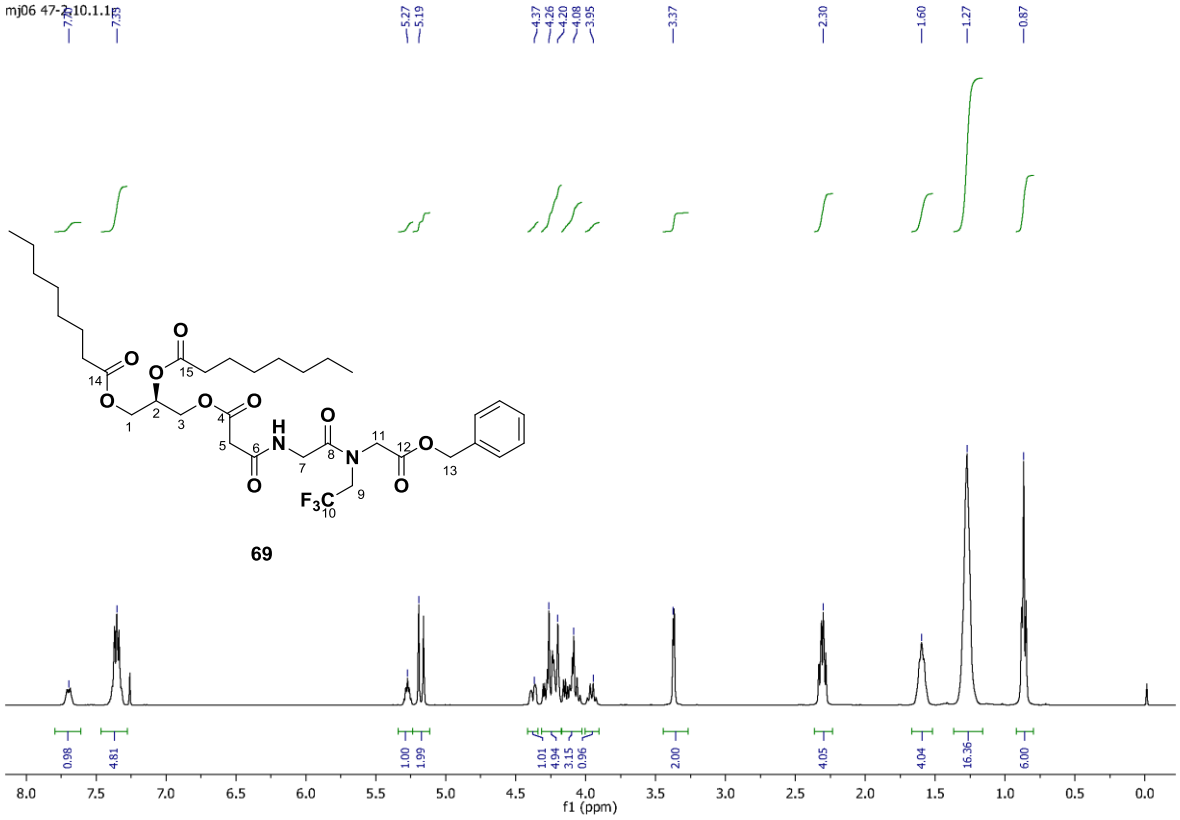
7.35
5.27
5.19
4.37
4.26
4.20
4.08
3.95
3.37
2.30
1.60
1.27
0.87
0.98
4.81
1.00
1.99
1.01
4.94
3.15
0.96
2.00
4.05
4.04
16.36
6.00
f1 (ppm)

69

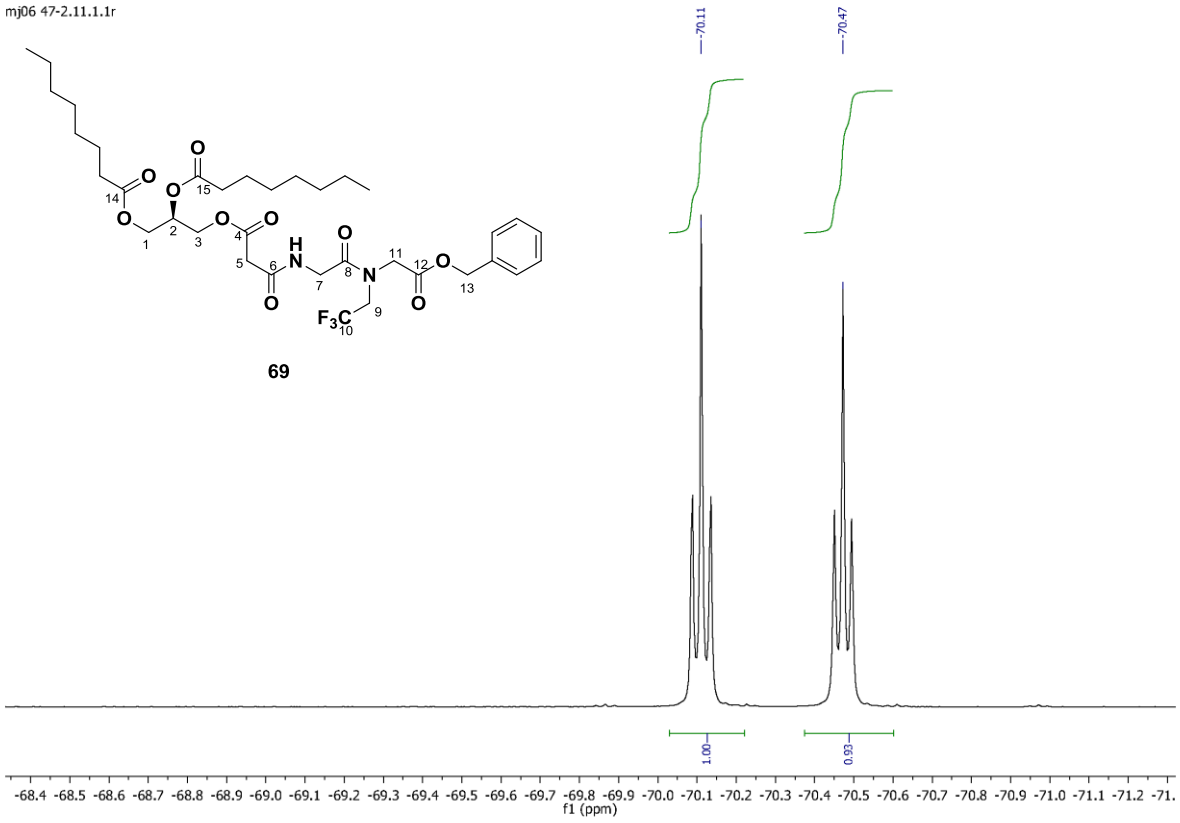
mj06 47-2.11.1.1r
-70.11
-70.47
1.00
0.93
f1 (ppm)

69

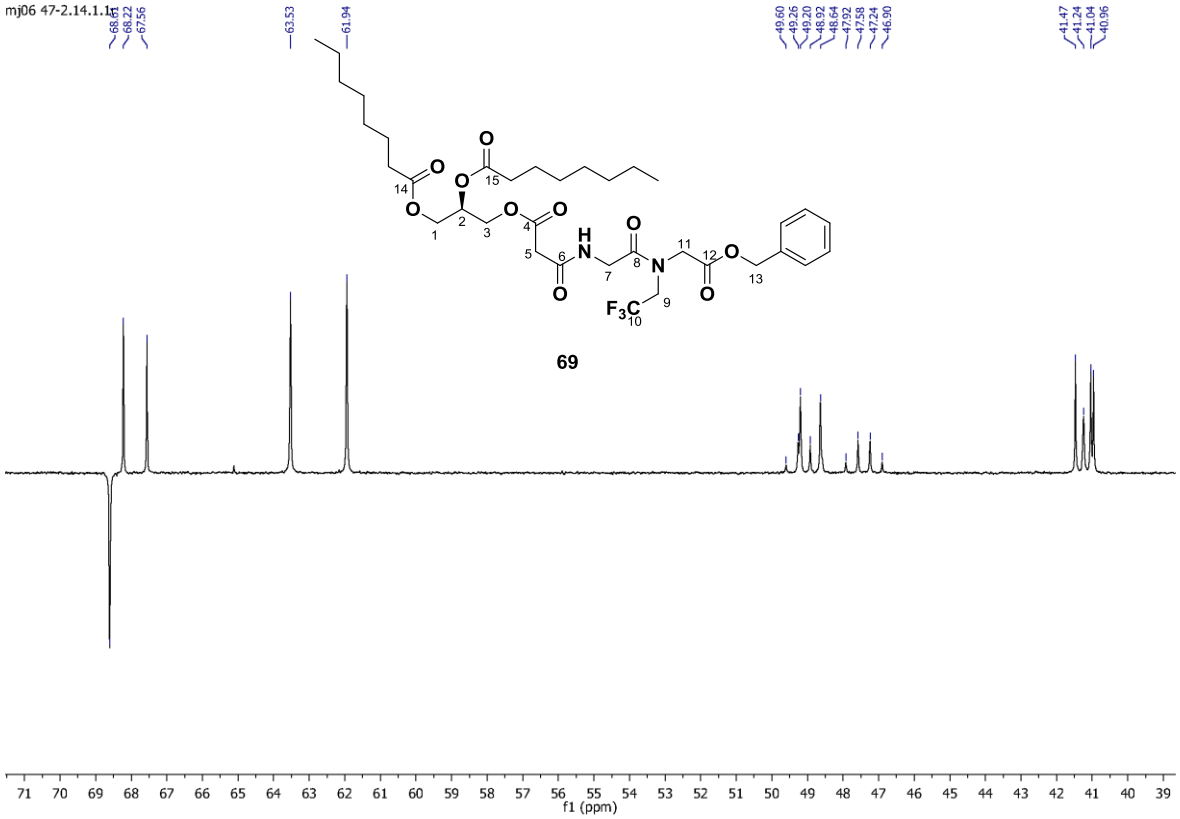
mj06 47-2.14.1.1r
68.61
68.22
67.56
63.53
61.94
49.60
49.26
49.20
48.92
48.64
47.92
47.58
47.24
46.90
41.47
41.24
41.04
40.96
69
71 70 69 68 67 66 65 64 63 62 61 60 59 58 57 56 55 54 53 52 51 50 49 48 47 46 45 44 43 42 41 40 39
f1 (ppm)

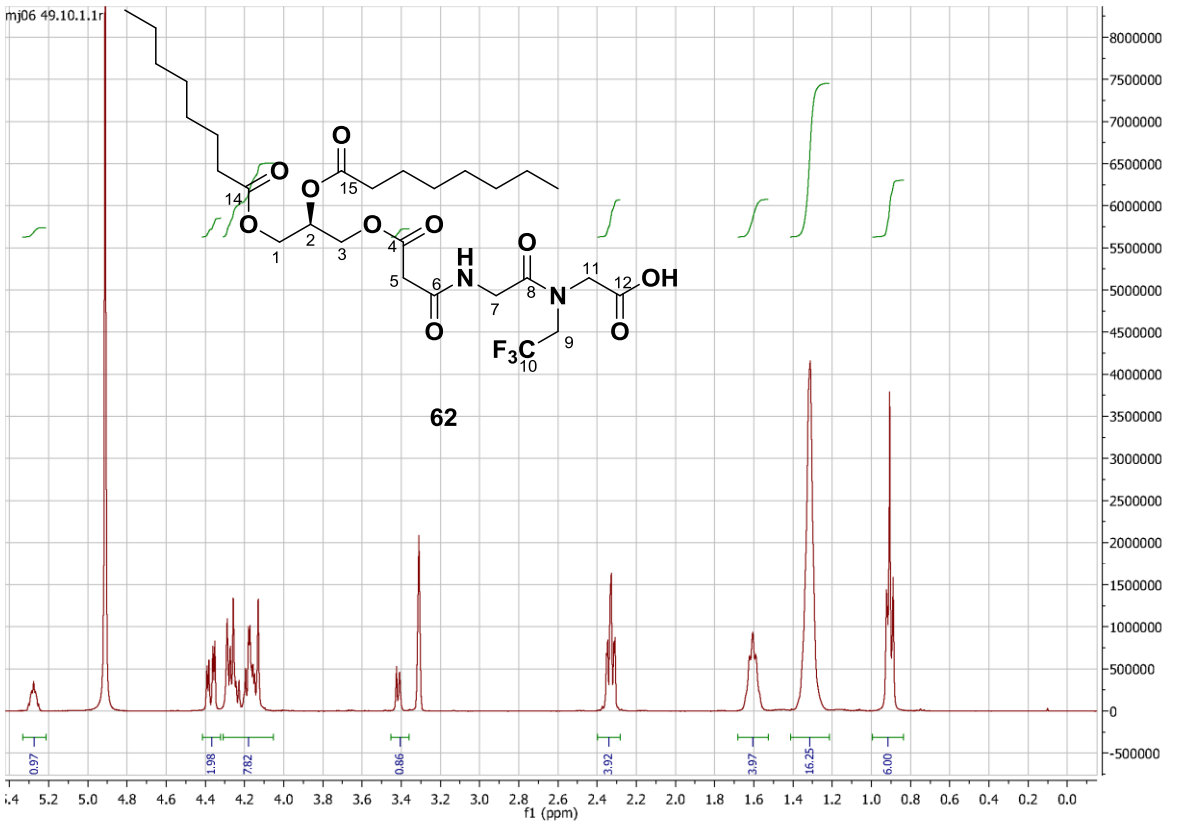
mj06 49.10.1.1r
62
8000000
7500000
7000000
6500000
6000000
5500000
5000000
4500000
4000000
3500000
3000000
2500000
2000000
1500000
1000000
500000
0
-500000
0.97
1.98
7.82
0.86
3.92
3.97
16.25
6.00
5.4 5.2 5.0 4.8 4.6 4.4 4.2 4.0 3.8 3.6 3.4 3.2 3.0 2.8 2.6 2.4 2.2 2.0 1.8 1.6 1.4 1.2 1.0 0.8 0.6 0.4 0.2 0.0
f1 (ppm)

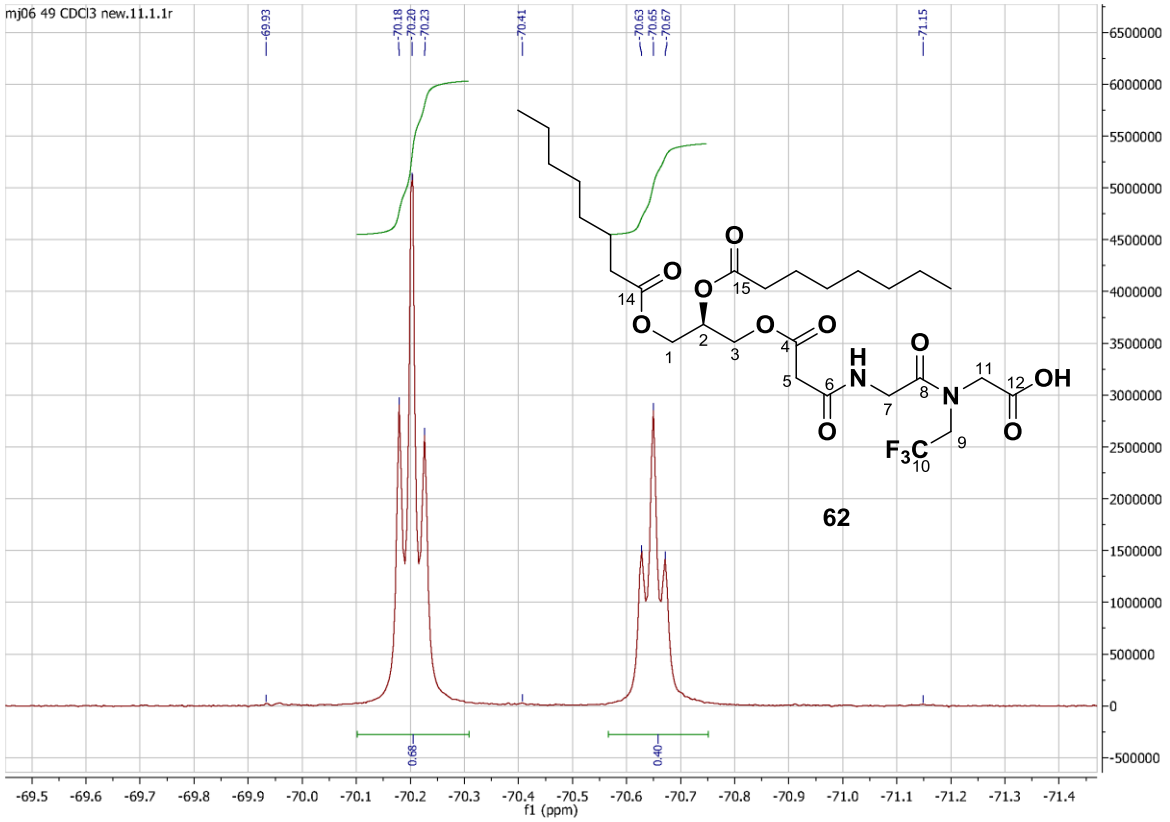
mj06 49 CDCl3 new.11.1.1r
-69.93
-70.18
-70.20
-70.23
-70.41
-70.63
-70.65
-70.67
-71.15
0.68
0.40
f1 (ppm)
62

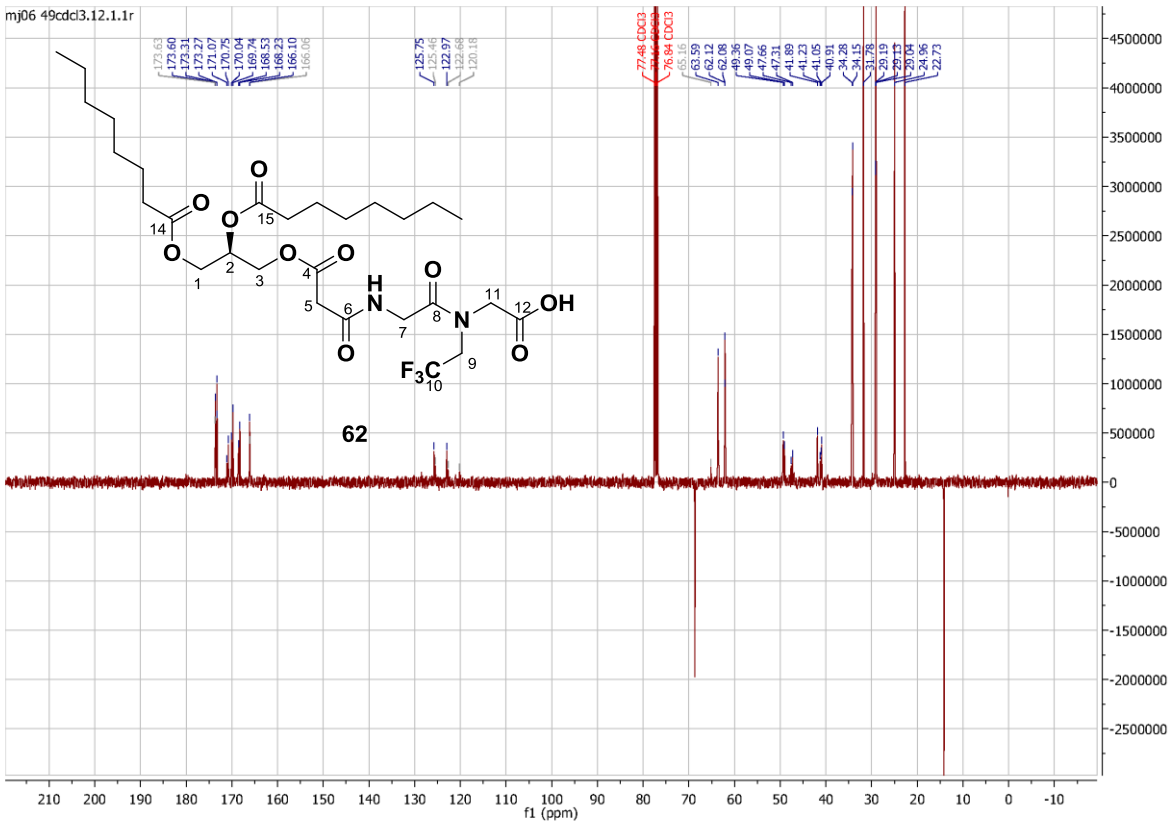
mj06 49cdcl3.12.1.1r
f1 (ppm)
62

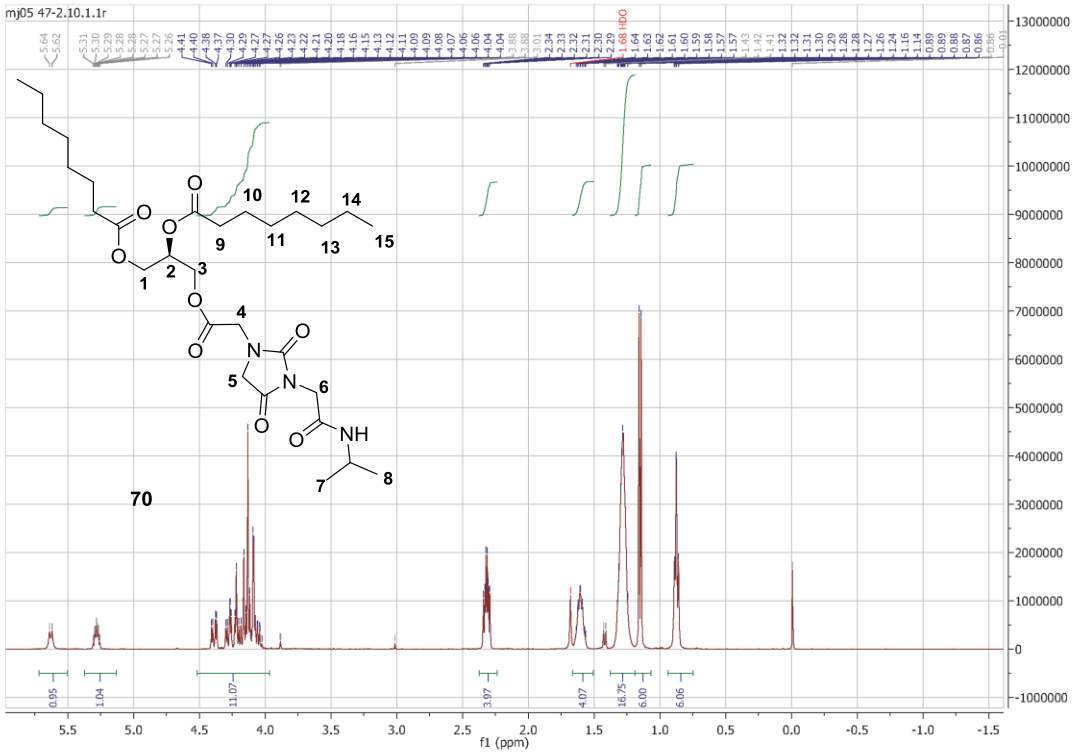
mj05 47-2.10.1.1r
70
f1 (ppm)

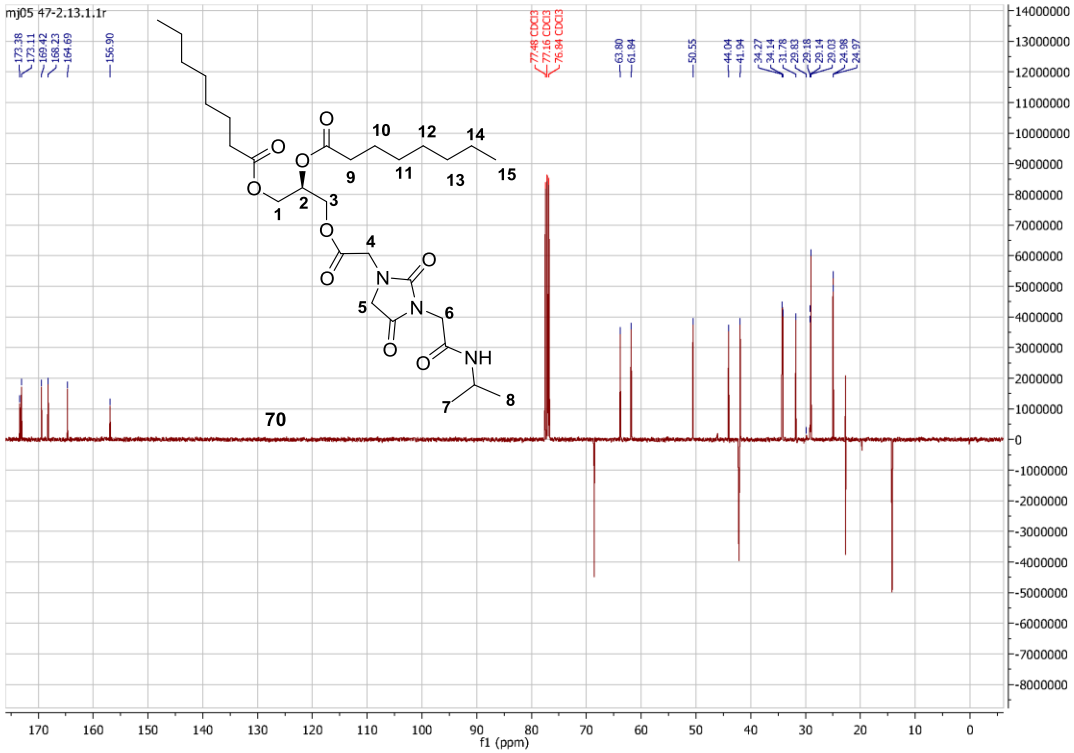
mj05 47-2.13.1.1r
70
f1 (ppm)

7.4. Supplementary Figures

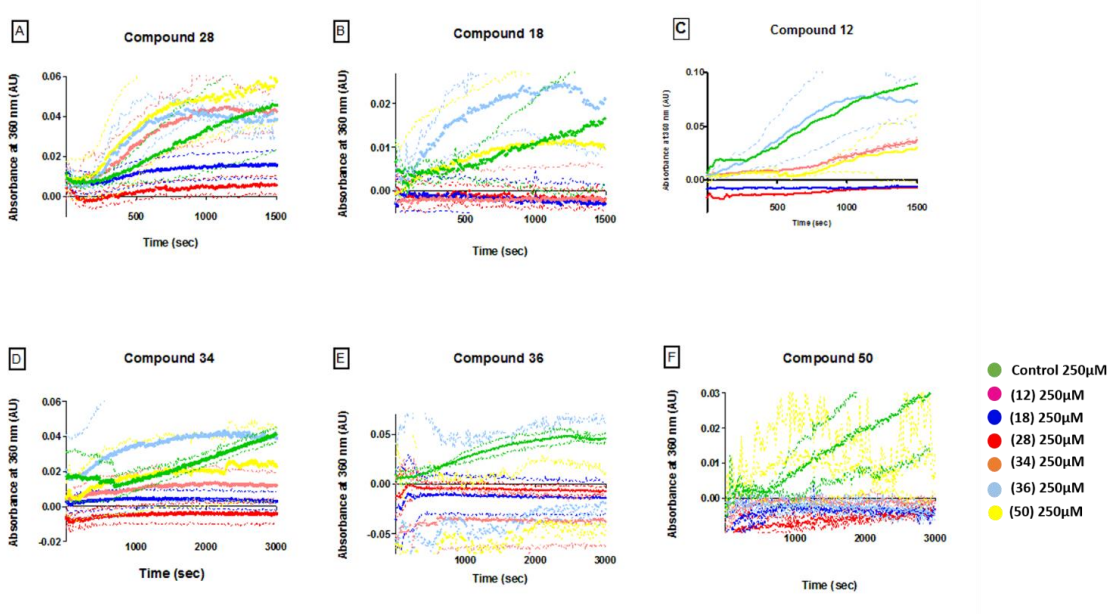

Figure **S1** The dephosphorylation activity of PRL-3 toward the PI(4,5)P_2 analogues, at 5 different concentrations (25, 50, 100, 200 and 250 µM). The slopes are shown until 1500-3000 seconds of measurements because of the signal variation observed after that time point in all assays, which could either be due to the precipitation of the protein or the interaction of the analogues with the photoactive component in the assay. A) Absorbance measurements of compound **28**. B) Absorbance measurements of compound **18**. C) Absorbance measurements of compound **34**. D) Absorbance measurements of compound **12**. E) and F), Absorbance measurements of compounds **36** and **50**, respectively: those compounds were not active against PRL-3. Graphs are shown with error bars, depicted as dotted lines above and below each respective curve. The lower the signal intensity, the higher the relative error in the assay[18,19,120], leading to error bars that would mask other curves.

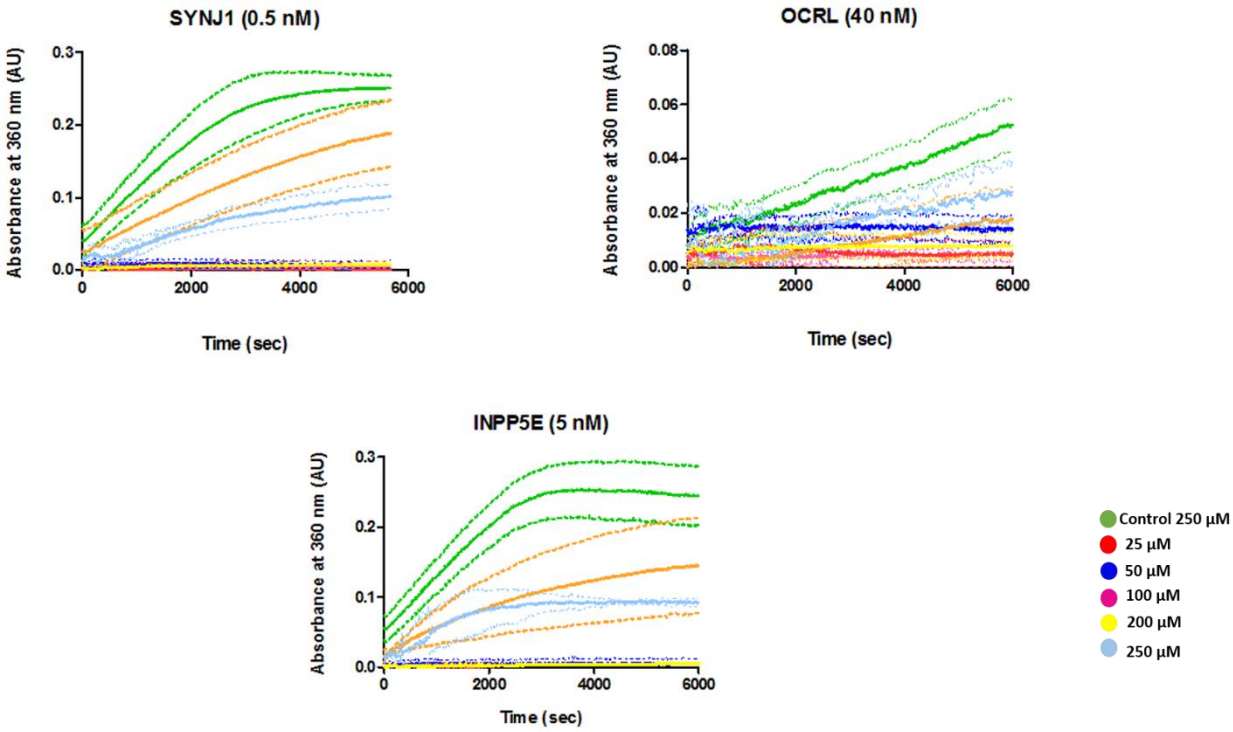

Figure **S2** Activity of the six synthesized analogues with three different PI(4,5)P_2-metabolizing phosphatases, with respect to the parent substrate (control) PI(4,5)P_2. The results shown in the graphs take into consideration the error margins (dotted lines above and below each curve) of each experiment replicates.

References

(1) Moorhead, G. B. G., Wever, V. D. E., Templeton, G., and Kerk, D. (2009) Evolution of protein phosphatases in plants and animals. *Biochem. J 409*, 401–409.

(2) Cohen, P. T. W. (2004) Protein Phosphatases (Ariño, J. n., and Alexander, D. R., Eds.), pp 1–20. Springer Berlin Heidelberg, Berlin, Heidelberg.

(3) Cohen, P. (2002) The origins of protein phosphorylation. *Nat. Cell Biol. 4*, E127–E130.

(4) Alonso, A., Sasin, J., Bottini, N., Friedberg, I., Friedberg, I., Osterman, A., Godzik, A., Hunter, T., Dixon, J., and Mustelin, T. (2004) Protein tyrosine phosphatases in the human genome. *Cell 117*, 699–711.

(5) Manning, G., Plowman, G. D., Hunter, T., and Sudarsanam, S. (2002) Evolution of protein kinase signaling from yeast to man. *Trends Biochem. Sci. 27*, 514–520.

(6) Hunter, T. (2003) Protein phosphorylation: what does the future hold?, in *Life Sciences for the 21st Century* (E. Keinan, I. Schechter, and M. S., Ed.), pp 191–223. Wiley-VCH.

(7) Tonks, N. K. (2006) Protein tyrosine phosphatases: from genes, to function, to disease. *Nat. Rev. Mol. Cell Biol. 7*, 833–846.

(8) Fahs, S., Lujan, P., and Köhn, M. (2016) Approaches to Study Phosphatases. *ACS Chem. Biol. 11*, 2944–2961.

(9) Li, X., Wilmanns, M., Thornton, J., and Köhn, M. (2013) Elucidating human phosphatase-substrate networks. *Sci. Signal. 6*, rs10.

(10) Tonks, N. K. (2013) Protein tyrosine phosphatases - From housekeeping enzymes to master regulators of signal transduction. *FEBS J. 280*, 346–378.

(11) Brautigan, D. L. (2013) Protein Ser/Thr phosphatases--the ugly ducklings of cell signalling. *FEBS J. 280*, 324–345.

(12) Duan, G., Li, X., and Köhn, M. (2015) The human DEPhOsphorylation database DEPOD: a 2015 update. *Nucleic Acids Res. 43*, D531–D5315.

(13) Shi, Y. (2009) Review Serine / Threonine Phosphatases : Mechanism through Structure. *Cell 139*, 468–484.

(14) Chen, M. J., Dixon, J. E., and Manning, G. (2017) Genomics and evolution of protein phosphatases. *Sci. Signallig 54*, 1–18.

(15) Hsu, F., and Mao, Y. (2015) The structure of phosphoinositide phosphatases: Insights into substrate specificity and catalysis. *Biochim. Biophys. Acta 1851*, 698–710.

(16) Liu, Y., and Bankaitis, V. A. (2010) Phosphoinositide Phosphatases in Cell Biology and Disease. *Prog. Lipid Res. 49*, 201–217.

(17) Oganesian, A., Poot, M., Daum, G., Coats, S. A., Wright, M. B., Seifert, R. A., and Bowen-Pope, D. F. (2003) Protein tyrosine phosphatase RQ is a phosphatidylinositol phosphatase that can regulate cell survival and proliferation. *PNAS 100*, 7563–7568.
(18) Hoeger, B., Rios, P., Berteotti, A., Hoermann, B., Duan, G., and Köhn, M. (2017) Mutational Analysis of a Conserved Glutamate Reveals Unique Mechanistic and Structural Features of the Phosphatase PRL-3. *ACS Omega 2*, 9171–9180.
(19) McParland, V., Varsano, G., Li, X., Thornton, J., Baby, J., Aravind, A., Meyer, C., Pavic, K., Rios, P., and Köhn, M. (2011) The metastasis-promoting phosphatase PRL-3 shows activity toward phosphoinositides. *Biochemistry 50*, 7579–7590.
(20) Rios, P., Li, X., and Köhn, M. (2013) Molecular mechanisms of the PRL phosphatases. *FEBS J. 280*, 505–524.
(21) Xie, L., Zhang, Y. L., and Zhang, Z. Y. (2002) Design and characterization of an improved protein tyrosine phosphatase substrate-trapping mutant. *Biochemistry 41*, 4032–4039.
(22) Foy, M., Anézo, O., Saule, S., and Planque, N. (2017) PRL-3/PTP4A3 phosphatase regulates integrin β1 in adhesion structures during migration of human ocular melanoma cells.
(23) Sharlow, E. R., Wipf, P., Mcqueeney, K. E., Bakan, A., and Lazo, J. S. (2014) Investigational inhibitors of PTP4A3 phosphatase as antineoplastic agents. *Expert Opin. Investig. Drugs 23*, 1–13.
(24) Zhang, Z.-Y. (1998) Protein-Tyrosine Phosphatases: Biological Function, Structural Characteristics, and Mechanism of Catalysis. *Crit. Rev. Biochem. Mol. Biol. 33*, 1–52.
(25) Kozlov, G., Cheng, J., Ziomek, E., Banville, D., Gehring, K., and Ekiel, I. (2004) Structural Insights into Molecular Function of the Metastasis-associated Phosphatase PRL-3. *J. Biol. Chem. 279*, 11882–11889.
(26) Xiao, J., Engel, J. L., Zhang, J., Chen, M. J., Manning, G., and Dixon, J. E. Structural and functional analysis of PTPMT1, a phosphatase required for cardiolipin synthesis.
(27) Ríos, P., Nunes-Xavier, C. E., Tabernero, L., Köhn, M., and Pulido, R. (2014) Dual-Specificity Phosphatases as Molecular Targets for Inhibition in Human Disease. *Antioxid. Redox Signal. 20*, 2251–2273.
(28) Tautz, L., Critton, D. A., and Grotegut, S. (2013) Protein Tyrosine Phosphatases: Structure, Function, and Implication in Human Disease, pp 179–221. Humana Press, Totowa, NJ.
(29) Bessette, D. C., Qiu, D., and Pallen, C. J. (2008) PRL PTPs: mediators and markers of cancer progression. *Cancer Metastasis Rev 27*, 231–252.
(30) Thura, M., Qader Omer Al-Aidaroos, A., Peng Yong, W., Kono, K., Gupta, A., Bin Lin,

Y., Mimura, K., Paul Thiery, J., Cher Goh, B., Tan, P., Soo, R., William Hong, C., Wang, L., Joyce Lin, S., Chen, E., Young Rha, S., Cheol Chung, H., Li, J., Nandi, S., Fung Yuen, H., Zhang, S.-D., Khay Guan, Y., and Zeng, Q. (2016) PRL3-zumab, a first-in-class humanized antibody for cancer therapy. *JCI Insight 1*, 1–15.

(31) Xing, X., Peng, L., Qu, L., Ren, T., Dong, B., Su, X., and Shou, C. (2009) Prognostic value of PRL-3 overexpression in early stages of colonic cancer. *Histopathology 54*, 309–318.

(32) Wang, Z., Cai, S.-R., He, Y.-L., Zhan, W.-H., Zhang, C.-H., Wu, H., Peng, J.-J., Xu, J.-B., Zhang, X.-H., Wang, L., and Song, W. (2009) Elevated PRL-3 expression was more frequently detected in the large primary gastric cancer and exhibits a poor prognostic impact on the patients. *J. Cancer Res. Clin. Oncol. 135*, 1041–1046.

(33) Wang, L., Peng, L., Dong, B., Kong, L., Meng, L., Yan, L., Xie, Y., and Shou, C. (2006) Overexpression of phosphatase of regenerating liver-3 in breast cancer: association with a poor clinical outcome. *Ann. Oncol. 17*, 1517–1522.

(34) Polato, F., Codegoni, A., Fruscio, R., Perego, P., Mangioni, C., Saha, S., Bardelli, A., and Broggini, M. (2005) PRL-3 phosphatase is implicated in ovarian cancer growth. *Clin. Cancer Res. 11*, 6835–9.

(35) Al-Aidaroos, A. Q. O., and Zeng, Q. (2010) PRL-3 phosphatase and cancer metastasis. *J. Cell. Biochem. 111*, 1087–1098.

(36) Ming, J., Liu, N., Gu, Y., Qiu, X., and Wang, E.-H. (2009) PRL-3 facilitates angiogenesis and metastasis by increasing ERK phosphorylation and up-regulating the levels and activities of Rho-A/C in lung cancer. *Pathology 41*, 118–126.

(37) Liu, Y., Zhou, J., Chen, J., Gao, W., Le, Y., Ding, Y., and Li, J. (2009) PRL-3 promotes epithelial mesenchymal transition by regulating cadherin directly. *Cancer Biol. Ther. 8*, 1352–9.

(38) Sun, Y., Carroll, S., Kaksonen, M., Toshima, J. Y., and Drubin, D. G. (2007) PtdIns(4,5)P2 turnover is required for multiple stages during clathrin- and actin-dependent endocytic internalization. *J. Cell Biol. 177*, 355–367.

(39) Rubio, T., and Köhn, M. Regulatory mechanisms of phosphatase of regenerating liver (PRL)-3.

(40) Krndija, D., Münzberg, C., Maass, U., Hafner, M., Adler, G., Kestler, H. a, Seufferlein, T., Oswald, F., and von Wichert, G. (2012) The phosphatase of regenerating liver 3 (PRL-3) promotes cell migration through Arf-activity-dependent stimulation of integrin α5 recycling. *J. Cell Sci. 125*, 3883–9382.

(41) Forte, E., Orsatti, L., Talamo, F., Barbato, G., De Francesco, R., and Tomei, L. (2007) Ezrin is a specific and direct target of protein tyrosine phosphatase PRL-3.

(42) Zheng, P., Liu, Y.-X., Chen, L., Liu, X.-H., Xiao, Z.-Q., Zhao, L., Li, G.-Q., Zhou, J., Ding, Y.-

Q., and Li, J.-M. Stathmin, a New Target of PRL-3 Identified by Proteomic Methods, Plays a Key Role in Progression and Metastasis of Colorectal Cancer.
(43) Mizuuchi, E., Semba, S., Kodama, Y., and Yokozaki, H. (2009) Down-modulation of keratin 8 phosphorylation levels by PRL-3 contributes to colorectal carcinoma progression. *Int. J. Cancer 124*, 1802–1810.
(44) Fang, X.-Y., Song, R., Chen, W., Yang, Y.-Y., Gu, Y.-H., Shu, Y.-Q., Wu, X.-D., Wu, X.-F., Sun, Y., Shen, Y., and Xu, Q. (2015) PRL-3 Promotes the Malignant Progression of Melanoma via Triggering Dephosphorylation and Cytoplasmic Localization of NHERF1. *J. Invest. Dermatol. 135154*, 2273–2282.
(45) Prl, V., Jeong, K., Kang, D., Lee, E., Shin, A., Jin, B., Park, Y., Lee, C., Kim, E., Jeon, Y. H., Kim, E. E., and Kim, Y. (2014) Structure and Backbone Dynamics of Vanadate-Bound PRL-3: Comparison of 15 N Nuclear Magnetic Resonance Relaxation Pro fi les of Free and Vanadate-Bound PRL ‑ 3. *Biochemistry 53*, 4814–4825.
(46) Kim, K.-A., Song, J.-S., Jee, J., Sheen, M. R., Lee, C., Lee, T. G., Ro, S., Cho, J. M., Lee, W., Yamazaki, T., Jeon, Y. H., and Cheong, C. (2004) Structure of human PRL-3, the phosphatase associated with cancer metastasis. *FEBS Lett. 565*, 181–187.
(47) Bunney, T. D., and Katan, M. (2010) Phosphoinositide signalling in cancer: beyond PI3K and PTEN.
(48) He, R., Zeng, L.-F., He, Y., Zhang, S., and Zhang, Z.-Y. (2013) Small molecule tools for functional interrogation of protein tyrosine phosphatases. *FEBS J. 280*, 731–750.
(49) Cole, P. A., Courtney, A. D., Shen, K., Zhang, Z., Qiao, Y., Lu, W., and Williams, D. M. (2003) Chemical Approaches to Reversible Protein Phosphorylation. *Acc. Chem. Res. 36*, 444–452.
(50) Vintonyak, V. V, Waldmann, H., and Rauh, D. (2011) Using small molecules to target protein phosphatases. *Bioorg. Med. Chem. 19*, 2145–2155.
(51) Pathak, M. K., Dhawan, D., Lindner, D. J., Borden, E. C., Farver, C., Yi, T., and Center, T. C. (2002) Pentamidine Is an Inhibitor of PRL Phosphatases with Anticancer Activity. *Mol. Cancer Ther. 1*, 1255–1264.
(52) Daouti, S., Li, W., Qian, H., Huang, K.-S., Holmgren, J., Levin, W., Reik, L., McGady, D. L., Gillespie, P., Perrotta, A., Bian, H., Reidhaar-Olson, J. F., Bliss, S. a, Olivier, A. R., Sergi, J. a, Fry, D., Danho, W., Ritland, S., Fotouhi, N., Heimbrook, D., and Niu, H. (2008) A selective phosphatase of regenerating liver phosphatase inhibitor suppresses tumor cell anchorage-independent growth by a novel mechanism involving p130Cas cleavage. *Cancer Res. 68*, 1162–1169.
(53) Hoeger, B., Diether, M., Ballester, P. J., and Köhn, M. (2014) Biochemical evaluation of virtual screening methods reveals a cell-active inhibitor of the cancer-promoting

phosphatases of regenerating liver. *Eur. J. Med. Chem. 88*, 1–12.
(54) Ballester, P. J. (2011) Ultrafast shape recognition : method and applications. *Futur. Med. Chem. 3*, 65–78.
(55) Ballester, P. J., and Richards, W. G. (2006) Ultrafast Shape Recognition to Search Compound Databases for Similar Molecular Shapes. *Wiley Intersci. 28*, 1711–1723.
(56) Zhang, H., Kozlov, G., Li, X., Wu, H., Gulerez, I., and Gehring, K. PRL3 phosphatase active site is required for binding the putative magnesium transporter CNNM3.
(57) Ballester, P. J., Finn, P. W., and Richards, W. G. (2009) Ultrafast shape recognition: Evaluating a new ligand-based virtual screening technology. *J. Mol. Graph. Model. 27*, 836–845.
(58) Best, M. D., Zhang, H., and Prestwich, G. D. (2010) Inositol polyphosphates, diphosphoinositol polyphosphates and phosphatidylinositol polyphosphate lipids: structure, synthesis, and development of probes for studying biological activity. *Nat. Prod. Rep. 27*, 1403–1430.
(59) Michell, R. H. (2008) Inositol derivatives: evolution and functions. *Nat. Rev. Mol. Cell Biol. 9*, 151–161.
(60) Cho, W., and Stahelin, R. V. (2005) MEMBRANE-PROTEIN INTERACTIONS IN CELL SIGNALING AND MEMBRANE TRAFFICKING. *Annu. Rev. Biophys. Biomol. Struct 34*, 119–51.
(61) Sprong, H., van der Sluijs, P., and van Meer, G. (2001) How proteins move lipids and lipids move proteins. *Nat. Rev. Mol. Cell Biol. 2*, 504–513.
(62) Toker, A. Phosphoinositides and signal transduction.
(63) Corvera, S. (2001) Phosphatidylinositol 3-Kinase and the Control of Endosome Dynamics: New Players Defined by Structural Motifs. *Traffic 2*, 859–866.
(64) Czech, M. P. (2000) PIP2 and PIP3: Complex Roles Minireview at the Cell Surface movements of the PI3K rather than PIP3 itself. Now, effective reagents for localization of PIP2 and PIP3 within cells have become available with the discovery. *Cell 100*, 603–606.
(65) Di Paolo, G., and De Camilli, P. Phosphoinositides in cell regulation and membrane dynamics.
(66) Pendaries, C., Tronchère, H., Plantavid, M., and Payrastre, B. (2003) Phosphoinositide signaling disorders in human diseases. *FEBS Lett. 546*, 25–31.
(67) Vicinanza, M., Dangelo, G., Campli, A. Di, and De Matteis, M. A. Phosphoinositides as regulators of membrane trafficking in health and disease.
(68) Wymann, M. P., and Schneiter, R. (2008) Lipid signalling in disease. *Nat. Rev. Mol. Cell Biol. 9*, 162–176.
(69) Lemmon, M. A. (2008) Membrane recognition by phospholipid-binding domains.

Nat. Rev. Mol. Cell Biol. 9, 99–111.
(70) Wymann, M. P., Zvelebil, M., and Laffargue, M. Phosphoinositide 3-kinase signalling – which way to target?
(71) Wymann, M. P., and Schneiter, R. (2008) Lipid signalling in disease. *Nat Rev Mol Cell Biol. 9*, 162–176.
(72) Krauss, M., and Haucke, V. (2007) Phosphoinositide-metabolizing enzymes at the interface between membrane traffic and cell signalling. *EMBO Rep. 8*, 241–6.
(73) Poccia, D., and Larijani, B. (2009) Phosphatidylinositol metabolism and membrane fusion. *Biochem. J. 418*, 233–46.
(74) Sasaki, T., Takasuga, S., Sasaki, J., Kofuji, S., Eguchi, S., Yamazaki, M., and Suzuki, A. (2009) Mammalian phosphoinositide kinases and phosphatases. *Prog. Lipid Res. 48*, 307–343.
(75) Harris, S. J., Parry, R. V, Westwick, J., and Ward, S. G. (2008) Phosphoinositide lipid phosphatases: natural regulators of phosphoinositide 3-kinase signaling in T lymphocytes. *J. Biol. Chem. 283*, 2465–9.
(76) HURLEY, J. (2006) Membrane binding domains. *Biochim. Biophys. Acta - Mol. Cell Biol. Lipids 1761*, 805–811.
(77) Hurley, J. H., and Misra, S. (2000) Signaling and Subcellular Targeting by Membrane-Binding Domains. *Annu. Rev. Biophys. Biomol. Struct. 29*, 49–79.
(78) Lemmon, M. A. (2003) Phosphoinositide recognition domains. *Traffic 4*, 201–13.
(79) Lemmon, M. A. (2007) Pleckstrin homology (PH) domains and phosphoinositides. *Biochem. Soc. Symp. 74*, 81–93.
(80) Lemmon, M. A., and Ferguson, K. M. (2000) Signal-dependent membrane targeting by pleckstrin homology (PH) domains. *Biochem. J 350*, 1–18.
(81) Mclaughlin, S., Wang, J., Gambhir, A., and Murray, D. (2002) PIP 2 AND PROTEINS: Interactions, Organization, and Information Flow. *Annu. Rev. Biophys. Biomol. Struct 31*, 151–75.
(82) Hirose, K., Kadowaki, S., Tanabe, M., Takeshima, H., and Iino, M. (1999) Spatiotemporal dynamics of inositol 1,4,5-trisphosphate that underlies complex Ca2+ mobilization patterns. *Science 284*, 1527–30.
(83) Kutateladze, T. G. (2006) Phosphatidylinositol 3-phosphate recognition and membrane docking by the FYVE domain. *Biochim. Biophys. Acta 1761*, 868–77.
(84) Bravo, J., Karathanassis, D., Pacold, C. M., Pacold, M. E., Ellson, C. D., Anderson, K. E., Butler, P. J., Lavenir, I., Perisic, O., Hawkins, P. T., Stephens, L., and Williams, R. L. (2001) The crystal structure of the PX domain from p40(phox) bound to phosphatidylinositol 3-phosphate. *Mol. Cell 8*, 829–39.

(85) Canals, D., Roddy, P., and Hannun, Y. A. (2012) Protein phosphatase 1 alpha mediates ceramide-induced ERM protein dephosphorylation. *J. Biochem. 287*, 10145–10155.
(86) Holmes, A. B., Margaret Brimble, P. A., Conway, S. J., Gardiner, J., A Grove, S. J., Johns, M. K., Lim, Z.-Y., Painter, G. F., J E Robinson, D. E., Schieber, C., Thuring, J. W., S-M Wong, L., Yin, M.-X., Burgess, A. W., Catimel, B., Hawkins, P. T., Ktistakis, N. T., and Stephens, L. R. (2010) Synthesis and biological evaluation of phosphatidylinositol phosphate affinity probes. *Org. Biomol. Chem. 8*, 1477–520.
(87) Ozaki, S., Watanabe, Y., Ogasawara, T., Kondo, Y., Shiotani, N., Nishii, H., and Matsuki, T. (1986) Total synthesis of optically active myo-inositol 1,4,5-tris(phosphate). *Tetrahedron Lett. 27*, 3157–3160.
(88) Potter, B. V. L. (1990) Recent Advances in the Chemistry and Biochemistry of lnositol Phosphates of Biological Interest. *Nat. Prod. Rep. 7*, 1.
(89) Billington, D. C. (1989) Recent Developments in the Synthesis of myo-Inositol Phosphates. *Chem. Soc. Rev. 18*, 83–122.
(90) Kiely, D. E., Abruscato, G. J., and Baburao, V. (1974) A synthesis of (±)myo-inositol 1-phosphate. *Carbohydr. Res. 34*, 307–313.
(91) Kubiak, R. J., and Bruzik, K. S. (2003) Comprehensive and Uniform Synthesis of All Naturally Occurring Phosphorylated Phosphatidylinositols involving inositol phospholipids (PIPn) and phosphates *6061*, 960–968.
(92) Watanabe, Y., Komoda, Y., Ebisuya, K., and Oxaki, S. (1990) An efficient phosphorylation method using a new phosphitylating agent, 2-diethylamino-1,3,2-benzodioxaphosphepane. *Tetrahedron Lett. 31*, 255–256.
(93) Yu, K.-L., and Fraser-Reid, B. (1988) A novel reagent for the synthesis of myo-inositol phosphates: N,N-Diisopropyl dibenzyl phosphoramidite. *Tetrahedron Lett. 29*, 979–982.
(94) Watanabe, Y., Nakahira, H., Bunya, M., and Ozaki, S. (1987) An efficient method for phosphorylation of inositol derivatives. *Tetrahedron Lett. 28*, 4179–4180.
(95) Cooke, A. M., Noble, N. J., Payne, S., Gigg, R., and Potters, B. V. L. (1989) Synthesis of myo-lnositol 1,4-Bisphosphate-5-phosphorothioate. *J. Chem. Soc., Chem, Commun. 120519*, 269–271.
(96) Dreef, C. E., Elie, C. J. J., Hoogerhout, P., van der Marel, G. A., and van Boom, J. H. (1988) Synthesis of 1-O-(1,2,-Di-O-Palmitoyl-SN-Glycero-3-phospho-D-myo-inosital 4,5-bisphosphate: an analogue of naturally occuring (Ptd)Ins(4,5)P2. *Tetrahedron Lett. 29*, 6513–6516.
(97) Baudin, G., Glänzer, B. I., Swaminathan, K. S., and Vasella, A. (1988) A Synthesis of 1

D - and 1 L -myo-Inositol 1,3,4,5,-Tetraphosphate. *Helv. Chim. Acta 71*, 1367–1378.
(98) Vacca, J. P., deSolms, S. J., R. Huff, J., Billington, D. C., Baker, R., Kulagowski, J. J., and Mawer, I. M. (1989) The total synthesis of myo-inositol polyphosphates. *Tetrahedron 45*, 5679–5702.
(99) Anderson, R. J., Osborne, S. L., Meunier, F. A., and Painter, G. F. (2010) Regioselective Approach to Phosphatidylinositol 3,5-Bisphosphates: Syntheses of the Native Phospholipid and Biotinylated Short-Chain Derivative. *J. Org. Chem 75*, 3541–3551.
(100) Xu, Y., Sculimbrene, B. R., and Miller, S. J. (2006) Streamlined Synthesis of Phosphatidylinositol (PI), PI3P, PI3,5P 2 , and Deoxygenated Analogues as Potential Biological Probes. *J. Org. Chem. 71*, 4919–1928.
(101) Conway, S. J., and Miller, G. J. (2007) Biology-enabling inositol phosphates, phosphatidylinositol phosphates and derivatives. *Nat. Prod. Rep. 24*, 687.
(102) Potter, B. V. L., and Lampe, D. (1995) Chemistry of Inositol Lipid Mediated Cellular Signaling. *Angew. Chemie Int. Ed. English 34*, 1933–1972.
(103) Irvine, R. F., and Schell, M. J. (2001) Back in the water: the return of the inositol phosphates. *Nat. Rev. Mol. Cell Biol. 2*, 327–338.
(104) Hatch, A. J., and York, J. D. (2010) SnapShot: Inositol Phosphates. *Cell 143*, 1030–1030.e1.
(105) Chakraborty, A., Kim, S., and Snyder, S. H. (2011) Inositol Pyrophosphates as Mammalian Cell Signals. *Sci. Sig. 4*, re1.
(106) Gillaspy, G. E. (2011) The cellular language of myo-inositol signaling. *New Phytol. 192*, 823–839.
(107) Michell, R. H. (2011) Inositol and its derivatives: Their evolution and functions. *Adv. Enzyme Regul. 51*, 84–90.
(108) Lee, J.-Y., Kim, Y., Park, J., and Kim, S. (2012) Inositol polyphosphate multikinase signaling in the regulation of metabolism. *Ann. N. Y. Acad. Sci. 1271*, 68–74.
(109) Croze, M. L., and Soulage, C. O. (2013) Potential role and therapeutic interests of myo-inositol in metabolic diseases. *Biochimie 95*, 1811–1827.
(110) Billington, D. C., Baker, R., Kulagowski, J. J., Mawer, I. M., Vacca, J. P., Jane, S., Huff, J. R., Sharp, M., and Point, W. (1989) The Total Synthesis of myo-lnositol Phosphates via myo-lnositol Orthoformate. *J. Chem.Soc. Perkin. Trans. I* 1423–1429.
(111) Thomas, M. P., Mills, S. J., and Potter, B. V. L. (2016) The “Other” Inositols and Their Phosphates: Synthesis, Biology, and Medicine (with Recent Advances in myo-Inositol Chemistry). *Angew. Chem. Int. Ed. Engl. 55*, 1614–50.
(112) Billington, D. C., Baker, R., Kulagowski, J. J., Mawer, I. M., Vacca, J. P., DeSolms, S. J.,

and Huff, J. R. (1989) The total synthesis of myo-inositol phosphates via myo-inositol orthoformate. *J. Chem. Soc. Perkin Trans. 1 1*, 1423–1429.
(113) Pettitt, T. R., Dove, S. K., Lubben, A., Calaminus, S. D. J., and Wakelam, M. J. O. (2006) Analysis of intact phosphoinositides in biological samples. *J. Lipid Res. 47*, 1588–1596.
(114) Bruzik, K. S., and Tsai, M.-D. (1992) Efficient and Systematic Syntheses of Enantiomerically Pure and Regiospecifically Protected myo-Inositols. *J. Am. Chem. Soc 114*, 6361–6374.
(115) Zhang, H., Xu, Y., Markadieu, N., Beauwens, R., Erneux, C., and Prestwich, G. D. (2008) Synthesis and biological activity of phosphatidylinositol-3,4,5-trisphosphorothioate. *Bioorg. Med. Chem. Lett. 18*, 762–766.
(116) Miller, D. J., Bashir-Uddin Surfraz, M., Akhtar, M., Gani, D., and Allemann, R. K. (2004) Removal of the phosphate group in mechanism-based inhibitors of inositol monophosphatase leads to unusual inhibitory activity. *Org. Biomol. Chem. 2*, 671–688.
(117) Dinkel, C., Moody, M., Traynor-Kaplan, A., and Schultz, C. (2001) Membrane-Permeant 3-OH-Phosphorylated Phosphoinositide Derivatives. *Angew. Chemie Int. Ed. 40*, 3004–3008.
(118) Vajanaphanich, M., Schultz, C., Rudolf, M. T., Wasserman, M., Enyedi, P., Craxton, A., Shears, S. B., Tsien, R. Y., Barrett, K. E., and Traynor-Kaplan, A. (1994) Long-term uncoupling of chloride secretion from intracellular calcium levels by lns(3,4,5,6)P4. *Nature 371*, 711–714.
(119) Schultz, C. (2010) Challenges in studying phospholipid signaling. *Nat. Chem. Biol. www.nature.com/naturechemicalbiology 6*.
(120) Bru, M., Kotkar, S. P., Kar, N., and Kohn, M. (2012) Development of a solid phase synthesis strategy for soluble phosphoinositide analogues. *Chem. Sci. 3*, 1893–1902.
(121) Poon, K. W. C., and Dudley, G. B. (2006) Mix-and-Heat Benzylation of Alcohols Using a Bench-Stable Pyridinium Salt.
(122) Paterson, I., and Coster, M. J. (2002) Total synthesis of altohyrtin A (spongistatin 1): An alternative synthesis of the CD-spiroacetal subunit. *Tetrahedron Lett.*
(123) Dvorakova, M., Nencka, R., Dejmek, M., Zbornikova, E., Brezinova, A., Pribylova, M., Pohl, R., Migaud, M. E., and Vanek, T. (2013) Organic & Biomolecular Chemistry Synthesis of alkylcarbonate analogs of O-acetyl-ADP-ribose. *Org. Biomol. Chem 11*.
(124) Yu, K.-L., and Fraser-Reid, B. (1988) A novel reagent for the synthesis of myo-inositol phosphates: N,N-Diisopropyl dibenzyl phosphoramidite. *Tetrahedron Lett. 29*, 979–982.
(125) Gregory, M., Meng-Xin, A., Yin, A., Mcconville, M. J., Williams, E., Bullock, A. N.,

Conway, S. J., Burgess, A. W., Catimel, B., and Holmes, A. B. (2015) Synthesis of Highly Water-Soluble Adamantyl Phosphoinositide Derivatives. *Aust. J. Chem. 68*, 543–548.
(126) Bru, M., Kotkar, S. P., Kar, N., and Köhn, M. (2012) Development of a solid phase synthesis strategy for soluble phosphoinositide analogues. *Chem. Sci. 3*, 1893–1902.
(127) Roberts, S. J., Stewart, A. J., Sadler, P. J., and Farquharson, C. (2004) Human PHOSPHO1 exhibits high specific phosphoethanolamine and phosphocholine phosphatase activities. *Biochem. J. 382*, 59–65.
(128) Sun, J.-P., Luo, Y., Yu, X., Wang, W.-Q., Zhou, B., Liang, F., and Zhang, Z.-Y. (2007) Phosphatase activity, trimerization, and the C-terminal polybasic region are all required for PRL1-mediated cell growth and migration. *J. Biol. Chem. 282*, 29043–51.
(129) Atkins, W. M. (2005) Non-Michaelis-Menten kinetics in cytochrome P450-catalyzed reactions. *Annu. Rev. Pharmacol. Toxicol. 45*, 291–310.
(130) Kisseleva, M. V., Wilson, M. P., and Majerus, P. W. (2000) The isolation and characterization of a cDNA encoding phospholipid- specific inositol polyphosphate 5-phosphatase. *J. Biol. Chem. 275*, 20110–20116.
(131) Billcliff, P. G., Noakes, C. J., Mehta, Z. B., Yan, G., Mak, L., Woscholski, R., and Lowe, M. (2015) OCRL1 engages with the F-BAR protein pacsin 2 to promote biogenesis of membrane-trafficking intermediates. *Mol. Biol. Cell 27*, 90–107.
(132) Chang-Ileto, B., Frere, S. G., Chan, R. B., Voronov, S. V, Lien Roux, A., and Di Paolo, G. (2011) Synaptojanin 1-Mediated PI(4,5)P 2 Hydrolysis Is Modulated by Membrane Curvature and Facilitates Membrane Fission. *Dev. Cell 20*, 206–218.
(133) Guo, S., Stolz, L. E., Lemrow, S. M., and York, J. D. (1999) SAC1-like domains of yeast SAC1, INP52, and INP53 and of human synaptojanin encode polyphosphoinositide phosphatases. *J. Biol. Chem. 274*, 12990–5.
(134) McPherson, P. S., Garcia, E. P., Slepnev, V. I., David, C., Zhang, X., Grabs, D., Sossini, W. S., Bauerfeind, R., Nemoto, Y., and De Camilli, P. (1996) A presynaptic inositol-5-phosphatase. *Nature 379*, 353–357.
(135) Aguilar, R. C., Madhivanan, K., and Ramadesika, S. (2016) Role of Ocrl1 and Inpp5E in primary cilia assembly and maintenance: a phosphatidylinositol phosphatase relay system? *Res. Rep. Biol. 7*, 15.
(136) Mao, Y., Balkin, D. M., Zoncu, R., Erdmann, K. S., Tomasini, L., Hu, F., Jin, M. M., Hodsdon, M. E., and De Camilli, P. (2009) A PH domain within OCRL bridges clathrin-mediated membrane trafficking to phosphoinositide metabolism. *EMBO J. 28*, 1831–42.
(137) Lee, K., Kang, H. J., Xia, Y., and Chung, S. J. (2011) Recent Advances in Protein Tyrosine Phosphatase Detection Using Chemical Probes. *Anticancer. Agents Med. Chem. 11*, 54–63.

(138) Jain, A. N. (2000) Morphological similarity: A 3D molecular similarity method correlated with protein-ligand recognition. *J. Comput. Aided. Mol. Des. 14*, 199–213.